SANDIA REPORT

SAND2004-4859
Unlimited Release
Printed October 2004

Natural Gas Production Problems: Solutions, Methodologies, and Modeling

John C. Lorenz, Scott P. Cooper, Bill W. Arnold, Paul M. Basinski, James M. Herrin, John F. Holland, Russell G. Keefe, Rich Larson, William A. Olsson, Christopher A. Rautman

Prepared by
Sandia National Laboratories
Albuquerque, New Mexico 87185 and Livermore, California 94550

Sandia is a multiprogram laboratory operated by Sandia Corporation,
a Lockheed Martin Company, for the United States Department of Energy's
National Nuclear Security Administration under Contract DE-AC04-94AL85000.

Sandia National Laboratories

Issued by Sandia National Laboratories, operated for the United States Department of Energy by Sandia Corporation.

Available to DOE and DOE contractors from
U.S. Department of Energy
Office of Scientific and Technical Information
P.O. Box 62
Oak Ridge, TN 37831

Telephone: (865)576-8401
Facsimile: (865)576-5728
E-Mail: reports@adonis.osti.gov
Online ordering: http://www.osti.gov/bridge

Available to the public from
U.S. Department of Commerce
National Technical Information Service
5285 Port Royal Rd
Springfield, VA 22161

Telephone: (800)553-6847
Facsimile: (703)605-6900
E-Mail: orders@ntis.fedworld.gov
Online order: http://www.ntis.gov/help/ordermethods.asp?loc=7-4-0#online

SAND 2004-4859
Unlimited Release
Printed October-2004

Natural Gas Production Problems: Solutions, Methodologies, and Modeling

Team Members and Authors

John C. Lorenz, Scott P. Cooper, James M. Herrin, and Russell G. Keefe
Geophysical Technology Department

Bill W. Arnold
Total System Performance Assessment

William A. Olsson
Geomechanics Department

John F. Holland
Structural Mechanics Engineering Department

Christopher A. Rautman
Geotechnology and Engineering Department

Sandia National Laboratories
P.O. Box 5800
Albuquerque, NM 87185-0706

Rich Larson
Vermejo Park Ranch
P.O. Drawer E
Raton, NM 87740

Paul M. Basinski
El Paso Production Company
Nine Greenway Plaza
Houston, TX 77046

Ron Broadhead
New Mexico Bureau of Geology and Mineral Resources
801 Leroy Place
Socorro NM 87801-4796

Thomas W. Engler
Petroleum and Natural Gas Engineering Department
New Mexico Institute of Mining and Technology
801 Leroy Place
Socorro NM, 87801

Gus Holm
Vermejo Park Ranch
P.O. Drawer E
Raton, NM 87740

Curt McKinney
Devon Energy Corporation
20 North Broadway
Oklahoma City, OK 73102-8260

Connie D. Knight
Consulting Geologist
Golden, CO 80401

Abstract

Natural gas is a clean fuel that will be the most important domestic energy resource for the first half the 21st century. Ensuring a stable supply is essential for our national energy security. The research we have undertaken will maximize the extractable volume of gas while minimizing the environmental impact of surface disturbances associated with drilling and production. This report describes a methodology for comprehensive evaluation and modeling of the total gas system within a basin focusing on problematic horizontal fluid flow variability. This has been accomplished through extensive use of geophysical, core (rock sample) and outcrop data to interpret and predict directional flow and production trends. Side benefits include reduced environmental impact of drilling due to reduced number of required wells for resource extraction.

These results have been accomplished through a cooperative and integrated systems approach involving industry, government, academia and a multi-organizational team within Sandia National Laboratories. Industry has provided essential in-kind support to this project in the forms of extensive core data, production data, maps, seismic data, production analyses, engineering studies, plus equipment and staff for obtaining geophysical data.

This approach provides innovative ideas and technologies to bring new resources to market and to reduce the overall environmental impact of drilling. More importantly, the products of this research are not be location specific but can be extended to other areas of gas production throughout the Rocky Mountain area. Thus this project is designed to solve problems associated with natural gas production at developing sites, or at old sites under redevelopment.

This page intentionally left blank.

Table of Contents

List of Figures

1.0 INTRODUCTION

This study is primarily concerned with issues related to domestic natural gas development because unlike crude oil or refined petroleum products, natural gas cannot be easily imported from overseas. To import natural gas it must be liquefied, carried under pressure within cryogenic tankers and unloaded at facilities specifically designed to safely handle this product. Each of these transportation items is extremely expensive and will require significant lead-time to build. There are currently five such facilities in the United States but finding additional communities along the coast that would accept a new facility may be difficult.

Given the limited natural gas resources in Canada, along with their own energy demands, and the fact that Mexico is a net importer of natural gas from the U.S.A., natural gas must be an internally-sourced United States commodity. Small independent gas companies are the primary producers in the U.S.A. yet within their companies they do not have the technical expertise to engage in the type of research we can provide. Nevertheless, demand for natural gas is anticipated by the Energy Information Administration (EIA) to increase by 50% or 10 trillion cubic feet by 2020. It is also important to recognize that besides home heating, natural gas is primarily used to generate electricity. In a statement to the U.S. Chamber of Commerce's National Energy Summit in 2001, Energy Secretary Spencer Abraham cited figures from the EIA showing a 45% increase in demand for electrical power over the next 20 years, but without corresponding increases in domestic production. Without increasing domestic production, natural gas shortages and associated electrical power blackouts can be anticipated and, in fact, have already occurred. Therefore, natural gas has become vital to our national energy security.

1.1 PURPOSE OF STUDY

The study site is the Raton Basin in northeastern New Mexico and southeastern Colorado. Since commercial production began in late 2000, the Raton Basin has become the second most active coalbed methane field in the U.S. and contains an estimated 18 trillion cubic feet of natural gas.

Much of the natural gas in the Raton Basin is disseminated within numerous thick, naturally fractured, rock (sandstone) layers that do not readily allow fluids, including natural gas, to flow through them. These sandstones are officially described as 'tight' signifying that they are not conducive to fluid movement. The only way these tight sandstones can actually produce natural gas is if the sandstones contain fractures (are naturally broken). These breaks or fractures allow fluid movement within the open areas between the broken sections of rock and create a natural plumbing system enabling fluids to move within the sandstones. Each of these sandstone layers can be a separate resource having its own distinct plumbing system.

The thick, naturally fractured, tight sandstones within the Raton Basin are not being developed because the system of stress-sensitive fractures and stress-controlled fluid flow is very poorly understood. The stress field and fracture orientations and distributions in the basin are complicated by the presence of numerous impermeable, igneous rock units. Stress systems (*in situ* and applied stresses) control both the formation of natural fractures and their response to pressure changes during production; thus understanding the stresses is very important in optimizing resource recovery from this or any other basin. The stress field in combination with the natural fracture system also controls the directionality of fluid flow. An understanding of this directionality is fundamental for efficient well placement and resource development.

The final product of this work is a systematic approach for the development of 1) an exploration and extraction methodology applicable to many other basins, 2) a model of the Raton Basin, the parameters of which can be easily changed for application to other basins, 3) a thorough understanding of these variables permitting operators to efficiently develop the resource with fewer wells (cheaper) and minimal environmental impact (cleaner), 4) the exploration methodology and model can be designed such that the possible sequestration (i.e. underground storage) of produced liquids and gases (such as CO_2) can be addressed in the development stage of a basin.

1.2 LOCATION AND GEOLOGIC SETTING

The Raton Basin (Figure 1) is located along the Colorado-New Mexico state line. It is an elongate, asymmetric, Laramide-age sedimentary basin. The greater Raton Basin extends over approximately 4,000 mi^2. The coal section, which is within the Raton Mesa portion of the basin, covers an area of over 2100 square miles (Tyler et al., 1995). The basin is bordered on the west by the Sangre de Cristo Mountains, to the north by the Wet Mountains, to the northeast by the Apishapa Arch, to the east by the Las Animas Arch and to the southeast and south by the Sierra Grande Uplift. The basin was formed during the Laramide orogeny as tectonic activity uplifted the Sangre de Cristo Mountains and created numerous folds and reverse faults across the basin.

The western margin of the basin has numerous thrust faults and is highly deformed. In contrast the eastern limb gently dips, 1-2 degrees, toward the west. The basin is highly asymmetrical with its synclinal axis parallel and near to the Sangre de Cristo uplift. The Raton Mesa part of the basin is defined as the area that contains the stratigraphic units above the Trinidad Sandstone/Pierre Shale contact. The overlying units were deposited in the basin as the basin was subsiding. Deposition into the basin was followed by broad uplift of the entire Rocky Mountain area and subsequent erosion of stratigraphic units.

Tertiary volcanism was common throughout the basin followed by Rio Grande rift extension leading to the western side of the Sangre de Cristo Mountains being dissected by normal faults that down dropped the western portion of these Laramide age mountains into the Rio Grande Rift. Detailed discussion of the tectonic history and stratigraphy of this area are in sections 1.2.1 and 1.2.2.

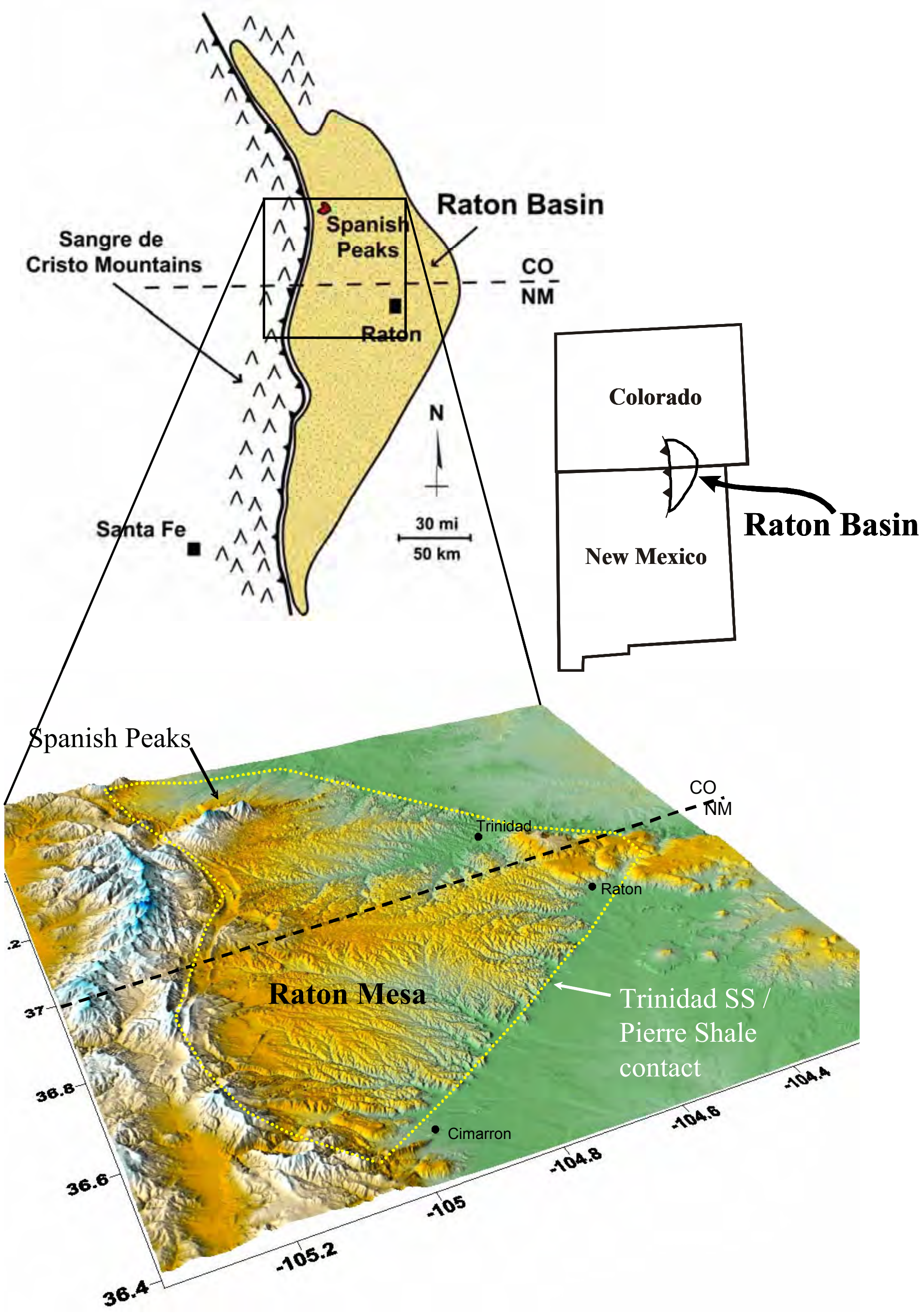

Figure 1: Maps of the greater Raton Basin (defined structurally) and Raton Mesa (a geographic province within the basin); the latter is the area of coal-bed methane production.

1.2.1 Stratigraphy

Tertiary deposition within the basin was directly tied to ongoing orogenic activity. In Late Cretaceous time the Raton area was the southern extension of the Rocky Mountain Foreland Basin. Formations deposited along what was then the coast of the Western Interior Seaway include the Pierre Shale, Trinidad Sandstone and the Vermejo Formation (Figures 2 and 3). East directed thrusting continued and eventually isolated the Raton Basin from the main foreland basin as evidenced by conglomerates within the Raton Formation. Tectonic activity continued into Paleocene time with the associated deposition of the Poison Canyon Formation. Further activity continued into Eocene time with deposition of the Cuchara, Huerfano and Farasita Formations. It is only within Eocene time that the Sangre de Cristo Mountains became a source of sediment (Merin et al., 1988; Tyler et al., 1995).

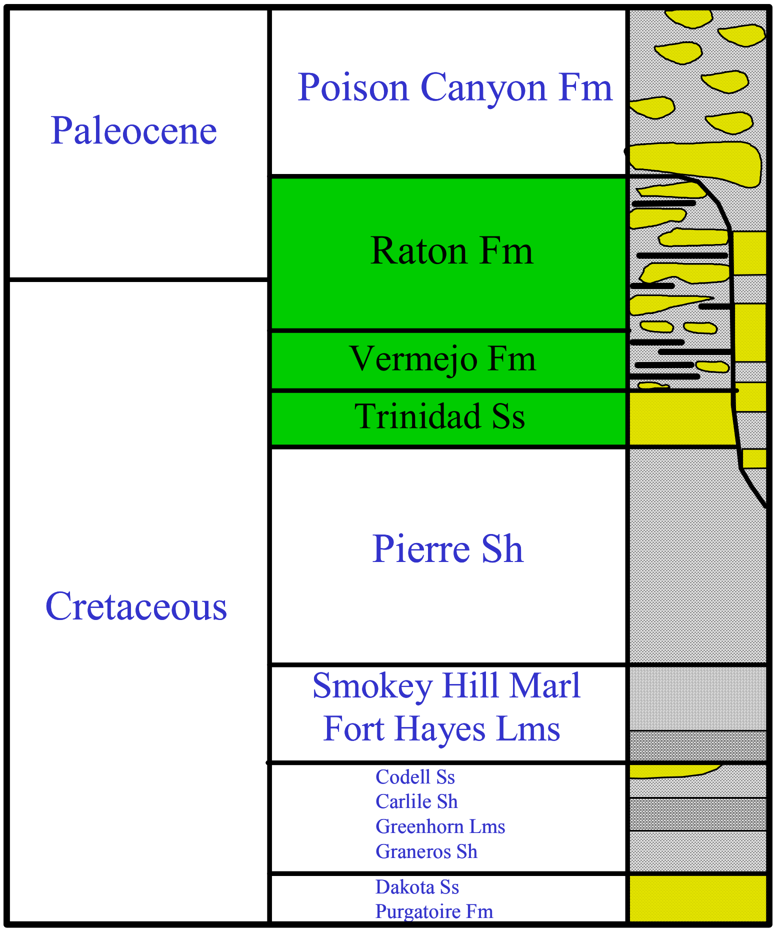

Figure 2: Partial geologic column of the Raton Basin area (modified after Dolly and Messier, 1977). Units highlighted in green are those of interest with respect to coal-bed methane production.

Figure 3: Outcrop exposures of the major coalbed methane producing intervals; Raton and Vermejo Formations along the NE flank of the Vermejo Park anticline.

The youngest deposits preserved within the Basin are preserved only within the Colorado portion of the Basin and consist of the Chuchara, Huerfano, and Farasita formation (Eocene-Oligocene?). Other units, now eroded away, overlaid these formations. This is evidenced by the Spanish Peaks which are an intrusive igneous complex that was buried at least a kilometer below the paleosurface (Johnson, 1968; Hemmerich, 2001) but are now well exposed as resistant mountains (Figure 1). Sills and dikes across the basin are inferred to have been emplaced at reconstructed depths of at least 5,000 ft. The cover removed from the New Mexico portion of the basin may have exceeded 8,000 ft (Hemmerich, 2001). Discordent overlying sediments of the Miocene age Devils Hole Formation contains abundant volcanic detritus much of which is correlative with erosion of these intrusive volcanic rocks. Rock units within the zone of coal-bed methane production interest include the Raton Formation, Vermejo Formation, and the Trinidad Sandstone (Figure 2).

Upper Cretaceous and Tertiary Rocks

Poison Canyon Formation

The Poison Canyon Formation overlies the Raton Formation and at the western edge of the basin it interfingers and truncates the Raton Formation (Pillmore, 1969). At certain locations in the northern and western portions of the basin the Poison Canyon is in unconformable contact with the underlying Pierre Shale (Figures 2 and 3; Dolly and Messier, 1977). This formation is composed of lenticular coarse-grained arkosic sandstones and micaceous sandy mudstones and varies in thickness from 0 to 2500 ft (0 - 760 m) across the basin.

Raton Formation

The Raton Formation underlies the Poison Canyon Formation and overlies the Vermejo Formation (Figure 2). It varies in thickness from 0 - 2075 ft (0 – 630 m) across the basin (Dolly and Meissner, 1977). It is composed of a variety of sandstones, siltstones, mudstones, conglomerates, coals and carbonaceous shales associated with a fluvial depositional type of environment. Pillmore and Flores (1987) divide the formation into three lithofacies; Upper Coal Zone, Barren Series, and the Lower Coal Zone (Figure 4). Coal seams in the Raton Formation are thinner, more numerous, and less continuous than those of the underlying Vermejo Formation. Maximum seam thickness is 8 feet, but typical average thickness is only 1.5 feet. The coal-bearing zones of the Raton may contain up to 50 individual seams with a net thickness of more than 80 feet (24 m). Additional data on the coal beds is provided in Section 2.08 (Production).

AGE	FORMATION NAME	GENERAL DESCRIPTION	
PALEOCENE	Poison Canyon Formation	Sandstone: Coarse to conglomeratic; beds 15-50 ft thick; interbeds of yellow-weathering, clayey sandstone. Thickens to west at expense of underlying Raton Formation	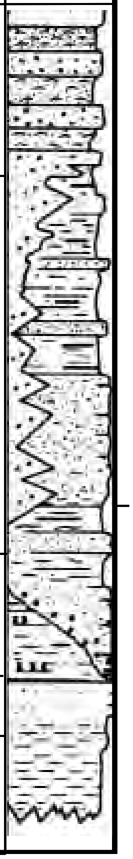
UPPER CRETACEOUS	Raton Formation	Formation intertongues with Poison Canyon Formation to the west Upper Coal Zone: Very fine grained sandstone, siltstone, and mudstone with carbonaceous shale and thick coal beds Barren Series: Mostly very fine grained sandstone with minor mudstone, siltstone, carbonaceous shale, and thin coal beds Lower Coal Zone: Same as upper coal zone; coal beds mostly thin and discontinuous; conglomeratic sandstone at base; locally absent	
	Vermejo Formation	Sandstone: Fine- to medium-grained; also mudstone, carbonaceous shale, extensive, thick coal beds. Local sills	
	Trinidad Sandstone	Sandstone: Fine- to medium-grained; contains casts of *Ophiomorpha*	
	Pierre Shale	Shale: Silty in upper 300 ft; grades up to fine-grained sandstone; contains limestone concretions	

K-T Boundary

Figure 4: Generalized stratigraphic section of the rock units discussed within this report and located on the Raton Mesa (modified from Pillmore and Flores, 1987).

The Upper Coal Zone ranges in thickness from 590 to 1100 ft (180 – 335 m). Flood plains and swamps were the environments of deposition for this unit. Therefore it contains sequences of crevasse-splay sandstones, mudstones, siltstones and shales along with carbonaceous shales and coals. Lenticular coal beds range in thickness from 3 to 6 ft (1 – 2 m; Pillmore and Flores, 1987).

The Barren Series varies in thickness from 600 ft (180 m) in the western side of the basin to 180 ft (55 m) on the eastern side. A series of fluvial and flood plain environments were the environments of deposition. There are numerous lenticular fluvial channel sandstones as well as mudstones and siltstones associated with the flood plain. Thin coal seams and limited carbonaceous shales can also be found within the Barren Series.

The Lower Coal Zone was deposited on an alluvial plain containing numerous fluvial channels, crevasse splays, and flood plain deposits. The thickness of this zone ranges from 300 ft (90 m) in the western portions of the basin to 100 ft (30 m) in the eastern sections. A basal conglomeratic sandstone is observed in parts of the basin ranging in thickness from 0 to 50 ft (0 to 15 m). The K-T boundary, evidenced by an iridium layer, is found near the contact of the Lower Coal Zone with the overlying Barren series (Pillmore and Flores, 1987).

Vermejo Formation

The Vermejo Formation ranges in thickness from 380 ft (115 m) to 0 ft, the thickest sections are along the western side of the basin. It was deposited landward of the Trinidad Sandstone in fluvial, deltaic and back-barrier environments. As expected from deposition within these paleoenvironments the Vermejo Formation is composed of alternating beds of sandstone, siltstone, shale, carbonaceous shale, and coal. The Vermejo Formation was also found to intertongue with the Trinidad sandstone in the area between Cimarron and Dawson along the southwestern edge of the Raton Mesa. This suggests some relative change in shoreline transgression and possible sea level change during deposition.

Individual coal beds within the Vermejo Formation can be as much as 14 feet thick, however typical coal bed thickness is 2.5 feet (1 m). Individual coal beds within the Vermejo Formation can be as thick as 14 ft (4 m). The Vermejo Formation can contain as many as 25 coal beds with a net thickness exceeding 40 feet (12 m). Additional data on Vermejo Formation coal beds is provided in Section 2.08 (Production).

Trinidad Sandstone

The Trinidad Sandstone is a laterally extensive tabular fine-grained sandstone that was deposited as the leading eastward edge of the prograding coastline of the Cretaceous Interior Seaway (Pillmore and Mayberry, 1976; Billingsley, 1977). It was deposited in barrier and delta type environments as evidenced by the numerous trace fossils, mainly *Ophiomorpha* (Figure 5) with some limited *Diplocraterion*.

Figure 5: Trinidad Sandstone with *Ophiomorpha* trace fossils.

Pierre Shale
The Pierre Shale is dark shale that coarsens and becomes siltier at the gradational contact with the overlying Trinidad Sandstone. The shale is 1300 – 2900 ft (550 – 580 m) thick and was deposited over a wide area within the Cretaceous Interior Seaway (Pillmore and Mayberry, 1976; Billingsley, 1977).

Underlying Rock Units
Below the previously described units, which are the primary units of interest for this report, is a thick Mesozoic and Paleozoic section. The entire stratigraphic column is shown in Figure 6. Some of the lower formations may be of interest concerning hydrocarbon production. For example the Dakota Sandstone is a proven tight gas reservoir in the San Juan Basin to the west of the Raton Basin.

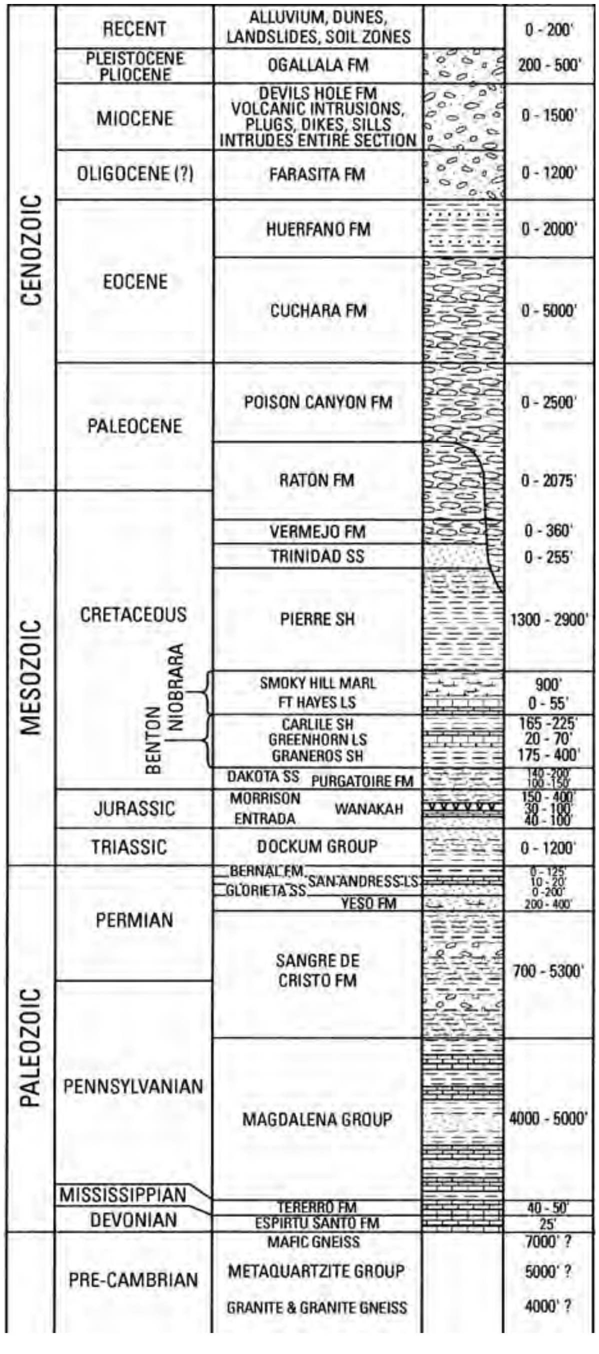

Figure 6: Generalized stratigraphic column of the northern Raton Basin (Dolly and Meissner, 1977; Johnson and Finn, 2001).

1.2.2 Tectonic Setting

The greater Raton Basin (Figure 7), located along the Colorado-New Mexico state line, it is an elongate, asymmetric, Laramide-age sedimentary basin, with an aerial extent of approximately 4,000 mi^2. The coal section, which is within the Raton Mesa portion of the basin, covers an area of over 2100 square miles (Tyler et al., 1995). The basin is bordered on the west by the Sangre de Cristo Mountains, to the north by the Wet Mountains, to the northeast by the Apishapa Arch, to the east by the Las Animas Arch and to the southeast and south by the Sierra Grande Uplift (Figure 7; Baltz, 1965). An intrabasinal arch known as the Cimarron Arch separates the northern Raton Basin from the shallower Las Vegas sub basin.

The axis of the present-day Raton Basin, the La Veta Syncline, trends roughly north-south and parallel to the Sangre de Cristo mountain range. The syncline bifurcates near the southern end of the Wet Mountains with the eastern axis named the Delcarbon Syncline (Close, 1988).

The depositional character (rock type and isopach thickness lines) of Paleozoic rock units in the basin indicates that an ancestral basin was formed in conjunction with the formation of the Ancestral Rockies during the Early Pennsylvanian. Baltz (1965) notes that this orogeny, which culminated in Late Pennsylvanian and Early Permian, was the most significant tectonic event, in the basin, from the Precambrian to the Late Cretaceous. While this paleobasin did not have the same orientation as the present-day Raton Basin (Read and Wood, 1947; Brill, 1952; Baltz, 1965: Woodward, 1984) this orogenic event did create the structural fabric that influenced the formation of geologic structures and subsequent sedimentation during the Laramide orogeny.

In Early Cretaceous time the Raton Basin was part of the regionally extensive Rocky Mountain geosyncline and accumulated over 3,500 ft (1060 m) of sediment primarily related to the Cretaceous Interior Seaway. During the initial phase of uplift in the Late Cretaceous the San Luis uplift was rising and providing the sediment source for the Trinidad Sandstone and Vermejo Formations (Baltz, 1965).

The major tectonic features of the present day Raton Basin were formed during the Laramide orogeny. The Laramide orogeny occurred over the time interval from Late Cretaceous to Early Tertiary (70 - 35 mya). The typical style of Laramide deformation includes basement-involved thrusts and sediment-filled forelands Dickenson et al., 1988). These Laramide-style deformation structures and syntectonic sedimentation are recorded in the Sangre de Cristo Mountains, and Culebra Range (a section of the Sangre de Cristo Mountains) and the Raton Basin (Figure 8). The eastern margins of the Sangre de Cristo Mountains have numerous high-angle reverse thrust faults that transposed Precambrian rocks over the Paleozoic section. These thrusts were primarily directed from the west toward the east. Overturned beds of Dakota Sandstone at the western edge of the Raton Basin in Vermejo Park Ranch suggest these thrusts cut the Cretaceous section and loaded the western margins of the basin (Figure 9). Subsequent erosion has removed traces of the overlying fault in this area. Numerous down dropped blocks break the western side of the Sangre de Cristo Mountains. These form the eastern edge of the Rio Grande Rift Valley. Underlying the fill of the San Luis Valley are the remnants of the Sangre de Cristo Mountains, as they existed prior to rifting approximately 27 mya. The deeper portions of the San Luis Valley have approximately 21,000 ft (6400 m) of Tertiary sediments overlying the remaining and buried

Cretaceous, Paleozoic and Precambrian rock units (Brister and Gries, 1994; Kluth and Schaftenaar, 1994).

Igneous rocks intruded the Raton Basin complex during the mid- to late Tertiary. These intrusives are in the forms of stocks, laccoliths, sills and dikes (Figure 10). The densest area of intrusive activity centers on the Spanish Peaks. However, numerous dikes and sills are found throughout the basin (Figure 10) (Johnson, 1961; Johnson 1968).

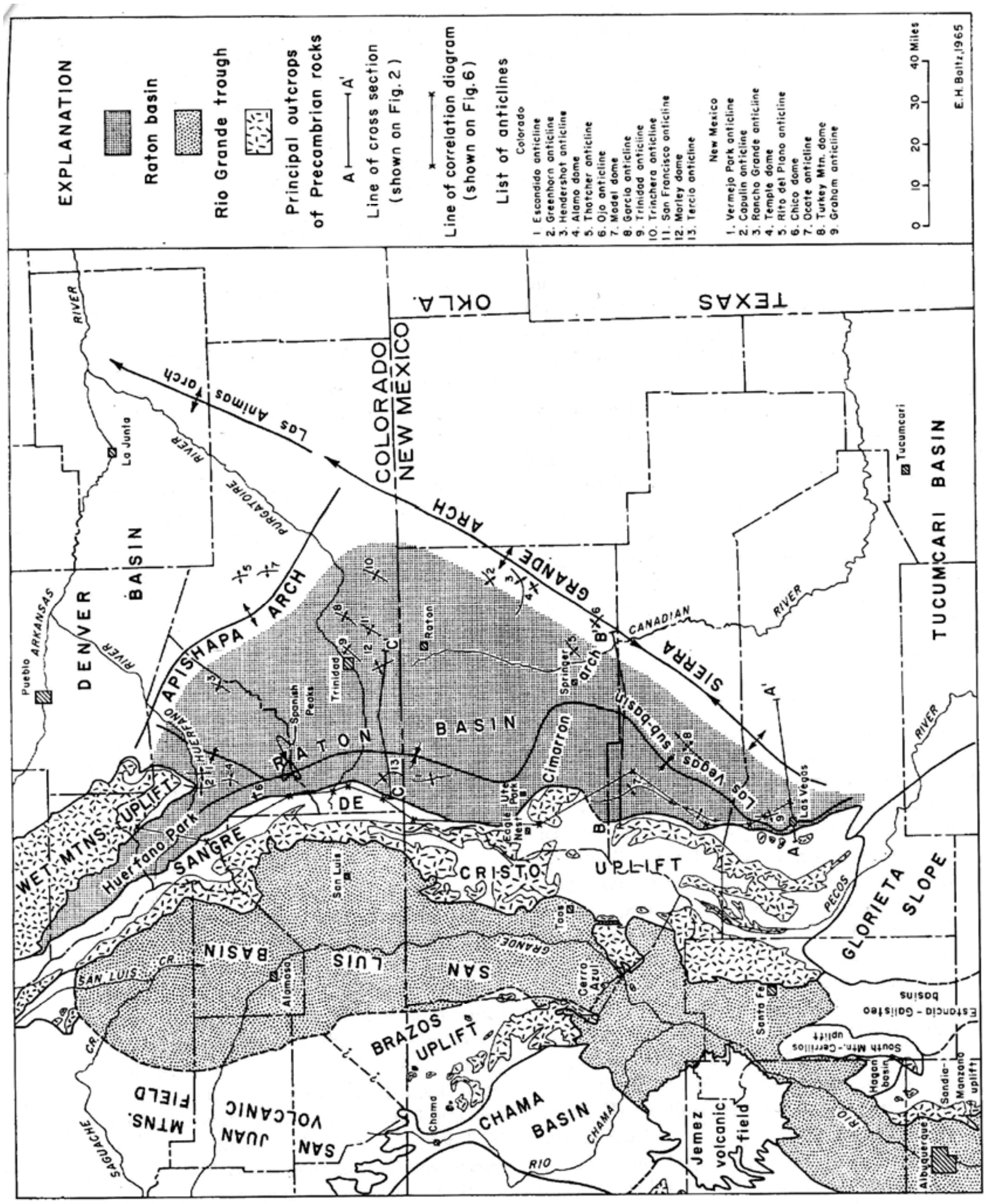

Figure 7: Raton Basin and major structures in southeastern Colorado and northeastern New Mexico (Baltz, 1965).

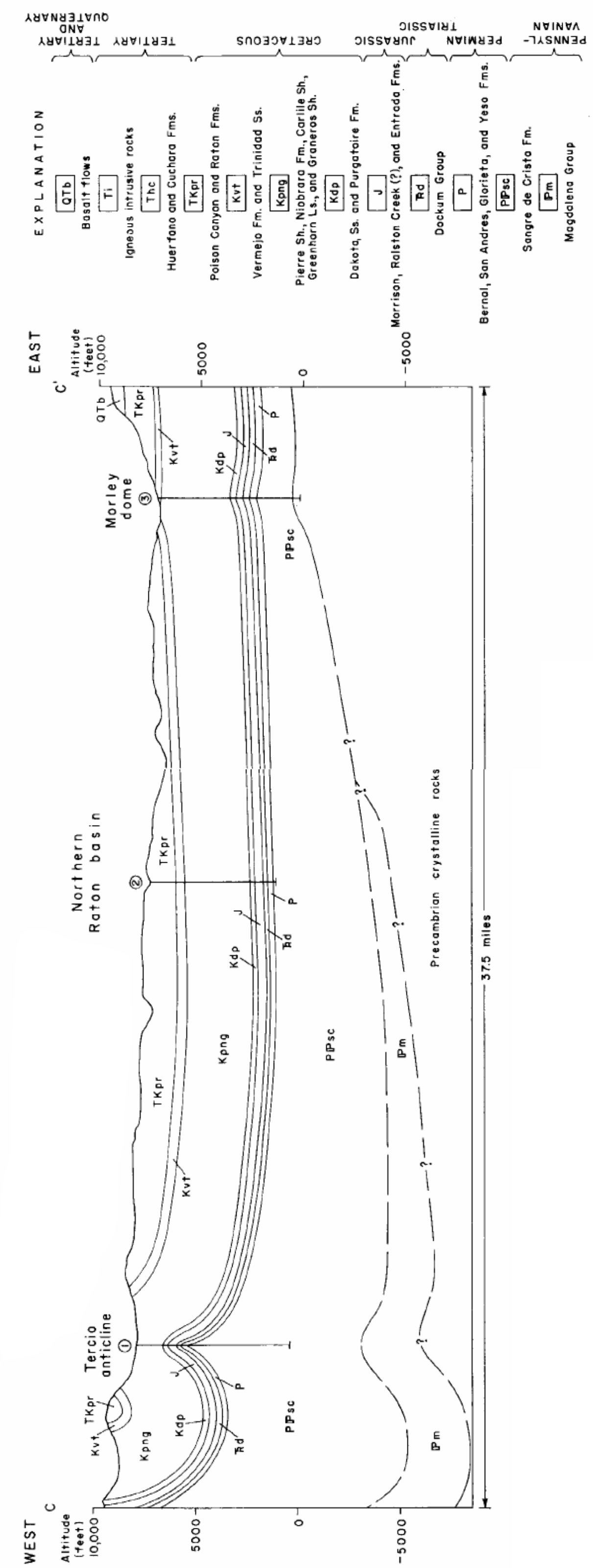

Figure 8: Diagrammatic cross section through the Raton Basin near and parallel to the New Mexico - Colorado state line.

Figure 9: Overturned beds of Cretaceous age Dakota Sandstone are evidence for an overlying thrust fault at the western margin of the Raton Basin on the Vermejo Park Ranch. Note people in lower left edge of photograph for scale.

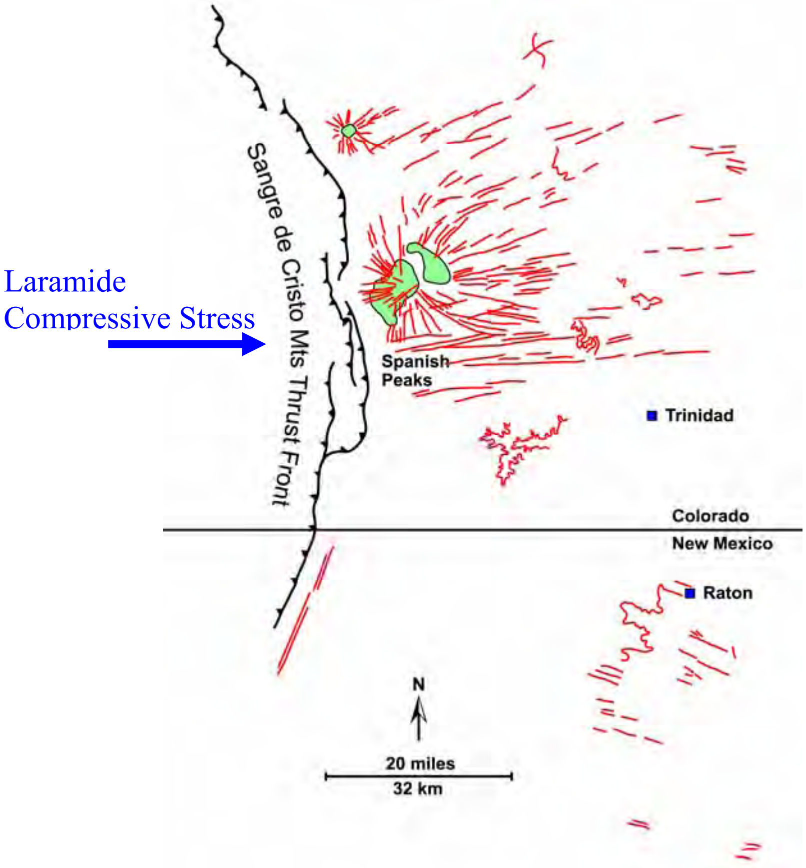

Figure 10: Map of larger scale intrusions within the Raton Basin. Due to the map scale numerous small dikes and sills are not shown. Volcanic intrusions are paleostress indicators.

A geologic sequence of events (deposition, coupled tectonism with deposition, and volcanic intrusion) from the Late Cretaceous to the present-day has combined to make the Raton basin a complex system. Figure 11 illustrates, in a simplified manner, the progressive sequence seen in the basin for the units above the Dakota Sandstone.

The igneous intrusions, late in the evolution of the basin, indicate that stresses within the basin were in a state of flux. Specifically, the vertical stress was either the maximum or intermediate stress during formation of the dikes, but was the minimum stress during formation of the sills (Figure 12).

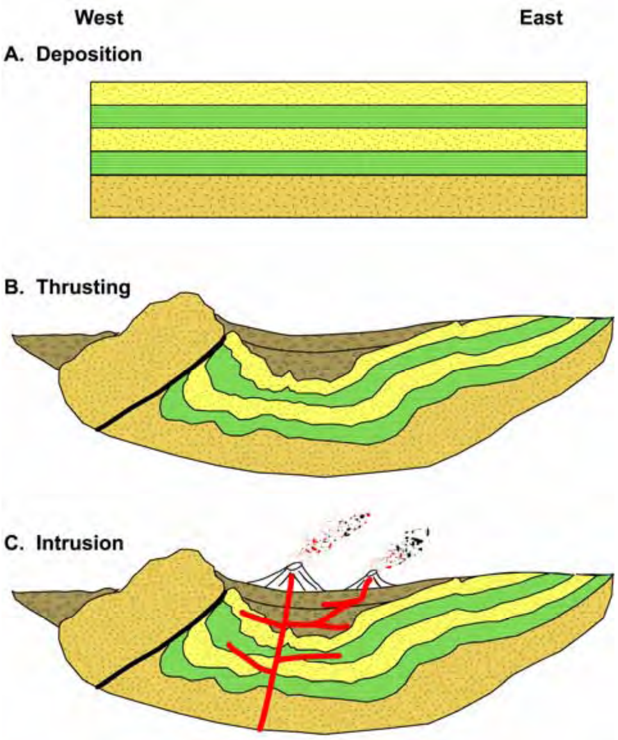

Figure 11: Simplified tectonic and depositional sequence of the Raton Basin. A) Initial deposition of sediments. B) Uplift and eastward thrusting of the Sangre de Cristo Mountains forms the basin. Syntectonic deposition also occurred within the basin at this time. C) Intrusion of magma into this geologic system formed laccoliths, stocks, dikes, and sills.

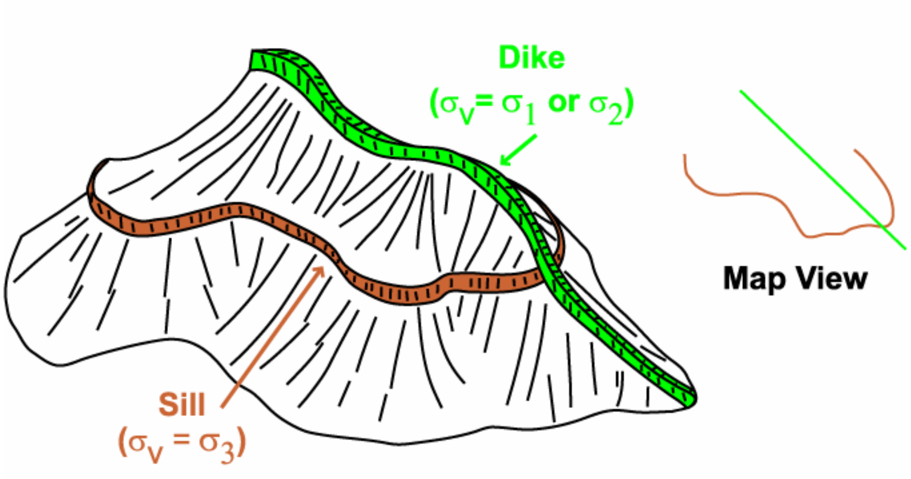

Figure 12: Emplacement conditions/requirements of a sill compared to a dike show that stresses were variable and changing across the basin during the period of igneous intrusion.

1.3 BACKGROUND

Fracture terminology

For simplicity, breaks in rock will be described as either extension fractures or shear fractures within this report, consistent with the terminology used within the petroleum industry. Extension fractures (also termed joints, or tensile fractures or dilation fractures or Mode I fractures: Pollard and Aydin, 1988), have displacements perpendicular to the fracture surfaces. Shear fractures have some displacement parallel to the fracture surface (also termed Mode II or Mode III fractures depending on displacement relative to the fracture front: Pollard and Aydin, 1988). Both extension and shear fractures can be formed in laboratory compression tests with specific orientations with respect to the applied stress. Extension fractures form perpendicular to the least compressive stress (σ_3), parallel to maximum compressive stress (σ_1) and bisect the acute angle between the conjugate shear fractures (Peng and Johnson, 1972; Long et al., 1997; Figure 13).

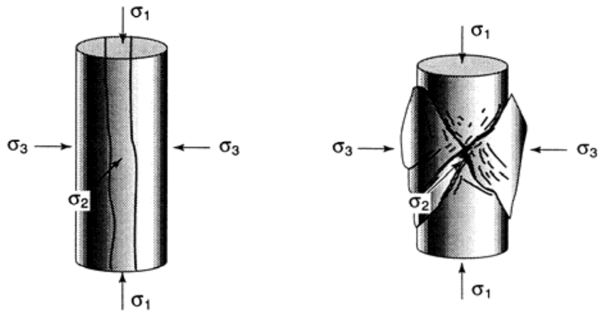
a) extension fractures

b) conjugate shear fractures

Figure 13: Extension and conjugate shear fractures as observed and created in laboratory compression tests (σ_1 – maximum principal stress; σ_2 – intermediate principal stress; σ_3 – minimum principal stress) (modified from Weijermars, 1997).

Fractures, fracture networks and faults can influence permeability and therefore fluid flow within an aquifer or petroleum reservoir (Lorenz and Finley, 1989; Lorenz and Finley, 1991; Teufel and Farrell, 1992). Permeability anisotropy has been observed in reservoirs with low matrix permeability and a well developed, open fracture system (Elkins and Skov, 1960; Lorenz and Finley, 1989; Teufel and Farrell, 1992), with the highest permeability parallel to the fractures. Significant interaction between the fracture surface and the matrix allows better drainage of the rock matrix. This matrix/fracture interaction could allow for a substantial increase in recoverable hydrocarbon reserves. This is also true for cleats in coal which are in many cases extension fractures.

In contrast, mineralized fractures and deformation bands (small-displacement faults, characterized by cataclasis and/or pore reduction through compaction) are typically characterized by significant permeability reduction (Nelson, 1985; Antonellini and Aydin, 1994; Antonellini et al., 1994). Where fractures are mineralized or the rock is cut by deformation bands, the rock matrix is more permeable than the bands, so the rock is most permeable parallel to, and between, fractures and deformation bands. Therefore, within a given rock volume containing mineralized fractures and/or deformation bands there will be an overall permeability decrease and possible reservoir compartmentalization.

Partially mineralized fractures may still have some permeability. However, there could be a significant reduction in the interaction between the remaining open fracture fluid pathway and the rock matrix (Nelson, 1985). Either mineralized or partially mineralized fractures could have the effect of decreasing the total amount of recoverable reserves.

Reasonable predictions of permeability anisotropy require an understanding of controls on the distribution and orientation of such features. As will be discussed in this report and as previous work shows (Cooper et al., 2001; Lorenz and Cooper, 2001; Lorenz and Cooper, 2002) these features can have predictable orientations with regard to large-scale structures such as the Sangre de Cristo thrust front and local structures such as anticlines.

1.4 TECHNICAL PROBLEM AND APPROACH

1.4.1 The Technical Problems with Natural Gas Production

Unlike crude oil or refined petroleum products, natural gas cannot be easily imported from overseas. To import natural gas it must be liquefied, carried under pressure within cryogenic tankers and unloaded at facilities specifically designed to safely handle this product. Each of these transportation items is extremely expensive and will require significant lead-time to build. Finding additional communities along the coast that would accept such a facility may also be difficult.

Given the limited natural gas resources in Canada, along with their own energy demands, and the fact that Mexico is a net importer of natural gas from the U.S.A., natural gas must be an internally sourced United States commodity. Small independent gas companies are the primary producers in the U.S.A. yet within their companies they do not have the technical expertise to engage in extensive research. Nevertheless, demand for natural gas is anticipated by the Energy Information Administration (EIA) to increase by 50% or 10 trillion cubic feet by 2020. It is important to recognize that besides home heating, natural gas is primarily used to generate electricity. In a statement to the U.S. Chamber of Commerce's National Energy Summit, Energy Secretary Spencer Abraham cited figures from the EIA showing a 45% increase in demand for electrical power over the next 20 years, but without corresponding increases in domestic production. Without increasing domestic production, natural gas shortages and associated electrical power blackouts can be anticipated and, in fact, have already occurred. Therefore, natural gas has become vital to our national energy security.

Since commercial production began in late 2000, the Raton Basin has become the second most active coalbed methane field in the U.S. and contains an estimated 18 trillion cubic feet of natural gas. Much of the natural gas in the Raton Basin is disseminated within numerous thick, naturally fractured, rock (sandstone) layers that do not readily allow fluids, including natural gas, to flow through them. These sandstones are officially described as 'tight' signifying that they are not conducive to fluid movement. The only way these tight sandstones can actually produce natural gas is if the sandstones contain fractures (are naturally broken). These breaks or fractures allow fluid movement within the open areas between the broken sections of rock and create a natural plumbing system enabling fluids to move within the sandstones. Each of these sandstone layers can be a separate resource having its own distinct plumbing system.

The thick, naturally fractured, tight sandstones within the Raton Basin are not being developed because the system of stress-sensitive fractures and stress-controlled fluid flow is very poorly understood. The stress field and fracture orientations and distributions in the basin are complicated by the presence of numerous impermeable, volcanic rock units. Stress systems (*in situ* and applied stresses) control both the formation of natural fractures and their response to pressure changes during production; thus understanding the stresses is very important in optimizing resource recovery from this or any other basin. The stress field in combination with the natural fracture system also controls the directionality of fluid flow. An understanding of this directionality is fundamental for efficient well-placement and resource development.

Current pre-drill fracture detection technologies emphasize the use of expensive 3D seismic surveys, and analytical techniques that use seismic attribute analysis. The proposed work seeks to develop a system that, in a three-stage process, will allow gas explorationists to predict fractures ‘pre-drill’ in poorly explored basins using only a very few boreholes combined with modern fracture analysis logs and 2D seismic surveys that are less expensive (by a factor of 10) and less damaging to the environment. This project provides an alternate method of fracture prediction that is amenable to the limited budgets of independent oil and gas operators.

The large whole-core data set made available by industry underpins this study. It will be integrated with geophysical logs and field data (note: core refers to long cylindrical rock samples retrieved from boreholes).

1.4.2 Technical Approach

The technical approach can be subdivided according to five project objectives.

1. Develop a correlation between fractures and rock type. Thorough rock and fracture descriptions are used to quantify field sites and core along with fracture analysis using state of the art geophysical tools (e.g. Formation MicroScanner and Dipole Sonic Imaging).
2. Evaluate rock types in the subsurface via conventional geophysical data. Emphasis has been placed on determining the rock types most likely to contain fractures because these will be the rock units most likely to contain producible natural gas reserves.
3. Geomechanical and numerical modeling of the current and past stress history of the basin was accomplished through reconstruction of the geologic stress history and available in-situ stress data. The Sandia-developed large deformation, nonlinear finite element code JAS3D (Blanford et al., 2001) will be used for the geomechanical modeling. This code has been successfully used for various oil & gas applications, including, for example, regional-scale modeling of stresses in the area of the Courthouse Branch point of the Moab Fault, Utah. Models of this type require a constitutive model for each of the rock layers used with an appropriate set of material parameters for those layers. This modeling will provide control on the regional orientation and distribution of fractures (i.e. the reservoir plumbing system) and whether the plumbing system is likely to be damaged during production.
4. Integrate 1, 2 and 3 above to produce a conceptual model of the orientation of the various

fracture systems and the number of fractures within the basin and to predict where undrilled fracture trends are likely to be present.

5. Pre-drill fracture prediction. The success of new wells in intercepting predicted fracture trends would serve as a basis for extrapolating this work to other basins.

1.4.3 Why this Approach is Appropriate

A significant volume of the vast natural-gas resource base in the United States is currently uneconomic to produce, even at current gas prices in excess of $5 per million cubic feet. Current exploration and development in the Raton Basin is focused exclusively on coalbed methane. The thick sections of gas-saturated sandstones that are also present in the basin are not being developed because the system of fracture-controlled permeability is so poorly understood. In order to produce this much-needed gas resource in an effective and prudent manner with minimal environmental impact, a comprehensive grasp of the total in-situ gas system is required, and can best be realized through an assisted, cooperative, and integrated effort that incorporates scientific and technical expertise not available even to sizeable independent producers such as El Paso Production or private land holders such as Vermejo Park Ranch.

1.4.4 Assessment of Technical Risks

The Raton basin, like other Rocky Mountain basins, is a complex geological system. An understanding of the components of the system will never be complete in a mathematical sense, because geological databases are always incomplete and limited relative to the size of a geological system. However, a solid understanding of the important components and interactions of the Raton system is within the grasp of this project because of the multi-faceted, complementary approaches used during implementation of the project. The main risk in any similar endeavor is that industry partners might suffer a reversal where they could no longer be able to contribute data and corporate knowledge.

2.0 STUDIES APPLIED TO METHODOLOGY

2.1 OUTCROP FRACTURE DATA

2.1.1 Introduction

Study of fractures in sandstones and limestones and cleats in coals within the Raton Basin of Colorado and New Mexico indicates a NW-SE to NE-SW primary fracture orientation (Figure 14). However, closer inspection of the data shows that there is significant variability and complexity within these fracture and cleat patterns. These observations will be used as focal points for discussion in the following sections.

2.1.2 Technical Approach

The questions of fracture origins, orientations, distributions, intensities, and effects on reservoirs within the Raton Basin were addressed through a combination of outcrop and subsurface studies. This section addresses the outcrop study. Outcrops of Dakota Sandstone, Niobrara Limestone, Trinidad Sandstone, Vermejo Formation, Raton Formation, Poison Canyon Formation and certain igneous sills and dikes across the Raton Basin were located and assessed for their contribution to fracture characterization and interpretations of fracture origin. While fracture characteristics were recorded from all these lithologies the Trinidad Sandstone was the most cited single unit. This is primarily because it has the most consistent lithologic characteristics. It is laterally continuous, tabular, and composed of the same material across the basin. The other coal bearing units of production interest (Vermejo, and Raton Formations) are composed of laterally discontinuous fluvial sandstones and were the second most recorded formations (Figure 15).

The outcrops studied were on private and public lands. A number of sites were on the Vermejo Park Ranch. The Ranch has had little concentrated research with regard to fracture interpretation done prior to this study. In other parts of the basin numerous outcrops that may have contributed to the study were inaccessible due to location on private lands (the majority of the basin is privately owned). Other outcrops were inaccessible due to steep topography or cover (which is common on the higher elevations of the basin). Fracture characteristics such as orientation, spacing, length, mineralization, surface ornamentation, and geometric relationships to local structure were noted, though not all criteria were displayed at each outcrop. These data were amassed in field notes and distilled into the rose diagrams and descriptions presented in this section. Raw data and location information for each site are available in Appendix D. In addition to the subsurface and outcrop studies, a literature search was made in order to provide the background for a synthesis of the fractures within the context of the local and regional structures and tectonics. Parts of this synthesis are detailed in previous and following sections.

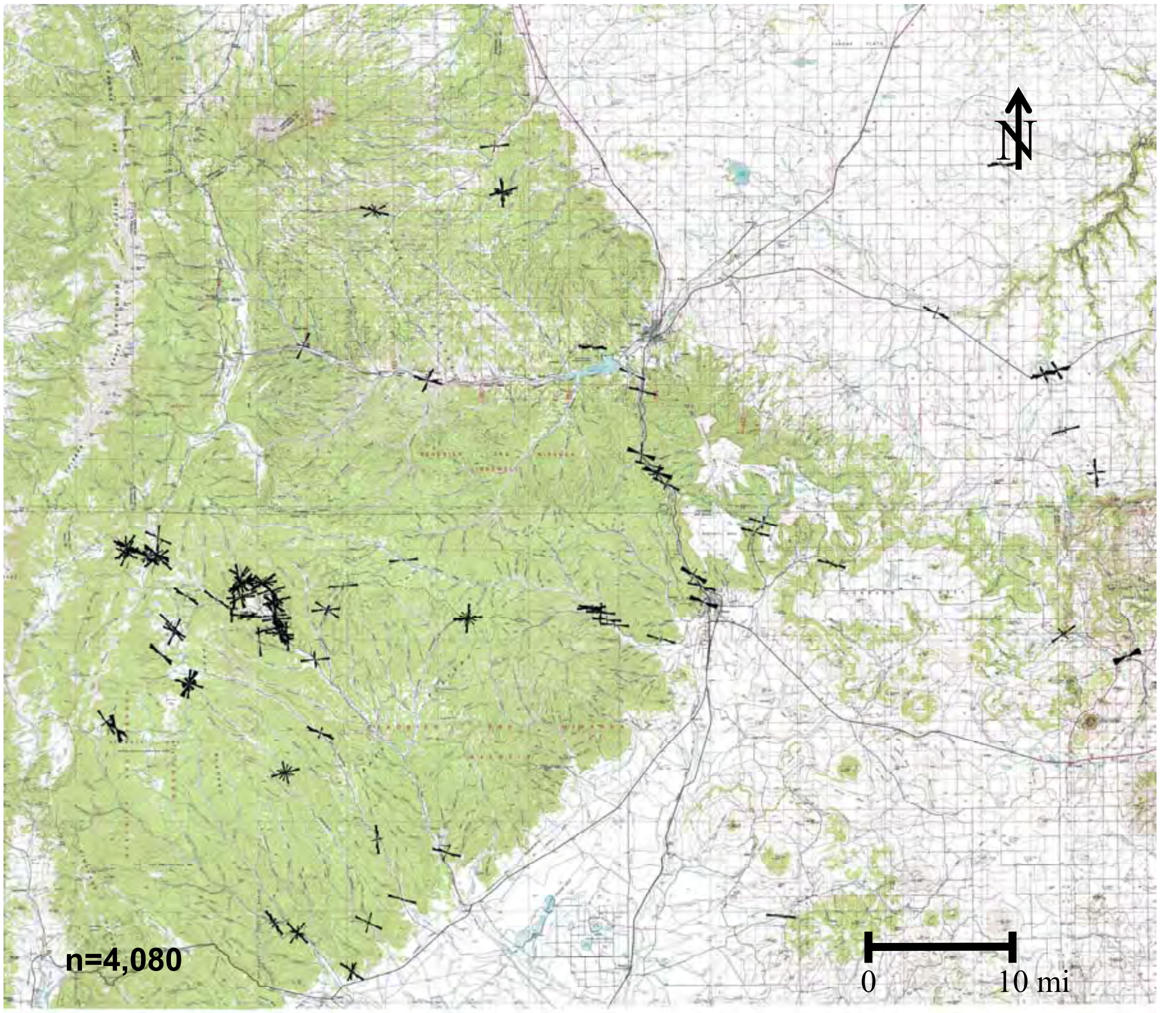

Figure 14: Map of fracture orientations across the Raton Basin (n=4,080).

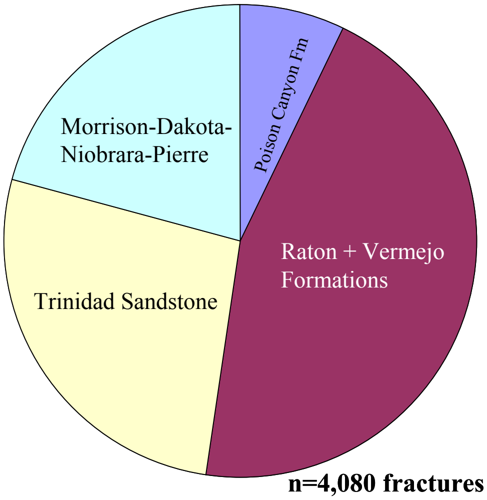

Figure 15: Majority of the outcrop fracture data are from the Trinidad Sandstone and the Vermejo-Raton interval.

Figure 16: A. Formation of fractures in extension is evidenced by plumose structure. This example is from the Vermejo formation. B. Many of these fractures are parallel in strike.

2.1.3 Previous Work

Numerous workers have described the stratigraphy, igneous rock units and emplacement, structure, fractures and coal beds and production potential of the Raton Basin, these include but are not limited to; Baltz, 1965; Billingsley, 1977; Brister and Gries, 1994, Brill, 1954; Carter, 1956; Close, 1988; Close and Dutcher, 1990; Dolly and Meissner, 1977; Flores, 1987; Flores and Tur, 1982; Flores and Pillmore; 1987; Flores and Bader, 1999;Harbour and Dixon, 1959; Hemborg, 1998; Hemmerich, 2001; Hoffman and Brister, 2003; Johnson, 1961; Johnson, 1968; Johnson and Wood, 1956; Johnson and Finn, 2001; Jurich and Adams, 1984; Knopf, 1936; Lee, 1917;Merry and Larsen, 1982; Merrin et al., 1988, Muller, 1986; Ode, 1957; Penn and Lindsey, 1996; Pillmore, 1969, 1976, 1991; Pillmore and Flores, 1984, 1987; Pillmore and Hatch, 1976; Pillmore and Mayberry, 1976; Read and Wood, 1947;Rose et al., 1986; Scott et al., 1990;Speer, 1976; Stevens et al., 1975; Strum, 1985; Tremain, 1980; Wood et al., 1957; Woodward, 1984; Woodward 1987; Woodward, 1995; (numerous maps have been draw of areas within the basin, please refer to the bibliography for a listing). All of these workers helped broaden the geologic understanding of the basin and the scope of this project. Nevertheless one particular worker stands out. Charles Pillmore spent the majority of his career working within the Raton Basin and is acknowledged here for his detailed and dedicated research.

Given the volume of work described above it is interesting to note that very little work has been done to characterize natural fractures within the basin. Close (1988) has provided the most detailed study of coal cleat orientation and an initial review of fractures within the sandstone units. To summarize some of Close's observations; coal face cleats are everywhere near perpendicular to the Sangre de Cristo thrust front, fractures in sandstones parallel cleat orientations, and igneous dikes intruded pre-existing fractures. Close (1988), also notes that a detailed field check of fracture orientations should be carried out when looking at new production sites.

Our study concentrated on fractures in sandstones. Fractures were found, in many cases, to parallel the strike of face cleats in coals. Extensions fractures were also found to be nearly perpendicular to the thrust front. Conjugate shear fractures (not previously described in the Raton Basin) were also observed. These shear fractures are oriented such that the stresses required to form them are consistent with tectonic loading from the Sangre de Cristo Mountains. Local structures were found have significant control on fracture orientations. Fracture orientations around local structures were found to be more complex than the hypothesis that all face cleats and fractures are perpendicular to the thrust front. Also present-day in situ stresses from well logs indicate a 90^o rotation in the maximum horizontal compressive stress from the Laramide E-W compression associated with the Sangre de Cristo thrust to N-S. This rotation in stresses was previously inferred by changes in igneous dike emplacement over time (Muller, 1986; Close and Dutcher, 1990). Close and Dutcher further recognize that the stress rotation may be related to Rio Grande Rift extension along the western side of the present day Sangre de Cristo Mountains. The orientation of present day stresses relative to the natural fracture pattern has great implications with regard to production. Specifically, induced hydraulic fractures (used to enhance production) will be oriented perpendicular to and cut across the regional natural fracture set. The N-S maximum horizontal compressive stress state may close some of the natural fractures if the normal stress across the fracture plane is too large.

2.1.4 Fracture Data Relative to Specific Rock Units

Dakota Sandstone – eastern Raton Basin

Fractures at two locations within the Dakota sandstone on the eastern margin of the basin have a conjugate geometry, with a NW-SE bisector to the acute angle (Figures 17 and 18). Field data provides limited evidence of shearing along these fractures. This interpretation is supported by fracture surface information such as the presence of Riedel shear steps/surfaces and a lack of plumose structure (Figure 19). Some of the shear steps and surfaces in this area may be altered due to numerous root casts in a number of the sandstones (Figure 20). These data combined with data from the Niobrara Limestone provide a kinematic analysis of fracture formation in this part of the basin and is discussed in the following Niobrara Limestone section of this report.

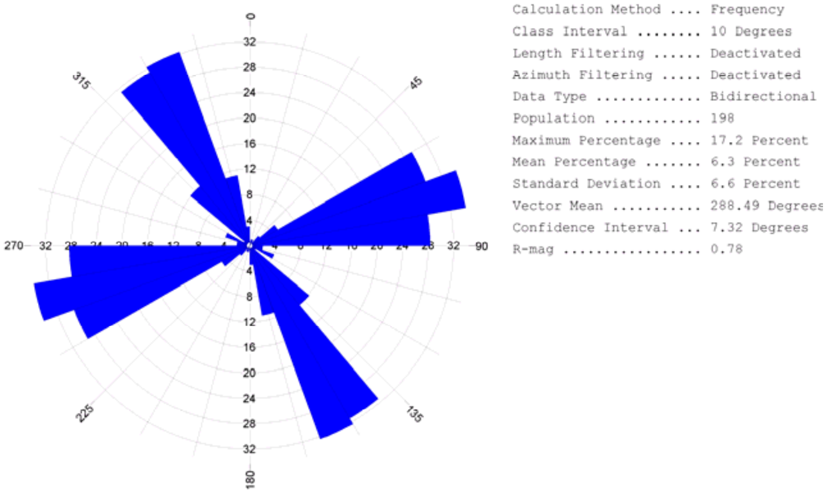

```
Calculation Method .... Frequency
Class Interval ........ 10 Degrees
Length Filtering ...... Deactivated
Azimuth Filtering ..... Deactivated
Data Type ............. Bidirectional
Population ............ 198
Maximum Percentage .... 17.2 Percent
Mean Percentage ....... 6.3 Percent
Standard Deviation .... 6.6 Percent
Vector Mean ........... 288.49 Degrees
Confidence Interval ... 7.32 Degrees
R-mag ................. 0.78
```

Figure 17: Rose diagram of fractures in the Dakota Sandstone near mileposts 374 and 375 on highway 160; n = 198.

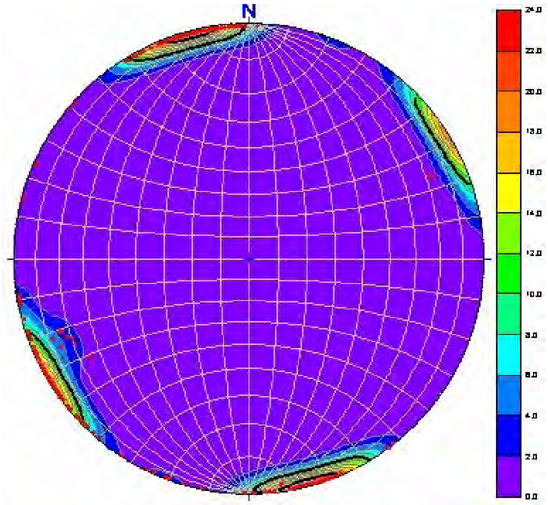

Figure 18: Pole to plane stereonet of fracture orientations within the Dakota Sandstone near mile markers 374 and 375 on Hwy 160; n=198. These data show the majority of fractures have near vertical dips and conjugate strikes.

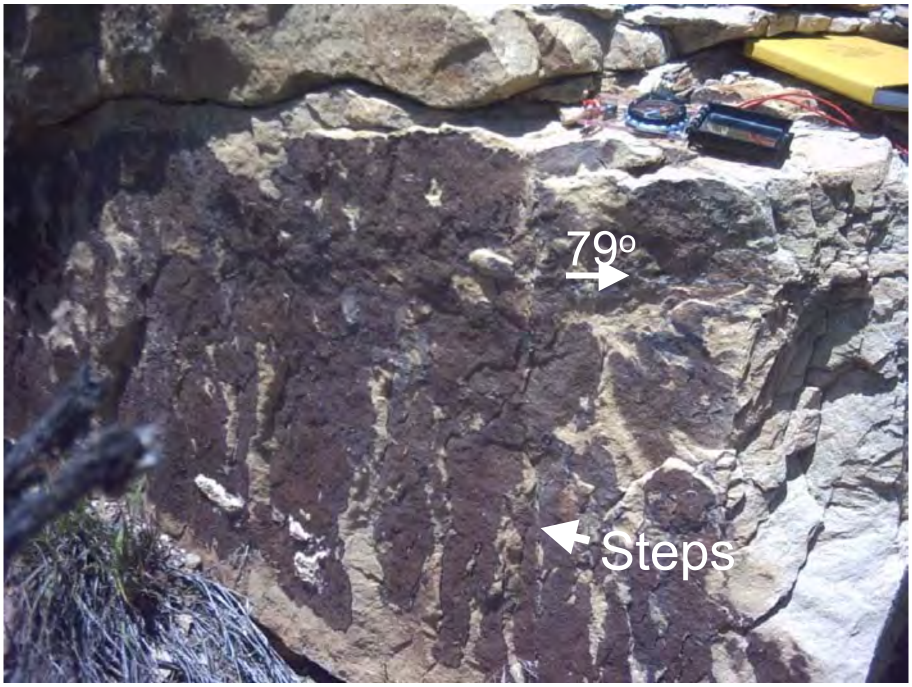

Figure 19: Riedel shear steps within the Dakota Sandstone near mile marker 374 on Hwy 160. The surface feature on this fracture plane indicates incipient right lateral movement.

Figure 20: Vertical root traces shown in this photograph may inhibit/alter the formation of shear steps as seen in Figure 19.

Dakota Sandstone – western Raton Basin

Exposures of the Dakota Sandstone along the western margin of basin are visible along what is locally called "The Wall". The outcrops contain near vertical to overturned beds of Dakota Sandstone (Figure 21). Deformation bands were observed within some of these sandstones. Deformation bands typically form in high porosity sandstones suggesting they formed early before the Dakota Sandstone was altered to its current low-porosity, well-cemented state. Bed-parallel stylolite surfaces and well developed bed-normal shear planes are also common at this location. The Dakota Sandstone at these locations is highly fractured with variable fracture orientations (Figure 22). However, once the bedding is rotated to horizontal many of the fractures strike parallel or perpendicular to the strike of the folded "Wall". This suggests that the fractures are genetically related to the formation of the fold along the western margin of the basin.

Figure 21: Photograph A shows an overturned portion Dakota Sandstone "Wall" along the western margin of the Raton Basin. Photograph B highlights deformation bands within the Dakota sandstone at this location. Deformation bands were also observed within the Raton Formation along the "Little Wall".

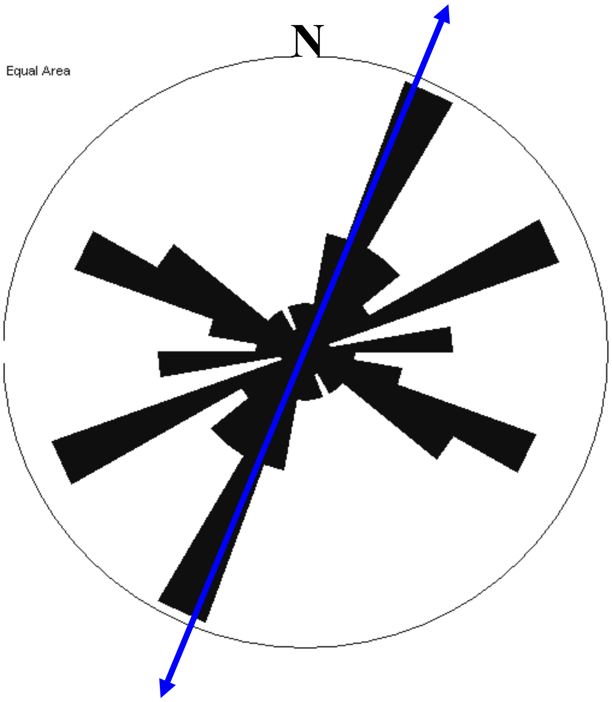

Figure 22: Rose diagram of fracture strikes from the Dakota Sandstone Wall (Figure 21) on the Vermejo Park Ranch (n=81). Fracture orientations are rotated back to horizontal. Strike of the folded "Wall" of Dakota Sandstone is shown as the blue arrow.

Niobrara Limestone – eastern Raton Basin

Fractures in the Fort Hayes Member of the Niobrara Limestone, located within ten miles of the previously described Dakota Sandstone outcrops on the eastern margins of the Raton Basin (Figures 17, 18, 19 and 20), have a more uniform extension-fracture pattern. Plumose structures are observed on the surfaces of the Niobrara fractures indicating these are extension fractures (Figure 23). Fractures were found to curve near intersections with normal faults, indicating stress reorientations near the faults. The main lobe of the Niobrara Limestone rose diagram (Figure 24) bisects the acute angle of the two nearby Dakota Sandstone fracture sets. This indicates these two seemingly dissimilar fracture patterns (extension fractures in the Niobrara and conjugate shear fractures in the Dakota) could most easily be interpreted as dynamically compatible fracture sets formed in a single stress regime, where σ_H was ESE and equal to σ_1 (Figure 25). Since the orientation of σ_H is nearly perpendicular to the Sangre de Cristo thrust front, this suggests horizontal tectonic loading by the thrust over 70 miles to the west. A geomechanical analysis of this hypothesis is provided in Section 2.2.

Figure 23: Plume structure on fracture surface within the Fort Hayes member of the Niobrara Limestone along Hwy 160 between mile markers 365 and 366.

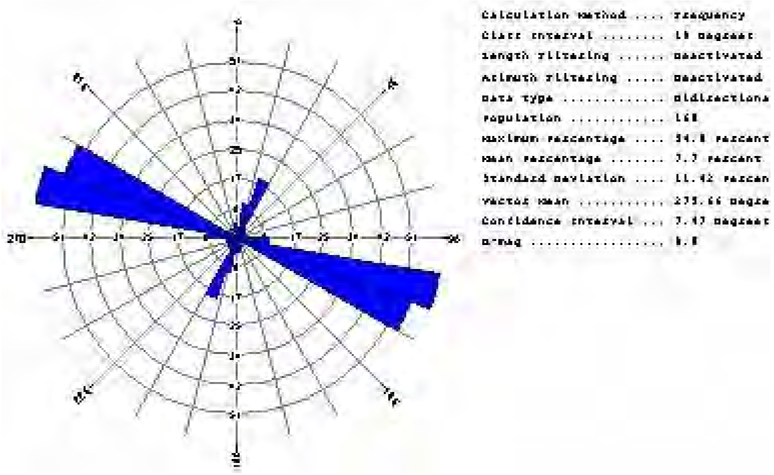

```
Calculation method .... Frequency
Class interval ........ 10 degrees
Length filtering ...... Deactivated
Azimuth filtering ..... Deactivated
Data type ............. Bidirectiona
Population ............ 168
Maximum percentage .... 34.8 Percent
Mean percentage ....... 7.7 Percent
Standard deviation .... 11.42 Percen
Vector mean ........... 275.66 Degre
Confidence interval ... 7.47 Degrees
R-mag ................. 0.8
```

Figure 24: Rose diagram of fractures within the Niobrara Limestone between milepost 365 and 366 on highway 160 (n=168). Note that the major fracture set strikes NW-SE and actually would bisect the acute angle of the fractures observed within the Dakota Sandstone (Figure 25).

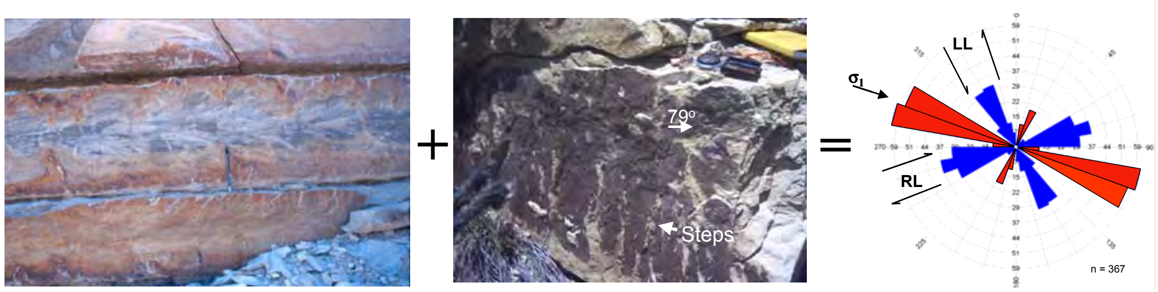

Niobrara Limestone

Dakota Sandstone

Figure 25: Diagram illustrating that these two sets of fractures are dynamically compatible. Comparison of fracture orientations and type within the Fort Hayes Member of the Niobrara Limestone (red) and Dakota Sandstone (blue), Highway 160 (n = 367) fits a kinematic interpretation wherein the maximum compressive stress was in the horizontal plane.

Fractures within the Niobrara Limestone south of Springer, NM have a conjugate geometry with one set oriented NW-SE and the other NE-SW (Figure 26). Interestingly, normal faults within this unit have a slightly dispersed N-S orientation that bisects the obtuse angle of the fracture sets (compare Figures 26 and 27). One hypothesis under consideration is that the fractures and faults formed under the same stress regime, where σ_H was E-W and equal to σ_1. Under these conditions the faults formed as reverse faults striking normal to σ_1. During the onset of Rio Grande Rift extension these faults would have been reactivated as normal faults. Figure 28 highlights the relationship wherein the extension fracture set (Figure 24) and the acute bisector of the conjugate facture set (Figure 26) strike roughly perpendicular to the Sangre de Cristo thrust front.

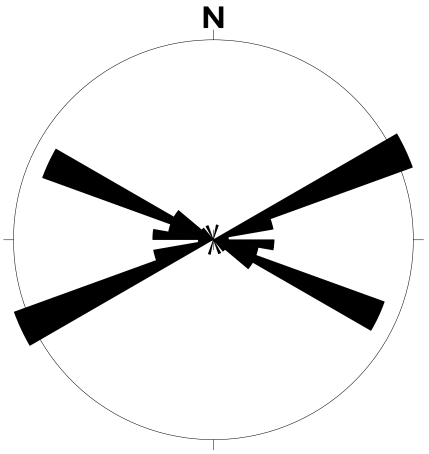

Figure 26: Rose diagram of fractures within the Niobrara Limestone south of Springer, NM. Ring equals 30%, n = 44.

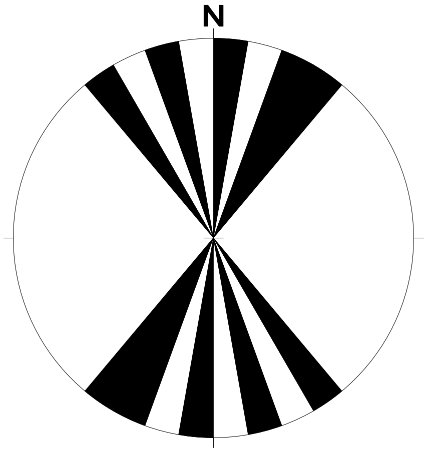

Figure 27: Rose diagram of faults within the Niobrara Limestone south of Springer, NM. Ring equals 20%, n = 5. Note the partial radial pattern and that this pattern bisects the obtuse angle of the fractures shown in Figure 26.

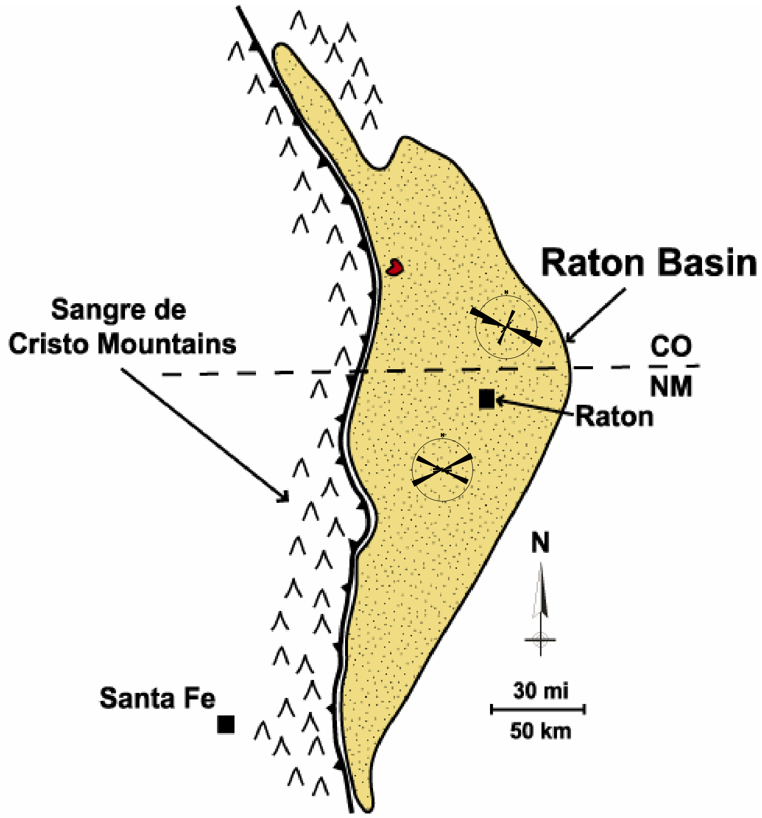

Figure 28: Rose diagrams of fracture orientations within the Niobrara Limestone.

Trinidad Sandstone

Fractures within the Trinidad sandstone along the eastern margins of the Raton Basin were found to be highly ordered, with the majority of fractures striking perpendicular to the Sangre de Cristo thrust front. Units that are thicker, such as a 15 m thick unit in the railroad cut near the southern edge of Trinidad Lake, typically have a very tightly constrained fracture pattern (Figure 29).

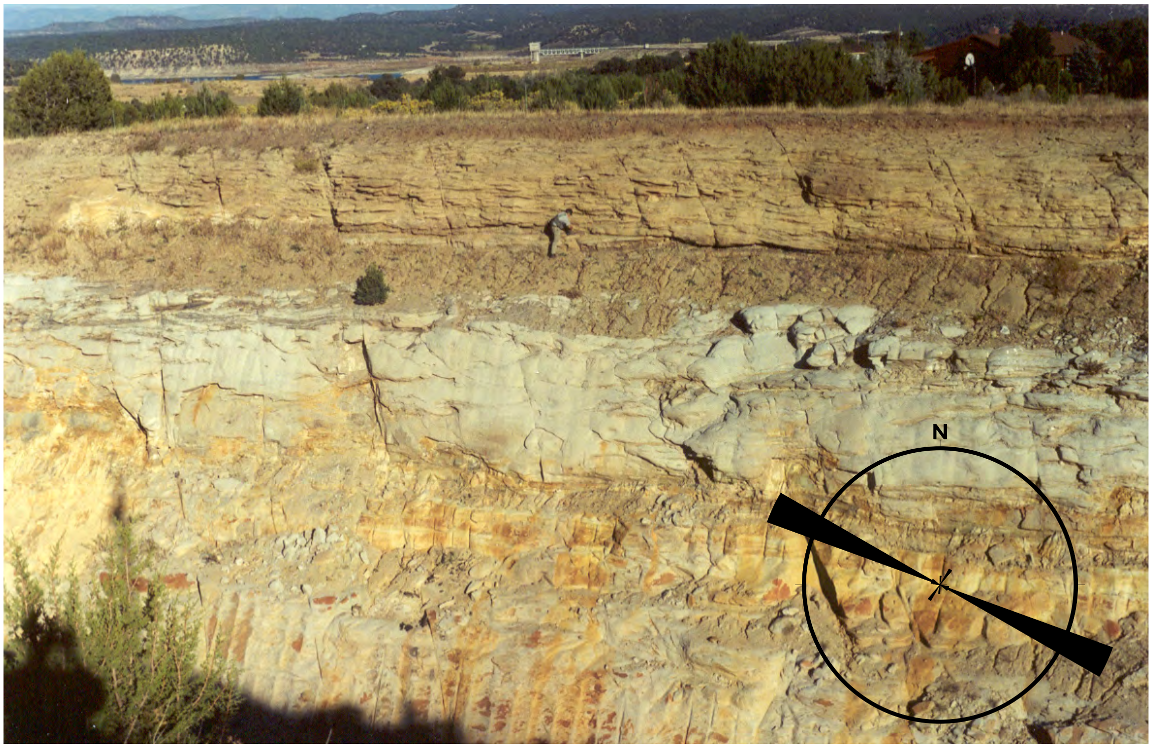

Figure 29: Photograph and rose diagram of fractures in a 15+ meter thick sandstone in a railroad cut near the SE corner of Trinidad Lake. Ring equals 60%, n = 25. Fracture orientations within this unit are highly ordered.

A second example of tightly constrained fracture orientations within the Trinidad Sandstone along the eastern edge of the basin is shown in Figure 30. Again these fractures are near normal to the Sangre de Cristo thrust front. Numerous other sites along this margin of the Raton Mesa were documented to also have this characteristic (Figure 31).

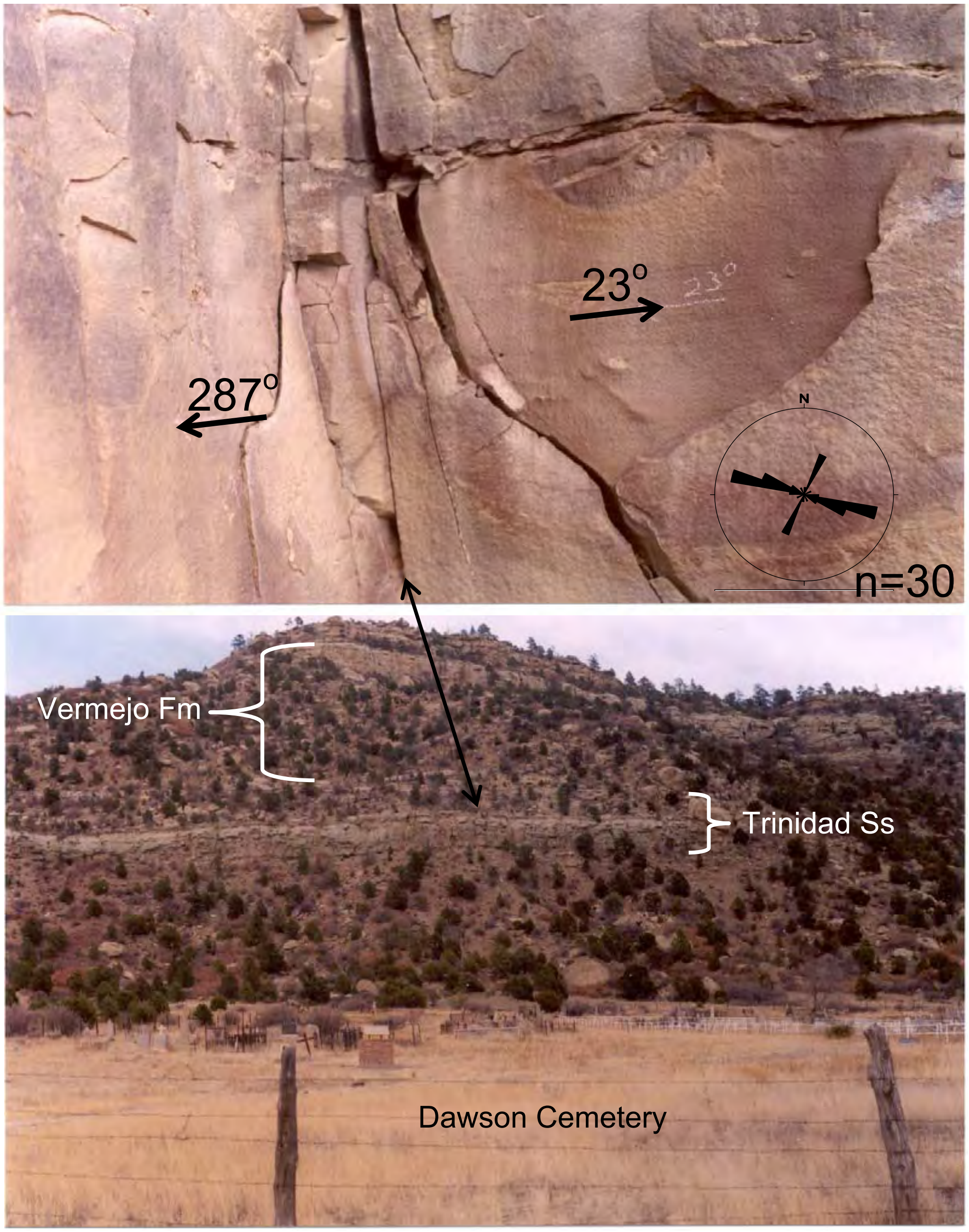

Figure 30: Fractures within the Trinidad sandstone near the Dawson Cemetery on the south eastern margins of the Raton Mesa show a distinct fracture patterns that is near normal to the Sangre de Cristo thrust front. Note that the fracture striking 23^{o} terminates at the intersection of the fracture striking 287^{o}. This relationship indicates the 23^{o} striking fracture is younger than the 287^{o} striking throughgoing fracture.

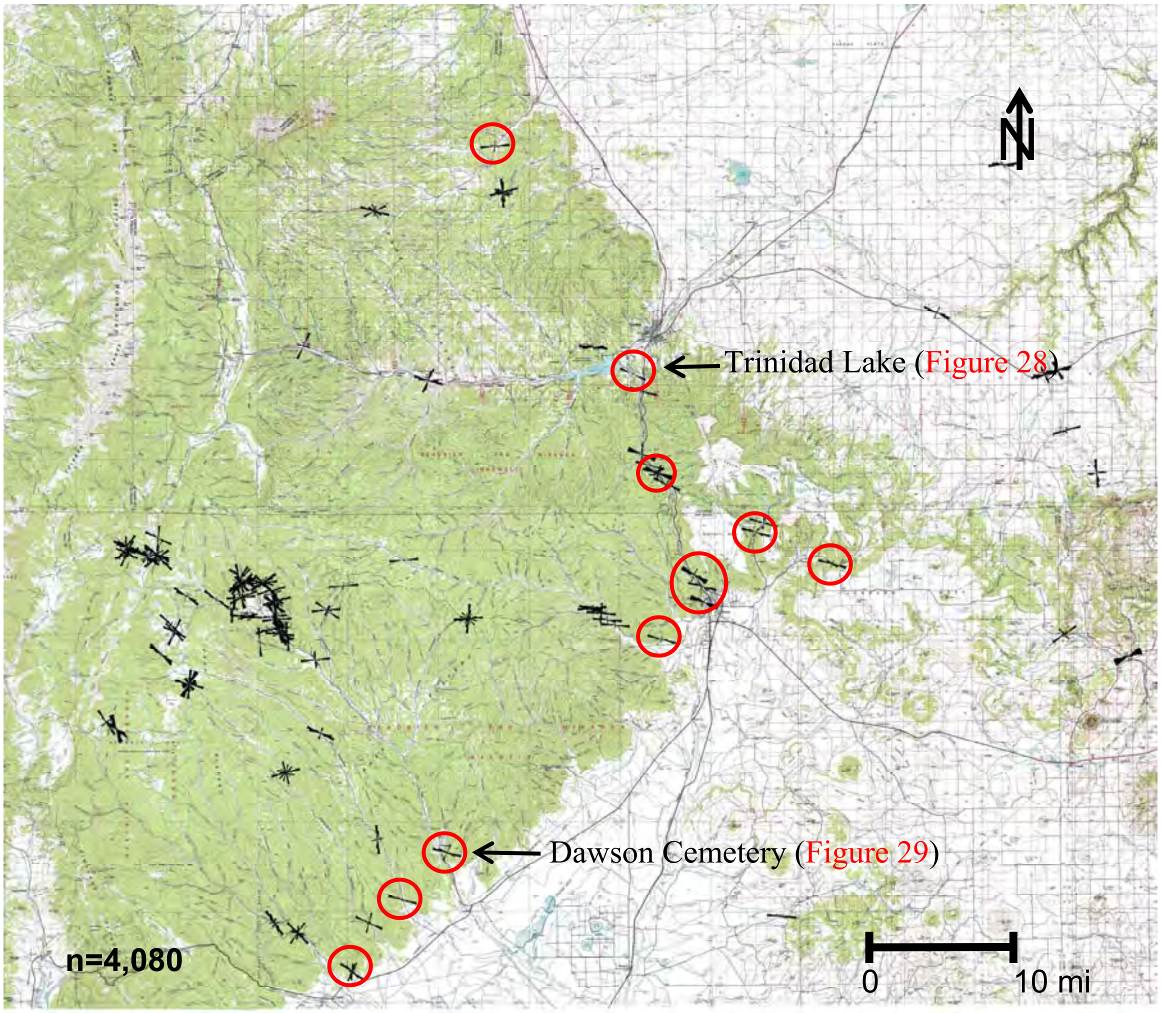

Figure 31: Map of fracture orientations across the basin. Some of the Trinidad Sandstone outcrop sites are located in red with the examples from Figures 29 and 30 highlighted.

In summary, fractures within the Trinidad Sandstone along the eastern margins of the Raton Mesa show a pattern wherein the primary (oldest throughgoing) fracture set is nearly perpendicular to the Sangre de Cristo thrust front. A younger secondary fracture set is typically perpendicular to the primary fracture set and may be related to stress relief due to unloading and/or to Rio Grande Rift extension. These characteristics were found at sites away from secondary structures such as faults, folds and igneous intrusives.

Vermejo and Raton Formations

Fractures in Vermejo Formation sandstones along the eastern margins of the Raton Mesa were found to be similar to those recorded in the Trinidad Sandstone; wherein there is one primary fracture trend that is nearly perpendicular to the Sangre de Cristo thrust front (Figure 32). This characteristic is clear only in areas east of the La Veta syncline and where there are no secondary structures such as faults and folds. Several examples of the fracture orientations along the eastern margin are illustrated in the following figures. Face cleats in coals were also found to be nearly parallel to fractures in the adjoining sandstones (Figure 33).

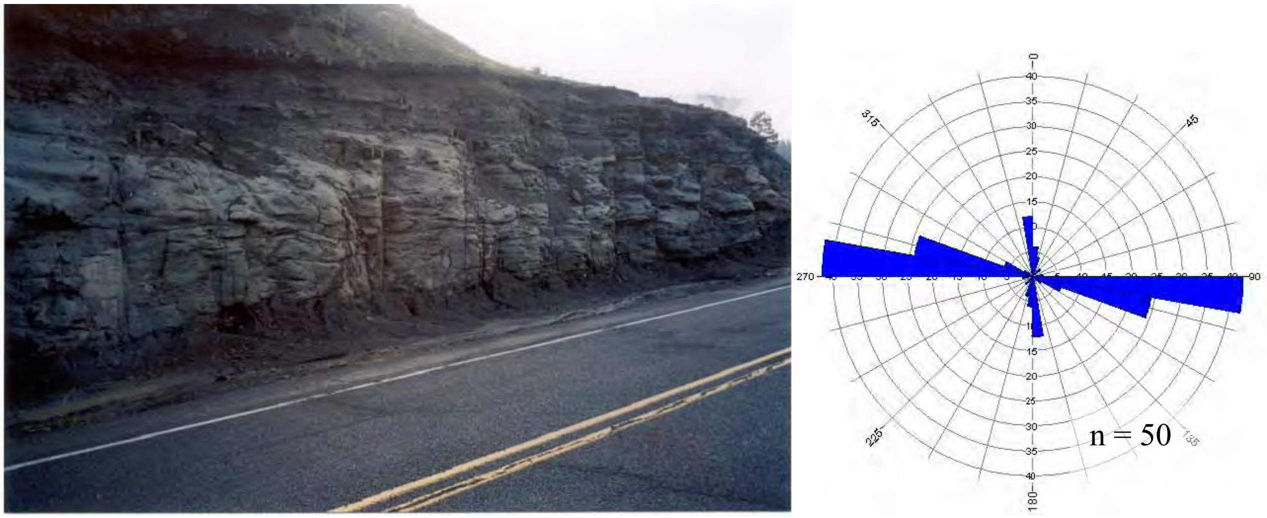

Figure 32: A) Uniform set of fractures within fluvial sandstones of the Vermejo Formation on Hwy 555 west of Raton, NM. B) Rose diagram illustrating fracture orientations at this site.

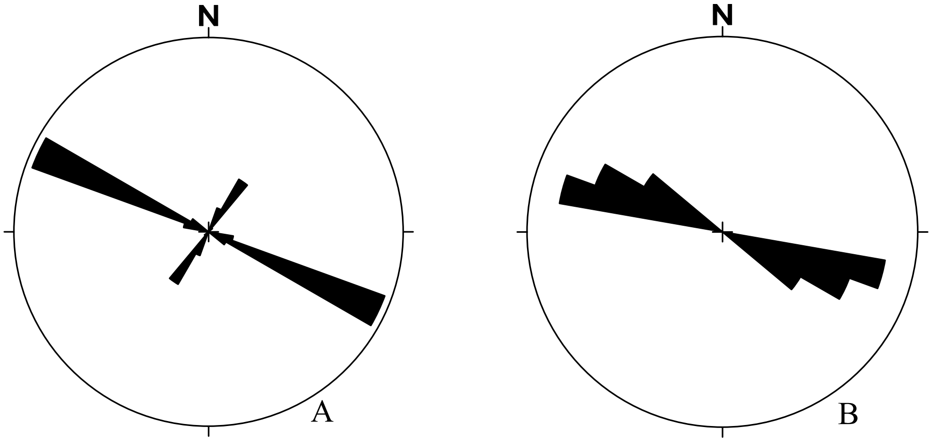

Figure 33: A) Rose diagram of fracture orientations within the Vermejo Formation at the Raton Overlook on the west side of Raton, NM (n=64). B) Rose diagram of face cleat orientation in a coal bed (n=26) directly underlying the sandstone shown in A. Note the near parallel strike of the fractures in the sandstone and the cleats in the coal.

Throughgoing fractures and face cleats on a frontage road two miles south of Trinidad are oriented WNW-ESE; similar to those shown in Figure 33. Fractures at this site are very ordered (Figure 34 A). Cross fractures and butt cleats are normal to the primary fracture and face cleat trends (Figure 34B).

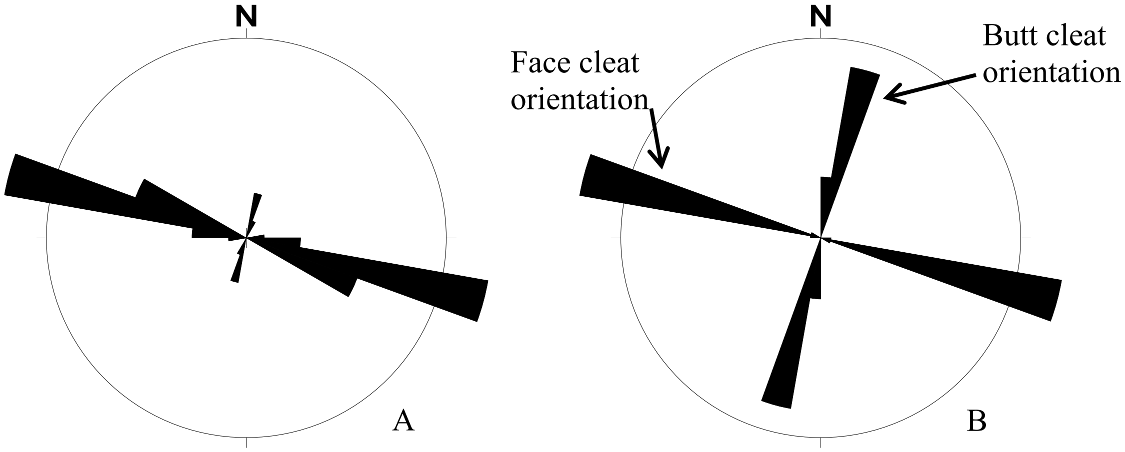

Figure 34: A) Rose diagram of fracture orientations in Vermejo sandstones on frontage road 2 miles south of Trinidad, CO. Ring equals 40%, n = 55. B) Rose Diagram of cleat orientations in Vermejo coals on frontage road 2 miles south Trinidad, CO. Ring equals 40%, n = 49.

Dip-slip slickensided faults within coals were also recorded at this location. A rose diagram of the orientation of these faults (Figure 35) shows a diverse distribution pattern. These faults have dip angles between 40^{o} to 60^{o}. One “spoke” of the rose diagram is notably longer, indicating some faults are parallel in nature. Significantly, this set of parallel faults is also parallel to the face cleat trend in the same coals (compare Figures 34 and 35). The other faults, those with a more diverse distribution, are interpreted to be related to compaction. Figure 36 highlights one location where the fault in the coal directly underlies a slump in the overlying sandstone. The slump is similar to ball and pillow sedimentary structures commonly associated with soft-sediment density differences (loading). Close inspection shows that coal beds are deflected upward and downward along these slumps, suggestive of early compaction. Shales from below also fill in the area of displacement (Figure 36).

Fractures and cleats within the Raton Formation along the eastern margins of the Raton Mesa show similar trends to those described within the Vermejo Formation. Examples from the Raton Formation along Hwy 12 west of Trinidad, CO show a primary WNW set of fractures and a NNE secondary fracture set (Figure 37 A and B).

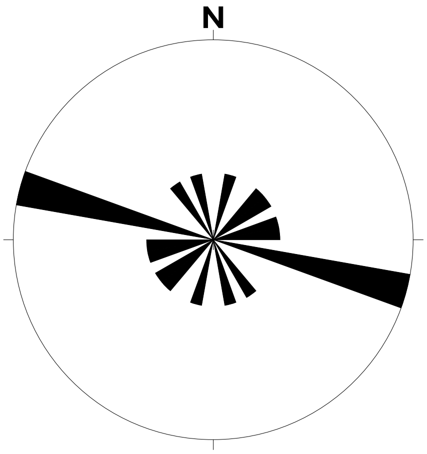

Figure 35: Slickensided faults in coal on frontage road 2 miles south of Trinidad., CO. Ring equals 30%, n = 10.

Figure 36: Slickensided fault in coal two miles south of Trinidad, CO. Fault at this location is located below a slump in the overlying sandstone. Underlying shale is squeezed into the fault plane and dislocation area near the point of the arrow. These relationships suggest the fault is related to early compaction.

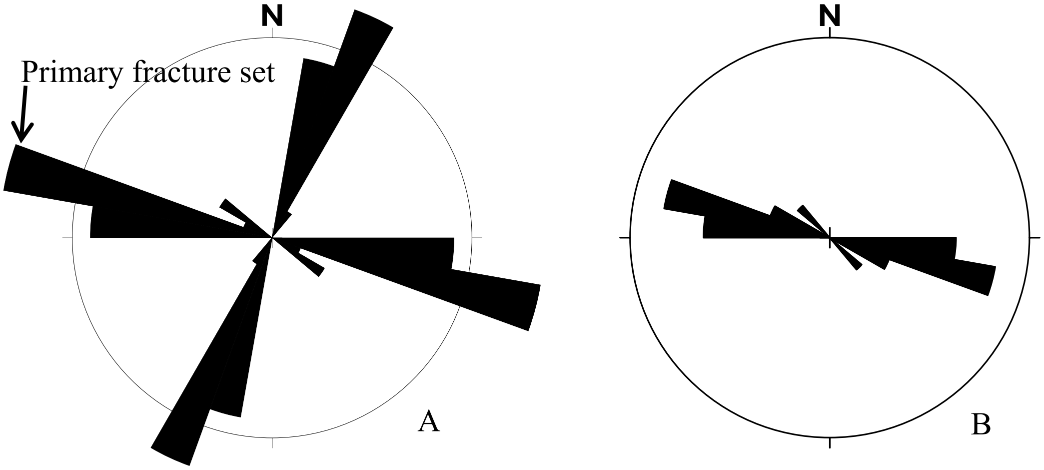

Figure 37: A) Rose diagram of primary throughgoing and secondary fracture orientations within Raton Fm sandstones near milepost 50 on Highway 12, n = 33. B) Rose diagram of the primary (oldest throughgoing) fracture set within Raton Formation sandstones on Hwy 12 near the intersection with county road 21.6, n=38.

In summary the oldest throughgoing fracture sets within the Vermejo and Raton Formations along the eastern margin of the Raton Mesa typically strike WNW and are parallel to face cleats within adjoining coals. This relationship is true only for those sites on the eastern side of the mesa and those sites at a distance from secondary structures such as faults, folds and igneous intrusions. A map of some typical Vermejo and Raton Formation locations and rose diagrams highlights this type of orientation characteristic (Figure 38).

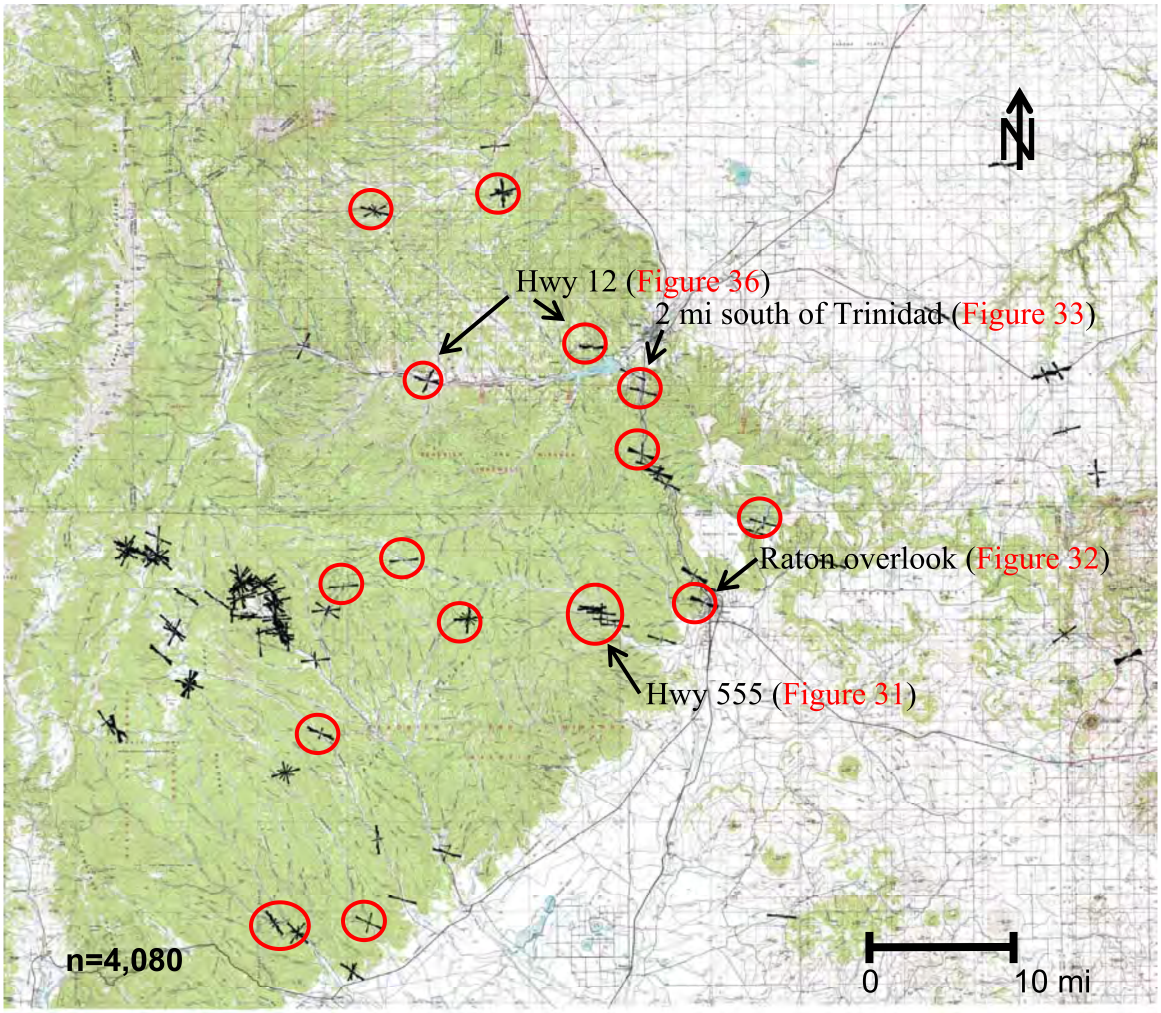

Figure 38: Map of fracture orientations across the basin. Some of the Vermejo and Raton Formation outcrop sites are located in red with examples from Figures 32, 33, 34, and 37 are highlighted.

Igneous rock units

Valdez sills

A site near Valdez CO, milepost 50 on Highway 12 west of Trinidad, provides an interesting comparison of fracture orientation within sandstones, an igneous sill and cleats within a coal bed (Figure 39). Extension fracture orientation is well constrained within a series of 10-30 cm thick sandstones above an igneous sill. Interestingly there is some parallelism between fracture orientation in these sandstones and the underlying sill (Figure 40). A comparison of the rose diagrams shows a slightly more distributed pattern and an extra set of fractures that strike NW-SE within the sill (Figure 41). The parallel nature of fractures in these differing rock units can be very apparent in the outcrop. Cleats within coals at this location have a more diverse pattern than the sandstones or the sill (Figure 42). In part this is due to different orientations of face cleats also having associated butt cleats at near right angles to the face cleat. It is also possible the diverse cleat pattern is due to compaction.

Figure 39: Photograph of a portion of the outcrop at milepost 50 on Highway 12 west of Trinidad, CO. Sandstones overlie an igneous sill and a coal bed at this site.

Figure 40: This photograph, oriented with the viewer looking straight down, illustrates the parallel nature of fractures in a sandstone and an igneous sill. The upper red colored rock unit is a sandstone. The intersection of two fractures forms a wedge pointing toward the top of the photograph within this unit. The dark colored wedge in the rock below the first wedge is within an igneous sill. Note the parallel nature of fractures within these two very different units, and the repetitive nature of these fractures.

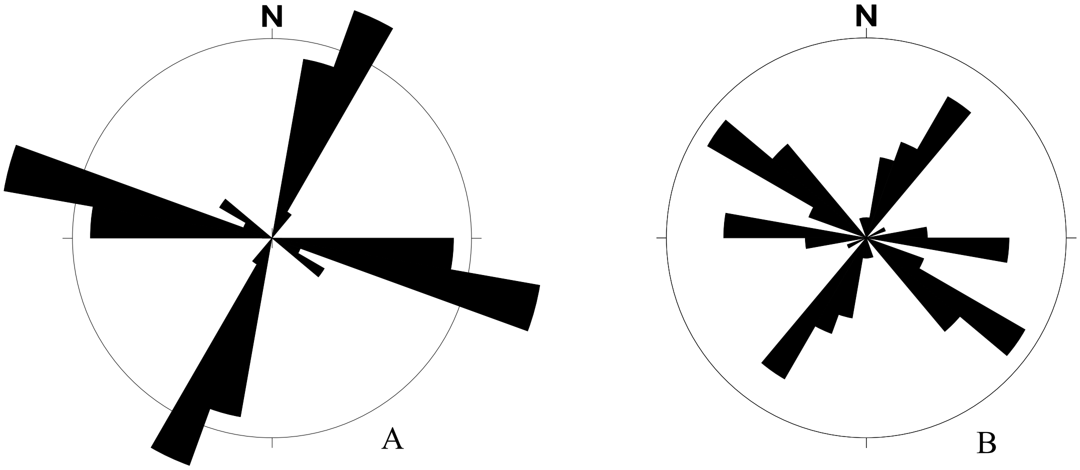

Figure 41: A) Rose diagram of fracture orientations within the sandstones, ring equals 20%, n = 33. B) Rose diagram of fracture orientations within the igneous sill, ring equals 20%, n = 49. There is a parallel relationship between many of the fractures within these two units of differing composition and age.

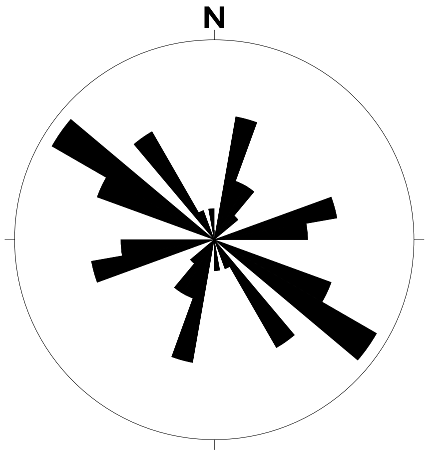

Figure 42: Rose diagram of cleat orientations within a Raton Formation coal bed underlying the sandstones and igneous sill of Figure 40, ring equals 20%, n=32.

Walsenburg dike

Evidence for high horizontal compressive stresses normal to dike walls during intrusion is present in a small borrow pit on the north side of the Walsenburg dike half a mile west of where the road north out of town cuts the dike. Thin sandstone beds contain small thrust planes that dip towards and away from the dike at shallow angles (less than 30 degrees). The thrust planes have dip-slip slickenlines that trend normal to the dike walls (Figures 43 and 44). These thrust planes suggest that the maximum compressive stress in the strata next to the dike was normal to the dike at the time of intrusion, despite the fact that the strike of the dike indicates that this was the orientation of the minimum regional compressive stress. This indicates that the opening of the dike added considerable stress to the surrounding rock.

This dike and numerous dikes within the basin are cut with myriad fractures. These fractures are typically of three sets, 1) oriented vertically, parallel to the fracture walls, 2) oriented vertically but normal to the fracture walls, and 3) oriented horizontal to sub-horizontal, normal to the fracture walls. Various phases of mineralization and extensive weathering along the fractures suggest that the fractures in the dikes formed a well connected plumbing system that allowed the percolation of mineralizing and weathering fluids, and that may have allowed the escape of much of the natural gas in the basin, leading to its present-day underpressured condition.

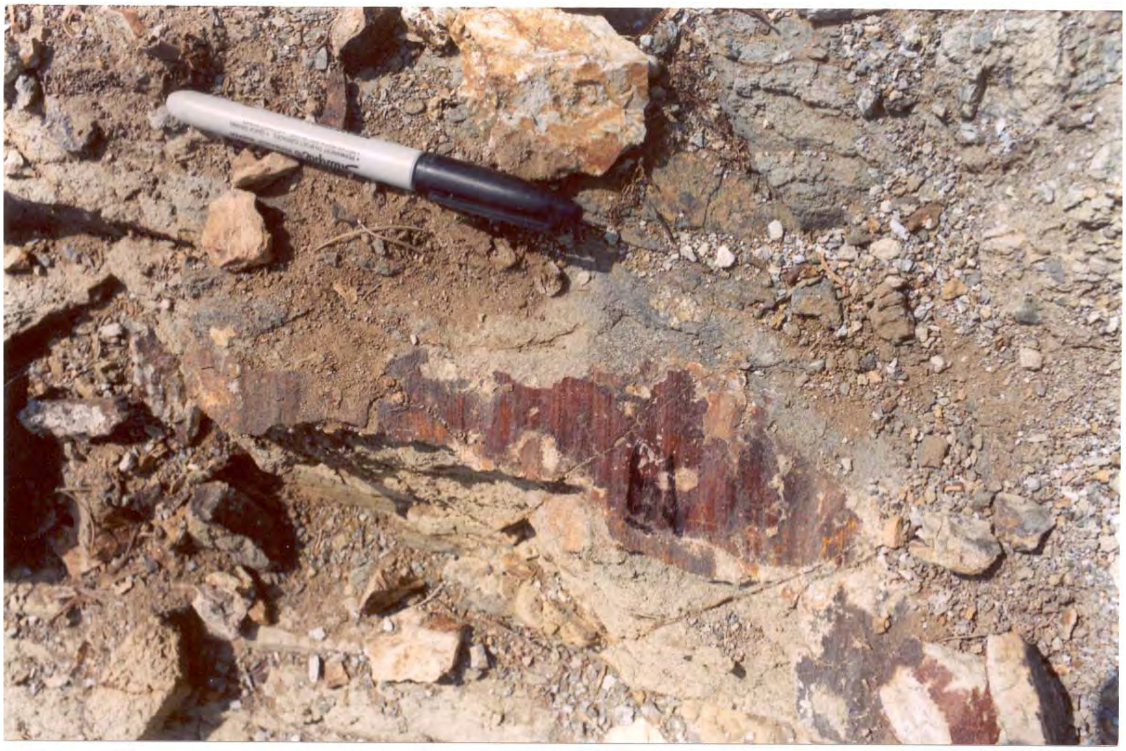

Figure 43: Low-angle thrust plane shown here has slickenline lineations striking perpendicular to the wall of the igneous dike. View is looking down (map view).

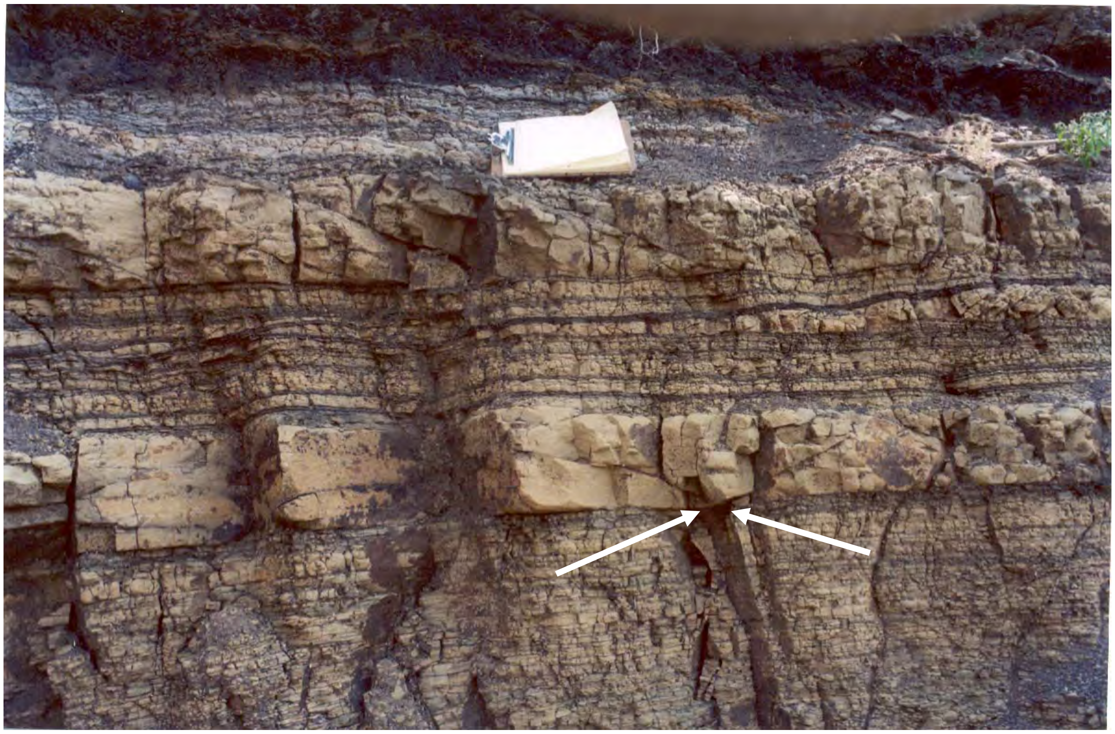

Figure 44: The thrust planes shown here indicate that the maximum compressive stress was normal to the dike at the time of intrusion. White arrows point in the direction and intersection point of two of the low angle thrust planes.

2.1.5 Fracture Data relative to Specific Structures

Morley anticline

Morley, Colorado is a coal-mining ghost town (Figure 45) situated at the center of a small-scale anticline on Interstate 25. A WNW primary extension fracture set is observed across the anticline. Base map after R.B. Johnson (1969) and modified from field observations is shown in Figure 46.

Figure 45: Photograph of the Morley church ruins; a small remnant of the mining town at the Morley anticline.

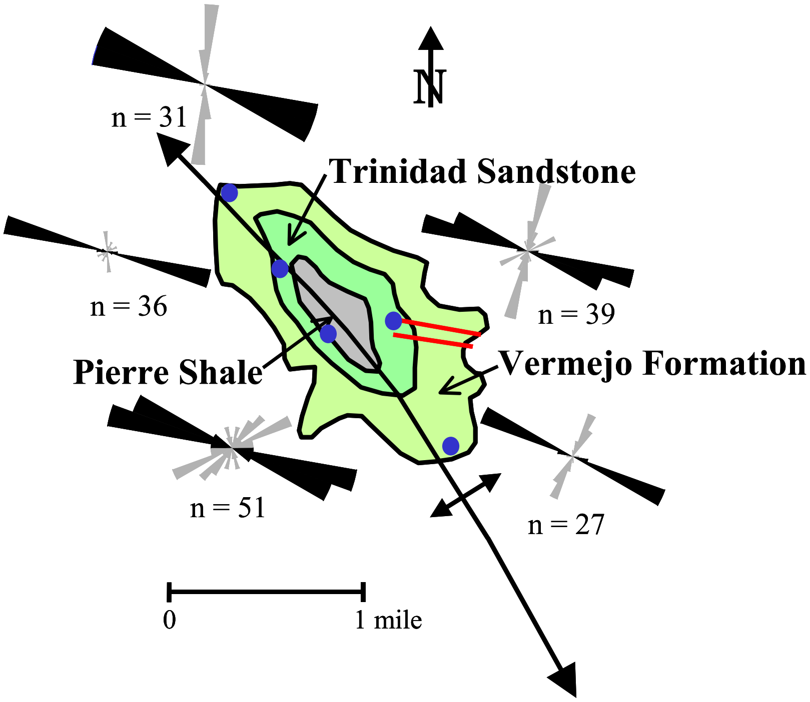

Figure 46: West-northwest oriented fractures are highlighted in black and are interpreted to predate fractures related to intrusion of Morley Dome. Red lines in the southeastern quadrant of the dome are igneous dikes. Gray cross fractures with variable strikes are probably related to the formation of the anticline.

The WNW oriented fractures in Figure 46 are the oldest set of fractures as determined by fracture cross-cutting relationships. Thus the WNW set of extension fractures are interpreted to predate the formation of the Morley dome because their orientations do not change regardless of position around the structure.

Two igneous dikes were also recorded in the southeastern quadrant of the dome (Figures 46 and 47). Fracture measurements in the sandstones adjacent to one of the dikes shows that there is an increase in fracture intensity with increased proximity to the dike. The interpretation is that intrusion of the dike (in a process similar to hydraulic fracturing of a production well) created a facture damage zone in the sandstones.

Figure 47: Scan-line of fractures within Vermejo Sandstones immediately adjacent to an igneous dike. Fracture intensity and number of fractures swarms increase with increased proximity to the dike.

Vermejo Park Anticline

Several sets of fractures are present in the Trinidad Sandstone around the Vermejo anticline (Figure 48). Some of these are interpreted to be related to eastward thrusting of the Sangre de Cristo thrust front, others are related to the formation of the Vermejo anticline, others are related to bending beds near the thrust front, to the irregular shape of the thrust and possibly east-west extension associated with the Rio Grande rift system.

There is an early though not always dominant set of approximately east-west striking extension fractures. These have been overprinted to varying degrees around the anticline by a strong south-southeast striking fracture set. Locally this younger set is the most obvious set of fractures, obscuring the earlier fractures. Fractures of both sets occur locally as very closely spaced swarms in the outcrops above the Vermejo Park Ranch headquarters buildings, suggestive of incipient faulting.

Several faults cut the Trinidad sandstone around the anticline. East-northeast striking normal faults were mapped in Spring Canyon on the northwestern edge of the anticline. We believe that these are not slump-block faults because they occur deep in the throat of the canyon and are locally cemented by sparry calcite crystals up to a centimeter in length. Blocks of this calcite up to 20 centimeters across occur in scree slopes, marking areas where faulting must be present but obscure, especially in the finer-grained deposits. Obscured, more recent slump blocks, trending east-west, are present on the southern margin of the anticline. Strata in these blocks did not maintain coherency, and the blocks are poorly defined, and these may be true, recent gravitational slumps.

A thrust within the Trinidad Sandstone places lower *Ophiomorpha* burrow bearing sandstone against upper non-*Ophiomorpha* bearing sandstone. The thrust has approximately 10-15m of vertical offset (Figure 49). It is filled with gouge and some calcite, and the adjacent strata in the hanging wall displays small back-thrust shear planes (Figure 50). Four to five miles north of this location in Spring Canyon a similar but smaller thrust was recorded (Figure 51).

Horizontally oriented conjugate fractures (i.e., plan-view X's) are present in the Raton Formation conglomerate on the eastern end of the anticline (Figures 52 and 53). At this site the more brittle quartzose Raton Formation conglomerate allowed the formation of conjugate shear fractures because of the different mechanical response to the same compressive stresses than less brittle rock units. With regard to conductivity, conjugate fracture systems are better connected and should provide a better reservoir plumbing system. The orientation of this conjugate system suggests significant east-west (to WNW-ESE) compression, probably during formation of the anticline or immediately prior to it. The previously described thrust faults in the Trinidad Sandstone (Figures 49, 50 and 51) and their orientations are also consistent with the high east-west compressive stresses suggested by the conjugate fractures found in the Raton Conglomerate.

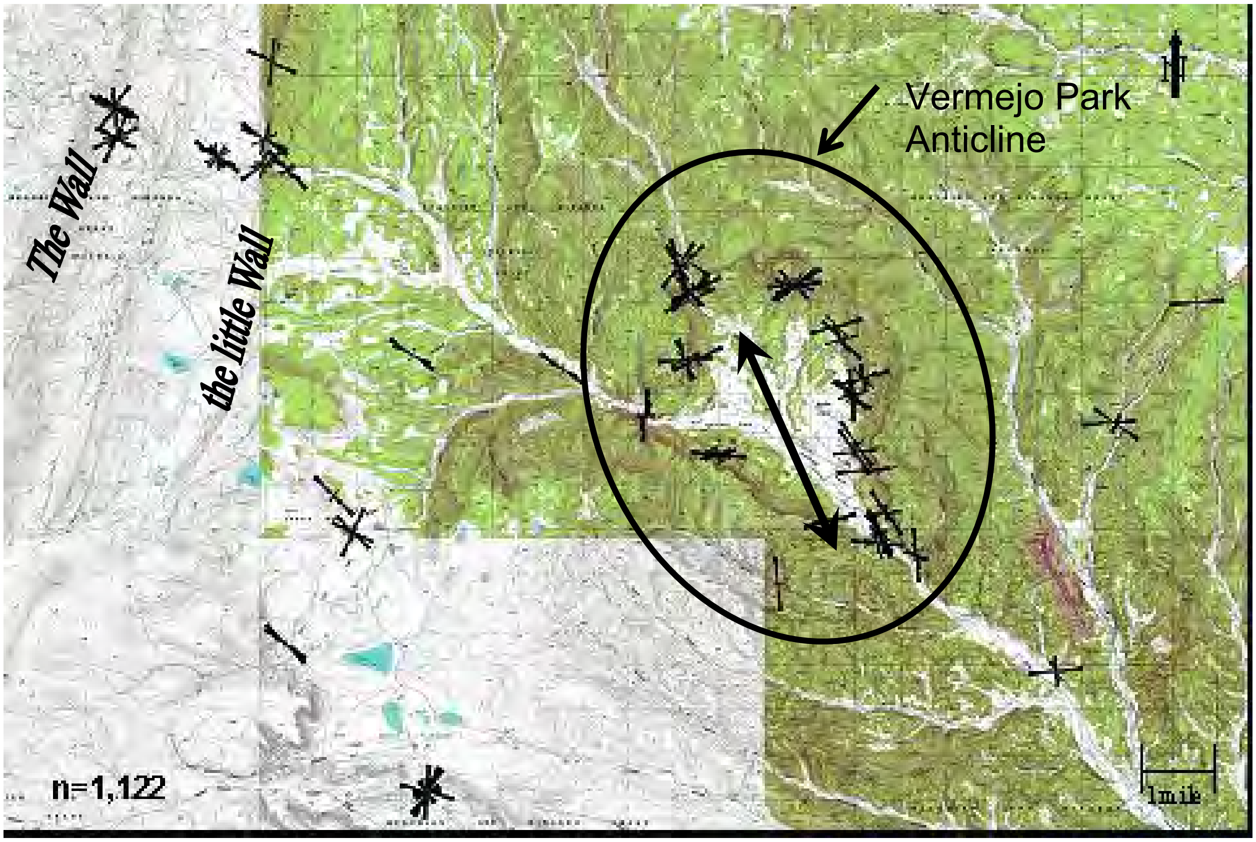

Figure 48: Fracture map close-up of area around the Vermejo Park Ranch Headquarters. Fractures in this area show a variety of orientations.

Figure 49: Photograph of a thrust within the Trinidad Sandstone along main road at the west side of the Vermejo Park Anticline.

Figure 50: Photograph of back thrust, striking parallel to the thrust fault but dipping east to intersect it.

Figure 51: Photograph of minor thrust fault within Trinidad sandstone near Spring Canyon on the northwest rim of the Vermejo anticline and 4-5 miles to north of the thrust in Figure 49. Orientation and sense of motion are similar.

Figure 52: Steps instead of plumose structures on fracture surfaces indicate an origin in shear rather than extension. Horizontal steps (like those shown above) indicate strike-slip movement.

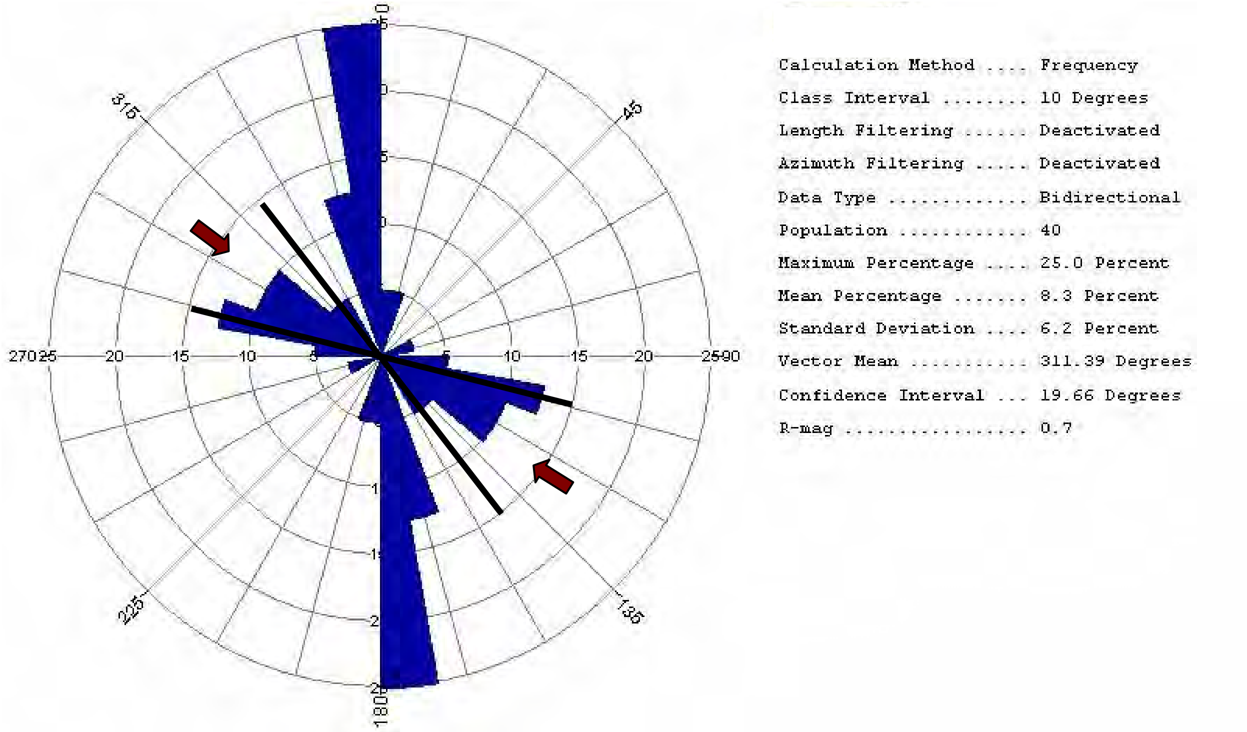

```
Calculation Method .... Frequency
Class Interval ........ 10 Degrees
Length Filtering ...... Deactivated
Azimuth Filtering ..... Deactivated
Data Type ............. Bidirectional
Population ............ 40
Maximum Percentage .... 25.0 Percent
Mean Percentage ....... 8.3 Percent
Standard Deviation .... 6.2 Percent
Vector Mean ........... 311.39 Degrees
Confidence Interval ... 19.66 Degrees
R-mag ................. 0.7
```

Figure 53: Conjugate shear fracture system within the Raton Conglomerate, n=40. This strike-slip system is displayed as an X in plan view and on the rose diagram above. Black lines and red arrows added to highlight the conjugate system and orientation of maximum compressive stress. The north-south lobe is a younger extensional fracture set superimposed on the conjugate shear fracture system.

2.1.6 Fracture Data Summary

The data show (Appendix G, Figures 31, 38, and 48) that there is a general E-W to WNW-ESE orientation to fractures and face cleats. This is most obvious along the eastern margins of the Raton Mesa within Trinidad Sandstone, Vermejo and Raton Formation outcrops. Some Dakota Sandstone outcrops on the eastern Margins of the basin have conjugate shear fractures, with a WNW-ESE bisector to the acute angle, indicative of horizontal shortening. Niobrara limestone outcrops have extension fractures striking WNW-ESE. Discussion of how these two differing fracture sets can be formed in the same area and under the same tectonic regime is discussed in section 2.1.7 "Mechanics of Natural Fracture Variability - Example 1".

Fractures nearer to the western margins of the Raton Basin typically have a more complex fracture system. Many of these varied fracture sets are found near local structures such as the Vermejo anticline. Some of these fractures have fracture characteristics indicative of shearing. Extension fracture sets were also recorded that are parallel and perpendicular to the axis of the fold and others are perpendicular (striking WNW-ESE) to the Sangre de Cristo thrust front. Fracture sets near the synclinal axis and along the tilted monoclinal fold at the western margin are parallel and perpendicular to the fold directions.

Extension fractures, roughly oriented E-W, are common in outcrops across the basin and yet subsurface data, in the form of cores and petrophysical logs, indicate that in the deeper part of the basin the common fracture set consists of east-west striking conjugate shear fractures whose acute angle bisector is vertical. The subsurface data are discussed in the sections of this report concerning well and core data (Sections 2.2 and 2.3). Through the use of Mohr-Coulomb failure criteria, we show in the following section (Example 2) how differences in rock strength and burial depth could create these differing fracture patterns within the same tectonic regime.

2.1.7 Mechanics of Natural Fracture Variability

Example 1: *Niobrara Limestone and Dakota Sandstone - eastern basin*

In the eastern part of the Raton basin there are vertical extension fractures in outcrops of the Niobrara limestone, and about 500 feet lower in the stratigraphic section there are conjugate, strike-slip, shear fractures in the Dakota sandstone. The strike of the extension fractures in the Niobrara limestone bisects the acute angle between the shear fractures in the Dakota sandstone. It is likely that the different mode of fracture is related to different magnitudes of confining stress.

At a deeper level in the basin, the stresses would be higher because of the increased weight of overburden. In this section, the vertical stress is considered to be the result of the weight of the rock plus any contained fluids acting on a unit horizontal area. In the remainder of this section stresses are considered to be effective stresses σ_{i} defined as total stress minus pore pressure: $\sigma_{\mathrm{i}} = \sigma_{\mathrm{i}}^{\mathrm{tot}} - \mathrm{p}$ where p is pore pressure and σ_i is any normal stress. An increase in the vertical effective stress $\Delta\sigma_{\mathrm{v}}$, caused by a change in depth Δz, is given by $\Delta\sigma_{\mathrm{v}} = \rho \mathrm{g}\Delta \mathrm{z}$, where ρ is the density of saturated rock. The gravitational constant is g. It is also assumed that the rock is drained, that is, the pore pressure is given simply the by hydrostatic gradient at any depth. The depth difference between these two formations induces about 500 psi (3.5 MPa) greater σ_v at the level of the Dakota sandstone.

A simple model for the rate of horizontal stress increase with depth is perfect lateral constraint. This condition requires that the changes of the two horizontal stresses be related to the vertical stress change by

$$\Delta\sigma_H = \Delta\sigma_h = \frac{\nu}{1-\nu}\Delta\sigma_v \tag{1}$$

where $\Delta\sigma_H$, $\Delta\sigma_h$ and $\Delta\sigma_v$ are, respectively, the increments of maximum and minimum horizontal stress, and vertical stress. Poisson's ratio is denoted by ν. Taking $\nu = 0.25$, the proportionality factor is 0.33. This means that the two horizontal principal stresses increase more slowly than the vertical stress with increasing depth. At the depth of the Dakota then, the vertical stress is about 3.5 MPa greater than in the Niobrara, but the horizontal stresses are only 0.88 MPa higher.

Figure 54 shows possible stress orientations for the two different fracture systems. At the shallower depth in the Niobrara, σ_3 must be perpendicular to the extension fractures, and σ_1 and σ_2 are only known to lie at some orientation in the plane of the fractures. Stress orientations for the conjugate shear fractures in the Dakota, however, are unique. For this system of small strike-slip faults, σ_1 must bisect the acute angle between sets, σ_3 bisects the obtuse angle between sets and both are normal to the line of intersection of the two sets. The intermediate stress σ_2 parallels the line of intersection of the two shear fracture sets and is normal to the other two principal stresses.

The simplest deduction with regard to the orientations of the fractures in the two rocks is to take σ_2 to be vertical at both depths, $\sigma_v = \sigma_2$, then $\sigma_H = \sigma_1$ (parallel to the extension fracture in the horizontal plane), and $\sigma_h = \sigma_3$. Thus the orientations of stresses are identical at both depths (Figure 54).

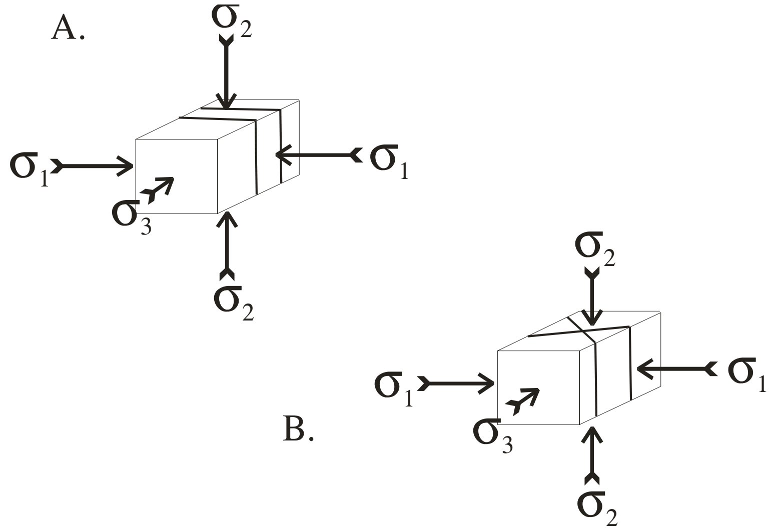

Figure 54: A) Stress orientations *consistent* with extension fractures. B) Stress orientations *required* for strike-slip shear fractures. The orientations for both systems of fractures are identical.

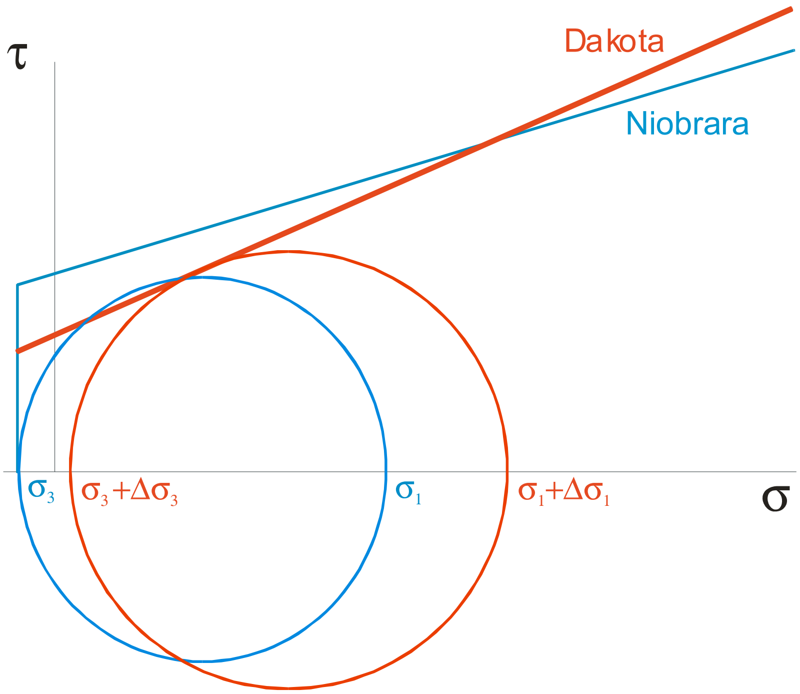

Figure 55: Mohr circles of the stress states in Niobrara limestone (blue) and Dakota sandstone (red), combined with the appropriate failure conditions for each rock type.

To understand how the difference in depth resulted in two different fracture modes with the same stress orientation, we need to study the stress states at the two depths and the respective failure conditions for the two rocks. The Mohr diagram (Figure 55) illustrates what could have been going on. The straight failure curves show qualitatively the differences between the strengths of the limestone and the sandstone. For example, the limestone (blue) is usually stronger at the τ-axis, but often has a lower slope than the sandstone (red). For extension fractures to form, σ_3 must have been negative (tension), and must have touched the tension cut-off. Elastic mismatch between layers is known to cause such tensions in the stiffer layers.

Five hundred feet (152 m) deeper, in the Dakota, higher stresses cause the stress circle for the sandstone (red) to be farther to the right, and larger. The existence of shear fractures indicates that it must have touched the shear failure line for sandstone (red). The minimum point on the circle was subject only to the condition that it must not have touched the tension cut-off. (The tension cut-off is about the same, 10 MPa, for all rocks.) The relative increases in stress with depth as calculated above are consistent with these constraints.

Example 2: *Extension fractures vs. shear fractures in a given rock unit*

A given rock layer contains vertical extension fractures in outcrop, but has shear fractures with a normal fault orientation at greater depth in the basin. The strikes of the extension fractures parallel the line of intersection of the normal shear fracture system. This problem differs from

Example 1 in two ways: (1) for this problem, the fractures are in the same rock unit, and (2) the deeper shear fractures are normal faults rather than strike slip. Figure 56 shows the likely orientations of the principal stresses responsible for the two systems of fractures. Recall from Example 1 that the requirements are that σ_1 and σ_2 must lie in the plane of an extension fracture, and that σ_3 must be normal to it. Analogous to the strike-slip faults of Example 1, for the system of small-scale normal faults of this problem, σ_1 must bisect the acute angle between sets, σ_3 must bisect the obtuse angle between sets and is normal to $\sigma_{1;}$ and σ_2 must parallel the line of intersection of the two shear fracture sets and is normal to the other two principal stresses.

In Figure 56 A, σ_1 was drawn to be in the horizontal plane because of other geological constraints. That stress orientation is also consistent with this problem. In three out of the four observed fracture systems, the direction of σ_1 is the same. As in Example 1, we can explore the possibility of failure in two different modes, extension fractures and shear fractures, using Mohr's diagram.

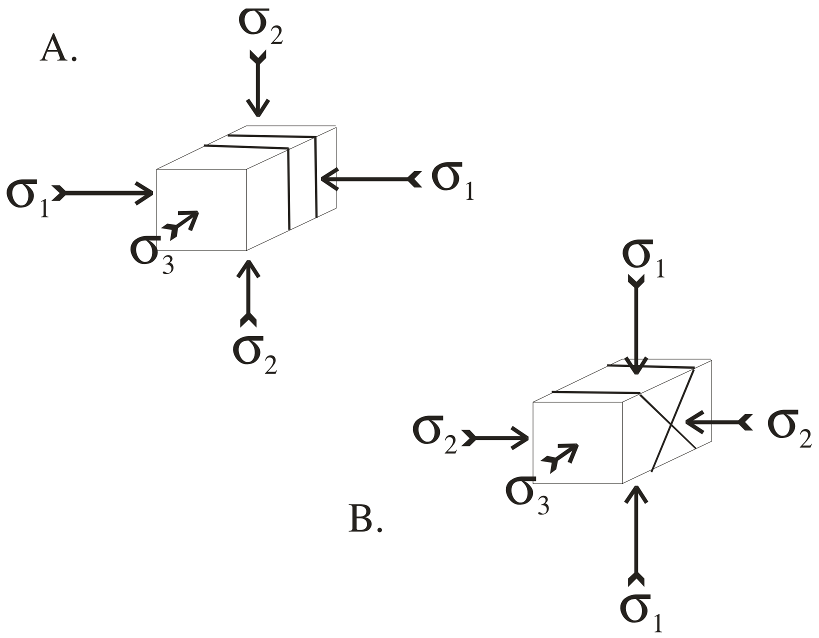

Figure 56: Block diagrams showing relations of stresses to fractures at two different depths. A) σ_1 and σ_2 are constrained only to lie in the fracture plane. B) The stress system shown is unique for conjugate normal fractures.

Let us take a look at a possible scenario for the extension fractures. For this problem, the fracture systems of interest occur in the same rock type, so only one failure curve is needed. Figure 57 shows such a posited failure curve having a tension cut-off. For the extension fractures to form, the maximum Mohr's circle must be tangent to the tension cut-off, and this will happen at $\sigma_h = \sigma_3$, to the left of the origin. The other two stresses, being compressive, will lie off to the right of the origin. As mentioned in Example 1, elastic mismatch may be responsible for the existence of tensile stress in certain layers. It is not possible to estimate the depth at which the extension fractures occurred because the exact mechanism for generating the tensile stress is unknown.

We need to make an assumption about the relative magnitudes of σ_v and σ_H. As before, without further information, they could be ordered either way for the extension fractures. Consistency between the two existing fracture systems, however, suggests that σ_1 was horizontal at the time of fracturing. Thus we will assume that σ_v is the intermediate stress and σ_H is the maximum stress. This is summarized in the top Mohr diagram. Now at a greater depth, the two horizontal stresses will be greater according to Equation 1, but they increase more slowly, about one-third the rate, than σ_v. Therefore, at some depth, σ_v will exceed σ_H and become the maximum stress. If the exterior circle increases sufficiently in diameter to touch the shear failure curve, normal fractures will form.

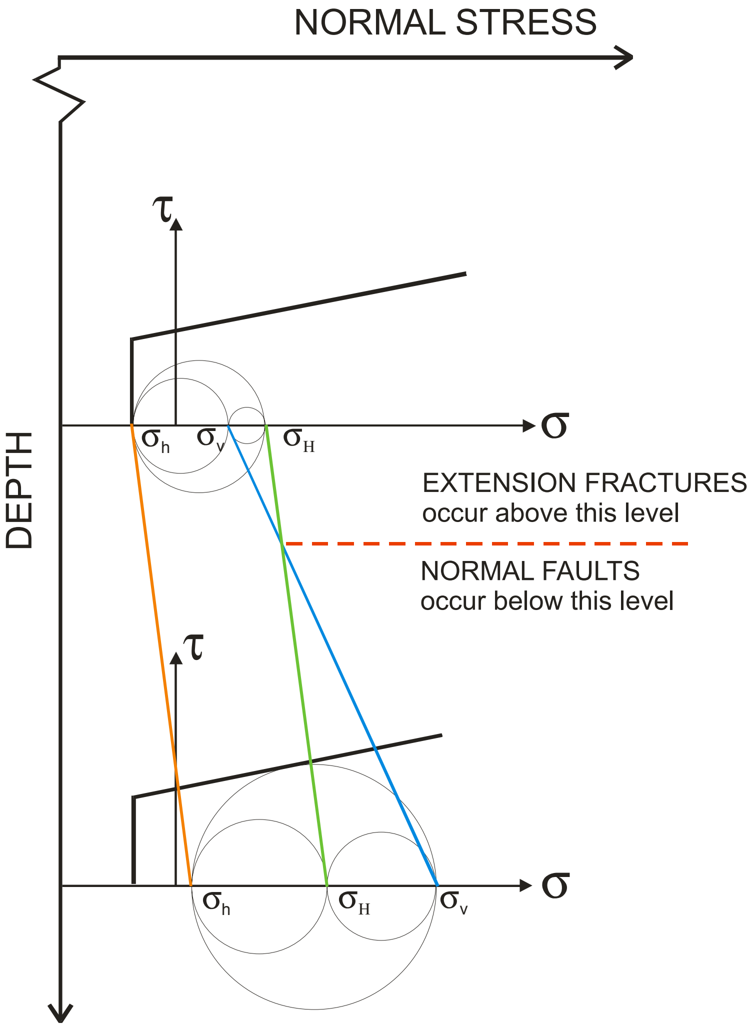

Figure 57: States of stress in relation to the failure condition at the two different depths referred to in the text.

The direction of $\sigma_2 = \sigma_H$ forces the alignment of the normal fracture strike to be parallel to that of the extension fractures. Therefore the change in fracture mode from extension to normal fault with increasing depth is likely due to increasing stress associated with greater depth of burial.

2.1.8 Discussion/Summary

This overview of fractures in outcrop within the Raton Basin details a complex fracture pattern related to lithology, local structure, compaction, and thrusting. The most ubiquitous fractures appear to be related to Laramide-age eastward thrusting of the Sangre de Cristo Mountains located at the western edge of the Raton Basin. This is evidenced by extension fracture orientations nearly normal to the thrust front and/or conjugate shear fractures with a bisector to the acute angle that is normal to the thrust front. These fractures and cleats trend roughly E-W to WNW-ESE and are found throughout the basin. It is important to note that these fractures and cleats are also found along the distant eastern margins of the basin over 75 miles from the thrust front. Fracture orientations and surface features at some of these distal locations are indicative of horizontal shearing. These include strike-slip style conjugate fracture sets having an E-W to WNW-ESE acute-angle bisector. Subsurface data in the form of cores and petrophysical logs indicate that, in the deeper part of the basin, the common fracture set consists of east-west striking conjugate shear fractures whose acute angle bisector is vertical. These data are discussed in the sections of this report concerning well and core data.

More complex fracture orientations are observed nearer the thrust front and to secondary structures. The fractures associated with secondary structures were formed by shearing and bending of beds across the Vermejo Park Anticline, by the irregular shape of the thrust front, by the bending of beds in areas of high structural curvature such as the near vertical to overturned beds at the western margins of the basin, and possibly to a stress reversal from approximately east west to north-south.

These data and inferences lead to the hypothesis that the western margins of the basin are more highly fractured and contain a more complex fracture system than eastern sections of the Raton Mesa. Given that rock units are more highly fractured in western areas, it can be hypothesized that western areas will in general have increased production rates and less anisotropic drainage relative to the eastern margins where a single primary fracture pattern may be typical.

2.2 CORE ANALYSES

Cores provide significant insights into the in situ fracture characteristics that are not afforded by outcrops and wellbore-image logs. Cores allow measurements of actual fracture apertures, provide analysis of fracture surfaces and mineralization, and allow for making distinctions between coring-induced and natural fractures. However, fracture strikes cannot be determined in the unoriented Raton basin cores.

Small-diameter cores (two, and two and a half inches in diameter) from seven of the more recent exploration and production wells drilled by the El Paso Production Company on the Vermejo Park Ranch were examined for natural fractures. Three of these cores were examined by contractor Ron Graichen, four cores were examined and analyzed by contractor Connie Knight, and the core reports are part of the Appendix of this report. Statistics from the four cores from wells VPRCH-30, 31, 32, and 34 allow a certain level of comparison of the fracture intensity and characteristics across the area of interest, as well as a comparison of fracturing by lithology.

Fractures are present in all of the cored lithologies: sandstones, siltstones, shales, coals, and igneous intrusives. Four types of fractures are present in the cores: 1) vertical extension fractures similar to those in outcrop, 2) a set of conjugate shear fractures with a vertical acute-angle bisector similar to the fractures seen in image logs, 3) small-scale thrust faults, and 4) compaction fractures in mudstones. The vertical to near-vertical extension fractures and the shear fractures are most common. More of the extension fractures occur in sandstones whereas most of the shear fractures are found in shales. A higher percentage of the total fractures are present in the shales and siltstones, but that merely reflects the fact that these lithologies represent a higher percentage of the core. The compaction fractures that are common in mudstones are ubiquitous throughout this lithology in all Rocky Mountain basins; they are rarely mineralized and, unless reactivated, do not add to the porosity or permeability of the reservoir systems, and will not be discussed further here.

Most of the rest of the cored fractures are mineralized with patchy calcite, and a thin layer of quartz druze often underlies the calcite. This is the most common mineralization sequence found in cored fractures up and down the Rocky Mountains. Other minor mineral phases in the Raton include local occurrences of iron pyrite, clay, and a local occurrence of bitumen. Despite mineralization, approximately half of the fractures retain at least 25% of the original fracture aperture. A higher percentage of remnant aperture is typical of larger fractures; sub-millimeter fractures tend to be more completely filled with mineralization.

The spacing of vertical fractures can be assessed in those cores where the core axis is slightly oblique to the planes of a set of fractures, and where fracture spacing is less than the core diameter. Numerous such fracture spacings could be measured in the four cores, and ranged from 0.02 ft to 1.1 ft. This range represents the low end of a much wider range of fracture spacings since the near-vertical core can not sample the wider fracture spacings. However, it does indicate that fractures are widely distributed and occur in all lithologies in the subsurface.

Absolute fracture orientations cannot be determined from these unoriented cores, but can be inferred to be parallel to the fracture orientations measured in nearby wellbores by wellbore-image logs. Most of the core fractures probably strike approximately east-west, with local exceptions. Fracture orientations relative to each other, however, can be measured in numerous examples in the core, where they are overwhelmingly parallel. Approximately three-quarters of the examples of fracture orientations relative to each other show a parallel relationship. However, intersecting fracture orientations were also noted locally, the intersection angles varying from 30 degrees up to 90 degrees.

The degree of fracturing varies significantly in the different cores. One measurement is the total number of fractures divided by the total number of feet cored. This is a gross measurement that suffers from various inaccuracies; i.e., it does not account for the possibility that more of the specific fracture-susceptible lithologies such as siltstone, or perhaps more of the less fracture susceptible lithologies such as the igneous intrusives may be cored in any given well. Moreover, it does not discriminate between the different types of fractures. However, it does provide a certain platform for a preliminary comparison between wells. Thus the ratio of fractures per foot of core varies from 0.32 in the VPRCH-34 well to 1.28 in the VPRCH-32 well, with intermediate values, 1.0 and 0.70, for wells VPRCH-30 and VPRCH-31, respectively.

Many of the inclined shear fractures show lineations on their surfaces indicating the direction of offset, and in fact these lineations do not record simple dip-slip motion. Many of the lineations record oblique-slip offset, with the rake of the lineations across the fracture surfaces deviating as much as 80 degrees from a simple, down-dip plunge. There is also significant evidence, in the form of superimposed lineations on a given fracture surface, for reactivation of many fracture planes.

Several fault zones were cored, as noted by fracture breccia and slickensided fault surfaces. These fault zones are compatible with the reactivated fractures noted above. A few thrust faults were cored, defined by planes with a low dip angle, evidence for shear on the surfaces, and suggestions of reverse-dip offset.

Another cored feature is a small dike filled with coal. Such features are present in several places in outcrop (Pillmore, 1976; Harbour and Dixon, 1959; Podwysocki and Dutcher, 1971), and apparently form where a heat source such as an igneous intrusive heats coal to its liquification temperature of about 400 degrees C.

2.3 WELL LOG ANALYSES OF FRACTURES

Detailed data on fractures from geophysical logging in four wells in the Raton Basin were analyzed to understand fracture patterns at depth. Locations of these wells are shown in Figure 58. These wells were logged to depths ranging from about 1600 ft. to about 2500 ft., primarily in the Raton and Vermejo Formations, with some penetration of the Trinidad Sandstone. Wells VPRC 73 and VPRC 87 are located near the synclinal axis of the Raton Basin in Colorado. Well VPRE 33 is located on the western limb of the basin axis and on the eastern side of the Vermejo Park Anticline. Well VPRD 71 is located near the western flank of the Raton Basin and to the southwest of the Vermejo Park Anticline.

The Formation Micro Imager (FMI) logging tool provides imaging of the formation based on the correlation of eight microresistivity traces measured around the circumference of the well bore. Real-time orientation knowledge of the position of the downhole tool allows measurement of both the dip and strike of bedding, fractures, and faults. Fractures that are open to invasion by the drilling mud are distinguished from closed fractures based on contrasts in electrical resistivity of the mud and the formation. Analyses of fracture orientations in this study have focused on open or partially open fractures for which an apparent hydraulic aperture has been estimated. Open fractures are more likely to interact with the local stress state and are more relevant to gas and water flow within the formation.

2.3.1 **Fracture Orientations from FMI Logs**

The orientations of open fractures from the FMI logs for the four wells are shown in Figure 59. Open fractures are defined as those for which a fracture aperture was estimated on the FMI logs.

The rose diagram of fracture strike for well VPRC 73 indicates two primary populations of fractures, one oriented approximately east-west and the other northeast-southwest. The east-west striking fracture set is numerically dominant in well VPRC 73. There is no consistent variation in fracture strike with lithology. The corresponding stereonet plot of fracture poles shows that fractures dip to the north and south for the east-west striking population and to the northwest and southeast for the northeast-southwest striking population. The density of the plotted poles on the stereonet indicates that more of the fractures dip to the north and northwest than to the south and southeast in the two populations.

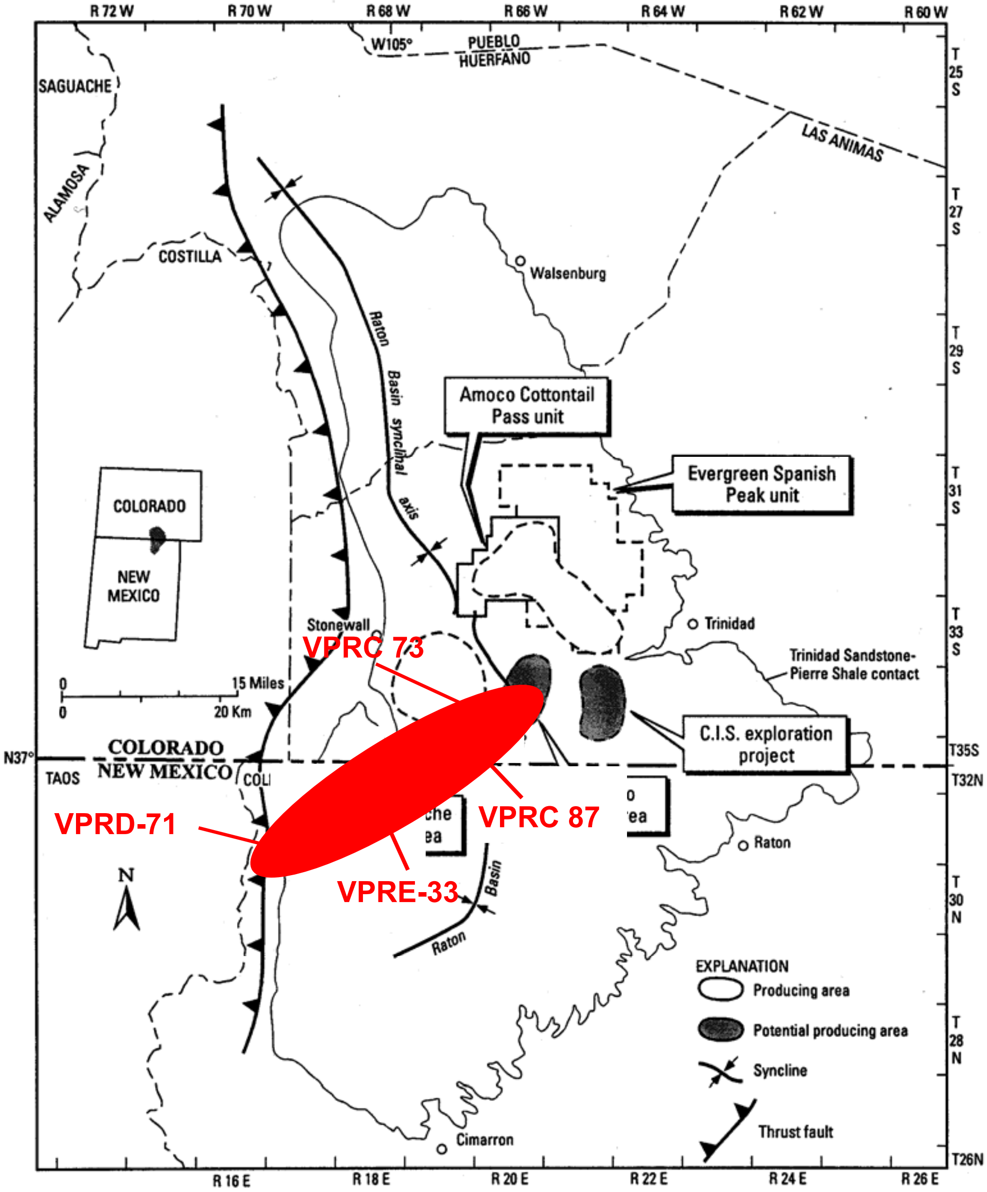

Figure 58: Map showing the approximate location of wells with detailed geophysical logging. Base map of the Raton Basin taken from Johnson and Finn (2001). Red ellipse added to mask precise locations to protect proprietary information.

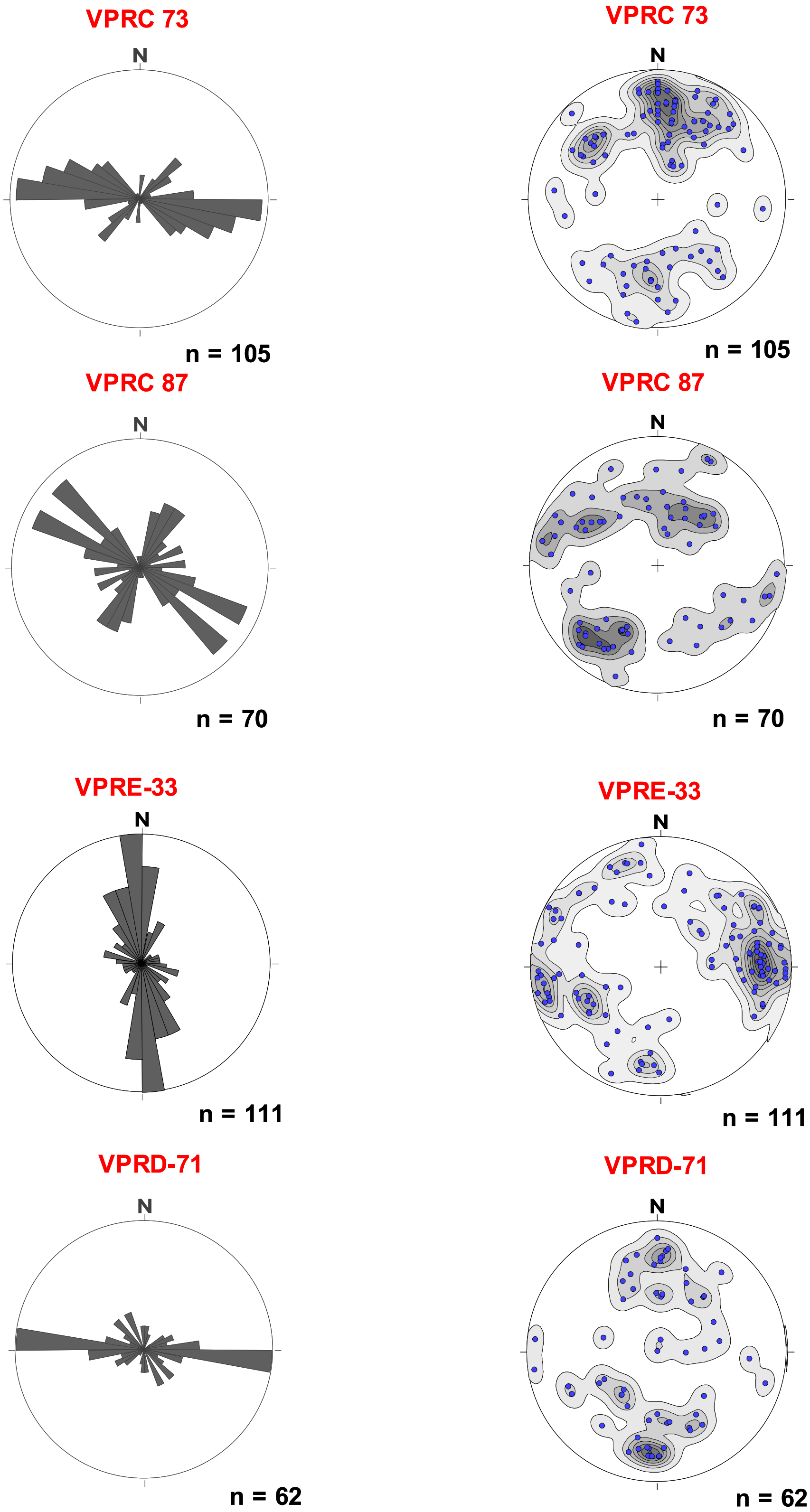

Figure 59: Orientations of open fractures from FMI logs of four wells. Plots on left show rose diagrams of fractures and plots on right show lower hemisphere stereonet plots of fracture poles.

The rose diagram of fracture strike for well VPRC 87 shown in Figure 59 shows two less-well-defined populations that are oriented approximately N55°W and N25°E. The corresponding stereonet plot of fracture poles indicates that these fracture sets dip to both the northeast and southwest, and northwest and southeast, respectively. The northeasterly dipping fractures have generally higher dip angles than the southwesterly dipping fractures.

The plots in Figure 59 for well VPRE 33 show a dominant population of fractures that strike approximately north-south and dip to the west. The fracture pattern in well VPRE 33 is probably strongly influenced by its location on the steeply dipping eastern limb of the Vermejo Park Anticline. Whereas there are general similarities in fracture patterns for the other three wells, VPRE 33 differs significantly.

The rose diagram and stereonet plots of fracture orientations for well VPRD 71 indicate a set of east-west striking fractures, with some random variations in strike within the population. Approximately equal numbers of fractures dip to the north and south.

It should be noted that fracture orientation data from vertical drill holes is inherently biased against the observation of fractures with high dip angles. Interpretation of the stereonet plots in Figure 59 should include the realization that high-angle fractures have been undercounted and that the frequency of poles near the circumference of the stereonet is significantly lower than in the actual population of fractures. The bias associated with fracture-orientation data from drill holes can be quantitatively corrected using the inverse of the cosine of dip. For example, the actual frequency of fractures dipping at 80° is greater than the apparent frequency by a factor of 5.8.

The fracture sets identified in these four wells do not readily correspond to conjugate sets resulting from horizontal compression. This is in contrast to the conjugate shear fracture sets resulting from horizontal compression identified in outcrop in the Raton Basin. Differences in fracture orientation patterns from the FMI logs and the observations in outcrop may be attributable to bias against steeply dipping fractures in the borehole logs. In addition, some fractures that would not be identified as open fractures in the FMI logs because of confining stress would be identified with the unloaded conditions in outcrop.

The east-west striking fracture set in wells VPRC 73 and VPRD 71 shown in Figure 59 is consistent with formation as a conjugate set in response to vertical compression, as indicated by the two oppositely dipping sub-sets evident on the stereonet plot. This fracture set would have formed with σ_1 in the vertical direction, σ_2 in an east-west orientation, and σ_3 in the north-south direction. This stress state is not consistent with the present north-south orientation of the maximum horizontal compressive stress, but is consistent with the west to east thrusting along the Sangre de Cristo range and thicker overburden in the Raton Basin during the Middle Tertiary. Similarly, the northwest-southeast striking fracture set observed in well VPRC 87 would have formed with σ_1 in the vertical direction, σ_2 in a northwest-southeast orientation, and σ_3 in the northeast-southwest direction. The difference in the inferred orientation of σ_2 in the two wells may be attributable to irregularities in the Sangre de Cristo thrust front.

The fracture pattern in well VPRE 33 is unique among the four wells in this analysis. Proprietary seismic data in this area of the Raton Basin indicate multiple, nearly vertical offsets in seismic reflectors that apparently correspond to north-south striking faults (Paul Basinski, personal communication, 2004). These faults may be related to strike-slip movement along a trend from the Vermejo Park Anticline to the Tercio Anticline. The fracture patterns observed in VPRE 33 are probably related to this larger-scale structural feature.

2.3.2 Fracture Orientation and Depth

To examine variations in fracture orientation with depth, the population of open fractures in each well has been divided into depth intervals, as shown in Figures 60a and 60b. Rose diagrams of fracture strike in well VPRC 73 are shown to the right of the graph in Figure 60a (upper) for depths of less than 800 ft, 800 ft to 1200 ft., and greater than 1200 ft. These diagrams indicate a shift in the dominant direction of fracture strike from east-west at the shallower depth interval to northeast-southwest in the deeper depth interval in well VPRC 73. Rose diagrams for depths of less than 1200 ft. and greater than 1200 ft. from well VPRC 87 are shown in Figure 60a (lower). The northeast-southwest striking fracture set becomes a more prominent component of the fracture population for depths greater than 1200 ft in well VPRC 87. Similar plots for well VPRE 33 in Figure 60b (upper) show very predominantly north-south strike to fractures at shallower than 1200 ft and three fracture sets at depths greater than 1200 ft. The two dominant fracture sets below 1200 ft depth in well VPRE 33 strike north northwest and north northeast. The plots for well VPRD 71 shown in Figure 60b (lower) indicate two fracture sets at depths of less than 800 ft, dominantly north-south fractures between 800 ft and 1200 ft depth, and one fracture set striking east-west for depths of greater than 1200 ft. It should be noted that only four open fractures were identified between 800 ft and 1200 ft, so the distribution of orientations is not statistically significant.

For wells VPRC 73, VPRC 87, and VPRE 33, the frequency of open fractures is significantly lower for depths of greater than 1200 to 1400 ft than for shallower depths, as shown in Figures 60a and 60b. Interestingly, this corresponds to the depth below which the variability in the direction of the maximum horizontal compressive stress decreases, as observed in wells VPRC 73 and VPRC 87 (see Section E below). The frequency of open fractures in well VPRD 71 does not show a similar pattern because there are very few open fractures at shallower depths and there are many open fractures near the base of the Vermejo Formation between 1400 and 1600 ft depth. Generally, these observations suggest that there may be a change in the stress state and fracture network at a depth of approximately 1200 to 1400 ft in this area of the Raton Basin.

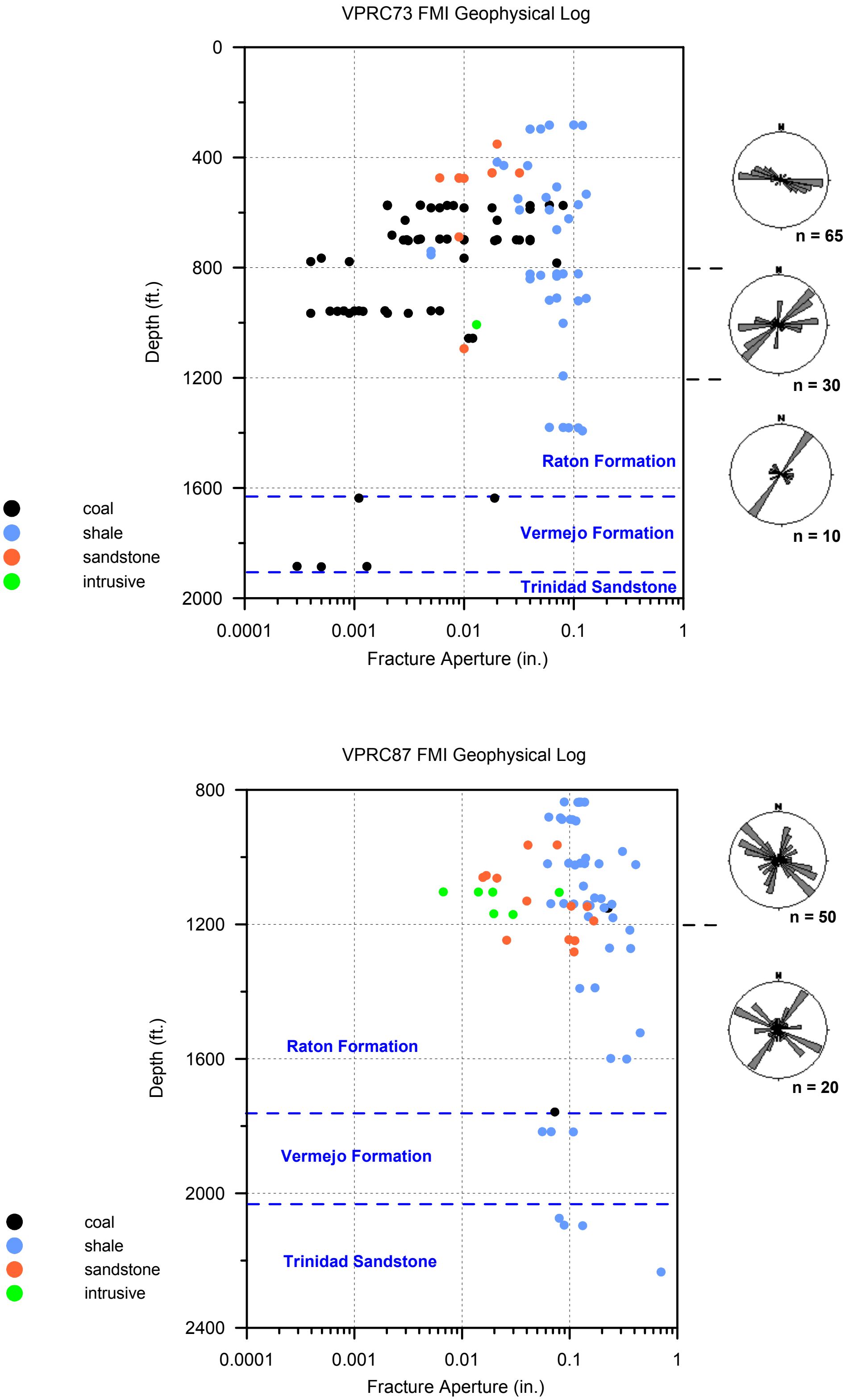

Figure 60a: Fracture hydraulic aperture estimated from the FMI logs for wells VPRC 73 and VPRC 87 versus depth. Lithology of fractures indicated by colored symbols. Rose diagrams of fracture strike are shown for different depth ranges to the right of the plot.

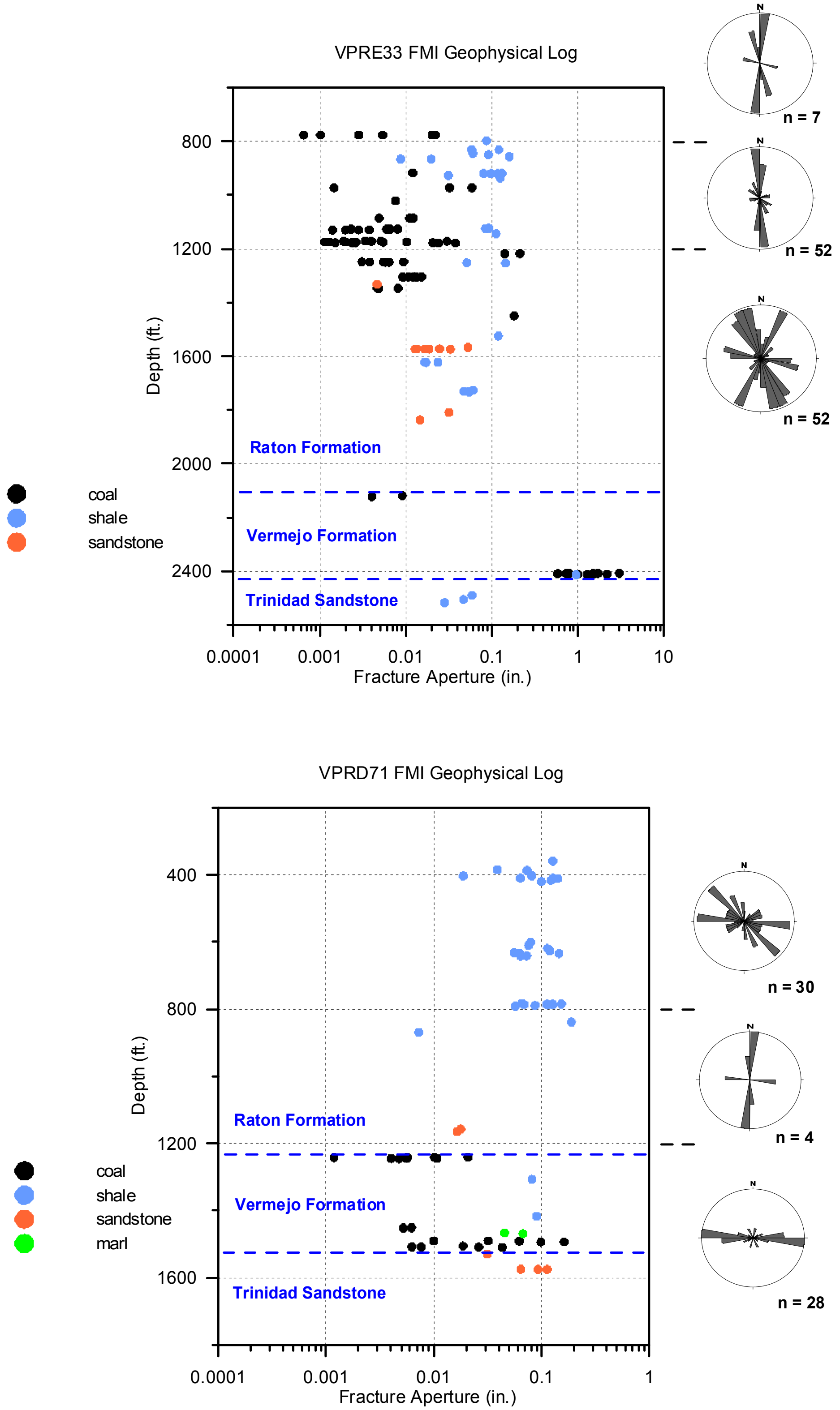

Figure 60b: Fracture hydraulic aperture estimated from the FMI logs for wells VPRE 33 and VPRD 71 versus depth. Lithology of fractures indicated by colored symbols. Rose diagrams of fracture strike are shown for different depth ranges to the right of the plot.

2.3.3 Fracture Orientation and Lithology

Open fractures from the FMI logs from the four wells were divided into groups based on the rock type in which they occur. Plots of the orientations of these fractures, classified by lithology are shown in Figures 61a and 61b. There are few systematic associations between fracture orientation and lithology apparent in these plots. It should be noted that the sample size of the number of fractures for some lithologic types is relatively small, calling into question the statistical relevance of the patterns of fracture orientations. In wells VPRE 33 and VPRD 71 there is a significant difference in the distributions of fracture orientation in the coals and shales (see Figure 4b). Fractures strike dominantly north-south in coals in well VPRE 33 and strike east-west in coals in well VPRD 71. The rose diagrams for shales in these two wells show somewhat similar, bimodal distributions of fracture strike. Differences in the mechanical characteristics of coal and shale may account for the contrasting fracture patterns.

Interestingly, the six steeply dipping fractures in an igneous intrusion penetrated by well VPRC 87 have a tightly clustered distribution striking just east of north. This orientation is approximately the same as the direction of maximum horizontal compressive stress estimated from ADI logs, as described in Section E below. These fractures may have formed as tension fractures in the cooling igneous body and the direction of the maximum horizontal stress was oriented in approximately north-south direction at that time. These observations suggest that the maximum horizontal stress had rotated from an east-west direction associated with Laramide thrusting to a north-south direction by the time this intrusive rock was formed.

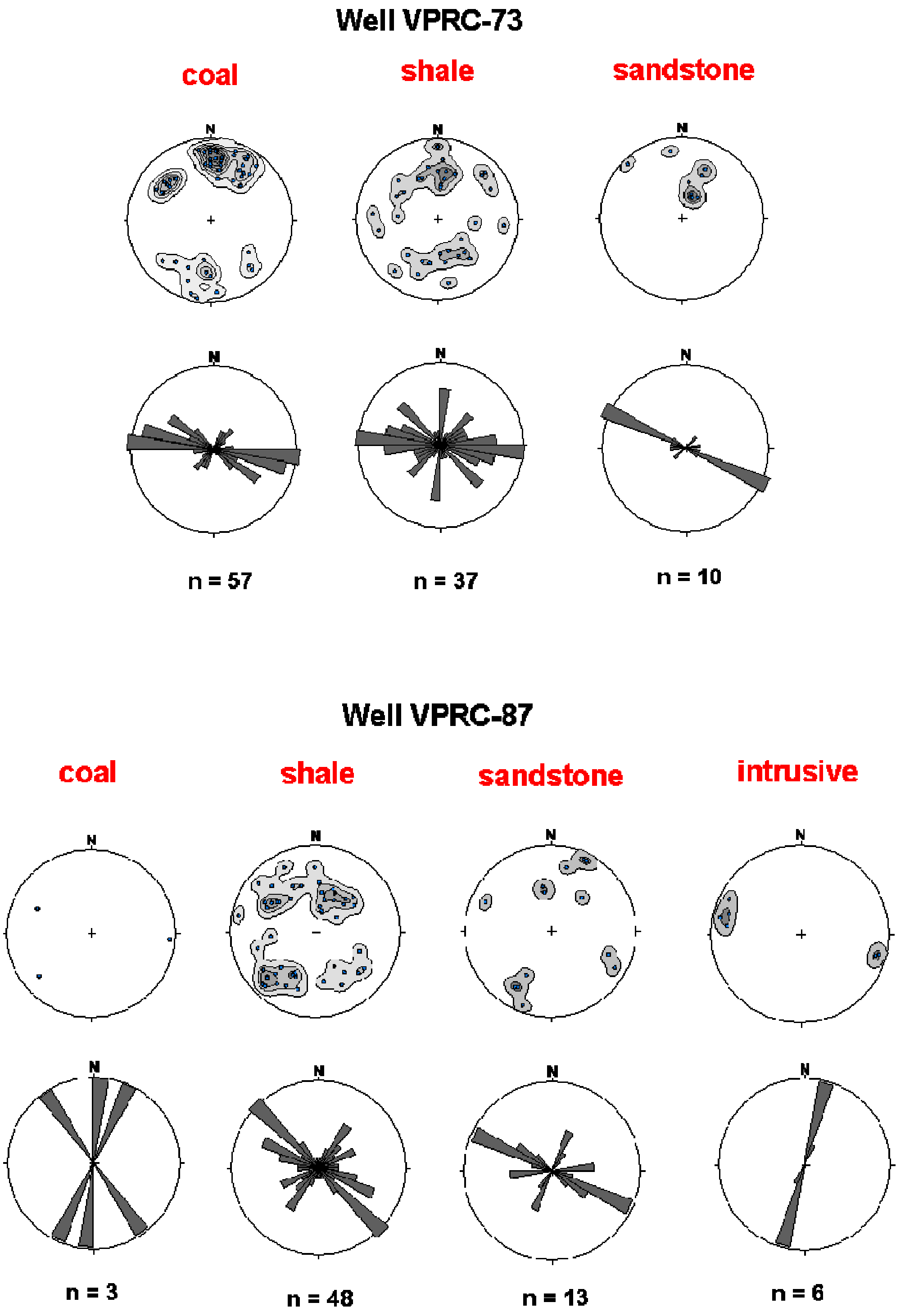

Figure 61a: Orientations of open fractures from FMI logs for wells VPRC 73 (above) and VPRC 87 (below), classified by lithology. Stereonet plots show lower hemisphere projections of fracture poles.

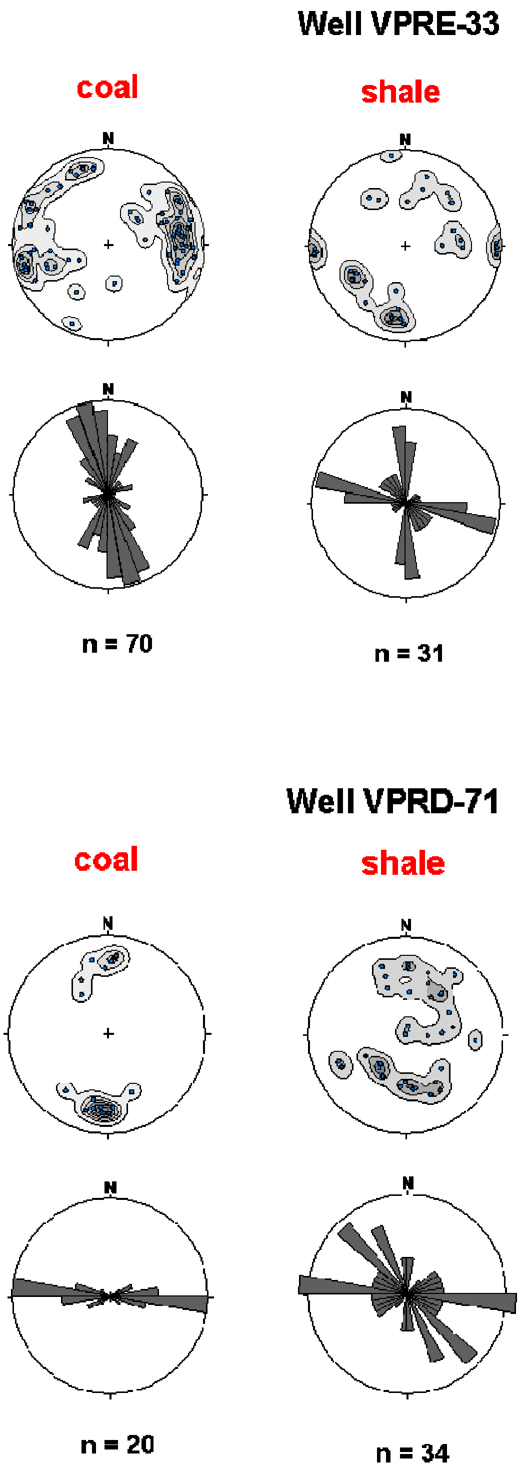

Figure 61b: Orientations of open fractures from FMI logs for wells VPRE 33 (above) and VPRD 71 (below), classified by lithology. Stereonet plots show lower hemisphere projections of fracture poles.

2.3.4 Fracture Aperture

Fracture hydraulic aperture is estimated for the open fractures on the FMI logs. This estimate is based on the assumption that the open fractures are invaded by the drilling fluid and that the contrast in resistivity between the fluid and the formation provides a basis for modeling the aperture of the fracture between the micro-resistivity pads on the FMI tool. Furthermore, the variation in fracture aperture along the trace in the borehole wall is used to calculate an effective hydraulic aperture, based on the cubic law of flow in fractures (Domenico and Schwartz, 1990.

Fracture hydraulic aperture as a function of depth and lithology is shown in Figures 60a and 60b for the four wells. The locations of formation contacts are also shown on these figures. The data from well VPRC 73 show a general decrease in fracture aperture with depth, primarily based on measurements from the coal beds. Fractures in shale do not show any apparent decrease in aperture with depth and have generally larger apertures than fractures in sandstone or coal. The data from wells VPRC 87, VPRE 33, and VPRD 71 do not show any systematic decrease in fracture hydraulic aperture with depth. Values of fracture aperture in shale are generally larger than in sandstone, coal, or intrusive sills in all of the wells, with the notable exception of a cluster of open fractures in coals of the lower Vermejo Formation in well VPRE 33.

There are some significant differences in average and clustered values of fracture aperture in the four wells. The values of fracture hydraulic aperture are significantly higher in VPRC 87 than in well VPRC 73. The apparent difference in average fracture aperture between the FMI logs could be related to the values of resistivity in the drilling mud. The measured values of resistivity of the mud in the two wells differ by almost a factor of two (1.8 ohms and 3.0 ohms, respectively for VPRC 73 and VPRC 87). If there is an error in the value of resistivity in the mud, this could account for the apparent contrast in average hydraulic aperture between the wells.

It should also be noted that wells VPRC 73, VPRE 33, and VPRD 71 are somewhat unusual relative to FMI logs from western coal basins with regard to the large number of open fractures identified in the coals (Randy Koepsell, Schlumberger, personal communication).

It is expected that fractures parallel to the direction of maximum horizontal compressive stress would be more open and exhibit a larger fracture aperture. The relationship between estimated fracture aperture and orientation relative to the local horizontal stress state from the FMI and ADI logs in wells VPRC 73 and VPRC 87 is shown in Figure 62. On these plots, low values of the difference between strike and the ADI azimuth correspond to the situation in which the fracture is nearly parallel to the direction of the maximum horizontal compressive stress at that depth. There is no indication of the expected relationship between fracture aperture and orientation relative to the stress state in the plots in Figure 62. There is a small, expected negative correlation, as shown by the red line regression for well VPRC 73, but the correlation for well VPRC 87 is, unexpectedly, somewhat positive. These findings are apparently contrary to observations of production interference in wells aligned north-south, approximately parallel to the maximum horizontal compressive stress (Paul Basinski, El Paso Production, personal communication). However, interference between wells may be attributable to fracture continuity and connectivity, rather than to larger fracture aperture in the north-south direction.

The lack of apparent correlation between fracture hydraulic aperture and orientation relative to the local stress state may to due to several factors. The estimate of fracture hydraulic aperture on the FMI log is a highly derivative value that is consequently subject to error from several sources. Another potentially complicating factor is the relationship between vertical stress and fracture aperture. The vertical stress relative to the horizontal stress is not quantified with the ADI logging and would impact fracture aperture, particularly for less steeply dipping fractures.

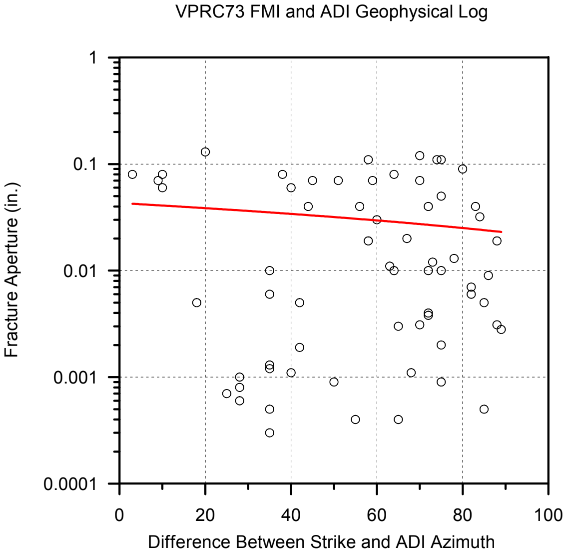

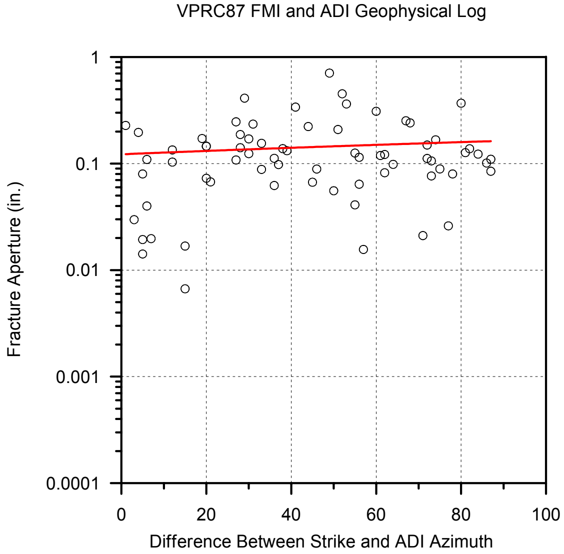

Figure 62: Fracture hydraulic aperture estimated from the FMI logs for wells VPRC 73 (upper) and VPRC 87 (lower) versus the angle between fracture strike and the local azimuth of the maximum horizontal compressive stress from ADI logs. The linear regression is shown as the red line in both plots.

2.3.5 Fracture Spacing

The spacing of fractures in the Raton Basin area was investigated by conducting a horizontal line survey of fractures in an exposed sandstone bed of the Vermejo Formation. Most of the fractures encountered in this survey were vertical or nearly vertical. The results of this survey are shown in Figure 63 as a probability plot. To construct this plot the values of fracture spacing were ranked and a value of cumulative probability was assigned to each ranked value, based on the number of observations. In Figure 63 the excedence (or cumulative) probability is plotted on a normal distribution scale and the fracture spacing is plotted on a log scale. The approximately linear distribution of the data points indicates that fracture spacing is log-normally distributed. The geometric mean or median of this distribution of fracture spacing is about 30 cm.

The results of this survey indicate a fairly dense distribution of vertical fractures in the sandstone of the Vermejo Formation, with a median spacing of only 30 cm. It is not clear how many of these fractures are related to near-surface unloading of stress and it should be noted that these results may significantly underestimate the fracture spacing in the subsurface. A log-normal distribution of fracture spacing is highly skewed and implies that many fractures are clustered with a relatively small spacing, but a few fractures are spaced relatively far from neighboring fractures.

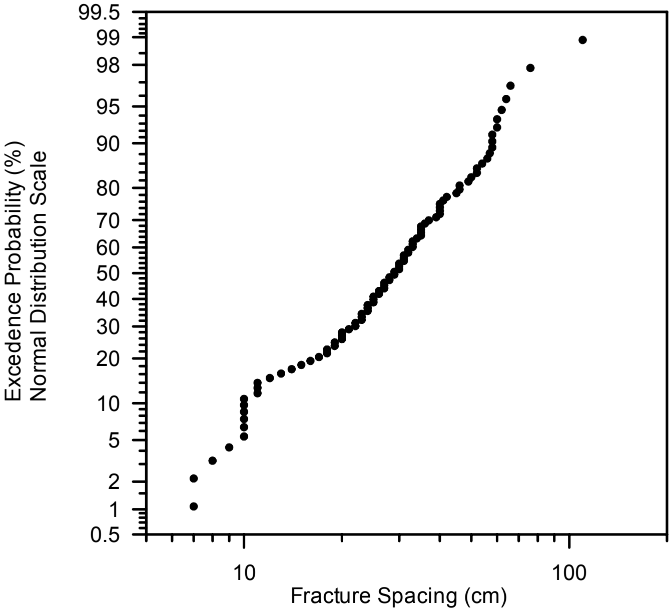

Figure 63: Probability plot of fracture spacing measured in a sandstone bed of the Vermejo Formation at the Maloya Lake spillway, Sugarite State Park, New Mexico.

2.4 WELL LOG ANALYSES OF STRESS

Measurements of *in situ* stress from geophysical logging in four wells in the Raton Basin (VPRC 73, VPRC 87, VPRE33, and VPRD 71) were analyzed to understand the present orientation of the stress field within the Basin. Locations of these wells are shown in Figure 58.

The ADI (or Dipole Shear Sonic Imager) logging tool detects anisotropy of the sonic shear-wave velocity within the formation. The acoustic anisotropy measured by this tool may be intrinsic or stress-induced in nature. Intrinsic anisotropy is due to preferential textural or fracture orientations within the rock; whereas, stress-induced anisotropy is imparted by differences in the horizontal stress state. The direction of fast shear-waves in the medium is aligned with intrinsic features or the maximum horizontal stress in the cases of intrinsic and stress-induced anisotropy, respectively. A consistent azimuth of maximum shear-wave velocity in a well, without a corresponding preferred fracture orientation or textural trend, is generally interpreted to be indicative of the direction of maximum horizontal stress.

2.4.1 Horizontal Stress from ADI Logs

Results of the ADI logging for the four wells are shown in Figures 64a and 64b. The plots on the left show the estimated azimuth of maximum horizontal compressive stress at 5 ft depth intervals and a smoothed curve of individual measurements using a running average. The plots on the right show the corresponding rose diagrams for the running average of the azimuth of maximum horizontal stress.

The average inferred direction of the maximum horizontal stress is approximately north-south in all four of the well logs. The average azimuth in wells VPRC 73, VPRC 87, and VPRE33 is between approximately N5^{o}E and N10^{o}E. The average azimuth in well VPRD 71 is somewhat different at approximately north. The variability in the individual measurements of the azimuth of maximum horizontal stress is noticeably greater in wells VPRC 73 and VPRC 87 than in wells VPRE33, and VPRD 71, particularly with regard to smaller-scale variations. There is no apparent geological explanation for this difference in variability at these locations. It is possible that differences in instrumentation and/or data processing account for these differences in variability.

The results of the ADI logging from these four wells indicate a consistent pattern of horizontal stress orientation at these four locations. This approximately north-south direction does not correspond to any dominant fracture set in wells other than VPRE 33 and indicates that the strong shear-wave anisotropy observed in the ADI logs is not related to preferential fracture orientation. These factors suggest that the ADI logging is sensitive to the regional stress state and that the stress regime is equivalent at the scale of the approximately 20 miles distance separating these wells. The average orientation of the maximum horizontal stress is more north-south in well VPRD 71 and this may be due to its location closer to the thrust front on the western margin of the Raton Basin. The thrust front is essentially north-south in this area; whereas, it strikes in a more northeasterly direction further to the north.

The present approximately north-south orientation of the maximum horizontal stress is about 90^{o} different than the orientation during the formation of the Raton Basin. The Raton Basin formed in response to west to east compression and thrusting during Laramide orogenic activity. Consequently, the maximum horizontal stress is inferred to have been approximately east-west during filling of the basin. The rotation of the maximum horizontal stress from east-west to north-south inferred from the ADI logging is consistent with conclusions that the stress regime rotated in the late Oligocene, based on the history of igneous intrusions (Close and Dutcher, 1990). The present north-south orientation of the maximum horizontal compressive stress may be a consequence of an extensional tectonic regime related to the Rio Grande rift system located to the west of the Raton Basin. Extension in the Rio Grande rift is in the east-west direction.

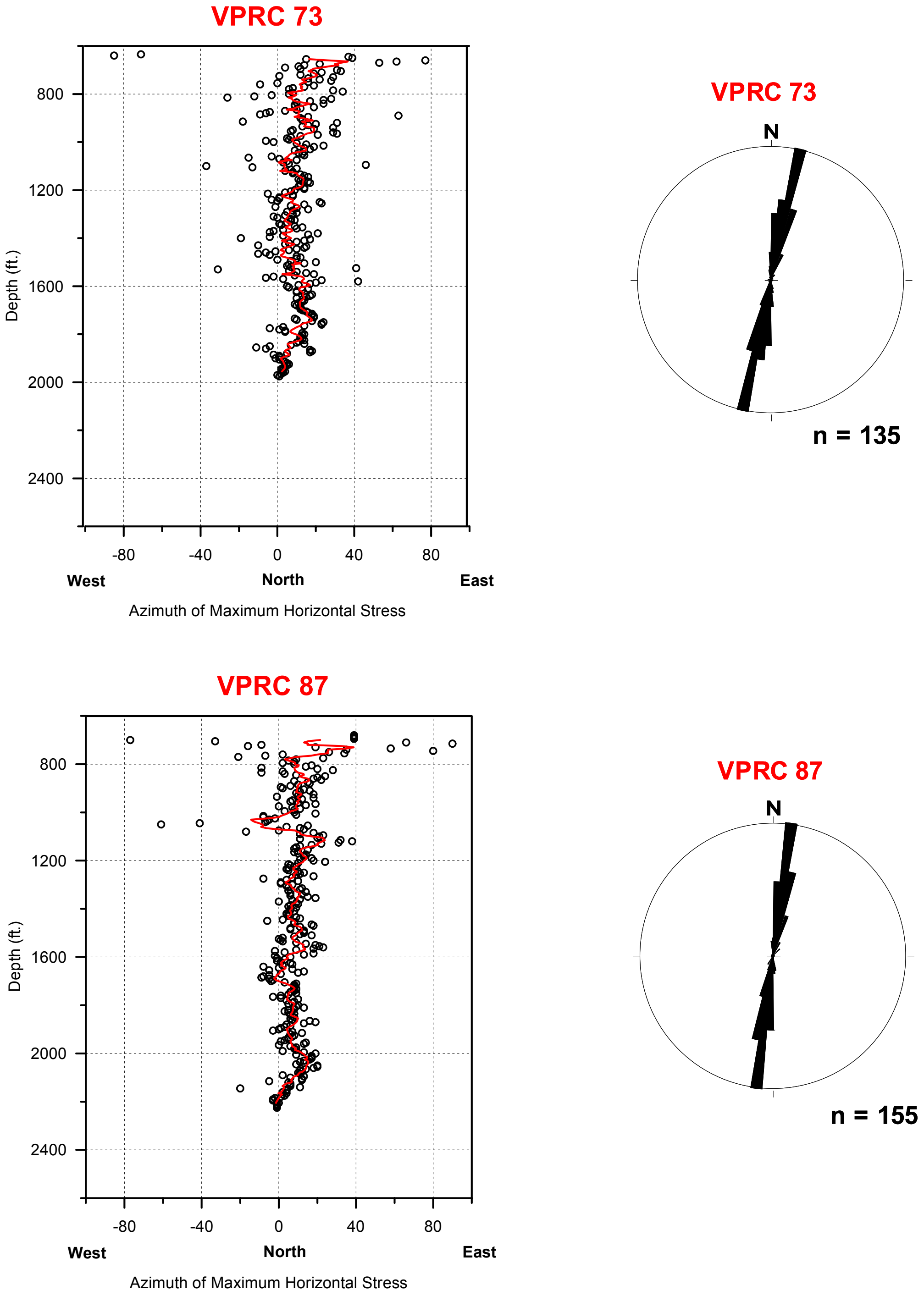

Figure 64a: Azimuth of the maximum horizontal compressive stress from the ADI logs from wells VPRC 73 and VPRC 87 versus depth. The red line shows the running average (over a 50 ft. window) of the azimuth of maximum horizontal stress. The rose diagrams to the right plot the corresponding values of the running average of the azimuth.

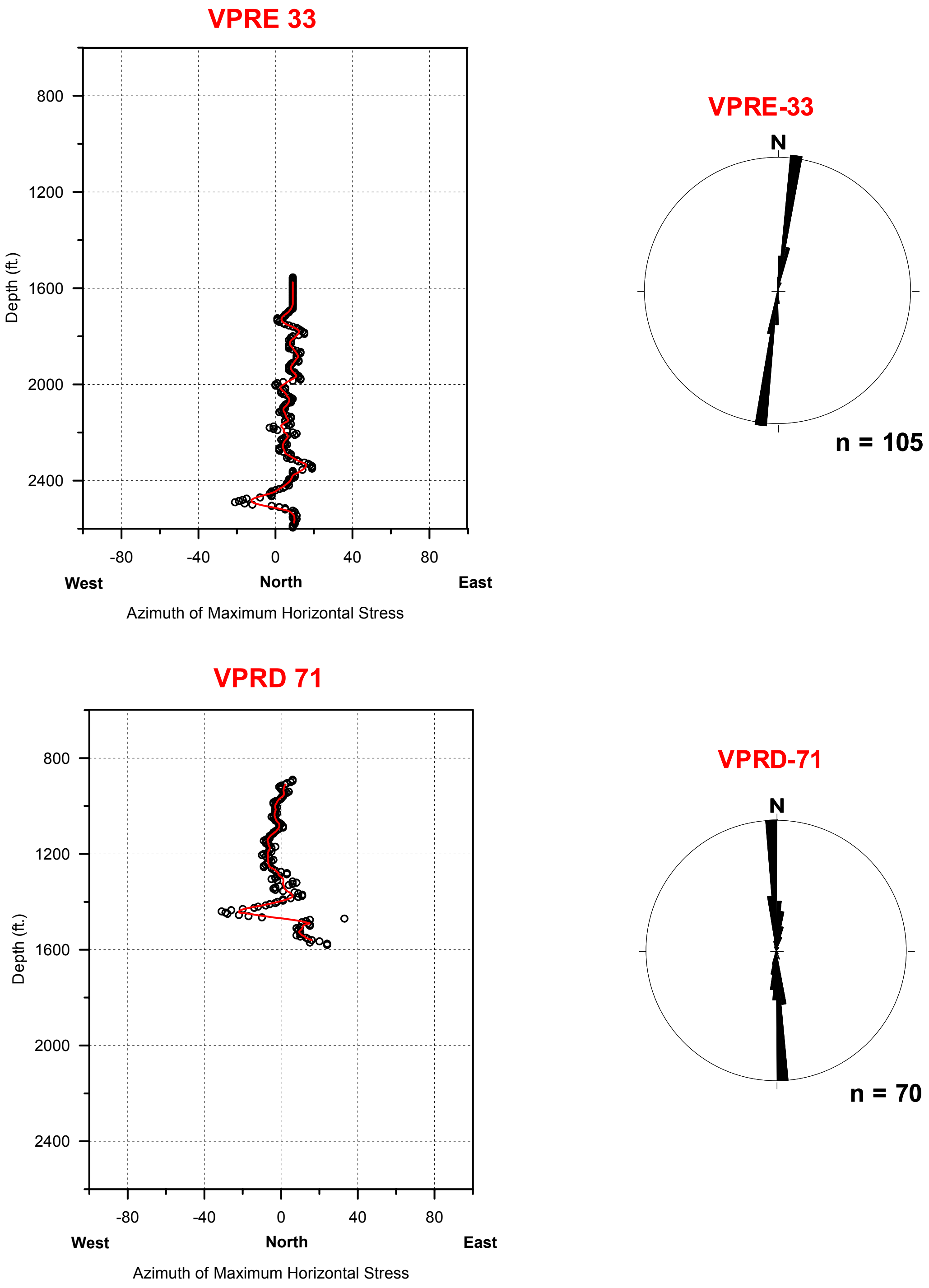

Figure 64b: Azimuth of the maximum horizontal compressive stress from the ADI logs from wells VPRE 33 and VPRD 71 versus depth. The red line shows the running average (over a 50 ft. window) of the azimuth of maximum horizontal stress. The rose diagrams to the right plot the corresponding values of the running average of the azimuth.

2.4.2 Horizontal Stress and Depth

The ADI logs from wells VPRC 73 and VPRC 87 indicate a noticeable decrease in the variability in the direction of the maximum horizontal compressive stress with depth (Figure 64a). The standard deviation in the direction in well VPRC 73 is 20^o for depths of less than 1200 ft. and is 9^o for depths greater than 1200 ft. For well VPRC 87, the standard deviation in the direction is 22^o for depths of less than 1200 ft and is 7^o for depths of greater than 1200 ft. The results for wells VPRE 33 and VPRD 71 do not show this pattern of decreasing variability with depth.

At shallower depths, the local stress state may be somewhat decoupled from stratigraphically adjacent units across fractures or bedding planes, leading to greater variability in the azimuth of the maximum horizontal compressive stress. With increasing confining pressure at depth, the stress state is more strongly coupled across such discontinuities and the variability in the orientation of the stress state decreases. The topographic relief of approximately 200-400 ft. near wells VPRC 73 and VPRC 87 could potentially influence the distribution of stress at shallower depths.

In addition, the ADI logs from wells VPRC 73 and VPRC 87 indicate a slight northerly rotation in the direction of the maximum horizontal compressive stress with depth. The mean direction of maximum horizontal compressive stress is N12^{o}E for depths of less than 1200 ft. and is N8^{o}E for depths of greater than 1200 ft in well VPRC 73. The mean direction of maximum horizontal compressive stress is N11^{o}E for depths of less than 1200 ft. and is N7^{o}E for depths of greater than 1200 ft in well VPRC 87. There is not a clear change in the azimuth of maximum horizontal stress in well VPRE 33, although all of the ADI logging in this well is at depths of greater than 1200 ft. The results for well VPRD 71 seem to show a more complex change in direction with depth, with the direction rotating to the west of north between 900 and 1200 ft depth and then rotating generally back to the east to a depth of 1600 ft.

There is an irregular but consistent, repetitive 30 to 50 ft thick “motif” within the shear wave velocity pattern, primarily within the upper parts of the section, in both the VPRC 87 and VPRC 73 wells. The motif consists of an irregularly clockwise uphole stress rotation that abruptly shifts by 20 to 50 degrees counter-clockwise at the top of the pattern. Typically the abrupt shifts occur within shaley intervals, but the shift at 1060 ft on the ADI log correlates to a highly fractured interval within what appears to be a sandstone on the FMI log (see Figures 65 and 66). Similar, but somewhat larger scale patterns are evident in the ADI logs for wells VPRE 33 and VPRD 71 shown in Figure 64b. The abrupt shift in the ADI log at about 1470 ft depth in well VPRD 71 also correlates with a highly fractured interval in the FMI log.

We suggest that the abrupt shift in orientation of the shear-wave velocity anisotropy orientation at the top of a motif occurs at sub-horizontal shear zones, probably thrust faults. Such stress deviations would be easily explained by the stress changes expected in proximity to shear zones. If this is the case, several small, horizontal thrust planes cut the upper part of the section, and in fact similar features can be found in outcrop. These zones of altered stress may in fact be production targets if they can be traced into reservoirs.

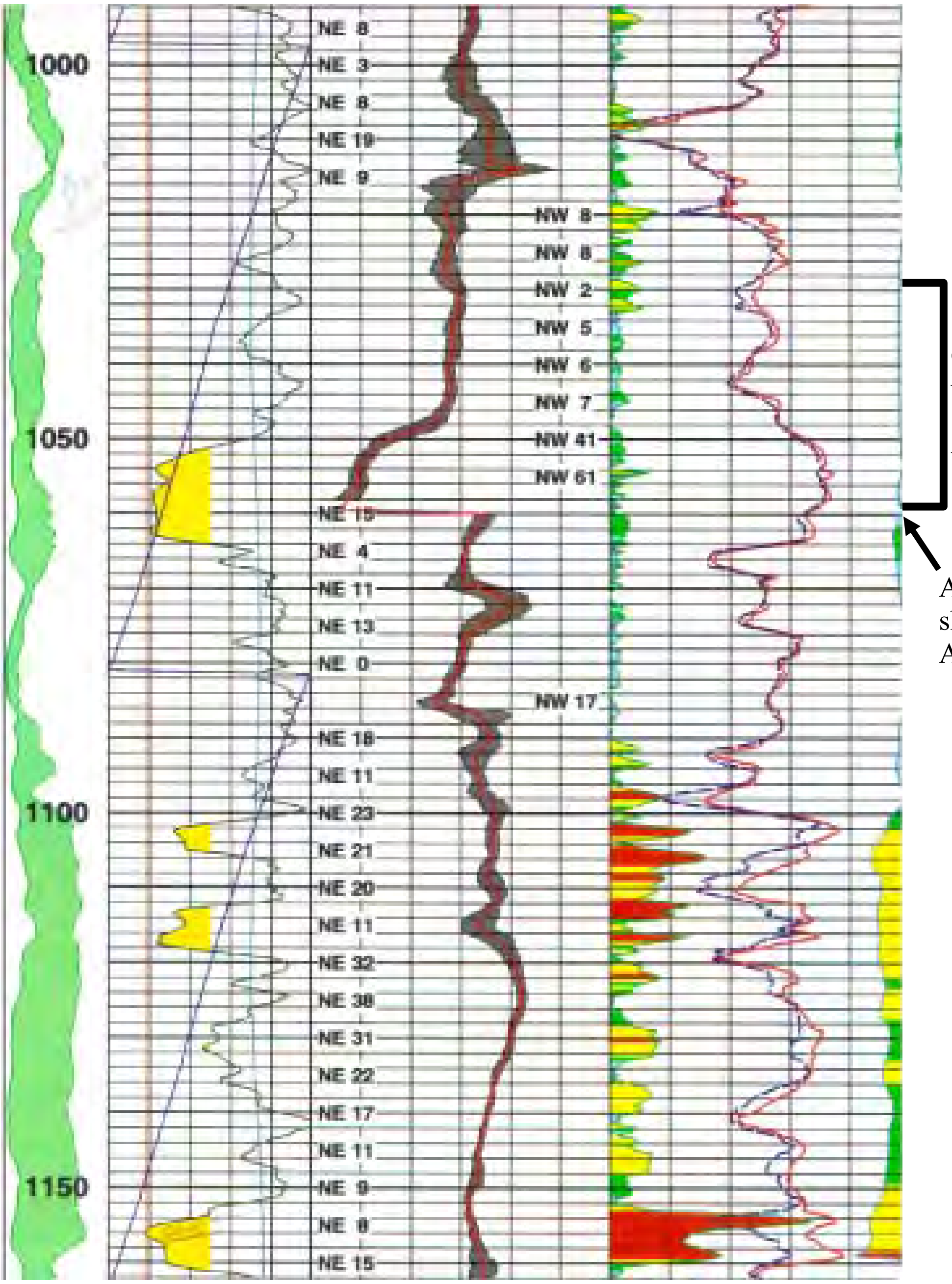

Clockwise uphole stress rotation

Abrupt shift in ADI

Figure 65: An example of the irregular uphole stress rotation typical within upper sections of the VPRC 87 and 73 holes. An abrupt shift at 1060 ft correlates to a fractured interval in the FMI log (Figure 66).

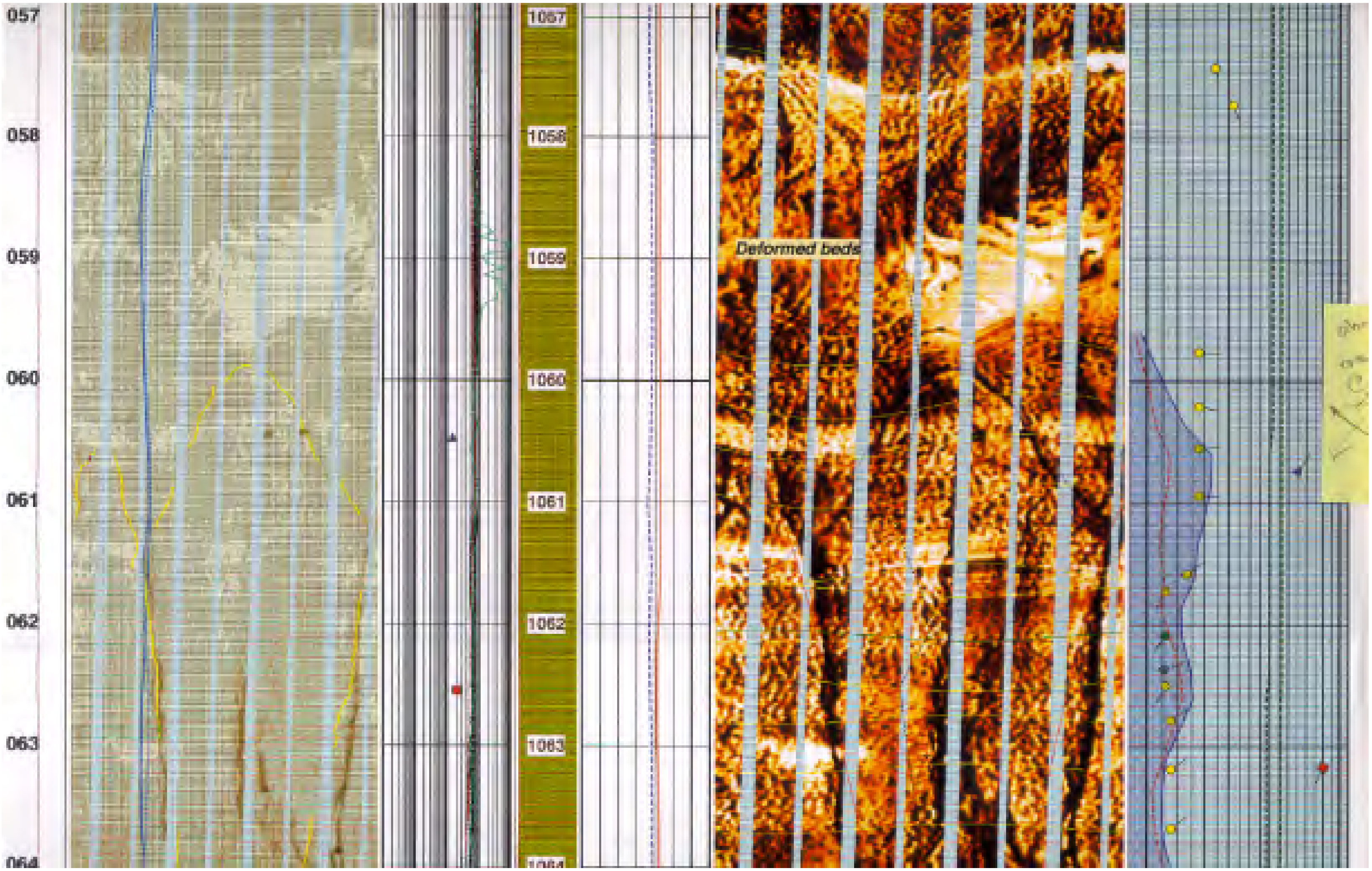

Figure 66: Highly fractured zone at 1060 ft correlates to an abrupt shift in the stress orientation on ADI log (Figure 65).

2.4.3 Relationship Between Horizontal Stress and Fractures

As indicated in the results presented above, the direction of maximum horizontal compressive stress, based on the ADI logging, is consistently oriented in an approximately north-south direction in the four wells used in the analysis. Results from the FMI logging of open fractures indicate that, with the exception of well VPRE 33, there are very few fractures that are optimally oriented to be open and highly permeable (i.e., parallel to the maximum horizontal stress). In contrast, there are numerous fractures oriented parallel to the maximum horizontal stress in well VPRE 33, suggesting higher permeability aligned in a north-south direction at that location.

2.5 IN SITU STRESS CONDITIONS IN THE RATON BASIN DURING THE FORMATION OF SILLS AND DIKES

2.5.1 Background

Dikes and sills are both intrusive igneous bodies that were formed by the injection of magma into solid host rocks. Both have roughly tabular shapes. By definition, sills are oriented approximately horizontally, and dikes approximately vertically. In the case of the Raton basin the host rocks are sedimentary layers that were nominally horizontal at the time of intrusion. Therefore, dikes cut the sedimentary layers perpendicularly, whereas sills are parallel to the layers. The mechanism of formation of both is thought to be tensile fracture of the host rock caused by the fluid pressure of the intruding magma. A key feature of these structures is that they lie in planes normal to the minimum principal compression (*Anderson*, 1951).

Hubbert and Willis (1957) aptly compared these natural hydraulic fractures to the man-made ones emanating from boreholes. In addition to pushing the rock walls open against the minimum compression, hydraulic fractures, either natural or man-made, must also break the host rock at the tip of the fracture.

2.5.2 Elastic Geomechanical Model

At the outset we must choose a constitutive relation for the host rock. Though there is evidence to the contrary such as time-dependence, nonlinearity and presence of discontinuities, the basic elastic model has been very successful for this type of problem because the time scale of fracture and injection is short. Examination of the elastic model will shed light on the relation of the orientations of dikes and sills to the stress boundary conditions.

The basic constitutive assumptions are that the intruded rock mass is homogeneous, isotropic elastic. In a later section, a layer of differing elastic properties is included. If the pores are fluid filled, the stresses are the effective values. The standard rock mechanics convention is adhered to such that compressive stresses and strains are taken to be positive and ordered as $\sigma_1 > \sigma_2 > \sigma_3 > 0$ and $\varepsilon_1 > \varepsilon_2 > \varepsilon_3 > 0$, respectively.

The surface of the earth, which is a free surface and thus a principal surface, is taken to be locally horizontal so that the remaining two principal surfaces are vertical. The vertical normal stress is induced by the overburden weight.

In the absence of tectonic stress, horizontal normal stress has been taken either as equal to the vertical stress (hydrostatic), or as given by a uniaxial strain condition, which is tantamount to lateral confinement (*Price*, 1966). Here we take the horizontal strain to be zero at the outset and thus assume the uniaxial strain condition. This condition derives from the fact that in an undisturbed basin, the symmetry suggests that as vertical load increases, the Poisson-induced lateral motion is restricted by the adjoining material.

Constitutive Equations

The problem is set up by erecting a right handed coordinate system (e, s, v) such that v is vertical (positive downward) and e increases to the east, s increases to the south. The elastic constitutive relations in three dimensions are (*Timoshenko and Goodier*, 1970)

$$\sigma_{\mathrm{e}} = \frac{\nu \mathrm{E}}{(1+\nu)(1-2\nu)}\Theta + \frac{\mathrm{E}}{1+\nu}\varepsilon_{\mathrm{e}} \qquad (1)$$

$$\sigma_{\mathrm{s}} = \frac{\nu \mathrm{E}}{(1+\nu)(1-2\nu)}\Theta + \frac{\mathrm{E}}{1+\nu}\varepsilon_{\mathrm{s}} \qquad (2)$$

$$\sigma_{\mathrm{v}} = \frac{\nu \mathrm{E}}{(1+\nu)(1-2\nu)}\Theta + \frac{\mathrm{E}}{1+\nu}\varepsilon_{\mathrm{v}} \qquad (3)$$

where σ_{i} is normal stress, ε_{i} is normal strain and i = (e, s, v). Young's modulus is E, ν is Poisson's ratio, and the volume strain is $\Theta = \varepsilon_{\mathrm{e}} + \varepsilon_{s} + \varepsilon_{\mathrm{v}}$.

Boundary Conditions for a Simple Sedimentary Basin

There are several situations in which dikes or sills could form, but here the problem will be set up to be consistent with the probable stress system responsible for the formation of the Raton Basin. This is the same stress system for any elongate basin compressed normal to its long axis. First, we examine the basic situation in which the stresses derive from the overburden only. For this case, as pointed out above, the horizontal strains are constrained to be zero $\varepsilon_{\mathrm{e}} = \varepsilon_{\mathrm{s}} = 0$ and by symmetry $\sigma_{\mathrm{e}} = \sigma_{\mathrm{s}}$. The vertical stress is reckoned to be $\sigma_{\mathrm{v}} = \rho \mathrm{gv}$ where ρ is wet rock density, and g is acceleration due to gravity. As is Section 2.1.7 all stresses are taken to be effective stresses as defined in that section. Inserting these conditions into equations (1–3) results in great simplification to

$$\sigma_{\mathrm{v}}(\mathrm{v}) = \rho \mathrm{gv} \qquad (4)$$

$$\sigma_{\mathrm{e}}(\mathrm{v}) = \frac{\nu}{1-\nu}\rho \mathrm{gv} \qquad (5)$$

$$\sigma_{\mathrm{s}}(\mathrm{v}) = \frac{\nu}{1\text{-}\nu}\rho \mathrm{gv}. \qquad (6)$$

The argument v is shown explicitly for the stress to emphasize that the stresses vary with depth. It is interesting to note that of the two elastic constants appearing in the constitutive equations, only the Poisson ratio ν remains in equations (4–6). Thus the only material parameters appearing in the model are Poisson’s ratio ν and density ρ. Equations (4–6) show that the horizontal stresses are always less than the overburden stress. Compare this to the other common starting point of hydrostatic conditions, where the horizontal stresses are equal to the vertical stress.

Poisson's ratio ranges from about 0.1 to 0.3 depending on rock type and therefore $0.11\sigma_v < \sigma_e = \sigma_s < 0.43\sigma_v$. That is, the horizontal stresses are 0.11 to 0.43 of the vertical stress.

Tectonic Stress

Additional tectonic stress along one direction, in this case the east-west σ_e, can be accounted for with the system

$$\sigma_e = \sigma_t \tag{7}$$

$$\varepsilon_s = 0 \tag{8}$$

$$\sigma_v = 0. \tag{9}$$

This is a plane strain problem wherein the deformation is restricted to the vertical, east-west plane. The tectonic stress σ_t is taken to be independent of depth, but may vary with time. This system of stresses would tend to create an elongate basin, characterized by buckling of layers if the magnitude of tectonic stress was great enough.

The basic principal for creation of a fluid-filled crack is that the crack must lie in the plane of σ_1 and σ_2, and is normal to σ_3. The simplest criterion of formation is that $p \geq \sigma_3^{tot} + T_0$, where p is the magma pressure in the crack and T_0 is the tensile strength of the host rock. T_0 is a very low number for rock, and is vanishingly small for a bedding plane. Therefore, if magma pressure is just slightly greater than the minimum compressive stress a sill or dike is likely to form.

Propagation could be discussed in terms of fracture toughness rather than tensile strength, but this would not add any important insights for the problem at hand.

Boundary Conditions for a Sedimentary Basin Under Tectonic Stress

The problem under consideration is one of linear elasticity and therefore the two previous problems can be superposed. This is tantamount to adding the oriented tectonic stress to the simple sedimentary basin. Adding equations (4–6) to equations (7–9) results in

$$\sigma_v(v) = \rho g v \tag{10}$$

$$\sigma_e(v) = \frac{\nu}{1-\nu}\sigma_v + \sigma_t \tag{11}$$

$$\sigma_s(v) = \frac{\nu}{1 - \nu}\sigma_v + \nu\sigma_t \quad (12)$$

The vertical stress σ_v is still governed by gravity and density of the overlying rocks plus any fluids contained in them. The driving stress σ_e is the component of stress induced by the vertical stress plus the independent, east-west tectonic stress. The north-south stress is comprised of elastic components arising from vertical loading and the tectonically applied stress.

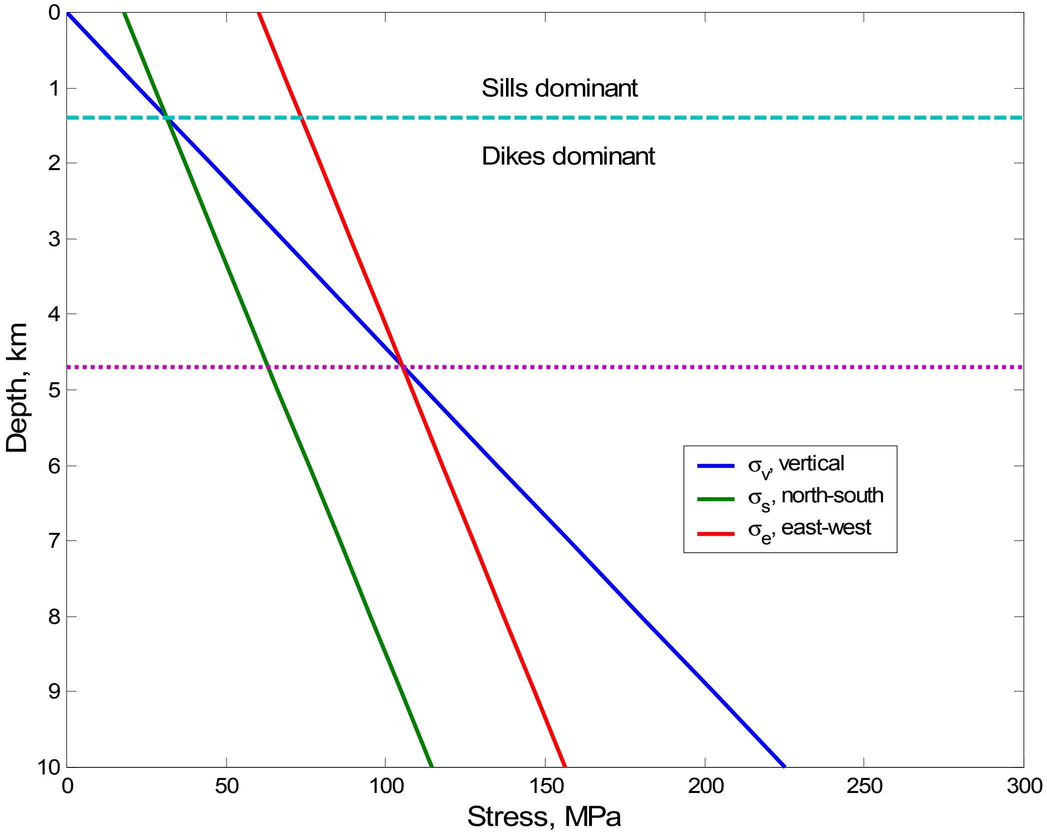

Figure 67: The three normal stresses σ_v (vertical stress, blue line), σ_e (east-west stress, red line), and σ_s (north-south stress, green line), plotted against depth. Above the dashed line, the relative stress magnitudes promote the formation of sills. Below the dashed line, dikes are more likely to form. Below the dotted line, the maximum and intermediate stresses exchange directions within the planes of the dikes, but this has no effect on orientation of the intrusion. Poisson's ratio is taken as 0.3 and σ_t = 60 MPa.

2.5.3 Implications for Dikes and Sills in the Raton Basin

The relationship of dikes to sills can be easily seen by choosing some realistic values for the parameters ν, ρ and σ_t. As noted above $0.1 \le \nu \le 0.3$. The density of sedimentary rock is taken to be 2300 kg m^{-3}, which may vary with porosity and pore filling. For illustration, the tectonic stress was taken to be $\sigma_t =$ 60 MPa. Figure 67 shows the three coordinate stresses plotted against depth. At the surface v = 0 so that

$$\sigma_v(0) = 0 \qquad (13)$$

$$\sigma_e(0) = \sigma_t \qquad (14)$$

$$\sigma_s(0) = \nu\sigma_t \qquad (15)$$

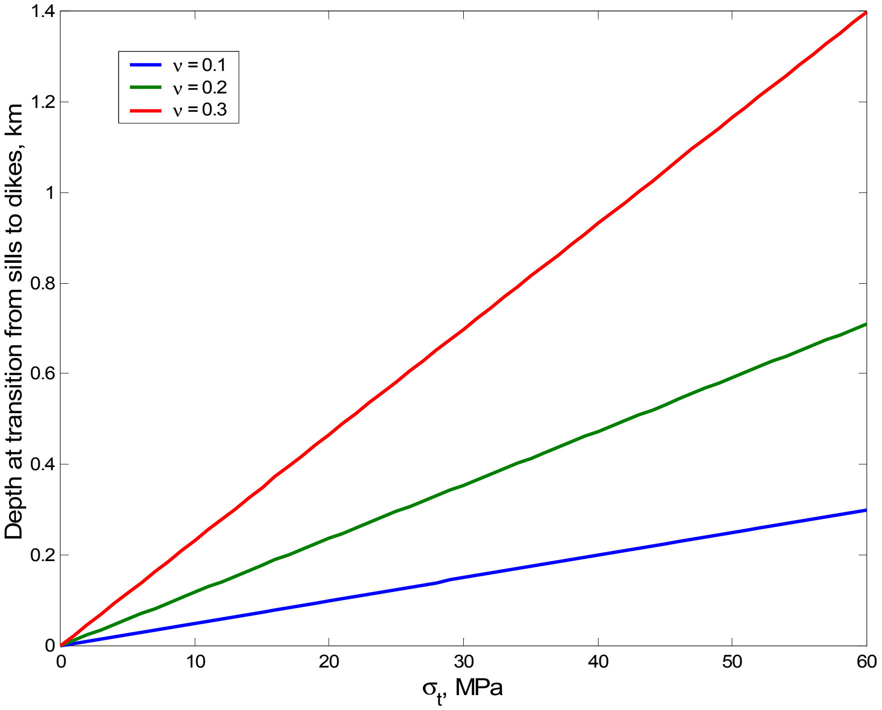

Figure 68: Depth below which dikes predominate and above which sills predominate plotted against tectonic stress for several values of ν. Density ρ was taken to be 2300 kg m^{-3}.

The slope of the vertical stress is 23 MPa km^{-1}. The vertical stress is zero at the surface and increases linearly with depth. The stress in the east-west direction σ_e starts at 60 MPa at the surface and increases less rapidly with depth than σ_v because of the factor $\nu/(1-\nu)$. The north-south stress σ_s increases at the same rate as σ_e, but starts out at the surface at only $\nu\sigma_e = 18$ MPa.

The important consequence of the different rates of increase of the horizontal stresses with respect to the vertical stress is that although $\sigma_v \le \sigma_s \le \sigma_e$ at the surface, σ_v surpasses σ_s at a depth of 1.5 km. At depths less than v = 1.5 km, the stresses are ordered $\sigma_v \le \sigma_s \le \sigma_e$ and therefore, $\sigma_v = \sigma_3$, that is, the vertical stress is the minimum compressive stress. Any hydraulic fracture to form at depths shallower than v = 1.5 km will then be a sill. Similarly, below 1.5 km the stresses are ordered $\sigma_s \le \sigma_v \le \sigma_e$ or $\sigma_s = \sigma_3, \sigma_v = \sigma_2$ and $\sigma_e = \sigma_1$. Therefore, below v = 1.5 km, any hydraulic fracture to form must be vertical and consequently it would be a dike. In this case, the dikes, would lie in the plane of σ_1 and σ_2 and strike east-west. Below 4.7 km, the stresses are ordered such that $\sigma_s = \sigma_3, \sigma_e = \sigma_2,$ and $\sigma_v = \sigma_1$. A hydraulic fracture forming below 4.7 km, is also a dike, but σ_1 and σ_2 have exchanged directions—they still lie in the east-west plane of the dike.

Additional information can be gained by examining the relation between the critical depth as a function of σ_t for various values of ν. The density is also a factor but does not vary as rapidly relative to the other two variables. The depth of transition from sills to dikes is plotted against σ_t in Figure 68 for selected values of ν. For higher values of ν the effect of tectonic stress magnitude is greater. In fact for the smaller values of 0.1 to 0.2 for ν the effect of tectonic stress is much less than that for $\nu = 0.3$, the value used in Figure 67. Poisson's ratio tends to smaller values in rocks of lower elastic modulus E (*Jaeger and Cook*, 1969), and this often correlates with increased porosity. Clearly, the orientations of dikes and sills can be used to determine the direction of one axis of the stress tensor, σ_3. Estimates of the magnitude of σ_t can be made from Figure 2, or by equating equations (10) and (12), if the depth of emplacement could be estimated.

A question of some importance is when, relative to subsidence, did the intrusives form? For example, further subsidence combined with additional sedimentation could easily lead to dikes being higher in the stratigraphic section than sills. Thus, the ages of the dikes and sills by independent means is also an important consideration It is possible that further considerations of this type could lead to a better estimate of the rock properties in the Raton basin or boundary conditions on the basin at the time of formation of the intrusives.

2.5.4 Depression of the Sill-to-Dike Transition Depth

Clearly, for a given density, the factors controlling the relative magnitudes of the three stresses during the emplacement of tabular intrusions in this scenario are the Poisson's ratio and the tectonic stress σ_t. The roles of both ν and σ_t were examined in Figure 68. It is clear from that figure, that for larger values of ν, the transition depth increases for a model with no layering. The question of included layers and how they might behave is now addressed.

Uniform Host Rock with an Included Layer of Coal

In this section $\nu = 0.2$ is used for the host rock (a better value for sedimentary rocks), and the response of an included layer of coal with $\nu = 0.4$ is examined. This value for coal was suggested by Paul Basinski (El Paso Production Company) and is supported by data from *Peng* (1978). Inclusion of a layer with a value of ν different from the host rock broaches the issue of the conditions at the layer interfaces, i.e., bedding surfaces. There is a continuum of conditions there, bounded by the extreme cases of welded and frictionless interfaces. Let us determine if this problem can be done analytically. The difference in kinematics between these two cases is depicted in

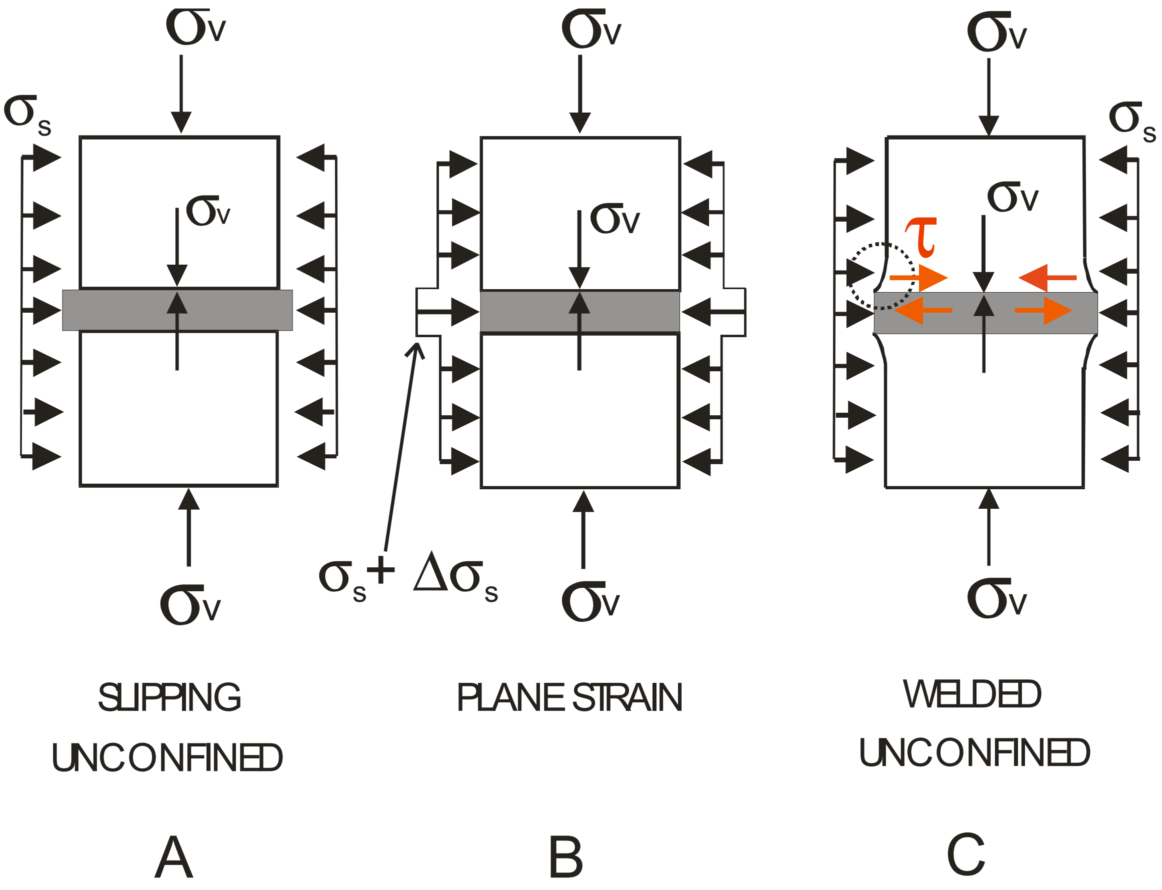

Figure 69: A) Three-layer model with frictionless contacts. Loaded vertically with σ_{v} and laterally with σ_s. Both σ_{v} and σ_s are continuous across the bedding planes. The coal layer is allowed to "squeeze out". B) Same with sufficient additional σ_s applied to push coal layer back to the original size. Vertical stress continuous, σ_s discontinuous at contacts. C) Same three-layer model with welded contacts. Applied vertical and lateral stresses are continuous. The additional lateral deformation of the coal induces shear stresses along the contacts and distorts the host rock as indicated in the dotted circle.

Figure 69, which shows the results for a three-layer model with the coal in the middle (gray shading), ignoring gravity. The boundary stresses are σ_{v} vertical and σ_s lateral for the frictionless case in A and the welded case in C. This sketch corresponds to looking east-west. In the frictionless case A, the coal layer extrudes out the sides, which are loaded with a uniform lateral stress σ_s. This results is a sharp discontinuity in the horizontal displacements at the bedding surfaces. For welded conditions C, the larger ν for the coal still causes more lateral displacement for coal, but now the coal exerts a drag on the surrounding rock, and vice versa, setting up shear stresses as shown in red.

The surrounding rock, being stiffer and welded to the coal, prevents the coal from extending laterally to an extent as great as that in the frictionless case. The displacement is now continuous across the bedding surfaces (circled in Figure 69C). The induced shear stresses cause the principal stresses to rotate from vertical and horizontal.

The application of sufficient additional lateral stress to the frictionless model, (Figure 69A) calculated with knowledge of nothing more than the vertical stress σ_v and ν for coal, pushes the coal layer back to the same width as the surrounding rock (Figure 69B). In this problem, the vertical stress remains continuous from top to bottom of the model, even at the coal/rock interfaces as required by stress equilibrium. The lateral stress is not continuous across the interfaces, but is not required to be by equilibrium conditions (See *Appendix*). Because the interfaces are frictionless, no shear stresses arise, and thus the normal stresses remain the principal stresses everywhere in the model. Calculation of σ_v and σ_s is therefore independent of the existence of the layer, and depends only on the depth and the local value of ν, and the condition of zero-displacement at the lateral boundaries. The mathematical details of equilibrium conditions are given in the *Appendix*.

For the welded condition, the unknown resistance to lateral expansion of the coal caused by the surrounding rock makes it difficult to estimate the stress increment required to enforce plane strain on the model in Figure 69C.

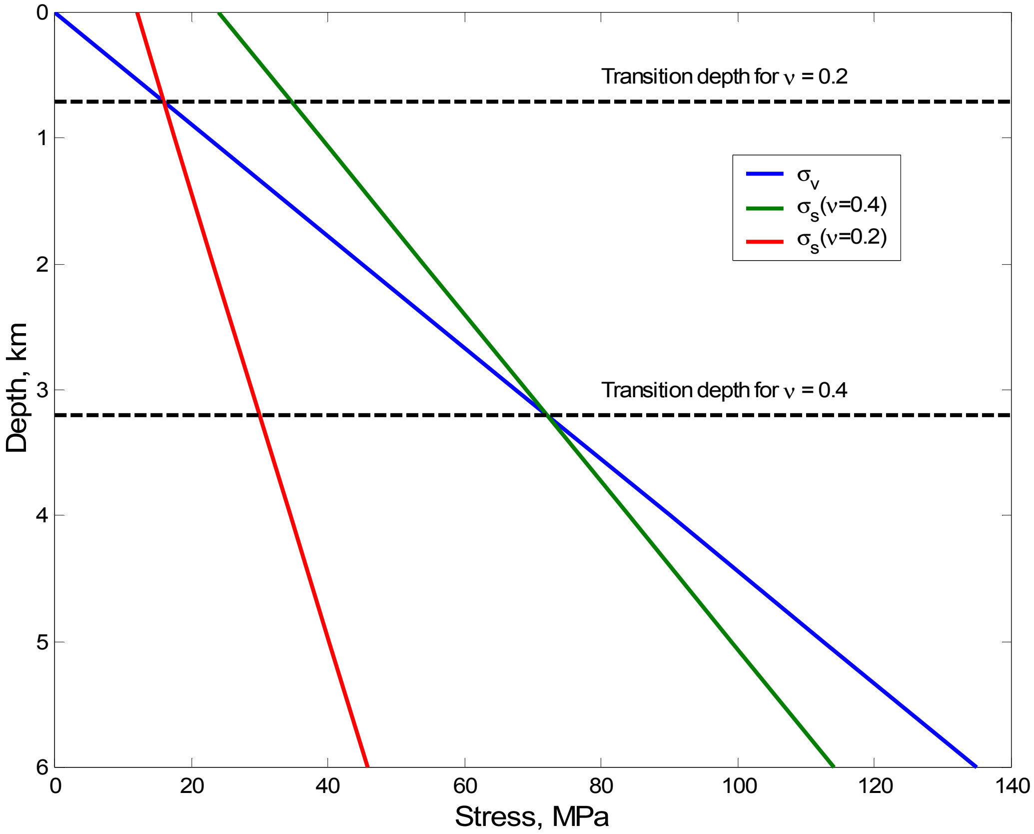

Figure 70: Vertical stress σ_{v} and σ_{s} plotted against depth for $\nu=0.2$, typical of sedimentary rocks, and $\nu=0.4$, representative of coal. The depth where σ_{v} exceeds σ_{s} is the transition depth from sills to dikes. This transition occurs at 0.72 km (2362 ft) for $\nu=0.2$. For $\nu=0.4$, the transition occurs at 3.21 km (10,531 ft).

Figure 70 shows the results of assuming in that calculation that the lateral stress is independent of which layer is being considered. This plot shows σ_{v} for a gradient of 23 MPa km^{-1} and $\sigma_{\mathrm{t}} = 60$ MPa as in Figure 1. As the maximum stress σ_{e} is largest of the three stresses, and is always equal to σ_{1}, it is not involved in locating the transition depth and is omitted for clarity. Two lines, one for $\nu = 0.2$ and the other for $\nu = 0.4$ are shown as red and green, respectively. These are calculated from equation (3). This plot shows that for an non-layered model of $\nu = 0.2$ the transition depth is 0.72 km (2362 ft), and that for a non-layered model of $\nu = 0.4$, the transition depth is 3.21 km (10531 ft). In the light of the argument presented in the previous paragraph, one may correctly interpret this to show that an embedded layer with $\nu = 0.4$ could allow the intrusion of sills to depths of 3.21 km even while embedded in material that allows sills to form only to a depth of 0.72 km. Thus the sill-to-dike transition depth is depressed 2.49 km below the level of the host rock.

A value for the transition depth $\mathrm{v}_{\mathrm{transH}}$ for a particular geographic location can be calculated for the host rock by equating eqn. (1) and eqn. (3) to get

$$\mathrm{v}_{\mathrm{transH}} \quad = \quad \frac{\nu_{\mathrm{H}}}{\rho \mathrm{g}}\left[\frac{1}{(1-\nu_{\mathrm{H}})}\sigma_{\mathrm{v}}+\sigma_{\mathrm{t}}\right].$$

Simply enter the appropriate ρ for the local geologic column, and assign some reasonable average value to ν_{H} for the host rock. The reasonable value for the tectonic stress σ_{t} is somewhat arbitrary and is left to the experience of the investigator. Next, enter the value of ν_{C} for coal and recalculate according to

$$\mathrm{v}_{\mathrm{trans\,C}} \quad = \quad \frac{\nu_{\mathrm{C}}}{\rho \mathrm{g}}\left[\frac{1}{(1-\nu_{\mathrm{C}})}\sigma_{\mathrm{v}}+\sigma_{\mathrm{t}}\right].$$

The transition depth in coal $\mathrm{v}_{\mathrm{transC}}$ is independent of the transition depth in the host rock.

2.5.5 Finite Element Model

To broaden the applicability of the geomechanical model, its response with welded bedding surfaces was investigated. A commercially available partial differential equation solver called ***FlexPde©*** was used to solve the two-dimensional static equilibrium equations of elasticity with gravity, as written in the *Appendix* (*Timoshenko*, 1970). Stress boundary conditions were given by equations (1–3). The model dimensions were 10 km wide by 10 km deep (Figure 71). A coal layer is modeled at a depth of 2.2 km and was taken to be 0.3 km thick. (This unrealistically large thickness was used for clarity of display and has no effect on the results.) The top and bottom layers have $\nu = 0.2$ and the included coal layer (Fig. 5, gray) has $\nu = 0.4$. The small rectangular inset in the lower right of the figure shows relative dimensions, location of the coal, and the vertical line shows the axis of the plot. The red numerals are keyed to the plot.

The gravity induced vertical stress σ_v is shown in green as a function of depth. The calculated values of both σ_e (purple) and σ_s (red) are also shown as functions of depth. The horizontal dotted black line indicates the sill-to-dike transition at a depth of 0.7 km, the same as calculated previously for frictionless interfaces to within plot-reading error. The vertical stress is continuous with depth as discussed earlier; it is the gravity stress ρgv. The lateral stresses, however, are both strongly discontinuous at the rock/coal interfaces. The maximum σ_e jumps about 30 MPa in the coal layer and remains the maximum principal stress. The minimum σ_s lateral stress jumps about 35 MPa in the coal layer and surpasses the vertical stress σ_v there by 10 MPa, becoming the intermediate stress in the coal layer. As the vertical stress is the minimum principal stress in the coal, any intrusions that may form would therefore be sills.

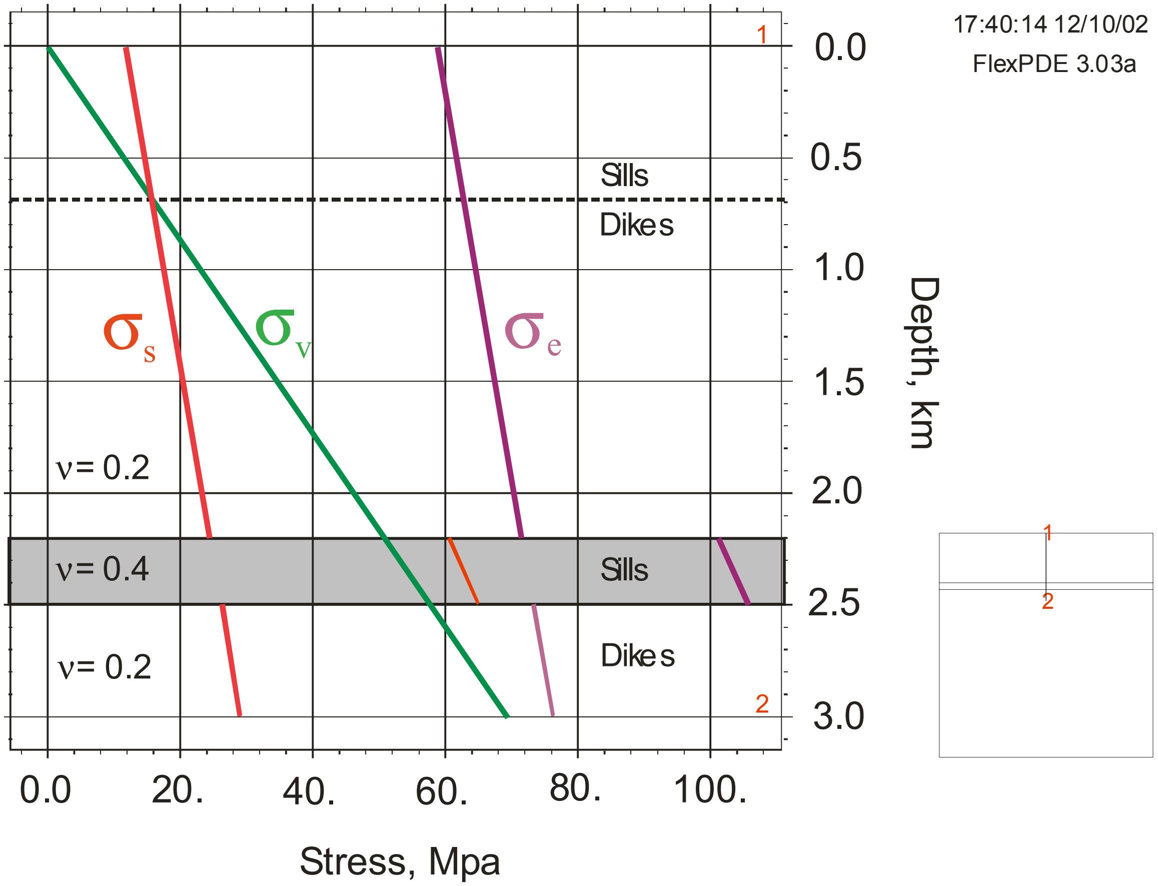

Figure 71: Two-dimensional, elastic model. The host rock is uniform sedimentary rock with $\nu = 0.2$ containing a single layer of coal (gray) with $\nu = 0.4$. The vertical line indicated by the red numerals 1 and 2, is the line along which the stresses were plotted.

It is pointed out that the stress profiles are more complicated at the lateral edges of a finite size model. This has no effect on the problem at hand, however, as the boundaries in the real situation are far away.

2.5.4 Conclusions

The geomechanical model developed here for sill and dike development in the Raton Basin has shown the following:

1. The transition depth separating sills from dikes is greater for materials with higher Poisson ratios.
2. Whether the interfaces between coal and surrounding rock are welded or freely slipping is immaterial to the calculations.
3. The formation of sills in a given layer is independent of the possibility of enclosing layers having different Poisson ratio. Therefore, the sill-to-dike transition depth can be calculated for the host rock and coal independently, using equations 4 and 5.
4. Sills may have formed in coals to depths as great as 3.21 km. This compares favorably with the reconstructed depth for the coals of 2.44 km. In the absence of coals the transition depth would have been nearer 720 meters.

Appendix

Recall the that the Cartesian coordinate system used in this analysis was (e, s, v) representing the geographic coordinates. The two-dimensional stress equilibrium equations including gravity body force $\mathbf{F}_v$ in the v-direction are

$$\frac{\partial \sigma_s}{\partial s} + \frac{\partial \tau_{vs}}{\partial v} = 0$$

$$\frac{\partial \tau_{vs}}{\partial s} + \frac{\partial \sigma_v}{\partial v} + F_v = 0$$

Existence of the derivative $\partial \sigma_s / \partial s$ requires that σ_s be continuous in the s-direction but not the v-direction. Similarly, existence of $\partial \sigma_v / \partial v$ requires that σ_v be continuous in the v-direction but not the s-direction. The existence of the derivatives of shear stress is satisfied because τ_{vs} is zero everywhere.

2.6 MECHANICAL ANALYSIS OF THE RATON BASIN

The finite element analysis of the Raton Basin represents an initial attempt at numerically simulating the geologic evolution of the Raton Basin. It is hoped that understanding the development of the aggregate stress state in the basin may lead to a predictive model for the exploration of potential natural gas reserves within the basin.

The model can be described as a regional model in that we are attempting to ascertain the mechanical response of the Raton Basin from a large east-west cross-section of the basin. Individual geologic structures such as dikes, sills, faults, and disjointed material layering are not included in this model. The effects of such geologic structures on the stress and displacement fields in the basin are better addressed by smaller and more detailed models. It is hoped that the regional model does provide adequate computational resolution for understanding the development of the Raton Basin.

The computer codes used to create the finite element meshes, analyze the models, pre-, and post process the data were developed at Sandia National Laboratories in Albuquerque, NM (Sandia). The finite element mesh was created by CUBIT (Cubit, 2000) a three-dimensional mesh generating code. The analysis was performed using JAS3D (Blanford, 2001), a quasi static three-dimensional finite element code. The transfer of model information (stress and displacement fields) from one model to another is accomplished with MAPVAR (Wellman, 1999), a finite element model, data mapping program. Additional software was also written by the analyst specifically for this project to facilitate the modeling of the layer deposits and variable extraction from the data base.

2.6.1 Model Description

The finite element analysis models the geologic history of the Raton Basin from 74.5 million years ago (Mya) to the present era. During this time span the geologic structure that will eventually form the Raton Basin undergoes horizontal compression from the Laramide thrust on its western flank and gravity loading from layer deposits and erosion. Figure 72 shows the plan view of the Raton Basin with the region of interest shaded in the figure.

Model Geometry and Boundary Conditions

The finite element model of the Raton Basin represents a 87 Km slice of the Raton Basin (Keefe, 2002). The western boundary of the model is the Laramide thrust fault boundary and the model extends approximately 10 Km beyond the eastern edge of the basin. An additional 10 Km were appended the eastern edge of the basin in order to reduce boundary condition effects upon this region of interest. Figure 73 shows the boundary conditions of the model. The east (right) side of the model is restrained against horizontal displacement and is free to move vertically. The west (left) side of the model has a horizontal displacement boundary and is free to move vertically. The north and south boundaries (out-of-plane) of the model are restrained against horizontal displacement. In solid mechanics terms this is a plane strain model.

The finite element model is composed of 55,616 hexagonal elements (8-node bricks) and 113,100 nodes. The average element in the mesh is roughly 100 m on a side and thin material layers have a minimum of three elements through their depths.

Constitutive Model

The geology of the Raton Basin is very complex and not fully characterized, particularly in regions of the basin close to the Laramide thrust fault. Adding to the modeling uncertainty there is a limited database of mechanical properties defined for the rocks in the basin. As a result mechanical properties for the material layers are largely derived from representative rock properties. The geology of the Raton Basin is modeled by seven material layers whose properties are derived from averaging the various rock types making up the individual geologic units (Cooper, 2002). Figure 74 shows a close up view of the material layers on the western edge of the model.

The mechanical response of the rock layers is modeled using Sandia’s soil and crushable foam constitutive model (Stone, 1995). In the soils and foams material model mechanical response is defined by dilational and deviatoric properties of the material. The dilational response of the material is controlled by the pressure (mean stress) and the volumetric strain (natural strain). The pressure is defined as a function of the volumetric strain. In the case where a pressure versus volumetric curve is not specified by the analyst the dilational response is linear with the slope of the pressure versus volumetric strain curve being the bulk modulus of the material (Figure 75). The deviatoric response of the material is governed by a yield surface defined as a parabolic function of the pressure (Figure 75). Tensile failure of the material can be approximated by specifying a tensile stress limit (negative) on the pressure axis.

The pressure dependent yield surface allows the analyst to use failure criteria that can be defined in terms of a pressure variable and can create a smooth surface of revolution about the pressure axis. The Drucker-Prager (Desai, 1984) failure criterion meets these requirements and it defines a conical failure surface (truncated cone if a tensile stress limit is specified) when rotated about the pressure axis. The Drucker-Prager criterion is defined as a linear function of pressure in the soil and foams material model. The Mohr-Coulomb failure criterion could not be used as it defines a six sided prismatic solid centered about the pressure axis.

The dilational response of the rock layers is modeled using the default linear function in the soils and foams material model due to the lack of pressure and volumetric strain data.

Figure 76 depicts the Young’s modulus and Poisson’s ratios for the rock layers from the stiffest material (granite) to the softest (mid-Cretaceous units). In Figure 77 the Mohr-Coulomb failure parameters are similarly ordered from the strongest (granite) to the weakest (mid-Cretaceous units; Cooper, 2002).

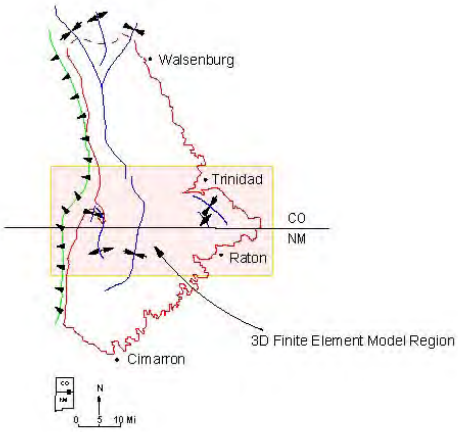

Figure 72: Region of interest.

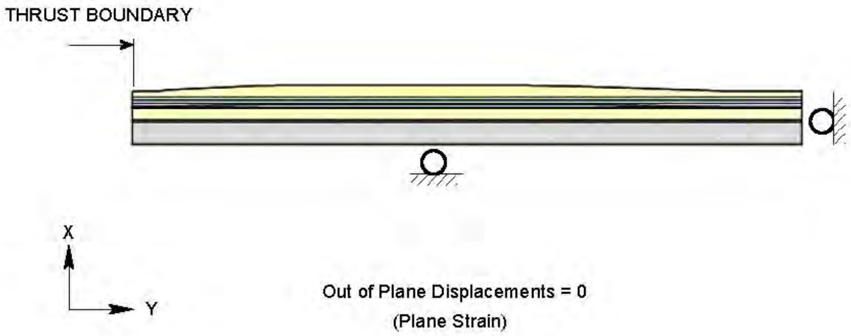

Figure 73: Model boundary conditions.

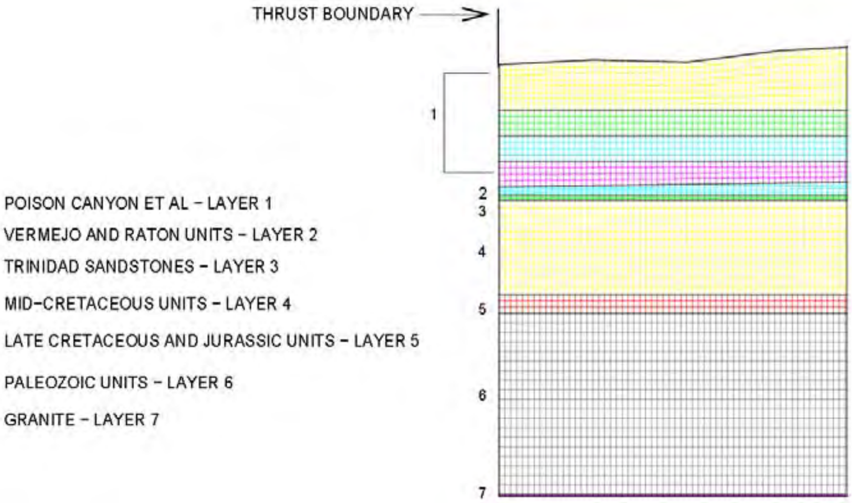

Figure 74: Mesh detail left-hand side of model.

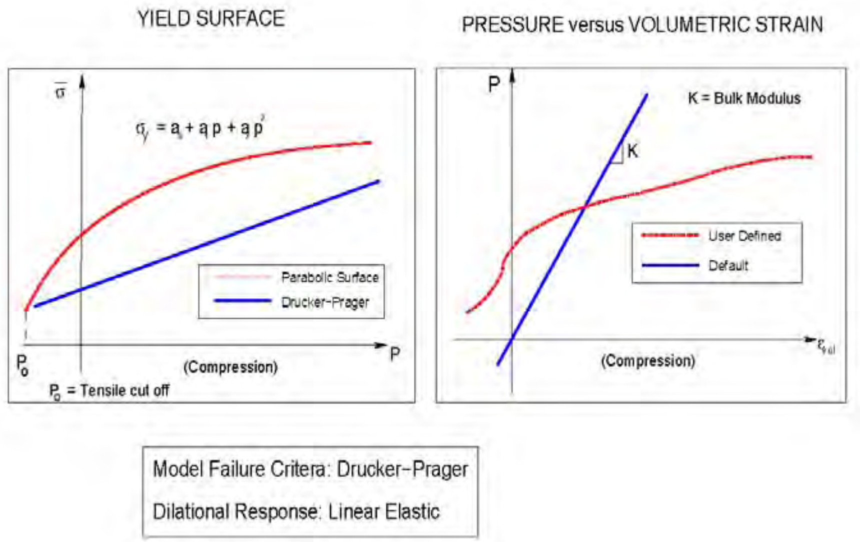

Model Failure Critera: Drucker-Prager

Dilational Response: Linear Elastic

Figure 75: Soil and foams material model.

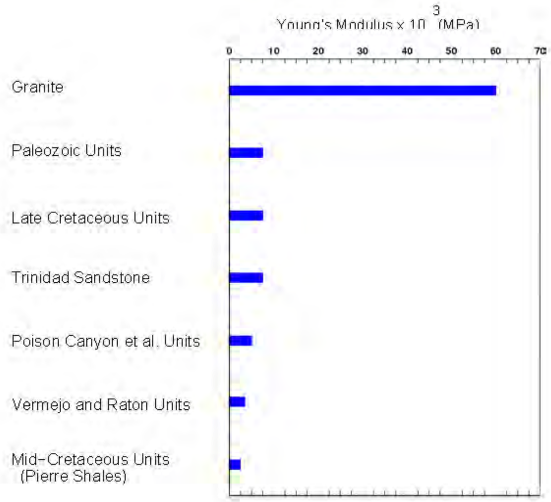

Figure 76: Young's moduli.

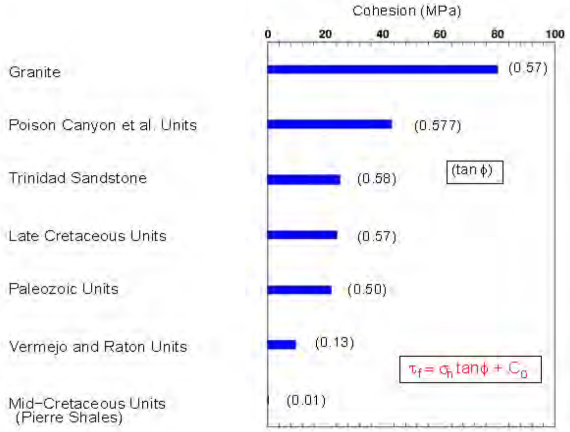

Figure 77: Mohr-Coulomb failure criteria.

2.6.2 Load History

The loading history of the Raton Basin model is depicted in Figure 78. In the figure the Laramide thrust history, the expected creation dates of the material layers, and other relevant geologic events are depicted on the time line.

Early and Late Laramide Thrust Histories

In the analysis the horizontal movement of the Laramide thrust is modeled as a bilinear displacement function. The abrupt change in the curve's slope marks boundary between the early and late Laramide thrust periods. The assumption of linear thrust movement in the model is admittedly simplistic as the true fault movement is more likely characterized by intermittent and varying rates of movement. From the present geologic evidence the early Laramide thrust began approximately 74.5 Mya, moved at an average rate of 120 m/Myr to about 62 Mya. In the late Laramide period thrust fault activity increased and the thrust fault moved at an average rate of 444 m/Myr and ending movement at 44 Mya.

Regional Strain Across the Basin

The Laramide thrust has been estimated to move 9500 m eastward over it's 30.5 million years (Myr) of activity. The effects of the thrust faulting were felt far beyond the eastern edge of the Raton Basin. It is the consensus of the project group that the average horizontal strain developed within the Raton Basin is on the order of two percent. This translates to a maximum horizontal displacement of 1745 m being applied to western flank (left-side) of the model.

Deposit Process of Material Layers

Four of the seven material layers from the Mid-Cretaceous units down to the base Granite are assumed to be in situ prior to the start of the Laramide thrust. The remaining three geologic units are deposited or "birthed" over the course of the Laramide thrust. The deposit of the geologic units is modeled as discrete loading events, reflecting the rapid (geologically speaking) lay down of the material. The Trinidad Sandstones are deposited 71.3 Mya, followed by the Vermejo and Raton units at 62 Mya, and finally the Poison Canyon *et al.* units are deposited in three discrete loading events starting at 40 Mya and ending at 37 Mya. The decision to break the Poison Canyon *et al.* units deposit into three parts, 40 Mya, 38 Mya, and 37 Mya, was based upon two concerns. One being the greater thickness of the geologic unit relative to the previous units and that multiple deposits over time would be more realistic. The other concern was the numerical stability of the finite element calculation if a large load is instantaneously applied to the model.

The in situ stress state of the material layers (pre-existing and deposited) was chosen to be lithostatic (horizontal components of stress are equal to the vertical stress) for modeling purposes. The classic, elastic solution for plane strain, gravity loaded models calculates the ratio of the horizontal stresses to the vertical stress to be $\nu/(1+\nu)$ where theν is the Poisson's ratio of the material. In most geologic settings the elastic solution underestimates the actual stress ratio. Usually the ratios of horizontal to vertical stresses are closer to unity and thus were set to a lithostatic stress state in the analysis. An exception to the lithostatic condition was made for the last component layer of the Poison Canyon *et al.* units. It was in the analyst's opinion that given the proximity of the free surface a lower stress ratio was more realistic and therefore the elastic solution stress ratio was used.

The assumption of the discrete creation of the material layers implies that erosion is non-existent during the Laramide thrust. While the lack of erosion during the Laramide thrust is not realistic in the model, there is an absence of data indicating the extent of this process. It can be said that the rate of layer building was faster than the rate of erosion during the period of 74.5 to 44 Mya timeframe. The erosion that is analyzed in the model occurs later than 44 Mya.

The creation of material layers in the model made the analysis a stop and start process. The calculation was halted at the time when the layer was to be deposited. The in situ stresses and material properties in the new layer were computed, mapped onto the model, and the calculation restarted. The JAS3D code outputs a restart file at user specified intervals during a calculation. The restart file contains all the state variables required to restart the calculation. It is important to note that the geometries of all the “to be deposited” layers were carried along in the finite element model from the start of the analysis. The material properties of these layers; stiffness, strength, and density were set at very low values prior to their “birth”. For example the Trinidad Sandstone unit had a pre-deposit density of 2.320e-06 kg/m^3 and a bulk modulus 0.333 MPa. The post deposit values for these variables were respectively set at 2320 kg/m^3 and 5643.94 MPa. Setting the material properties to very low values minimizes their effect upon the lower layers in the model and produces a near zero stress states within the materials themselves. Custom software was written to edit the restart file to enable this process.

Post Laramide Thrust and Erosion to the Present Era

The post Laramide thrust period is dominated by erosion whereas the previous period of thrust activity was characterized by layer building. Figure 79 shows the top surface of the Poison Canyon *et al*. units at the end of the Laramide thrust with intermediate surfaces between it and the present era surface profile. The rate of erosion from 44 Mya to the present era is unknown and in the absence of data the decision was made to model the erosion from the post Laramide thrust surface to the present era topography in five discrete steps. The intermediate surfaces were derived by linear interpolation between the post Laramide and present era surfaces. In the figure each curve is annotated with the time of formation in the model.

The analysis of the erosion of Poison Canyon *et al.* units was simpler than the modeling of the layer deposit during the Laramide thrust period. JAS3D has a material death option that allowed the removal of the erosion layers and eliminated the need for stopping and restarting the calculation[1]. To model the erosion the part of original model defining the Poison Canyon *et al.* units was re- meshed, going from the original three layers to the five layers defining the erosion geometry. Stresses, displacements, and other state variables were then mapped using the MAPVAR code onto the new mesh from all seven geologic units to create a new restart file. The analysis could continue from this point with the new mesh and restart file.

---

[1] JAS3D also has a material birth option, but it did not work properly for creating material layers in the Raton Basin model.

Rio Grande Extension

Approximately 26 Mya the geologic structures west of the Laramide thrust fault underwent a large north-south extension. Four Myr after that event the maximum principal stress (compression) in the Raton Basin rotated 90° from an east-west direction to a north- south direction. There is a lack of agreement among the geologists and engineers on this project over how or if the Rio Grande extension affected the swing in maximum principal stress direction in the Raton Basin. A plausible case can be made that the Rio Grande extension west of the thrust fault relaxed the thrust load on the Raton Basin and thereby reduced the maximum horizontal stress in the east-west direction. The reduction in the east-west compressive stress may have been enough to allow the north-south horizontal stress to dominate. Another opinion is that the rotation in the stress direction was due to processes, not fully understood, occurring within the Raton Basin itself. The main process for driving the stress rotation being the erosion of the overburden. In the current analysis the effects of the Rio Grande extension are not included in the model and will be considered when more field evidence is gathered and greater consensus among the researchers is reached. However in the analysis the erosion of the overburden includes output occurring at both the time of the Rio Grande extension and the time of the stress direction reversal in the Raton Basin.

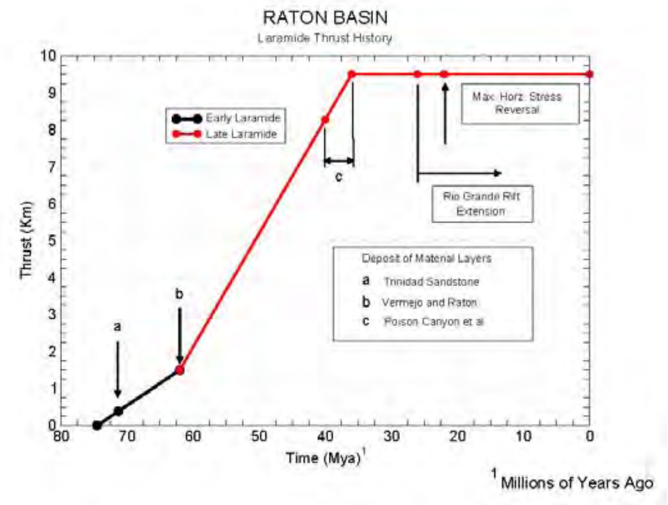

Figure 78: Laramide thrust loading history.

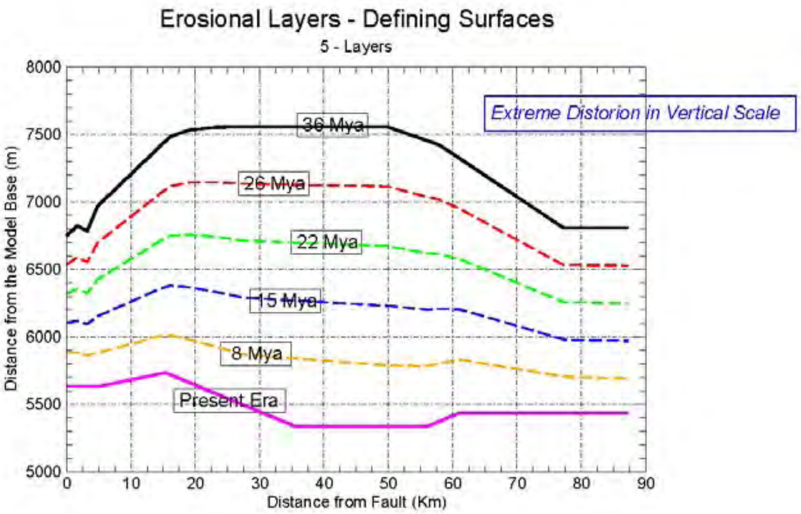

Figure 79: Post Laramide thrust topographies.

2.6.3 Model Results

JAS3D outputs a plot file containing the time histories of the stresses, displacements, and user selected variables for every element (stresses) and node (displacements) in the mesh. From this data the user can derive principal stresses, principal stress directions, and other variables of interest. In the Raton Basin analysis the stresses, displacements, principal stresses, and principal stress direction components were written to the plot file.

Formation of the Raton Basin

One of the encouraging predictions made by the finite element model was the formation of a basin-like structure as interpreted from the deformation of deep layers in the model at the end of the Laramide thrust. The basin formation was not a monotonic process, but one in which the layers were alternatively extended and compressed vertically in response to the thrust fault movement and the deposit of the overburden layers. There was a possibility the model could have predicted a dome structure instead of a basin due to the thrust fault loading and the fact that all the geologic units with the exception of the Poison Canyon *et al.* underwent plastic deformation from the loading. However, there is evidence to suggest that the compliance of one of the geologic units influenced the structure formation.

Influence of the Pierre Shales (Mid-Cretaceous Units)

The vertical displacement of the Raton Basin was dominated by its weakest and softest material, the Mid-Cretaceous units (Figures 76 and 77). The mechanical behavior of the Mid-Cretaceous units was in turn influenced by the Pierre Shales that comprised 90 percent of the unit's volume. The Mid-Cretaceous units failed completely or go "plastic" soon after the start of the Laramide thrust. Figure 80 shows vertical displacement profiles for selected times from the analysis. The displacement profiles clearly show the Mid-Cretaceous units extending under thrust loading and compressing with the creation of overburden layers. The layer compression being the greatest with the deposit of the Poison Canyon *et al.* units. The stronger and stiffer layers above and below the Mid-Cretaceous units show relatively little vertical displacement under the same loads. Figure 81 shows another perspective of the vertical deformation of the Mid-Cretaceous units with the plots of the units' extension for times before and after the creation of the Poison Canyon *et al.* units, and in the present era. There is a slight extension of the layer after the erosion of the overburden which is expected, but the bowl shape remains intact.

Analytical Results

At this time there is very little available field data from Raton Basin that can be used to compare predictions made by the finite element model. Of particular interest is the orientation of maximum (compressive) principal stress. It is known from the few available fracture logs that with increasing depth the orientation the maximum principal stress is tending towards north-south.

The principal loading on the Raton Basin is the Laramide thrust and it is not surprising that the predicted orientation of the maximum principal stress is east-west in all the geologic units at the end of the Laramide thrust period 36 Mya. In the post Laramide thrust era the erosion of the overburden in the model did produce a rotation of the maximum principal stress from the east-west direction to the north-south direction in parts of the Mid-Cretaceous units. Available field data shows the north-south direction trend starting in the Vermejo and Raton units. The model does not show this and predicts the maximum principal stresses orientation in the units above the Mid-Cretaceous remaining in an east-west direction. Also the orientation of the maximum principal stress in the geologic units beneath the Mid-Cretaceous is predicted to be east-west.

Figure 82 shows the rotation of the maximum principal stress orientation from the end of the Laramide thrust to the current era.

Figure 83 shows the variation in maximum principal stresses in the top four geologic units over a distance of 50 Km from the thrust front. The stresses plotted are from the mid-layer of each unit. There is general trend of the magnitude of the maximum principal stresses increasing with depth. However the Trinidad Sandstones are the major exception to this trend. This is due to the unit's higher stiffness and strength relative to the other layers depicted. The "undulations" of the maximum principal stresses across the basin reflect the effect of the ground surface topology upon the stresses. The Poison Canyon *et al.* units show the greater oscillation when compared with the deeper Mid-Cretaceous units.

Figures 84 and 85 show the strike and dip angle profiles for the maximum principal stresses across the basin. For visual clarity the strike and dip angle profiles for the Mid-Cretaceous units are plotted separately in Figure 85. The maximum principal stress directions for the three geologic units above the Mid-Cretaceous are nearly uniform in orientation. The strike angle is 90 degrees (east-west) and the dip angles are either zero degrees (horizontal) or close to it. The dip angles predicted for the Poison Canyon *et al.* layer showed some deviation from zero probably due to ground surface effects. The Mid-Cretaceous units show the greatest variation in strike angle and dip angles of the four layers. It should be noted that this unit is the softest and weakest of the four and the difference between the minimum and maximum principal stresses is close to zero. Thus any a slight change in the stress state can cause the principal stress directions to switch directions.

Figures 87 through 90 show the strike and dip profiles for the minimum principal stresses for each layer.

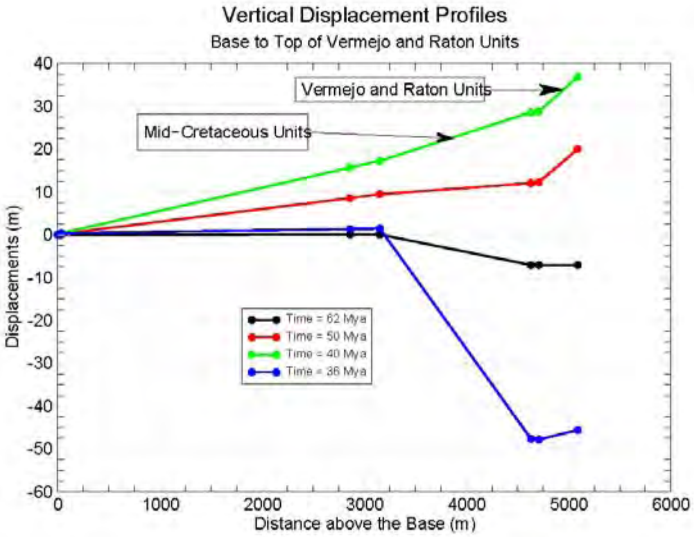

Figure 80: Vertical displacement profiles at 40 km.

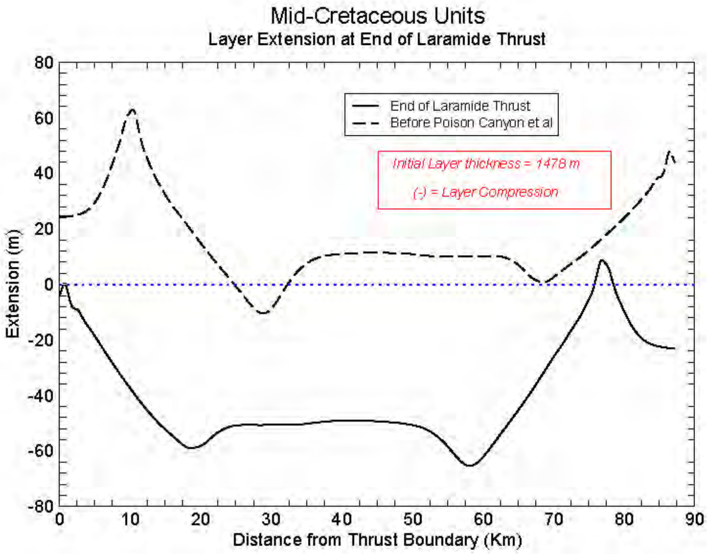

Figure 81: Mid-Cretaceous layer extension.

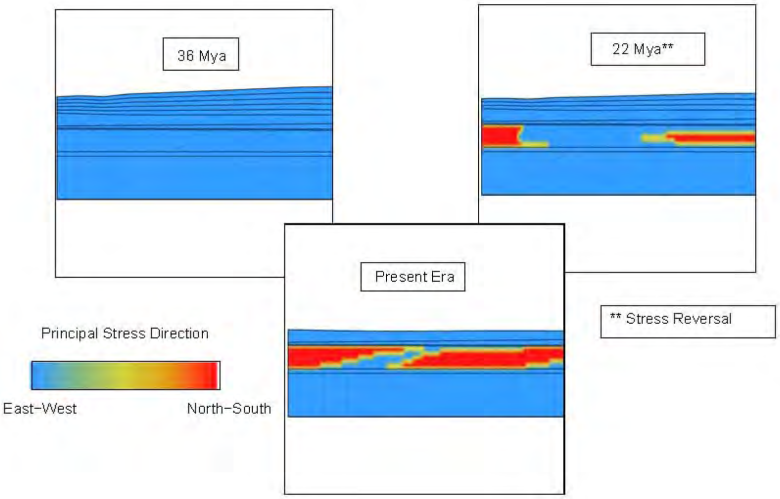

Figure 82: Maximum principal stress orientation.

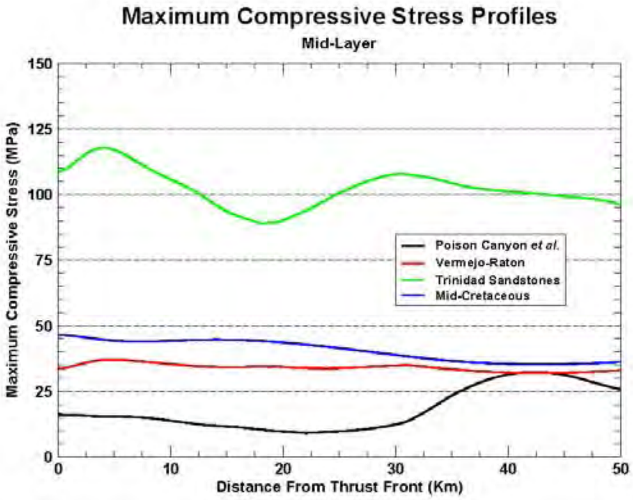

Figure 83: Maximum compressive Stress Profiles

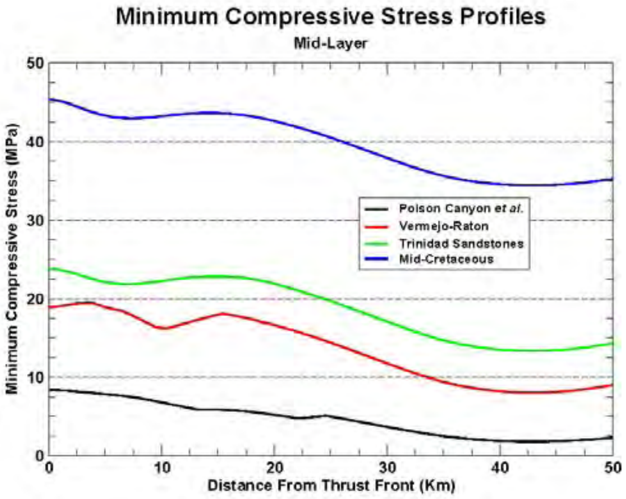

Figure 84: Minimum Compressive Stress Profiles

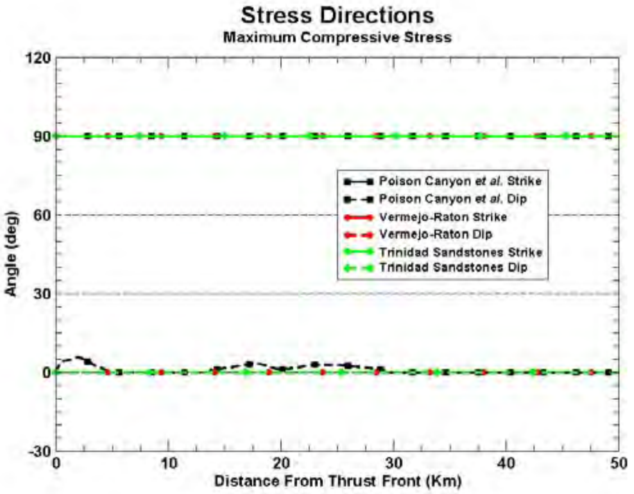

Figure 85: Strike and Dip Angle Profiles - Max. 1

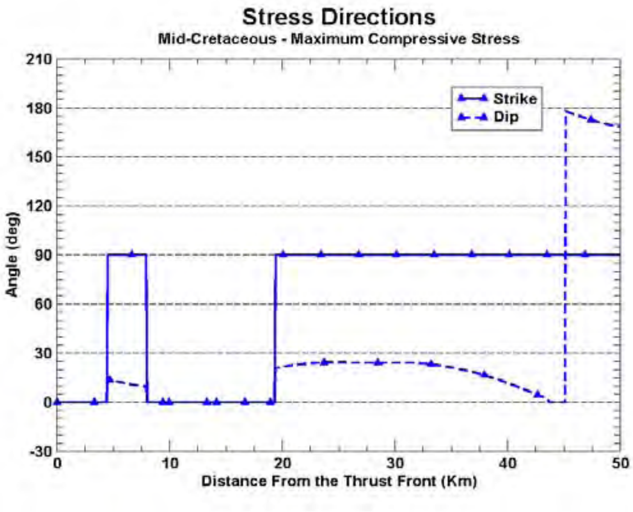

Figure 86: Strike and Dip Angle Profiles - Max. 2

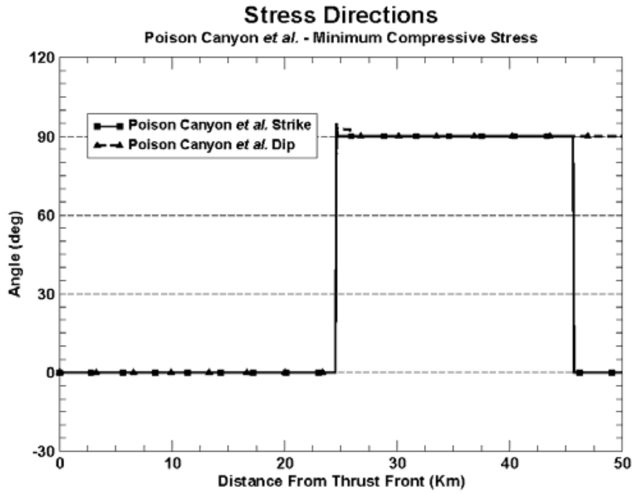

Figure 87: Strike and Dip Angle Profiles - Min. 1

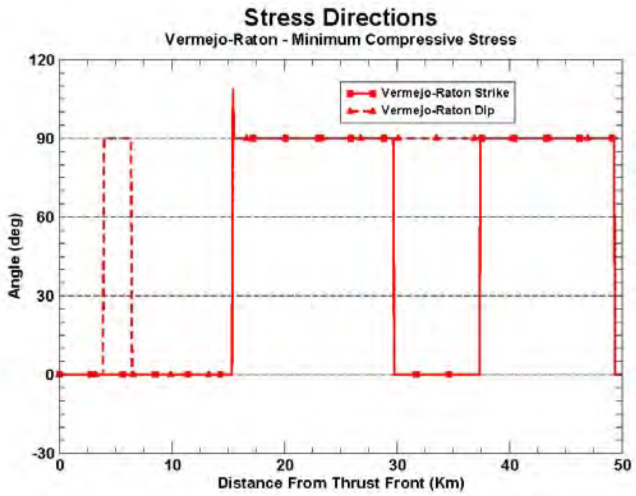

Figure 88: Strike and Dip Angle - Min. 2

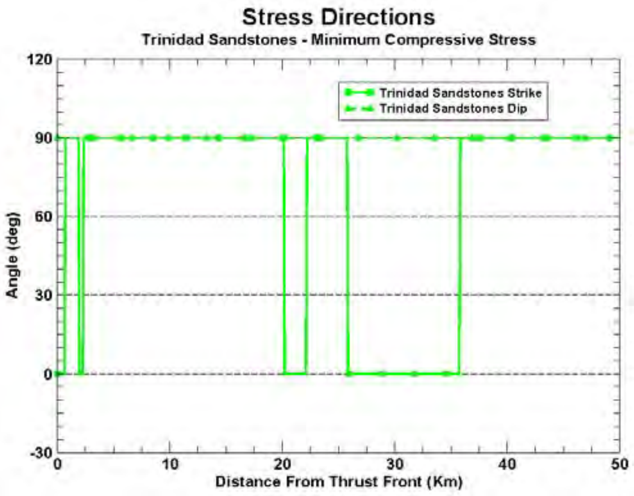

Figure 89: Strike and Dip Angle Profiles - Min. 3

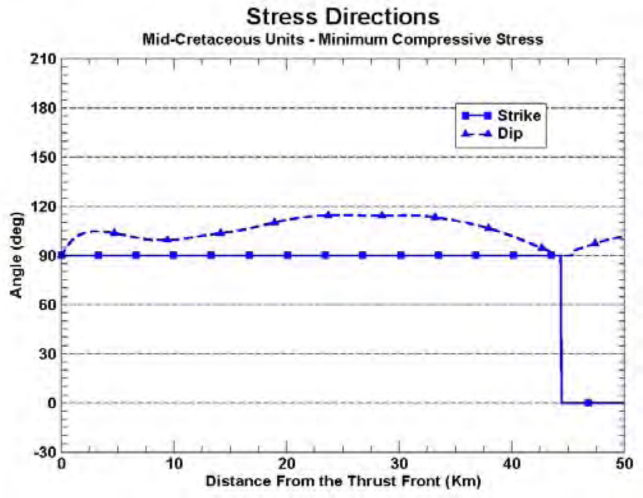

Figure 90: Strike and Dip Angle - Min. 4

2.6.4 Future Modeling Efforts

The finite element model discussed in the previous sections represents a first attempt at understanding the evolution of the Raton Basin. The following are suggestions where future modeling efforts could proceed.

Full Three-dimensional Models

As noted in section 2.6.1 the finite element model represented a two-dimensional slice of the basin and on this model plane strain boundary conditions were applied. When the modeling project began two and half years ago our knowledge of the basin geology was limited and a two-dimensional geometry was deemed appropriate. A "true" three-dimensional model would allow us to model more realistic loading scenarios by incorporating the variations in north-south topography, geology, and boundary conditions.

Three-dimensional models will require a much greater level of effort than was needed for the first model. Computational times can be expected at a minimum to quadruple and construction of the finite element mesh will be major task in itself. As an alternative to building large, basin scale models it may be more productive to construct smaller, high resolution models of regions within the Raton Basin that are of interest to the natural gas industry. The boundary and initial conditions of these models can be derived from larger and simpler models.

Greater Detail in Material Layer Modeling

The current finite element model used seven materials to model the rock response of the Raton Basin. This was very simplistic considering the complex layering of materials within both the basin and the geologic units themselves. Future models will require a larger number of rock materials, more sophisticated material modeling, model fluid pore pressures, and account for the spatial variation of the rock properties within the mechanical units. More sophisticated material models will be required to account for creep and stress relaxation behavior in materials such as coal and shale, and material discontinuities such as fault surfaces may be needed in the finite element model. Nonlinear material behavior and discontinuities will definitely have an effect upon the stress magnitudes and orientations within the mechanical units. Parallel to these efforts is that more material testing and spatial mapping of the representative rock types and geologic features will be required.

Improved Boundary Conditions

The present finite element model had its base restrained against vertical deformation. It is shown in several cross-sections made of the basin that the deep rock layers on the western flank of the Raton Basin underwent large vertical movement in response to the Laramide thrust and material deposits. It may be useful to build and analyze finite element models that capture this kinematic behavior. An effort was being made to develop such a model, but was curtailed due to budget shortfalls.

Given that our knowledge of the loading of Raton Basin will always be limited and subjected to interpretation, it may be useful to perform parametric analyses where different loading scenarios can be explored. For example the effects of different thrust loading rates and magnitudes upon the present era stress state could be explored.

2.7 PRODUCTION ANALYSES

2.7.1 Production History

Petroleum exploration in the Raton Basin dates from as early as 1896. Natural gas for local consumption was produced from the Garcia Field in Las Animas county, Colorado, and from the Wagon Mound Field in Mora county, New Mexico. A moderate quantity of oil was produced from the Cretaceous Codell Formation in Colorado, and many exploration wells throughout the basin have had gas shows from Lower and Upper Cretaceous clastic formations (Woodward, 1984). With no pipeline to carry natural gas to market, most petroleum exploration before 1980 was targeted at oil which could be transported by truck or rail. Results of this exploration were disappointing, partly due to the very low permeability of the Cretaceous formations and an apparent lack of suitable hydrocarbon traps in the Raton Basin.

A new exploration approach began in the 1980's in which wells were drilled with the intention of draining gas from coal seams. One of the first pilot projects to exploit this coalbed methane (CBM) resource was Amoco's Cottontail Pass unit in Colorado (Johnson and Finn, 2001). Evergreen Resources began drilling in the same area of the basin and began the first commercial production of coalbed methane in 1993. Meanwhile, in the New Mexico portion of the basin, Pennzoil drilled several CBM exploratory wells in 1989. However, lack of a pipeline to drain this portion of the basin, along with low gas prices and an expiration of CBM tax credits forced these wells to be shut in to await the extension of the pipeline system into New Mexico. The pipeline finally arrived, and the first commercial production from the New Mexico side started in October 1999. Between January 1999 and May 2004, approximately 475 billion cubic feet of gas (BCFG) were produced from nearly 2000 wells in the Raton Basin (Figures 91, 92).

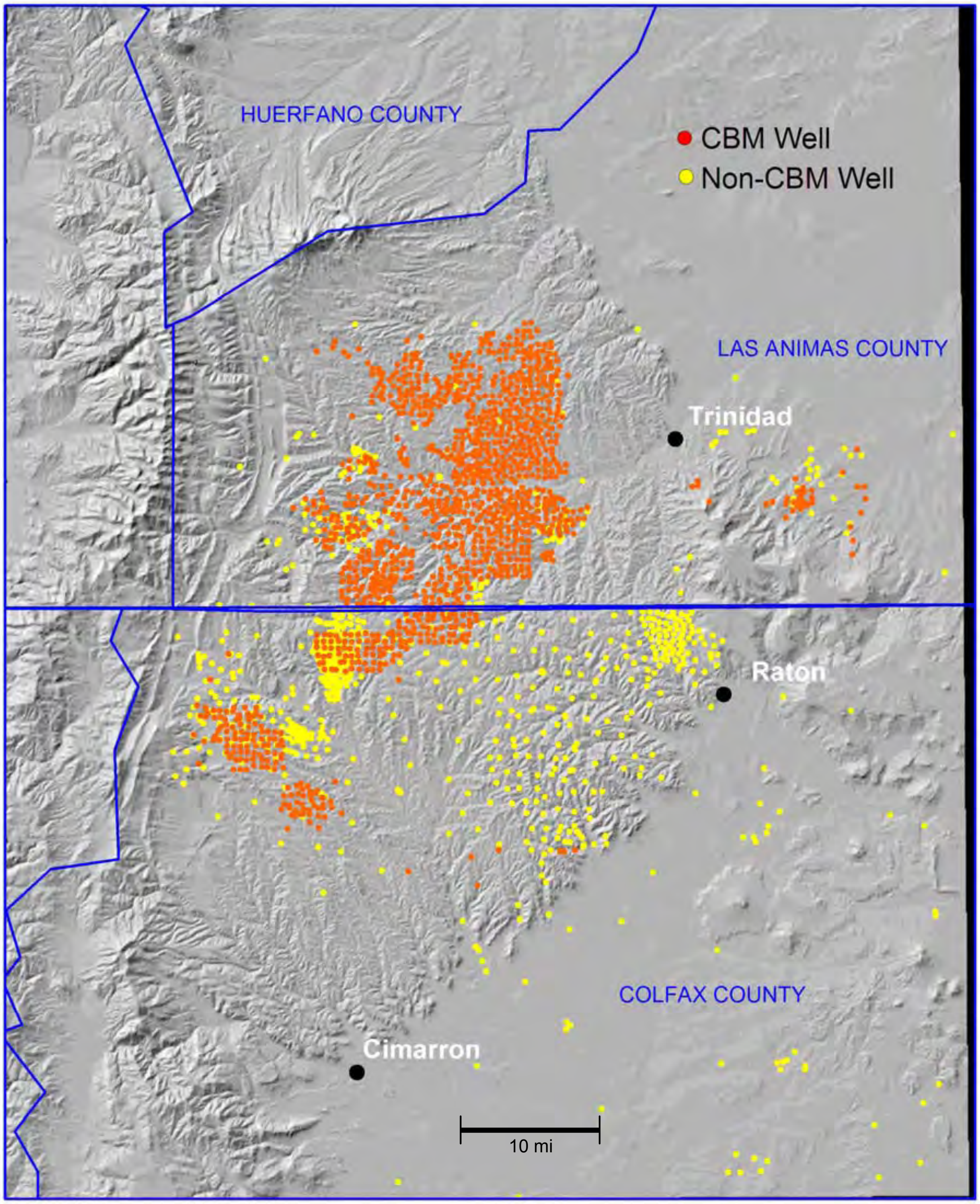

Figure 91: Distribution of wells in the Raton Mesa Region as of December 2002 (includes producing CBM wells, as well as shut in wells, mine wells, and stratigraphic holes.)

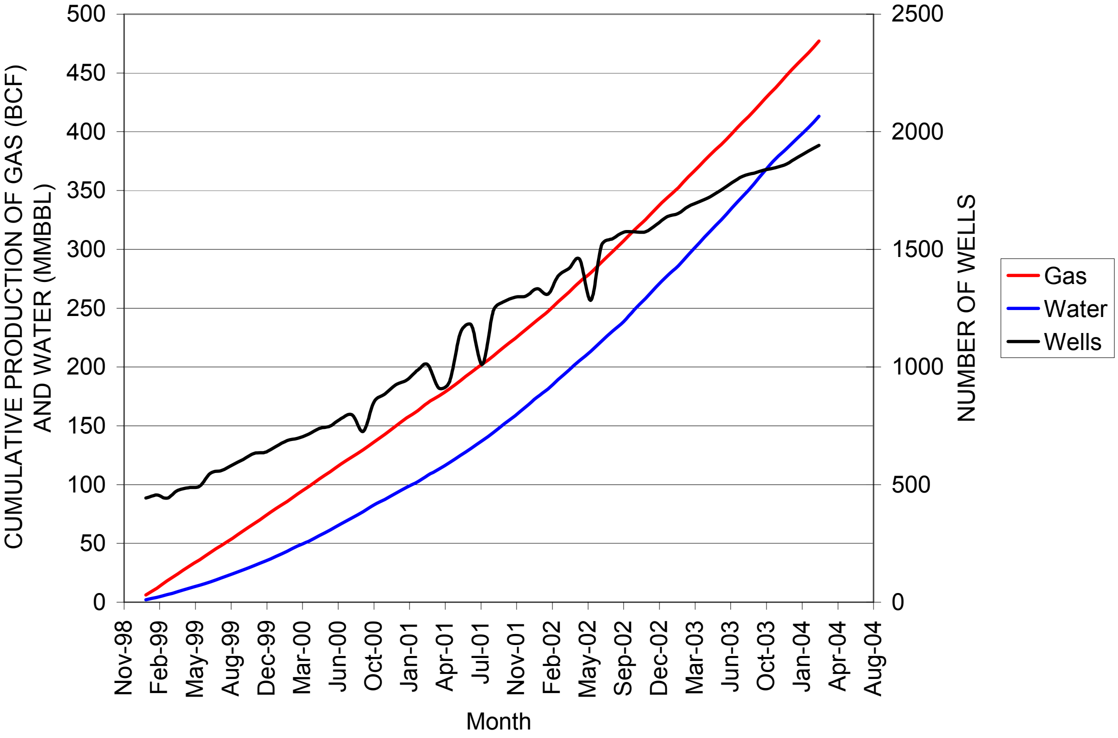

Figure 92: Cumulative production and number of producing CBM wells in the Raton Basin from 01/1999 to 06/2004.

2.7.2 Coalbed Methane

Coalbed methane (CBM) is classified as an unconventional hydrocarbon resource, as the coal seam acts as both a source rock and reservoir rock. During the natural process by which peat is transformed to coal, large amounts of methane are stored within the fabric of the coal. The system of natural fractures in coal, termed cleats, may also store a certain volume of free gas, but a much larger volume may be bound at the molecular level to the large surface area of the coal matrix. Thermal maturity, along with other factors such as coal rank and type, determine the volume of gas generated during the coalification process. The amount of gas that can be stored within the coal matrix is a direct function of pressure. That is, as a coal bed is buried and subjected to greater lithostatic and hydrostatic stress, it is capable of storing more methane in its matrix. Conversely, if a coal bed is brought nearer to the surface of the earth, either through tectonic means or removal of overburden, gas is desorbed from the coal matrix as the overall pressure of the system is reduced.

In a typical coalbed methane operation, a well is drilled through the coal seams of interest, completed and stimulated to enhance the natural cleat system. The pressure of the system is reduced by pumping off formation water to reduce the hydrostatic stress. Due to this pressure requirement, little gas may flow during the initial stages of production, and it is difficult to estimate the ultimate recovery of gas from a CBM well during the first few weeks or months of production. Following this “dewatering” stage, however, gas will begin to flow more readily and reach a somewhat steady rate of production. As methane is depleted from the coal matrix, the well begins a decline phase in gas production, similar to that seen in conventional gas wells (Figure 93). Currently, 7% of the gas production in the U.S.A. is from coal beds, and interest in CBM exploration and production is growing (Nuccio, 2002). It is estimated that U.S. basins contain at least 700 trillion cubic feet (TCF) of coalbed methane in place, with about 100 TCF in recoverable reserves.

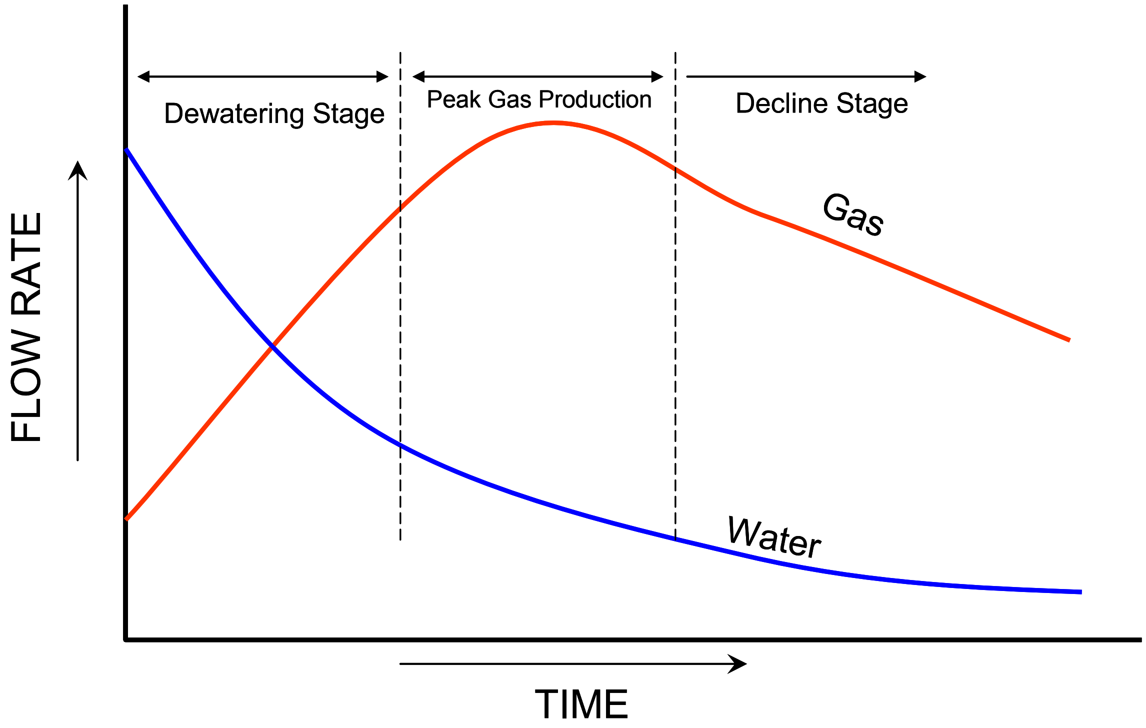

Figure 93: Idealized production behavior of a typical coalbed methane well. Pressure in the coal seam is reduced by pumping off formation water. Methane production increases with decreasing formation pressure.

2.7.3 CBM Resources in the Raton Basin

Coal has been mined in the Raton Mesa region for more than a century. Coal seams from both the Vermejo and Raton formations were mined along the eastern edge of the mesa, where these formations outcrop in cliff exposures, as well as near the center of the basin where drainage channels have exposed these formations. Estimates of coal volumes vary, ranging from 1.5 billion tons of combined Vermejo and Raton coal, to 5 billion tons in the Vermejo Formation alone (Johnson and Finn, 2001). It is generally accepted among most sources that there is at least 1.5 billion tons of demonstrated coal resources within Raton Mesa region (Hoffman and Brister, 2003). Rank of these coals is mostly high volatile 'C' bituminous to medium volatile bituminous. Anthracite and graphite locally occur near the many Tertiary igneous intrusions in the basin. Vitrinite reflectance values range from less than 0.57% along the edges of the basin to 1.58% along the Purgatoire River (Johnson and Finn, 2001). Coals having reflectance values greater than 0.8% are generally considered favorable for coalbed methane exploration.

Measured gas content values range from 115-492 cubic feet per ton for Vermejo coals, and from 23-193 cubic feet per ton for Raton coals (Tyler et al., 1995).

Estimates of coalbed gas reserves in the Raton Basin vary, but most sources cite a figure of about 18 TCF of gas in place, which includes contributions from coals in both the Vermejo and Raton formations. Estimates are based on average aggregate coal thickness, coal density (mass per unit area), aerial extent of coal, and average coal rank (to determine amount of gas generated per unit mass). For the Raton Basin, it was assumed that only half the amount of gas generated has remained trapped in the coal beds (Jurich and Adams, 1984).

2.7.4 CBM Operations in the Vermejo Park Ranch Unit

Distribution of wells and on-line dates

Data from CBM wells in the Raton Basin—including monthly gas and water production volumes, completion procedures, and well locations—that are reported to state regulatory agencies are available to the public via internet database interfaces. Some data for this report were provided by the Colorado Oil and Gas Conservation Commission Information System and the New Mexico Oil and Natural Gas Administration and Revenue Database. Detailed production and geologic data concerning CBM operations in the New Mexico portion of the basin were provided by El Paso Raton LLC. Since much of the detailed outcrop study was also focused on the New Mexico side, the remainder of this chapter will chiefly focus on the production characteristics of this part of the basin. It should be recognized that geologic heterogeneities and hydrologic systems vary widely across the greater Raton Basin, so findings and hypotheses applicable to the southern half of the basin may not apply in the northern half.

Commercial coalbed methane production from the New Mexico side began in October 1999 on the Vermejo Park Ranch (VPR) Unit. Wells are grouped into five geographic sub-unit 'Pods' labeled A, B, C, D, and E (Figure 94). The size of each Pod ranges in size from approximately 10 to 20 square miles and contains up to 100 wells. Pods A, C, and E in the northern part of the Vermejo Park Ranch unit are separated from Pods D and B by the Vermejo Park Anticline. This structural dome exposes the Pierre shale at its core and the Vermejo and Raton formations along its rim. Wells are absent in this area due to the simple fact that the producing intervals are exposed to near atmospheric pressure and are not likely to contain much gas.

Current well spacing is approximately 160 acres, and spotting of individual wells is dependent on environmental and aesthetic concerns. Most wells are drilled through the Trinidad sandstone and terminate in the Pierre shale at an average depth of 2,000 feet. The primary target in both the Colorado and New Mexico portions of the basin are the coals within the Vermejo Formation. Though they be thinner and less continuous, coals of the Raton Formation are sometimes completed with the Vermejo coals to supplement production, especially when they occur at depths greater than 900 feet. Once the coals of interest are identified by wireline petrophysical methods, they are fracture stimulated to enhance the natural cleat system. Water is pumped from the well to initiate coal gas desorption. In compliance with Vermejo Park Ranch environmental requirements, pump jacks are driven by electric motors, and produced water is injected into deeper formations (e.g., the Cretaceous Dakota Formation). Gas and water are transported to compressor stations or injection wells via underground plumbing.

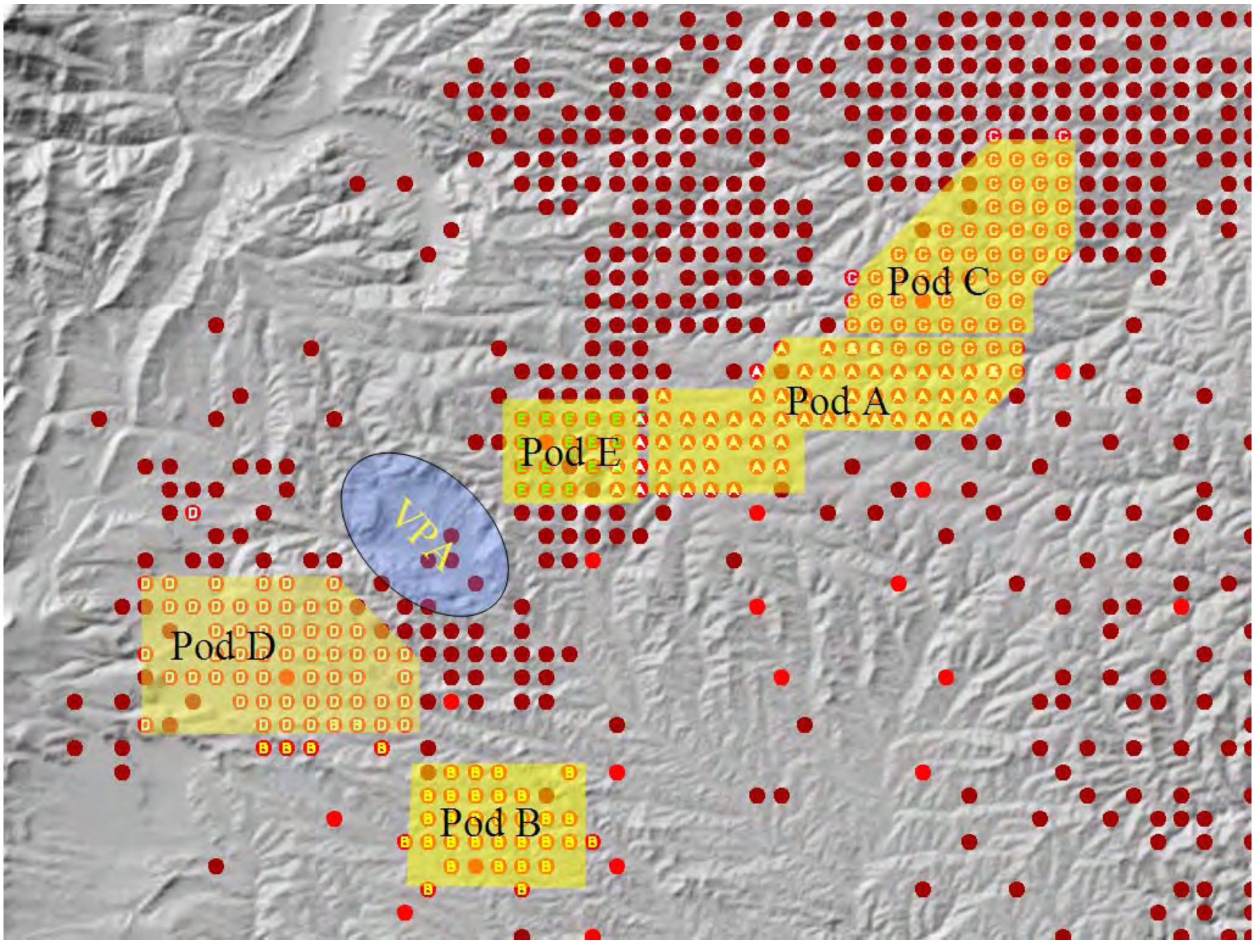

Figure 94: Subset of Figure 1, showing arrangement of CBM wells operated by El Paso Raton LLC in the New Mexico portion of the Raton Basin. Note position of well "Pods" relative to the Vermejo Park Anticline (VPA).

2.7.5 Pod-scale Characteristics

Drilling Activity

Figure 95 shows the drilling activity of the Vermejo Park Ranch unit from September 1999 to January 2004. The stepped appearance of the drilling program reflects the cessation of drilling activities during certain wildlife-sensitive seasons. As can be seen from the Pod breakdown, the first wells drilled were in Pods A and C—those areas near the Colorado border which extended CBM production from the productive fields already established in Colorado. During the second year of drilling, Pods D and B in the south were explored, as was Pod E the following year. As of January 2004, El Paso Raton LLC was operating 423 wells on the Vermejo Park Ranch unit. At present, drilling continues in all Pods.

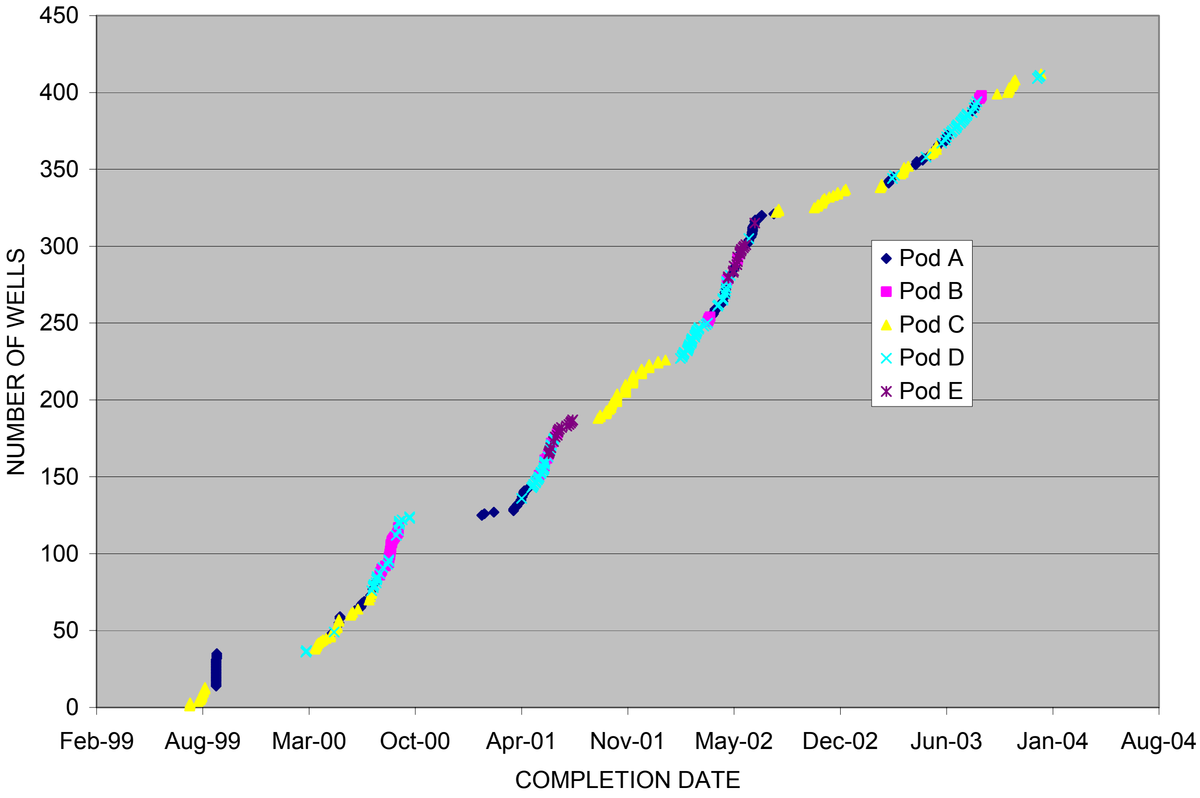

Figure 95: Chart showing development of CBM program on the Vermejo Park Ranch Unit.

Gas and Water Production

As of October 2003, more than 28 billion cubic feet (BCF) of gas had been produced, along with nearly 24 million barrels of water. The average VPR coalbed methane well produces 100 thousand cubic feet (MCF) of gas per day, however that figure is not uniform across the lease. Figure 96 shows that after four years of production, most wells in Pods A, B, C, and E have settled into a production rate of 2.5 million cubic feet (MMCF) of gas per well per month. The exception are those wells in Pod D which show an average monthly production as high as 9 MMCF per well. At times, some individual wells in Pod D produced more than one million cubic feet of gas per day.

The disparity in production characteristics between those wells in the southern portion of the lease (Pods D and B) and those in the north (A, C, and E) is shown in the production graphs for each Pod (Figures 97-101). Pod D production is remarkable for the low volumes of water produced and high volumes of gas. Pod B has produced little gas, but little water as well. Cumulative gas to water ratio for Pod D is 3.6 (MMCF/MBBL) and for Pod B is 2.7. The gas to water ratios for pods A, C, and E, however, are 0.67, 0.63, and 0.23, respectively.

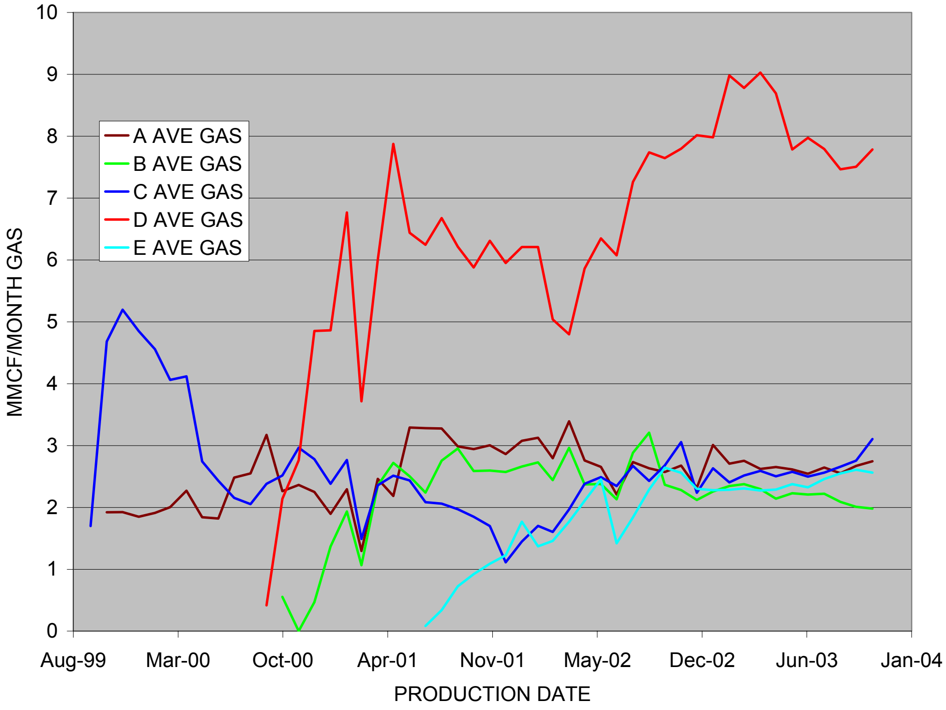

Figure 96: Average monthly gas production per well. Most wells in Pods A, B, C, and E are currently producing an average of 2.5 million cubic feet of gas per month. In contrast, the average production from wells in Pod D is three times greater.

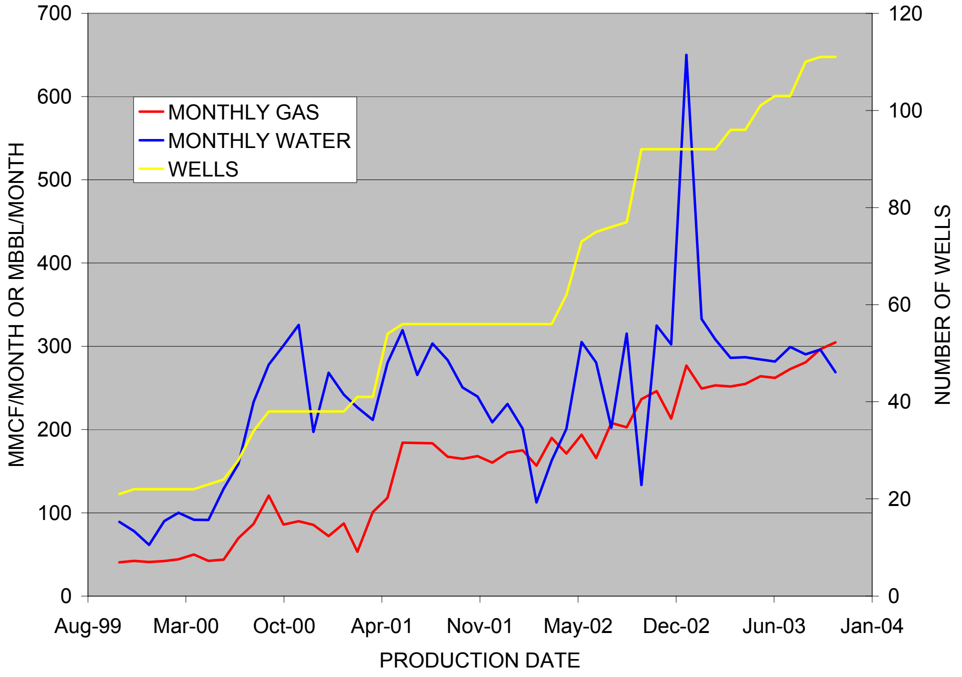

Figure 97: Summary of monthly gas and water production from Pod A wells.

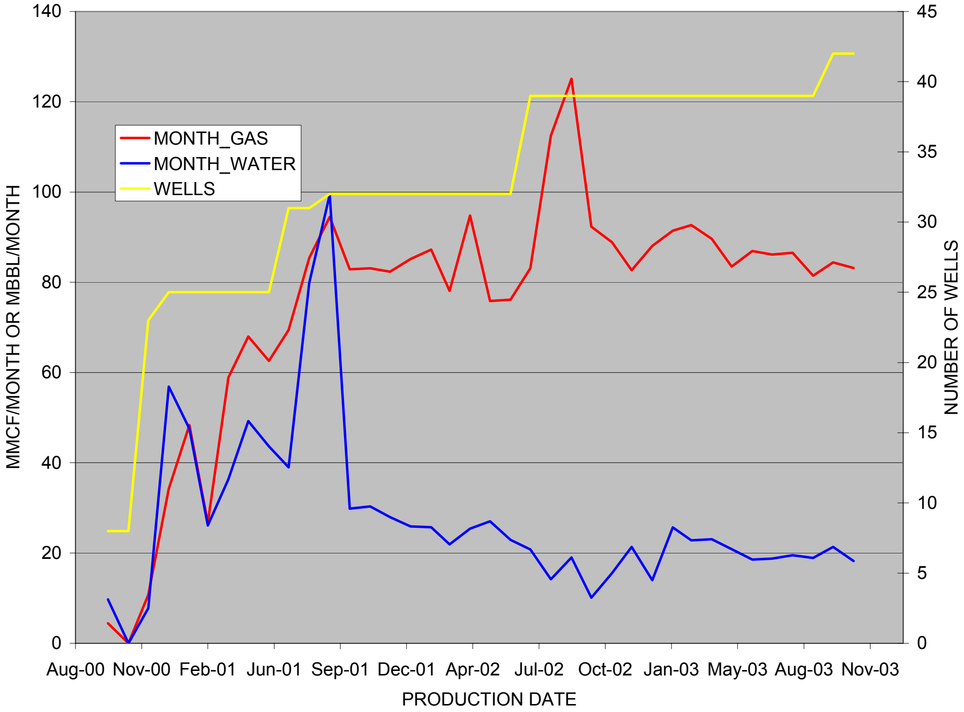

Figure 98: Summary of monthly gas and water production from Pod B wells. Note significant drop in water production after one year of production and relatively modest gas production.

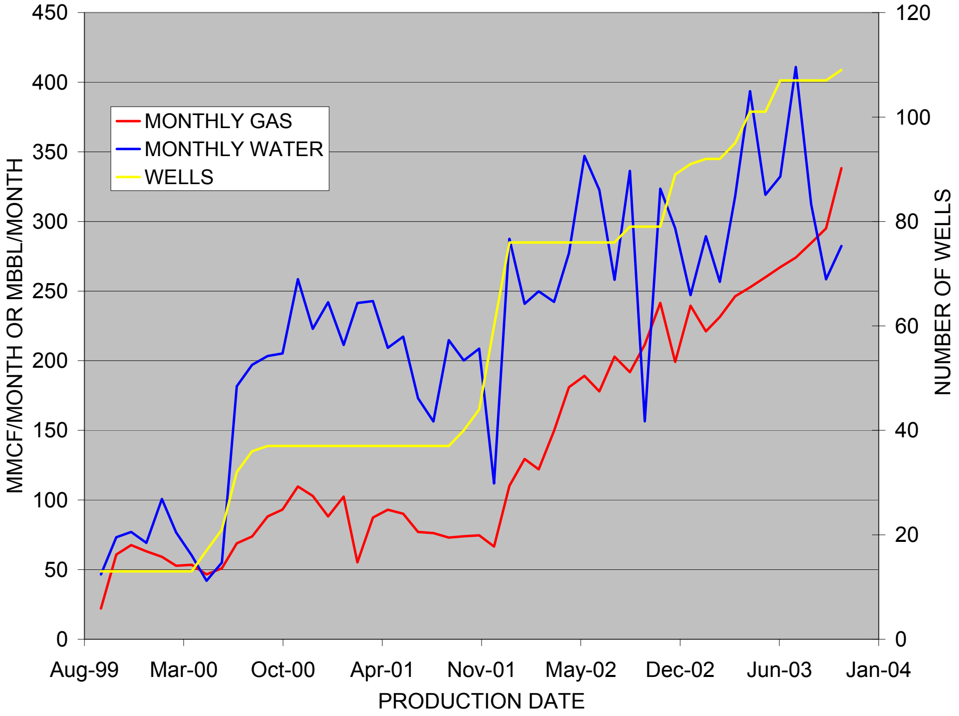

Figure 99: Summary of monthly gas and water production from Pod C wells.

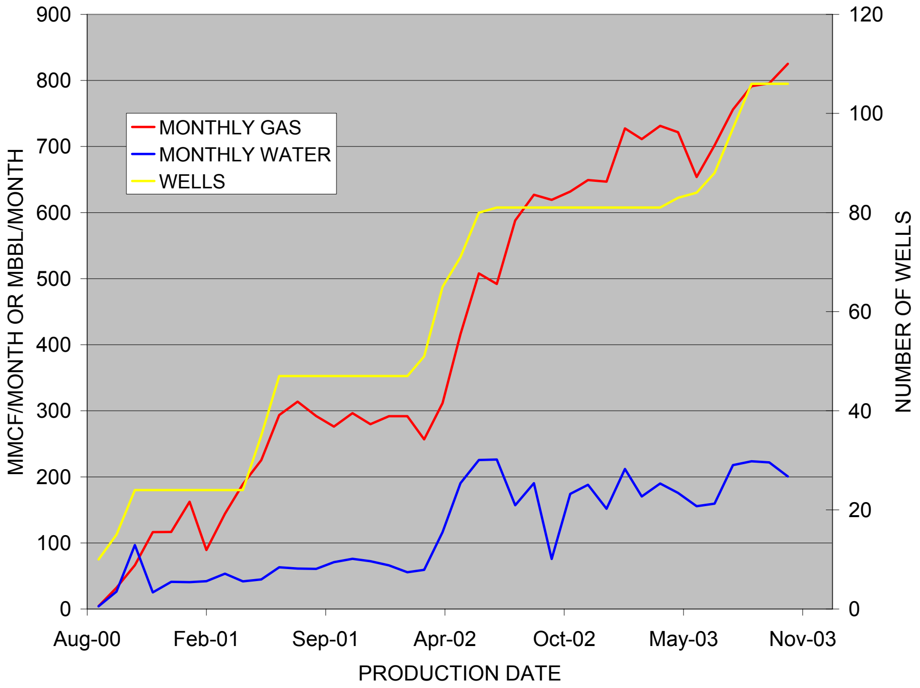

Figure 100: Summary of monthly gas and water production from Pod D wells. Note relatively low water production and very high gas production rates.

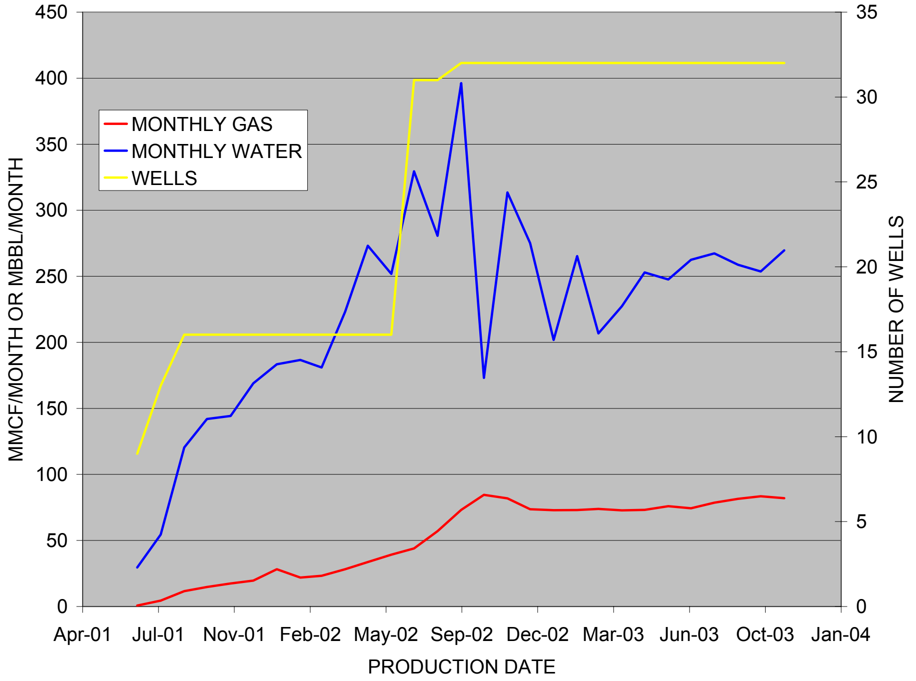

Figure 101: Summary of monthly gas and water production from Pod E wells. This pod is characterized by relatively high water and low gas production. Note, however, that this is the youngest pod of wells within the Vermejo Park Ranch Unit.

Water Quality

In many coalbed methane-producing regions in the U.S., the quality of produced water determines whether it must be injected back into the earth or if it may be discharged on the surface. While all produced water on the VPR lease is injected back into deeper aquifers, water quality characteristics could be useful in identifying different ground water systems which, in turn, could provide insight into coalbed gas potential. Average values of total dissolved solids (TDS) in units of milligrams per liter for Pods A, C, D, and E are 2,800, 5,400, 4,600, and 2,500, respectively. In contrast, Pod B has an average TDS value of 12,900 mg/L. This seems to be a local anomaly, as compared to the entire basin. In general, TDS values increase from west to east across the greater basin. This indicates a general west-to-east movement of groundwater from recharge areas near the Sangre de Cristo Mountains, where aquifer strata are upturned and exposed at the surface, to outcrops and drainages in the eastern end of the basin.

2.7.6 Individual Well Production Curve Characteristics

Observing gas and water production characteristics on a pod-by-pod basis gives some idea of geographical trends in CBM production, but looking at production curves from individual wells exposes vast differences in production behavior across the basin, and even among wells in the same pod. This section will highlight just four end-member examples which were identified among the VPR wells.

Typical coalbed methane wells initially produce large volumes of water and little gas. As hydrostatic pressure is reduced in the reservoir, more and more methane desorbs from the coal surface. As a result, the water and gas production curves from such a typical well should look similar to those in Figure 93. A gas incline curve is paired with a water decline curve during the de-watering phase. Many wells, especially those within Pods A and C, exhibit this behavior. An example from Pod A is given in Figure 102.

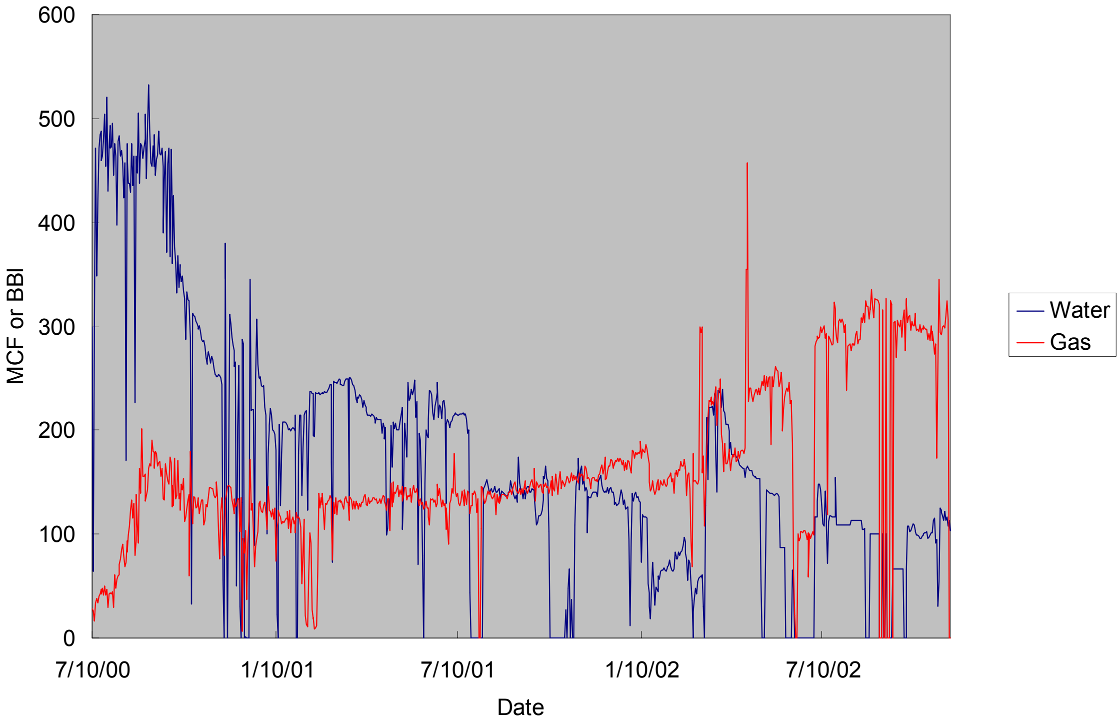

Figure 102: Example of gas and water production curves for a single well in Pod A. Compare with the idealized CBM production behavior in Figure 93. Wells of this type exhibit high initial water production and little gas production. Withdrawal of water from the formation decreases hydrostatic pressure and induces methane gas to desorb from the coal matrix. As formation pressure is reduced further, more gas desorbs from the coal, resulting in a gas incline curve.

Three other end-member production behaviors were identified which diverge from the standard CBM model. One, an example of which is shown in Figure 103, is characterized by water and production curves which remain fairly parallel. That is, an increase in gas production is matched by an increase in water production; a decrease in gas production is paired with a decrease in water production. There may be a slight lag of a few days between peaks or troughs of the water and gas curves. Another end-member example is given in Figure 104. In this case, there is a local peak in gas production which occurs nine months to one year after the well comes on line. After this local peak, gas production decreases for a few months and then increases again, surpassing flow rates of the earlier peak. Finally, another production behavior observed in some wells consists of a high initial gas flow rate followed by a continuous decline in gas production (Figure 105). Very little water is produced in this type of well. Hypotheses concerning these end-member production types are in the Discussion section.

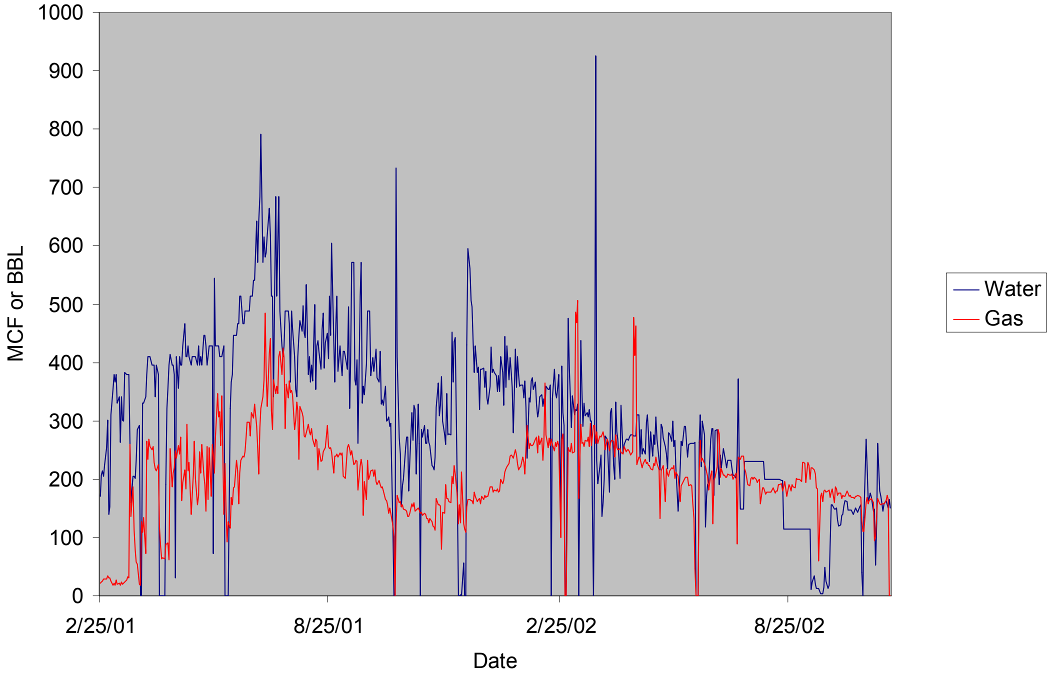

Figure 103: Gas and water production curves from a single well in Pod A. Contrast this production behavior with than in Figure 12. There is no well defined water decline, gas incline curve. Instead, peaks on water production are typically followed soon after by a peak in gas production.

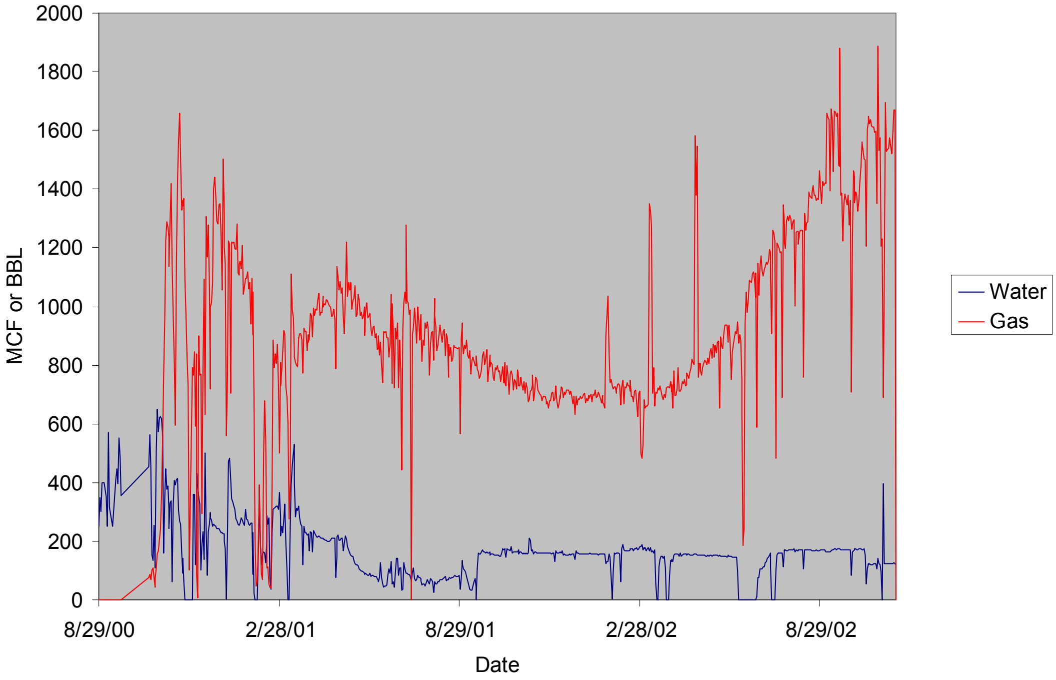

Figure 104: An example, from Pod D, of a well that exhibits high gas production early in its history, followed by a decline in gas production, and then a gas incline curve.

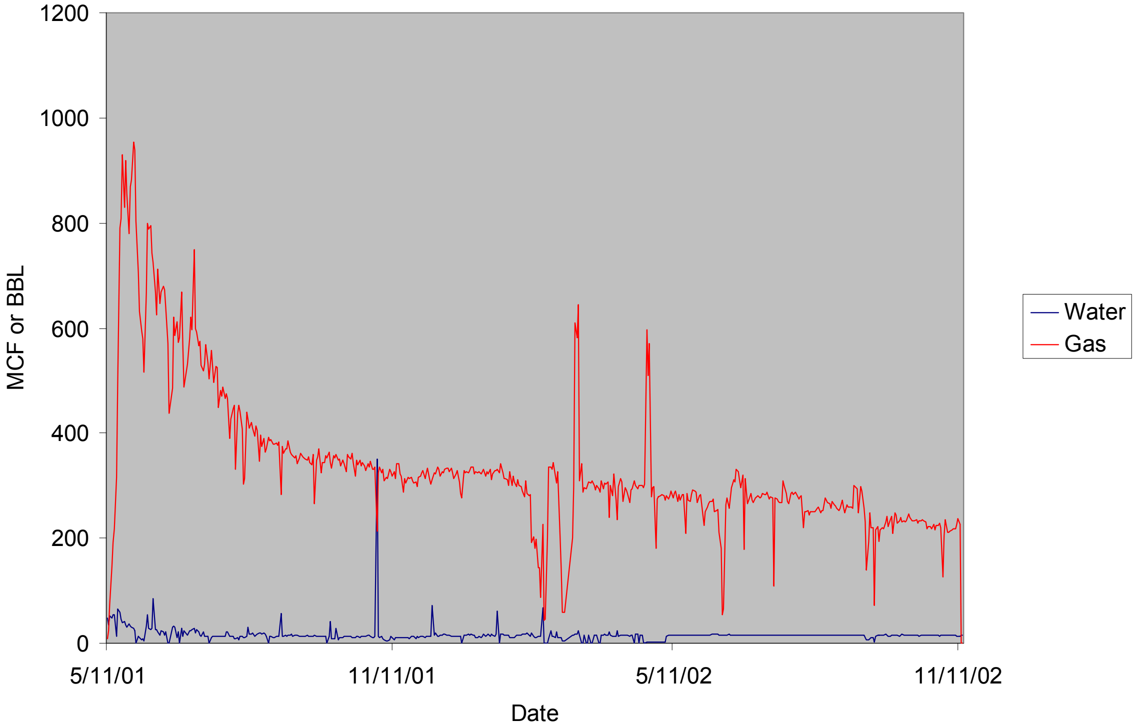

Figure 105: An example of high gas, very low water production typical of many wells in Pod D. Production behavior such as this would be more likely anticipated in a conventional gas reservoir rather than a coalbed methane field.

2.7.7 Resource Potential of the Raton Mesa Region

Notwithstanding the spotty pre-1990 oil and gas exploration attempts, gas exploration and production is relatively new in the Raton Basin. New infrastructure and technology have established coalbed methane as the most important hydrocarbon resource in the basin. Producing gas from the Trinidad Sandstone, the basal conglomerate of the Raton Formation, and sandstone lenses within the Vermejo and Raton formations has experienced mixed results. These clastic rocks, although having very low matrix permeability values, stand a good chance of being charged with gas from the adjacent coal beds. The presence of natural fractures would greatly enhance bulk permeability, facilitating gas flow to the wellbore, and detailed fracture studies such as the one described in this report would aid exploration and production strategies for low-permeability fractured sandstone reservoirs in the Raton Basin. Operators in both New Mexico and Colorado have generally not completed wells in these non-coal intervals for fear of excessive water production, however some very promising gas shows have been noted in the Trinidad Sandstone, and at least one well is producing gas from the Raton Conglomerate in the VPR unit. In some areas, gas may be trapped within the sandstones by a regional capillary seal, and such a "basin-centered" gas accumulation has been proposed for the Raton Basin (Johnson and Finn, 2001).

2.7.8 Discussion: Vermejo Park Ranch CBM Production

The nature of coalbed methane production—the requirement that wells must be dewatered, sometimes for many months before economic quantities of gas begin to flow—makes it very difficult to predict reserve estimates or ultimate recovery based on early production characteristics. At the time of this writing, the oldest of El Paso's Vermejo Park Ranch wells have only been producing for four years, and the company's exploration strategy is constantly being modified with each new well drilled. However, some general observations can be made about relationships between gas production, water production, geography, geology, and hydrology of the VPR unit.

The most striking contrast in production behavior is seen in the very different gas-to-water ratios between Pod D and B wells, and those of Pods A, C, and E. Water production rates and cumulative volumes exhibited by most wells in Pods A, C, and E are comparable to most CBM wells in Colorado and CBM wells in other basins. The low water production in Pods D and B is anomalous, and points to a different hydrologic system in this area. The most salient geologic feature separating Pods B and D from Pods A, C, and E is the Vermejo Park Anticline. Whether this structure is indeed solely responsible for the differences in water production between the northern and southern wells is uncertain. Pods D and B, despite being adjacent to each other, exhibit very different water chemistry values, suggesting these two areas are host to different hydrologic systems. No obvious surface features hint at a geologic structure separating the two regions. As noted in this report, the Vermejo and Raton formations are quite heterogeneous, consisting of laterally discontinuous lenses of sandstone, shale, siltstone, and coal. It is reasonable to assume that hydrologic flow units are also restricted laterally and vertically, and could account for the very different water production behavior among wells that are relatively closely spaced.

Alternatively, low water production in the wells of the southern part of the unit could be a result of their separation, by capillary seal, from the wells to the north. Figure 106 illustrates how this capillary seal, which cuts across lithologic boundaries, could isolate the productive intervals of Pods D and B in a basin-centered type gas deposit. Wells of Pods A, C, and E would produce from intervals above this seal, and be exposed to the regional groundwater and meteoric water systems. Rainfall rates do not appreciably differ from Pod D to Pod C, and there is no evidence to suggest greater recharge on the northeast side of the Vermejo Park Anticline than on the southwest side.

Variability in the gas and water production curves from individual wells could help answer these questions. The first example, shown in Figure 102, exhibits a general gas incline curve, water decline curve, and has no peculiar features that would suggest it is not a "typical" coalbed methane well. The second example (Figure 103) is more problematic. Both gas and water production curves behave similarly. Increased cumulative water production does not bring about greater gas flow rates. The third example (Figure 104) shows a spike in gas production during the early history of the well. The latter portion of the recorded production shows an increase in gas flow rate with continued dewatering, just as one would expect from a typical coalbed methane. The early peak may be evidence of free gas being produced directly from the cleat or natural fracture system. Significant pressure reduction is not necessary to produce this free gas—only a pressure gradient from the formation to the wellbore is required. However, only a limited amount of free gas can be stored in the fracture network, and once this resource has been depleted, the well's gas flow rate declines until a sufficient quantity of water is pumped off the formation, beginning liberation of gas adsorbed onto the coal matrix. In the final example (Figure 105), gas production is high to begin with, continuously declines, and water production is minimal throughout. This is the 'hyperbolic' type decline curve one would expect to see in a conventional or basin-centered gas reservoir.

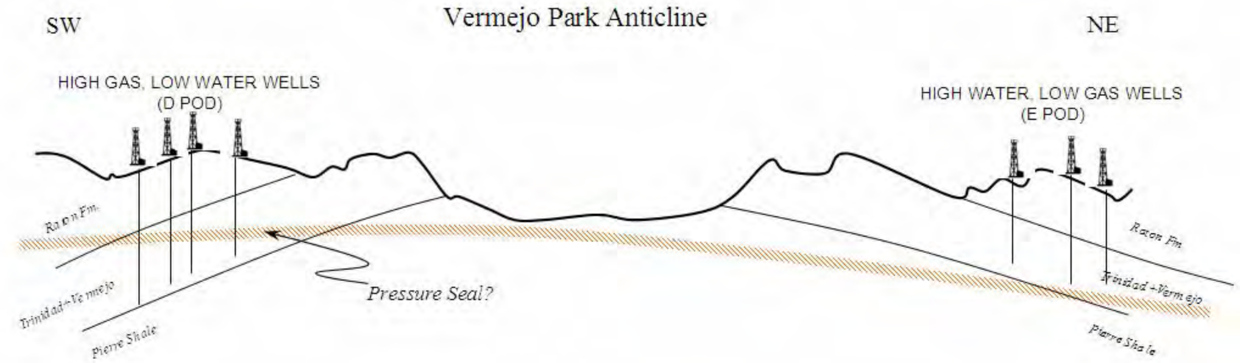

Figure 106: Conceptual cross section of Vermejo Park anticline illustrating one hypothesis for the differing gas to water ratios on either side of the structure. Production from Pod D southwest of the anticline may be from a basin-centered gas accumulation, which is isolated from meteoric waters by a capillary seal. Evidence includes low water production, high values of dissolved solids in the produced water, and increased water production at shallower depths.

2.8 GEOSTATISTICAL ANALYSIS OF WELL PRODUCTION

Coal-bed methane production can be influenced by multiple factors, including fracture network characteristics, local geologic structure, regional stress, coal thickness, depth, hydrology, and pressure history. In addition, there may be significant spatial continuity (i.e., clustering) of gas production that reflects spatial trends in the underlying geological controls on production rates. Understanding the relative importance of influential factors and the spatial continuity of their impacts potentially contributes to the optimization of production development (Arnold et al., 2004).

This section describes statistical and geostatistical analyses of gas and water production in coal-bed methane production wells. Average daily gas and water production from 235 coal-bed methane wells in four El Paso Production development pods in the Raton Basin were analyzed. A statistical analysis of factors potentially influencing production was conducted using the stepwise linear regression method, which estimates the relative importance of independent variables or correlation to production. The factors or independent variables in the regression analysis include coal thicknesses, slope of the structural surface of the Trinidad Sandstone, groundwater total dissolved solids, and duration of production. The geostatistical method of variogram analysis was used to assess the spatial continuity in production.

2.8.1 Estimates of Gas and Water Production

A database of gas production was compiled from information from the El Paso Production Company. Average daily gas and water production were calculated from the data on cumulative production and the number of producing days. Gross coal thicknesses in the Vermejo Formation and the Raton Formation for each well were also contained in the information from the El Paso Production Company. Average total dissolved solids values in groundwater produced from the wells were also compiled. A map plotting the values of average daily gas production is shown in Figure 107. Note in Figure 107 that the production wells are grouped into two general areas.

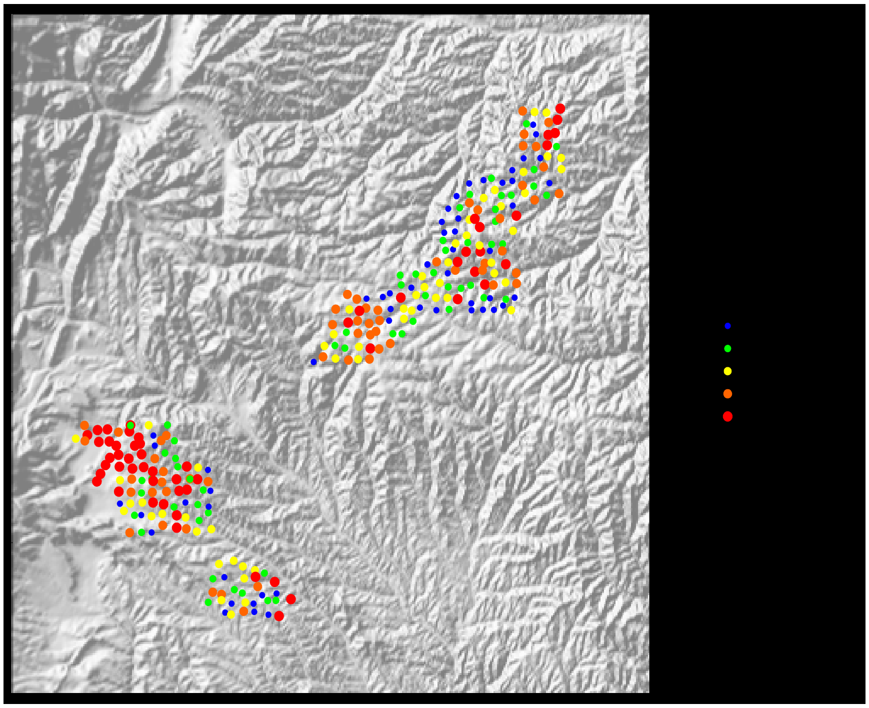

Figure 107: Average daily gas production in El Paso Production wells.

2.8.2 Stepwise Linear Regression Analysis

Data on the structural surface of the Trinidad Sandstone were derived from a hand-contoured structural map of the southern portion of the Raton Basin supplied by the El Paso Production Company. The contours on this map were digitized and used to produce a gridded representation of the surface. Several quantities were calculated from this gridded structural surface, including the local dip, the first derivative of the surface parallel and perpendicular to the direction of maximum horizontal stress, and the second derivative parallel and perpendicular to the direction of maximum horizontal stress. Figure 108 shows the digital representation of the structural surface of the Trinidad Sandstone as the lower surface, overlain by the topographic surface. Note that the perspective view shown in Figure 108 is from approximately the southeast. The color scale superimposed on the structural surface of the Trinidad Sandstone indicates the first derivative, or dip, of the surface. The steeper dips along the western margin of the Raton Basin, especially along the eastern limbs of the Vermejo Park anticline and the Tercio anticline, are clearly shown in the figure. Estimated values of quantities related to the slope of the structural surface at well locations are incorporated into the production database and used in the regression analysis.

Topographic Surface

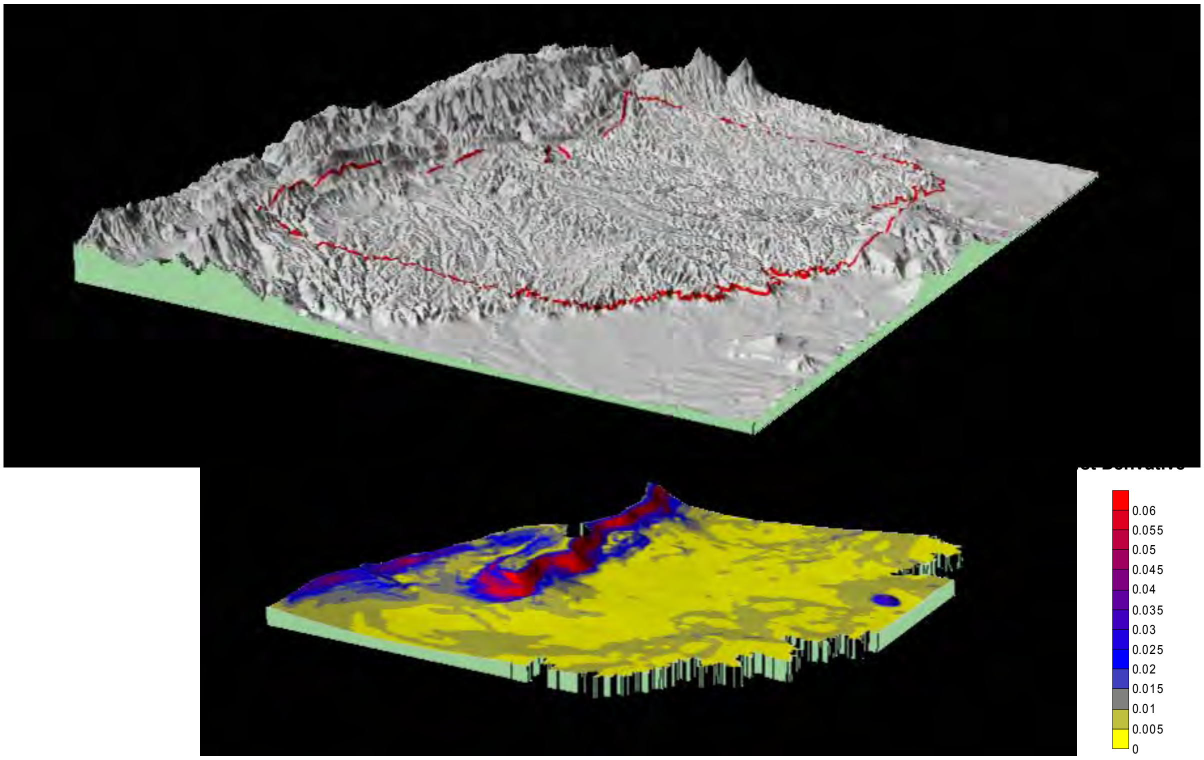

Structural Surface of the Trinidad Sandstone

Figure 108: Topographic surface and structural surface of the Trinidad Sandstone in the southern Raton Basin. The dip, expressed as the first derivative of the structural surface of the Trinidad Sandstone, plotted as the color scale.

The method used to explore the relationships between gas (and water) production and potentially influential geological factors in this study was stepwise regression, a form of regression analysis. Stepwise linear regression varies from commonly used multiple regression techniques in that stepwise regression, in addition to calibrating a predictive equation, uses statistical criteria for selecting which of the predictor variables will be included in the final regression equation. The stepwise process consists of building the regression equation one variable at a time by adding at each step the variable that explains the largest amount of the remaining unexplained variation (Haan, 1994). The coefficient of determination R^2, represents the fraction of the total variation that is explained by the linear relationship between the input variables and the dependent variable (production in this case). The change in the coefficient of determination, as each variable is added into the regression equation, is used to determine the relative importance of each variable. Rank transformation of variables was used in this sensitivity analysis to reduce potential non-linearity between the independent and dependant variables.

The results of the stepwise linear regression analysis of average daily gas production are shown in Table 1. These results indicate that a regression or correlation model using six of the independent variables has a value of about 0.19 for the coefficient of determination. The total thicknesses of the coal in the Vermejo and Raton Formations, as the first two variables in the stepwise regression model, have a R^2 value of about 0.14. This indicates that these two variables account for about 14% of the variability in observed average daily gas production.

These regression analysis results show that there is not a strong correlation between the average daily gas production and the potentially controlling variables used in the analysis. Even taken in aggregate, the independent variables account for only about 19% of the variability in gas production. This indicates that these independent variables probably have very little predictive value for potential gas production, at least within the context of the regression model developed in this study.

Table 1. Stepwise Linear Regression Analysis Results for All Independent Variables Versus Average Daily Gas Production, n=235.

Step	Variable	R^2	ΔR^2	Correlation
1	Gross Vermejo Coals Thickness	0.0975	0.0975	Positive
2	Gross Raton Coals Thickness	0.1412	0.0437	Negative
3	First Derivative – Trinidad Sandstone – S85°E	0.1669	0.0257	Negative
4	Groundwater Total Dissolved Solids	0.1830	0.0161	Negative
5	Second Derivative – Trinidad Sandstone – N5°E	0.1879	0.0049	Negative
6	First Derivative – Trinidad Sandstone – N5°E	0.1899	0.0020	Positive

Significantly better correlation exists between the independent variables and the average daily water production. The results of the stepwise regression analysis for average daily water production are shown in Table 2. As indicated in these results, about 48% of the variability in the average daily water production can be accounted for by the eight independent variables listed for the regression model. About 37% of the variations in water production can be explained by just two of the variables, the first derivative of the structural surface of the Trinidad Sandstone parallel to the direction of maximum horizontal stress and the total dissolved solids in the groundwater.

The regression analysis results for average daily water production do show a weak to moderate correlation to the independent variables. Although water production from wells is of secondary importance with regard to coal-bed methane production, it does impact the economics of gas production because of potential costs associated with the disposal of water. Consequently, the regression model for average daily water production may have potential value with regard to planning production well locations.

Table 2. Stepwise Linear Regression Analysis Results for All Independent Variables Versus Average Daily Water Production, n=235.

Step	Variable	R^2	ΔR^2	Correlation
1	First Derivative – Trinidad Sandstone – N5°E	0.2214	0.2214	Negative
2	Groundwater Total Dissolved Solids	0.3717	0.1503	Negative
3	Number of Gas Producing Days	0.4418	0.0701	Negative
4	First Derivative – Trinidad Sandstone – S85°E	0.4586	0.0168	Positive
5	Gross Vermejo Coals Thickness	0.4679	0.0093	Negative
6	Second Derivative – Trinidad Sandstone – N5°E	0.4732	0.0053	Negative
7	Gross Raton Coals Thickness	0.4770	0.0038	Negative
8	First Derivative – Trinidad Sandstone	0.4808	0.0038	Negative

2.8.3 Geostatistical Analysis of Production

The spatial continuity of gas and water production was analyzed using the geostatistical technique of variography. A variogram quantifies the variability in a particular variable as a function of the separation distance between locations at which the variable is measured (Issaks and Srivastava, 1989). It is based on the intuitive concept that measured values of a quantity in a heterogeneous system should be more similar for locations that are closer together than for locations that are farther apart. The degree of spatial continuity of a variable within the system is typically quantified using a value called the "range" of the variogram. The range is the limit of spatial continuity and is the distance beyond which values for a particular variable are essentially uncorrelated.

Variograms of average daily gas production for two production areas of the El Paso Production wells are shown in Figure 109. The variograms in this figure are omnidirectional, meaning that the pairing of observations is made in any (and all) directions. The lag distance is the separation distance between pairs of wells and the variogram is the measure of variability in average daily gas production. The points plotted on the graphs are the values from the production database and the number by each point is the number of data pairs used to calculate that variogram value. The blue curves on the plots are models approximately fitted to the plotted points. The values of the range from the plotted variogram models are shown for each area. Note that the range in Area 1 (1300 m) is significantly less than the range in Area 2 (4200 m).

The results in Figure 109 indicate that values of average daily gas production for wells that are farther apart than about 1300 m in Area 1 are essentially unrelated; whereas, wells that are closer than 1300 m tend to have similar (either high or low) rates of gas production. In Area 2, the estimated range of 4200 m indicates that the distance over which gas production is related is significantly larger.

Variograms can also be constructed so that the pairing of observations is directionally restricted. Multiple directionally restricted variograms of average daily gas production were constructed to assess potential variations in spatial continuity as a function of direction. Each variogram only considered pairs of wells that were within 30^o of the azimuth of interest and a value of the range was estimated for each variogram. The results of this analysis for both of the production areas are shown in Figure 110 as a polar plot of the estimated range as a function of azimuthal direction. The results for Area 1 indicate that spatial continuity in gas production is approximately isotropic and the range is about 1200 m to 2000 m. The results for Area 2 show that the spatial correlation in gas production is anisotropic, with significantly greater continuity in the NW-SE direction than in the NE-SW direction. The correlation range in gas production for Area 2 varies from about 2000 m to 6000 m, depending on direction.

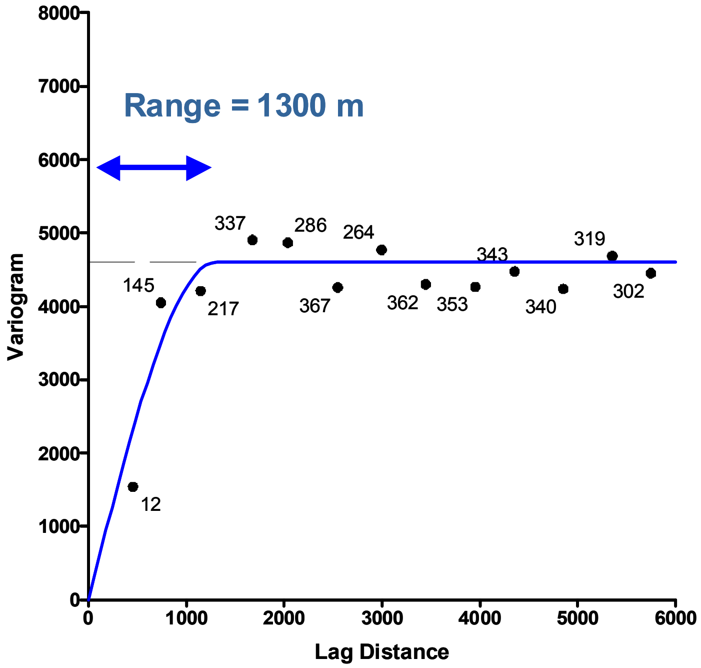

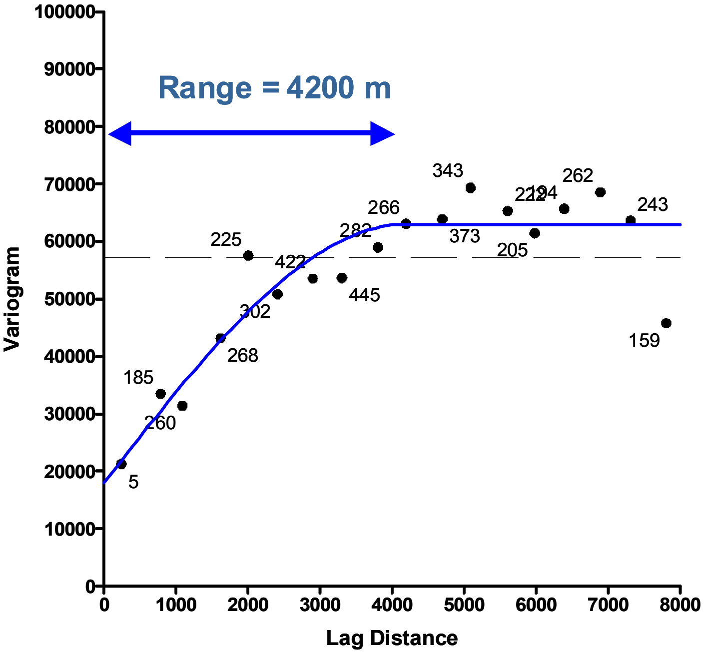

Figure 109: Omnidirectional variograms of average daily gas production in El Paso Production wells for Area 1 (above) and Area 2 (below) in the Raton Basin.

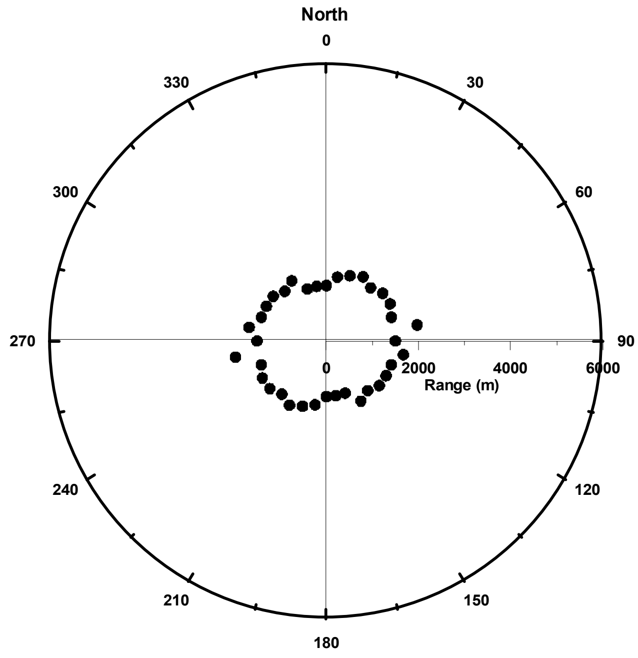

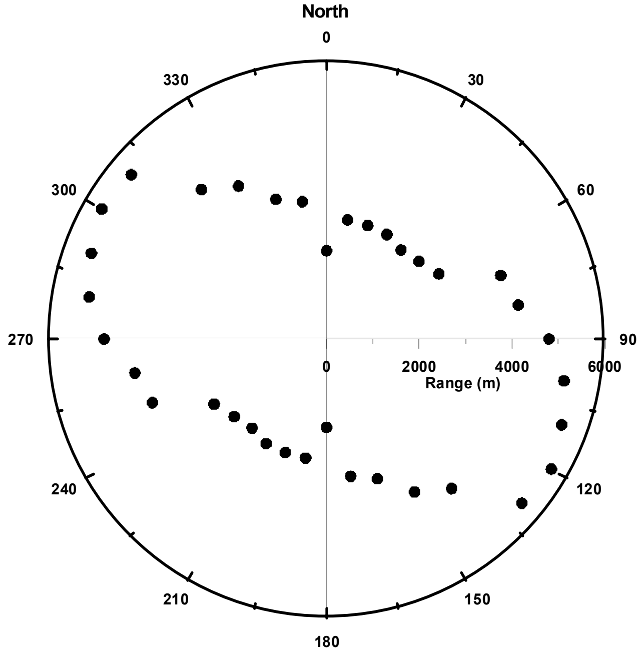

Figure 110: Polar plots of variogram range of average daily gas production in El Paso Production wells as a function of direction for Area 1 (upper) and Area 2 (lower) in the Raton Basin.

To illustrate the style of spatial continuity in gas production and the differences between Area 1 and Area 2, simulations of the heterogeneous distribution of potential gas production were performed. These simulations were generated using the values of the range and the degree of anisotropy indicated in the analyses above. In other words, these simulations honor the geostatistical characterization derived from the variograms of average daily gas production. These simulations were generated using the sequential gaussian simulation method described in Deutsch and Journel (1998). In addition, it should be noted that these are unconditional simulations, meaning that they do not correspond to the values at the actual values of average daily gas production at individual wells. The resulting simulations are shown in Figure 111.

The simulated distributions of relatively high and low gas production potential shown in Figure 111 for Area 1 and Area 2 are qualitatively consistent with the characteristics of spatial continuity identified in the variogram analysis. Regions of high or low production potential in Area 1 are smaller and more randomly distributed than in Area 2. The regions of high or low production potential in the simulation of Area 2 are larger and have a longer extent in the NW-SE direction than in the NE-SW direction.

The patterns of spatial continuity in gas production identified in this analysis are, by inference, related to spatial continuity in underlying geological characteristics of the system that control gas production. The relatively small scale of spatial correlation in gas production observed in Area 1 suggests that the geological controls on rates of gas production are local and not related to any larger-scale structural or stratigraphic geological features. In contrast, the relatively larger scales of spatial continuity in gas production in Area 2, especially in the NW-SE direction, suggests that there are larger, through going geological features related to the potential for gas production. The longer spatial correlation in the NW-SE direction in Area 2 does not correspond to preferred orientations of open fractures observed in well VPRD 71 from this area (see Figure 2). Consequently, it is unlikely that the greater spatial continuity in gas production in the NW-SE direction is related to fracture orientations. It is possible that the greater spatial correlation in gas production in the NW-SE direction in Area 2 is related to greater stratigraphic continuity, particularly of coal beds favorable to production, in that direction.

These results on spatial correlation in gas production have potential implications for exploration and production strategies. In Area 1, the lack of spatial continuity in gas production potential implies that drilling offsets from existing wells, either high- or low-production wells, can be essentially random. In contrast, the anisotropic spatial correlation of gas production in Area 2 suggests differing drilling offset strategies from high- versus low-production wells. Examination of the simulation for Area 2 in Figure 111 illustrates that if there is an existing high-production well, a location to the NW or SE is more likely to have high gas production potential; whereas an offset to the NE or SW is likely to have lower gas production potential. However, if there is an existing low-production well, an offset to the NE or SW is more likely to be a location with higher gas production potential than an offset to the NW or SE.

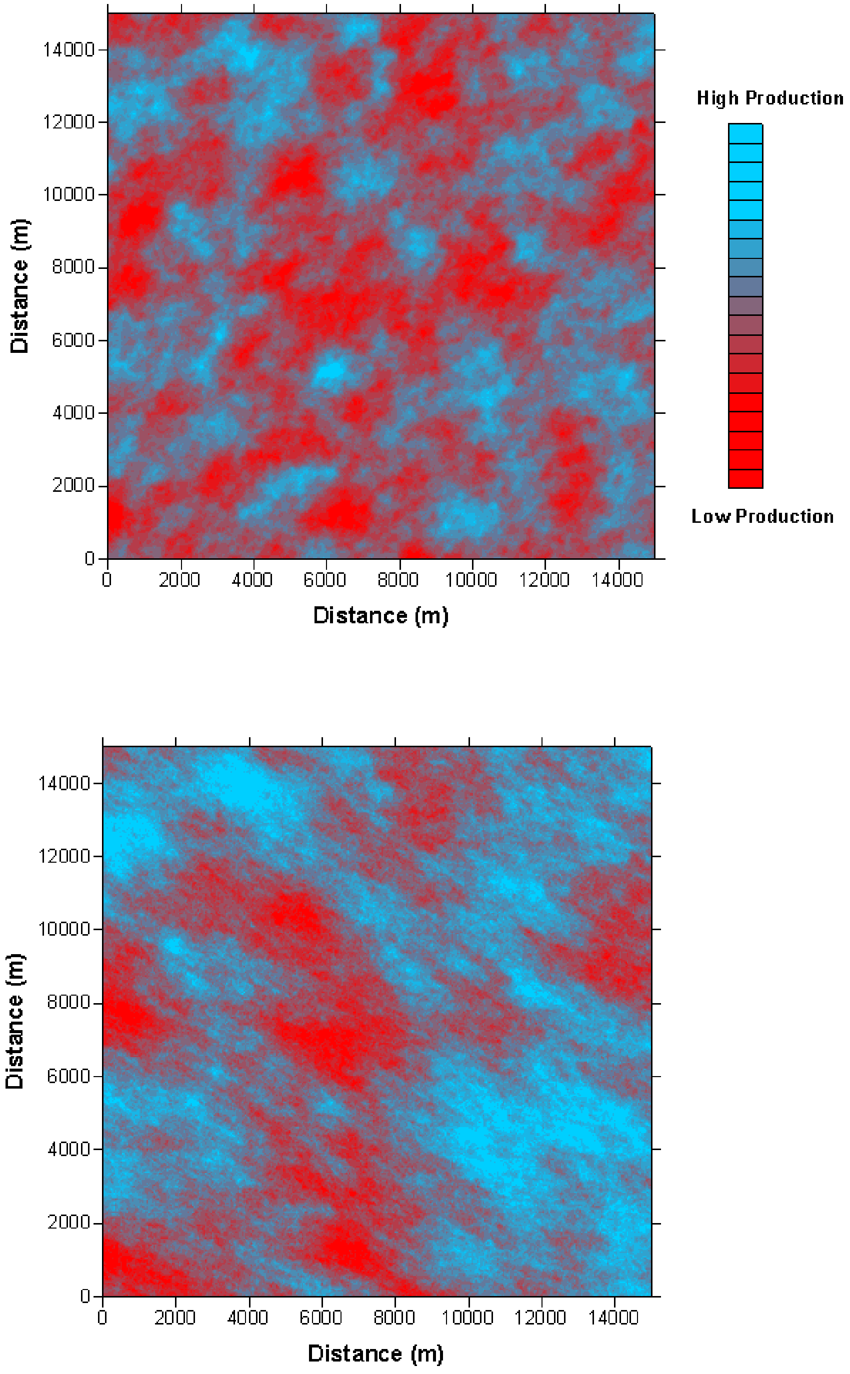

Figure 111: Unconditional simulations of relative average daily gas production, based on differing anisotropic values of variogram range, for Area 1 (upper) and Area 2 (lower) in the Raton Basin.

3.0 SYNTHESIS AND CONCLUSIONS

3.1 RATON BASIN TECTONICS

3.1.1 Topography vs. Structure

The Raton basin is unique among the Rocky Mountain basins in that it is marked by a topographic upland, commonly referred to as the Raton Mesa. Cather (2002) suggests that this highland mesa resulted from a point source for the basin filling strata, a basin-scale alluvial fan of sorts, although Merin et al. (1988), citing Tweto (1975), suggest that there were several sediment sources for the sediments that filled the Raton basin in the Late Cretaceous and Early Tertiary time, northwest and southwest of the basin but now deeply buried under the San Luis valley. Suppe et al. (1975) suggested that the Raton highlands are caused by a northeast-southwest trending linear upwarp, created by a migrating hot spot, although little has been made of this idea by later geologists working in the area. If this hot spot theory is valid, it might help to explain the thermal anomaly that extends eastward from the Rio Grande Rift province of high heat flow and encompasses the Raton basin (Edwards et al., 1978), and it would explain some of the anomalous stress orientations in the basin, discussed elsewhere.

3.1.2 Basin Margins

The gas-bearing Vermejo and Raton formations thin and lap eastward onto the broad Sierra Grande arch. The formations crop out at the eastern margins of the basin above cliffs created by the pairing of erosion-resistant Trinidad Sandstone and the underlying, easily weathered, slope-forming Pierre Shale. Strata dip gently westward from this basin margin to the synclinal basin axis, which is slightly west of the center of the basin, where they reverse and dip eastward. Dip angle increases westward to the western margin where the strata are abruptly upturned, locally to the vertical, and even overturned.

The western margin is a complex structure composed of multiple thrust horizons and repeated sections. Many of the published cross sections (i.e., Clark, 1966; Rose and Everett, 1986) can be interpreted to indicate that the eastward-dip of the strata at the western basin margin resulted from an insertion of under thrust layers wedged and jammed into the basin below the Late Cretaceous and Tertiary strata, uplifting them. Lindsey (1998) suggested that the basin axis moved eastward during deposition as the western margin was progressively compressed by thrusting and uplifted. Higher in the section, Precambrian rocks have been thrust eastward over the top of these same strata, resulting in stratigraphic inversion. Keller and Gridley (1990), based on a gravity low at the western margin of the basin, estimate that these Precambrian rocks have been thrust eastward by about 50 kilometers. Miocene and younger normal faulting related to extension along the Rio Grande basin has truncated the thrust system and buried its proximal, western regions deeply under the San Luis valley (i.e., Brister and Gries, 1994).

However, the western margin of the Raton basin is not a uniform, curved, overthrust front. Thrust faults are more numerous and most obvious north of the New Mexico-Colorado border, whereas normal faults are more common to the south. Merin et al. (1988) have suggested that the thrust-fault western margin of the Raton basin in Colorado transitions into a right-lateral wrench fault southward across the border into New Mexico. Although some thrusts are still present in New Mexico, they are fewer in number and perhaps have less eastward displacement. Cather (2002) suggests that the Pecos-Picuris fault zone, 40 km west of the present western margin of the Raton basin, is a transpressive, dextral, strike-slip fault, that accommodated 37 kilometers of lateral offset during Laramide tectonism. The interplay between this major fault zone and the nearby Raton-margin fault that combines eastward-directed thrusting and right lateral strike-slip motion is unclear, but north-south oriented strike-slip faulting is compatible with other structures in the Raton basin.

A component of right-lateral strike-slip faulting may explain the skewing of natural fracture strikes from the radiating pattern that would be expected of fractures that formed normal to the curved western thrust front during a purely thrust/indentation mode of deformation. A combination of thrust indentation and right-lateral shear offset would have produced a Laramide stress trajectory that favored an east-southeast/west-northwest maximum horizontal stress and related fractures.

3.1.3 Vermejo Park and Tercio Anticlines

Several structures are present within the basin, the largest being the Vermejo Park and Tercio anticlines. These are compound structures, related to Laramide strike-slip faulting in combination with contemporary thrusting and laccolithic intrusion. Different published maps (e.g., Pillmore, 1976; Woodward and Snyder 1976; Cather, 2002) have drawn structure contours that may or may not connect these two anticlines depending on the prejudices of the author: the sparse drill-hole data between these two features permits either interpretation. However, proprietary seismic data (Basinski, personal communication, 2003) suggest that they are related to each other via a north-south trending, right-lateral strike-slip zone. Seismic coverage consists of a single east-west line between the two structures and thus the north-south extent of the wrench zone cannot be determined, but the absence of this significant strike-slip zone in a seismic line south of the Vermejo Park anticline strongly suggests that this fault zone is the link between the two anticlines, and that the Vermejo Park anticline is the uplifted accommodation zone at the termination of the wrench fault. The natural fracture data gathered during this study show that the regional, east-west striking extension fracture pattern is significantly disrupted in the vicinity of the Vermejo Park anticline, indicating that the local stresses were significantly altered by the local structural complexities.

Spear (1976) wrote opaquely of deep-seated thrust faulting beneath the Vermejo Park and Tercio anticlines, and presumably he had wellbore data to substantiate this description, but these data are no longer available. However, this interpretation is compatible with outcrop data gathered from the west side of the Vermejo Park anticline during this study that include examples of small (a few centimeters to a few tens of meters offset), eastward directed thrust faults, and which probably reflect larger thrusts at depth.

The third and final part of the compound history of these structures, or at least of the Vermejo Park anticline, is an underlying laccolithic intrusion. Several other anticlinal structures in and near the Raton basin (the Morley dome, Stevens et al., 1992, and the Turkey Mountains uplift) are known or speculated to be underlain by laccoliths. Pillmore cited two 1926 drillholes that penetrated igneous rock below the Vermejo Park anticline, and Brian Brister (personal communication, 2003) actually located cuttings from these wells and is in the process of analyzing them for their age. Brister reports igneous rock at subsurface depths of 3200 ft and 3700 ft. The structure contours on the top of the Precambrian surface (Woodward and Snyder, 1976) do not reflect any anomaly over the Vermejo Park anticline, but this is probably more due to a lack of control than to the actual absence of basement-involved structure in the area.

In summary, our interpretation is that the Tercio and Vermejo Park anticlines were formed as uplifts along a transpressive splay off of the western-margin thrust/wrench-fault margin of the basin where it jogged eastward into the basin. Right-lateral motion was accommodated along a connecting wrench fault, culminating at a southern terminus in uplift of the Vermejo Park anticline. Uplift of this anticline was enhanced by intrusion of an igneous laccolith, probably facilitated by and localized along the deep-seated faults of the system.

3.1.4 Other Structures within the Raton Basin

Numerous anticlines, faults, and other structures are present within the Raton basin, including some that have not yet been mapped or described. Many of these were actively forming during deposition of the gas-bearing Late Cretaceous and Early Tertiary strata, as indicated by otherwise unexplained thickening and thinning of strata across the basin, and by evidence of intra-formational, syn-sedimentary deformation of the strata documented elsewhere in this report.

Different stratigraphic picks have led different authors to map different thickening and thinning trends within the same formations, but the overall trends are similar. Interestingly, the Vermejo Formation apparently *thickened* over the site of the future Vermejo Park anticline (Pillmore, 1976), suggesting that this area was the locus of a structural sag that was later inverted into the uplift, and strengthening the evidence for an underlying wrench-fault system where structural inversions are common along the length of the fault. Stevens et al., 1992, map coal isopachs that show thinning eastward from the basin axis (due to non-deposition and change of facies to marine strata) and westward (due to more proximal depositional environments that were not conducive to coal formation and/or uplift of the western margins during deposition.) In fact, many of the strata initially deposited at the western margins of the basin were uplifted sufficiently to be eroded, reworked, and re-deposited farther eastward as the Poison Canyon Formation.

Stevens et al. (1992) suggest that thinner coals along the Purgatoire River reflect a paleo-high during deposition, and in fact several authors (Harbour and Dixon, 1959; Johnson et al., 1966) have suggested that the Vermejo Formation itself is thinner or even absent along this trend. It is unclear whether this is non-deposition due to local, syn-sedimentary uplift or whether coal deposition was largely displaced by a sandstone channel system. Merry and Larsen (1982) map sandstone thicks offset from coal thicks elsewhere in the basin, but this is a common depositional pattern, thus not necessarily the result of structural complications.

Regardless, there are several anomalies in addition to thinner coals associated with the Purgatoire River valley. One is a higher coal rank and higher gas content of the coals (Close and Dutcher, 1990; Flores and Bader, 1999). Interestingly, Merry and Larsen (1982) did not map a similar pattern in vitrinite reflectance but rather suggested that coal ranks increase in proximity to the Spanish Peaks intrusions, a trend which is not apparent on any of the other published coal rank or vitrinite reflectance maps. Other Purgatoire River anomalies include a local abundance of sill intrusions and what appears in satellite imagery to be stressed vegetation. The reason(s) for these anomalies are not apparent but they may be related to the difference in production north and south of the Vermejo Park anticline.

3.1.5 Timing

Subsidence of the Raton basin and deposition of the gas-bearing strata initiated about 80 million years ago, accelerating as thrust faulting worked its way eastward. Cather (2002) suggests that subsidence increased between 72 and 71 million years ago, probably related to an increase in the rate of thrusting. Timing on wrench faulting at the western margin of the basin cannot be constrained, although it was probably concurrent with thrusting. Rio Grand rifting in general began between 27 and 25 million years ago (Miggins et al., 2002), about the same time that intrusion began in the Spanish Peaks area. Johnson et al (1966) and Lindsey et al (1986) report that apatite fission track data suggest that rapid uplift and cooling of the strata began about 19 million years ago, possibly in association with renewed Rio Grande rifting at about 15 million years.

3.1.6 Erosion

A significant but poorly constrained amount of material has been stripped off of the Raton basin by erosion during these periods of uplift. The Spanish Peaks stand up some 6000 ft above the general surface of the surrounding basin; they are intrusives, indicating that they were intruded into strata of at least that thickness that is now missing. Harbour and Dixon (1959) suggest that at least 7000 ft of section has been removed from the overburden of the basin during two phases: late Laramide and post Pliocene. Close and Dutcher (1990) estimate the removed strata to have been somewhat less but at least 5000 ft in thickness, whereas Hemmerich (2001) estimates that some 8000 ft of strata have been removed from the New Mexico portion of the basin.

3.1.7 Stresses

Observations made on the present-day in situ stresses in the Raton basin are presented elsewhere in this report, but some reports have been published by other authors. Stevens et al. (1992) suggested that an east-west maximum horizontal compressive stress prevailed from Laramide time through to Miocene time, when a north-south trending maximum compressive stress developed related to initiation of the Rio Grande rift. The east-west stress is compatible with the background fracture pattern across the basin, and the north-south stress in compatible with measurements of the present-day, in situ stress. Muller, 1986, pegged the stress rotation at 22 million years, or early Miocene, while Close and Dutcher (1990) suggest that the stress rotation occurred somewhat earlier, during the Late Oligocene.

3.2 Implications for Production

The data presented in this report can be used to further the understanding of the hydrocarbon system of the Raton basin and to improve the probabilities of successful drilling for natural gas, but they do not add up to a "drill-here" map. There are just too many variables in the system and the constraints on the variables are too loose. This is highlighted by the geostatistical analyses (chapter 2.8) which show that even an accounting for eight of the different variables that are commonly used to predict and assess production potential is insufficient to fully characterize the wide range in observed production in the Raton basin.

Although discouraging from the exploration standpoint, this highlights the importance of obtaining as much information as possible from wells as they are drilled and from other sources (i.e., seismic) early in a development program in order to successfully drive it. In this respect, the Raton basin study has described a methodology, components of which will assume varying significance in other basins but the whole of which affords a comprehensive and integrated approach to understanding the fracture and stress history of a basin. The relationships documented here can be used to intelligently spot well locations and choose drilling practices, as follows:

1. Structures in the Raton basin such as the Morley and Vermejo Park anticlines are associated with local fracture populations that include both background, thrust-front-normal fractures and good developments of secondary fracture sets trending oblique to the background fractures, and should therefore have good interconnected fracture permeability. Such structures are good exploration targets. Given the origin of these structures as thrust and laccolith-related anticlines, there could be more of them hidden within the basin and gravity surveys might prove to be a good exploration tool.

2. The oblique relationship between east-west background fracture strikes and the north-south present-day maximum horizontal compressive stress is not reason enough to predict that the in situ fractures have been or will be squeezed shut and would therefore be ineffective permeability mechanisms. The wellbore-image logs suggest that east-west striking fracture apertures are not any narrower than the apertures of north-south fractures, and in fact the apertures do not decrease with the increasing confining stresses at deeper horizons in any of the four wells for which data are available. Either the prevailing stress magnitudes (which were not measured) are insufficient to cause fracture closure, or the rock within which the fractures occur is sufficiently stiff that the fracture apertures are not particularly sensitive to changes in stress magnitudes. This suggests that fracture-related permeability will not significantly diminish under stress changes caused by decreasing pore pressures during production. This is particularly true since drawdown of the already low in situ pore pressures should not cause significant changes in the in situ effective stress magnitudes.

3. The regional, background fracture pattern is approximately east-west, which means that north-south laterals from horizontal wells would be most effective in intersecting the most fractures. However, there are parts of the basin, such as along the wrench fault between the Tercio and Vermejo Park anticlines and perhaps closer to the western margin of the basin, where north-south striking regional fractures seem to dominate. Recognition of the

existence of these local structural and fracture domains allows an operator to optimally orient horizontal wellbore azimuths and to spot vertical step-out wells according to the local conditions.

4. The placement of step-out wells relative to existing wells is a problem in any play. The Raton geostatistical study suggests that in areas of high anisotropy in the similarity of production characteristics (which is not the same thing as an anisotropy in drainage area), a step-out well from a poor producer has a higher probability of good production if it is offset along the narrow axis of anisotropy, whereas a step-out from a good producer is more likely to also have good production if it is offset along the long axis of the ellipse. This tactic must be played carefully against knowledge of fracture-controlled elliptical drainage patterns, where step-out well locations in drained areas should be avoided. Placement of step-outs is less critical in areas of relatively isotropic lateral variability in production characteristics.

5. The highly fractured dikes and sills that cut through the basin and the enhanced fracturing in the strata in the adjacent strata are probably responsible for venting gas to the atmosphere over geologic time and leaving the basin in its present, underpressured condition. Anecdotal reports indicate that gas is being produced locally from completions within the igneous units, but the low igneous matrix permeabilities suggest that these completions are probably also connected to other, conventional reservoir units. Similar dikes and sills are present in other Rocky Mountain basins although not in such profusion, and they are probably not good reservoir targets.

6. Fracture spacing in reservoir sandstones is log-normal, meaning that there are few widely spaced fractures and significantly more closely spaced fractures. The ultimate in close fracture spacing is a fracture swarm, commonly associated with a fault or incipient fault. Fracture swarms make good reservoirs as long as they have not tapped large water reservoirs in deeper parts of the stratigraphic section, but they are hard to locate prior to drilling.

7. Fractures are present in all lithologies at reservoir depths. The core and image-log data show that significant fracturing is present in the subsurface shales: such fracturing is either obscured by weathering or not present in outcrops, and outcrop studies therefore do not lend themselves to good shale fracture studies.

8. In the Raton basin it appears that fractures in these fine-grained strata are open and conductive at depth, providing potential paths of communication between adjacent sandstone reservoirs. In fact, the average relative fracture widths in shales, as measured from image logs, are greater than they are in any other lithology. This condition is not apparent in other Rocky Mountain basins where fractures in the muddy intervals are typically poorly developed and, where present, closed by high magnitude in situ confining stresses. The difference may have to do with shallower Raton depths of interest as well as with the high degree of tectonism and resulting internal deformation within the strata that fill the Raton basin.

9. Plan-view conjugate shear fractures are present in several parts of the stratigraphic succession, including within the Raton Conglomerate, the Dakota Sandstone, and limestones of the Fort Hayes Member of the Niobrara Formation at various locations in the Raton basin. Conjugate fractures have the potential to be highly interconnected and their presence should significantly enhance the quality of a reservoir. The conjugate fractures in the Dakota sandstone are both good and bad, however: at the western margin of the basin they have developed as deformation bands, i.e., shear features that degrade rather than enhance permeability. On the eastern margin of the basin, stress and depth of burial conditions in the Dakota sandstone were such that good, intersecting, high permeability fracture conduits developed. Modeling of the stress conditions and rock properties as presented here, can point to the conditions under which the desirable types of conjugate fractures rather than deformation bands developed, leading to a rationale for targeting conjugate fractures at depth. Conversely, outcrop observations provide constraints on such modeling as well as the basic data to put into models.

10. Syn-sedimentary deformation seems to be more common, or rather, perhaps, more obvious, in the Raton basin than in other Rocky Mountain basins. This deformation has controlled the orientations of many of the fluvial lenticular sandstone reservoir bodies, turning them to strike across the regional paleo-slope and 90 degrees to their expected trend. In following such reservoir trends it is useful to know that such potential quirks exist.

11. Similarly, there are many horizontal and sub-horizontal thrust planes that cut the section. These planes formed both during and after sedimentation, are difficult to recognize in wellbores, even when image logs and cores are available. They may be important as permeability conduits, and they controlled local fracture populations, local stress orientations, and commonly, sedimentary distribution patterns as noted above.

12. Hydraulic stimulation fractures grow in the direction parallel to the maximum horizontal compressive stress except where the horizontal stress anisotropy is low, in which case local planes of weakness such as faults and natural fractures can control the direction of hydraulic fracture growth. The horizontal stress anisotropy is an unknown in the Raton basin, but it is reasonable to expect it to be relatively small given the observed stress rotation and the absence of north-south compressive structures. Hydraulic fractures should propagate in a north-south direction, parallel to the observed present-day maximum horizontal compressive stress, but given the predominant east-west fracture orientations, there should be significant hydraulic fracture tortuosity as these stimulation fractures jog and side step as they cross the natural fractures. This can be a good way to access the natural fracture permeability, but it can also lead to stimulation fractures that do not reach as far into the formation as planned due to the extra energy consumed in propagating irregular fractures. In the vicinity of VPCH-33 however, where the hydraulic fractures should propagate parallel to the dominant natural fracture trend, it will be easier to inject the hydraulic fracture as it follows and exploits pre-existing planes of weakness. However, the hydraulic fracture may not access regions of the reservoir that would have been drained by the natural fracture system anyway.

3.3 Environmental Considerations

Several environmental issues exist with production of coal bed methane. These include construction of facilities, noise, access to well sites, number and spacing of wells, size of the well pad, production and disposal of water, and draw down of water tables. There are also possible benefits to production of good quality water for irrigation and possible sequestration of green house gases (CO_2) during an enhanced recovery phase. Possible working solutions to mitigate or reduce the impact of CBM production on the environment are discussed below.

In other Rocky Mountain basins, such as the San Juan Basin, each major productive stratigraphic unit has been developed at a separate stage in resource development. As a result, most areas have required a separate set of wells for each major gas-producing layer. For example, in the San Juan Basin, separate wells are used to produce gas from vertically arrayed rock layers such as Fruitland coals, Pictured Cliffs sandstones, and Dakota sandstones. These three rock units are present throughout the same geographic area of the basin at different depths but each has been developed separately. Work done during the course of this project indicates that simultaneous development of multiple producing horizons using the same boreholes for production of methane from coalbeds as well as tight, naturally fractured sandstones would reduce the total number of wells needed to extract gas from the basin, with a resulting reduction in the need for drill pads and haul roads.

Another approach to drilling and accessing producing intervals is directional drilling. Using this report to review the type and orientation of fracture most likely to be encountered at a particular site in the basin, a well could be designed to enter the producing interval and to intersect the greatest number of fractures. This approach has the benefit of draining a large area and enhancing production. This approach could also be used to drill under large scale obstacles such as large scale structures negating the need for roads and pipeline into topographically challenging areas. One such area on the Vermejo Park Ranch property could be the Ash Mountain area south and west of the Castle Rock Park production area. Wells could be placed along the perimeter of Ash Mountain within the already sited areas of Castle Rock Park and drill under the mountain negating the need for additional surface disturbances such as well pads, roads, pipelines, and electric lines on Ash Mountain itself but nevertheless recovering the reserves in that area.

To mitigate water issues it would be best to have several observation wells to obtain a continuing database of water levels and quality across an area of interest. Many variables can lower water level besides production such as drought or minimal snow pack. Thus gathering data over a long period of time starting well before production begins till long after production has ceased is recommended. This approach could allow water related issues and problems to be addressed and solved earlier rather than later.

In environmentally sensitive areas, such as the Raton Basin, the use of 2D seismic data rather than the more invasive 3-D seismic would minimize surface disturbances. This approach has the benefit of also being much less expensive. However, such an effort would require a approach similar to that used in this report of integrating surface, well log, core and production and tectonic modeling to fill in that missing third dimension of seismic data. In areas of fracture controlled production these types of data can be more valuable than seismic data. This is in part due to the fact seismic methods cannot directly record data from or measure fractures.

An understanding of the reservoir and its associated fracture system as provided in this report can help in future enhanced recovery programs or carbon sequestration efforts. Enhanced understanding of the directional nature of fluid flow will allow CO_2 to be safely and efficiently sequestered and used to enhance recovery of the methane resource.

The methodology outlined in this report can be used to maximize the extractable volume of gas in any basin while decreasing the number of boreholes needed to produce this gas. This creates the opportunity to minimize surface disturbances associated with natural gas production while actually increasing the economic viability of a basin.

4.0 RECOMMENDATIONS FOR FUTURE WORK

The Raton basin still has secrets. The hydrocarbon content and reservoir potential of the stratigraphic section below the Trinidad-Vermejo-Raton formations are largely untested, and although these deeper strata crop out at the edges of the basin, their fracture characteristics have not been extrapolated into the deep subsurface via modeling and they have not been sampled by numerous cores or logs.

The relative importance of strike-slip vs. overthrust motion at the western margin of the basin has still to be assessed and the effects of this type of combined structure on stresses and fractures on the basin-filling strata remain speculative.

The presence of what appears to be strike-slip faulting, splaying off the thrust front along the western margin of the basin and running beneath the Tercio anticline, ultimately connecting it with Vermejo Park anticline where it abruptly terminates, was largely unsuspected until late in study, and its origin, as well as its effects on the nearby fracture patterns, should be more fully assessed. The few data available from the vicinity of this structure come from a single wellbore-image log, but they suggest that there are significantly anomalous fracture characteristics in that region. A short field study should be carried out to document whether, and if so, how, the fracture patterns vary as strata are affected by the underlying fault zone. Given unlimited funds, a modern, three-dimensional seismic coverage would be ideal for documenting the presence and extent of this and similar structures.

This work has documented the presence of both vertical and lateral fracture domains within the basin, but the extents and limits of these domains are still poorly defined. Assessments of the fracture distributions and orientations, and of stress characteristics, should be continued via coring and logging programs, at least until such time as the extent of variability in these characteristics and the reasons for it become apparent. The in situ stress magnitudes have not been measured, and although they can be estimated for a given depth and pore pressure, the magnitude of the anisotropy in the present day horizontal stresses, the presence of which is so obvious from the geophysical logs, can only be guessed at. Stress magnitudes generally control fracture permeability, and are there fore also important inputs for both reservoir and tectonic models.

Logging core is a labor- and time-intensive undertaking, but fractures in more of the numerous cores from the basin should be assessed statistically. The distributions of different fracture types by lithology have been assessed for individual wells, but the inter-well differences or similarities in those distributions, and kinematic reconstructions based on fracture characteristics and distributions, have not been attempted.

The possibility of obtaining core and a wellbore-image log from the same hole is a project that we discussed with El Paso Production Company but the timing, funding, and logistics never meshed. Such a comparison would have calibrated the image logs, allowing a better distinction between induced and natural fractures. It would also have quantified the fracture aperture signatures and allowed recognition of shear vs. extension fractures in the logs.

The geostatistical approaches started here can and should be continued as they hold the promise of being able to assess production variability. Such assessments can be relatively blind, i.e., predictions made on the basis of observed trends but in the absence of an understanding of the reasons for that variability and those trends, but they can also be used to support and to advance the geological insights and understandings of the reservoir systems.

This study has not seriously addressed the reasons for significant differences in volume of co-produced formation water from the gas wells on the northeast vs. the southwest side of the Vermejo Park anticline. Several potential reasons for this difference have been considered, including differences in depth to production, local faults that may introduce meteoric waters to the formations at depth, differences in topographic relief, and local seals within the producing horizons, but none of these factors have been rigorously assessed, in large part because the data base is not well enough defined to support rigorous investigation. For example, production records are for the whole producing interval in a given well: they do not, because it is not economically feasible, isolate individual gas-producing zones for testing and monitoring. However, it may be possible to instrument several dedicated closely spaced wells and subdivide the production horizons by zone, monitoring production of gas and water under different conditions, and looking for inter-well interference in a controlled manner.

Further basin modeling efforts would include plan-view, lateral distributions of irregular boundaries, stress trajectories, and strains, and would provide predictions for the lateral distributions of fracture susceptibility and orientations. Such a modeling effort would better integrate the rock-mechanics models of strains, and would use log and outcrop observations of fractures and stresses as known tie points to constrain the model. Further research into the production characteristics of the wells drilled into the basin could concentrate on trying to tie known production variability to various geologic characteristics.

Much of the present work has concentrated on the southern, New Mexican half of the Raton basin as a matter of efficiency. Access to large tracts of land containing many significant outcrops was easily obtained from a single landowner (the Vermejo Park Ranch), and the surface land ownership overlaps nicely with the mineral rights holdings of a single company (El Paso

Production Company) which has been more than generous in sharing production and logging data. Continued work in the basin should expand northward into Colorado, where similar numbers of reserves are present. Evergreen, recently bought by Pioneer Natural Resources, was the major holder of mineral rights in this area; Evergreen had been unresponsive to our efforts to work with them but Pioneer might be more approachable. However, patchwork surface ownership by numerous private individuals seriously complicates outcrop examinations.

5.0 ACKNOWLEDGEMENTS

This study has been funded by Sandia's internal Lab Directed Research and Development (LDRD) program. It was proposed, funded, and started at a time when California was suffering from rolling brown-outs and local blackouts, a probable forerunner of future energy shortages. We would like to express appreciation to the LDRD office for continued support for the three year project, and for the vision to see that research in fossil energy will be critical to maintaining the US energy supply levels for the next few decades while we develop the technology for alternative energy sources. In addition, we would like to thank the U.S. Department of Energy, National Energy Technology Laboratory (Tom Mroz, Project Manager), which supported a separate but related study of the sedimentological aspects of the Raton basin, part of which is reported here as a matter of efficiency and of combining all studies from the basin into one volume.

This study could not have proceeded without the assistance of the El Paso Production Company, in particular Paul Basinski. While cautious and deliberate in the release of data, El Paso gave us unlimited access to their cores, logs, and production and seismic data. These gave us invaluable insights into the third dimension, without which this study would have been severely hampered and limited in scope.

Personnel at the Vermejo Park Ranch, in particular Rich Larsen and Gus Holm, shared their considerable knowledge of the local geology and geography, and in addition provided invaluable access to the ranch holdings on the southern Raton basin. This gave us the ability to compare outcrops across a wide area and vastly improved the scope and efficiency of the field work effort. We were also lucky enough early in the project to participate in a field trip led by Chuck Pillmore (USGS, now deceased), who shared much of his vast experience in the basin.

Contractors Dr. Connie Knight and Mr. Ron Graichen are thanked for diligent logging of the cores as reported here, and Dr. Knight for pursuing the core fracture analyses. We thank Dr. David Holcomb and Dr. Norman Warpinski for their through and insightful reviews of this report.

6.0 REFERENCES/BIBLIOGRAPHY

Anderson, E. M., 1951, The Dynamics of Faulting and Dyke Formation with Applications to Britain: Oliver and Boyd, London, 206 p.

Antonellini, M., and Aydin, A., 1994, Effect of faulting on fluid flow in porous sandstones: Petrophysical properties: American Association of Petroleum Geologists Bulletin, v. 78, p. 355-377.

Antonellini, M., Aydin, A., and Pollard, D. D., 1994, Microstructure of deformation bands in porous sandstones at Arches National Park, Utah: Journal of Structural Geology, v. 16, p. 941-959.

Applegate, J.K., and Rose, P.R., 1985, Structure of the Raton basin from a regional seismic line; in Gries, R.R., and Dyer, R.C., eds., Seismic exploration of the Rocky Mountain region: Denver, Rocky Mountain Association of Geologists and Denver Geophysical Society, p. 259-266.

Arnold, B.W., M. Herrin, and P. Basinski, 2004, Statistical and geostatistical analyses of coal-bed methane production in the Raton Basin, New Mexico and Colorado (abstract), American Association of Petroleum Geologists 2004 Annual Convention, April 18-21, Dallas, TX.

Baltz, E.H., 1965, Stratigraphy and history of Raton Basin and notes on San Luis Basin, Colorado-New Mexico: American Association of Petroleum Geologists Bulletin, v. 49, no. 11, p. 2041-2075.

Billingsley, L.T., 1977, Stratigraphy of the Trinidad Sandstone and associated formations Walsenburg area, Colorado, in Veal, H.K., ed., Exploration Frontiers of the Central and Southern Rockies: Rocky Mountain Association of Geologists Guidebook, p. 235-246.

Blanford, M. L., Heinstein, M. W., Key, S. W., September 2001,"JAS3d A Multi-Strategy Iterative Code for Solid Mechanics Analysis Users' Instructions, Release 2.0", SANDxx-0000, Sandia National Laboratories, Albuquerque, NM.

Brister, B.S., and Gries, R.R., 1994, Tertiary stratigraphy and tectonic development of the Alamosa basin (northern San Luis Basin), Rio Grande rift, south-central Colorado, in Keller, G.R., and Cather, S.M., Basins of the Rio Grande Rift: Structure, Stratigraphy, and Tectonic Setting, Geological Society of America Special Paper 291, p.39-58.

Brill, K.G., 1952, Stratigraphy of the Permo-Pennsylvanian zeugogeosyncline of Colorado and northern New Mexico: Geological Society of America Bulletin, v. 63, p. 809-880.

Byerlee, J. D., Friction of rocks, *Pageoph* 116, 615-, 1978.

Carter, D.A., 1956, Coal deposits of the Raton Basin, in McGinnis, C.J., ed., Geology of the Raton Basin, Colorado: Rocky Mountain Association of Geologists Guidebook, p. 89-92.

Clark, K.F., 1966, Geology of the Sangre de Cristo Mountains and adjacent areas, between Taos and Raton, New Mexico, in Northrop, S.A., and Read, C.B., eds., New Mexico Geological Society Seventeenth Field Conference Guidebook of the Taos—Raton--Spanish Peaks Country, New Mexico and Colorado, p. 57-65.

Close, J.C., 1988, Coalbed methane potential of the Raton Basin, Colorado and New Mexico: Southern Illinois University at Carbondale, Ph.D. dissertation, 432p.

Close, J.C., and Dutcher, R.R., 1990, Update on coalbed methane potential of Raton Basin, Colorado and New Mexico: Society of Petroleum engineers, Proceedings, 65th Technical Conference, SPE Paper 20667, p.497-512.

Close, J.C., and Dutcher, R.R., 1990, Prediction of permeability trends and origins in coalbed methane reservoirs of the Raton Basin, New Mexico and Colorado, in Bauer, P.W., and others, eds., Tectonic development of the southern Sangre de Cristo Mountains, New Mexico: New Mexico Geological Society Guidebook, Forty-First Field Conference, p.387-395.

Cooper, S.P., Lorenz, J.C., and Goodwin, L.B., 2001, Lithologic and structural controls on natural fracture characteristics Teapot Dome, Wyoming: Sandia National Laboratories Technical Report, SAND2001-1786, 73p.

Cooper, S. P., June 26, 2002, "Raton Basin", *Xcel* spreadsheet file attached to e-mail.

CUBIT Development Team, April 18, 2000,"CUBIT Mesh Generation Environment Volume 1: Users Manual", SAND94-1100, Sandia National Laboratories, Albuquerque, NM.

Delaney, P.T., Pollard, D.D., Ziony, J.I., and McKee, E.H., 1986, Field relationships between dikes and joints: emplacement processes and paleostress analysis: Journal of Geophysical Research v. 91, p. 4920-4938.

Desai, C. S., Siriwardane, H. J., 1984,"Constitutive Laws for Engineering Materials with Emphasis on Geologic Materials", Prentice-Hall Inc.,Englewood Cliffs, NJ.

Deutsch, C.V. and A.G. Journal, 1998, GSLIB Geostatistical Software Library and User's Guide, Oxford University Press, New York, second edition.

Dickinson, W.R., Klute, M.A., Hayes, M.J., Janecke, S.U., Lundin, E.R., McKittrick, M.A., and Olivares, M.D., 1988, Paleogeographic and paleotectonic setting of Laramide sedimentary basins in the central Rocky Mountain region: Geological Society of America Bulletin, v. 100, p. 1023-1039.

Dolly, E. D., and Meissner, F. F., 1977, Geology and gas exploration potential, Upper Cretaceous and Lower Tertiary strata, northern Raton basin, Colorado, Exploration frontiers of the central and southern Rockies: Rocky Mountain Association of Geologists Field Conference Guidebook, p. 247-270.

Domenico, P.A. and F.W. Schwartz, 1990, Physical and Chemical Hydrogeology, John Wiley and Sons, New York.

Dunn, D. D., LaFountain, L. J., and R. E. Jackson, Porosity dependence and mechanism of brittle fracture in sandstones, *J. Geophys. Res.* 78, 2403-2417, 1973.

Elkins, L. F., and Skov, A. M., 1960, Determination of fracture orientation from pressure interference: Petroleum Transactions, American Institute of Mining Engineers, v. 219, p. 301-304.

Epis, R.C., and Chapin, C.E., 1975, Geomorphic and tectonic implications of the post-Laramide, late Eocene erosion surface in the southern Rocky Mountains, in Geological Society of America Memoir 144, p. 45-74.

Flores, R.M., 1987, Sedimentology of Upper Cretaceous and Tertiary siliciclastics and coals in the Raton Basin, New Mexico and Colorado, in Lucas, S.G., and Hunt, A.P., eds., Northeastern New Mexico: New Mexico Geological Society 38th Annual Field Conference, p. 255-264.

Flores, R.M., and Tur, S.M., 1982, Characteristics of deltaic deposits in the Cretaceous Pierre Shale, Trinidad Sandstone, and Vermejo Formation, Raton Basin, Colorado: The Mountain Geologist, v.19, no. 2, p. 25-40.

Flores, R.M., and Pillmore, C.L., 1987, Tectonic control on alluvial paleoarchitecture of the Cretaceous and Tertiary Raton Basin, Colorado and New Mexico, in Ethridge, F.G., Flores, R.M., and Harvey, M.D., eds., Recent developments in Fluvial Sedimentology: Society of Economic Paleontologists and Mineralogists Special Publication 39, p. 311-321.

Flores, R.M., and Bader, L.R., 1999, A summary of Tertiary coal resources of the Raton Basin, Colorado and New Mexico, in Resource assessment of selected Tertiary coal beds and zones in the Northern Rocky Mountains and Great Plains region, United States Geological Survey Professional Paper 1625-A, p. SR1-SR35.

Geldon, A.L., 1989, Ground-water hydrology of the central Raton Basin, Colorado and New Mexico: U.S. Geological Survey, Water-Supply Paper 2288, 81p.

Haan, C., 1994, Statistical Methods in Hydrology, Iowa State University Press, sixth printing. Harbour, R.L., and Dixon, G.H., 1959, Coal Resources of the Trinidad-Aguilar area, Las Animas and Huerfano counties, Colorado: U.S. Geological Survey, Bulletin 1072-G, p. 445-489.

Hemborg, H.T., 1998, Spanish Peak Field, Las Animas County, Colorado: Geologic Setting and Early Development of a Coalbed Methane Reservoir in the Central Raton Basin: Colorado Geological Survey Resource Series 33, p. 1-34.

Hemmerich, M., 2001, Cenozoic denudation of the Raton Basin and vicinity, northeastern New Mexico and southeastern Colorado, determined using apatite fission-track Thermochronology and Sonic Logs Analysis: New Mexico Institute of Mining and Technology, Master’s thesis report, 75p. plus appendices.

Hoffman, G., and B. Brister, 2003, New Mexico's Raton Basin coalbed methane play: New Mexico Geology, v. 25, p. 95-110.

Howard, W.B., 1982, The hydrogeology of the Raton Basin, south-central Colorado: Indiana University, Master's thesis, 95p.

Hubbert, M. K., and D. G. Willis, 1957, Mechanics of hydraulic fracturing: Petrol. Trans. AIME, vol. 210, 153–166.

Hugmann, R. H. H., III, and M. Friedman, Effects of texture and composition on mechanical behavior of experimentally deformed carbonate rocks, Amer. Assoc. Petrol. Geol. Bull. 63, 1478-1489, 1979.

Issacs, E.H. and R.M. Srivastava, 1989, An Introduction to Applied Geostatistics, Oxford University Press, New York.

Jaeger, J. C., and N. G. W. Cook, 1969, Fundamentals of Rock Mechanics: Chapman and Hall, London, 585 p.

Johnson, R.B., 1961, Patterns and origin of radial dike swarms associated with West Spanish Peak and Dike Mountain, south-central Colorado: Geological Society of America Bulletin, v. 72, p. 579-590.

Johnson, R.B., 1968, Geology of the igneous rocks of the Spanish Peaks region, Colorado: U.S. Geological Survey Professional Paper 594-G, p. 1-47.

Johnson, R.B., and Baltz, E.H., 1960, Probable Triassic rocks along eastern front of Sangre de Cristo Mountains, south-central Colorado: American Association of Petroleum Geologists, v. 44, no. 12, p. 1895-1902.

Johnson R.B., and Wood, G.H., Jr., 1956, Stratigraphy of Upper Cretaceous and Tertiary rocks of Raton Basin, Colorado and New Mexico: American Association of Petroleum Geologists Bulletin, V.40, no. 4, p. 707-721.

Johnson, R.B., Dixon, G.H., and Wanek, A.A., 1966, Late Cretaceous and Tertiary stratigraphy of the Raton Basin of New Mexico and Colorado, in Northrop, S.A., and Read, C.B., eds., Guidebook of Taos-Raton-Spanish Peaks Country, New Mexico and Colorado: New Mexico Geological Society 17th Field Conference, p. 88-98.

Johnson, R.C., and Finn, T.M., 2001, Potential for Basin-Centered Gas Accumulation in the Raton Basin, Colorado and New Mexico, in Nuccio, V.F., and Dyman, T.S., eds., Geologic Studies of Basin-Centered Gas Systems: United States Geological Survey Bulletin 2184-B, p. 1-14.

Jurich, D., and Adams, M.A., 1984, Geologic overview, coal and coalbed methane resources of Raton Mesa region, Colorado and New Mexico, in Rightmire, C.T., Eddy, G.E., and Kirr, J.N., eds., Coalbed Methane Resources of the United States: American Association of Petroleum Geologists Studies in Geology Series 17, p. 163-184.

Kauffman, E.G., 1977, Geological and biological overview – Western Interior Cretaceous basin, in Kauffman, E.G., ed., Cretaceous facies, faunas, and paleoenvironments across the Western Interior basin: The Mountain Geologist, v.6, p. 227-245.

Keefe, R. G., June 24, 2002,"2D stratigraphic column data", e-mail.

Kirby, S. H., and J. W. McCormick, Inelastic properties of rocks and minerals: strength and rheology, Chap. 3, p. 139-280, in: CRC Handbook of Physical Properties of Rocks. Ed. Robert S. Carmichael, CRC Press, 1984.

Kluth, C.F., and Schaftenaar, C.H., 1994, Depth and geometry of the northern Rio Grande rift in the San Luis Basin, south-central Colorado, in Keller, G.R., and Cather, S.M., Basins of the Rio Grande Rift: Structure, Stratigraphy, and Tectonic Setting, Geological Society of America Special Paper 291, p.27-37.

Knopf, A., 1936, Igneous geology of the Spanish Peaks region, Colorado: Geological Society of America Bulletin, v. 47, p. 1727-1784.

Law, B. E., and Dickinson, W.W., 1985, Conceptual model for origin of abnormally pressured gas accumulations in low-permeability reservoirs: American Association of Petroleum Geologists Bulletin, V.69, p. 1295-1304.

Lee, W.T., 1917, Geology of the Raton Mesa and other regions in Colorado and New Mexico, in Lee, W.T., and Knowlton, F.H., eds., Geology and paleontology of the Raton Mesa and other regions in Colorado and New Mexico: U.S. Geological Survey Professional Paper 101, p. 9-37.

Lee, W.T., 1924, Coal resources of the Raton coal field, Colfax County, New Mexico, United States Geological Survey Bulletin 752, 254p.

Lindsey, D.A., Andriessen, P.A.M., and Wardlaw, B.R., 1986, Heating, cooling, and uplift during Tertiary time, northern Sangre de Cristo range, Colorado: Geological Society of America Bulletin, v. 97, p. 1133-1143.

Long, J. C. S., A. Aydin, S. R. Brown, H. H. Einstein, K. Hestir, P. A. Hsieh, L. R. Myer, K. G. Nolte, D. L. Norton, O. L. Olsson, F. L. Paillet, J. L. Smith, and L. Thomsen, 1997, Rock Fracture and Fluid Flow, Washington, D.C., National Academy Press, 551p.

Lorenz, J.C., and Cooper, S.P., 2001, Tectonic setting and characteristics of natural fractures in Mesaverde and Dakota Reservoirs of the San Juan Basin, New Mexico and Colorado, Sandia National Laboratories Technical Report, SAND2001-0054, 77p.

Lorenz, J. C., Cooper, S. P., 2001, Interpreting fracture patterns in sandstones interbedded with ductile strata at Salt Valley Anticline, Arches National Park, Utah, Sandia National Laboratories, Albuquerque, NM, SAND Report, SAND2001-3517, 26p.

Lorenz, J. C., and Finley, S. J., 1991, Regional fractures II: Fracturing of Mesaverde Reservoirs in the Piceance Basin, Colorado: American Association of Petroleum Geologists Bulletin, v. 75, p. 1738-1757.

Lorenz, J. C., and Hill, R. E., 1991, Subsurface fracture spacing: comparison of inferences from slant/horizontal core and vertical core in Mesaverde reservoirs: Society of Petroleum Engineers Paper 21877: Joint Rocky Mountain Section Meeting and Low-Permeability Reservoir Symposium, p. 705-716.

Merry, R.D., and Larsen, V.E., 1982, Geologic investigations of the methane potential of western U.S. coalbeds: Gas Research Institute Project CE-807083, 155p.

Meissner, F.F., 1980, Examples of abnormal fluid pressure produced by hydrocarbon generation: American Association of Petroleum Geologists Bulletin, v. 65, p. 749.

Meissner, F.F., 1981, Abnormal pressures produced by hydrocarbon generation and maturation and their relationship to processes of migration and accumulation: American Association of Petroleum Geologists Bulletin, v. 65, p. 2467.

Merin, I.S., Everett, J.R., and Rose, P.R., 1988, Tectonic evolution and structural geology of the Raton Basin, Colorado, in Sloss, L.L., ed., Sedimentary cover – North American Craton, U.S.: Geological Society of America, Decade of North American Geology, v. D-2, p. 170-179.

Muller, O.H., 1986, Changing stresses during emplacement of the radial dike swarm at Spanish Peaks, Colorado: Geology, v. 14, p. 157-159. Muller, O.H., and Pollard, D.D., 1977, The stress state near Spanish Peaks, Colorado, determined from a dike pattern: Pure and Applied Geophysics, V. 115, p. 69-86.

Nelson, R. A., 1985, Geologic analysis of naturally fractured reservoirs, Contributions in petroleum geology and engineering: Houston, Gulf Publishing Company, 360 p.

Nuccio, V. F., 2002, Coalbed Methane--"What is it"--"Where Is It"--"And Why All the Fuss?" in S. D. Schwochow, and V. F. Nuccio, eds., Coalbed Methane of North America II, Rocky Mountain Association of Geologists.

Odé, H., 1957, Mechanical analysis of the dike pattern of the Spanish Peaks area, Colorado: Geological Society of America Bulletin, v. 68, no. 5, p. 567-576.

Olsson, W. A., Grain size dependence of yield stress in marble*, J. Geophys. Res*. 79, 4859-4862, 1974.

Penn, B.S., Lindsey, D.A., 1996, Tertiary Igneous Rocks and Laramide Structure and Stratigraphy of the Spanish Peaks Region, South-Central Colorado: Road Log and Descriptions from Walsenburg to La Veta (First Day) and La Veta to Aguilar (Second Day): Colorado Geological Survey Department of Natural Resources Open-File Report 96-4, Field Trip No. 28, (not consecutively numbered).

Peng, S. S., 1978, Coal Mine Ground Control: John Wiley & Sons, 450 p.

Peng, S., and A. M. Johnson, 1972, Crack growth and faulting in cylindrical specimens of Chelmsford granite: International Journal of Rock Mechanics and Mining Science, v. 9, p. 37-86.

Pillmore, C.L., 1969, Geology and coal deposits of the Raton coal field, Colfax County, New Mexico: The Mountain Geologist, v. 6, no. 3, p. 125-142.

Pillmore, C.L., 1976, Commercial coal beds of the Raton coal field, Colfax County, New Mexico, in Ewing, R.C., and Keus, B.S., eds., Guidebook to Vermejo Park Northeastern New Mexico: New Mexico Geological Society Guidebook, Twenty-Seventh Field Conference, p. 227-247.

Pillmore, C.L., 1976, The York Canyon coal bed, in Ewing, R.C., and Keus, B.S., eds., Guidebook to Vermejo Park Northeastern New Mexico: New Mexico Geological Society Guidebook, Twenty-Seventh Field Conference, p. 249-251.

Pillmore, C.L., and Flores, R.M., 1984, Field Guide and discussion of coal deposits, depositional environments and the Cretaceous-Tertiary boundary, southern Raton Basin, in Lintz, J., Jr., ed., Western Geological Excursions: Geological Society of America Annual Meeting Guidebook, v.3, p. 1-51.

Pillmore, C.L., 1991, Geology and coal resources of the Raton coal field, in Molina, C.L., Jobin, D.A., O'Connor, J.T., and Kottlowski, F.E., Coalfields of New Mexico: Geology and Resources: U.S. Geological Survey, Bulletin 1972-D, p. 46-68.

Pillmore, C.L., and Hatch, J.R., 1976, Geochemical data on selected coal beds, Raton coal field, Colfax County, New Mexico: U.S. Geological Survey Open-File Report 76-542, 26 p.

Pillmore, C.L., and Flores, R.M., 1987, Stratigraphy and depositional environments of the Cretaceous-Tertiary boundary clay and associated rocks, Raton Basin, New Mexico and Colorado, in Fassett, J.E., and Rigby, J.K., Jr., eds., The Cretaceous-Tertiary boundary in the San Juan and Raton Basins, New Mexico and Colorado: Geological Society of America Special Paper 209, p. 111-130.

Pillmore, C.L., and Maberry, J.O., 1976, The depositional environment and trace fossils of the Trinidad Sandstone, southern Raton Basin, New Mexico, in Ewing, R.C., and Keus, B.S., eds., Guidebook to Vermejo Park Northeastern New Mexico: New Mexico Geological Society Guidebook, Twenty-Seventh Field Conference, p. 191-195.

Pollard, D. D., and A. Aydin, 1988, Progress in understanding jointing over the past century: Geological Society of America Bulletin, v. 100, p. 1181-1204.

Podwysocki, M.H. and Dutcher, R.R., 1971, Coal dikes that intrude lamprophyre sills, Purgatoire river valley, Colorado: Economic Geology, v. 66, p. 267-280.

Price, N. J., *Fault and Joint Development*, Pergammon, Oxford, 1966.

Read, C.B., and Wood Jr., G.H., 1947, Distribution and correlation of Pennsylvanian rocks in the late Paleozoic sedimentary basins of northern New Mexico: Journal of Geology, v. 55, p. 220-236.

Roehler, H.W., and Danilchik, 1980, *in* Carter, L.M., eds., Proceedings of the fourth Symposium on the Geology of Rocky Mountain Coal, Colorado Geological Survey Resource Series 10, p. 13.

Rose, P.R., Everett, J.R., and Merin, I.S., 1986, Potential basin-centered gas accumulation in Cretaceous Trinidad Sandstone, Raton Basin, Colorado, in Spencer, C.W., and Mast, R.F., eds., Geology of Tight Gas Reservoirs: American Association of Petroleum Geologists Studies in Geology Series 24, p. 111-128.

Sales, J.K., 1983, Collapse of Rocky Mountain basement uplifts, in Lowell, J.D., ed., Rocky Mountain foreland basins and uplifts: Rocky Mountain Association of Geologists, p.70-97.

Scott, G.R., Wilcox, R.E. and Mehnert, H.H., 1990, Geology of volcanic and subvolcanic rocks of the Raton-Springer area, Colfax and Union Counties, New Mexico: U.S. Geological Survey Professional Paper, 1507, 58 p.

Speer, W.R., 1976, Oil and gas exploration in the Raton Basin, in Ewing, R.C., and Kues, B.S., eds., Guidebook of Vermejo Park, northeastern New Mexico, New Mexico Geological Society Guidebook, Twenty-Seventh Field Conference, p. 217-226.

Spencer, C.W., 1987, Hydrocarbon generation as a mechanism for overpressuring in the Rocky Mountain region: American Association of Petroleum Geologists Bulletin, v.71, p. 368-388.

Spencer, C.W., 1989, Review of characteristics of low-permeability gas reservoirs in Western United States: American Association of Petroleum Geologists Bulletin, v. 73, no.5, p. 613-629.

Steven, T.A., 1975, Middle Tertiary volcanic field in the southern Rocky Mountains, in Curtis, B.F., ed., Cenozoic History of the Southern Rocky Mountains: Geological Society of America Memoir 144, p. 75-94.

Stevens, S.H., Lombardi, T.E., Kelso, B.S., and Coates, J.M., 1992, A geologic assessment of natural gas from coal seams in the Raton and Vermejo Formations, Raton Basin: Advanced Resources International, Inc., topical report prepared for the Gas Research Institute under contract no. 5091-214-2316, GRI 92/0345, 84 p.

Stone, C. M., 1995,"SANTOS - A Two-Dimensional Finite Element Program for Quasistatic Large Deformation, Inelastic Response of Solids", SAND90-0543, Sandia National Laboratories, Albuquerque, NM.

Strum, S., 1985, Lithofacies and depositional environments of the Raton formation (Upper Cretaceous-Paleocene) of northeastern New Mexico: North Carolina State University M.S. thesis, 81 p.

Teufel, L. W., and Farrell, H. E., 1992, Interrelationship between in situ stress, natural fractures, and reservoir permeability anisotropy: A case study of the Ekofisk Field, North Sea, In Proceedings of Fractured and Jointed Rock Conference, Lake Tahoe, Ca, June 3-5, 1992, not consecutively numbered.

Timoshenko, S. P., and J. N. Goodier, *Theory of Elasticity*, McGraw-Hill, New York, 1970.

Tschudy, R.H., Pillmore, C.L., Orth, C.J., Gillmore, J.S., and Knight, J.D., 1984, Disruptions of the terrestrial plant ecosystem at the Cretaceous-Tertiary boundary, Western Interior: Science, v. 225, no. 4666, p. 1030-1034.

Tremain, C.M., 1980, The coalbed methane potential of the Raton Mesa coal region, Raton Basin, Colorado: Colorado Geological Survey Open-File Report 80-4, 48 p.

Tyler, R., Kaiser, W.R., Scott, A.R., Hamilton, D.S., and Ambrose, W.A., 1995, Geologic and Hydrologic Assessment of Natural Gas from Coal: Greater Green River, Piceance, Powder River, and Raton Basins, Western United States: Gas Research Institute Report of Investigations No. 228, 219p.

Weimer, R.J., 1960 Upper Cretaceous stratigraphy, Rocky Mountain area: American Association of Petroleum Geologists Bulletin, v. 44, no. 1, p. 1-20.

Weijermars, R., 1997, Principles of Rock Mechanics, Alboran Science Publishing, 360 p.

Wellman, G. W., March 1999, "MAPVAR - A Computer Program to Transfer Solution Data Between Finite Element Meshes", SAND99-0456, Sandia National Laboratories, Albuquerque, NM.

Wood, G.H., Johnson, R.B., and Dixon, G.H., 1957, Geology and coal resources of the Starkville - Weston area, Las Animas County, Colorado: U.S. Geological Survey, Bulletin 1051, scale 1:31680, 68p.

Woodward, L.A., 1984, Potential for significant oil and gas fracture reservoirs in Cretaceous rocks of Raton Basin, New Mexico: American Association of Petroleum Geologists Bulletin, v. 68, no. 5, p. 628-636.

Woodward, L.A., 1987, Oil and gas potential of the Raton Basin, New Mexico, in Lucas, S.G., and Hunt, A.P., Northeastern New Mexico: New Mexico Geological Society Guidebook, p. 331-338.

Woodward, L.A., 1995, Regional Tectonic Control of Laramide (Late Cretaceous-early Tertiary) Fractures in the Raton Basin, New Mexico - Implications for Horizontal Drilling in Cretaceous Shales: American Association of Petroleum Geologists Bulletin, v. 79, p. 148A.

7.1 Maps

Andreasen, G.E. and Kane, M.F., 1961, Isostatic compensation in the Sangre de Cristo Mountains, New Mexico [paper 391]: U.S. Geological Survey, Professional Paper 424-D, scale 1:856000.

Bass, N.W., 1947, Structure contour map of the surface rocks of the Model anticline, Las Animas County, Colorado: U.S. Geological Survey, Oil and Gas Investigations Preliminary Map OM-68, scale 1:42240.

Budding, K.E. and Kluender, S.E., 1983, Mineral resource potential map of the Spanish Peaks Wilderness Study Area, Huerfano and Las Animas Counties, Colorado: U.S. Geological Survey, Miscellaneous Geologic Investigations Map MF-1542-C, scale 1:50000.

Budding, K.E. and Lawrence, V.A., 1983, Geochemical map of the Spanish Peaks Wilderness Study Area, Huerfano and Las Animas Counties, Colorado: U.S. Geological Survey, Miscellaneous Geologic Investigations Map MF-1542-B, scale 1:50000.

Budding, K.E. and Lawrence, V.A., 1983, Reconnaissance geologic map of the Spanish Peaks Wilderness Study Area, Huerfano and Las Animas Counties, Colorado: U.S. Geological Survey, Miscellaneous Geologic Investigations Map MF-1542-A, scale 1:50000.

Cordell, L., Keller, G.R., and Hildenbrand, T.G., 1982, Complete Bouguer gravity map of the Rio Grande Rift, Colorado, New Mexico, and Texas: U.S. Geological Survey, Geophysical Investigations Map GP-949, scale 1:1000000.

Danilchik, W., Schultz, J.E., and Tremain, C.M., 1979, Content of adsorbed methane in coal from four core holes in the Raton and Vermejo Formations, Las Animas County, Colorado: U.S. Geological Survey, Open-File Report OF-79-762, scale 1:48800.

Danilchik, W., 1979, Geologic and coal outcrop map of the Madrid quadrangle, Las Animas [County], Colorado: U.S. Geological Survey, Open-File Report OF-79-377, scale 1:24000.

Danilchik, W., 1979, Geologic and coal outcrop map of the Weston quadrangle, Las Animas County, Colorado: U.S. Geological Survey, Open-File Report OF-79-927, scale 1:24000.

Dempsey, W.J., and Page, E., 1963, Aeromagnetic map of parts of southern Colfax, northern Mora, and western Harding Counties, New Mexico: U.S. Geological Survey, Geophysical Investigations Map GP-355, scale 1:250000.

Harbour, R.L. and Dixon, G.H., 1956, Geology of the Trinidad-Aguilar area, Las Animas and Huerfano Counties, Colorado: U.S. Geological Survey, Oil and Gas Investigations Map OM-174, scale 1:31680.

Harbour, R.L. and Dixon, G.H., 1959, Coal resources of the Trinidad - Aguilar area, Las Animas and Huerfano Counties, Colorado: U.S. Geological Survey, Bulletin 1072-G, scale 1:31680.

Johnson, R.B., Wood, G.H., and Harbour, R.L., 1958, Preliminary geologic map of the northern part of the Raton Mesa region and Huerfano Park in parts of Las Animas, Huerfano, and Custer Counties, Colorado: U.S. Geological Survey, Oil and Gas Investigations Map OM-183, scale 1:63360.

Johnson, R.B., 1969, Geologic map of the Trinidad quadrangle, south-central Colorado: U.S. Geological Survey, Miscellaneous Geologic Investigations Map I-558, scale 1:250000.

Luedke, R.G. and Smith, R.L., 1978, Map showing distribution, composition, and age of late Cenozoic volcanic centers in Arizona and New Mexico: U.S. Geological Survey, Miscellaneous Investigations Series Map I-1091-A, scale 1:1000000.

Luedke, R.G., 1993, Maps showing distribution, composition, and age of early and middle Cenozoic volcanic centers in Arizona, New Mexico, and west Texas: U.S. Geological Survey, Miscellaneous Investigations Series Map I-2291-A, scale 1:1000000.

Molenaar, C.M., Cobban, W.A., Merewether, E.A., Pillmore, C.L., Wolfe, D.G., and Holbrook, J.M., 2001, Regional stratigraphic cross sections of Cretaceous rocks from east-central Arizona to the Oklahoma Panhandle: U.S. Geological Survey, Miscellaneous Field Studies Map MF-2382.

Northrup, S.A., Sullwold, H.H., MacAlpin, A.J., and Rogers, C.P., 1946, Geologic maps of a part of the Las Vegas basin and of the foothills of the Sangre de Cristo Mountains, San Miguel and Mora Counties, New Mexico: U.S. Geological Survey, Oil and Gas Investigations Preliminary Map OM-54, scale 1:42240.

Pillmore, C.L., 1964, Geologic map of the Catskill SW quadrangle, Colfax County, New Mexico: U.S. Geological Survey, Open-File Report OF-64-123, scale 1:24000.

Pillmore, C.L., 1965, Geologic map of the Catskill NE quadrangle, Colfax County, New Mexico: U.S. Geological Survey, Open-File Report OF-65-122, scale 1:24000.

Pillmore, C.L., 1965, Geologic map of the Catskill SE quadrangle, Colfax County, New Mexico: U.S. Geological Survey, Open-File Report OF-65-121, scale 1:24000.

Pillmore, C.L., 1966, Geologic map of the Catskill NW quadrangle, New Mexico and Colorado: U.S. Geological Survey, Open-File Report OF-66-104, scale 1:24000.

Pillmore, C.L., 1969, Geologic map of the Casa Grande quadrangle, Colfax County, New Mexico and Las Animas County, Colorado: U.S. Geological Survey, Geologic Quadrangle Map GQ-823, scale 1:62500.

Pillmore, C.L. and Scott, G.R., 1994, Geologic map of the Clifton House quadrangle, showing fossil zones in the Pierre Shale, Colfax County, New Mexico: U.S. Geological Survey, Geologic Quadrangle Map GQ-1737, scale 1:24000.

Scott, G.R., 1986, Historic trail maps of the Raton and Springer 30' x 60' quadrangles, New Mexico and Colorado: U.S. Geological Survey, Miscellaneous Investigations Series Map I-1641, scale 1:100000.

Scott, G.R., 1986, Geologic map and structure contour map of the Springer 30' x 60' quadrangle, Colfax, Harding, Mora, and Union Counties, New Mexico: U.S. Geological Survey, Miscellaneous Investigations Series Map I-1705, scale 1:100000.

Scott, G.R., and Pillmore, C.L., 1993, Geologic and structure-contour map of the Raton 30’x 60’ quadrangle, Colfax and Union Counties, New Mexico, and Las Animas County, Colorado: U.S. Geological Survey, Miscellaneous Investigations Series Map I-2266, scale 1:100000.

Staatz, M.H., 1986, Geologic map of the Pine Buttes quadrangle, Colfax County, New Mexico: U.S. Geological Survey, Geologic Quadrangle Map GQ-1591, scale 1:24000.

Staatz, M.H., 1987, Geologic map of the Tres Hermanos Peak quadrangle, Colfax County, New Mexico: U.S. Geological Survey, Geologic Quadrangle Map GQ-1605, scale 1:24000.

Tur, S.M. and Flores, R.M., 1980, Lithologic descriptions of measured sections of Upper Cretaceous Trinidad Sandstone, northern Raton Basin, Colorado: U.S. Geological Survey, Open-File Report OF-80-818, scale 1:24000.

Wanek, A.A., Read, C.B., Robinson, G.D., Hays, W.H., and McCallum, Malcolm, 1959, Geologic map of the Philmont Ranch quadrangle, New Mexico: U.S. Geological Survey, Open-File Report OF-59-126, scale 1:48000.

Wanek, A.A., 1962, Geologic map of the southeastern part of the Raton coal field, Colfax County, New Mexico: U.S. Geological Survey, Open-File Report OF-62-148, scale 1:48000.

Wanek, A.A., 1963, Geology and fuel resources of the southwestern part of the Raton coal field, Colfax County, New Mexico: U.S. Geological Survey, Coal Investigations Map C-45, scale 1:48000.

Wanek, A.A., Read, C.B., Robinson, G.D., Hayes, W.H., and McCallum, Malcolm, 1964, Geologic map and sections of the Philmont Ranch region, New Mexico: U.S. Geological Survey, Miscellaneous Geologic Investigations Map I-425, scale 1:480000.

Wood, G.H., Johnson, R.B., Eargle, D.H., Duffner, R.T., and Major, Harold, 1951, Geology and coal resources of the Stonewall-Tercio area Las Animas County, Colorado: U.S. Geological Survey, Coal Investigations Map C-4, scale 1:31680.

Wood, G.H., Johnson, R.B., and Dixon, G.H., 1956, Geology and coal resources of the Gulnare, Cuchara Pass, and Stonewall area, Huerfano and Las Animas Counties, Colorado: U.S. Geological Survey, Coal Investigations Map C-26, scale 1:31680.

7.0 APPENDICES

APPENDIX A

Advantages and Limitations of Different Methods for Assessing Natural Fractures in the Raton Basin of Colorado and New Mexico

Presented at:
The Conference on Naturally Fractured Reservoirs, hosted by the Mewbourne School of Petroleum and Geological Engineering and the Oklahoma Geological Survey, Oklahoma City, OK, June 4, 2002. The presentation was accompanied by the 20-page proceedings paper in Appendix A.

Citation:
Rautman, C.A., Cooper, S.P., Arnold, B.W., Basinski, P.M., and Lorenz, J.C., 2002, Advantages and limitations of different methods for assessing natural fractures in the Raton Basin of Colorado and New Mexico: Conference on Naturally Fractured Reservoirs, June 3-4, 2002, Oklahoma City, OK

Advantages and Limitations of Different Methods for Assessing Natural Fractures in the Raton Basin of Colorado and New Mexico

Christopher A. Rautman[1], Scott P. Cooper[1], Bill W. Arnold[1], Paul M. Basinski[2],
Thomas H. Mroz[3], and John C. Lorenz[1]

[1]Sandia National Laboratories, Albuquerque, New Mexico
[2]El Paso Production Company, Houston Texas
[3]National Energy Technology Laboratory, Morgantown, West Virginia

ABSTRACT

A suite of three sets of fracture data, derived from outcrops, wellbore-image logs, and core in the Raton Basin, NM, provides an opportunity for comparison. Each data source provides a unique view of the fracture system, and a model based on any single source is significantly different from one derived from the combined data.

The dominant fractures in outcrop are present in sandstones and carbonates. Two types of fractures can be related to horizontal compressive stresses derived from Laramide thrusting at the western edge of the basin: extension fractures that strike approximately east-west, and conjugate fracture pairs where the bisector of the acute fracture-intersection angle is horizontal and also strikes east-west. Shear planes sub-parallel to bedding are also present but are commonly obscured.

In contrast, wellbore-image data suggest that the dominant subsurface fractures consist of conjugate fractures with an east-west strike and a vertical acute-angle bisector, and that they are preferentially developed in shales and coals. Vertical fractures in sandstones, common to outcrops, are relatively rare in the image logs. Wellbore-image and related logs also highlight bedding-parallel shear planes that are associated with zones of more intense fracturing, and give an indication of the present-day, maximum horizontal compressive stress orientation.

Data from an associated, extensive data base of small-diameter cores show four fracture sets: vertical extension fractures similar to those in outcrop except that they are developed in shales and siltstones; conjugate shear fractures with a vertical acute-angle bisector similar to those seen in the wellbore-image logs; small scale thrust faults; and randomly oriented compaction fractures. Identification of fracture strikes is not possible from unoriented drill core.

Each fracture data set has advantages and limitations. Cores and logs are biased against intersecting vertical fractures. Logs provide better vertical coverage than cores and give indications of fracture orientation, but do not provide any information on fracture surface or mineralization characteristics. Outcrops may display fracture patterns related to stresses that have not affected equivalent subsurface strata, and fractures in shales are poorly exposed in the outcrop, yet outcrops provide three-dimensional data. Reliance on any single data source for fracture detection and characterization results in an incomplete fracture model.

INTRODUCTION

Naturally occurring fractures are important in the production of hydrocarbons in many sedimentary basins. In fact, fractures (natural or induced) may be the only means of establishing commercial production from reservoirs with low matrix permeability. Additionally, in some non-conventional reservoirs, including the coal bed methane projects now being widely developed in the United States, cleats and fractures are the principal permeable conduits for the production of natural gas.

Given the importance of naturally occurring and induced fractures to successful hydrocarbon production, a major challenge facing explorationists is how best to characterize the fracture system of a given basin or potentially productive unit. An integrative study of fracturing and its relationship to the inferred evolution of stresses is underway in the Raton Basin of northeastern New Mexico and southeastern Colorado. Observations are being compiled from surface outcrops around the margins and within the basin, down-hole geophysical imaging logs, and extensive cored stratigraphic test wells drilled for an ongoing coal bed methane and fractured sandstone-play.

Each principal source of data provides a unique view of the overall fracture system. However, results to date suggest that each unique view is somewhat biased, and that integration of multiple data sources is required for development of a complete fracture model. This report describes some preliminary observations from the higher stratigraphic units within the Raton Basin, and it discusses the relative advantages and limitations of each of the different observational methods.

THE RATON BASIN PROJECT

Location and Geologic Overview

The Raton Basin (fig. 1) is an elongate, asymmetrical, Laramide sedimentary basin divided roughly in half by the Colorado-New Mexico state line. The western margin of the Late Cretaceous Rocky Mountain Foreland Basin in this area has been uplifted and deformed by Laramide uplift and east-directed thrusting of the Sangre de Cristo basement block. Coarse-grained, arkosic sediments were shed eastward into a subsiding Raton Basin, now isolated from the main foreland basin by tectonic activity. A generalized stratigraphic section of the Raton Basin is presented in figure 2.

The principal preserved basin fill of the Raton Basin includes the Vermejo Formation (Late Cretaceous in age), the Raton Formation (latest Cretaceous and Paleocene) and the Poison Canyon Formation (Paleocene). Younger deposits, now preserved only within the Colorado portion of the basin, consist of the Cuchara, Huerfano, and Farasita formations (Eocene–Oligocene?). Overlying Miocene sediments of the Devils Hole Formation contain abundant volcanic debris, much of which is correlative with the emplacement of the shallow intrusive centers now known as the Spanish Peaks. Intrusive sills and smaller laccoliths, as well as bedding-discordant dikes, are present in many locations throughout the basin. In parts of the basin, the topographic surface is underlain by portions of the Ogallala Formation (Plio-Pleistocene) of the High Plains.

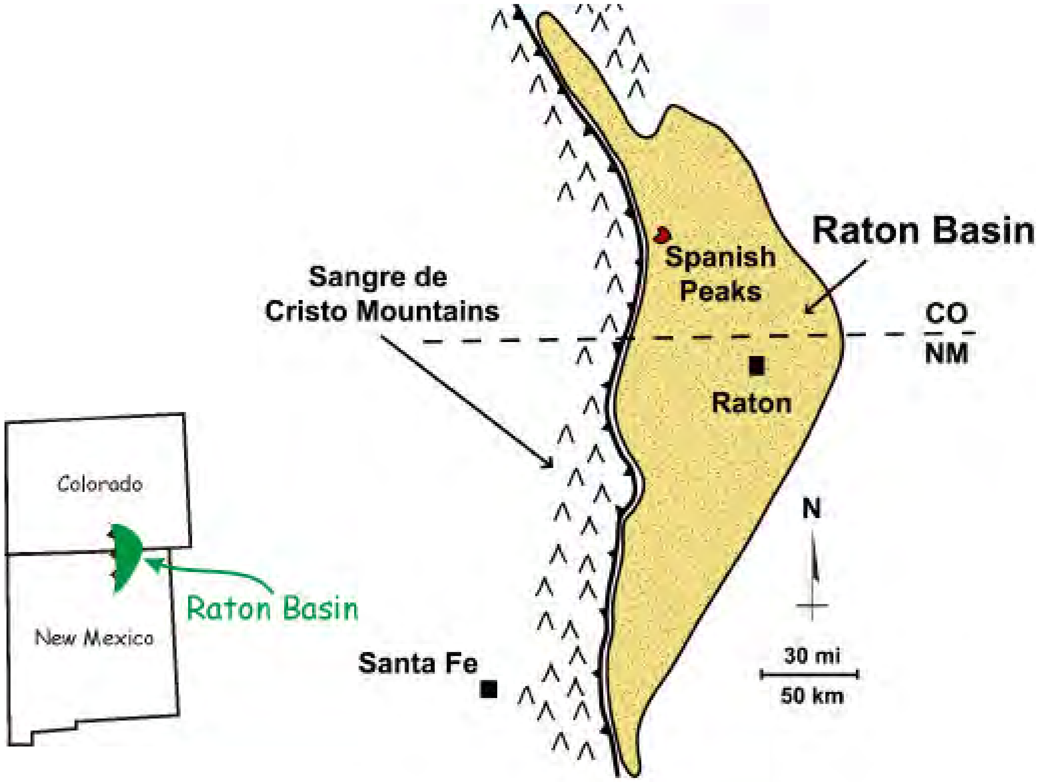

Figure 1. Index map showing the location and extent of the Raton Basin in northeastern New Mexico and southeastern Colorado.

The younger Tertiary sediments and volcanic rocks (Cuchara Formation and overlying rocks) have been removed from the New Mexico portion of the basin by erosion. Sills throughout the basin have been inferred to have been intruded at reconstructed depths of at least 5,000 ft, and the total thickness of cover that may have been removed from the New Mexico portion of the basin may exceed 8,000 ft (Hemmerich, 2001).

The principal methane production and potential resource is associated with thin, now relatively shallow (~1500–2500-ft depth) coal seams of in the Upper Cretaceous and Lowermost Tertiary sedimentary section. However, numerous thick, naturally fractured, low-permeability sandstones are interbedded in this portion of the sedimentary sequence, and these fractured units may contain significant gas resources for which the source rocks are the included coals. The existence and extent of fractured sandstone reservoirs in the Raton Basin is yet to be determined.

The presence of numerous bedding-parallel igneous sills within the section suggests an unconventional stress state, wherein the overburden stress was not necessarily the maximum principal stress at the time of intrusion during deep burial. Additionally, the deeper mid-Tertiary burial and later exhumation of the New Mexico portion of the basin, in conjunction with heating related to subvolcanic intrusive activity late in the geologic history of the area in a complex and poorly understood sequence of events, has resulted in a basin in which the fluids are underpressured at present. The stress field has also been reconfigured by late Tertiary uplift and erosion and by regional extension related to the opening of the Rio Grande Rift. Because stress systems con-

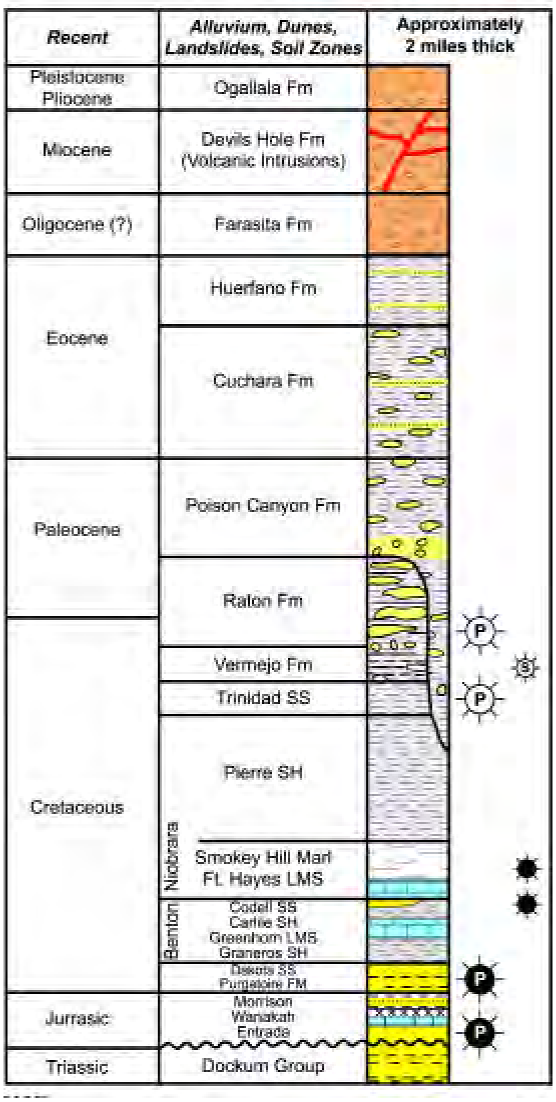

Figure 2. Geologic column of the Raton Basin area. Symbols to the right of the column indicate gas (white/ open symbols) and oil (black/closed symbols) shows (s) and/or production ("P") (modified after Dolly and Meissner, 1977).

trol both the formation of natural fractures and the response of those fractures to pore-pressure changes during production and recovery of hydrocarbons and related fluids, understanding of the geometry of both stresses and fractures would be a significant step toward optimizing recovery of natural gas from the Raton Basin.

Fracture Studies in Outcrop

Outcrop studies have focused on exposures of resistant Dakota Sandstone and stratigraphically higher rock units along the margin of the main Raton Basin, as well as on resistant sandstones and coals of the Raton Formation within the basin. A large number of fractures in outcrop appear to be near-vertical extension fractures. These features occur throughout the vertical section in the New Mexico portion of the basin, and they appear to be oriented roughly east–west and normal to the bounding thrust of the Sangre de Cristo Mountains (figs. 3–4).

Figure 3. Near-vertical, uniformly dipping extension fractures in the Trinidad Sandstone. (a) Roadcut exposure (note circled geologist for scale); (b) rose diagram of fracture strikes.

Figure 4. Near-vertical, parallel extension fractures in outcrop of a sandstone unit of the Vermejo Formation (Upper Cretaceous).

A somewhat less-evident style of fracturing is vertically dipping conjugate-fracture pairs. These sets are developed both in sandstones and in limestones (fig. 8), and there appears to be spatial and/or stratigraphic variation in the orientation of the acute-angle bisectrix of the conju-

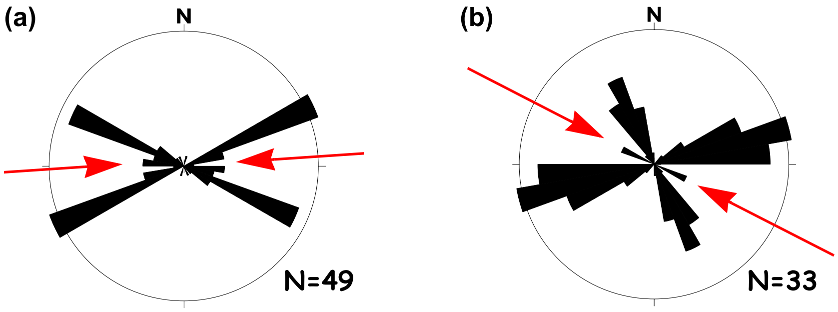

Figure 5. Rose diagrams showing differing orientations of fracture strikes for conjugate fracture sets in different positions within the Raton Basin. (a) South-eastern portion, Ft. Hayes Limestone; (b) eastern portion, Dakota Sandstone. Approximate acute-angle bisectrices shown by red arrows (dips are essentially vertical).

gate pairs (fig. 5). The bisector of the acute angle formed by the conjugate fracture pair reflects the orientation of the maximum principal stress during formation.

There are also more complex styles of fracturing and additional potential spatial controls on fracturing at the basinal scale. Figure 6 shows an example of a highly fractured outcrop of Dakota sandstone. However, this outcrop is located on the western margin of the Raton Basin near the bounding thrust fault, and the strata are, in fact, overturned. The nature and orientation(s) of the different types of fractures at this location have not yet been determined.

At another location, both sandstones and included sills exhibit parallel fracture patterns that are suggestive of vertically dipping conjugate shears (fig. 7). However, closer examination of

Figure 6. Factures developed in an outcrop of the Dakota Sandstone at the western margin of the Raton Basin close to the bounding thrust fault. Unit is overturned at this location.

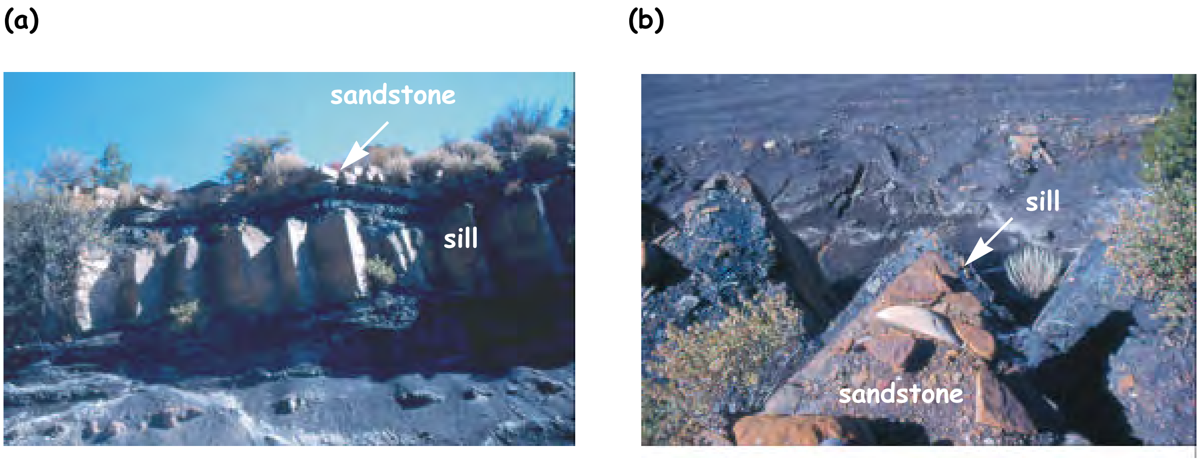

Figure 7. Parallel extensional fracturing in sandstone and igneous sill. (a) normal outcrop view; (b) view looking vertically downward, showing parallelism of fractures.

Figure 8. Conjugate fracture sets developed in outcrop of the Ft. Hayes Limestone Member of the Niobrara Formation (Upper Cretaceous). View is vertically downward.

the outcrop indicates that the fracture surfaces exhibit definite plumose structures, implying that the style of fracturing is almost unquestionably extensional in nature. Such close-up examination of what are moderately large mesoscale features is possible only in outcrop exposure, and the angular relationships alone might lead to a wholly different structural interpretation.

Large-scale regional changes in fracturing styles are suggested by the sequence of rose diagrams presented in figure 9. These orientation measurements are all from sandstone and have been collected from a west-to-east transect through the north-central Raton Basin along the course of the Purgatoire River. Notable is the change from two intersecting sets of extensional fractures on the west closest to the bounding thrust fault and the later Rio Grande Rift, through a single dominant set of extensional fractures in the central portion of the basin, to a set of conjugate shear fractures closer to the eastern margin of the basin. Although speculative at this time, the presence of north-trending extensional fractures in the westernmost portion of the Raton Basin is compatible with an influence of east-west directed extension associated with opening of the Rio Grande Rift to the west of the Sangre de Cristo Mountains.

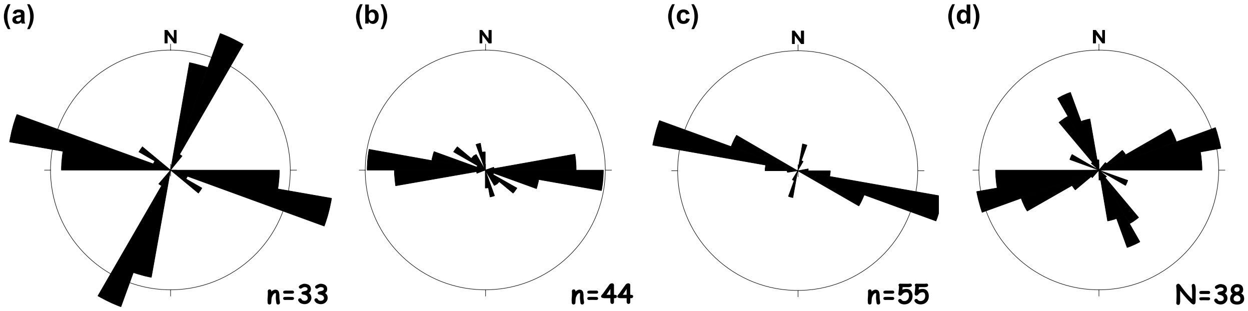

Figure 9. West-to-east transect of the Raton Basin along the Purgatoire River valley just north of the New Mexico-Colorado state line showing differences in fracture style with position within the basin. All fractures are in sandstone. (a) Two perpendicular sets of extensional fractures; (b) a single set of extensional fractures; (c) a dominant set of extensional fractures with a weak secondary set at 90 degrees and with a slightly different implied orientation of maximum horizontal compressive stress than (b); (d) conjugate shear fractures with a bisecting minor set of extension fractures.

Fracture Studies Through Wireline Geophysical Imaging

Two principal types of downhole geophysical imaging tools have been used to date for observation of fracture patterns in the subsurface: the Formation Micro-Imager (FMI™) log and the Anisotropic Dipole Imager (DSI™) log[1]. FMI and DSI logs have been run in selected full-diameter wells for El Paso Production Company as part of their El Paso-Raton, LLC, coal bed methane project.

Formation Micro-Imager Log

The FMI or microresistivity logging tool provides imaging of the formation based on the correlation of eight very high-resolution, shallow resistivity traces measured around the circumference of the wellbore. Real-time orientation knowledge of the position of the downhole tool allows measurement of both the dip and strike of bedding, fractures, and faults. Fractures that are open to invasion by the drilling mud are distinguished from closed fractures based on contrasts in electrical resistivity of the mud and the formation. Analyses of fracture orientations in this study have focused on open or partially open fractures for which an apparent hydraulic aperture has been estimated. Open fractures are more likely to interact with the local stress state and are more relevant to gas and water flow within the formation.

---

[1] The use of trade, product, industry, or firm names is for descriptive purposes only and does not imply endorsement by the Sandia National Laboratories or by the U.S. Government.

Fractures in the wells examined to date exhibit two more-or-less well-defined fracture sets. One set, striking roughly east–west, dominates the data from one borehole, whereas a second borehole in the same part of the basin exhibits two subequally developed populations. These fracture sets are shown both in rose-diagram format and on lower-hemisphere stereonets in figure 10.

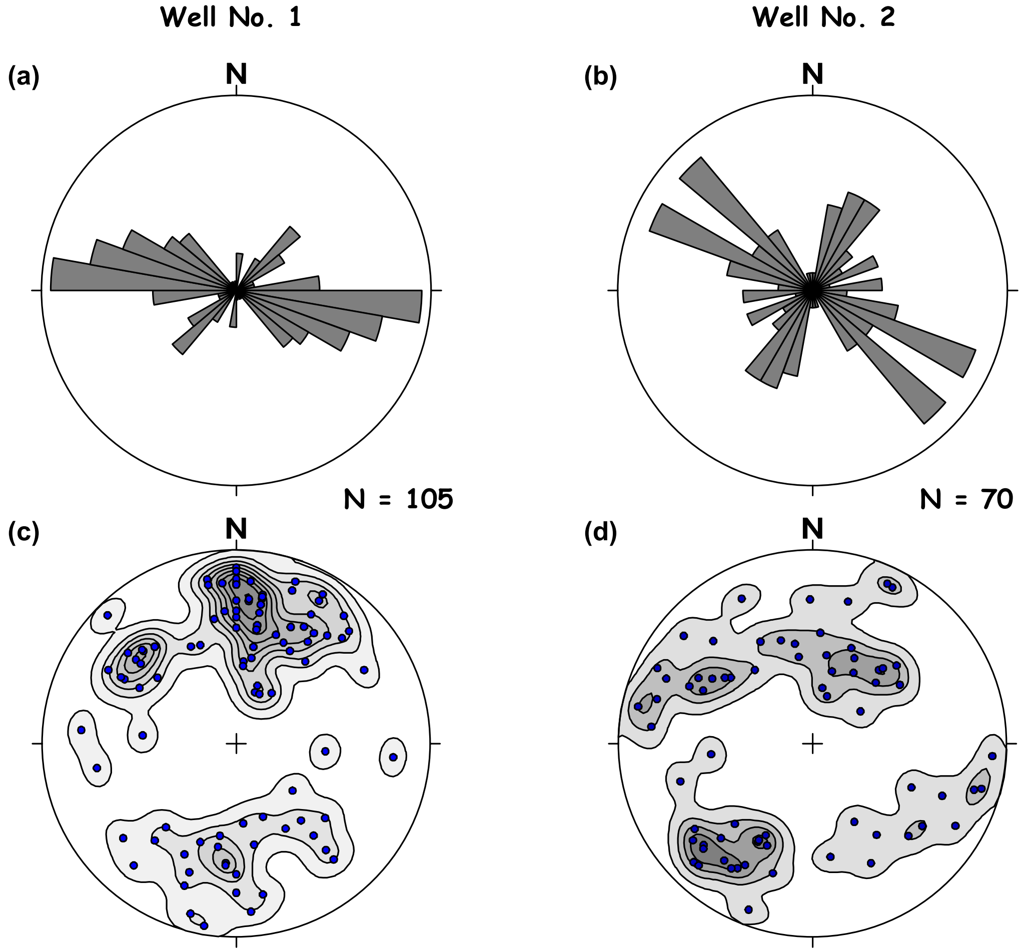

Figure 10. Orientations of open and partially open fractures as inferred from FMI logs from two holes in the southernmost Colorado portion of the Raton Basin. (a) and (b) Rose diagrams of fracture strikes; (c) and (d) lower-hemisphere stereonet diagrams for the same fracture populations shown in the rose diagrams immediately above showing poles to the fracture planes.

The stereonet presentation of figure 10(c) indicates that the east–west fracture set in the one borehole exhibits a dominantly southward dip. The less well-developed set, striking northeast–southwest, also dips southward (indicated by the cluster of poles in the northwest quadrant). Relatively few of the northeast-trending fractures appear to exhibit northerly dips.

The distribution of orientations in the second well for the northeasterly striking fractures, shown in figure 10(d), also indicates a dominance of generally southeastward dips, although the spread of these orientations appears more broad. Dips of the second, although numerically dominant set in this second borehole exhibit roughly equal number of fractures dipping southwest and northeast. North-dipping fractures of this set exhibit more steeply dipping fracture planes than do the southwest-dipping fractures.

Dipole Sonic Log

The DSI (or dipole sonic imager) logging tool detects anisotropy of the sonic shear-wave velocity within the formation. The acoustic anisotropy measured by this tool may be intrinsic in nature or stress induced. Intrinsic anisotropy is caused by preferential textural or fracture orientations within the rock, whereas stress-induced anisotropy is imparted by differences in the horizontal stress state. The direction of fast shear-waves in the medium is aligned parallel either to the dominant intrinsic features or to the maximum horizontal stress. A consistent azimuth of maximum shear-wave velocity in a well, without a corresponding preferred fracture orientation or textural trend, is generally interpreted to be indicative of the direction of maximum horizontal stress.

The DSI logs that have been examined thus far from the northernmost New Mexico and southernmost Colorado portion of the Raton Basin exhibit quite similar characteristics with relation to the direction of horizontal stress throughout the penetrated section, as indicated by the four rose diagrams of figure 11. The mean maximum horizontal compressive stress is just slightly east of north in three of the four drill holes and only very slightly west of north in the fourth. The fact that the maximum horizontal stresses inferred from the DSI logs are highly consistent and oriented almost perpendicularly to the dominant trend of the fractures identified by the FMI analysis suggests that the measurements are, in fact, reflecting the true in-situ stress conditions. The presence of some two dozen borehole-wall breakouts on the eastern and western sides of the drill holes also suggests that the present-day maximum horizontal compressive stress is oriented north–south.

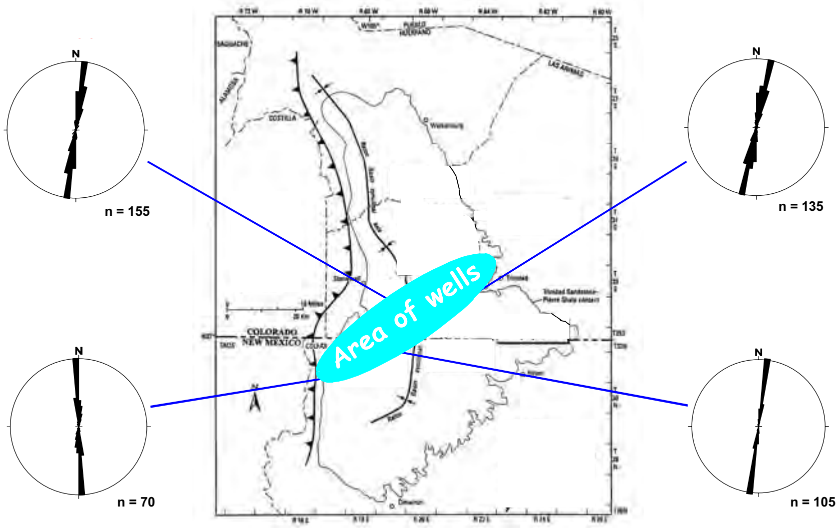

Figure 11. Rose diagrams showing consistency in orientation of present-day maximum horizontal stress in the central Raton Basin, as determined from DSI logging tool data. Precise locations obscured to protect proprietary data.

The variability of the maximum horizontal stress appears to decrease with depth, suggesting an increase in the anisotropy ratio of the stresses in the horizontal plane with increasing depth. The standard deviation of measured azimuths below roughly 1,200 ft is less than half the variability observed for measurements taken above this depth. In addition to a decrease in variability of orientation with depth, the inferred mean horizontal compressive stress appears to rotate to a more north-south orientation in observations made below 1,200 ft in depth. This trend is quite evident in the drill hole represented by figure 12.

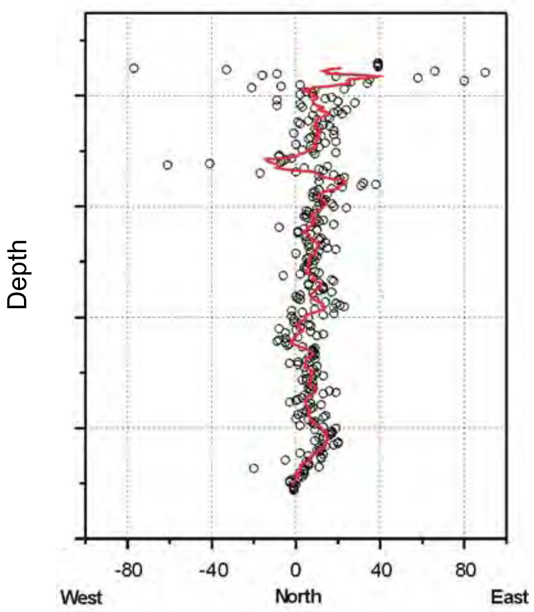

Figure 12. Measured azimuths of the maximum horizontal compressive stress (open circles) at 5-ft intervals inferred from DSI logs as a function of depth from a well drilled in the southernmost Colorado portion of the Raton Basin. The solid line indicates a 50-ft moving-average orientation. 200-ft depth ticks.

Fracture Studies of Continuous Core

Continuous wireline, small-diameter (NX- or HQ-type; approximately 2.0–2.5-inch maximum diameter) cores have been obtained from a 18 holes drilled as stratigraphic tests from near the surface to the Trinidad Sandstone (fig. 2) by El Paso-Raton, LLC, and its predecessor organizations operating a coal bed methane play, principally in the New Mexico portion of the Raton Basin. Core recovery for three holes examined in detail thus far is generally excellent. Layout of the core under quasi-controlled conditions in a core warehouse allows close examination of fractures, including measurement of dip (relative to the core-axis only in unoriented drill core), fracture coatings, mineralization and alteration of the fracture or adjoining wall rock, the nature of fracture terminations, associations with specific lithologic types, and the presence or absence of striae (slickensides) on the fracture surface(s). Evaluation of fractures observed in core is probably less advanced than analyses of fracturing in the Raton Basin by the other two methods. However, the preliminary data suggest that there are four distinctly different types of fractures.

Near-vertical extension fractures (zero to about 10 degrees to core axis; fig. 13) are well developed locally in the section overlying the Trinidad Sandstone. Although some extension fractures are present in sandstones, the overwhelming dominant lithologic association of near-vertical fractures is with finer-grained rocks, principally siltstones and silty mudstones. Not all vertical fractures are necessarily parallel. Some instances of near-vertical fractures can be demonstrated to exhibit strikes nearly 90-degrees apart. Extension fractures are almost the only class of fracture present in the more massive sandstone intervals; multiple near-parallel sets of fractures separated by a centimeter or less [fig. 13(b)] may also be present in these lithologic horizons. Plumose structure (fig. 14) may be present on some of these fractures.

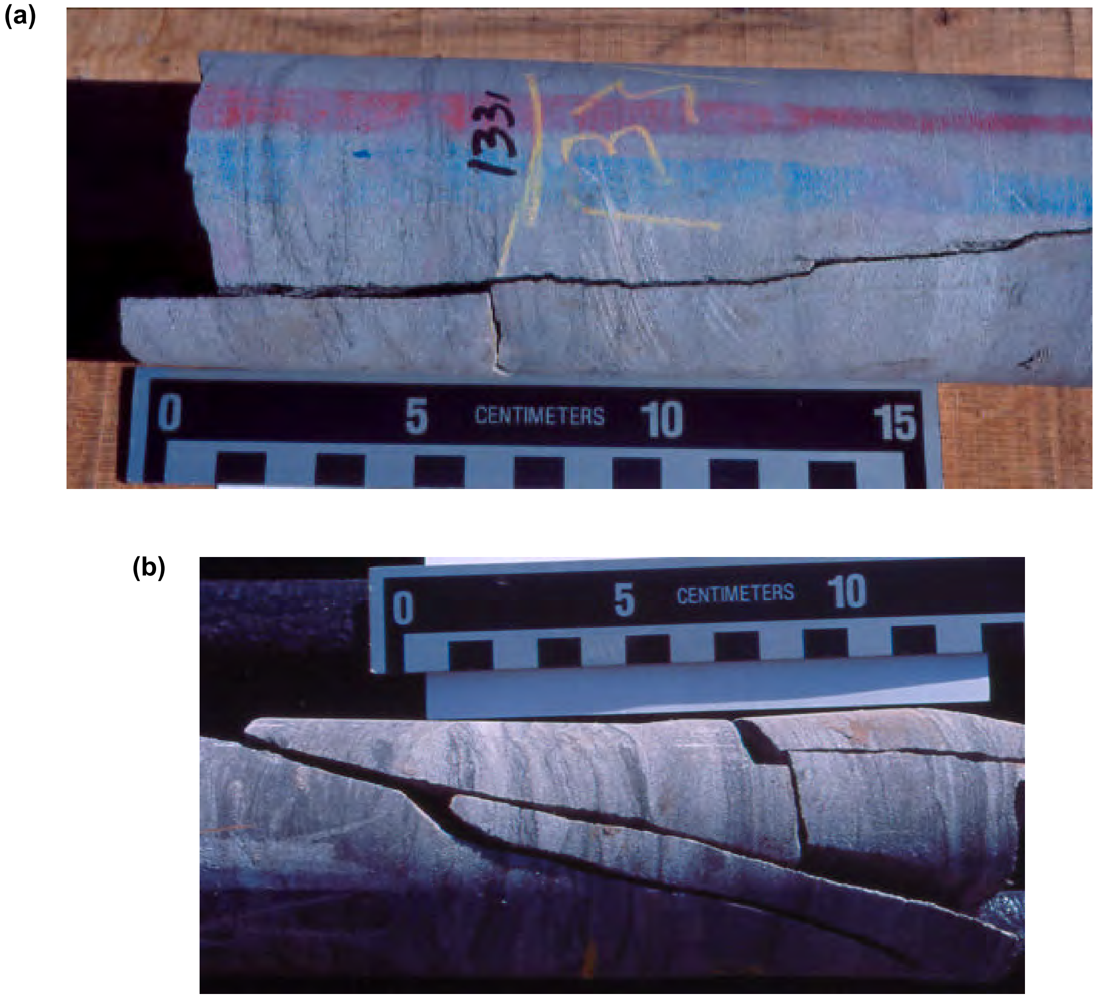

Figure 13. Near-vertical (approximately parallel to core axis) extension fractures in sandstones of the Raton Formation in core. Stratigraphic top is to the left. (a) Typical expression; (b) example of parallel fracturing.

A small number of intervals of intrusive igneous rock have been logged in the core from the Raton Basin. These intervals are inferred to represent sills on an outcrop scale, although smaller-scale cross-cutting relationships with the host rock, mostly carbonaceous mudstone and

Figure 14. Plumose structure on an extension-fracture surface in core from the Raton Formation.

coal, are visible in core. The intrusive rocks are broadly intermediate in composition, porphyritic, and somewhat altered. The only class of fracturing observed in the small set of sills logged to date are near-vertical extension fractures.

What appear to be conjugate fracture sets are present in the core, again principally associated with the finer grained portion of the lithologic section. These fractures dip dominantly between 20–30 and 70 degrees (forming angles of 30 to 70 degrees to the core axis); strike orientations are unknown, as none of the stratigraphic-test core was oriented during collection. Demonstration of the conjugate nature of fractures is difficult in drill core that is only 2 or so inches in diameter. However, reconstruction of significant lengths of core to its original continuous relative position by matching drilling- and handling-induced breaks does demonstrate the alternate-dipping nature of at least some inclined fractures in these cores (fig. 15). The acute-angle bisectrix of identifiable conjugate fracture sets, which reflects the orientation of the principal compressive stress at the time of formation, may be either near vertical or in the horizontal plane; however vertical principal compressive stresses appear to be predominant.

Because of the dominance of finer-grained lithologies associated with these inclined/conjugate fracture sets, a large number of fracture planes exhibit poorly to well-defined slickensides indicative of relative movement. The majority of slickensides rake roughly 10 to 20 degrees to the dip of the overall fracture plane, as indicated in figure 16(a). A very few slickensides rake at a high angle, 70–80 degrees, to the dip of the fracture plane [fig. 16(b)]. Slickensides may also be present on “bedding” planes that are nearly perpendicular to the core axis. Compositional layering may be present at significant angles to the nominally normal-to-core-axis direction, indicating local cut-and-fill sedimentary structures. That the sense of shearing is aligned with the orientation of fractures themselves is demonstrated by the photograph of figure 17.

A third, although rare, class of fracture observed in drill core consists of inclined fractures for which reverse-sense movement (thrust faulting) can be demonstrated. Such movement is strongly indicated by slight step features on the fracture surfaces that are most compatible with a reverse sense of movement. Very thin (less than one millimeter) carbonate coatings on some

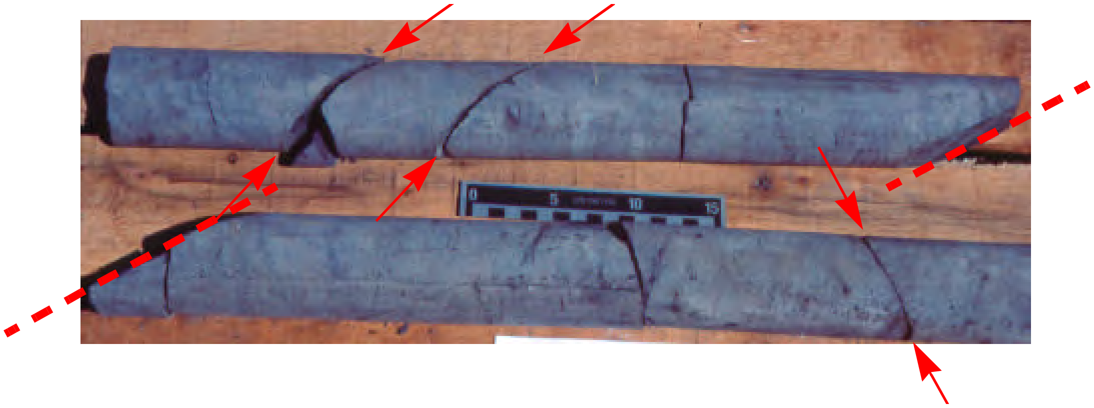

Figure 15. Reconstruction of in-situ core configuration for a reconstructed four (4) feet of core demonstrating the conjugate nature of a fracture set (solid arrows) in siltstone of the Raton Formation. The dashed lines indicate matched halves of the same fracture plane; Stratigraphic top is to the left and the core reads like a book from left to right and from top to bottom; scale is in centimeters.

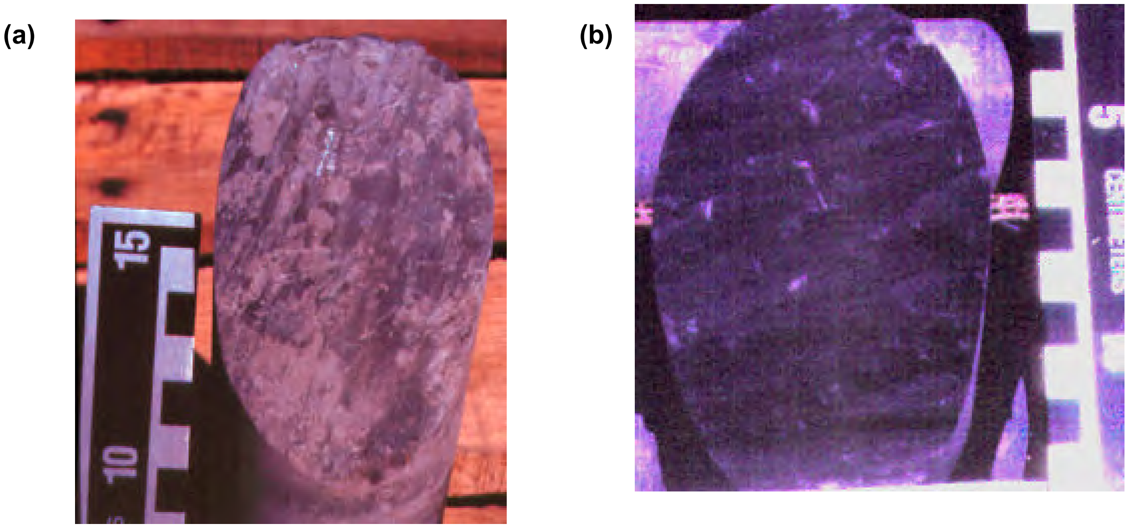

Figure 16. Examples of slickensides on fracture surfaces in siltstone from the Raton Formation. (a) Slicks rake at a low angle to the dip of the fracture; (b) slicks rake at a high angle to dip. Stratigraphic top is up in both images; scale is in centimeters.

slickensides also can be interpreted as suggesting deposition in pressure “shadows” of slight irregularities on the fracture surface. In some cases, the impression is that the last sense of movement was more-or-less up-dip.

An additional class of fracturing observed in core is ubiquitously distributed throughout the fine-grained portion of the section, particularly in the mudstones. These features appear to be randomly oriented “compaction” fractures (fig. 18). Typically, a compaction fracture is of short extent (many are less extensive than the diameter of the core), abruptly curved or otherwise non-

Figure 17. Shear fractures in muddy siltstone of the Raton Formation. Note alignment of slickensides on the outward-facing fracture with the dip direction of the other two fractures.

planar, slickensided, and can be observed to die-out into unfractured material over a short distance. Additionally, previously unbroken core may fracture (at least partially) along these planes during handling associated with examination of the core. Given the markedly different initial porosities and mechanical properties of muddy sediments and sands shortly after deposition, it would not seem surprising that significant differential compaction during dewatering and consolidation might occur, creating these fractures a syndepositional features.

Figure 18. Compaction fracture in fine-grained silty mudstone of the Raton Formation.

Calcareous coatings are evident on many fractures seen in the core. At least two types of calcite are present: white and reddish orange (iron stained). Most observed calcite coatings coat only part of the fracture, and may be observed to fill irregularities associated with slickensides and other mesoscopic irregularities on the fracture planes. Typically, these fractures are open (pieces separated) in the core box; these coatings are dislodged relatively easily from the fracture wall. In distinct contrast, some fractures are completely healed ("tight") by carbonate minerals. These "vein-fill" fractures may be either completely or partially filled by white carbonate material. Mesoscopic porosity up to a millimeter or two in diameter is visible in some of the wider (2–3-mm maximum width) vein-fill-type fractures. Interestingly, carbonate fracture coatings are more abundant in the finer-grained lithologies, and may be present even in the so-called compaction fractures, including those initially tight features that open up upon handling of the core during logging activities.

DISCUSSION

The purpose of this paper is not only to describe the location-specific (preliminary) results of ongoing fracture studies in the Raton Basin, but also to compare and contrast the advantages and limitations of three different methods for assessing the natural fracture system: outcrop studies, downhole geophysical imaging, and core examination. Using each of the observational methods separately, it is possible to construct separate "fracture models" to summarize briefly the more general interpretations obtained to date.

Fracture Model Based on Outcrop Observations

Based solely on the observations possible in outcrops, the conceptual model of fracturing in the Raton Basin can be summarized as follows:

1. Vertical extension fractures and vertical conjugate fracture sets dominate the sequence,
2. Strikes of extension fractures are dominantly east-west,
3. Strikes of the acute-angle bisectrix of conjugate fracture sets are also east-west, implying an east-west orientation for the maximum horizontal compressive stress during formation of these fractures,
4. Fractures are concentrated in brittle rock types: sandstones, limestones, and intrusive sills, and
5. There is abundant evidence for thrust (reverse-motion) faulting on a mesoscopic (outcrop) scale.

Fracture Model Based on Borehole Imagery

Based solely on the results of the downhole geophysical imagery (DSI and FMI logging tools), the conceptual model of fracturing in the Raton Basin may be summarized as follows:

1. Fracturing appears dominated by east-west striking, inclined conjugate fracture sets,
2. Fractures are concentrated in finer-grained strata and coals,
3. The maximum *present-day* horizontal principal stress is probably oriented north-south,
4. Open fractures (under the prevailing stress regime) are oriented east-west; this may be important evidence with respect to the open or closed nature of certain fracture sets, and
5. There is some evidence for thrust (reverse-motion) faulting.

Fracture Model Based on Core Examination

Based solely on examination of small-diameter continuous core, the conceptual model of fracturing in the Raton Basin may be summarized as follows:

1. Both near-vertical extension fractures and inclined, probable conjugate fracture sets are present; strikes of fractures cannot be determined from unoriented core,
2. Fractures are distinctly more abundant in finer grained strata, including both mudstones and silty units,
3. Compaction fractures are ubiquitous in the most fine-grained rock types; these fractures were sufficiently open at one time to allow the deposition of thin carbonate veinlets, and
4. There is some minor evidence for thrust (reverse-motion) movement on some fractures; this evidence is on a “micro-” (hand-sample) scale, in contrast to a mesoscopic outcrop scale.

Biases and Differences Identifiable in the Three Fracture Data Sets

The first and most obvious difference among the three fracture data sets, and one that would be capable of inducing significant bias in resulting interpretations, is the difference in fracture abundances identifiable through outcrop studies vs. those studies that emphasize subsurface observations. Fractures observable in outcrop are dominated by those that are present in brittle rock types, specifically sandstones, limestones, and sills. Although both near-vertical extension fractures and conjugate fracture sets were identified in outcrop, the profound dominance of fracturing in the finer and more ductile rock types identifiable where exposures are not biased by weathering and erosion is completely missed. Mudstones and siltstones are poorly exposed generally in the Raton Basin, and such exposures as do exist are affected by surficial weathering process and by the presence of swelling clays. The bias of outcrop studies generally toward resistant (and typically brittle) rock types is quite well known.

Recognition of the presence of the large suite of very small-scale compaction fractures identified through core examination — and perhaps of the role that may have been played by differential compaction in the development of these and other fractures in fine grained sediments — is not possible using the outcrop data set. The degree of disruption of the mudstones and their included features by surface weathering is simply too extreme. These compaction features also have not been identified in the downhole geophysical imagery, perhaps because they are too small and discontinuous to have attracted attention in the logging of production wells that are of relatively large diameter Although the compaction fractures as we have identified them through core examination are probably not important to permeability of the coal bed methane reservoirs, they nevertheless do appear to be significant features in the subsurface and may provide insights that might be relevant into the origins of other fractures.

A second major difference among the differing data sets is that absolute orientation data are necessarily absent from subsurface studies that utilize unoriented drill core. Given the significant added expense of obtaining oriented cores, the lack of absolute orientation data is not surprising in most stratigraphic studies. The impact of unoriented drill core with respect to absolute fracture orientations (and, indeed, on other types of planar geologic features) is sometimes compensated for by drilling of core holes in other than vertical orientations. The existence of a known fabric to the geology transected by such inclined boreholes (“horizontal” sedimentary bedding in basin interiors, for example), allows general reconstruction of the true orientation of core segments in three-dimensional space, and thus allows reconstruction of the approximate orientations of planar features such as fractures.

In addition, in the case of the Raton Basin coal bed methane play, the lack of oriented core may be mitigated to some extent by the apparently highly consistent orientation of the stress field, at least within limited regions. Throughout many of the producing areas drilled to-date, drilling-induced fractures, specifically those resulting from well stimulation procedures, appear to reflect the north-south maximum horizontal compressive stress deduced from the dipole-sonic logging (e.g., fig. 10). Although one must be wary of circular reasoning when extending such inferences into other parts of a basin where the stress regime may be different, this may be an situation where "external" information from a relatively small number of drill-stem tests can provide significant insight into the orientations of fractures at depth.

Another bias that affects data acquired from vertical boreholes, whether that data is from core examination or from downhole geophysical measurements, is the well-known bias against intersecting near-vertical fractures. This bias may account for the apparent lack of vertical extension fractures observed in the downhole geophysical imagery data set compared especially to the results of the outcrop studies and the core examination. Still another potential effect when comparing fracture-frequencies to lithology between drill hole and outcrop studies is the bed-thickness effect. If the resistant layers in outcrop are more massively bedded than the (poorly exposed) finer-grained strata, fracture spacings may be more widely spaced in the more brittle rocks, further decreasing the likelihood of encountering numerous fractures in core or log-based studies.

Alternatively, any individual vertical borehole may yield an unreasonably high estimate of the frequency of vertical fracturing if the vagaries of locating the hole collar lead to drilling the hole down a local zone of anomalously high fracture intensity (or even an individual fracture). Additionally, unless drilling procedures are closely controlled (e.g., penetration rates and resulting weight-on-bit), the coring operation itself may induce near-vertical fractures in certain rock types and under certain in-situ stress regimes. Petal fractures (fig. 19), which are also generally interpreted to be coring-induced, have been observed in some intervals of core.

Interpretation of stress conditions across the basin and across the differing fracture data sets is, of course, one step removed from the more-or-less objective description of extant fractures. However, at this preliminary stage in this study, some pronounced differences in stress inferences have become apparent. These involve principally the description and interpretation of conjugate fracture sets.

Specifically, the dominance of one or the other direction of conjugate fracture pairs appears potentially different between outcrop studies and the downhole imagery interpretations. Comparison of the rose diagrams of figures 5 and 10(a) and (b) indicates markedly subequal proportions of orientations in outcrop and markedly unequal proportions of orientations from the downhole geophysics. Additionally, although there is some spatial variability in orientation of the inferred maximum horizontal stress in the outcrop data, this variation is on a basinal scale (fig. 9) and in all cases is compatible with broadly east–west oriented compression.

Figure 19. Drilling-induced petal fracture in siltstone of the Raton Formation. Stratigraphic top is to the left.

Perhaps a final, illustrative bias or difference among the three data sets for the purposes of this discussion involves the time-sequence of changes in the stress regime across techniques. This example involves the (direct?) inference of the current stress regime showing the orientation of the maximum horizontal compressive stress as north–south using the DSI logging tool. Although the orientations of the principal horizontal stress shown by the rose diagrams of figure 11 is fully consistent with the current-day extensional regime that produced the Rio Grande rift to the west of the uplifted Sangre de Cristo basement block (fig. 1), this orientation is at almost 90 degrees to the direction of movement(s) along the thrust faults separating the basin from the basement block to the west. Thus, although there is no overt conflict in the observations because the stress field is known to have changed through time, knowledge of the timing of changing tectonic regimes and the age of formation of different fracture features is required for proper interpretations in any local area.

CONCLUSIONS

The existence of fracture data sets from three distinctly different sources in the Raton Basin project, and the both obvious and more subtle-but-yet significant differences among them, has prompted more than one wag to draw comparisons with the well-known parable regarding the three blind men and the elephant. Each of the proverbial men examines a different portion of the beast — the trunk, a leg, the tail — and arrives at a completely different conclusion regarding the overall nature and characteristics of the elephant. Although the differences among the three Raton Basin data sets may not be quite so glaring, and indeed, the commonalities among the three data sets led to identification of vertical extension fractures, inclined conjugate fracture sets, the existence of thrust-type displacements, and a profound reorientation of the stress regime at some time during the geological history of the basin, it is clear that the most complete model of natural fractures in a coal bed methane or fractured sandstone reservoir system is likely to be one that combines observations and interpretations from all three methods of observation.

The project is as-yet in an early stage of investigation. Future activities will focus on resolving issues related to spatial variability of orientations of different fracture types and the implications of such spatial variability to the stress history and the types of fractures and orientations to be expected at any given locality of interest. Additional emphasis will be placed on understanding the fracture characteristics of the various sills, dikes, and sill complexes that are a characteristic feature of the Raton Basin. The disparate locations studied by the geophysical investigations, core study, and outcrop exposures with respect to the topographically and geologically prominent intrusive center of the Spanish Peaks may significantly impact our understanding of the overall fracture system. Additionally, intrusive relationships among dikes and sills and their individual fracture systems, together with potential age-dating of selected intrusive rocks may provide important constraints on the change from a compressive stress regime to one of regional extension.

REFERENCES

Dolly, E. D., and Meissner, F. F., 1977, Geology and gas exploration potential, Upper Cretaceous and Lower Tertiary strata, northern Raton basin, Colorado, Exploration frontiers of the central and southern Rockies: Rocky Mountain Association of Geologists Field Conference Guidebook, p. 247-270.

Hemmerich, M., 2001, Cenozoic denudation of the Raton Basin and vicinity, northeastern New Mexico and southeastern Colorado, determined using apatite fission-track thermochronology and sonic log analysis: M.S. thesis, New Mexico Institute of Mining and Technology, Socorro, N. Mex.

ACKNOWLEDGMENTS

Ronald E. Graichen, of Winlock, Washington, assisted in logging the core provided by El Paso Production, operator of the El Paso-Raton, LLC, operation in northeastern New Mexico. The New Mexico Bureau of Geology and Mineral Resources curates core from the Raton Basin project and provided examination facilities.

Sandia is a multiprogram laboratory operated by Sandia Corporation, a Lockheed Martin Company, for the U.S. Department of Energy, under contract DE-AC04-94AL85000.

CONTACT INFORMATION

Christopher A. Rautman
Sandia National Laboratories
Underground Storage Technology Department
P.O. Box 5800; MS-0706
Albuquerque, NM 87185
505-844-2109
carautm@sandia.gov

APPENDIX B

Methodology for Specifying Failure Conditions for Sedimentary Rocks

Introduction

A critical need for the mechanical modeling of a geological structure from the point of view of a rate-independent, pressure-dependent constitutive model is the failure condition. A failure condition may be specified by several different but uniquely related functions. Some of these are the Mohr (or Mohr-Coulomb), the Griffith, and the Drucker-Prager. These can be examined in the book on rock mechanics by *Jaeger and Cook* (1969). For simplicity in this discussion I will use the most basic relation of standard rock testing; that is, maximum principal stress difference as a function of confining pressure (minimum principal stress). For the confining pressure range of interest to us, this relation is approximately linear such that

$$\sigma_1 - \sigma_3 = \sigma_o + (B-1)\,\sigma_3. \tag{1}$$

Here, $\sigma_1 > \sigma_3 > 0$ are the maximum and minimum compressive stresses, respectively. The coefficient B-1 derives from the simpler but equivalent relation

$$\sigma_1 = \sigma_o + B\,\sigma_3. \tag{2}$$

The constant σ_o is the unconfined compressive strength.

We begin to break the problem down by recognizing that in the geographic and geologic area that concerns us, there are at least 4 sedimentary rock types that will need to be included in the mechanical analysis (igneous rocks and unconsolidated surface materials are excluded): sandstone, limestone, shale, and coal. This is further complicated by the fact that there may be several different varieties of each rock.

The direct approach to this type of problem is to measure in the laboratory, for the 4 or more types of rocks encountered, the parameters required by the constitutive models of the codes used for the boundary value problem.

In a layer-cake problem, where there are not too many layers, and the layers are continuous across the model, the direct approach would make sense. If, however, there are, say, three different sandstones and two different limestones and possibly two types of shale this would lead to a very large amount of testing because to establish (1) requires tests at a minimum of two confining pressures. In addition some replication would be desirable. Given the time and budgetary constraints of the project, it may be best to address the issue of material properties using the methodology described in below.

Strength of sandstones

To the uninitiated it may seem that every sandstone with a different name would have a different and completely unpredictable set of material properties. Similarly there are a myriad of different limestone and shale formations, and so on. For the case of sandstones, it has been convincingly shown, that an underlying, intrinsic property of this rock type controls the strength (*Dunn et al*., 1973). This intrinsic property is the porosity. Figure 1 shows regression curves for maximum principal stress difference (hereafter referred to more simply as stress difference) versus porosity in percent in log-log space.

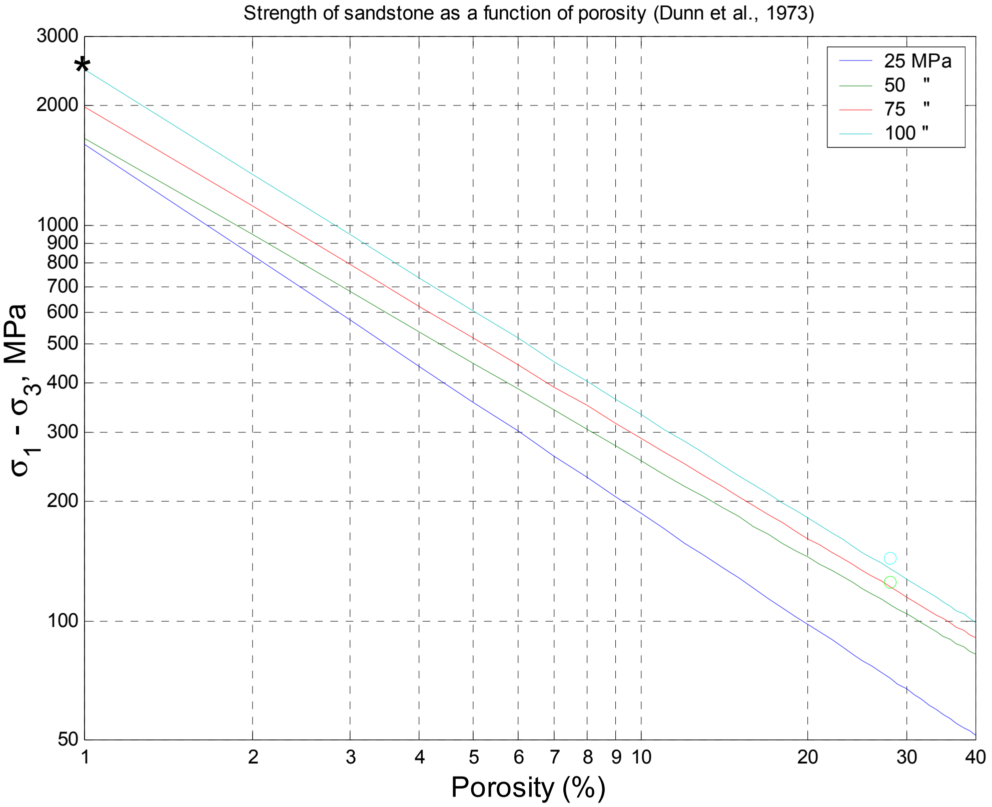

Figure 1: Maximum stress difference at failure for various sandstones plotted against porosity. Lines for the four different confining pressures indicated in the upper right. Circles are Sandia data for Castlegate sandstone of 28% porosity. The confining pressures for Castlegate are indicated by the same color code as the lines: cyan is 100 MPa, and (light) green is 50 MPa.

This plot was constructed for a variety of sandstones with porosities ranging from 2% to 24%. The asterisk indicates the strength of the mineral quartz, that provides an upper bound on strength for quartzose rocks at vanishing porosity. Also shown is our own data (*Olsson*, unpublished; *Olsson*, 1999) for Castlegate sandstone that has a porosity of 28%. This provides and independent check of the relations given in *Dunn et al*. (1973). The sandstones studied by *Dunn et al*. (1973) had different types of cement, suggesting the dominance of the porosity as the most influential variable.

Figure 2 shows this data as a plot of equation (1) for the different porosities studied by *Dunn et al.* (1973).

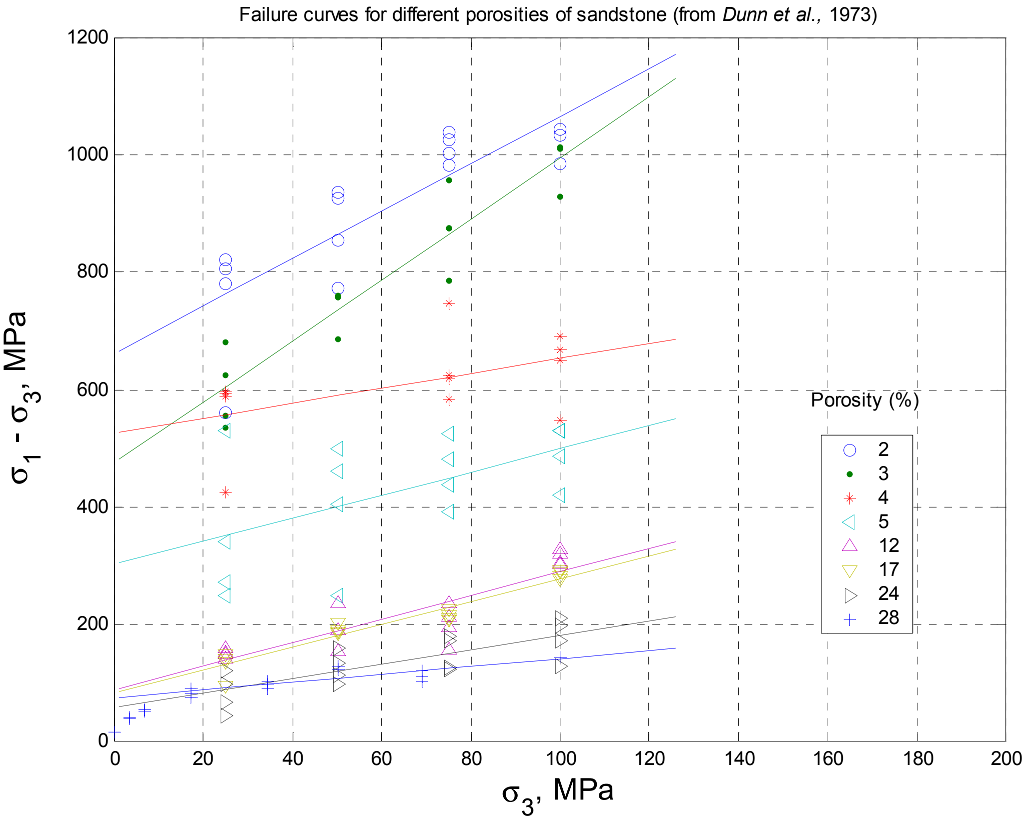

Figure 2: Strength versus confining pressure for sandstones of differing porosities. The 28-percent-porosity rock is from *Olsson* (unpublished, and 1999) for Castlegate sandstone.

The diagram in Figure 2 can be considered a contour map of the strength of sandstones. The individual contours are the failure curves for the individual rocks. Interpolation looks to be straight forward as there are no sharp kinks etc., the surface is just a sloping, plane for rocks with porosity between 3% and 24%. In fact, the rocks with the lowest porosities, 2 and 3%, were actually quartzites; that is, they had undergone some amount of metamorphism, destroying the porosity through grain growth. Therefore, for normal sedimentary sandstones, the two curves at the top can be deleted.

In Figure 3, the data have been replotted from a different perspective in the same 3-space (σ_3, porosity, σ_1 - σ_3) to emphasize the simplicity of the interrelationships of these variables. The data for the two quartzites have been omitted as there is none of this very strong metamorphic rock in the modeled area. The lines in the (σ_3, σ_1 - σ_3) planes are linear fits to the strength-confining pressure data. (The surface in this figure is not a regression surface.)

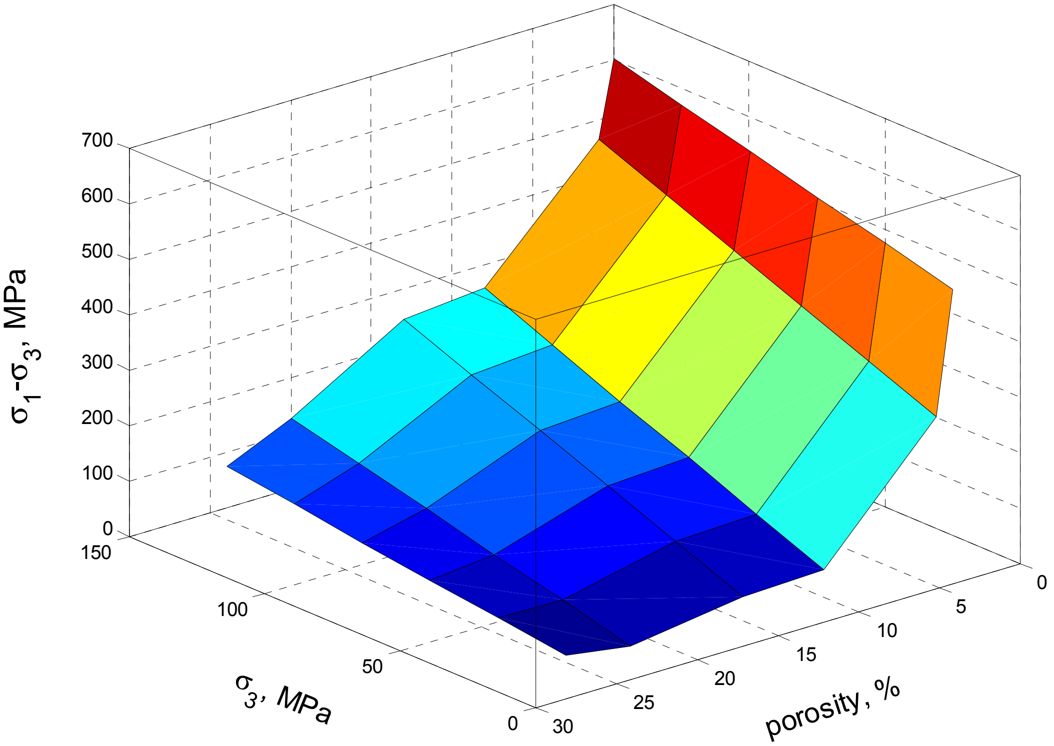

Figure 3: Strength versus confining pressure and porosity for sandstones. Same data set as Figure 2 with the quartzites omitted.

One of two approaches could now be taken. Either actually determine the porosities of the sandstones of interest, or simply choose a value that is thought to be representative of the types of sandstones that may be found in a particular area such as aeolian, beach, or deltaic.

Strength of shale

Shales, which are clastic rocks of measurable porosities, do not fit into this scheme because the minerals are layered silicates and deformation can be intra- and inter-granular. Also, the rock is very anisotropic in its properties. It is fortunate that there exist data on the strength of Pierre shale (*Kirby and McCormick*, 1984) for confining pressures that include the range we might be interested in. In Figure 4 data for Pierre shale has been added to the data set.

Strength of coal

Coal is another important rock in the basin. Fortunately there is a set of data for a sub-bituminous coal from Wyoming (*Kirby and McCormick*, 1984) that may be similar in its mechanical properties to the coal in the section from the Raton basin. The failure curve for coal has also been added to the strength plot in Figure 4.

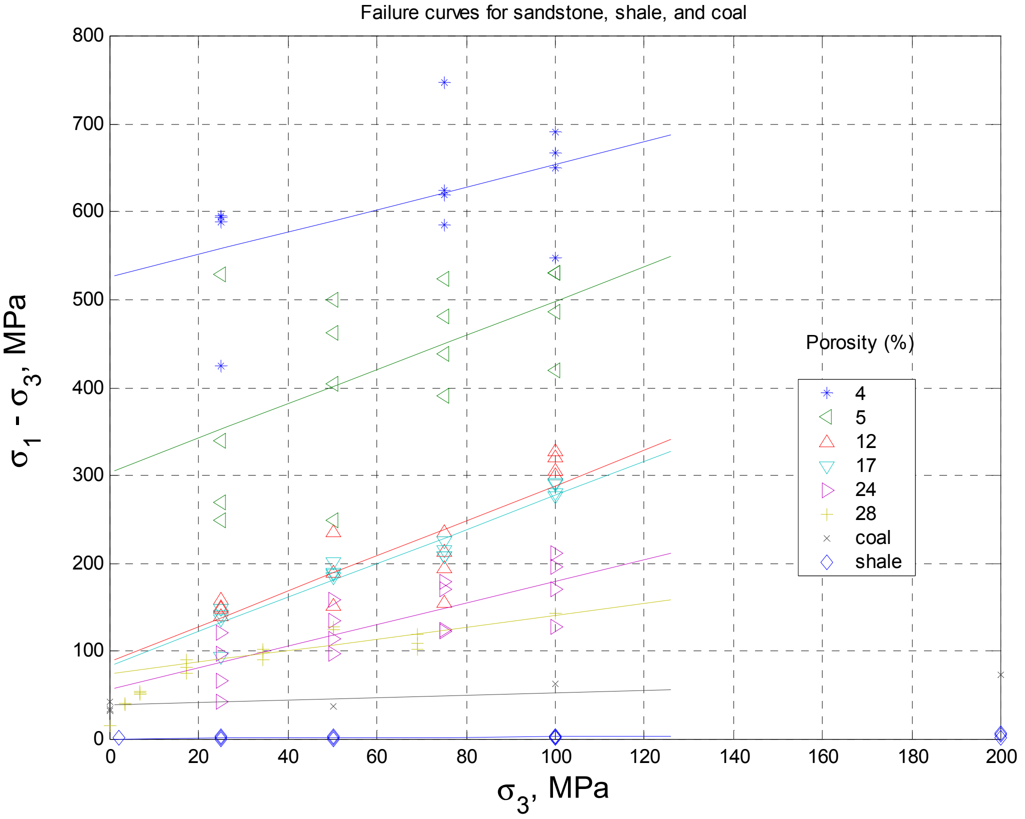

Figure 4: Strength map for clastic rocks and coal that may be typical of the Raton basin. Same as Figure 2 with the addition of curves for Pierre shale and sub-bituminous coal from Wyoming. Note that shale has a very low σ_o and vanishingly small (B-1). See Table 1.

Strength of limestone

The last rock type that concerns us for modeling the basin mechanics is limestone. As with sandstone, previous work by *Olsson* (1974) shows that an intrinsic variable controls the strength of calcite based rocks--limestones and marbles. The controlling intrinsic variable for limestone strength is the grain size. *Olsson* (1974) showed that the strength varies as the inverse of the square root of the grain size, and that this can be explained in terms of the length of slip bands or twin lamellae in calcite. The strongest limestones are those with smallest grain size, and Solenhofen limestone is one of the finest grained limestones ever studied, with an average grain diameter of 0.005 mm. A search of the literature showed that the other end of the grain size continuum was occupied by Yule and Yamaguchi marbles with a grain size of 3.5 mm. Data at different confining pressures is tabulated for Solenhofen and Carrara marble in *Kirby and McCormick* (1984). Carrara has a grain size of 2.2 mm and is thus very near to the lower bound in strength. In fact because the strength varies only slowly with grain size at these large sizes, the data for Cararra is assumed to be representative of the weakest limestones. The strength curves for these two rocks, Solenhofen and Carrara, are taken to serve as upper and lower bounds, respectively, on the strength of limestones.

To compare the potential range of limestone strength with that of the clastic rocks, I have added the curves to the plot of Figure 4 and plotted all data needed for the Raton basin in Figure 5. The range of possible limestone strengths lies within the potential range of sandstone strengths. Further, the pressure dependence of carbonate rocks, as given by
B-1, is somewhat less than for the sandstones.

Hugman and Friedman (1979) extended the microstructural basis for strength of carbonate rocks to include several other limestones and dolomites. As a check on the upper and lower bounds shown in Figure 5, I have plotted their data (only obtained at 100 MPa confining pressure) for the two extremes of grain size they studied 0.22 and 1.56 mm as stars. The agreement is very good.

As with the porosity for sandstones, the most objective method to estimate the strength of the limestones present in a region would be to determine the grain size. But again, it may be possible to apply geologic reasoning to choose a representative grain size and thus an appropriate failure criterion.

Failure parameters σ_o and B-1 are summarized in Table 1 for all the rocks discussed above.

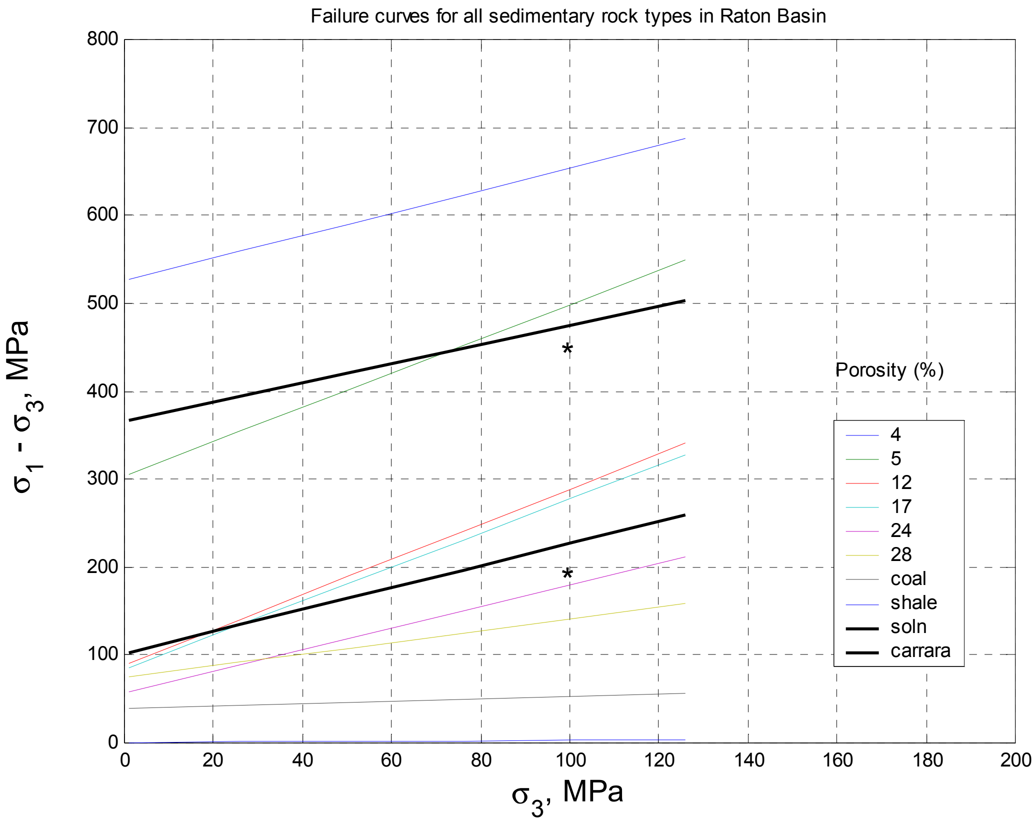

Figure 5: Failure curves for all major sedimentary rocks found in the Raton basin. All limestones fall between the two heavy black lines. The individual data points have been omitted for clarity. The two asterisks are for data from *Hugman and Friedman* (1979).

It is clear from Figure 5 that any estimate of sandstone and limestone failure criteria will give strengths far greater at all confining pressures than either coal or shale. Thus the presence of coal or shale layers will induce a very strong anisotropy in the sedimentary stack. If they were to be found in more lensoidal shapes, they would act as soft inclusions. This would appear to very much complicate the construction of a mechanical stratigraphy.

Mohr representation for the data

Some algebraic manipulation will show that σ_o and (B-1) of equation (1) can be related to C and ϕ of the Mohr (-Coulomb) relation

$$\tau = C + \tan\phi \, \sigma \qquad (3)$$

where τ is the shear stress and σ is the normal stress at the point of tangency of the failure envelope to the maximum stress circle at failure. The slope of the failure line is $\tan\phi$ where ϕ is the angle of internal friction. The relations between the constants in (1) and (3) are:

$\sin\phi = \tan(B\text{-}1)/(2 + \tan(B\text{-}1))$

$C = \sigma_o \tan\phi/\tan(B\text{-}1)$.

The parameters C and $\tan\phi$ are listed in Table 1 as well as the parameters σ_o and B-1 for equation (1).

Table 1: Failure parameters for sedimentary rocks.

Rock Type	σ_o (MPa)	B-1	C (MPa)	$\tan\phi$
Sandstone				
porosity = 2%	662	4	148	0.89
3	474	5.2	95	1.04
4	526	1.28	174	0.42
5	303	1.95	88	0.57
12	88	2.00	25	0.58
17	83	1.94	24	0.57
24	57	1.22	19	0.41
28	74	0.66	29	0.26
Pierre shale	0.26	0.028	0.13	0.01
Coal	39	0.15	18	0.07
Solenhofen limestone	366	1.09	127	0.38
Carrara marble	102	1.25	34	0.42

What about joints, faults and bedding surfaces?

So far we have considered intact rock strength. What do we do about the many discontinuities such as joints and bedding surfaces in the modeled volume? The simplest approach for like rock-on-rock, i.e., a joint through a bed, would be to apply

$$\tau = \mu\sigma \tag{3}$$

where τ is shear stress required for slip, σ is the normal stress, and μ is the coefficient of friction. The stresses τ and μ are referred to the plane of slip. According to *Byerlee* (1978), for many rock types at normal stresses below about 100 MPa, $\mu = 0.85$. My own experiments on surfaces of various kinds of tuff give $\mu = 0.6$ and greater. Therefore, it would be conservative to consider 0.85 as an *upper bound* on friction.

There appears to be little or no data concerning sliding of one rock type against another. The question of the magnitude of the strength of an interface between shale and a stronger rock thus has no clear answer, but it must be bounded above by the shear strength of the weaker material

Interrelationship of intact failure strength to frictional strength

This section is just a note to provoke thought on the concept of intact strength for layers that may have joints in them. Figure 6 is a sketch of how the frictional strength interacts with the intact strength for a given rock. The two circles represent failure stresses at two confining pressures for a rock and the failure envelope (blue line tanϕ = 0.6) is drawn tangent to the circles. The red line is the failure curve for frictional sliding based on Byerlee's law, μ = 0.85. For a particular state of stress in the region where the red line lies below the blue line, failure is predicted to occur at shear stress below intact strength on planes of orientation lying between E and F. The angle θ is measured between the normal to the sliding plane and the maximum compression direction. At any normal stress above (to the right) of the intersection of the blue and red lines, failure is by intact rock fracture. Note that if μ = 0.6, the friction line would lie parallel to the intact failure line, and sliding would generally precede/preempt 'intact' failure in rock layers that contained fractures.

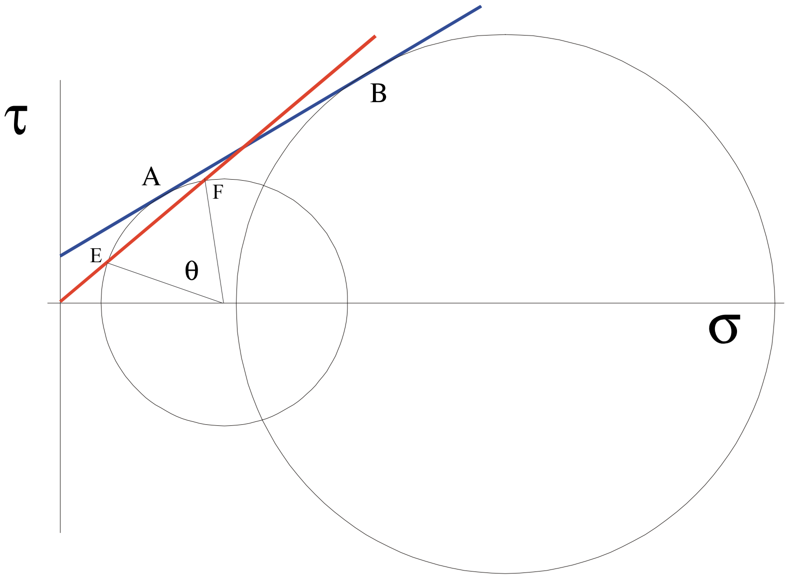

Figure 6: Mohr plot for intact (blue, tanϕ = 0.6) and friction on interface (red, μ = 0.85). Angular range over which slip occurs before intact failure given by θ.

Summary

This discussion suggested that it may be possible to choose reasonable strength parameters for the sedimentary rocks occupying the Raton basin without a systematic laboratory testing program. The proposed methodology is based on the proven concept that microstructural properties are related to strength for sandstones and limestones.

It is suggested that frictional strength may be chosen with acceptable accuracy by taking Byerlee's law (coefficient of friction = 0.85) as the upper bound.

Some simple interrelationships between intact and frictional strength were reviewed.

APPENDIX C

Calculated Reflection/Transmission Coefficient Curves for Shale overlying Basalt

Attached are three plots depicting seismic reflection and transmission coefficients, as functions of the angle of incidence θ of a plane P-wave onto a plane shale-basalt interface. The three plots correspond to different values of the seismic parameters assigned to the shale and basalt units:

Case 1: Strong impedance contrast.

Case 2: Average impedance contrast.

Case 3: Weak impedance contrast.

Values of compressional (P) wavespeed α, shear (S) wavespeed β, and mass density ρ assigned to shale (medium 1 - overlying) and basalt (medium 2 – underlying) are indicated on each plot. Reflection and transmission coefficient curves are displayed for the full range of incidence angles of the plane P-wave: $\theta = 0^o$ corresponds to normal incidence and $\theta = 90^o$ corresponds to grazing incidence.

The reason for considering three different cases is that the literature suggests that P wavespeed α and mass density ρ of both shale and basalt can vary quite widely, depending upon porosity, fluid saturation, mineral content, depth of burial, age, fracturing, vesiculation, etc. I selected values of α and ρ for the three cases from a brief literature search, and then calculated S wavespeed β by using the common assumption that the Poisson ratio of the two media is equal to 0.25.

On each plot, the top panel displays reflection coefficients and the bottom panel displays transmission coefficients. The curve that is most relevant to your situation is the "P-to-P" reflection coefficient curve labeled "R_{PP}" in the top panel. This curve is interpreted as the amplitude of a reflected plane P-wave, generated by an incident plane P-wave with unit amplitude onto the shale-basalt interface.

Clearly, these R_{PP} reflection coefficient curves exhibit significant variability between the three cases. Also, each curve varies strongly over incident angle θ in any individual case. The peak in the curve (at $\theta \approx 20^o$ for case 1, $\theta \approx 30^o$ for case 2, $\theta \approx 68^o$ for case 3) is referred to as a "critical angle effect", and indicates a very strong reflection characteristic. However, for most conventional seismic reflection work, the data acquisition geometry is such that the angle of incidence of the downgoing P-wave onto a subsurface reflecting horizon is less than the critical angle. Thus, we should concentrate on the portions of the R_{PP} curves ranging from $\theta = 0$ up to $\theta = \theta_{crit}$.

For the low angle (i.e., near-normal incidence) range, the numerical values of the three R_{PP} reflection coefficient curves are quite large. Conventional wisdom is that a shallow subsurface interface typically has a seismic reflection coefficient of about ~0.04, and a deep interface has a reflection coefficient of about half of that (~0.02). Thus, the present reflection coefficients are significantly larger in magnitude. Indeed, a reflection coefficient in the range of 0.4 to 0.6 (as in cases 1 and 2) would be regarded as atypically large. Even the weak impedance contrast case 3 yields a reflection coefficient above 0.1. Hence, *in the absence of other perturbing influences*, one would expect to observe a significant seismic reflected arrival (PP) from a shale-basalt interface of this type.

Of course, there are many reasons why a PP reflection might not be observed in the field recorded and processed seismic data. The two that we have discussed are 1) the subsurface shale-basalt interface is significantly more rugose than a simple plane, and hence would tend to scatter rather than coherently reflect seismic energy, and 2) a disturbed and/or highly variable shallow subsurface zone is scattering and attenuating the seismic waves, both downgoing and upcoming. I agree with the assessment made from the plotted field shot gathers that there is a noticeable “reflection event dimout” over a portion of the seismic line of interest (between shot points labeled 1101 and 1501). Subsequent processing of these data cannot be expected to create reflection event that are lacking in the field-recorded data. However, I do not understand why this event dimout constitutes strong evidence for a lack of a shallow subsurface problem affecting seismic reflection quality.

Dave Aldridge

Geophysical Technology Department
Sandia National Laboratories
Albuquerque, New Mexico, USA, 87185-0750

505-284-2823
dfaldri@sandia.gov

Case 1: shale over basalt, strong impedance contrast

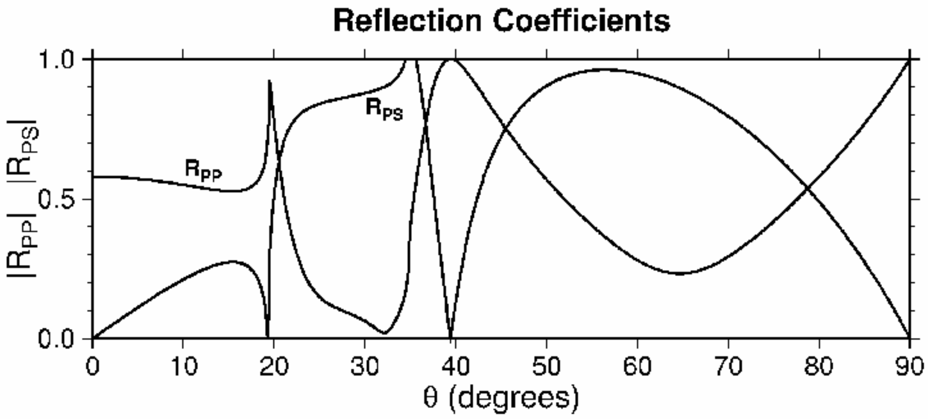
Reflection Coefficients

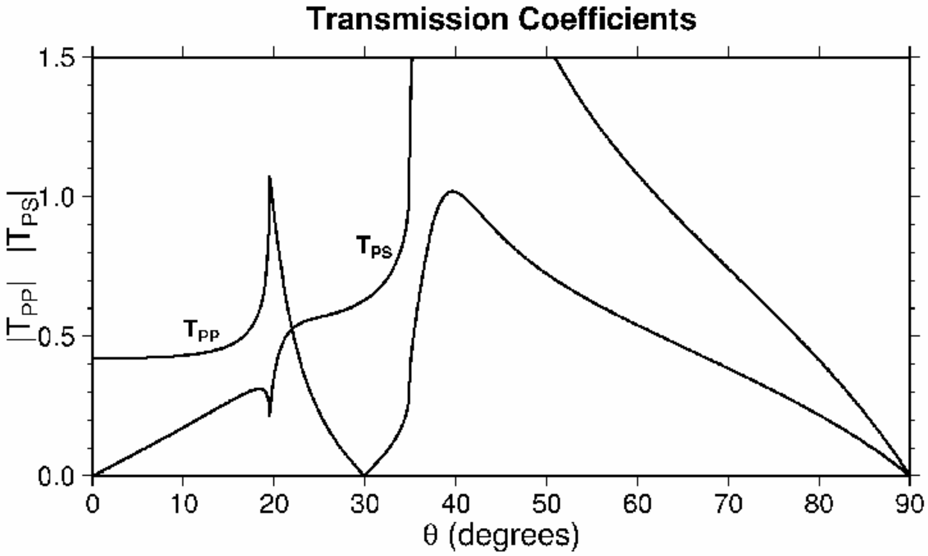
Transmission Coefficients

Plane P wave incident from medium 1

α_1=2.0 km/s β_1=1.2 km/s ρ_1=2.4 gr/cm^3 (shale)
α_2=6.0 km/s β_2=3.5 km/s ρ_2=3.0 gr/cm^3 (basalt)

critical angles: θ_{crit} = 19.5°, 34.9°

Case 2: shale over basalt, average impedance contrast

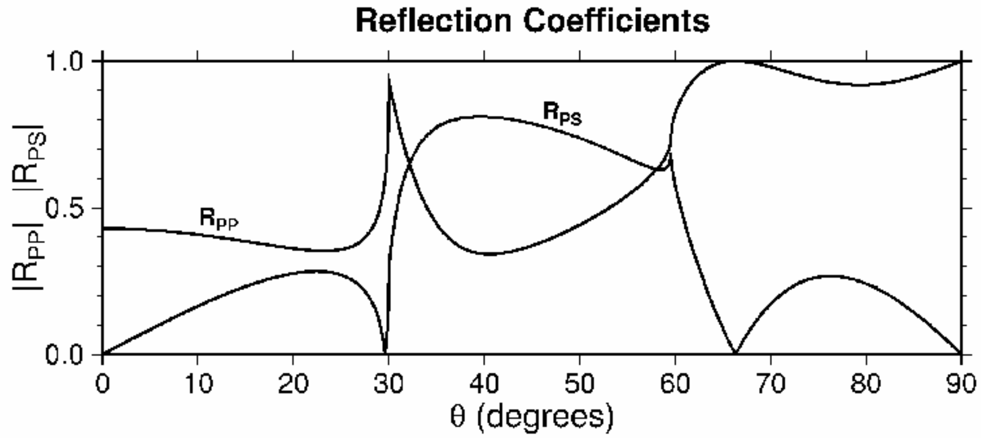

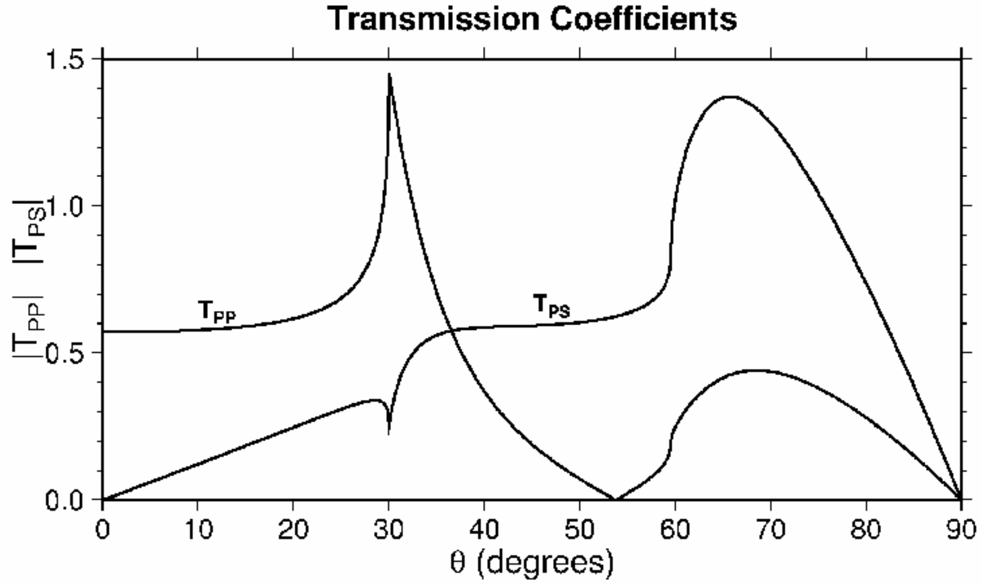

Plane P wave incident from medium 1

α_1=2.5 km/s β_1=1.4 km/s ρ_1=2.4 gr/cm^3 (shale)
α_2=5.0 km/s β_2=2.9 km/s ρ_2=3.0 gr/cm^3 (basalt)

critical angles: θ_{crit} = 30.0°, 59.6°

Case 3: shale over basalt, weak impedance contrast

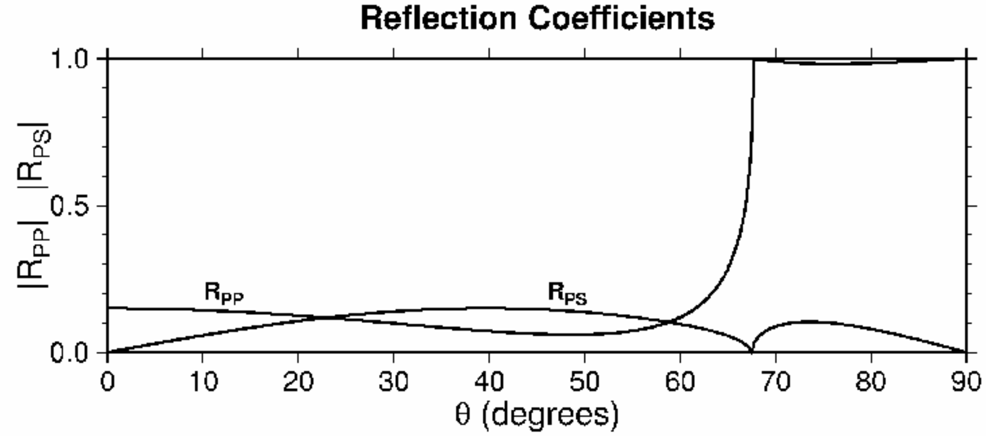

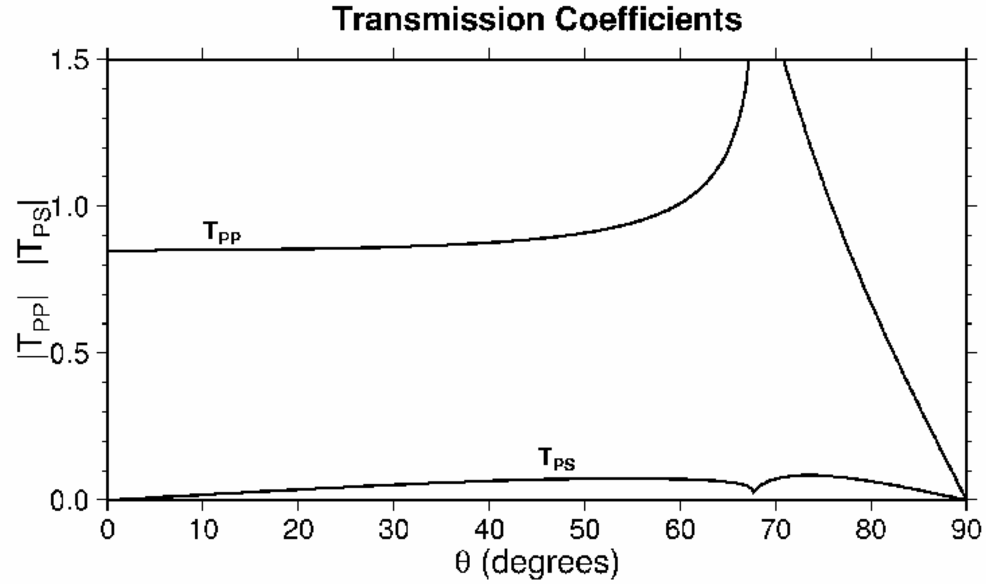

Plane P wave incident from medium 1

α_1=3.7 km/s β_1=2.1 km/s ρ_1=2.4 gr/cm^3 (shale)
α_2=4.0 km/s β_2=2.3 km/s ρ_2=3.0 gr/cm^3 (basalt)

critical angle: θ_{crit} = 67.7°

APPENDIX D

Raton Basin Field Trip

August 4&5, 2003
Vermejo Park
&
Southern Colorado

John C. Lorenz
Scott P. Cooper
Matt Herrin
Russell G. Keefe

Geophysical Technology

TABLE OF CONTENTS

Field Trip Stops

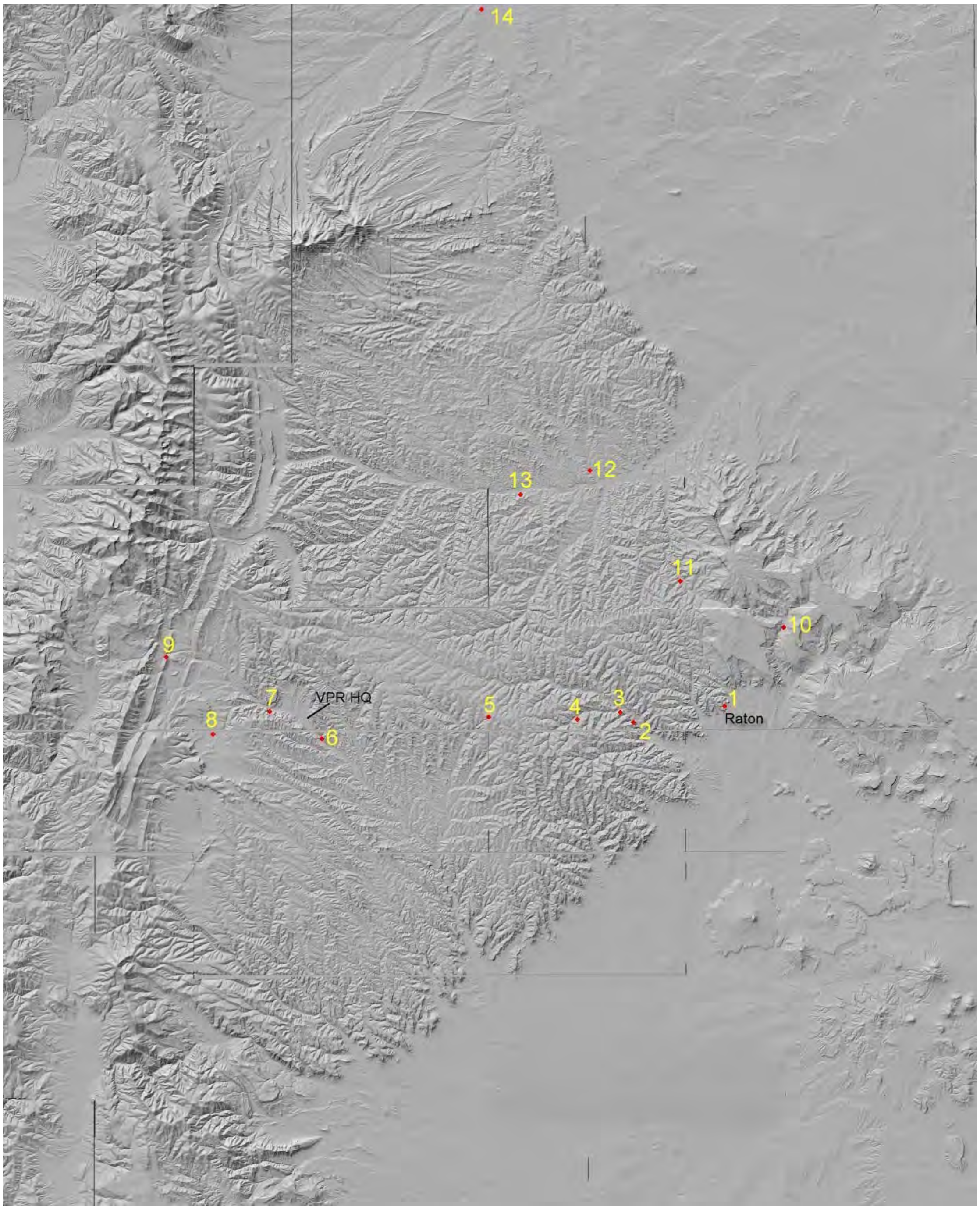

Actual order taken on August 4th & 5th:

Day 1: Stops 1, 2, 3, 4, 6, 9, 8, 7

Day 2: Stops 11, 12, 13, 14

Stop 1: Overview—Raton overlook and K/T boundary site

The Raton Basin (Figure 1) is a 150 x 120 mi north-south trending basin (Tremain, 1980) wherein the coal section covers an area of over 2100 square miles. It is bordered on the west by the Sangre de Cristo Mountains, to the north by the Wet Mountains, to the northeast by the Apishapa Arch, to the east by the Las Animas Arch and to the southeast and south by the Sierra Grande Uplift. The basin was formed during the Laramide orogeny as tectonic activity uplifted the Sangre de Cristo Mountains and created numerous folds and reverse faults across the basin. The western margin of the basin has numerous thrust faults and is highly deformed. In contrast the eastern limb gently dips, 1-2 degrees, toward the west. The basin is highly asymmetrical with its synclinal axis parallel and near to the Sangre de Cristo uplift.

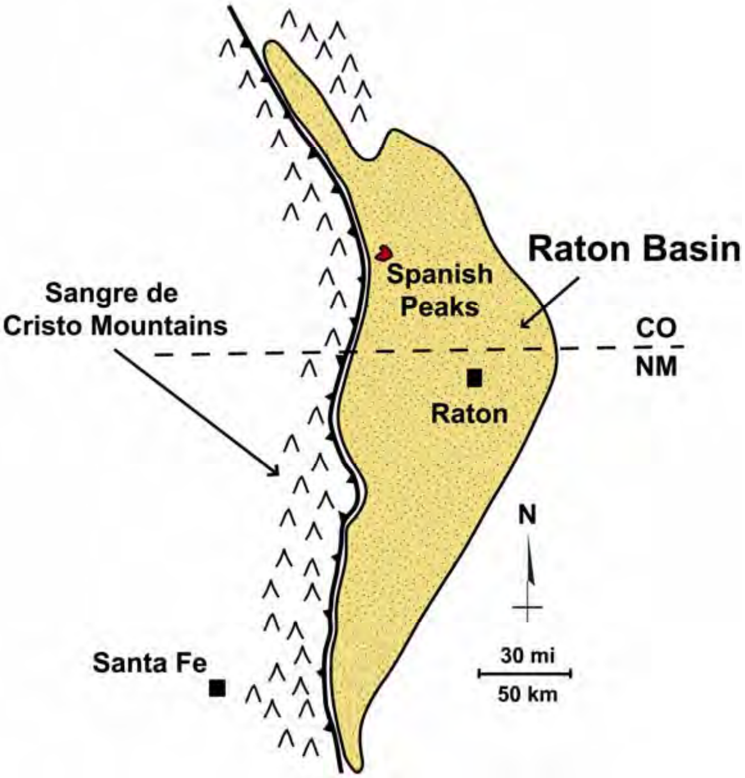

Figure 1: Map of the greater Raton Basin

Tertiary deposition within the basin was directly tied to ongoing orogenic activity. In Late Cretaceous time the Raton area was the southern extension of the Rocky Mountain Foreland Basin. Formations deposited along what was then the coast of the Western Interior Seaway included the Pierre Shale, Trinidad Sandstone and the Vermejo Formation (Figure 2). East directed thrusting continued and eventually isolated the Raton Basin from the main foreland basin as evidenced by conglomerates within the Raton Formation. Tectonic activity continued into Paleocene time with the associated deposition of the Poison Canyon Formation. Further activity continued into Eocene time with deposition of the Cuchara, Huerfano and Farasita Formations. It is only within Eocene time that the Sangre de Cristo Mountains became a source of sediment (Merin et al., 1988; Tyler et al., 1995).

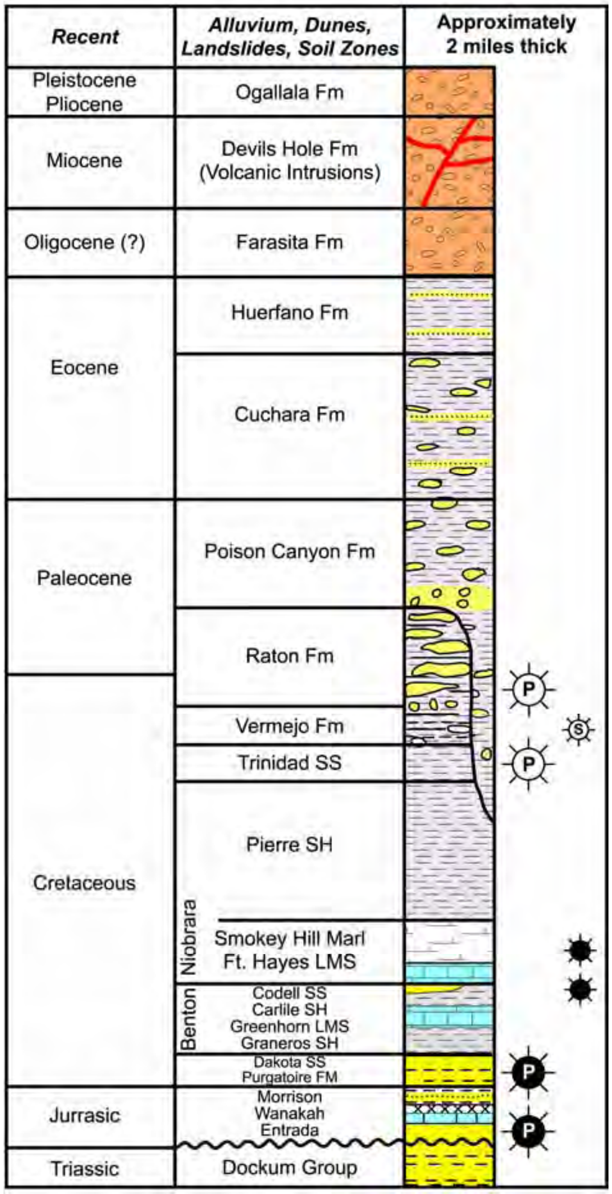

Figure 2: Geologic column of the Raton Basin area. Symbols to the right of the column indicate gas (white/open symbols) and oil (black/closed symbols) shows and/or production (modified after Dolly and Messier, 1977).

Igneous rocks intruded the Raton Basin complex during the mid- to late Tertiary eras. These intrusives are in the forms of stocks, laccoliths, sills and dikes (Figure 3). The densest area of intrusive activity centers around the Spanish Peaks and are 22-25 million years old (Penn and others, 1992). Numerous dikes and sills are also found throughout the basin (Figure 3). Recent sheet basalts capping the mesas in the Raton/Trinidad area are dated at 3.5 to 7.2 mya (Baldwin and Meulberger, 1959). The youngest volcanics are in the Capulin area, dated at 18,000 to 4500 years old (Kudo, 1976).

This geologic sequence of events (deposition, coupled tectonism with deposition, and volcanic intrusion) has combined to make the Raton basin a complex system.

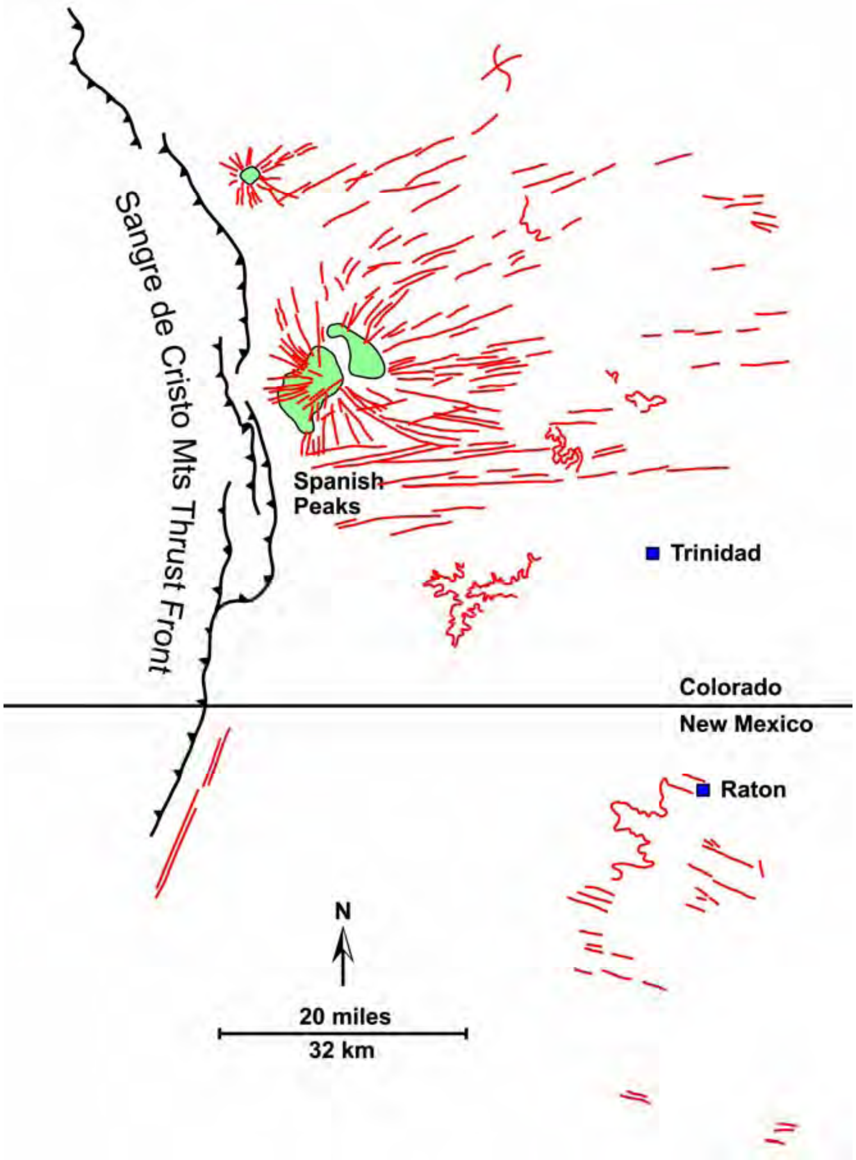

Figure 3: Map of larger scale intrusions within the Raton Basin. Due to the map scale numerous small dikes and sills are not shown. Volcanic intrusions are paleostress indicators.

K/T Boundary

K/T boundary Ir anomaly is 5 cm below a thin coal bed and at the top of a 2-3 cm thick kaolinite clay bed at this locality (Pillmore and Flores, 1984).

Stop 2: Fractures in road cut through Vermejo Fluvial sandstone, north and south sides of NM 555

This fluvial sandstone in the lower part of the Vermejo Formation is cut by numerous vertical extension fractures that strike essentially east-west, with a secondary/younger set of fractures striking north-south. Fractures cut vertically through the entire thickness of the two-meter-thick sandstone, and are stained with iron oxide. Some have remnant plumes suggesting an origin in extension. Maximum fracture spacing is half of the bed thickness, and most fractures are considerably more closely spaced. A well drilled into this sandstone would have good access to gas in the porosity via the fractures. Fractures of the same sets are more closely spaced in the thinner-bedded, more heterogeneous strata that are interbedded with the channel sandstone near the top. Most cleats in the associated coals are parallel to fractures in the sandstones, but locally cleating is oblique to the fractures, especially where sandstones directly overlie coal, suggesting that some shear occurs near this contact.

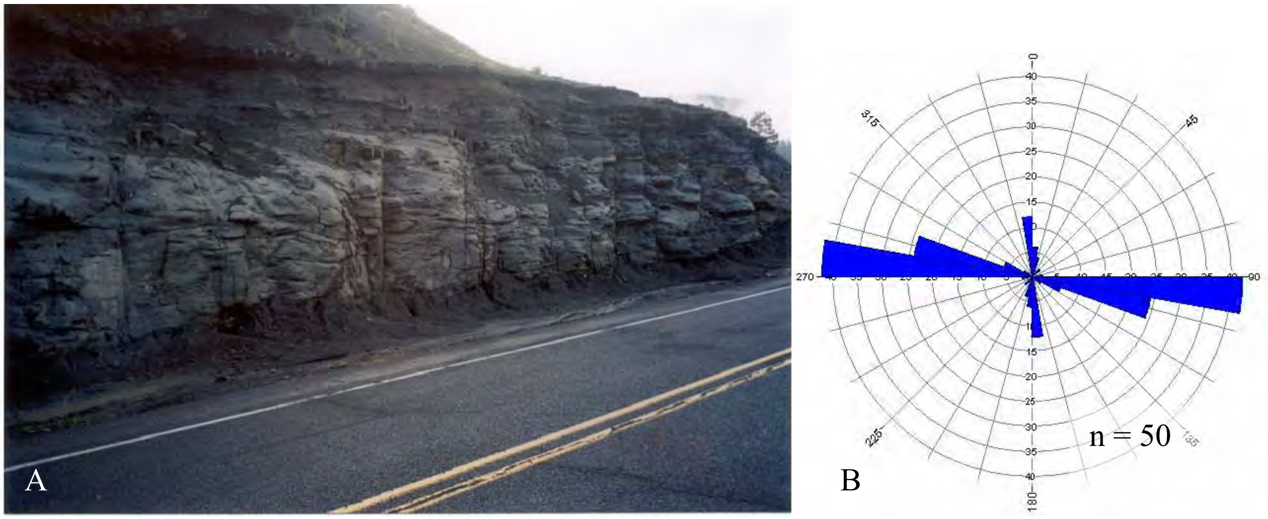

Figure 4: A) Fractures in fluvial sandstones of the Vermejo Formation on Hwy 555, and B) their orientations

Stop 3: Sills along the Canadian River north of Hwy 555

At this stop sills intrude the Vermejo Formation. A small coal dike, similar to one near the Vermejo Park Ranch headquarters is observed here. Coal liquefies at 450 degrees F. Transfer of plane of intrusion of sill suggests pushing the center of the earth down but this is probably an illusion. The sedimentary units are probably caught between the leading edge of two sills (or a bifurcation of a single sill). Fractures in the sills and adjoining sedimentary rocks can be similar.

Figure 5: A) Sills at this location can be difficult to distinguish from the baked siltstone units they intrude. B) Plume structures on fractures in sills. A thin coked coal bed overlies the sill.

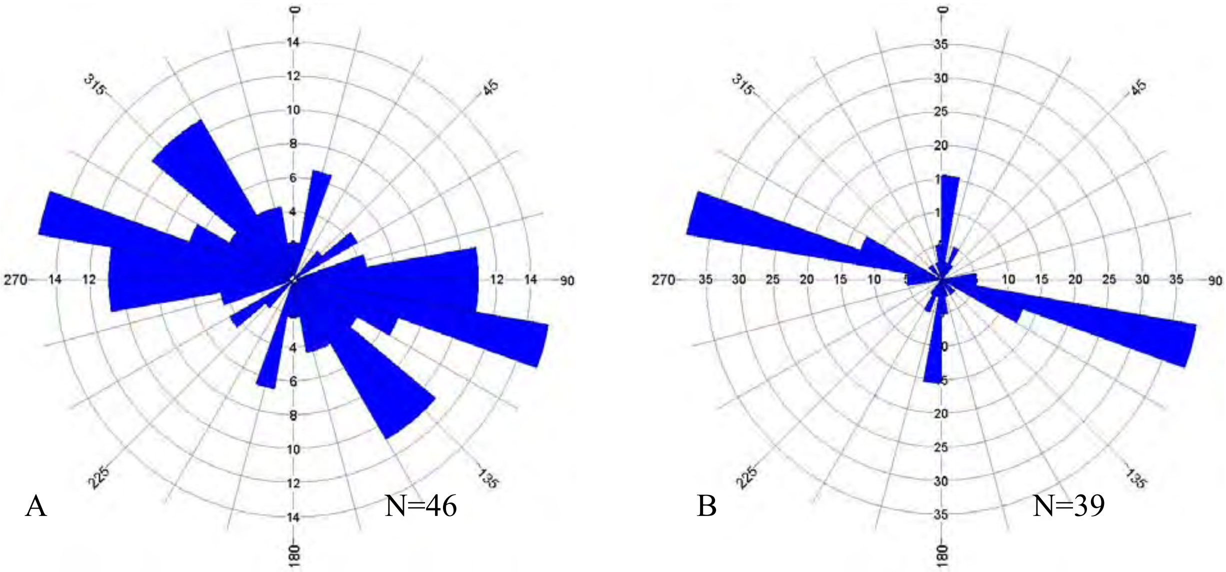

Figure 6: Fracture orientations within A) siltstone units, and B) sills.

Stop 4: The “Whale” syn-depositional structure between mile markers 12 and 13, south side of NM 555.

This large (20 meters diameter) sandbody of ambiguous origin was referred to Pillmore as a “foundered” sandstone in a photo caption found in a NMGS field guidebook. The unit was deformed by rotation around a horizontal, southeast-northwest trending axis (down on the northeast, up on the southwest) during deposition. Some of the muddy overbank strata were incorporated into the rotating unit and are now overturned. The overturned strata are found adjacent to the upper, western margin of the unit. Similarly deformed overbank strata are vertical on the lower, western margin of the unit. Evidence of syn-sedimentary deformation includes consistently steepening bedding within the sandstone and drag/smear near the lower contact. A two-meter-thick coal thins over the top of this unit, suggesting that it was a topographic high during deposition of the coal. The coal was apparently incorporated into the rotating block on the northeastern side, where the fluvial sandstone is considerably thicker than on the southwestern side.

The origin for this feature is ambiguous, but it may be related to syn-sedimentary deformation of more obvious genesis (slumping and intraformational thrusting) found elsewhere in the basin.

Figure 7: Syn-sedimentary deformation in "The Whale"

Figure 8: Progressively steeper bedding within the sandstone at lower edge of "The Whale". The black line was added to highlight bedding.

Stop 5: Syn-depositional fold in the Poison Canyon Formation along Hwy 555.

Laramide west-to-east thrusting formed the Sangre de Cristo Mountains and the Raton basin. The views at this local highlight the large-scale nature of this tectonic event.

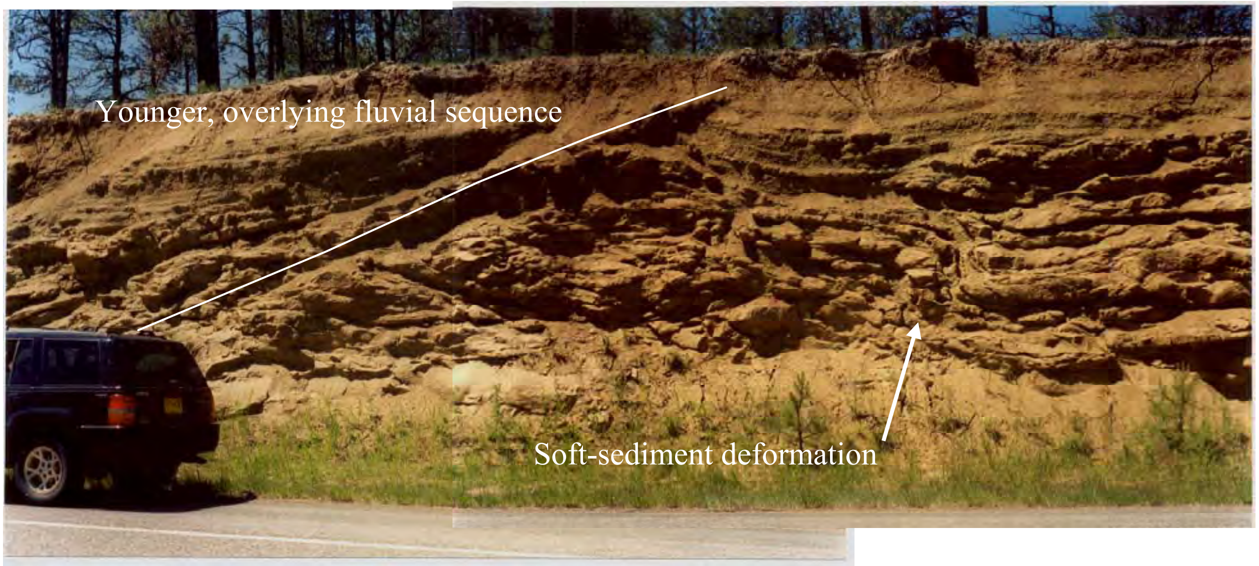

Figure 9: Prograding fluvial sequences and soft-sediment deformation structures wthin the Poison Canyon Formation can be observed here.

Stop 6: Raton Conglomerate, Reed Canyon

Conjugate fractures dictated by the more brittle nature of the quartzose Raton Conglomerate indicate a different mechanical response to the same compressive stresses than less brittle rock units. Conjugate fracture systems are better connected and should provide a better reservoir plumbing system.

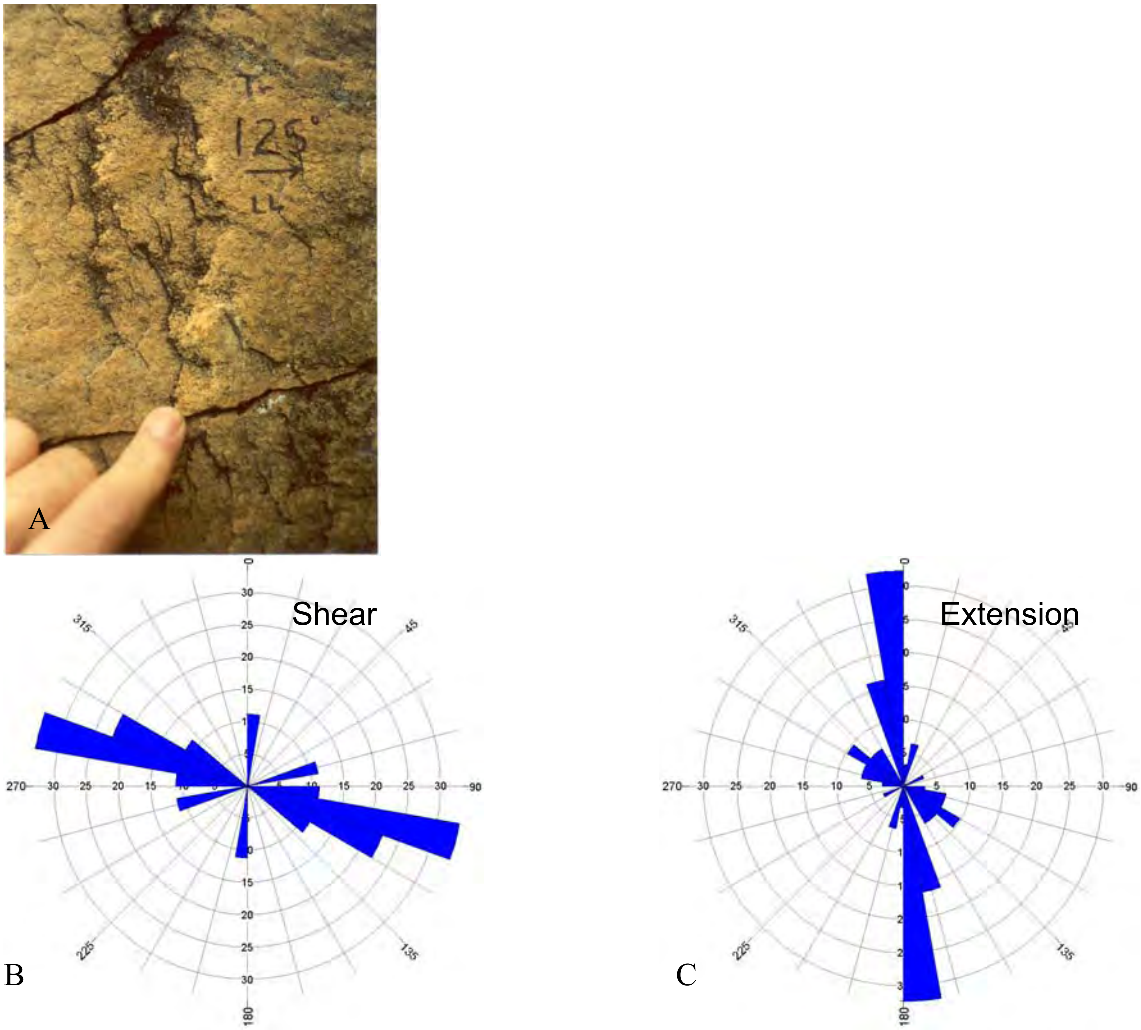

Figure 10: A) Steps instead of plumose structures on fracture surfaces indicate an origin in shear rather than extension. Shear indicators were found in the Raton Conglomerate in many locations around the Vermejo Park Ranch. Rose diagrams show difference in dominant orientation for shear fractures (B) versus extension fractures (C).

Stop 7: Trinidad thrust, west gate to Vermejo Park Anticline.

Figure 11: Thrust within the Trinidad Sandstone places lower *Ophiomorpha* burrow bearing sandstone against upper non-*Ophiomorpha* bearing sandstone (approximately 10-15 meters of vertical offset).

Figure 12: Photograph of back thrust, striking parallel to the thrust fault but dipping east to intersect it.

Figure 13: Photograph of minor thrust fault within Trinidad sandstone on west rim of the anticline, 4-5 miles to north of the thrust at stop 7. Orientation and sense of motion are similar.

Stop 8: Castle Rock Park stop with discussion concerning production.

Figure 14: Photograph of Bubbling Springs at east end of Castle Rock Park. Castle Rock, a remnant channel sandstone with cross-stratification indicating north-south paleoflow, is in the middle right of photograph.

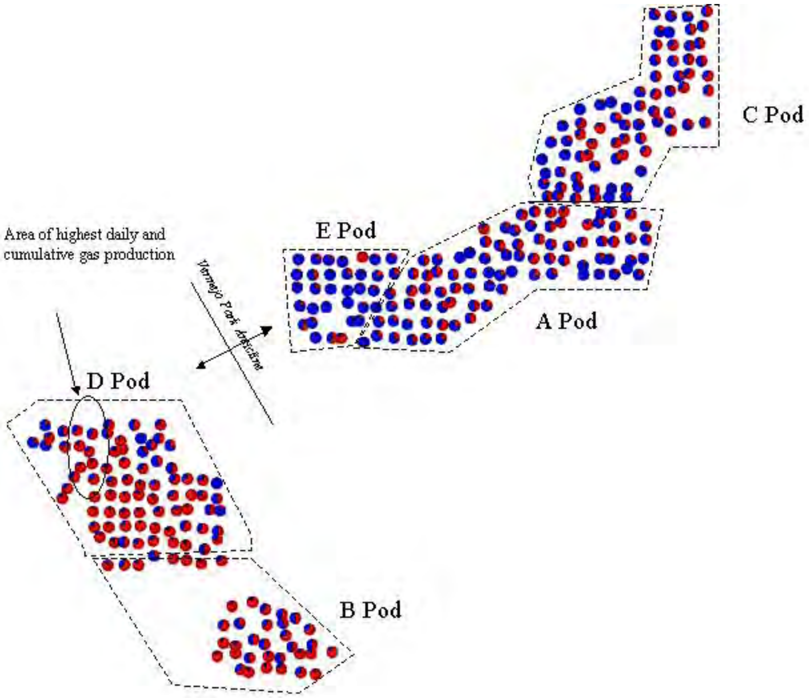

Figure 15: Pie chart map showing relative amounts of water (blue) and gas (red) produced on a daily averaged basis. The best gas producers of the lease are near where we are standing.

Stop 9: Overturned Dakota Sandstones at the western edge of the basin.

From our last stop, we drive toward the western edge of the structural basin. Note that as we drive down section, formations dip to the east at increasingly steeper angles, until at this stop the beds of the Dakota Formation are overturned to the west.

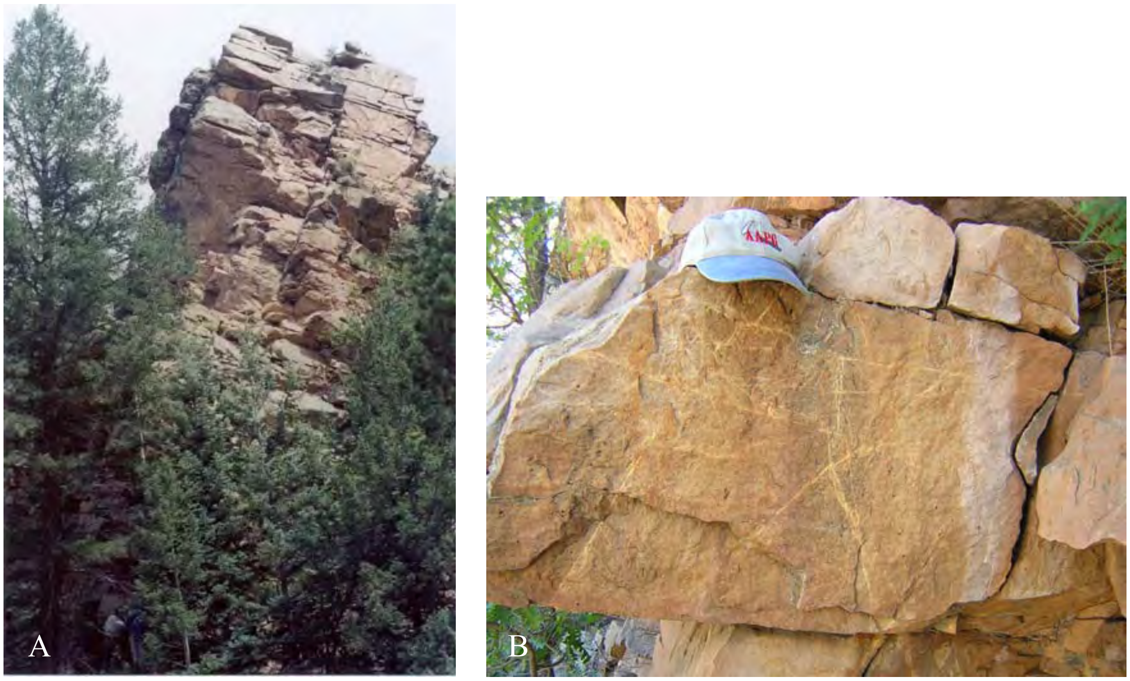

Figure 16: A) overturned wall of Dakota Formation. B) deformation bands within the well-silicified Dakota sandstone.

Deformation bands typically form in high porosity sandstones suggesting they formed early before the Dakota Sandstone was altered to its current low-porosity, well-silicified state. Bed-parallel stylolite surfaces and well developed bed-normal shear planes are also common at this location.

Stop 10: Syndepostional structures at Lake Maloya spillway

Detail of rollover sandstone and bounding fault: damp geologist for scale

Close-up of 15 cm thick fault smear (knife for scale). Smear consists of amorphous clay with coaly inclusions, suggesting incorporation/injection along the fault prior to lithification.

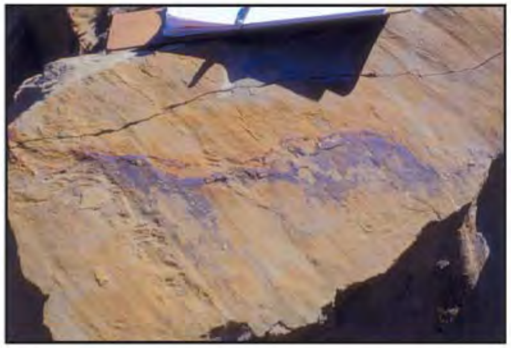

Fault surface where it cuts across sandstone (clip-board with pencil for scale). Low-relief lineations suggest some induration of the sand but lack of gouge and slickensides indicates it was not significant.

Photomosaic of syn-sedimentary growth faulting at the Maloya Lake spillway, Sugarite State Park, New Mexico.

Line drawing from photomosaic above

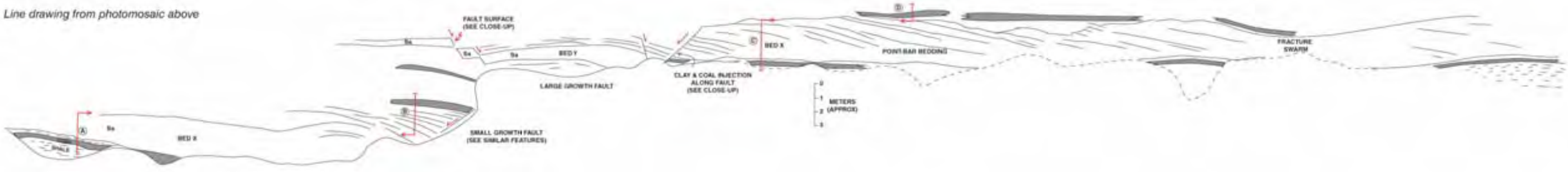

Sandstone thickens and rolls over into an east-west trending fault, implying that faulting was contemporaneous with deposition. Measured sections through the associated coaly strata suggest that the three-meter thick sandstone with lateral-accretion bedding to the right of the fault is equivalent to sandstone at the base of the exposure to the left of the outcrop, not to the rolled-over sandstone in the graben. Offset along the fault is therefore about 27 m.

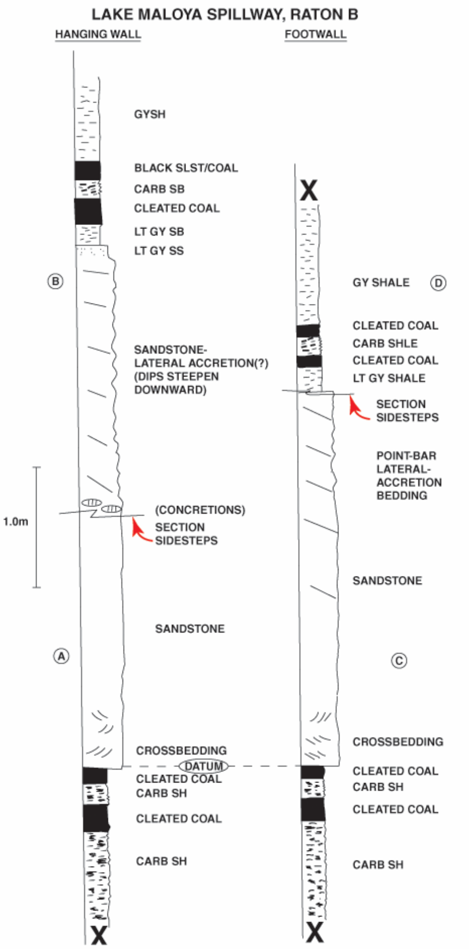

Figure 17: Composite sections through the sandstones and coals left and right of the fault (as indicated on the photomosaic/line drawing on previous page).

The sections above show that the sandstone at the lower left and associated coals—not the rollover sandstone in the graben—correlate best to the sandstone at the upper right.

Stop 11: Morley anticline

Morley, Colorado a coal-mining ghost town situated at the center of a small-scale anticline on Interstate 25.

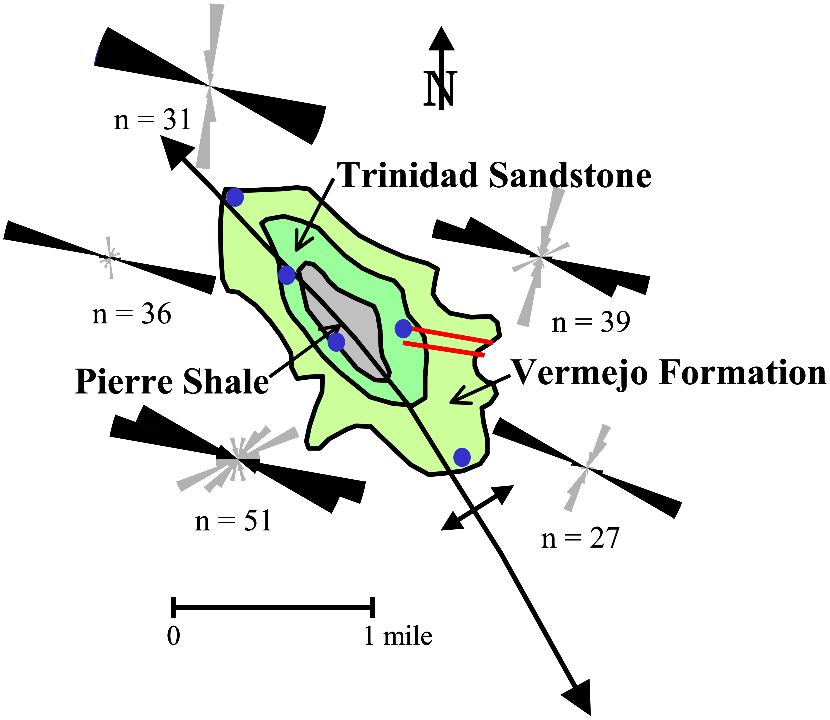

Figure 18: WNW primary extension fracture set is observed across the anticline. Base map after R.B. Johnson (1969), modified from field observations.

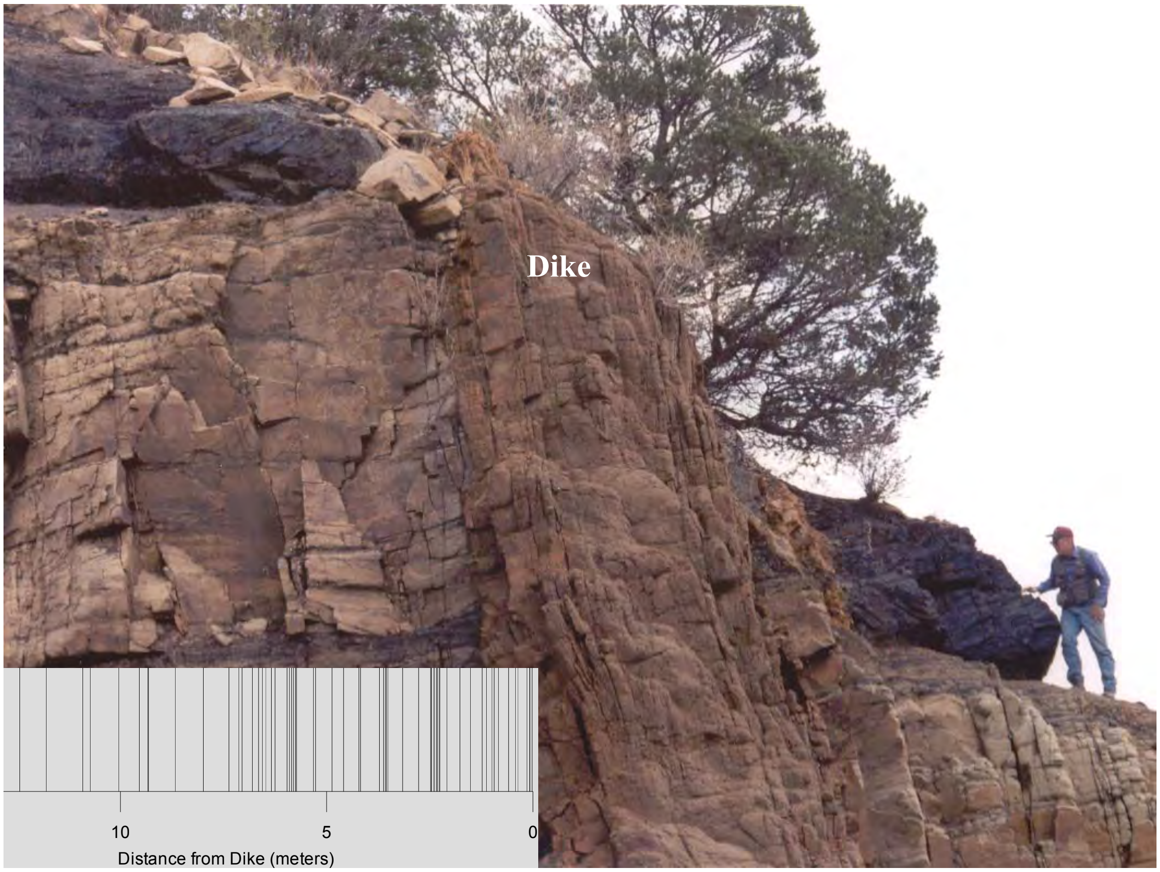

Figure 19: Fracture scan line shown above illustrates that the fractures within the Vermejo formation are related to emplacement of an igneous dike at SE side of the Morley anticline.

Stop 12: Synsedimentary deformation north of Cokedale, Colorado

This is one of numerous places within the Raton basin, typically in the Vermejo Formation, where syn-sedimentary deformation of the relatively unlithified strata took place. This deformation seems to have been related to down-slope slumping of sediment on a steep depositional slope, possibly aided by contemporaneous thrusting from the tectonic belt at the western margin of the basin.

A thrust fault is inferred to underlie the inclined strata because of the soft-sediment back thrusting found elsewhere (west of Ludlow) in similar features, and because of the compressive flow structures within the inclined strata. The angle of dip on these strata is too great to be a primary sedimentary feature. The strike of the thrust is assumed to be parallel to the strike of the inclined strata.

Deformation along this thrust apparently diverted drainage on the overlying depositional surface, as reflected by crossbedding vectors in the overlying sandstone that trend parallel to the strike of the inferred thrust and normal to the regional Late Cretaceous depositional slope.

Soft-sediment back-thrusting is less obvious than at Ludlow but present. Horizontal compression in the pre-lithification stage is also suggested by the blunt edge of the sandbody at the upper right and the apparent flow of the shaley sediments around it.

Angular relationship and erosional unconformity between inclined overbank strata and flat-lying fluvial strata above.

Thicker sandstone of the main fluvial channel to the right of previous photo, in erosional contact laterally against the deformed overbank strata that constrained the channel axis

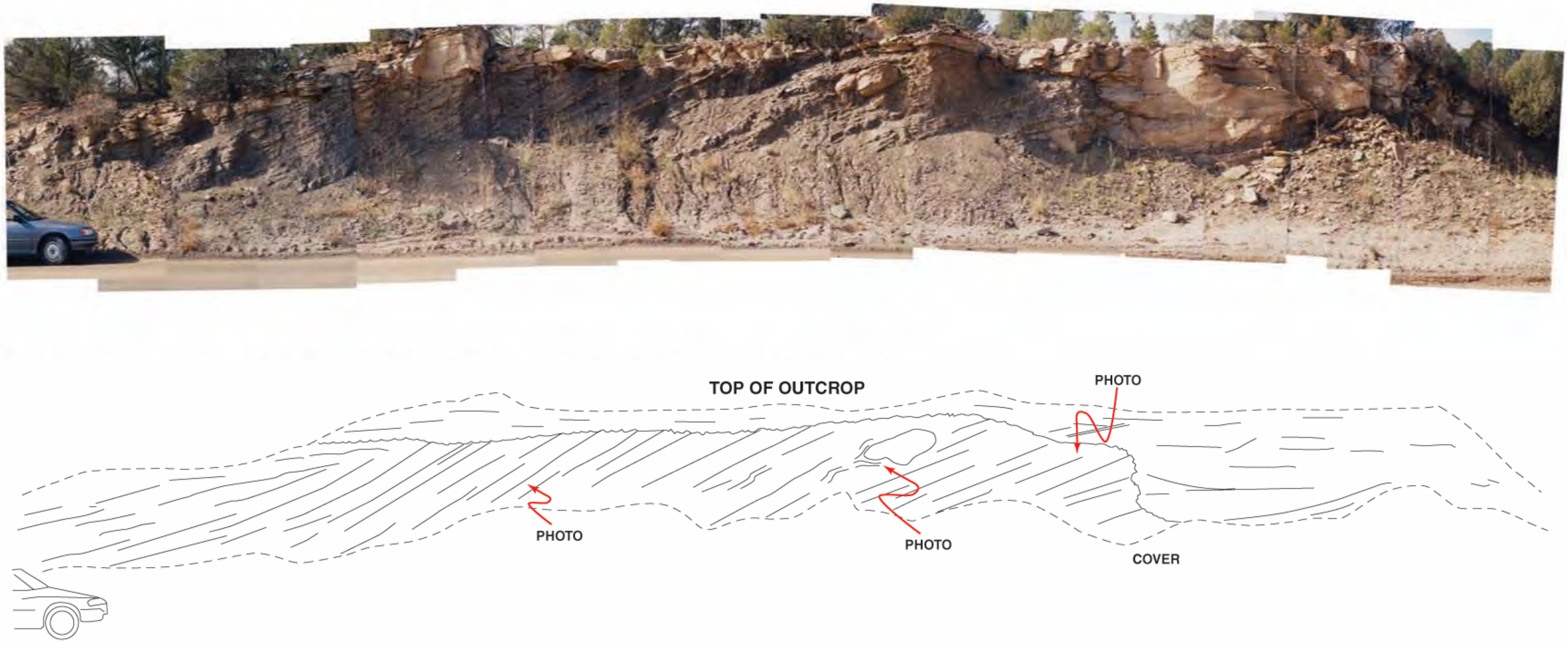

Line drawing from above photomosaic

Figure 20: Fluvial channel sandstone adjacent to and overlying/truncating deformed overbank strata. Dip of the deformed strata suggests thrusting towards 340^o.

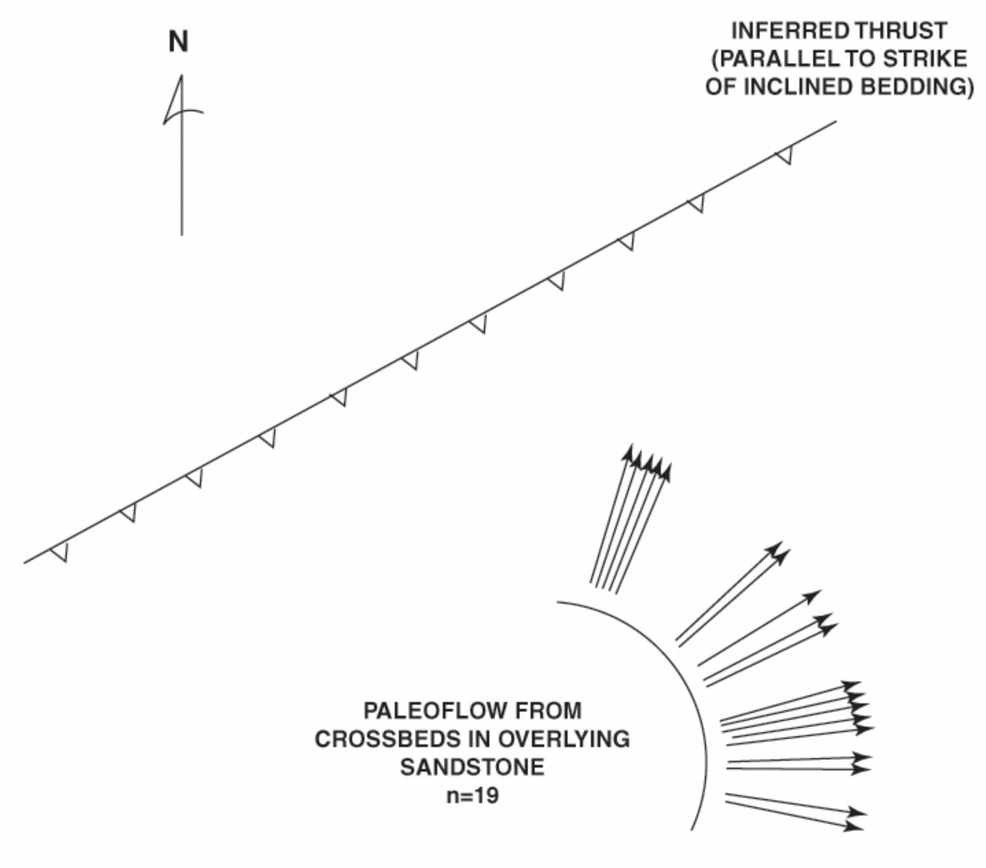

Figure 21: Paleoflow vectors derived from crossbedding measurements in the fluvial sandstone indicate flow towards the northeast, parallel to the strike of the inferred thrust fault.

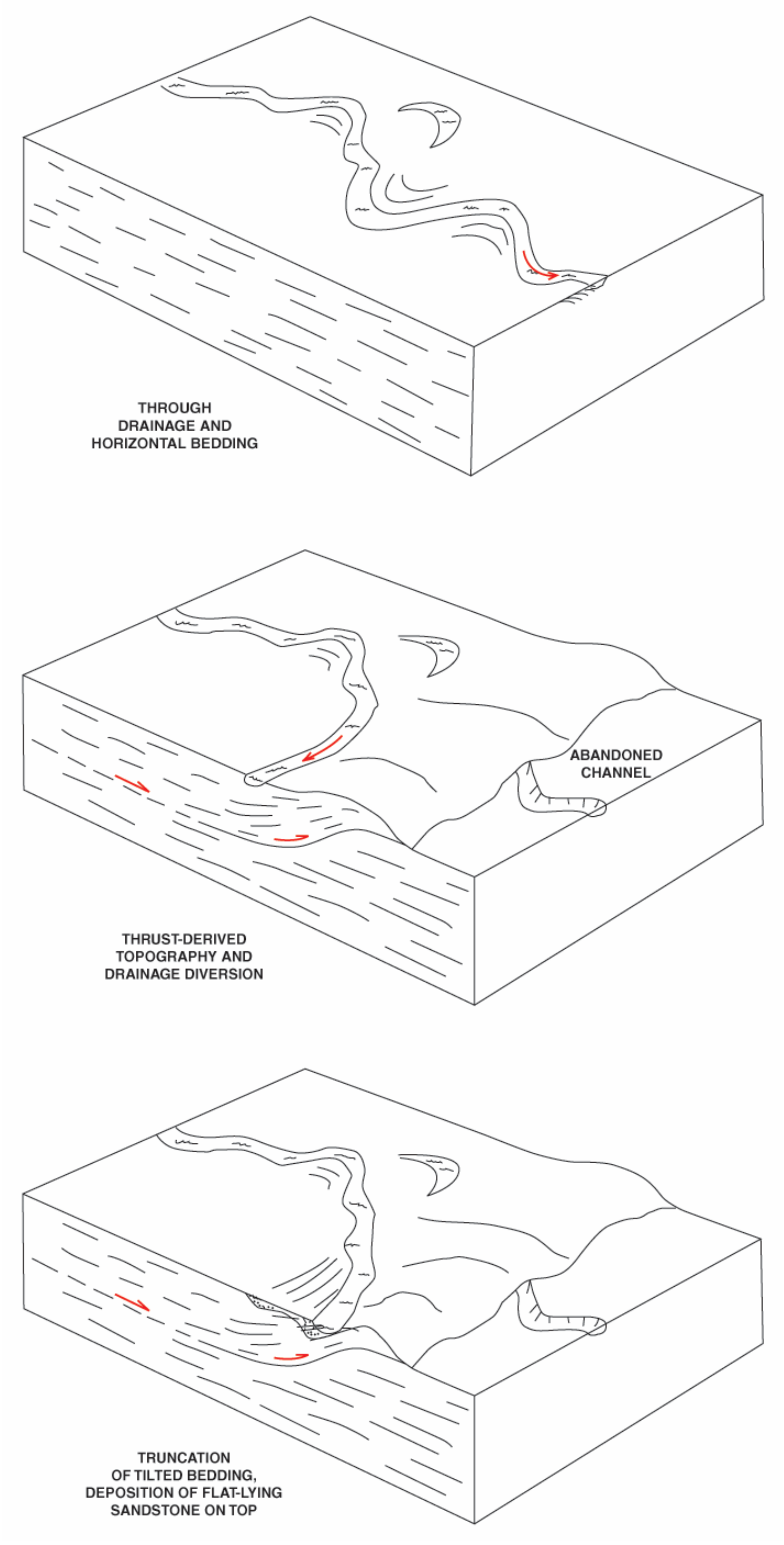

Figure 22: Suggested model to explain pre-lithification tilting and backthrusting of strata, with flat-lying fluvial strata in erosional contact above, at Ludlow and Cokedale sites.

Stop 13: Valdez sills

Stop 13, near milepost 50 on Highway 12 west of Trinidad, provides an interesting comparison of fracture orientation within sandstones, an igneous sill, and cleats within a coal bed. Extension fracture orientation is well constrained within a series of 10-30 cm thick sandstones above an igneous sill. Interestingly there is some parallelism between fracture orientation in these sandstones and the underlying dike. A comparison of the rose diagrams shows a slightly more distributed pattern and an extra set of fractures that strike NW-SE within the sill. The parallel nature of fractures in these differing rock units can be very apparent in the outcrop. Cleats within coals at this location have a more diverse pattern than the sandstones or the sill. In part this is due to different orientations of face cleats also having associated butt cleats at near right angles to the face cleat. It is also possible the diverse cleat pattern is due to compaction.

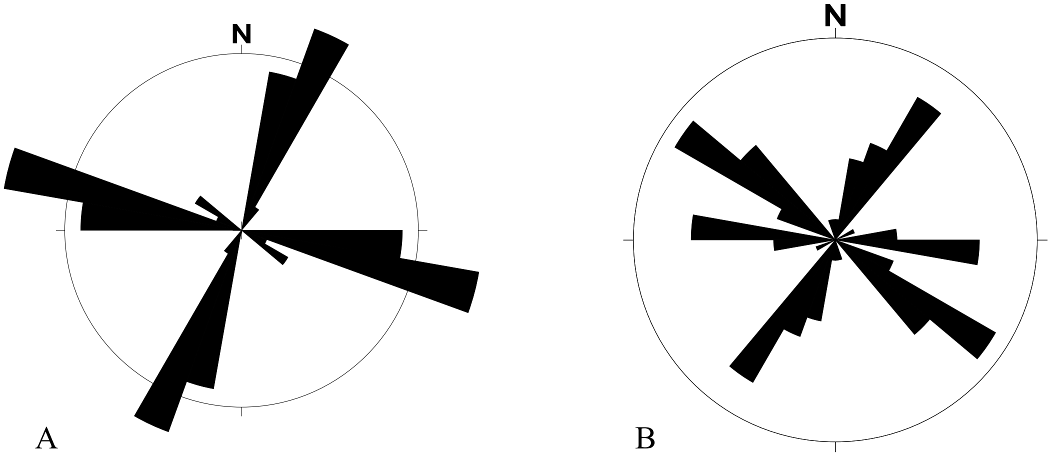

Figure 23: Rose diagram of fracture orientations within (A) sandstones, and (B) sill. There is a parallel relationship between many of the fractures within these two units of differing composition and age.

Figure 24: Photograph of a portion of the stop 13 outcrop. Sandstones overlie the igneous sill.

Figure 25: This photograph, oriented with the viewer looking straight down, illustrates the parallel nature of fractures in a sandstone and an igneous sill. The upper red colored rock unit is a sandstone. The intersection of two fractures forms a wedge pointing toward the top of the photograph within this unit. The dark colored wedge in the rock below the first wedge is within an igneous sill. Note the parallel nature of fractures within these two very different u nits and the repetitive nature of these fractures.

.

Stop 14: Walsenburg dike

Evidence for high horizontal compressive stresses normal to dike walls during intrusion is present in a small borrow pit on the north side of the Walsenburg dike half a mile west of where the road north out of town cuts the dike. Thin sandstone beds contain small thrust planes that dip towards and away from the dike at shallow angles (less than 30 degrees). The thrust planes have dip-slip slickenlines that trend normal to the dike walls. These thrust planes suggest that the maximum compressive stress in the strata next to the dike was normal to the dike at the time of intrusion, despite the fact that the strike of the dike indicates that this was the orientation of the minimum regional compressive stress.

The numerous dikes are cut with myriad fractures. These fractures are typically of three sets, 1) oriented vertically, parallel to the fracture walls, 2) oriented vertically but normal to the fracture walls, and 3) oriented horizontal to sub-horizontal, normal to the fracture walls. Various phases of mineralization and extensive weathering along the fractures suggest that the fractures in the dikes formed a well connected plumbing system that allowed the percolation of mineralizing and weathering fluids, and that may have allowed the escape of much of the natural gas in the basin, leading to it's present-day underpressured condition.

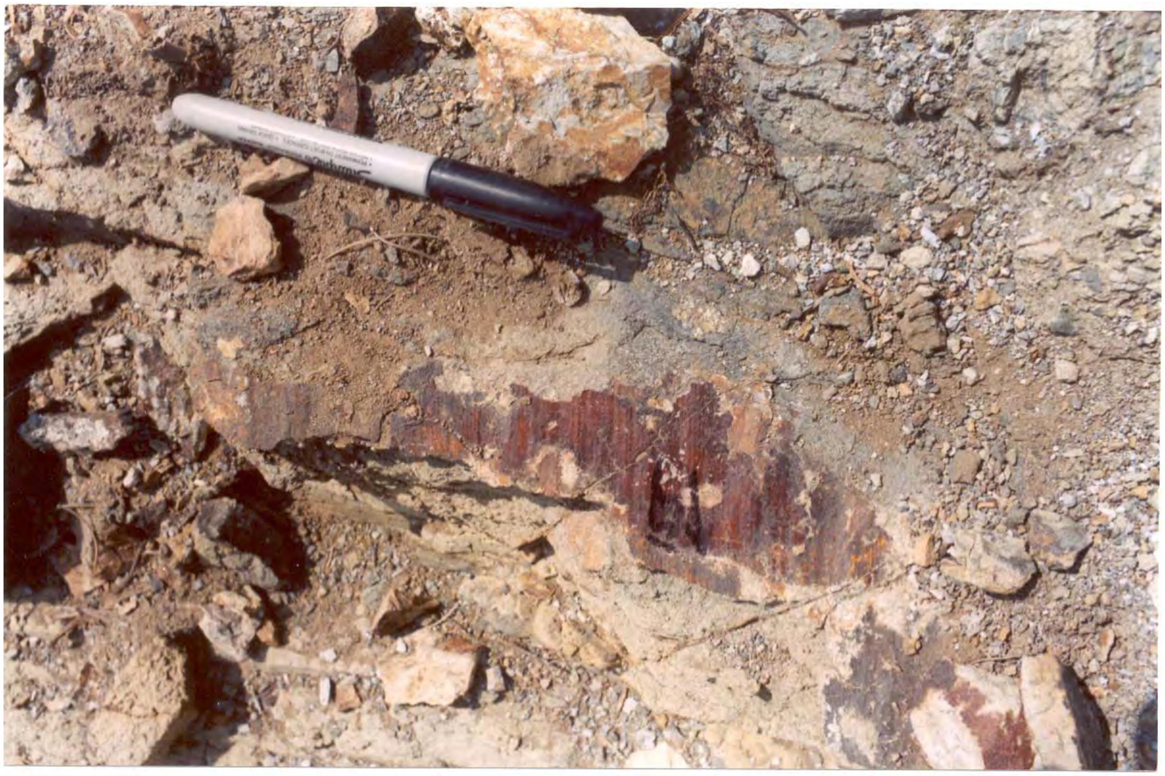

Figure 26: Low-angle thrust plane sown here has slickenline lineations striking perpendicular to the wall of the igneous dike.

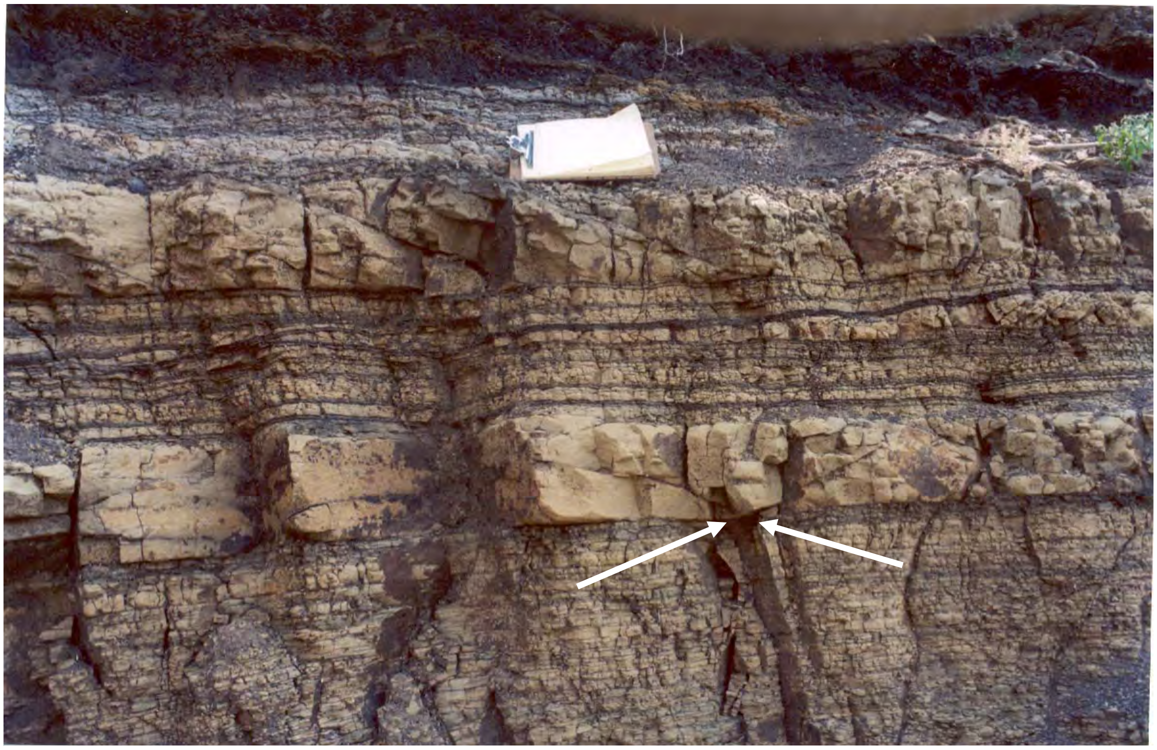

Figure 27: The thrust planes shown here indicate that the maximum compressive stress was normal to the dike at the time of intrusion. White arrows point in the direction and intersection point of two low angle thrust planes.

APPENDIX E

Core Log Reports: Constance N. Knight

Constance N. Knight
Independent Geologist

1800 Washington Ave
Golden, CO 80301
720-530-1387

This appendix contains core-logging reports prepared for the Sandia National Laboratory. These reports are part of a larger structural geology study being completed by John Lorenz and Scott Cooper. In that some reports refer to observations described in the earlier reports, it may help the reader to know the order in which the cores were logged. The cores were logged in the following order:

NLBSU 34
NLBSU 31
NLBSU 32
NLBSU 30

El Paso Well No: VPRCH 30

Summary of Fracture Characteristics Described in Core

Submitted to Sandia National laboratory
Raton Basin Project
By Constance N. Knight

Introduction

Well No. 30 VPRCH was cored continuously from near surface to a total depth of 1401 feet. The objective of this evaluation is to describe attributes of naturally occurring fractures below a depth of 1182'. Cores from the upper portion of the Vermejo Formation were not sent to Denver. Sandia personnel will log these cores at a later date. The entire core below a depth of 1182 feet was carefully examined for fracture occurrence. All natural fractures were logged with respect to: depth, host lithology, fracture dip, surface characteristics, and angular relationships with one another. Only one induced petal fractures was observed in this core.

Core from this well possessed a significant number of natural fractures. The purpose of this report is to summarize fracture characteristics and to compare fracture characteristics with those described in other wells. The first half of this report provides summary and specific information about the fractures. The second half provides photographs showing distinguishing features of the fracture types and the fracture angular relationships

Summary of Fracture Characteristics

Total fractures described: 219

All percentages presented below are presented as a fraction of the total 219 fractures unless otherwise noted.

Host Lithology

Host Lithology	Percentage of Fractures
Shale and claystone *	46%
Siltstone	38%
Sandstone	14%
Conglomerate	2%

* Almost all fine-grained clastics were determined to be shale.

Most (83%) of the described fractures occur in fine-grained rocks (siltstone and shale). Most of the fractures in described in previously logged cores (VPRCH 34, 32, and 31) also occur in fine-grained rocks. In this well, the number of extension fractures is approximately equal to the number of shears. (In well VPRCH 31, the majority of the fractures are extensional; in VPRCH 34 the majority of the fractures are shears; well VPRCH 32 has approximately the same number of extension fractures and shears.)

Types of Fractures (Extension vs. Shear)

Type of Fracture	**Percentage**
Extensional Fractures (Most fractures have surface plume structures. Some fractures also have evidence of shear, but this is usually not well displayed)	54%
Shears with a vertical component of relative motion	39%
Horizontal shears or bedding plane slip	7%

Number of Fractures sorted by Lithology

Lithology	**HZ Shears**	**Shears <35°**	**Shears 40°-65°**	**Shears 70°-90°**	**Extension Fractures**
Sandstone	0	2	1	1	27
Siltstone	3	9	12	6	53
Shale	12	16	31	8	33
Conglomerate	0	0	0	0	4
Coal	0	0	0	1	0
Totals	15	27	44	16	117

The table above shows five types of natural fractures. Fractures within these five categories are also presented with a Gamma Ray log as Figure 1. Fractures were identified as shear fractures only if they had evidence that movement had occurred, such as the presence of slickensides, surface polish, etc. Many fractures identified as extension fractures had plume structures, however some extension fractures were identified on the basis of angular relationships to other extension fractures and steep (vertical) dip angles.

Two intervals of highly broken core were identified as possible fault zones. These intervals possessed a large number of shear fractures. Possible fault zones are indicated on Figure 1and are listed below.

Possible fault zones: Intervals characterized by highly broken core and numerous shear fractures:

1307.3 – 1310.2
1369.9 – 1370.8

Shears Sorted by Dip Angle and Rake

Shear Angle	Percentage of total 219 fracs.	Rake Range	Apx. Avg. Rake	Comments Regarding Rake
Shears ≤35° dip	12%	5-90*	43°	62% of the shears ≤35°-exhibit rake.
Shears 40°-65° dips	20%	5-90*	27°	68% of the shears with dips of 40° - 65° exhibit rake
Shears 70° - 90° dips	7%	5-80	33°	56% of the fractures with dips of 70° - 90° exhibit rake.

The majority of the shear fractures exhibit oblique slip as evidenced by various amounts degrees of rake.

*Two fractures in this dip category have two sets of slickensides, which implies that these fractures may be recording two episodes of shearing.

* Two fractures in this dip category have two sets of slickensides, which implies that these fractures may be recording two episodes of shearing.

Relative Movement on Shears

When it was possible the relative movement on shears was observed. The table below presents the depths host lithology, and characteristics for 1 shears.

Depth	Lithology	Dip	Rake	Relative Movement
1291.6	Shale	90	0	Vertical/reverse

Fracture Fillings

Information regarding fracture fillings includes: 1. Percentage of filling material in individual fractures; 2. Mineralogy of the filling material; and 3. Fracture-aperture measurements. Percentages of filling materials were estimated by examining the facture faces. Some fractures appeared to be 100% filled with cementing material. However some such fractures exhibit well develop druze. The presence of druze implies that these fractures are partially open. The best druze development is associated with those fractures having the largest fracture apertures.

The table below summarizes fracture-filling data. These data should be used as estimates, not exact measurements.

% Fracture Filled	**No. Extension Fractures**	**No. Shears < 35°**	**No. Shears 40°-65°**	**No. Shears 70° - 90°**
< 10%	16	5	9	4
10% - 25%	10	6	12	5
26% - 49%	24	7	15	3
50% - 74%	14	3	2	3
75% - 100%	53	5	6	1
Total	117	26	44	16

Visual inspection at 10X revealed that approximately half of the extension fractures are less than 75% filled with cement. Several well-defined open extension fractures in sandstones exhibited less than 10% fracture filling. This is a contrast with most cored extension fractures found in the previous three logged wells. Extension fractures in other wells generally contained more cement (75% -100%). It is acknowledged that in some cases cementing materials were probably destroyed in the coring process.

For shear fractures, the degree of cementation is more variable than for extension fractures. Again, the estimates presented here should be considered to be imprecise variables.

Numbers of Fractures filled with Various Cements		
Cement Type	**Extension Fractures**	**Shear Fractures**
$CaCO_3$	95	43
Clay	0	15
Clay and $CaCO_3$	0	13
$CaCO_3$ and pyrite	8	0

The dominant fracture cement was calcite. Commonly extension fractures cemented with only calcite were relatively easy to break apart. Also, some of these fractures exhibited druze. However the occurrence of druze was less than in previously logged cores. The finer the fracture aperture, the finer the druze crystals.

Fracture Apertures

Fracture apertures range from <0.1 – 1.0 mm., with the average aperture approximately equal to 0.2 mm. In general the extension fractures observed in this well had smaller apertures and finer druze crystals than those observed in previously logged wells (VPRCH 34, 31, and 32). The following table lists fracture aperture measurements of healed fractures. In the case of open fractures with well-developed druze, the aperture measurement represents the thickness of the druze. Most of the estimates are from healed fractures.

Depth	Type of Fracture	Aperture mm	Druze
1121.5	Extension	0.1	
1183.1	Extension	0.6 - 1.0	Trace
1183.8	Extension	0.6 - 1.0	Trace
1196	Extension	<0.1	
1197.6	Extension	0.1	Trace
1198.5	Extension	0.1	
1225.8	Extension	0.1	
1226	Extension	0.1	
1226.5	Extension	0.2	Good
1227	Extension	0.4	Excel
1234.5	Extension	0.2	Good
1235.7	Extension	0.2	
1238.8	Extension	0.2	Good
1241.7	Extension	0.2	Excel
1252.2	Extension	0.2	V. fine
1252.2	Extension	0.2	V. fine
1252.8	Extension	0.2	V. fine
1255.8	Extension	0.1	Scattered - fine
1255.8	Extension	0.1	Scattered - fine
1284.4	Extension	0.1-0.3	Excel - fine
1288.5	Extension	<0.1	No
1288.5	Extension	<0.1	No
1288.6	Extension	<0.1	No
1294.4	Extension	<.01	
1294.6	Extension	<.01	
1294.8	Extension	<.01	
1312	Extension	0.2	No
1312.8	Extension	0.1	No
1313.2	Extension	0.2 - 0.5	No
1314.5	Extension	0.1	No
1314.9	Extension	1	No
1341.7	Extension	0.1	No
1341.9	Extension	0.1	No
1354.9	Extension	0.2	
1366.2	Extension	0.2-0.4	Scattered
1374.3	Extension	0.3	Scattered
1374.7	Extension	0.3	Scattered
1376.2	Extension	0.1 - 0.6	Scattered, fine

Fracture Spacing

Fracture spacing was determined for both extension and shear fractures. Two tables are presented below: one pertaining to extension fractures, and one pertaining to shears. For many fractures a "true" spacing (spacing perpendicular to the fracture surfaces) is measured. In cases where the vertical spacing of fractures would not permit such a measurement, the apparent spacing (vertical depth from one fracture midpoint to another) was measured. The true fracture spacing = sin (dip ∠) x (observed fracture spacing). True spacing measurements are presented in red, whereas observed fracture spacing measurements are presented in black.

Depth	**Fracture Spacing**
1135.5	0.03
1183.1	.05-0.1
1197.6	0.1
1198.5	0.01 - 0.03
1204.6	0.2
1218.9	0.02
1219.7	0.1
1220.3	0.15
1225.8	0.01-0.03
1226.5	0.17
1227	0.1
1234.5	0.06
1241.7	1
1252.2	0.05
1252.8	0.2
1255.8	0.05
1255.8	0.05
1288.5	0.1 - 0.3
1288.5	0.1 - 0.3
1320	0.02
1341.7	0.1
1343	1.1
1374.3	0.3

.

Shear Fracture Spacing		
Depth (ft)	Fracture spacing (ft)	Fracture Dip Angle
1136.3	0.1	60
1187.2	0.4	45
1226.2	0.2	70
1227.4	0.03-0.1	80
1245.8	0.05	60
1347.2	1	20
1348.2	0.05	30
1348.5	0.25	30
1357.7	0.2	25

Relationship of Fractures to sHmax Defined by a Possible Petal Fracture at 1295.5 feet

Only one possible petal fracture was identified. (See photos below.)

Depth	**Orientation Relative to Petal**	**Type of Fracture**
1294.4	Parallel	Vertical Extension
1294.6	Normal	Vertical Extension
1294.8	Parallel	Vertical Extension
1298.8	Normal	Vertical Extension
1298.9	30° Counter clockwise *	Vertical Extension

* See core photos on Page 16.

Summary of Fracture Strike Relationships

Because this core was not oriented, fracture dips and strikes cannot be directly obtained. However, the following table presents fracture strikes relationships that may be helpful in relating core to outcrop data. The number in each box refers to the number of fracture relationships. Fracture intersections in the 10° - 30° and 61° - 89° categories are mostly 30° and 60° intersections. Fractures in the 31° - 60° category are mostly approximately equal to 45°.

Intersection Angle	**Number of Fractures with Various Intersection Relationships**						
	EX/ EX	EX/Thrust	EX/>35 °Shear	EX / >70° Shear	>35° Shear / >35° Shear	>35° Shear / Thrust	Thrust/ Thrust
Parallel Strike	51	6	17	8	15	5	6
10° - 30° (30) **61° - 89° (60)**	8		8	1	3	1	1
31° - 60°(45)					7	1	
Normal (90°)	13	1	5			7	

EX/EX – Intersection of two extension fractures
EX/Thrust – Intersection of an extension fracture and a low angle shear (< 35°)
EX/>35° Shear – Intersection of an Extension fracture and a > 35° shear
EX/>70° Shear – Intersection of Extension fractures and a vertical (or near vertical) shear
>35° Shear/>35° Shear –Intersection for two higher angle shears
>35° Shear /Thrust – Intersection of a higher angle shear (> 35°) and a low angle shear (< 35°)

Fracture Length

Fracture length data for extension fractures and shears are presented below. Data for complete fractures (those fractures that possessed two terminations within the core) are presented separately from those of other fractures. For fractures that had one or no terminations within the core, a minimum fracture length is given.

Fracture Lengths for Extension and Sheer Fractures

	No. Fracs	Extension Fracture Lengths		No. Fracs	Shear Fracture Lengths	
		Length Range (ft)	Average Length (ft)		Length Range (ft)	Average Length (ft)
Complete fracture in core	26	0.1 – 1.2	0.4	2	0.1 – 0.9	0.5
Minimum Fracture Length	103	0.2 – 2.9	0.5	82	0.05 – 1.0	0.3

Miscellaneous Notes Regarding Fracture Characteristics

As previously noted, open extension fractures in well VPRCH 30 have less cement than in previously logged cores. It is acknowledged some of the fracture-filling materials have probably been destroyed in the coring and core-retrieval process. However, it is significant that many open vertical fractures in sandstones possess very little cement. Perhaps these fractures are propped open in the subsurface by differential horizontal stress.

In previous reports the possibility of fracture reactivation has been suggested. On page 7 of this report, the table shows that the strikes of most vertical shears are parallel to strikes of extension fractures. These strike relationships are also presented in some of the following photos.

The following photos are presented to document the types of factures and the fracture angular relationships. Several shears showed multiple sets of slickenlines. One example is shown in this report. In addition, two examples of fracture splays are presented in the photos below.

Figure 1: VPRCH 30 Gamma Ray Log and Fracture Summary

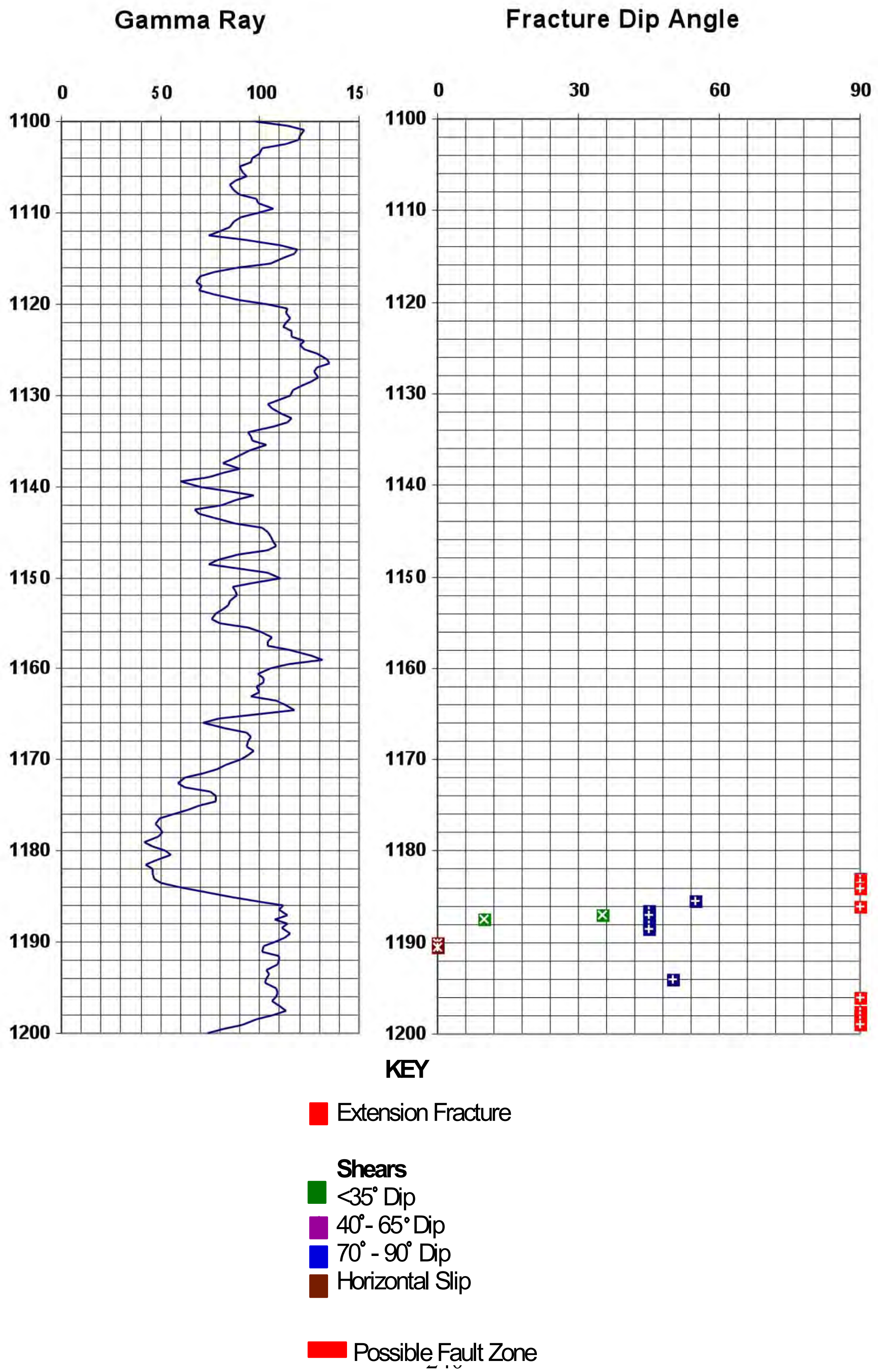

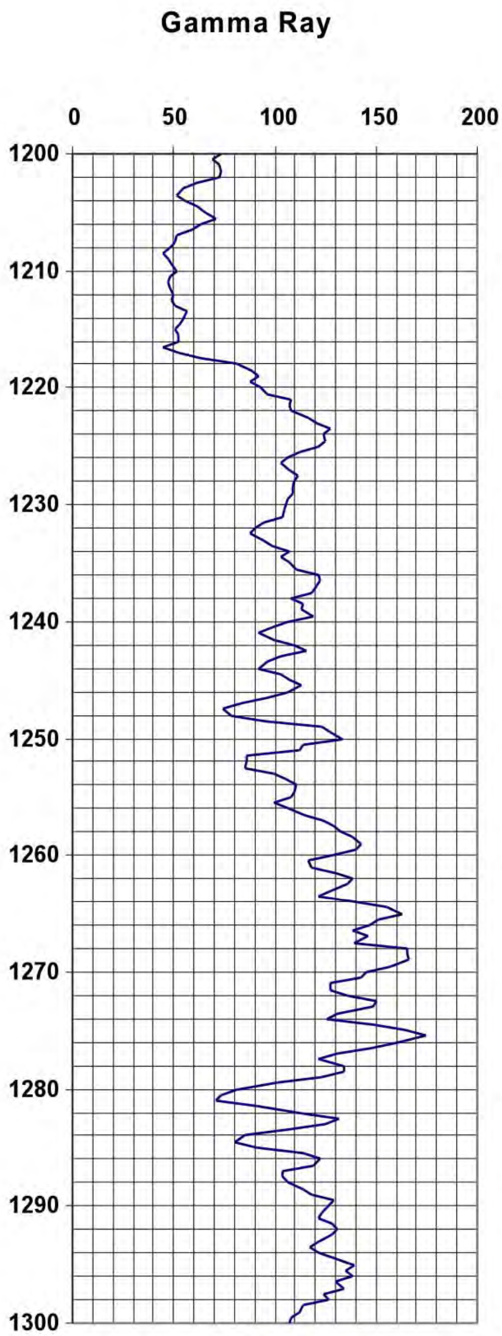
Gamma Ray
0
50
100
150
200
1200
1210
1220
1230
1240
1250
1260
1270
1280
1290
1300

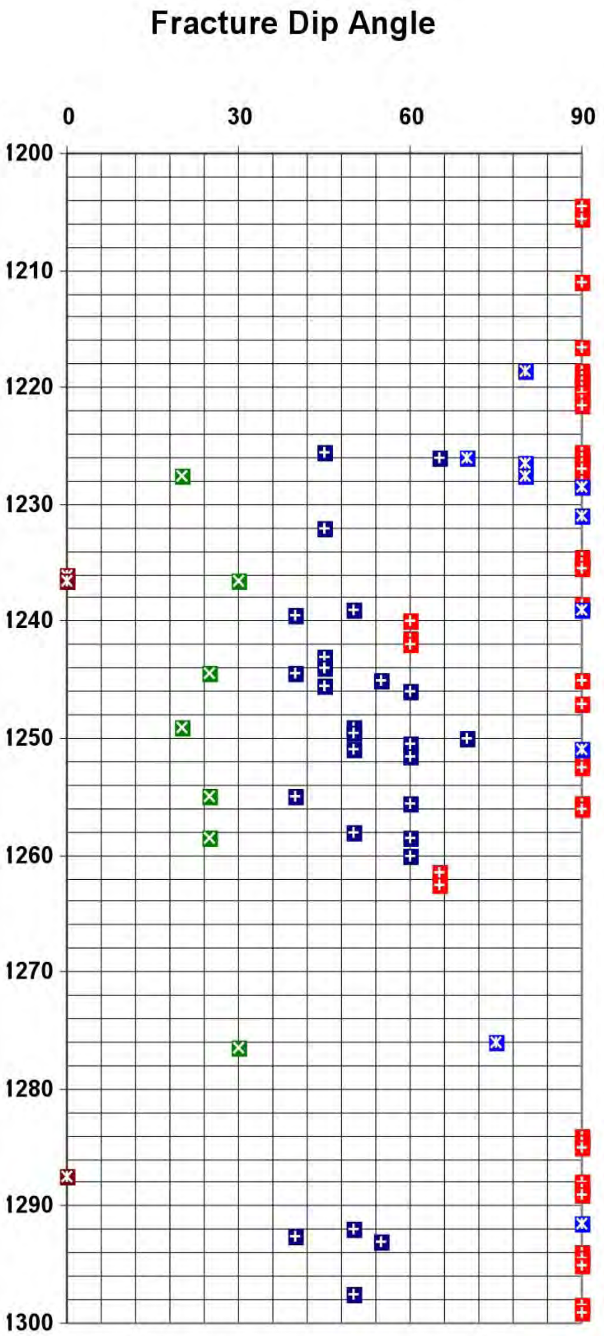
Fracture Dip Angle
0
30
60
90
1200
1210
1220
1230
1240
1250
1260
1270
1280
1290
1300

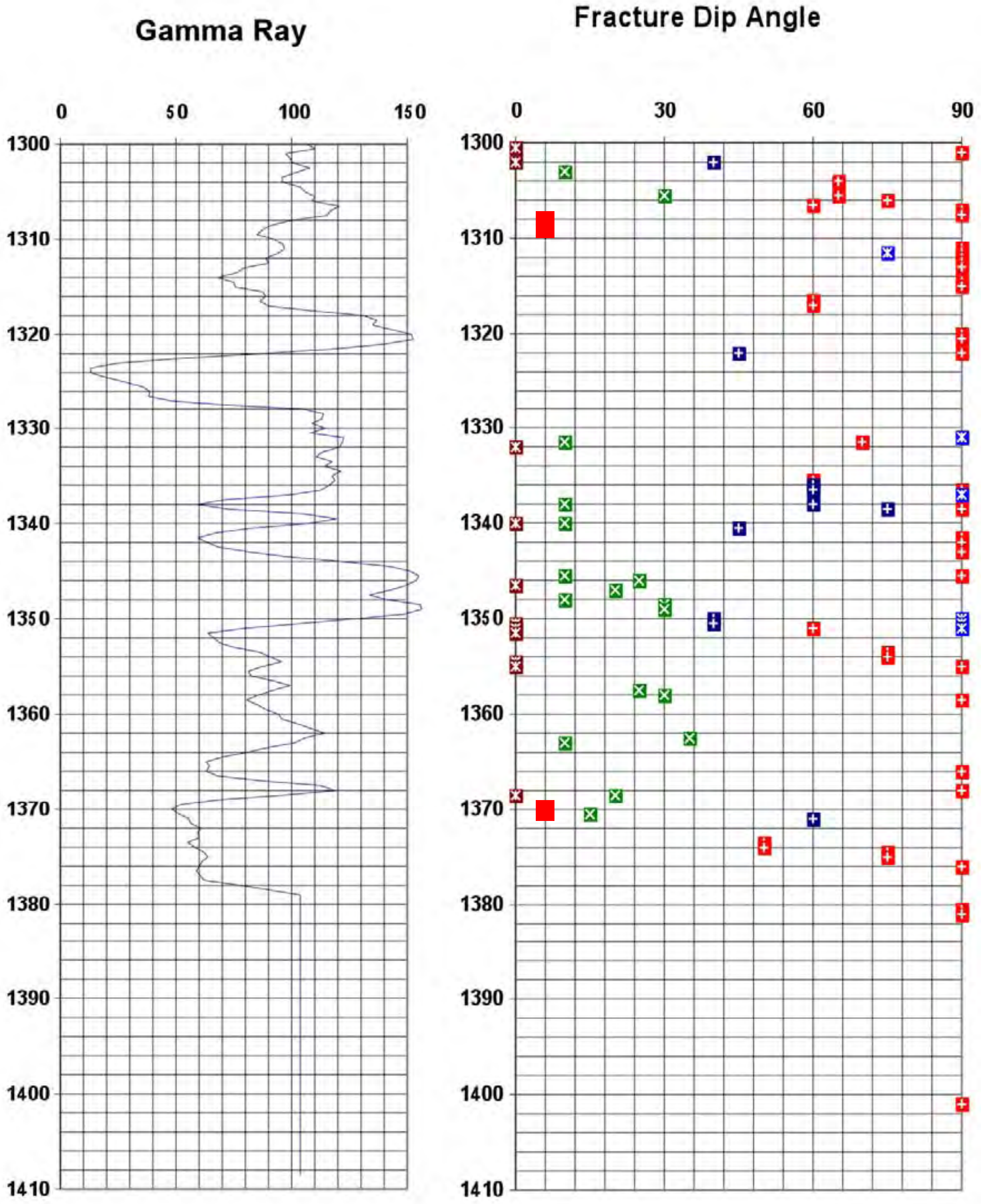
Gamma Ray
Fracture Dip Angle
0
50
100
150
0
30
60
90
1300
1310
1320
1330
1340
1350
1360
1370
1380
1390
1400
1410

Core Photographs

Examples of Extension Fractures

Parallel Vertical Extension Fractures

Depth: 1204’
Host Rock: Sandstone
Fracture spacing: 0.2 ft.

These fractures occur as open fractures in the core. Unlike most vertical fractures described in previously logged cores, these fractures possess little cement (5 – 10%).

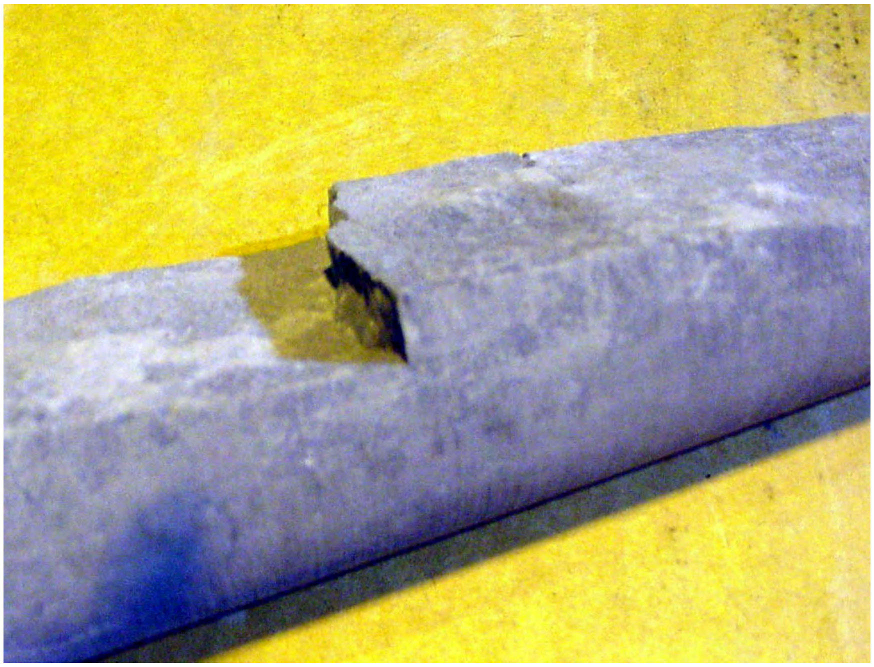

Parallel Vertical Extension Fractures

Depth:1219’
Host Rock: Siltstone
Fracture Spacing: 0.02 ft

Sometimes vertical fractures occur in a “stair-step pattern”.

A.

B.

Extension Fractures with Druze

Fracture A:
Depth: 1226.5’
Host Rock: Shale
Dip. Vertical
Aperture: 0.2 mm

Fracture B:
Depth: 1242.2’
Host Rock: Siltstone
Dip: 80°
Aperture: 0.2 mm

Fracture C:
Depth: 1320’
Host Rock: Shale
Dip: Vertical
Spacing: 0.02 ft

C.

A.

B.

Healed Vertical Extension Fractures

A:
Depth: 1252’
Host Rock: Sandy Siltstone
Spacing: 0.05 ft.
Aperture: 0.02 mm.
Fine Druze present

B:
Depth: 1314.5’
Host Rock: Sandstone
Spacing: 0.04 ft.
Aperture: 1.0 mm.
Druze not apparent

Strike Relationships of Three Extension Fractures

Depth: 1284’
Host Rock: Siltstone

Fractures A and C are vertical extension fractures with strikes normal to one another. Fracture B is near vertical. The strike intersection angle of fractures A and B is 30°. All fractures have well developed fines druze. Fracture apertures range from 0.1 mm to 0.3 mm.

Strike Relationships of Three Extension Fractures

Depth: 1305’ – 1306’
Host rock: Siltstone

Dip Angles: Fracture A - 65°
Fracture B – vertical
Fracture C - 60°

Fractures B and C are parallel. The strike intersection angle for Fractures A and B is 30°.

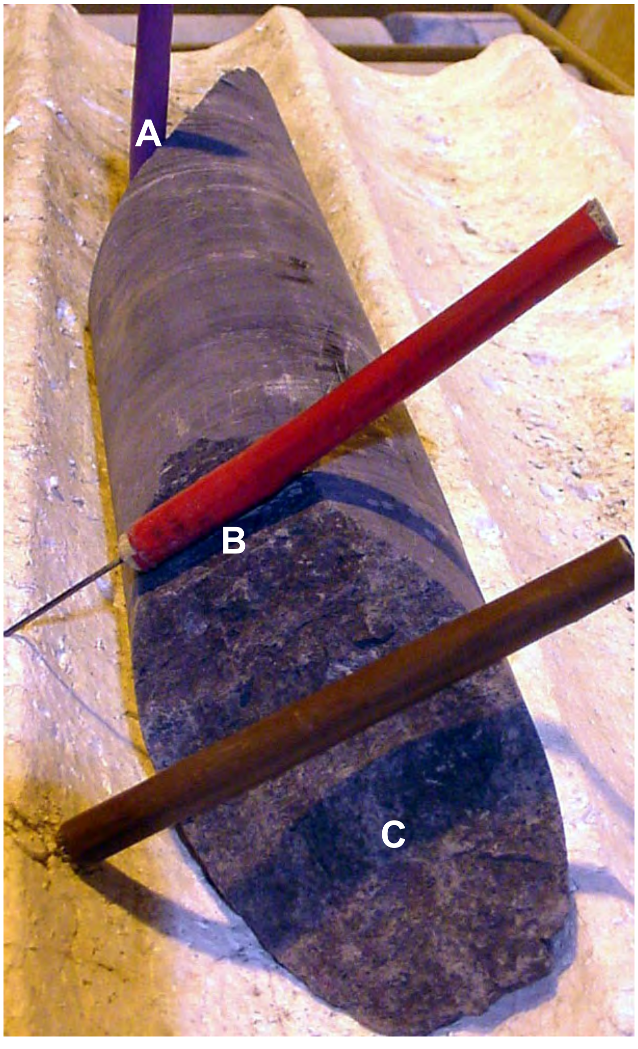

A.

B.

A: Possible petal fracture in a highly carbonaceous shale.
Depth: 1295.5'

B: The purple stick shows the strike of the petal fracture at 1295.5'. The red and yellow pencils show the strikes of two vertical extensions fractures that have a strike intersection angle of 30°. The extension fracture marked with the red stick strikes approximately normal to the petal fracture. The extension fracture marked with the yellow stick strikes approximately 30 clockwise from the petal fracture.

Examples of Shears

A: Fault Gauge Associated with Shear
Depth: 1251.1’
Host Rock: Siltstone
Fracture Dip: 65°
Approximately 0.7’ fault gauge. Possible slickenlines are shown with an arrow.

A.

B: Vertical fracture and Shear
Depth: 1291’ – 1292’
Host Rock: Siltstone
Fracture A: Vertical
Fracture B: 50° Dip
The upper termination of Fracture A is in siltstone, and the lower termination is at Fracture B. The fracture resembles vertical extension fractures; however it the fracture surface is smooth, and no plume structure is apparent. Fracture A and B are parallel

B.

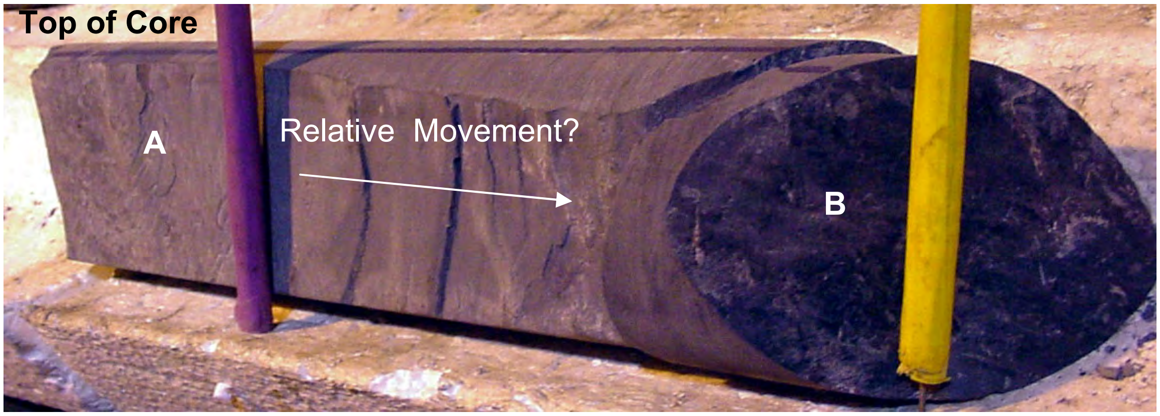

C.

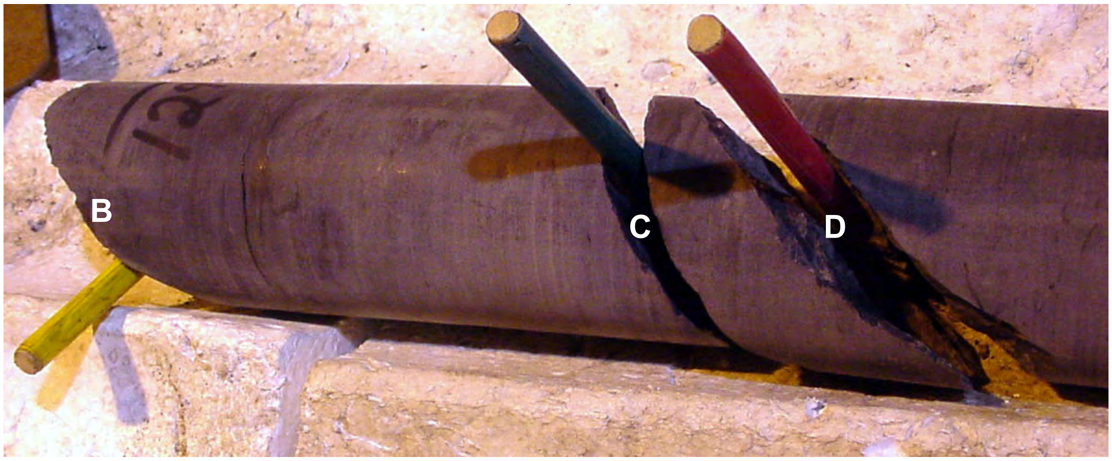

C: Continuation of the core seen in Figure B. Fractures C and D strike normal to Fracture C.

A.

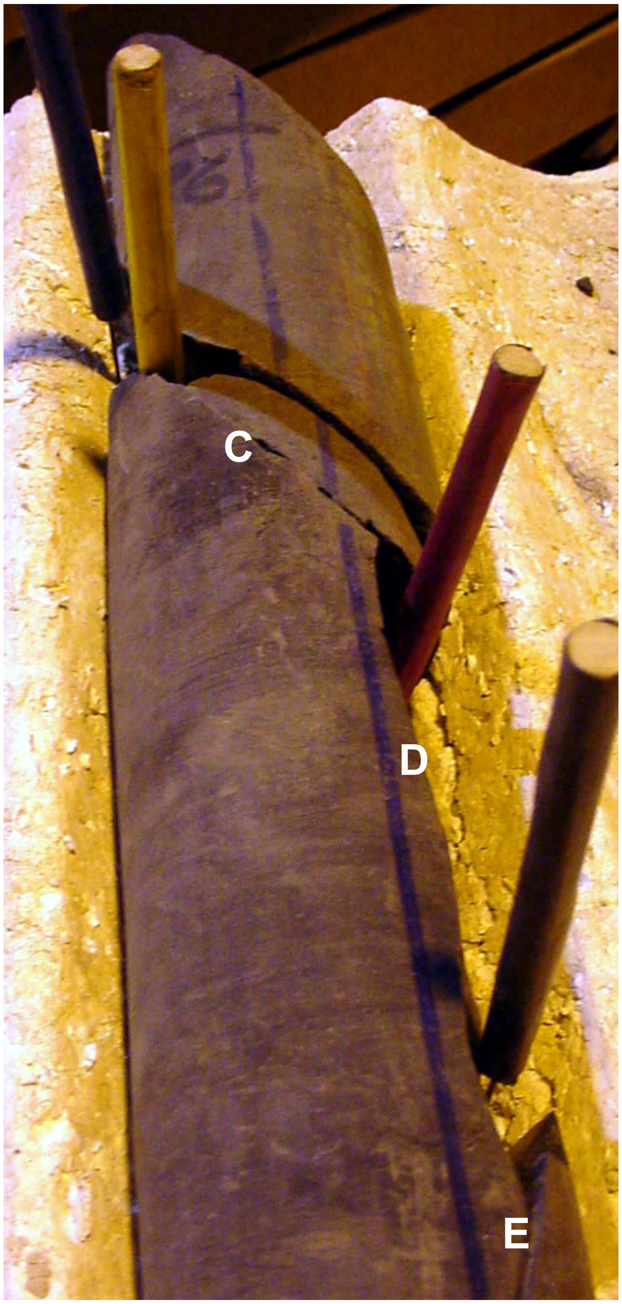

B.

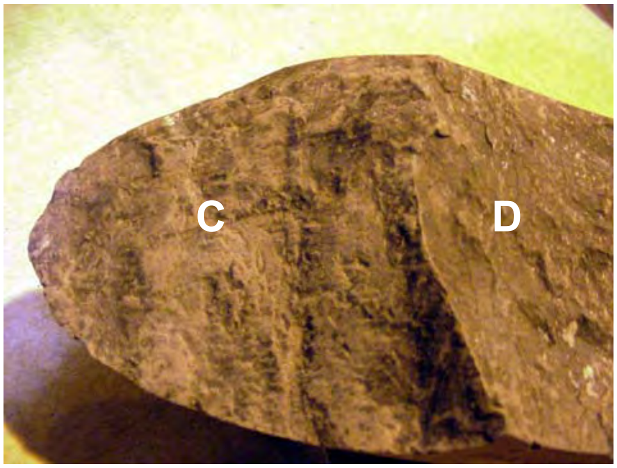

C.

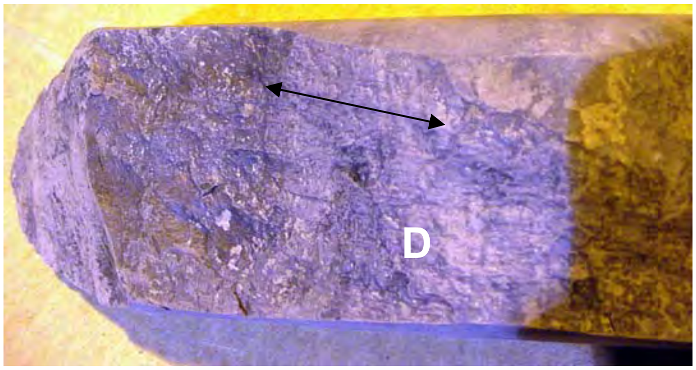

Parallel Shears and Extension Fracture

The photos shown in Figures A through E are from core depths 1336' – 1337'.

Fracture A is a vertical extension fracture. Fractures B and C are 60° dipping shears. The surface of Fracture C is shown in Figure B. Both fractures B and C exhibit 0° rake. Fracture D (shown in figure C) is classified as a vertical shear. The fracture surface is non-planar. (See figures C and D.) Near vertical slickenlines and patches of slickencryst are present on the surface of Fracture D.

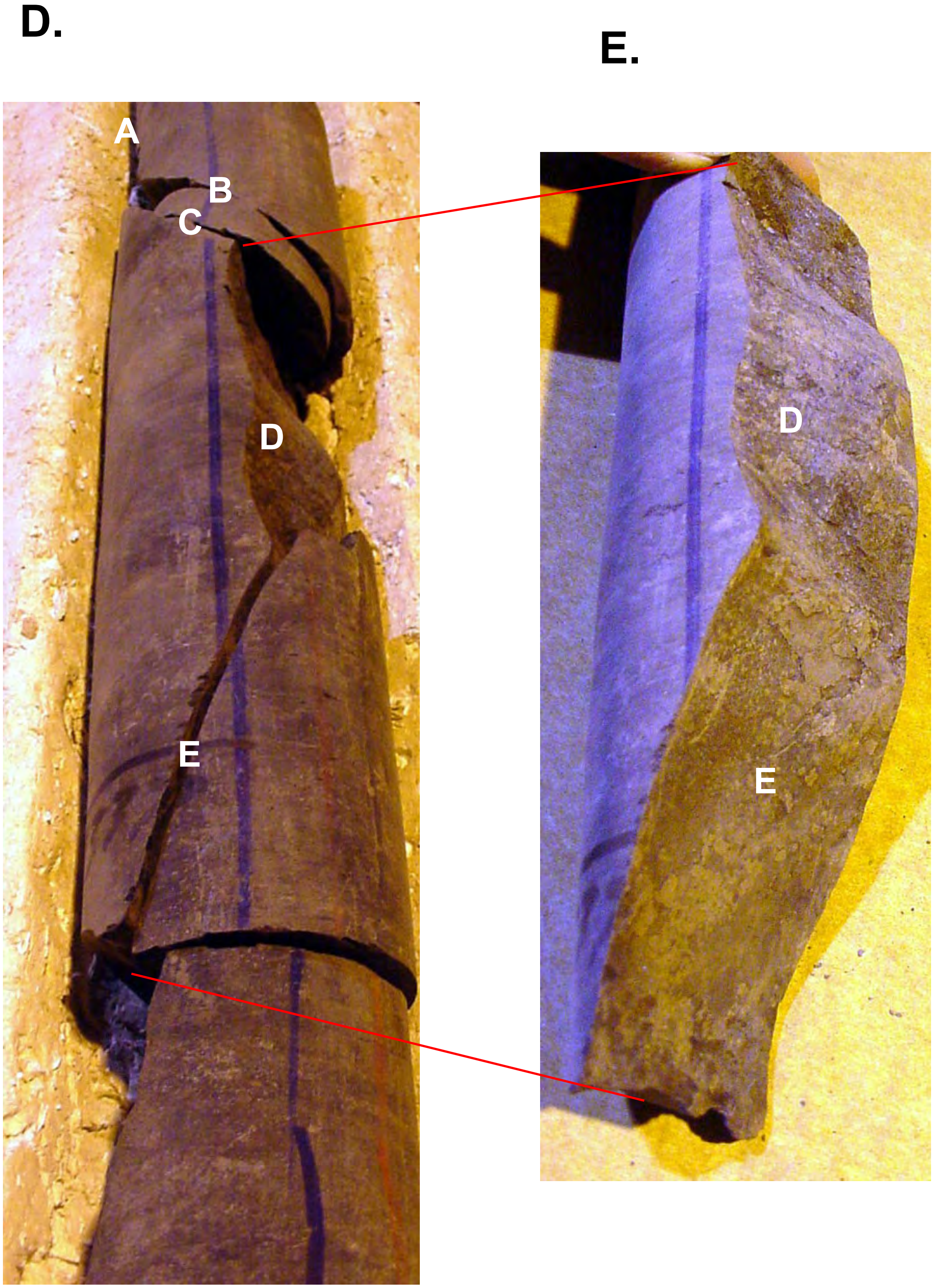

Fracture E is a vertical fracture that intersects Fracture D. The strikes of the two fractures intersect at a 0° to a 30° angle. The surface of the fracture is smooth and has patches of slickencryst.

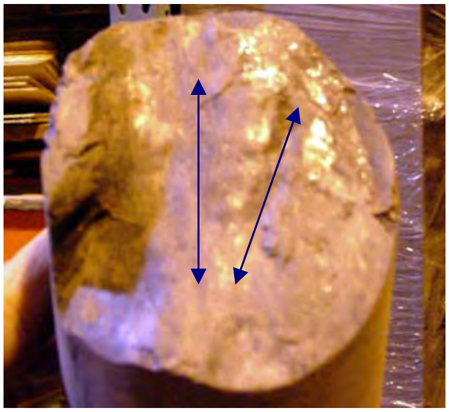

Shear with possibly two sets of Slickenlines

Depth: 1349.9
Host Rock: Shale
Dip Angle: 40°

Fracture Splays

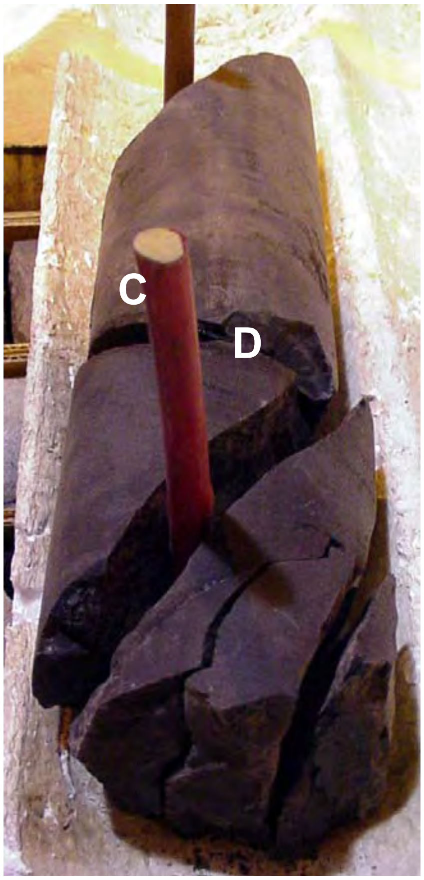

Shear fracture and Parallel Splay:

Depth: 1245
Host Rock: Shale

Fracture A: 45° dip

Shears B, C, and D are dip at 60° angles. Shears B ad C have 30 ° rake. Shear D has 0° rake.

Fracture Splay and Evidence of Lateral Slip – See next page

Photo A (on the next page) shows several feet of core with near vertical extension fractures. The colored probes are footage markers. Photo B. is an expanded view of the portion of the core outlined in red on Photo a. Fracture A is curved. The upper portion of Fracture A dips at a 60° angle, and the lower portion of Fracture A is vertical. Fractures A and B form somewhat of a splay. Photos C. and D. show a closer view of the Fracture A. The upper portion of the fracture has slickenlines with about an 80° rake. The red probe points to this portion of the fractures. The lower vertical portion of the fracture (yellow probe) has an extension plume. Photo E. shows the slickenlines on the upper portion of the fracture. They did not photograph well, but the lines show lateral slip.

A.

B.

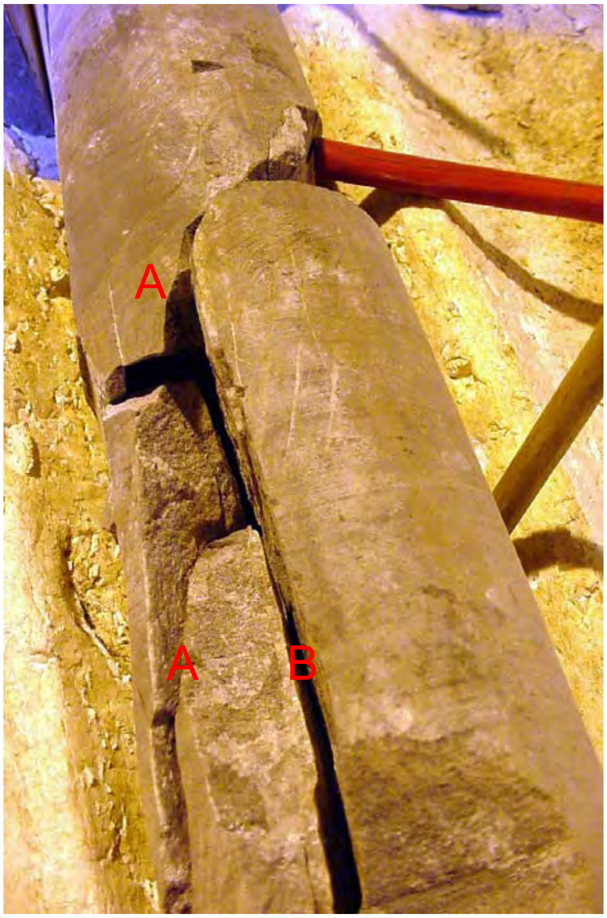

C.

D.

E.

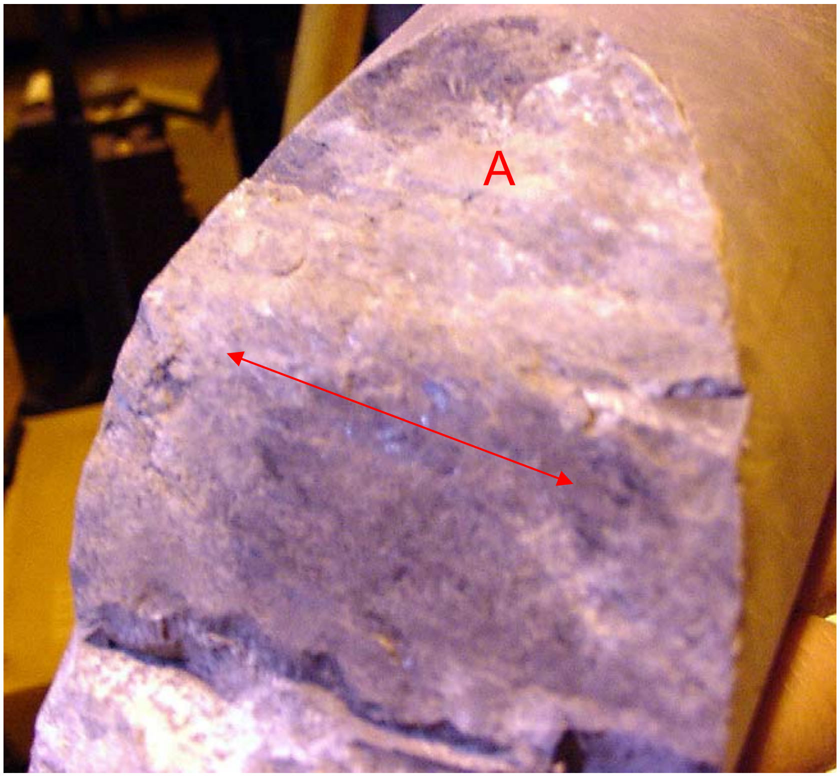

Extension and Shear Fracture Strike Relationships

A.

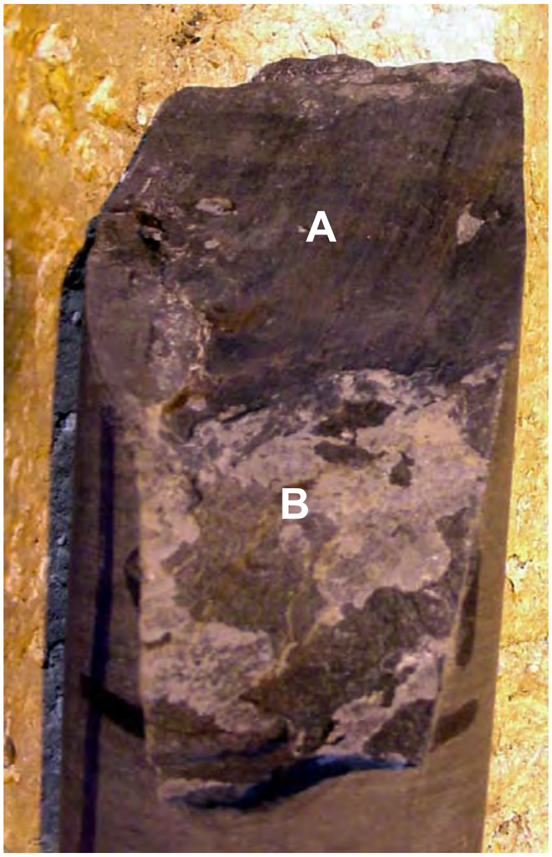

B

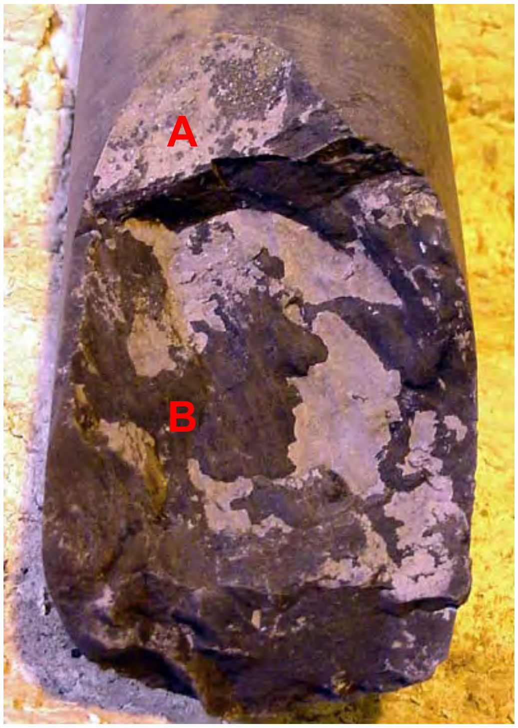

C.

Photo A: Parallel Extension Fracture and Shear
Depth: 1226.2’
Host Rock: Shale
Fracture A is a near vertical shear. Fracture B is a vertical extension fracture

Photo B: Parallel Extension Fracture and Shear
Depth: 1238.8’
Host Rock: Shale
Fracture A is a vertical extension fracture. Fracture B is a vertical shear

Photo C: Normal Extension Fractures and Shears
Depth: 1241’ – 1243’
Host Rock: Siltstone
Fracture strikes are shown with colored probes. The purple and yellow fractures are parallel extension fractures, each dipping at 60° angles. The red fracture is a 45°-dipping shear.

Extension Fractures and Shears

Fracture strikes are shown with colored probes. All of the fractures are extensional except for the fracture shown with the green probe and marked with an X. The red, brown and green (X) fractures have parallel strikes. The red and brown fractures dip at 60° angles, and the green (X) fractures dips at a 30° angle. The strikes of the blue and yellow fractures are parallel with one another. These two fractures have a strike intersection of 30° with the red, brown, and green fractures. The purple fracture is a vertical shear that strikes normal to the blue and yellow fractures.

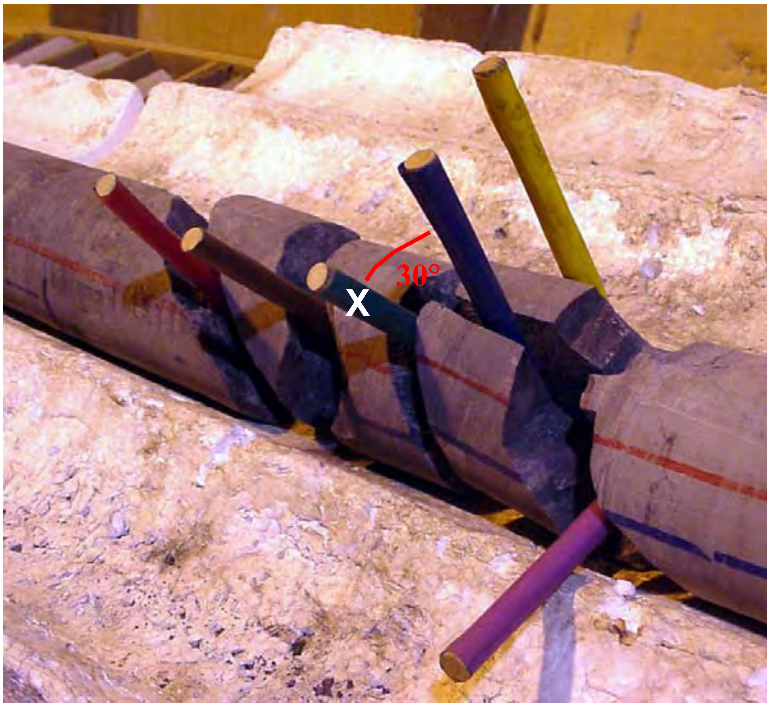

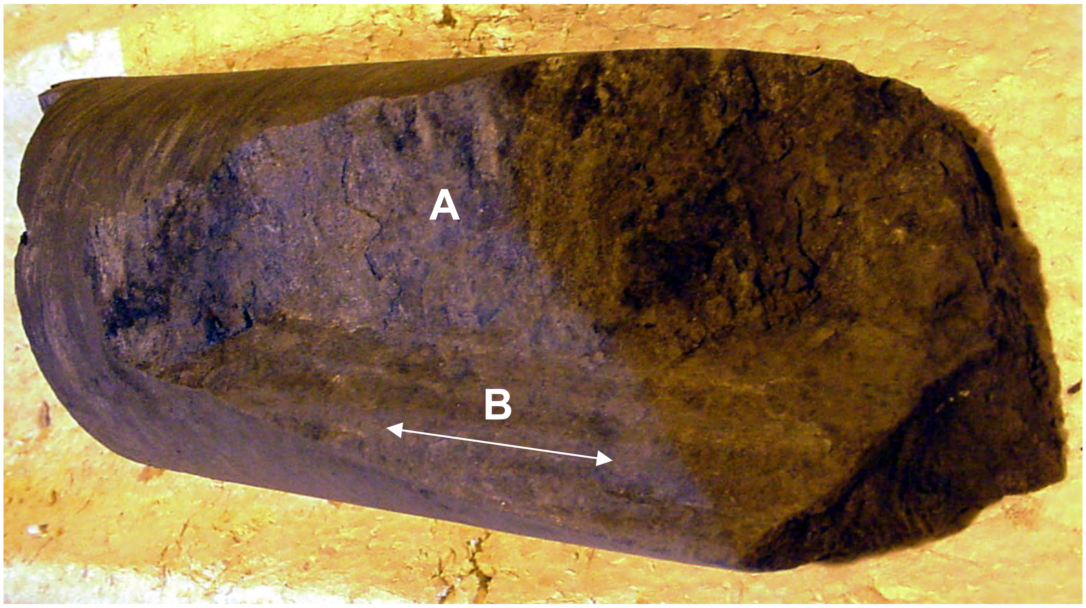

Intersecting Extension Fracture and Vertical Shear
Depth: 1332’
Host Rock: Siltstone

Fracture A is a vertical extension fracture. Fracture B is a vertical shear. The strike intersection angle of the two fractures is 30°.

A

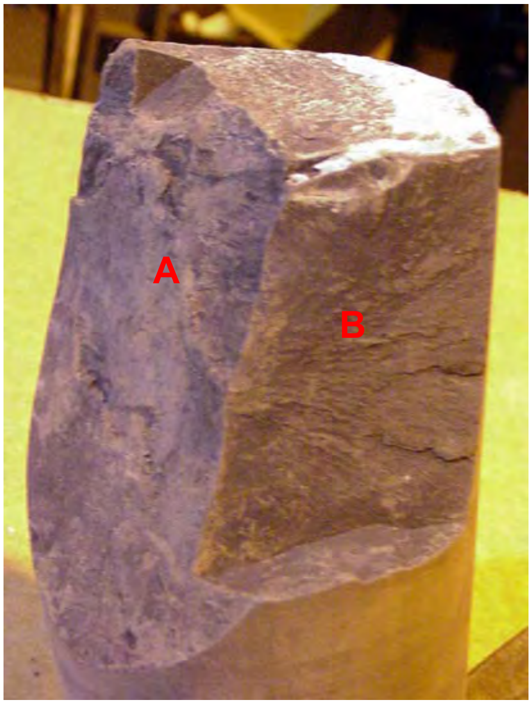

B

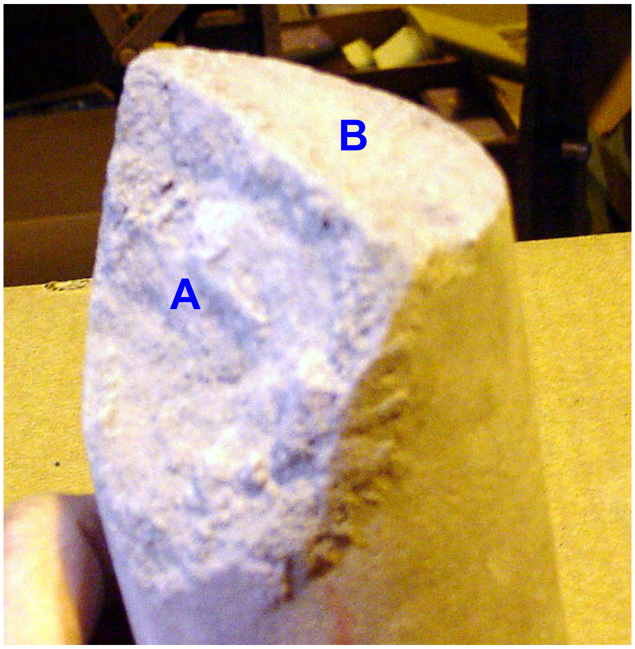

A.: Intersecting Vertical Shear and Vertical Extension Fracture

Depth: 1338.8’
Host Rock: Shale

Fracture A is a vertical shear with a smoothed fracture surface and slickencryst. Fracture B is an extension fracture with a plume structure radiating away from the Shear A. (In some instances, existing fractures form propagation barriers for extension fractures. However, if Shear A had formed prior to the Extension Fracture B, and if Shear A had been a barrier for extension fracture propagation, one might expect the plume to propagate toward Shear A rather than away from Shear A.)

B: Intersecting Thrust and Extension Fracture

Depth: 1370’
Host Rock: Sandstone

Fracture A is a 60°-dipping extension fracture. Fracture B is a 15°-dipping shear. The two fracture strikes are normal to one another. Fracture A has approximately 15% cement filling.

El Paso Well No: VPRCH 31

Summary of Fracture Characteristics Described in Core

Submitted to Sandia National laboratory
Raton Basin Project
By Constance N. Knight

Introduction

Well No. 31 VPRCH was cored continuously from near surface to a total depth of approximately 3,090 feet. The objective of this evaluation is to describe attributes of naturally occurring fractures below the Raton Conglomerate to total depth. The entire core below a depth of 2774 feet was carefully examined for fracture occurrence. All natural fractures were logged with respect to: depth, host lithology, fracture dip, surface characteristics, and angular relationships with one another.   Induced fractures were also noted, and wherever possible the orientations of natural fractures were described with respect to induced fractures. The strike of induced fractures parallels the direction of the maximum horizontal *in-situ* stress (sHmax). Since sHmax has been determined at a regional scale through other investigations, relating natural fractures to induced fractures can produce a reasonable estimation of true fracture strike and dip

Core from this well possessed a significant number of natural fractures. Many of the zones described in this report were associated with gas shows. Hopefully that some of the results of this study will aide in evaluating and developing the reservoir.

Summary of Fracture Characteristics

Total fractures described: 220

All percentages presented below are presented as a fraction of the total 220 fractures unless otherwise noted.

Host Lithology

Host Lithology	**Percentage of Fractures**
Shale and claystone *	42%
Siltstone	36%
Sandstone	21%
Coal	1%

* Almost all fine-grained clastics were determined to be shale.

Most (approximately 80%) of the described fractures occur in fine-grained rocks (siltstone and shale).

Types of Fractures (Extension vs. Shear)

Type of Fracture	Percentage
Extensional Fractures (Most fractures have surface plume structures. Some fractures also have evidence of shear, but this is usually not well displayed)	60%
Shears with a vertical component of relative motion	35%
Horizontal shears or bedding plane slip	3%
Fractures with both well developed plumes and evidence of shear, such as slickensides	2%

Extension fractures are the dominant fractures that were described in the VPRCH 31 well. Most "bleeding" gas shows encountered during drilling are associated with the presence of extension fractures.

Number of Fractures sorted by Lithology

Lithology	HZ Shears	Shears <35°	Shears 40°-65°	Shears 70°-90°	Extension Fractures	Extension/ Shear Fractures
Sandstone		4	1	1	38	2
Siltstone		4	12	10	52	1
Shale	7	8	24	16	36	1
Coal			1		1	
Conglomerate					1	
Totals	7	16	38	27	128	4

The table above shows five types of open fracture. Fractures within these five categories are also presented with a Gamma Ray log as Figure 1. Fractures were identified as shear fractures only if they had evidence that movement had occurred, such as the presence of slickensides, surface polish, etc. Many fractures identified as extension fractures had plume structures, however some extension fractures were identified on the basis of angular relationships to other extension fractures and steep (vertical) dip angles.

Some fractures have well-defined characteristics of both extension fractures and shears. The implication here is that the fractures initially formed as extension fractures and later were associated with offset movement.

Three intervals of highly broken core and a large number of shear fractures were identified as possible fault zones. In some cases, pieces of breccia were also observed. Possible fault zones are indicated on Figure 1. Fault intervals are: 2779.3 – 2780.3, 2789 – 2790, 2792.4 – 2792.7.

Shears Sorted by Dip Angle and Rake

Shear Angle	Percentage of total (100) fracs.	Rake Range	Apx. Avg. Rake	Comments Regarding Rake
Shears ≤ 35° dip	13%	5-80	40°	44% of the shears ≤35° exhibit rake.
Shears 40°-65° dips	32%	5-45*	20°	58% of the shears with dips of 40° - 65° exhibit rake
Shears 70° - 90° dips	11%	5-50*	20°	37% of the fractures with dips of 70° - 90° exhibit rake.

*Two fractures in this dip category each have two sets of slickensides, which implies that these fractures may be recording two episodes of shearing.

* One fracture in this dip category each have two sets of slickensides, which implies that these fractures may be recording two episodes of shearing.

Reverse offset was observed on several shears. The depths and dip characteristics of reverse shears are shown in the table below.

Reverse Shears	
Depth	Shear Dip Angle
2790.2	60°
2816.4	20°
2895.8	55°
2965.5	80°

Relationship of Fractures to sHmax as Defined by Petals

Depth of Fracture	Orientation Relative to Petal	Type of Fracture
2779	20° (measured clockwise)	60° dipping shear
2820	Sub-parallel - 10°	3 extension fractures
2974	Parallel	Extension Fracture

2976	Parallel	Extension Fracture
2977	Parallel	2 Extension Fractures
2978	Parallel	2 Extension Fractures
2979	Parallel	3 Extension Fractures

At several depths extension fractures occur parallel to sHmax. An orientation parallel to sHmax is optimal for gas production.

Relationship of Coal Cleats to sHmax	
Depth	Orientation with respect to sHmax
2813	Parallel

Fracture Fillings

Information regarding fracture fillings includes: 1. Percentage of filling material in individual fractures; 2. Mineralogy of the filling material; and 3. Fracture-aperture measurements. Percentages of filling materials were estimated by examining the facture faces. Many fractures appeared to be 100% filled with cementing material. However commonly such fractures exhibit well develop druze. The presence of druze implies that these fractures are partially open. The best druze development is associated with those fractures having the largest fracture apertures.

In some cases sets of extension fracture were observed to strike perpendicular to one another. It these cases, it was observed that druze were well develop on one set of parallel fractures however poorly developed on the complementary set of fractures. Fractures with the well-developed druze probably parallel the sHmax of the time the druze were formed.

% Fracture Filled	**No. Extension Fractures**	**No. Shears < 35°**	**No. Shears 40°-65°**	**No. Shears 70° - 90°**
< 10%	12	11	11	10
20% - 25%	2	1	4	3
25% - 49%	10	1	3	4
50% - 74%	6	1	8	3
75% - 100%	98	2	12	7
Total	128	16	38	27

On visual inspection at 10X, most of the extension fractures appeared to be over 75% filled with cement. Extension fractures exhibiting lower percentages of cementation were those extension fractures that were found open in the core boxes. Probably some of the cementing materials were destroyed in the coring process. For shear fractures, the degree of cementation is more variable that extension fractures. The estimates presented here should be considered to be imprecise variables.

Numbers of Fractures filled with Various Cements		
Cement Type	**Extension Fractures**	**Shear Fractures**
$CaCO_3$	97	21
Clay	5	23
Clay and $CaCO_3$	8	10
Clay and Pyrite	1	
$CaCO_3$ and Quartz	1	
$CaCO_3$ and pyrite	4	
*$CaCO_{3,}$ - Dead oil stain.	1(depth 2944')	

The dominant fracture cement was calcite. Commonly extension fractures cemented with only calcite were relatively easy to break apart. Also, these fractures commonly exhibited druze. The finer the fracture aperture, the finer the druze crystals. Those fractures cemented with pyrite were difficult to break apart. Such fractures had poor druze development.

Mineralized fractures were observed to extend into coal beds at the following depths: 2993.6, 2996.6, and 3016.9.

Fracture Apertures

Fracture apertures range from 0.1 – 2.0 mm., with the average aperture equal to 0.4 mm. The following table lists fracture aperture measurements of healed fractures. In the case of open fractures with well-developed druze, the aperture measurement represents the thickness of the druze. (Over 95% of the measurements are of healed fractures.)

Depth	**Fracture Aperture (mm)**	**Fracture Type**	**Druze**
2830.5	0.3 - 0.7	Extension	
2837	0.3	Extension	
2849.1	0.3 - 0.5	Extension	
2860	0.2 - 0.3	Extension	
2860.7	0.5	Extension	
2863.9	1.0	Extension	Well-developed (large crystals)
2867.2	1.0 - 1.5	Extension	Well-developed
2873.2	0.2 - 0.3	Extension	
2880.5	0.3	Extension	
2881.5	0.3 - 1.0	Extension	Well-developed
2886.6	0.2-0.3	Extension	Well-developed
2889.5	0.1-0.2	Extension	
2910	0.1-0.3	Extension	
2912	0.1-0.3	Extension	Well-developed

2916.1	0.3	Extension	
2916.5	1.0	Extension	
2917.5	0.1-0.3	Extension	Apparent
2919.7	0.5-1.0	Extension / Shear	
2932.2	0.1-1.0	Extension	Apparent
2958.8	0.5	Extension	
2959.7	0.2-0.3	Extension	Apparent
2960.7	0.2-0.3	Extension	Apparent
2962.2	0.1-0.2	Extension	
2962.3	0.1-0.2	Extension	
2962.6	0.1-0.2	Extension	
2965.4	0.1	Extension	
2965.5	1.0	Shear	
2974.3	0.1-0.2	Extension	
2974.9	0.1-0.2	Extension	Apparent
2979.7	0.1	Extension	
2982	2.5	Extension	Well-developed
2982.5	0.1	Extension	Well-developed
2982.7	0.5-1.0	Extension	Well-developed
2983.1	0.1	Extension	
2983.7	.05-1.0	Extension	
2984.1	.05-1.0	Extension	Apparent
2987.3	0.5 - 0.7	Extension	Apparent
2987.8	0.1-0.6	Extension	Apparent
2987.8	0.1-0.6	Extension	Apparent
2987.8	0.1-0.6	Extension	Apparent
2987.8	0.1-0.6	Extension	Apparent
2988.5	2.0	Extension	Well-developed
2992.2	0.2-0.5	Extension	
2992.3	0.1-0.3	Extension	
2993.2	0.1-0.3	Extension	
3002.3	0.5	Shear	
3009.5	0.1	Extension	
3010.1	0.1-0.2	Extension	
3011.6	0.5	Extension	Well-developed
3012.7	0.3	Extension	Well-developed
3013.3	0.1	Extension	

Fracture Spacing

Fracture spacing was determined for both extension and shear fractures. Two tables are presented below: one pertaining to extension fractures, and one pertaining to shears. Due to the highly fractured nature of this reservoir, for many fractures a “true” spacing (spacing perpendicular to the fracture surfaces) is presented. In cases where the vertical spacing of fractures would not permit such a measurement, the apparent spacing (vertical depth from one fracture midpoint to another) was measured. The true fracture spacing = sin (dip ∠) x (observed fracture spacing). True spacing measurements are presented in red, whereas observed fracture spacing measurements are presented in black. Considering the level of accuracy of this study, the difference between “true” and “observed” spacing is inconsequential

Extension Fracture Spacing	
Depth (ft)	Fracture Spacing (ft)
2819.1	1.3
2822.9	0.5
2826.7	1.4
2830.5	0.03
2836.1	1
2865.8	1
2867.2	1.8
2912	0.03
2912	0.1
2916.1	0.1
2957.4	0.075
2958.8	.05 - .15
2962.2	0.05
2974.9	0.1
2978.1	0.05
2978.2	0.05
2982	0.05
2982	0.05
2982.7	0.3
2983.1	0.05
2987.8	.025 - .15
2987.8	.025 - .15
2987.8	.025 - .15
2987.8	.025 - .15
2992.2	0.2
2992.3	0.15
2992.6	0.15
2993.4	0.4
3010.1	0.05
3012.7	0.15
3013.3	0.15

.

Shear Fracture Spacing		
Depth (ft)	Fracture spacing (ft)	Fracture Dip Angle
2782.2	0.3	60°

2782.6	0.4	30°
2788	0.3	80°
2790.2	0.3	60°
2794.2	1.5	75°
2803.1	0.5	70°
2803.5	0.5	70°
2816.8	0.1	80°
2894.8	1.0	50°
2998.3	0.7	55°

Summary of Fracture Strike Relationships

Because this core was not oriented, fracture dips and strikes cannot be directly obtained. However, the following table presents fracture strikes relationships that may be helpful in relating core to outcrop data.

Intersection Angle	**Number of Fractures with Various Intersection Relationships**					
	EX/EX	EX/Thrust	EX/>35°Shear	>35° Shear / >35° Shear	>35° Shear / Thrust	Thrust/ Thrust
Parallel Strike	55	4	5	17	2	1
Parallel Strike Opposite dips	1		1			
10° - 30°	2	1	7	1	1	
31° - 60°	7	1	9	1	2	
61° - 89°			1	1		1
Normal (90°)	11	3	2	4	2	

EX/EX – Intersection of two extension fractures
EX/Thrust – Intersection of an extension fracture and a low angle shear (< 35°)
EX/>35° Shear – Intersection of an Extension fracture and a higher angle (> 35°) shear
>35° Shear/>35° Shear –Intersection for two higher angle shears
>35° Shear /Thrust – Intersection of a higher angle shear (> 35°) and a low angle shear (< 35°)

Fracture Length

Fracture length data for extension fractures and shears are presented below. Data for complete fractures (those fractures that possessed two terminations within the core) are presented separately from those of other fractures. For fractures that had one or no terminations within the core, a minimum fracture length is given.

Fracture Lengths for Extension and Sheer Fractures						
	No. Fracs	**Extension Fracture Lengths**		**No. Fracs**	**Shear Fracture Lengths**	
		Length Range (ft)	**Average Length (ft)**		**Length Range (ft)**	**Average Length (ft)**
Complete fracture in core	16	0.1 – 1.0	0.4	0		
Minimum Fracture Length	104	0.1 – 6.1	0.7	62	0.05 – 1.2	0.2

Some notes about Fracture Terminations and Relative ages of Fractures

The following are some observations to keep in mind as the study continues.

Several fractures have characteristics of both extension and shear, i.e. plume structures and mineralized slickensides. (Usually the slickensides indicate oblique fault motion.) The implication here is that movement occurred after the extension fractures formed.

Also, some shears have two rake orientations. At depth 2920' an original tension fracture possesses two sets of slickenlines. One set exhibits dominantly dip slip movement with a rake of 70° to 80°. The other set of slickenlines are horizontal, implying lateral slip.

Two 60° dipping shears each possess two sets of slickenlines. The rakes of each are (0°, 20°) and (10°, 45°). In well VRPCH 34, a 50° dipping shear was observed to have two sets of slickenlines with rakes of 40° and 70.

In three cases, extension fractures were observed to terminate at shear fractures. The shears may have existed prior to the extension fractures, thus forming a "barrier" for extension fracture propagation. It is also possible that the extension fractures came first and then were offset for the shears.

In some cases where an sHmax determination can be made, druze development is more complete on extension fractures parallel to sHmax (as opposed to fractures normal to sHmax). This implies that the sHmax existing when the fractures became mineralized is the same as it is today. Perhaps the extension fractures were formed in the recent stress regime – in other words, the fractures are young.

Figure 1: VPRCH 31 Gamma Ray Log and Fracture

KEY

🟥 Extension Fracture

Shears

🟩 <35° Dip

🟪 40°- 65° Dip

🟦 70° - 90° Dip

🟫 Horizontal Slip

▬ Possible Fault Zone

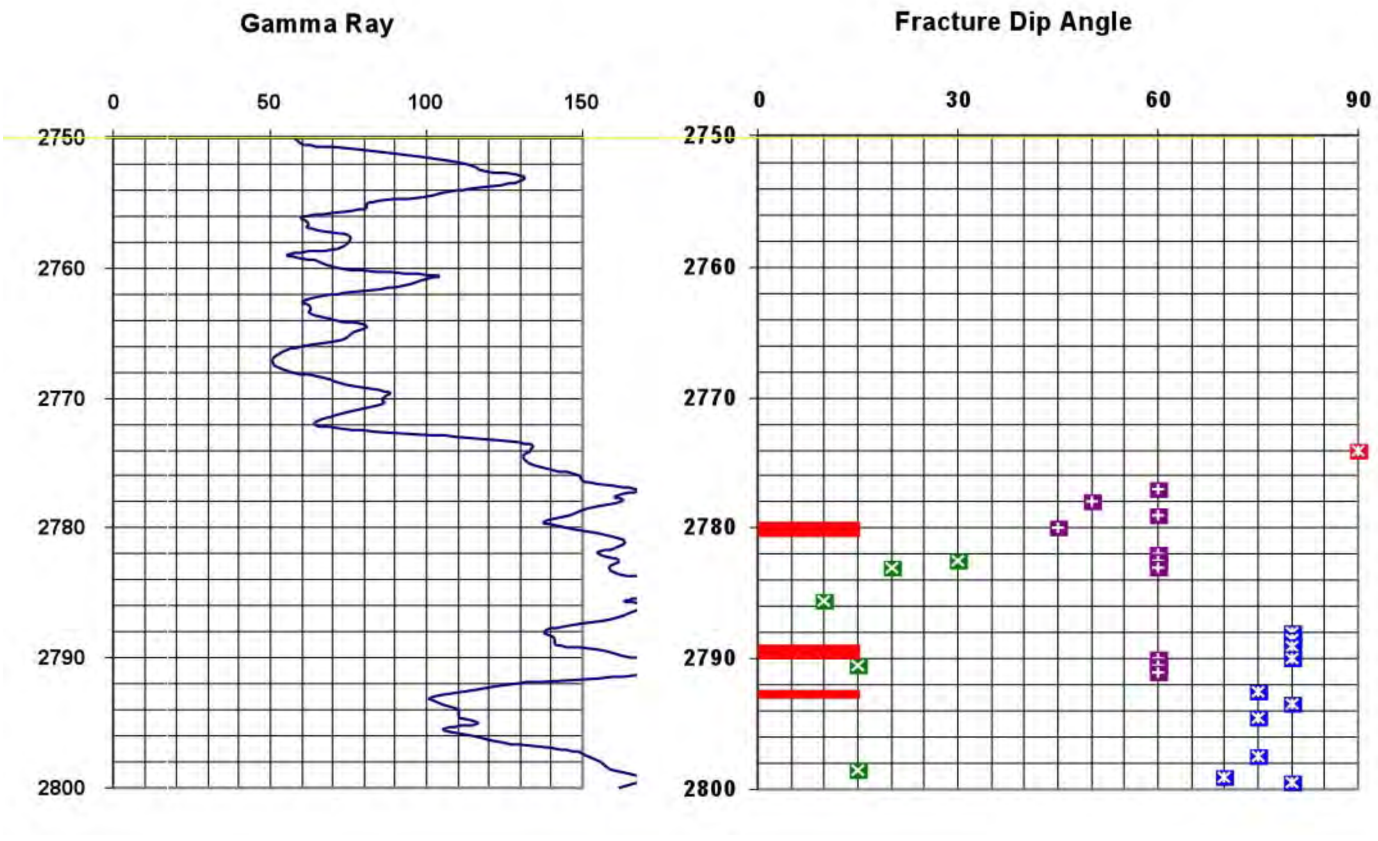

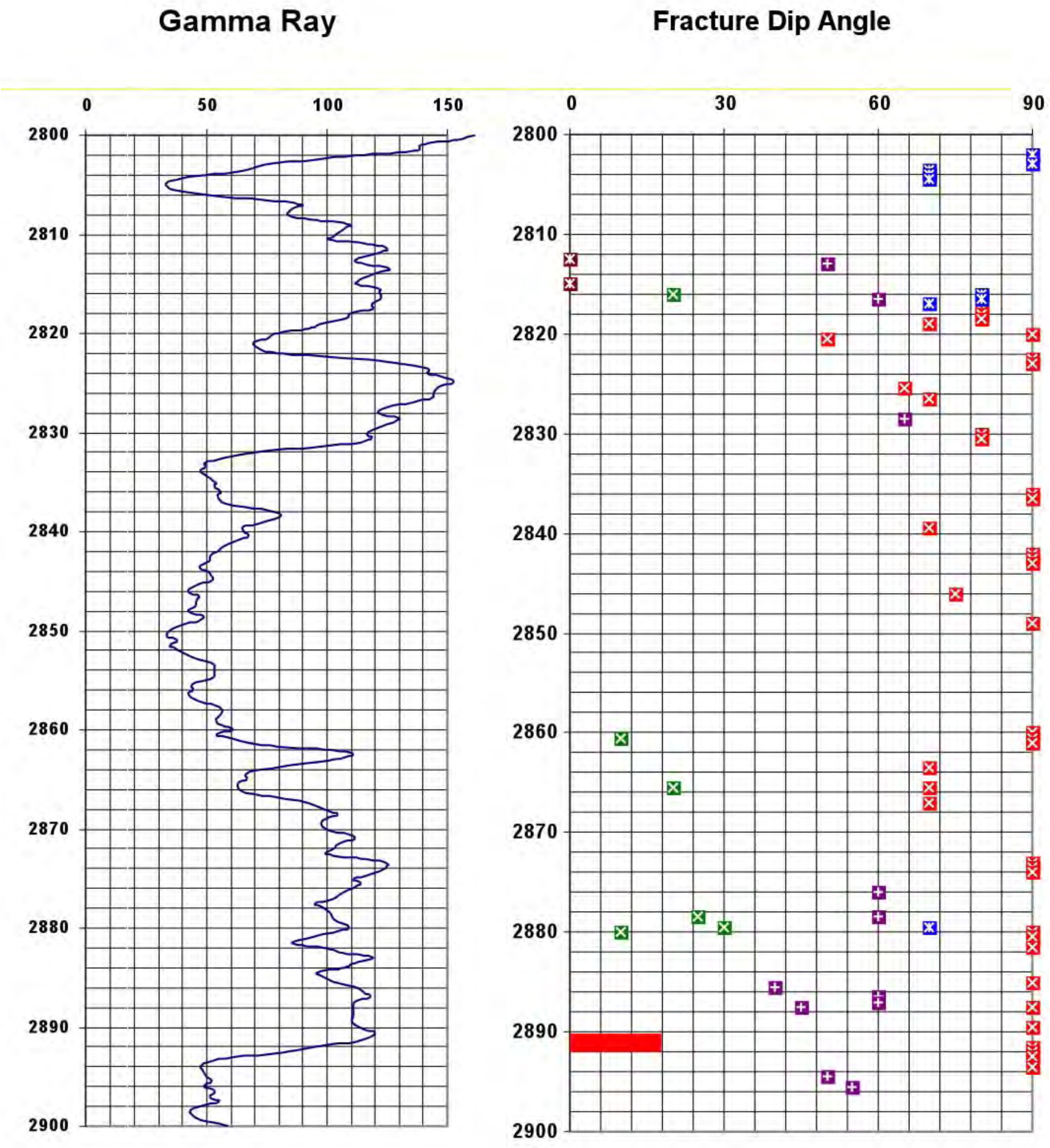
Gamma Ray
Fracture Dip Angle
0
50
100
150
0
30
60
90
2800
2810
2820
2830
2840
2850
2860
2870
2880
2890
2900

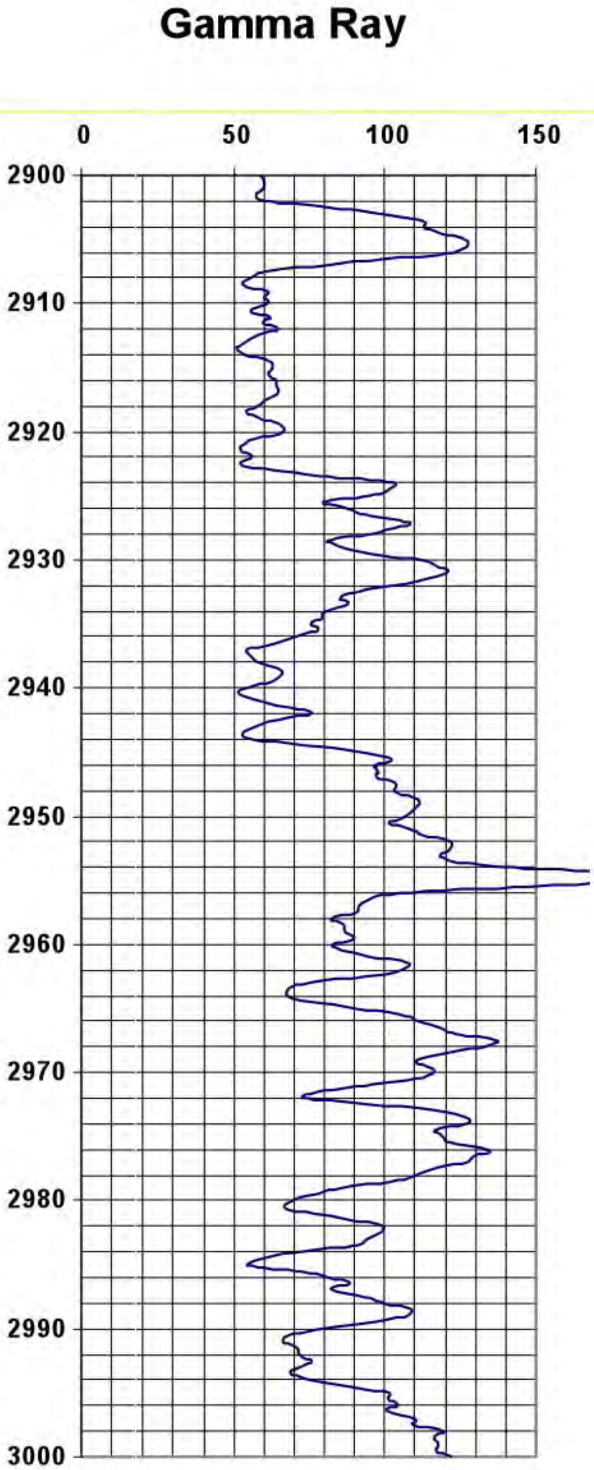
Gamma Ray
0
50
100
150
2900
2910
2920
2930
2940
2950
2960
2970
2980
2990
3000

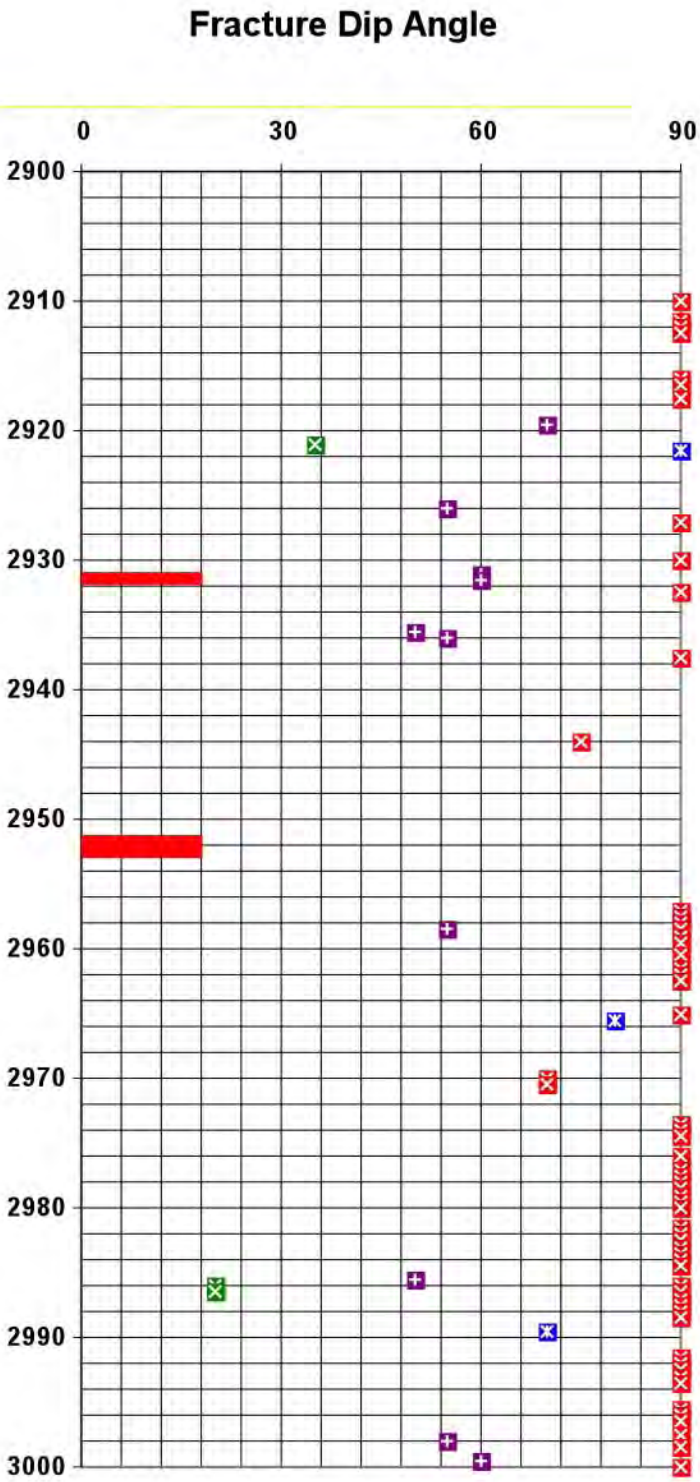
Fracture Dip Angle
0
30
60
90
2900
2910
2920
2930
2940
2950
2960
2970
2980
2990
3000

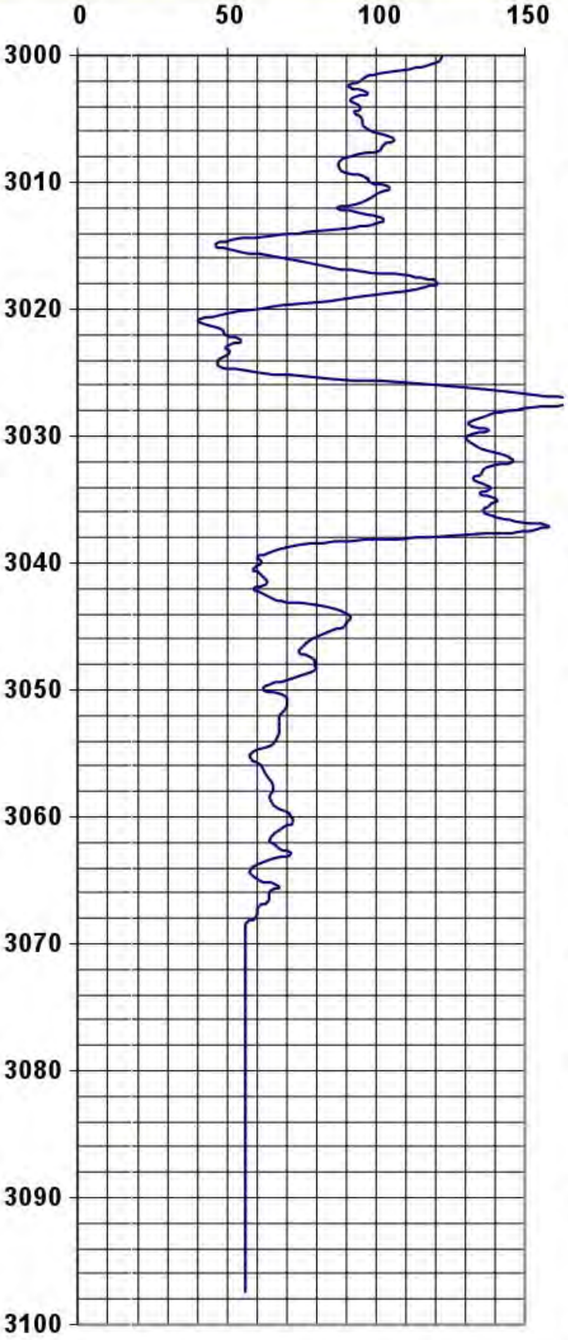

Gamma Ray

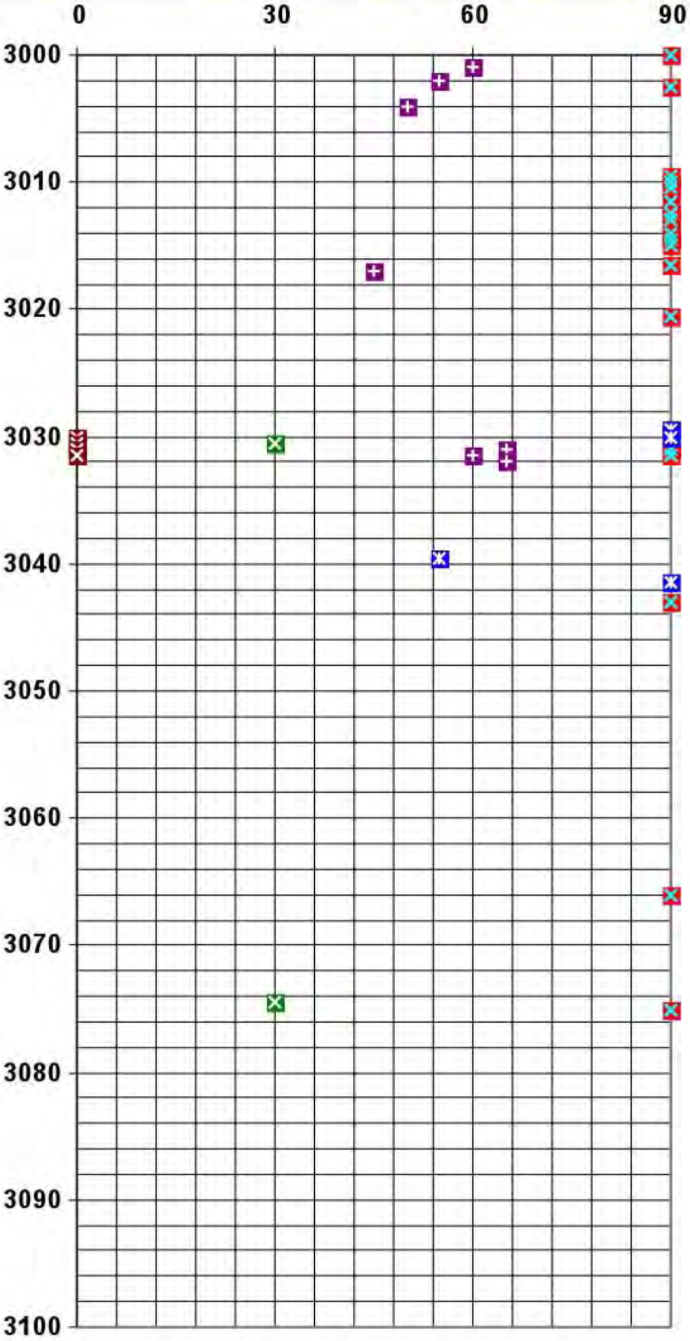

Fracture Dip Angle

Photographs are presented here to document some of the observations described above. (Over 150 photos were taken and are available digitally.)

Core Photographs – Examples of Shears

Possible Fault Zone

Depth: 2779'-1780'

Lithology: Shale

Slickensides and surface polish are common on core pieces. Pieces of breccia, possibly fault breccia, are also present within this interval.

Breccia

Two sets of shears with parallel to sub-parallel fracture strikes

Depth: 2782'

Host Rock: Shale

Fracture dips: A=60°, B=30°, C=60°, D=60°

The lower set of fractures (A&B) dip in opposite directions from the upper set (C&D). Pens, which are aliened with rake striations, indicate that movement on the lower set of fractures was normal to that on the upper set of fractures.

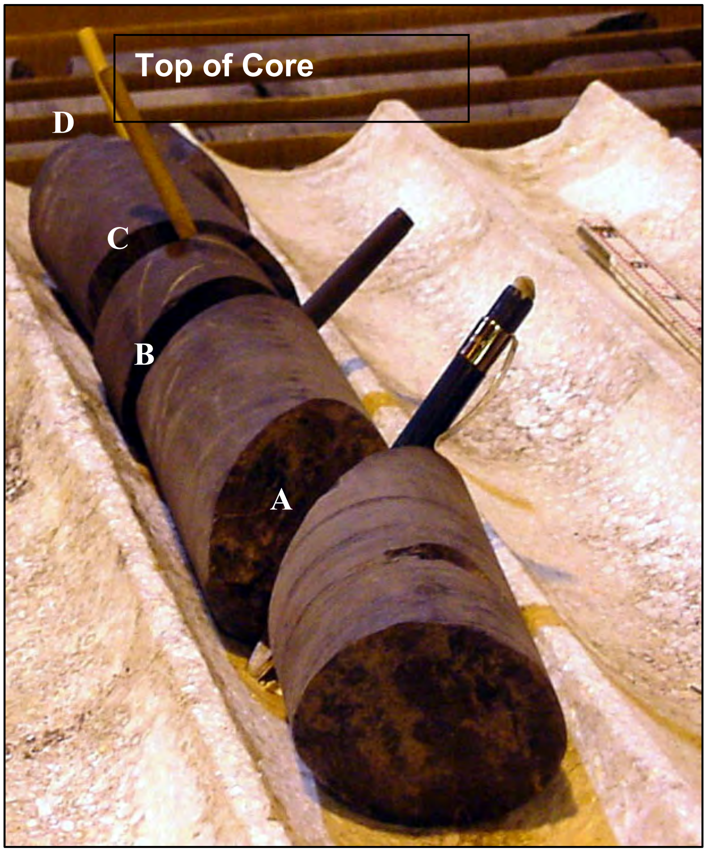

Shears with Parallel Strikes

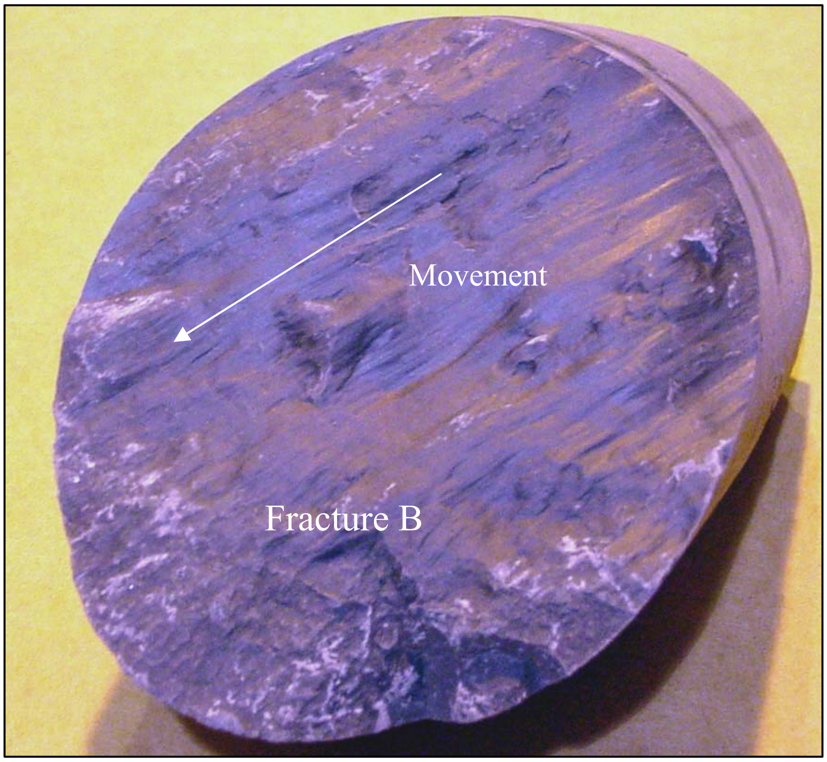

Depth: 2791-2792

Host Rock: Shale

The photo above shows orientations of shears with respect to one another. The photo on the right shows the surface of Fracture B

Dip angles: A = 80°
B = 60°
C = 60°
D = 60°

Surface markings on Fracture B imply reverse movement.

Shear Fracture

Depth: 2936’

Host Rock: Shale
Fracture Dip: 55°
Rake: 20°

This is a typical shear in shale. Slickenlines are shown with an arrow.

Shear with two sets of slickenlines

Depth: 2876

Host Rock: Shale

Fracture Dip: 50°
Although not clear in this photo, this fracture face shows two sets of slickenlines with rakes of 10° and 45°. This shear strikes 50° relative to an extension fracture above.

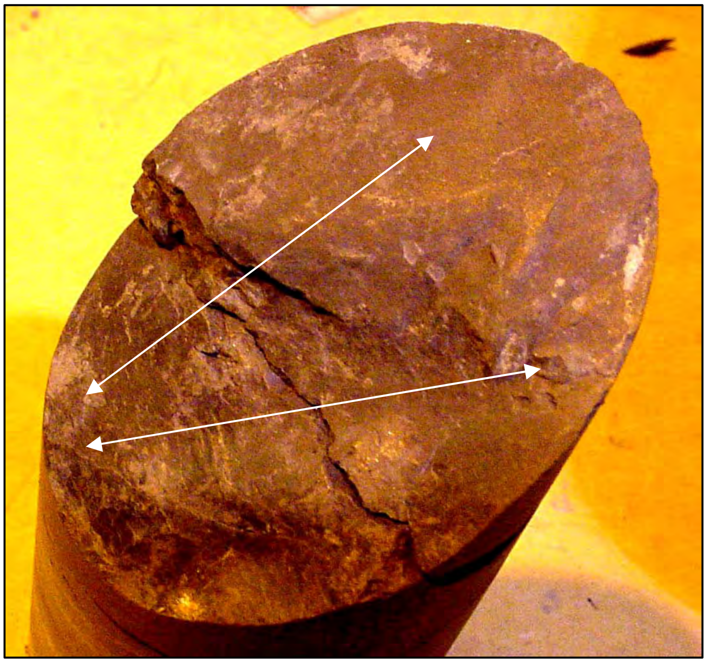

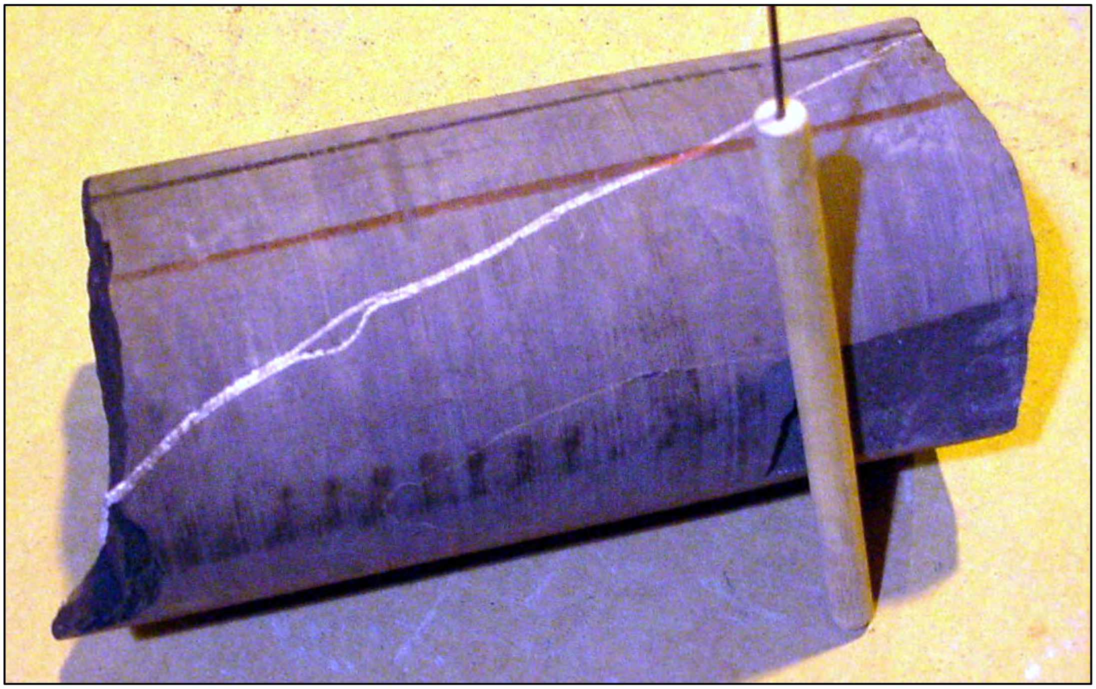

High Angle Reverse Fault

The upper photo shows the fracture in tact. The lower photo shows the fracture surface.

Depth: 2965

Host rock: Shale
Dip Angle: 80°
Fracture filling: $CaCO_3$
Rake: 5°
Fracture aperture: 1.0 mm

Core Photographs – Examples of Extension Fractures

Orientation of Extension Fractures relative to sHmax

Depth: 2817.3 – 2820.8 – An expanded view of the outlined area is presented below

Host Rock: Siltstone

A petal fracture is present in highly carbonaceous shale near the bottom of this cored interval. Strikes of extension fractures are shown with pencils. Three extension fractures (including Fracture A defined above) are parallel to the petal and thus to sHmax. Fracture B (defined below) is normal to sHmax.

Extension Fractures with Perpendicular Strikes (Section of core outlined above)

Depth: 2817.3 -

Host Rock: Siltstone
Fracture Filling: $CaCO_3$

These two extension fractures have normal strikes. Fracture A, which is oriented parallel to present day sHmax, has better druze development than fracture surface B, which is normal to present day sHmax, This implies that the sHmax existing when the fracture was mineralized is the same orientation as that today.

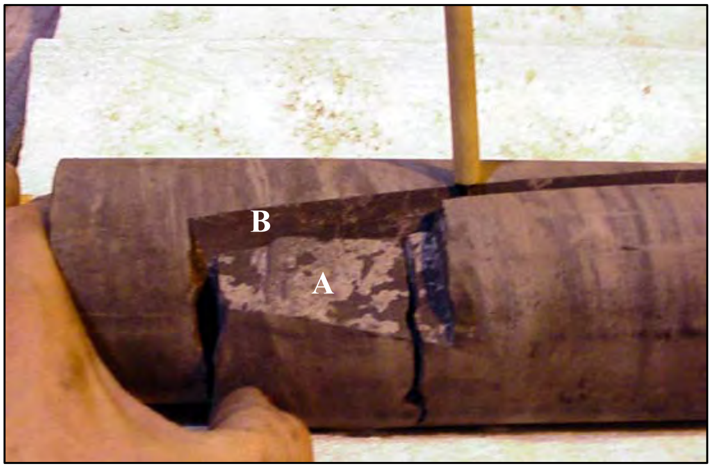

Druze on extension fracture surface

Depth: 2864’

Host Rock: Sandstone (fg)
Fracture Dip: 70°
Fracture Filling: $CaCO_3$ and Quartz

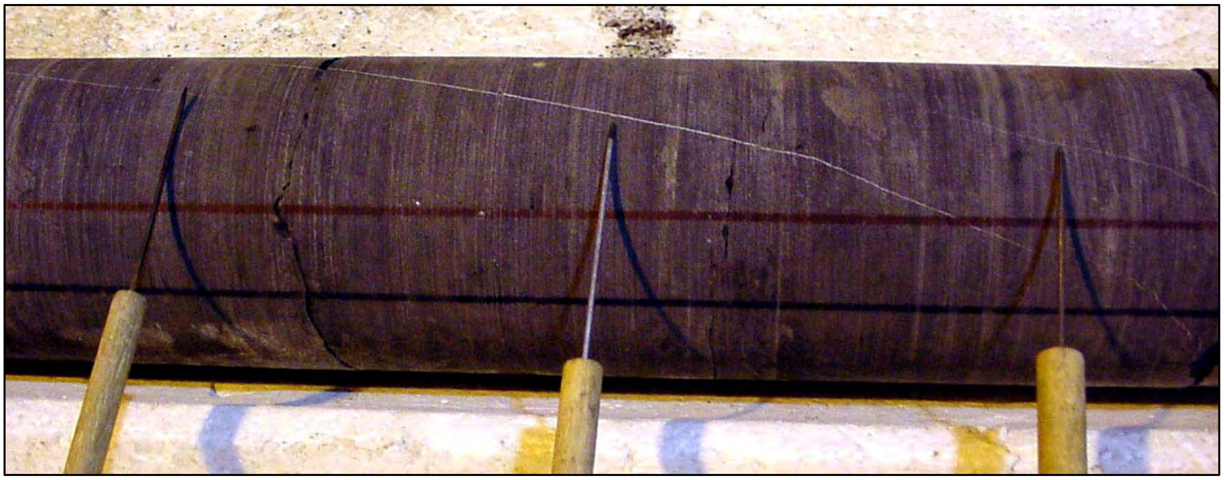

Three Parallel Hairline Extension Fractures

Depth: 2873’

Host Rock: Siltstone
Fracture Dip: Vertical
Fracture Apertures: 0.2 – 0.3 mm
Fracture Filling: $CaCO_3$

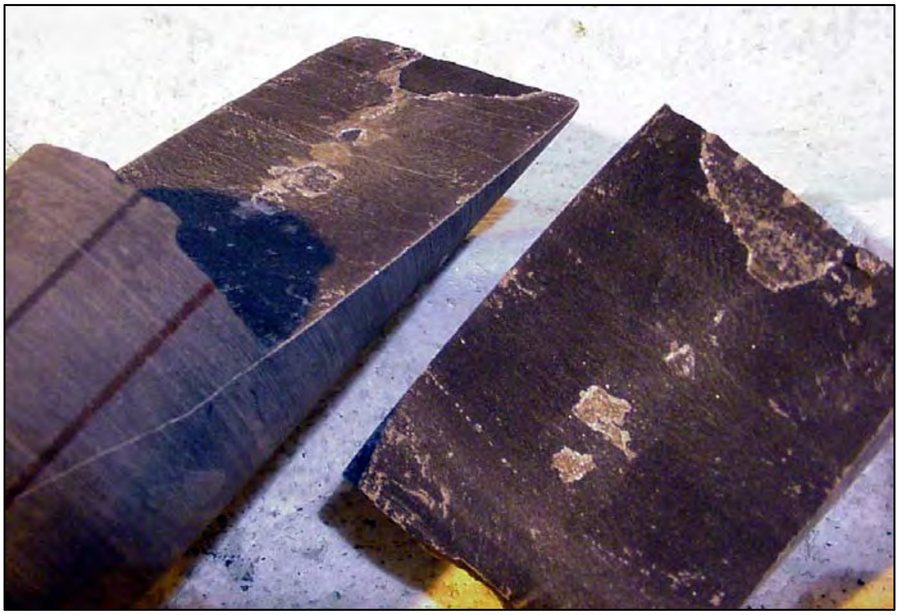

Extension Fracture (This fracture is the middle fracture in the photo shown above.)

Depth: 2873.5
Host Rock: Siltstone
Note finely crystalline druze on fracture surfaces

Extension Fracture

Depth: 2883 – 2885.5

Host Rock: Silty shale
Fracture Lengths: 2.2’
Fracture apertures: 0.3 – 1.0 mm
Fracture Filling: $CaCO_3$

Most of the fracture surface exhibits plume structures. However there is a suggestion of oblique slickenlines and surface polish on some of the surfaces

Slickenlines indicating oblique slip

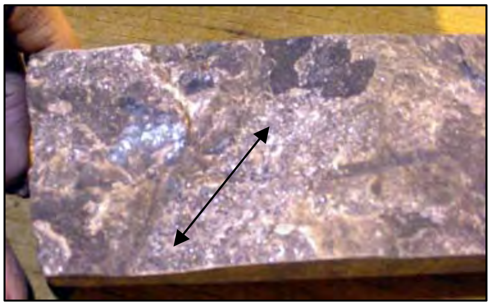

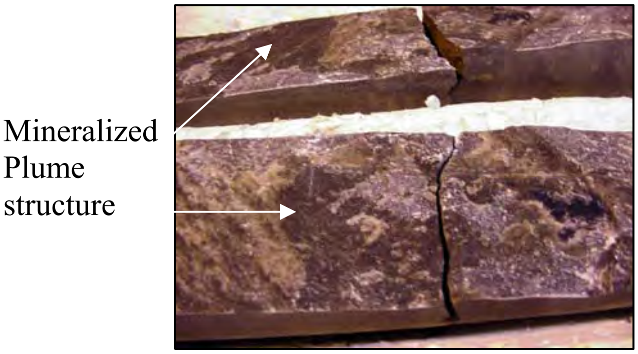

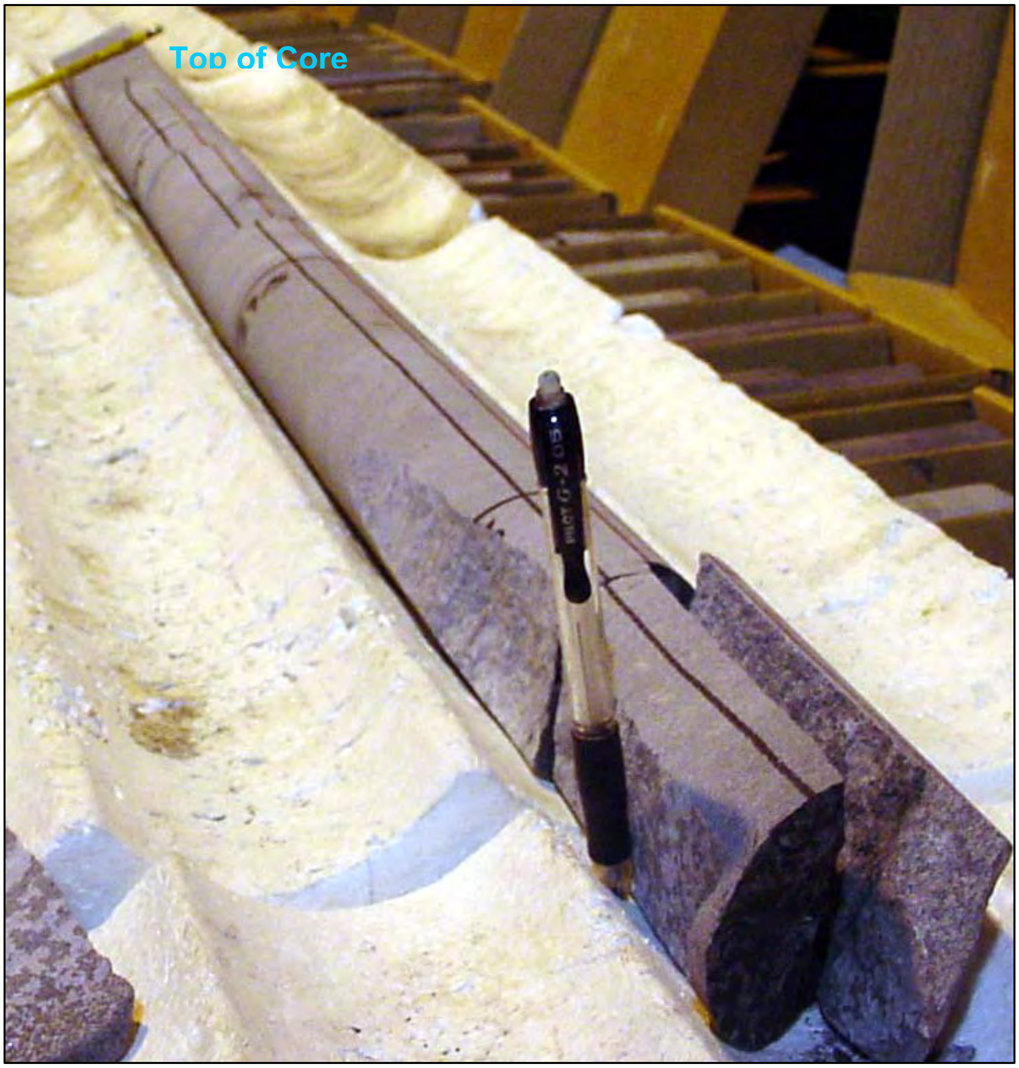

Extension Fractures with Parallel and Normal strikes

Depth: 2912 – 2916

Host Rock: Sandstone (fg)
Fracture Apertures: 0.1 – 0.3 mm
Fracture Filling: $CaCO_3$ with trace patchy pyrite

The pens parallel fracture strikes. Note the finely crystalline druze on fracture surfaces. The fracture spacing shown in the lower portion of the core is 0.1’.

Extension Fractures with Parallel Strikes

Depth: 2917' – 2922'

Host Rock: Sandstone (cg)

Fracture length:	0.6
Fracture Apertures:	0.1 – 1.0 mm.
Fracture Filling:	$CaCO_3$

The pens parallel the fracture strikes. Note well-developed drews on fracture surfaces.

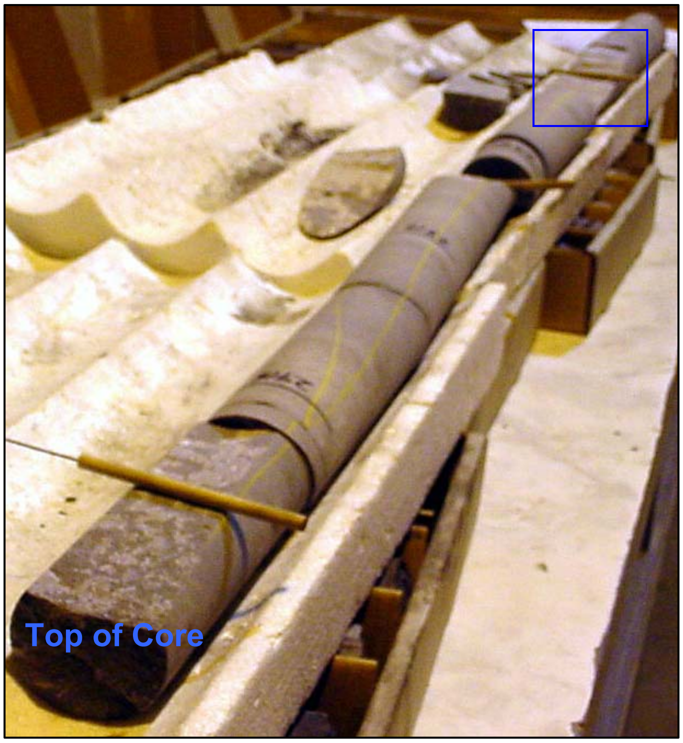

Extension Fracture Surface – from interval outlined in previous photo

Depth: 2920

Host Rock: Sandstone (cg)
Fracture Filling: $CaCO_3$

This mineralized surface shows two sets of slickenlines. One set implies oblique motion, while the other implies lateral slip.

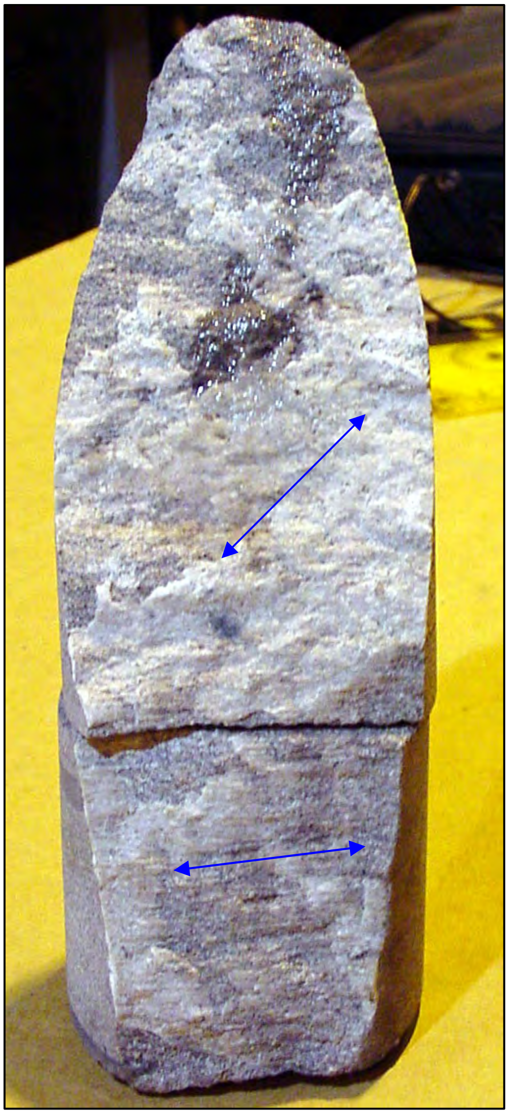

Closely Spaced Hairline Fractures

Depth: 2932’

Host Rock: Sandstone (vfg)
Fracture Length: 0.2 – 0.9 ft.
Fracture Spacing: .02’ to 0.1 ft.
Fracture Filling: $CaCO_3$
Fracture Apertures: 0.1 – 1.0 mm

Two Intersecting Extension Fractures

Depth: 2973

Host Rock: Sandstone (vfg)
Fracture Dips: Vertical
Fracture Filling: $CaCO_3$, trace pyrite
Apertures: 0.1 – 0.2 mm

These two fractures dip in opposite directions and have a strike intersection of 45°.
Drews is present, but not as well developed as in other sections of sandstone.

Orientation of Extension Fractures relative to *insitu* stress

The photo on the upper left shows a petal (induced) fracture at depth 2977.7'. This induced fracture, which identifies the orientation of sHmax is located at the top of the core photo to the right. The pens indicate fracture strikes and show that the lower two natural fractures strike parallel to the petal fracture.

Host Rock: Shale
Fracture apertures: 0.1 mm.
Fracture Filling: $CaCO_3$

Two Intersecting Extension fractures

Depth: 2992’
Host rock: Siltstone

Fracture Apertures: 0.2 to 0.5 mm
Fracture Filling: $CaCO_3$

Fracture-strike Intersection: 60°

Mineralized Extension Fracture in Coal

Depth: 3016’

Extension fractures identified in upper beds extend into the coal. Mineralized fractures were also found in coals at other depths (2993.6 and 2996.6).

Core Photographs – Examples of Extension / Shear Relationships

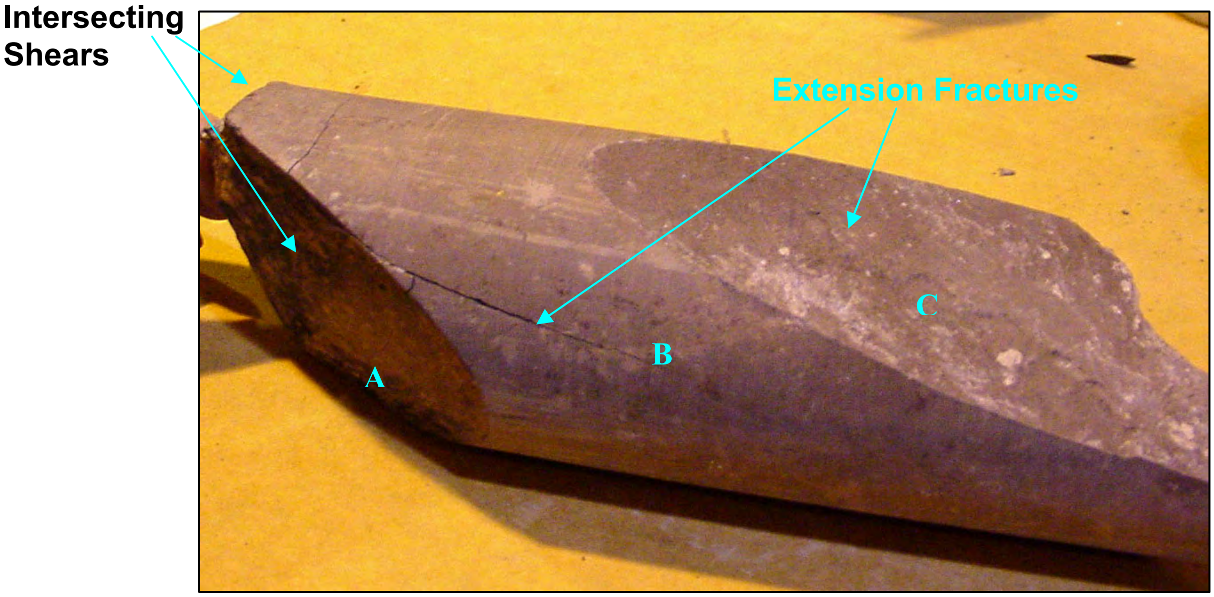

Intersecting Shears and Two Extension Fractures

Depth: 2830-31'

Two shear fractures have a strike intersection of 60°. Two extension fractures are parallel. The strike of shear fracture A is normal to the strike of extension fractures B and C.

Three Extension Fractures and on Low Angle Shear

Depth: 2863' – 2865'

Extension fractures A, C, and D are parallel to one another. These strikes are normal to low angle shear B. The dips on the extension fractures are 70°. The dip on Shear B is 20°.

Intersection of a Low Angle Shear and a Vertical Extension Fracture

Depth: 2880’

Host Rock: Shale

The strike of the extension fracture is parallel to that of the thrust shear

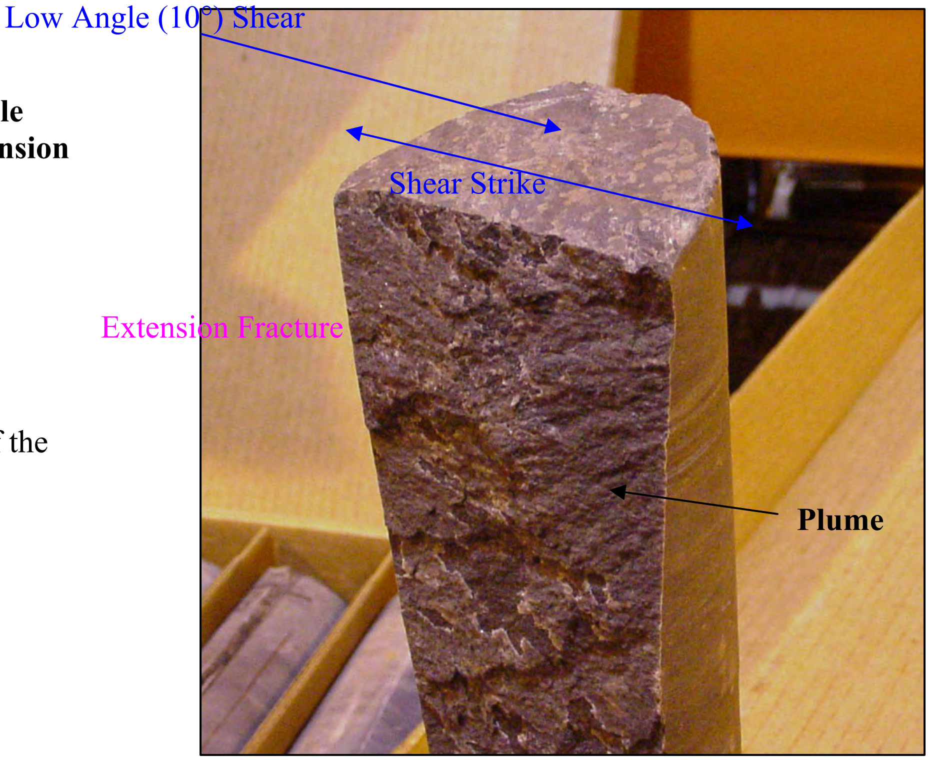

Intersection of a Low Angle Shear and a Vertical Extension Fracture

Depth: 2887’

Host Rock: Shale

Extension fracture A and low-angle shear B have parallel strikes.

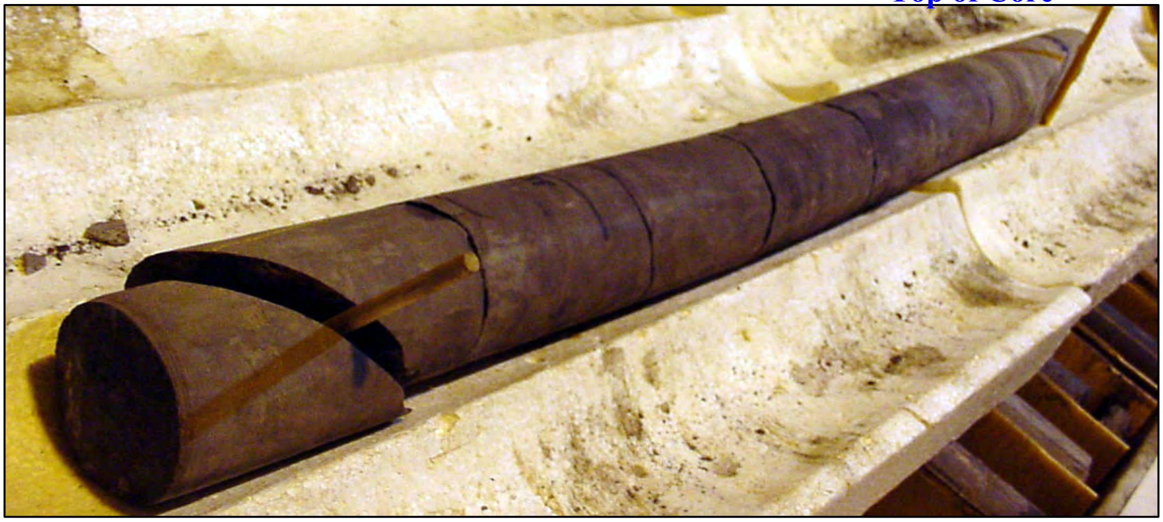

Extension Fracture and Shear

Depth: 2932 – 2935.5

This interval shows the strike relationship of a vertical extension fracture in sandstone and a 55°- dipping shear in shale. The pencils are aligned parallel to fracture strike. The strike intersection of these two fractures is 35°.

Vertical Fracture with Deal Oil Residue

Depth: 2944.1

Host rock: Sandstone

This fracture is highly cemented, and the break along the fracture is non-planar. The rock surrounding this fracture is well indurated and difficult to break apart.

El Paso Well No: VPRCH 32

Summary of Fracture Characteristics Described in Core

Submitted to Sandia National laboratory
Raton Basin Project
By Constance N. Knight

Introduction

Well No. 32 VPRCH was cored continuously from near surface to a total depth of 1433 feet. The objective of this evaluation is to describe attributes of naturally occurring fractures below the Raton Conglomerate to total depth. The entire core below a depth of 1090 feet was carefully examined for fracture occurrence. All natural fractures were logged with respect to: depth, host lithology, fracture dip, surface characteristics, and angular relationships with one another. Induced fractures such as petal fractures were not observed in this core.

Core from this well possessed a significant number of natural fractures. The purpose of this report is to summarize fracture characteristics and to compare fracture characteristics with those described in other wells. The first half of this report provides summary and specific information about the fractures. The second half provides photographs showing distinguishing features of the fracture types and the fracture angular relationships

Summary of Fracture Characteristics

Total fractures described: 414

All percentages presented below are presented as a fraction of the total 414 fractures unless otherwise noted.

Host Lithology

Host Lithology	Percentage of Fractures
Shale and claystone *	45%
Siltstone	35%
Sandstone	16%
Igneous Intrusion	4%

* Almost all fine-grained clastics were determined to be shale.

Most (80%) of the described fractures occur in fine-grained rocks (siltstone and shale). Most of the fractures in described in previously logged cores (VPRCH 34 and VPRCH 31) also occur in fine-grained rocks. However, in contrast with the core from VPRCH 31, in which most of the fractures were dominantly extensional, the majority of the fractures in Well VPRCH 32 are shears.

Types of Fractures (Extension vs. Shear)

Type of Fracture	Percentage
Extensional Fractures (Most fractures have surface plume structures. Some fractures also have evidence of shear, but this is usually not well displayed)	40%
Shears with a vertical component of relative motion	52%
Horizontal shears or bedding plane slip	8%

Shears are the dominant fractures the VPRCH 32 core. At least 4% of the total fracture population possessed both plumes as well as evidence of shears, such as slickensides.

Number of Fractures sorted by Lithology

Lithology	HZ Shears	Shears <35°	Shears 40°-65°	Shears 70°-90°	Extension Fractures
Sandstone	3	3	2	4	56
Siltstone	14	24	35	17	56
Shale	22	40	70	19	34
Igneous Sill			1	1	12
Totals	38	67	110	41	158

The table above shows five types of natural fractures. Fractures within these five categories are also presented with a Gamma Ray log as Figure 1. Fractures were identified as shear fractures only if they had evidence that movement had occurred, such as the presence of slickensides, surface polish, etc. Many fractures identified as extension fractures had plume structures, however some extension fractures were identified on the basis of angular relationships to other extension fractures and steep (vertical) dip angles.

Approximately 4% of the total number of fractures has well-defined characteristics of both extension fractures and shears. The implication here is that the fractures initially formed as extension fractures and later were associated with offset movement. It is possible that other steeply dipping fractures possess characteristics of both extension and sheer fractures, but that these features were not obvious in the cored sample.

Eight intervals of highly broken core were identified as possible fault zones. These intervals possessed a large number of shear fractures. Possible fault zones are indicated on Figure 1and are listed below.

Possible fault zones: Intervals characterized by highly broken core and numerous shear fractures:

1094-1099.5
1238.8 - 1239.1
1243 - 1244.5
1247.2-1249.8
1261.8-1262.4
1282-1283.4
1309-1309.9
1377.6 - 1378.5

Shears Sorted by Dip Angle and Rake

Shear Angle	Percentage of total (100) fracs.	Rake Range	Apx. Avg. Rake	Comments Regarding Rake
Shears < 35° dip	16%	5-90	24°	63% of the shears ≤35°-exhibit rake.
Shears 40°-65° dips	26%	5-80*	22°	70% of the shears with dips of 40° - 65° exhibit rake
Shears 70° - 90° dips	10%	5-70*	24°	59% of the fractures with dips of 70° - 90° exhibit rake.

The majority of the shear fractures exhibit oblique slip as evidenced by various amounts degrees of rake.

*One fracture in this dip category has two sets of slickensides, which implies that these fractures may be recording two episodes of shearing.

* One fracture in this dip category has two sets of slickensides, which implies that these fractures may be recording two episodes of shearing.

Relative Movement on Shears

When it was possible the relative movement on shears was observed. The table below presents the depths, host lithologies, and characteristics for 21 shears.

Depth	Lithology	Dip	Rake	Relative Movement
1237.2	Shale	45		Lateral
1379	Shale	90		Lateral
1156.6	Shale	50		Normal
1244.5	Sandstone	60	40	Normal
1262.4	Siltstone	55	20	Normal
1267.3	Shale	90		Normal
1345.5	Shale	90		Normal
1356.5	Siltstone	60		Normal
1093.6	Shale	15	25/5	Reverse
1190.9	Shale	90	20	Reverse
1242.1	Siltstone	60	60	Reverse
1246.3	Siltstone	70	40	Reverse
1268.3	Siltstone	65	45	Reverse
1280.1	Shale	70	45	Reverse
1306.5	Shale	20	20	Reverse
1307.6	Shale	45		Reverse
1307.9	Shale	45		Reverse
1308.2	Siltstone	30		Reverse
1313.8	Shale	15		Reverse
1339.6	Sandstone	80		Reverse
1194.4	Siltstone	45	10	Vertical

Fracture Fillings

Information regarding fracture fillings includes: 1. Percentage of filling material in individual fractures; 2. Mineralogy of the filling material; and 3. Fracture-aperture measurements. Percentages of filling materials were estimated by examining the facture faces. Many fractures appeared to be 100% filled with cementing material. However commonly such fractures exhibit well develop druze. The presence of druze implies that these fractures are partially open. The best druze development is associated with those fractures having the largest fracture apertures.

The table below summarizes fracture-filling data. These data should be used as estimates, not exact measurements.

% Fracture Filled	**No. Extension Fractures**	**No. Shears < 35°**	**No. Shears 40°-65°**	**No. Shears 70° - 90°**
< 10%	41	23	36	12
10% - 25%	11	15	16	5
26% - 49%	10	13	20	8
50% - 74%	11	8	15	7
75% - 100%	85	8	23	9
Total	158	67	110	41

On visual inspection at 10X, most of the extension fractures appeared to be over 75% filled with cement. Extension fractures exhibiting lower percentages of cementation were those extension fractures that were found open in the core boxes. Probably some of the cementing materials were destroyed in the coring process. For shear fractures, the degree of cementation is more variable than for extension fractures. Again, the estimates presented here should be considered to be imprecise variables.

Numbers of Fractures filled with Various Cements		
Cement Type	**Extension Fractures**	**Shear Fractures**
$CaCO_3$	103	80
Clay	9	36
Clay and $CaCO_3$	7	32
$CaCO_3$ and pyrite	10	4
*$CaCO_{3,}$ - Dead oil stain.		2

The dominant fracture cement was calcite. Commonly extension fractures cemented with only calcite were relatively easy to break apart. Also, these fractures commonly exhibited druze. The finer the fracture aperture, the finer the druze crystals. Those fractures cemented with pyrite were difficult to break apart. Such fractures exhibited poor druze development.

Fracture Apertures

Fracture apertures range from 0.1 – 1.0 mm., with the average aperture equal to 0.3 mm. The following table lists fracture aperture measurements of healed fractures. In the case of open fractures with well-developed druze, the aperture measurement represents the thickness of the druze. (Over 95% of the measurements are of healed fractures.)

Depth	**Type of Fracture**	**Aperture mm**	**Druze**
1128.8	Extension	1	Good
1131.9	Extension	0.3	Apparent
1132.3	70 deg. shear	0.7	Common
1132.3	70 deg. shear	0.7	Common
1135.3	Extension	0.3	

1137	Extension	0.3	
1137.5	Extension	.1-.2 avg, up to 1.0	Apparent
1137.5	Extension	.1-.2 avg, up to 1.0	Apparent
1175.9	Extension	0.1-0.2	
1176.3	Extension	0.1-0.3	
1176.6	Extension	0.3-0.6	
1177.1	Extension	0.4	
1177.3	Extension	0.1-0.3	Excellent
1177.4	Extension	0.1-0.5	Excellent
1181	Extension	0.2	
1188.3	Extension	0.1	
1189.5	Extension	0.2	
1203.8	Extension	0.1	Apparent
1204.2	Extension	0.1-0.4	
1204.5	Extension	0.1-0.4	
1205.3	Extension	0.1-0.4	
1206.3	Extension	0.1	
1206.8	Extension	0.1	
1207.3	Extension	0.1-0.4	
1208.5	Extension	0.2-0.3	
1208.6	Extension	0.2-0.3	Good
1210	Extension	0.1-0.4	Good
1210.5	Extension	0.5-1.0	Excellent
1212.5	Extension	1.0	Apparent
1213.9	Extension	0.1-0.2	
1215.9	Extension	0.7-1.0	Good
1216.3	Extension	0.1-1.0	Apparent
1216.4	Extension	0.2	Apparent
1217.5	Extension	0.1	
1221.7	Extension	0.1	
1223.4	Extension	0.1	Apparent
1223.4	Extension	0.1	Apparent
1223.4	Extension	0.5-1.0	Apparent
1246.8	Extension	0.1	
1260.6	Extension	0.1	
1266.5	Extension	0.1	
1271.3	Extension/Shear	0.3	Apparent
1287.1	Extension	0.1	
1290.6	Extension	0.2	
1312.6	Extension	0.2	
1315.9	Extension	0.1	
1324.4	Extension	0.1	
1333.3	Extension	0.2-0.3	Apparent
1334.8	Extension	0.1	
1339.6	Extension/Shear	1.0	

1342.7	Extension	0.1-0.2	Very fine
1344	Extension	0.3-0.5	
1344.1	Extension	0.1-0.3	
1345.5	Extension	0.1-1.0	

Fracture Spacing

Fracture spacing was determined for both extension and shear fractures. Two tables are presented below: one pertaining to extension fractures, and one pertaining to shears. Due to the highly fractured nature of this core, for many fractures a "true" spacing (spacing perpendicular to the fracture surfaces) is measured. In cases where the vertical spacing of fractures would not permit such a measurement, the apparent spacing (vertical depth from one fracture midpoint to another) was measured. The true fracture spacing = sin (dip ∠) x (observed fracture spacing). True spacing measurements are presented in red, whereas observed fracture spacing measurements are presented in black. Considering the level of accuracy of this study, the difference between "true" and "observed" spacing is inconsequential

Depth	**Fracture Spacing**
1137.5	.03-.6
1137.5	.03-.6
1162.7	0.15
1175.9	0.15
1176.6	0.1
1188.3	1.2
1204.2	0.05
1205.3	0.8
1206.3	1.0
1208.5	0.07
1208.5	0.07
1208.6	0.07
1210	.05-.0.1
1211.1	.06-1.5
1213.9	1.4
1215.9	.07-.13
1216.3	0.08
1217.5	0.3
1223.4	0.03
1223.4	0.05
1242.1	0.1
1246.1	1.6
1298	0.02 - 0.1
1303	0.05
1312.6	0.04
1312.7	0.03

1344	0.12
1344.1	0.15
1345.5	0.02-0.1
1375.3	0.1
1412.5	0.03
1413.1	0.3
1413.7	0.2
1414.5	0.13
1414.7	0.05
1422.2	0.1
1423.4	0.03
1424.3	0.15
1425.4	0.87
1425.6	0.05
1425.8	0.03

.

Shear Fracture Spacing		
Depth (ft)	Fracture spacing (ft)	Fracture Dip Angle
1123.6	0.4	60
1164.2	0.2	45
1166.1	0.2	90
1167.7	0.3	50
1168.3	0.8	50
1223.7	0.5	60
1223.8	0.2	60
1237.2	0.1	45
1239.6	0.2	45
1239.7	0.2	45
1240	0.03	45
1255.2	0.2	25
1276.8	0.65	60
1281.3	0.05	65
1289.6	0.15	55
1315.6	0.15	45
1380.2	0.1	70

Summary of Fracture Strike Relationships

Because this core was not oriented, fracture dips and strikes cannot be directly obtained. However, the following table presents fracture strikes relationships that may be helpful in relating core to outcrop data.

Intersection Angle	**Number of Fractures with Various Intersection Relationships**					
	EX/EX	EX/Thrust	EX/>35°Shear	>35° Shear / >35° Shear	>35° Shear / Thrust	Thrust/ Thrust
Parallel Strike	45	7	23	25	12	
Parallel Strike Opposite dips				9	1	6
10° - 30°	7			3	2	1
31° - 60°	7	3	12	14	4	1
61° - 89°	3		2	1		
Normal (90°)	8	6	12	7	3	3

EX/EX – Intersection of two extension fractures
EX/Thrust – Intersection of an extension fracture and a low angle shear (< 35°)
EX/>35° Shear – Intersection of an Extension fracture and a higher angle (> 35°) shear
>35° Shear/>35° Shear –Intersection for two higher angle shears
>35° Shear /Thrust – Intersection of a higher angle shear (> 35°) and a low angle shear (< 35°)

Fracture Length

Fracture length data for extension fractures and shears are presented below. Data for complete fractures (those fractures that possessed two terminations within the core) are presented separately from those of other fractures. For fractures that had one or no terminations within the core, a minimum fracture length is given.

Fracture Lengths for Extension and Sheer Fractures						
	No. Fracs	**Extension Fracture Lengths**		**No. Fracs**	**Shear Fracture Lengths**	
		Length Range (ft)	**Average Length (ft)**		**Length Range (ft)**	**Average Length (ft)**
Complete fracture in core	20	0.15 – 0.8	0.4	2	0.3-0.3	0.3
Minimum Fracture Length	122	0.05 – 2.8	0.5	179	0.02 – 0.8	0.16

Brief Discussion of Extension Fractures vs. Shears

In this and previous reports, fractures have in classified as either extension fractures or as shears. In most cases vertical, or near vertical, fractures are interpreted as extensional fractures. The VPRCH 32 core exhibited a relatively large number (41) of steeply dipping shears. In some cases, high angle shears parallel extension fractures. This angular relationship might support the reactivation of extension fractures.

Figure 1: Gamma Ray / Fracture Display

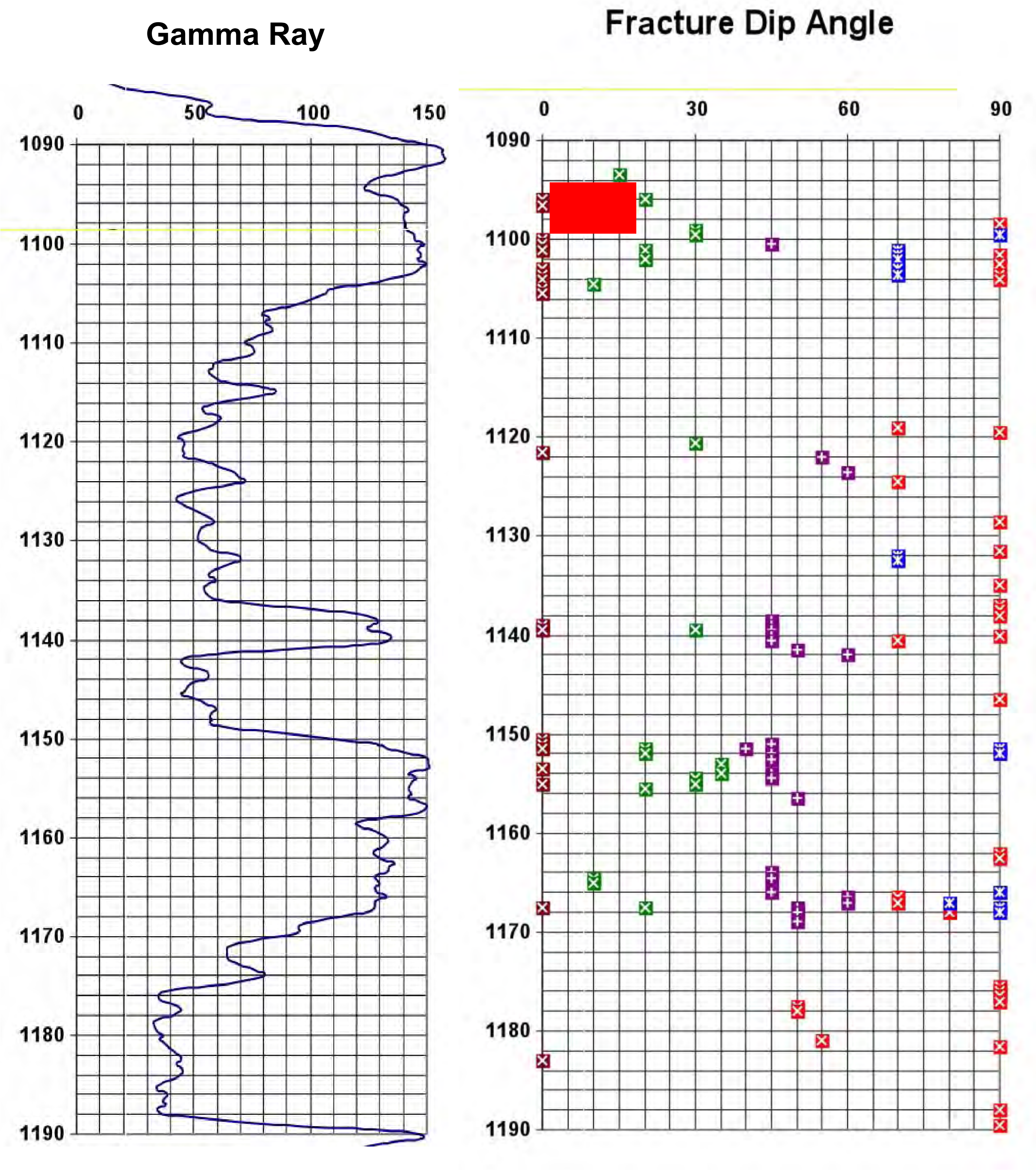

[redacted]

Gamma Ray

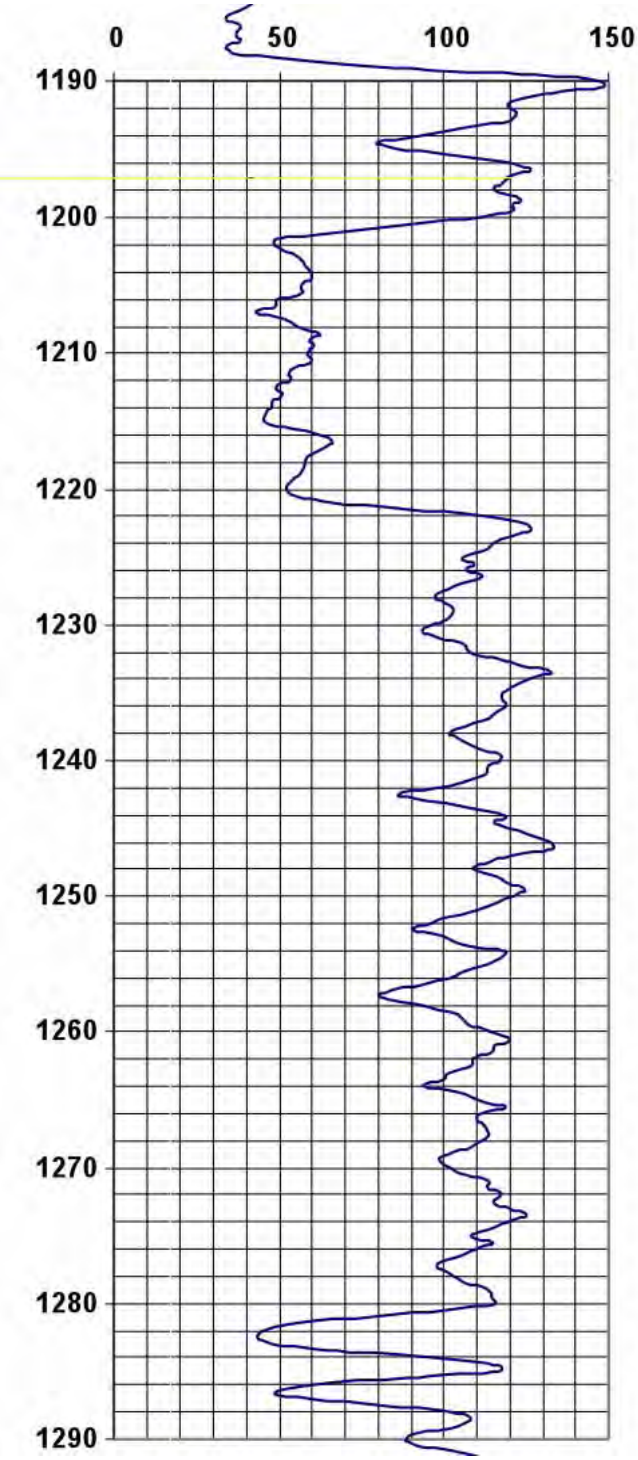

Fracture Dip

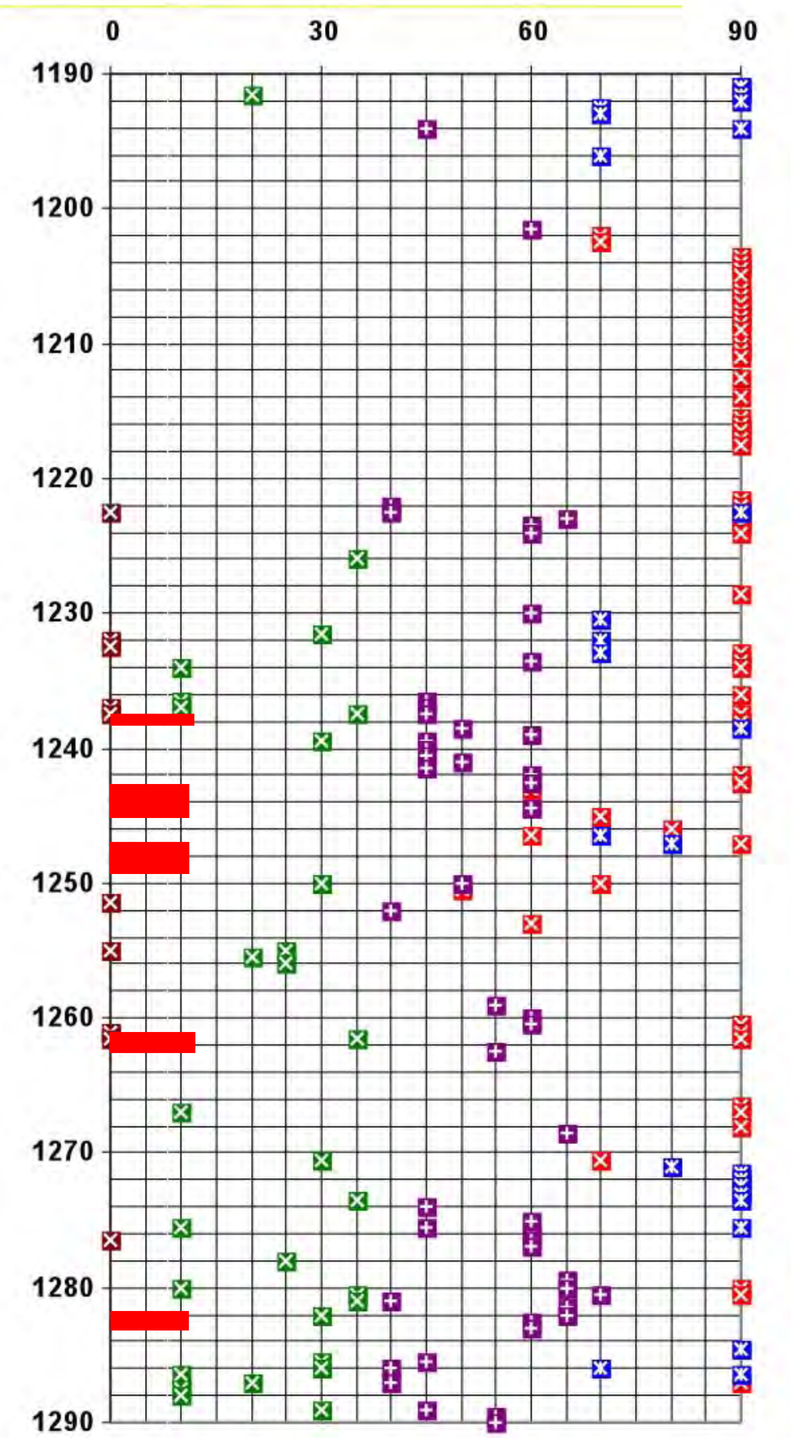

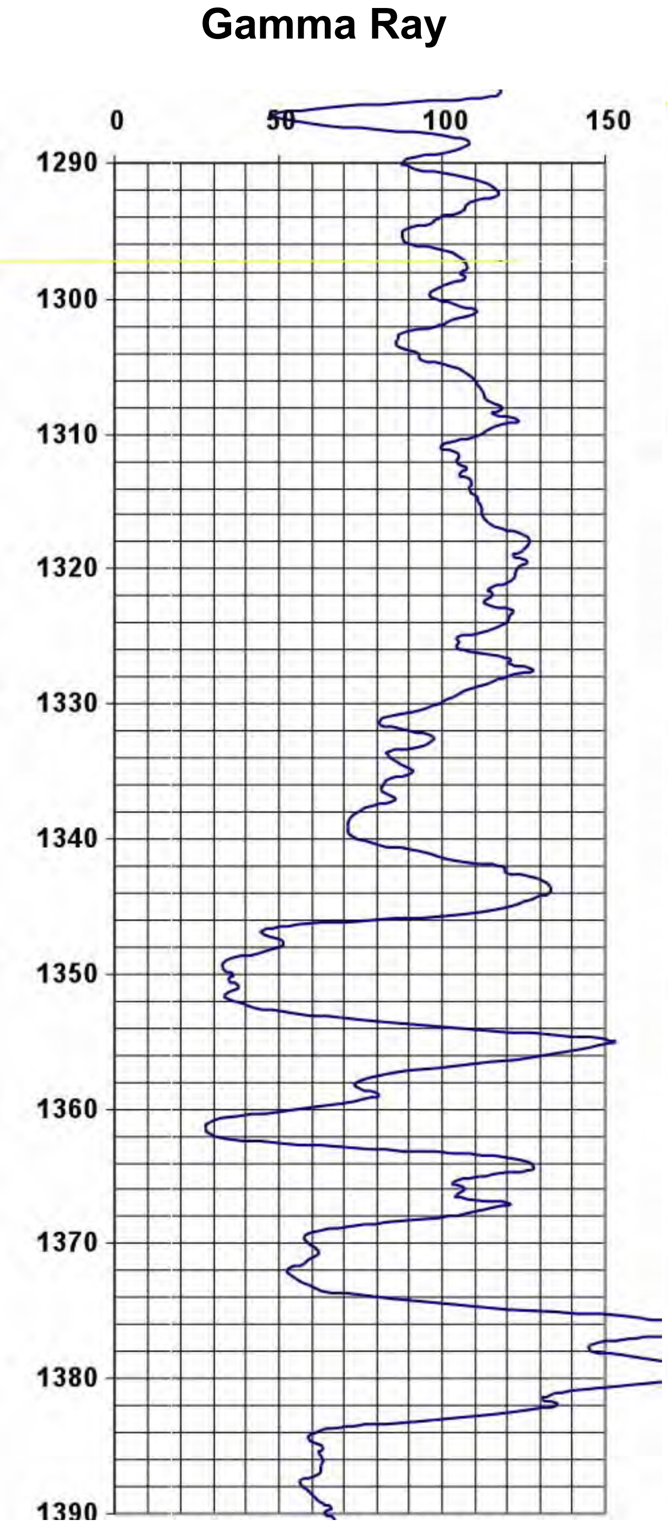
Gamma Ray
0
50
100
150
1290
1300
1310
1320
1330
1340
1350
1360
1370
1380
1390

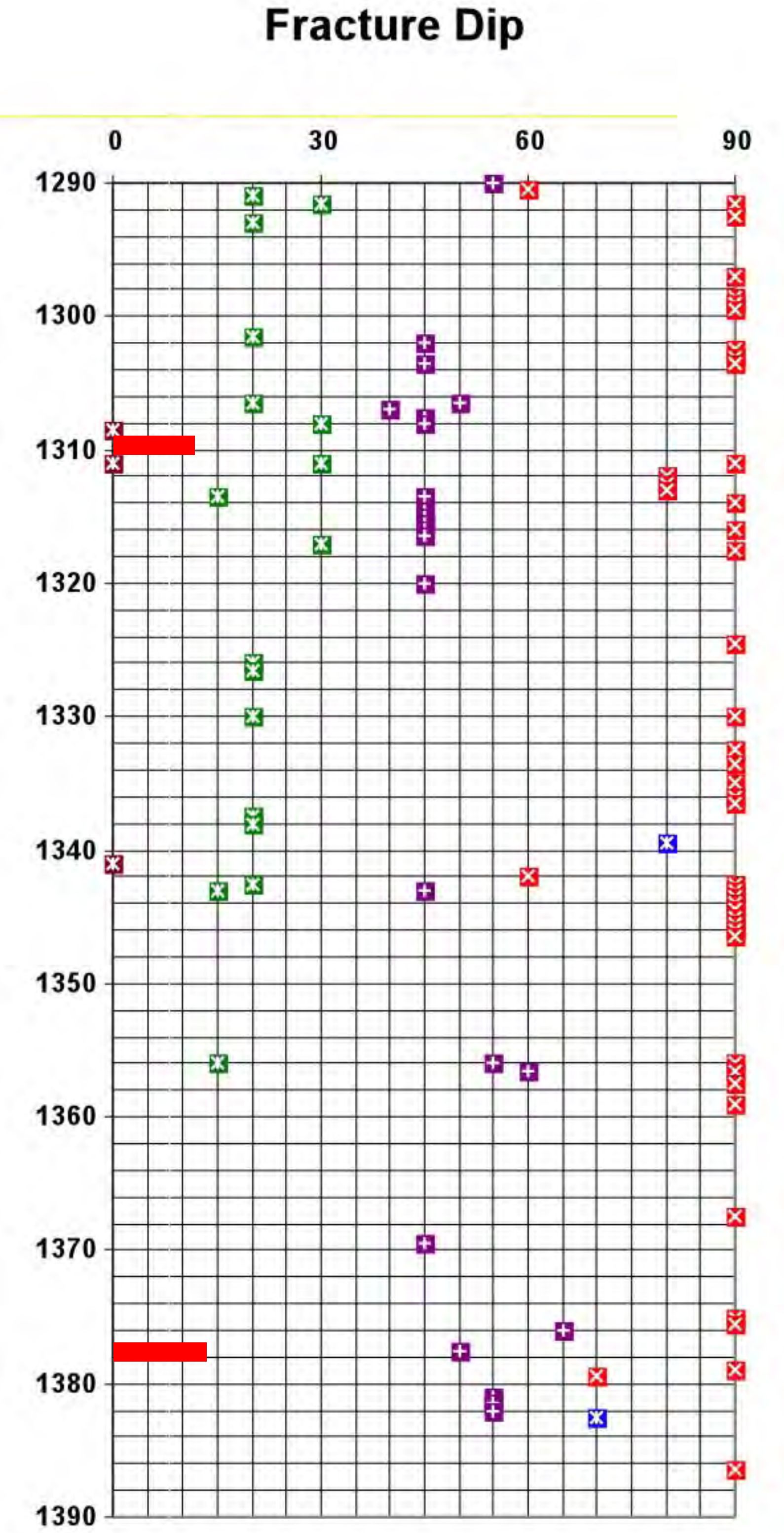
Fracture Dip
0
30
60
90
1290
1300
1310
1320
1330
1340
1350
1360
1370
1380
1390

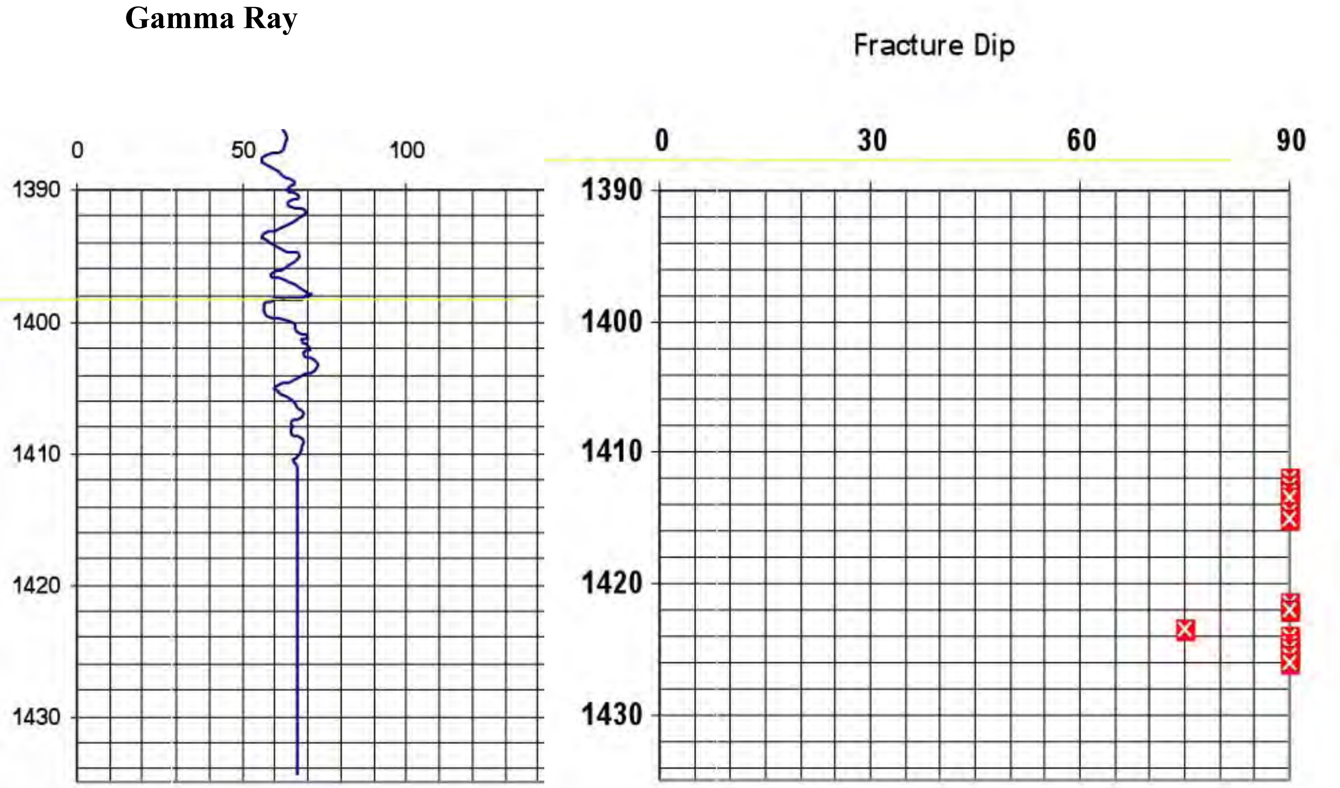

KEY

🟥 Extension Fracture

Shears

🟩 <35° Dip

🟪 40°- 65° Dip

🟦 70° - 90° Dip

🟫 Horizontal Slip

🟥 Possible Fault Zone

Core Photographs

Examples of Shears

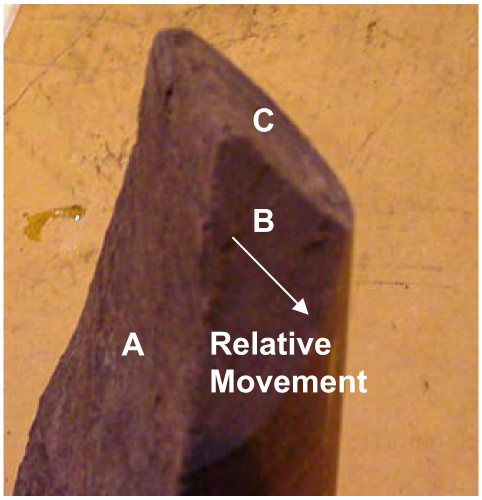

Fracture A

Three Intersecting Shears:

Depth: 1203.8’
Host Rock: Shale
Fractures A and C are parallel; Fracture B is normal to Fractures A and C. Fracture B exhibits oblique normal slip. Fracture A is a near vertical fracture exhibiting oblique slip.

Two Intersecting Parallel Shears

Depth: 1138.9’

Host Rock: Shale

Two parallel shears each dip at a 45° angle.

Parallel Shears

Depth: 1167.4’

Host Rock: Shale

Three shears have parallel strikes shown with the vertical colored pencils. Fractures A and C dip in the same direction. The fracture spacing is 0.3 ft. The Yellow pencil in aligned with bedding-plane slip striations. Bedding plane slip is normal to the strike of the shears.

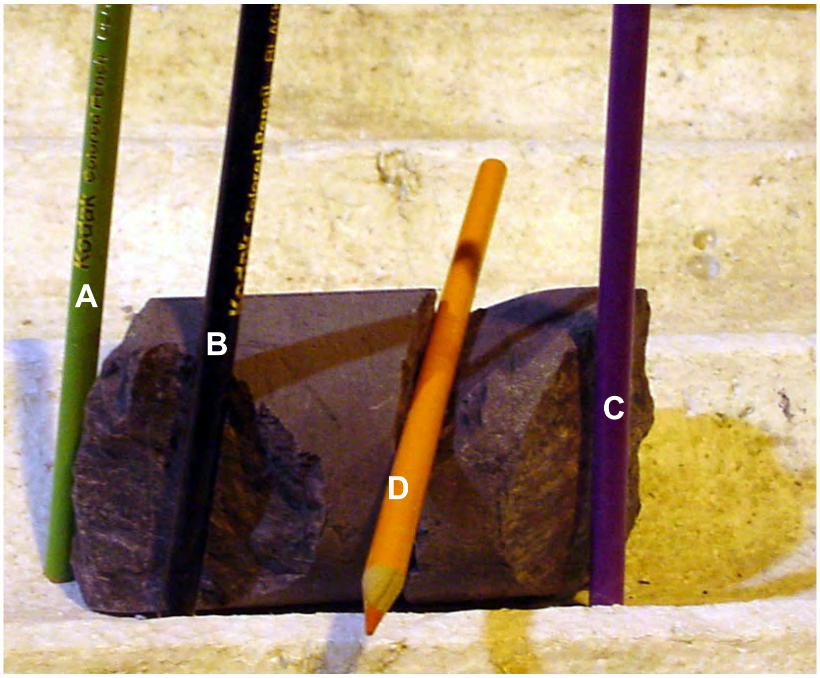

Two Shears Intersecting at a 45° Angle.

Depth: 1167.8’

Host Rock: Shale

Pencils are aligned parallel to the strike of each fracture.

Low Angle Shear With Lateral Slip

Depth: 1191.6’

Host Rock: Shale
Dip angle = 30°

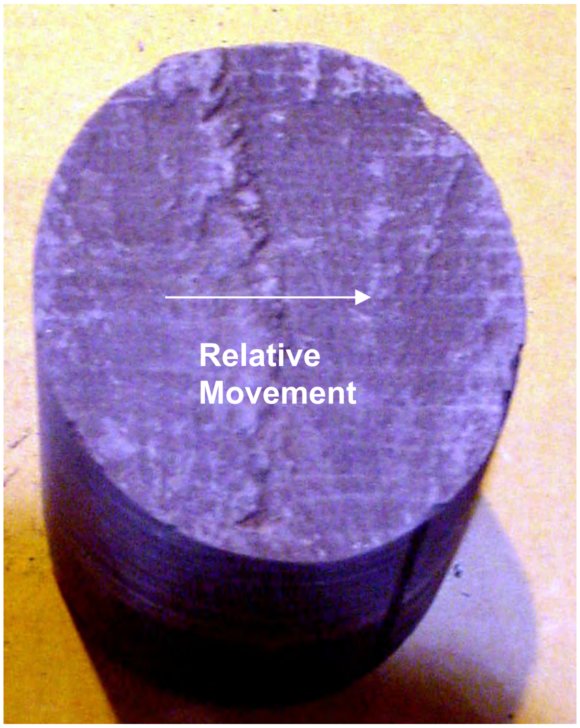

Vertical Fracture and Shear

Depth: 1194’

Host Rock: Siltstone

Fracture A
- Dip Angle = 90°
- Rake = 45°

Fracture B:
- Dip Angle = 45°
- Rake = 10°

Strike Intersection of Fractures A and B = 60°

The surface of Fracture A has a plume structure. Fracture B shows slickenlines.

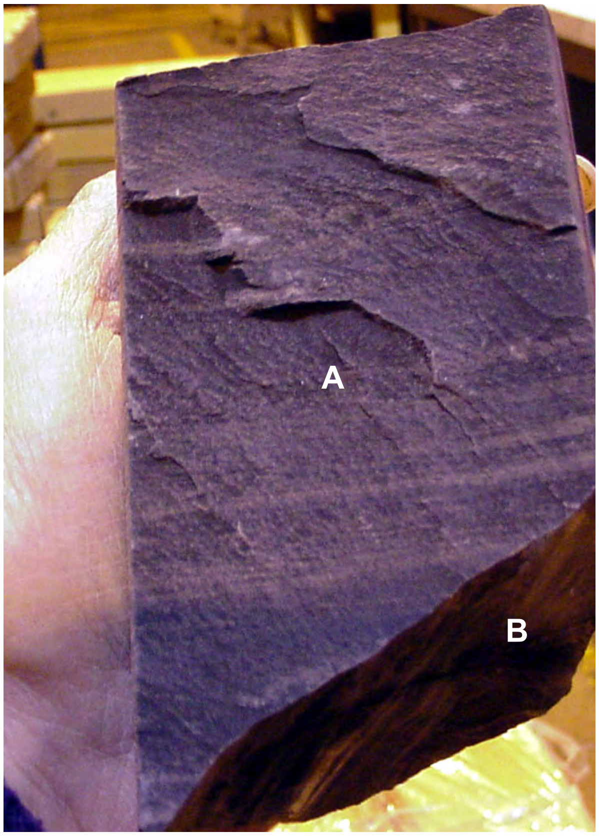

Vertical Fracture Exhibiting Lateral Slip

Depth: 1379’

Host Rock: Shale

Dip Angle = 90°
Rake = 90°

Vertical Fracture and Low-Angle Shear

Depth: 1267’

Host Rock: Siltstone

Fracture A:

Dip Angle: 90°

Fracture B:

Dip Angle: 10°

Strike Intersection of Fractures: 90°

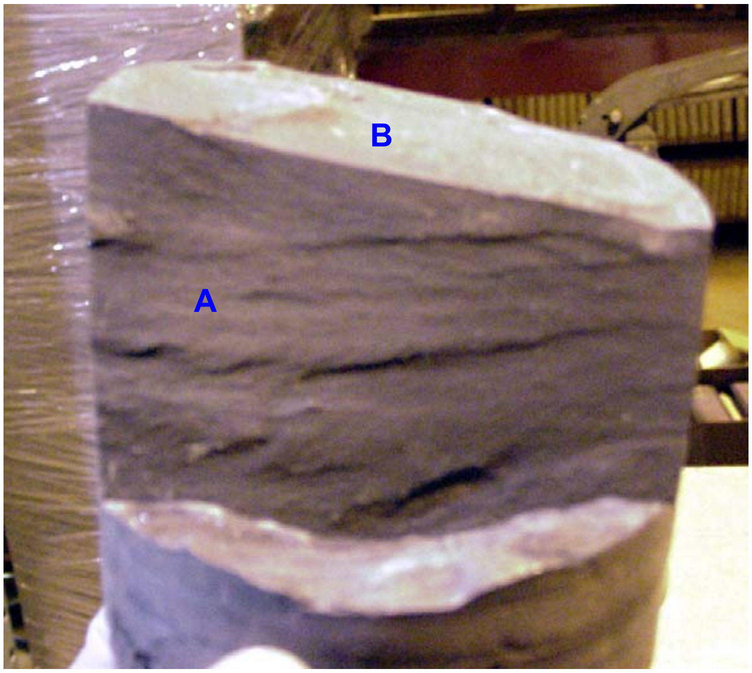

Reverse Fault

Depth: 1168.3

Host Rock: Siltstone

Dip Angle: 50°
Rake: 45°

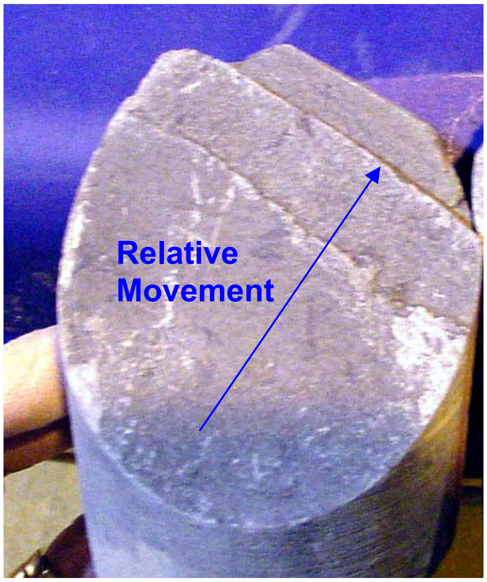

Three examples of Horizontal Bedding-plane Slip

Figure A
Host Rock: Sandstone (The previous two cores did not have well-defined horizontal slip in sandstones.)

Figure B
Host Rock: Siltstone
A Calcite filled horizontal fracture shows slip normal to underlying bedding-slip striations.

Figure C
Host Rock: Sandstone
Calcite Filled Horizontal Fracture

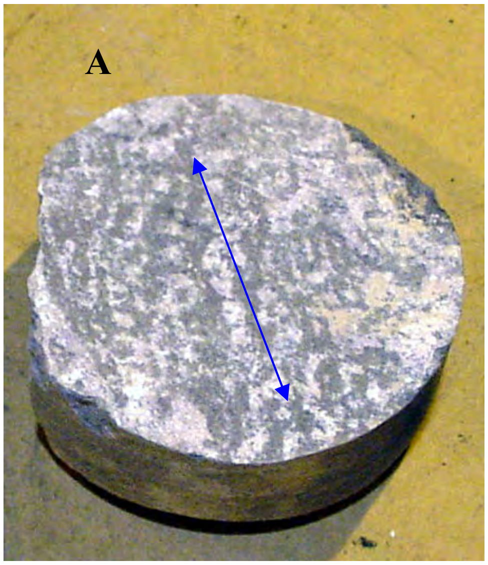

Depth: 1105.5

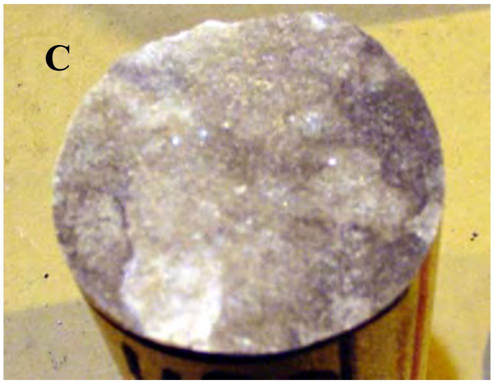

Depth: 1183’

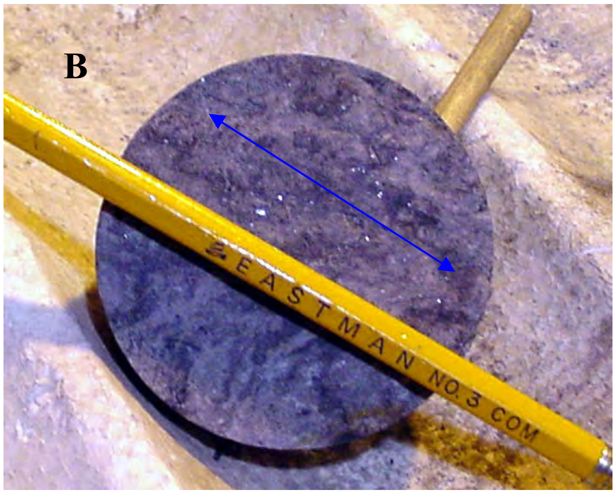

Depth: 1121.8

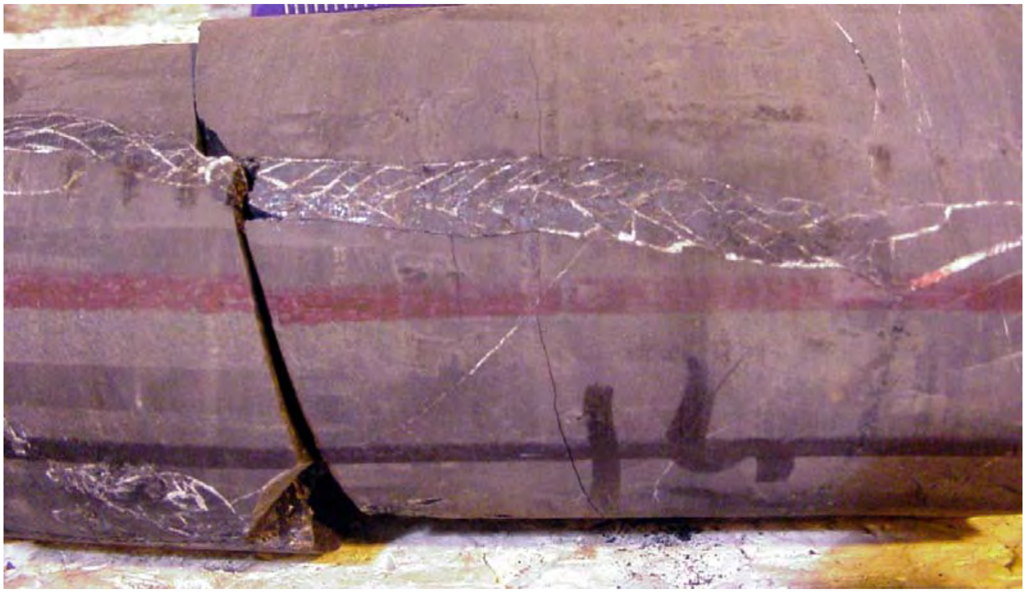

Depth: 1345

Coal Dike
Depth: 1345 – 1346
Host Rock: Shale
This small dike extends over 2.4 feet of core. A coal bed is present at 1345 feet.

Depth: 1346

Examples of Extension Fractures and Extension/Shear Relationships

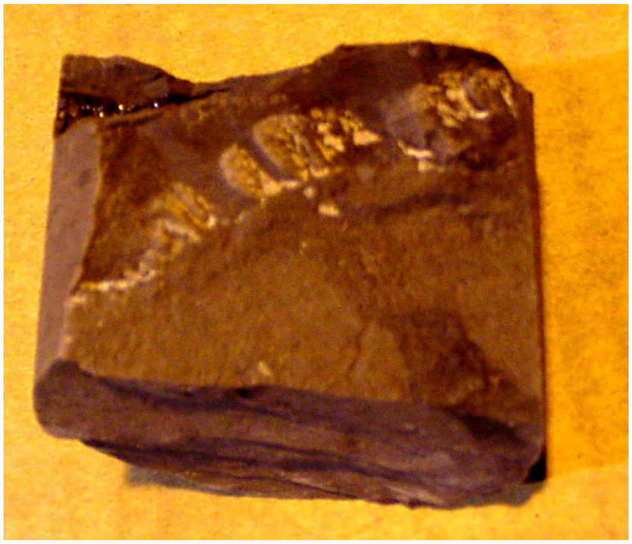

Termination of an extension Fracture
Depth: 1261.1 ‘
Host Rock: siltstone

Perpendicular Extension Fractures
Depth: 1192’
Host Rock: Shale

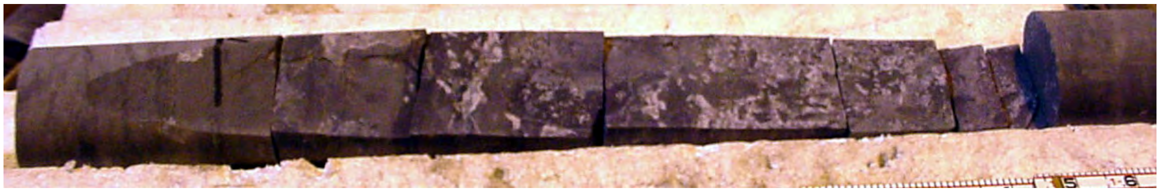

Extension Fracture
Depth: 1296’
Host Rock: Siltstone

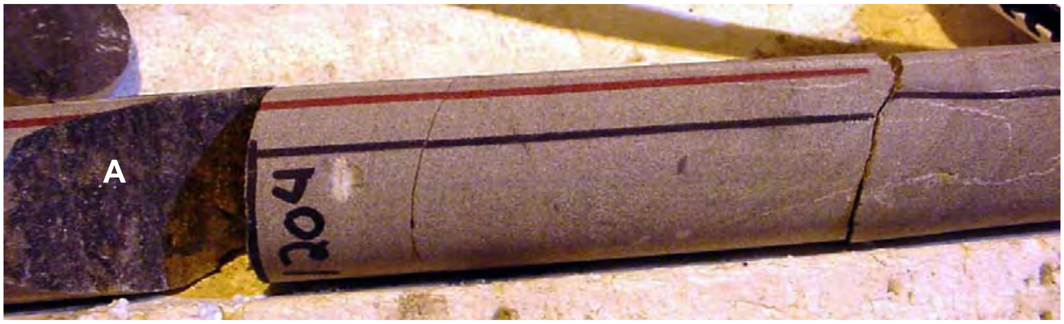

Parallel Extension Fractures
Depth: 1204’
Host Rock: Sandstone
Fracture A may have dead oil stain on the surface. The fracture spacing is 0.05.

Two Intersecting Extension Fractures

Depth: 1208.5’
Host Rock: Sandstone

Dip angles: 90°

Strike Intersection Angle: 45°
Discoloration may be due to iron staining.

Intersecting Extension/ Shear Fractures

Depth: 1284’

Host Rock: Igneous Sill

Both fractures are vertical. Fracture A appears to be extensional, whereas Fracture B appears to have slickenlines. The strike intersection angle is 60°.

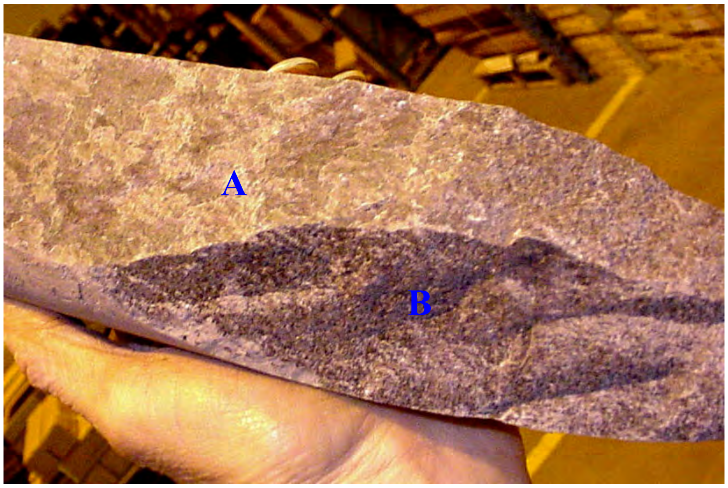

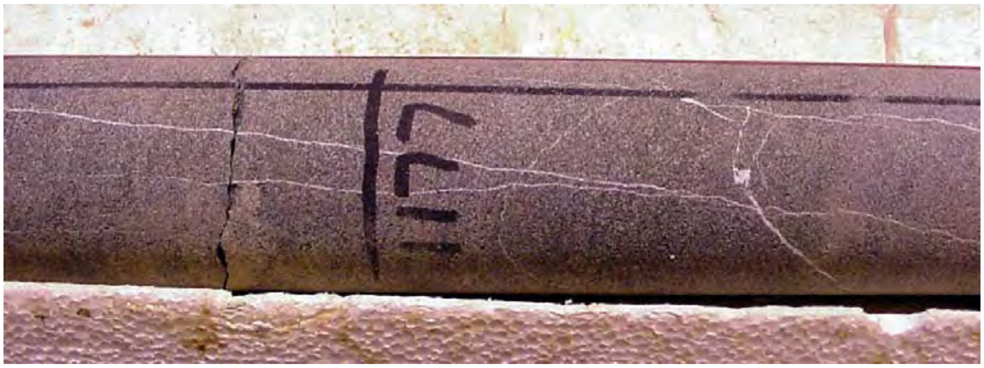

Multiple Extension Fractures

Depth: 1177’

Host Rock: Igneous Sill

Parallel Extension Fracture and Shear

Depth: 1246’

Fracture A:
- Host rock: Sandstone
- Dip Angle = 80°
- The fracture terminates at the bed boundary.

Fracture B:
- Host Rock: Siltstone
- Dip Angle = 40°
- Shear shows reverse relative movement.

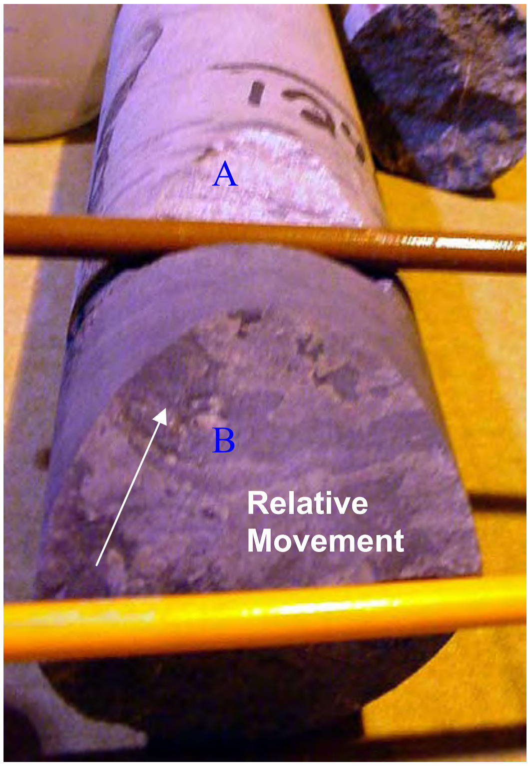

Possible Dead Oil Stain on Fracture

Depth: 1132’

Host Rock: Sandstone

Dip angle = 70°

Fracture was well cemented and difficult to break apart.

Multiple Extension Fractures

Depth: 1425’

Host Rock: Sandstone.
Large druze crystals are present on some of the fracture faces.

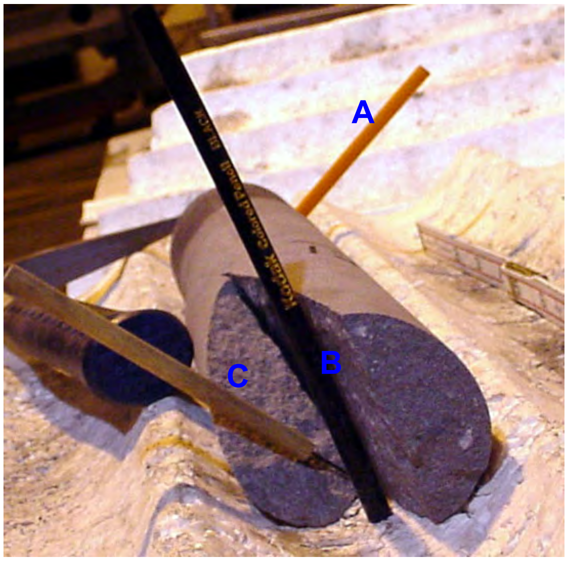

Three Intersecting Extension Fractures

Depth: 1201.4 – 1202.4

Fracture dip angles = 60 -70°
Host Rock: Sandstone

Fractures A and C strike normal to one another. The C-B strike intersection angle is 30°. The A-B strike intersection angle is 60°.

Calcite and Pyrite Fracture Filling

Depth: 1223.4
Host rock: Shale
The most common fracture filling is calcite. When pyrite is present, the fractures are more completely cemented and are difficult to break apart.

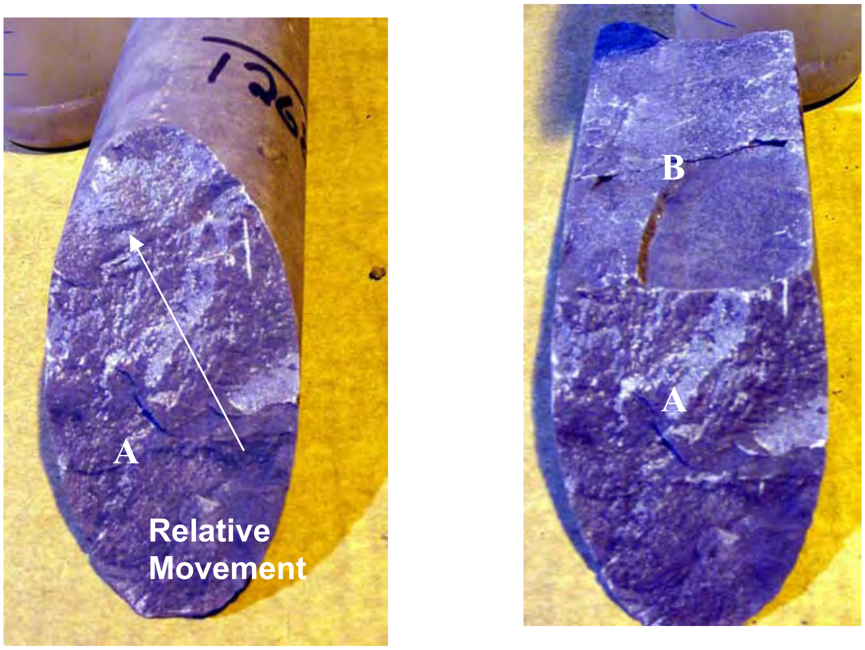

Intersecting Shear and Extension Fractures

Depth: 1268’
Fracture A is a reverse shear with a 65°- dip angle. Fracture B is a vertical extension fracture that terminates at Fracture A. The two fractures strike normal to one another

Extension Fracture and Shears

Depth: 1230’

Fracture A:	Shear Dip angle: 60° Rake: 20°
Fracture B:	Extension Dip angle: 70°
Fracture C:	Shear Dip angle: 70° Rake: 10°

Fractures A and B are parallel. The strike of Fracture C is 45° relative to Fractures A and B.

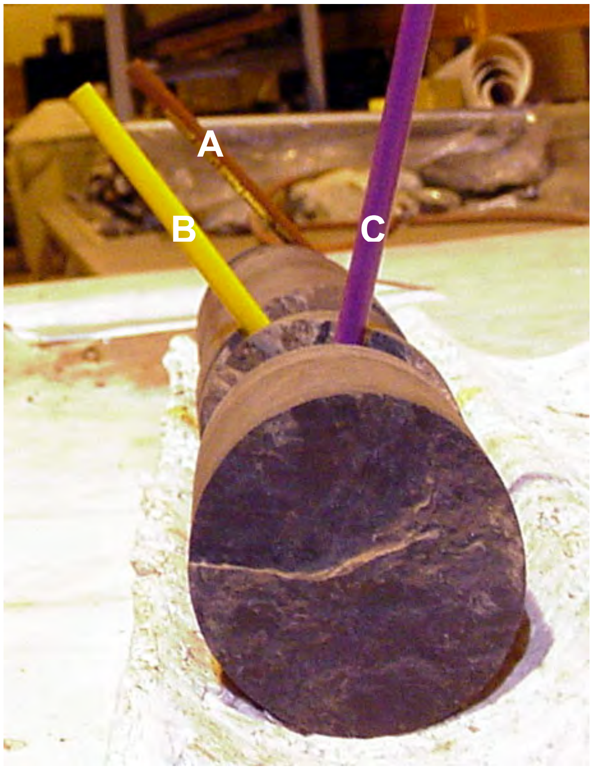

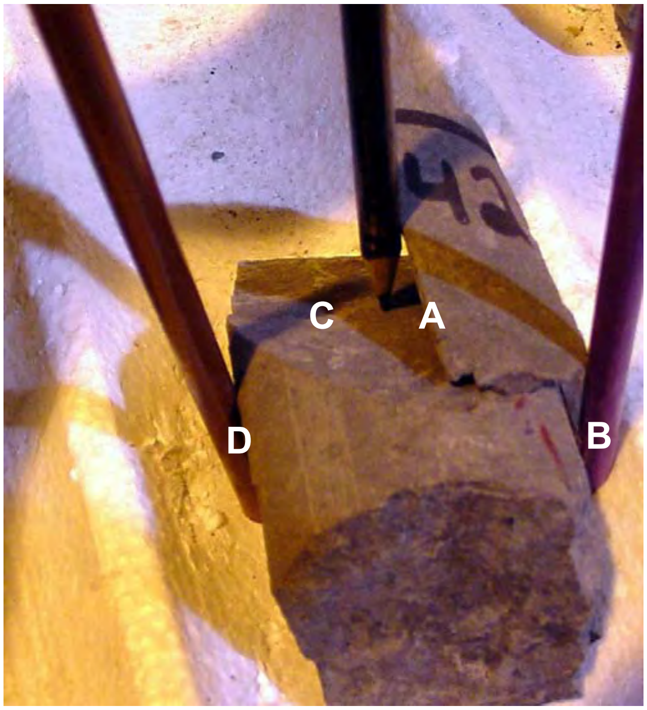

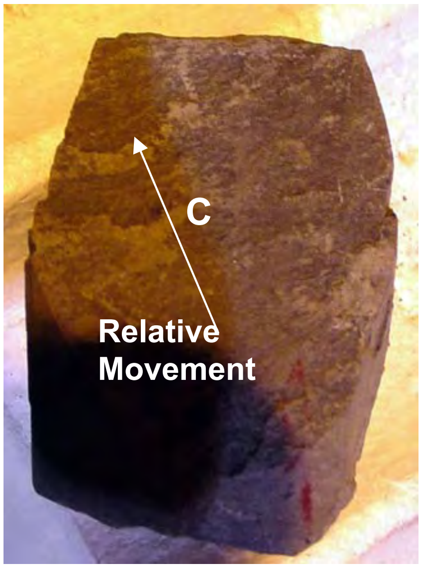

One foot of Fractured Core

Depth: 1242' – 1243'

Host Rock: Shale

Fractures A, B, and D are Parallel vertical Extension Fractures. Fracture A terminates at Reverse Shear C. Fractures B and D do not. The strike intersection between A and C is 70° Fractures E and F are shears, each dipping at 60°. The strike of Fracture E is parallel to Fracture C, but the dip direction is opposite. Fracture F strikes 45° relative to Fracture C. Fractures G are two sub-parallel extension fractures. Fracture H is a 40°- dipping shear. Fractures G and H are parallel. The strikes of G and H are parallel to Fracture F, but the dip directions are opposite.

Figure A: Vertical Extension Fracture with Calcite (and Pyrite) Filling
Depth: 1339’

A well- developed plume structure is present.

Two Vertical Fractures with evidence of Shear Movement – Possible Reactivated Fractures

Figure B: Calcite Filled Vertical Reverse Shear
Depth: 1271.3’The lower portion of the fracture surface has well-developed druze. The upper portion of the fracture shows a smoothed calcite crust.

Figure C: Vertical Fracture
Depth 1286’
Host Rock: Shale
The Calcite filling of this fracture is highly fractured.

Features Associated with Igneous Intrusion

Figure B: "Stylolitic"-like features
Depth: 1222'
Host Rock: Igneous Sill
Fine quartz veinlets are found at the base of an igneous sill.

Figure C: "Chicken-wire" fracturing
Depth: 1219'
Host Rock: Igneous Sill
A fine network of quartz veinlets are found in an igneous sill.

Fractured Coal Inclusion in Igneous Sill

Depth: 1374'

This small coal inclusion is highly fractured relative to the surrounding igneous rock.

Columnar Jointing

Depth 1352.8'

Host Rock: Altered Coal or High Carbonaceous Shale

Several feet of vertically jointed rock occurs in association with igneous intrusion. Calcite fracture fillings are common.

Interpreted Fault Zones

Possible fault zones (shown on Figure 1) were interpreted where intervals of core were highly broken and also possessed numerous shears. In some cases, “shattered” core, as shown here, is associated with these intervals

Depth: 1239

Depth: 1378’

El Paso Well No: VPRCH 34

Summary of Fracture Characteristics Described in Core

Submitted to Sandia National laboratory
Raton Basin Project
By Constance N. Knight

Introduction

Well No. 34 VPRCH was cored continuously from near surface to a total depth of approximately 2050 feet. The objective of this evaluation is to describe attributes of naturally occurring fractures below the Raton Conglomerate to total depth. The entire core below a depth of 1740 feet was carefully examined for fracture occurrence. All natural fractures were logged with respect to: depth, host lithology, fracture dip, surface characteristics, and angular relationships with one another. Induced fractures were also noted, and wherever possible the orientations of natural fractures were described with respect to induced fractures. The strike of induced fractures parallels the direction of the maximum horizontal *in-situ* stress (sHmax). Since sHmax has been determined at a regional scale through other investigations, relating natural fractures to induced fractures can produce a reasonable estimation of true fracture strike and dip.

Summary of Fracture Characteristics

Total fractures described: 100

All percentages presented below are presented as a fraction of the total 100 fractures unless otherwise noted.

Host Lithology

Host Lithology	Percentage of Fractures
Shale and claystone *	62%
Siltstone	28%
Sandstone	10%

Almost all fine-grained clastics were determined to be shale.

Types of Fractures (Extension vs. Shear)

Type of Fracture	Percentage
Extensional Fractures (No evidence of shear is present. Most fractures have surface plume structures.)	11%
Shears with a vertical component of relative motion	74%
Horizontal shears or bedding plane slip	15%

Number of Fractures sorted by Lithology

Lithology	HZ Shears	Shears <35°	Shears 40°-65°	Shears 70°-90°	Extension Fractures
Sandstone		1	2	2	4
Siltstone	1	4	13	5	7
Shale	14	13	24	10	
Total	15	18	39	17	11

Shears Sorted by Dip Angle and Rake

Shear Angle	Percentage of total (100) fracs.	Rake Range	Comments Regarding Rake
Shears ≤ 35° dip	18%	0° - 90°	Less than 30% of thrust shears (≤ 35° dip) exhibit rake.
Shears 40°-65° dips	49%	0° - 70°	Half of the shears with dips of 40° - 65° exhibit rake
Shears 70° - 90° dips	17%	0° - 30°	60% of the fractures with dips of 70° - 90° exhibit rake.

Relationship of Fractures to sHmax as Defined by Petals

Depth	Orientation Relative to Petal	Type of Fracture
1879-1880	Normal	Shear/Thrust
1896-1897	Normal	Shear (10° dip)
“	Oblique (70 deg)	Shear (70 deg dip)*
1944-1945	Normal	Shear (55 deg dip)

* Slickenlines are normal to petal

Relationship of Coal Cleats to sHmax	
Depth	Orientation with respect to sHmax
1746-1748	20 deg (sub parallel)
1864-1865	Parallel
1935-1936	Parallel to 10deg (sub parallel)
1938-1939	Parallel
1954-1955	Parallel

Fracture Filling

The following table presents numbers of fractures with respect to the percentage of fracture filling and fracture type. Percentages of filling materials were estimated by examining the facture faces. (Almost all of the described fractures were found open in the core. Only a couple of fractures were healed.)

% Fracture Filled	**No. Extension Fractures**	**No. Shears < 35°**	**No. Shears 40°-65°**	**No. Shears 70° - 90°**
< 10%	5	11	22	10
20% - 25%	4	3	4	6
25% - 49%		1	5	
50% - 74%		3	6	
75% - 100%	2	0	2	1
Total	11	18	39	17

The following table presents the type of fracture cements described. The most abundant fracture filling is clay.

Numbers of Fractures filled with Various Cements		
Cement Type	**Extension Fractures**	**Shear Fractures**
Clay	3	25
CaCO$_3$	1	8
Clay and CaCO$_3$	1	2
Quartz		1
Clay and trace Quartz	3	3
Dolomite ?		1
*CaCO$_3$, - Dead oil stn.		1

*At 1929 ft , a highly mineralized fracture contained possible deal oil residue on the fracture surface. The aperture of this fracture was estimated to be 1 – 2 mm.

Fracture Spacing

Fracture spacing determinations were made at four depths.

Depth	Fracture Type	Dip Angle	*Observed Fracture Spacing ft.
1769	Shear	50°	0.6
1802	Shear	50°	0.8
1886	Shear	50°	0.3
1949	Extension	80°	0.7

* The true fracture spacing (measured perpendicular to the fracture surfaces) = (sin(dip ∠) x (observed fracture spacing).

Summary of Fracture Relationships

Intersection Angle	**Number of Fractures with Various Intersection Relationships**				
	EX/EX	EX/Thrust	EX/>35°Shear	>35° Shear/>35° Shear	>35° Shear /Thrust
Parallel Strike	4			3	
Parallel Strike Opposite dips	1	1			
10° - 30°				1	1
31° - 60°			1		
61° - 89°				1	
Normal (90°)	1	1	1	3	1

EX/EX – Intersection of two extension fractures
EX/Thrust – Intersection of an extension fracture and a low angle shear (< 35°)
EX/>35° Shear – Intersection of an Extension fracture and a higher angle (> 35°) shear
>35° Shear/>35° Shear –Intersection for two higher angle shears
>35° Shear /Thrust – Intersection of a higher angle shear (> 35°) and a low angle shear (< 35°)

Fracture Length

Fracture length measurements are not reported in this report, because almost all of the fracture terminations were out of the core. Most fracture lengths for all types of fractures ranged from 0.1 to 0.3 feet. More pertinent information will be reported for the other wells.

Examples of Fracture Characteristics and Fracture Relationships

Shears

This information is provided to document shear characteristics and orientation information. Information is organized according to depth.

Parallel Shears that dip in opposite directions

Depth: **1743'**
Fracture description: Fracture dips: 50°
Rake: 0°-10°
Fracture spacing for each set of shears: 0.2 ft.
Fracture strike intersection: 90°
Host Rock: Shale

Bedding Plane Slip

Depth: **1752.2'**, Host Rock: Shale

A three-foot zone of shale from 1751 to 1753 is highly broken. Evidence for fracturing and bedding-plane horizontal slip is ample. Six fractures within two feet of core were described. Also, dislodged pieces of core possessing slickenlines are common. This zone may represent a fault zone intersecting the borehole.

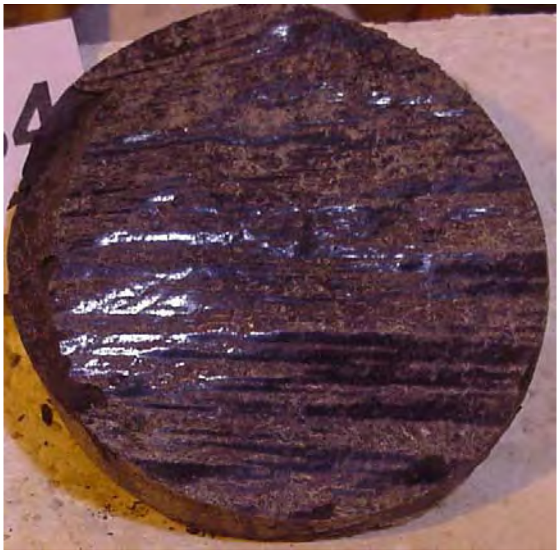

Sheer showing two sets of slickenlines

Depth: **1769.5'**
Fracture description: Fracture dip: 50°
Rake: 40° and 70°
Fracture Spacing: 0.6 ft.
Fracture strike intersection: parallel
Host Rock: shale

Two episodes of movement are implied by two sets of slickenlines. A fracture 0.6 feet deeper in the core has a sub-parallel strike to this fracture. The slickenlines of the lower fracture are perpendicular to those showing 40° rake in the photo.

(The slickenlines on this fracture face intersect at a 30° angle. On page 11 two small thrusts are shown to have strikes that intersect at a 30° angle.

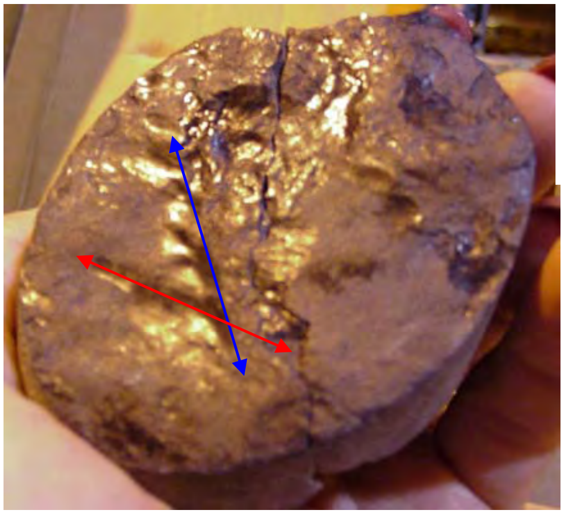

Small Reverse Fault

Depth: **1794.3'**

Host Rock: Siltstone

Dip of Fault = 60°
Rake = 0°

Reverse movement is interpreted from the patchy calcite filling.

Small Thrust Fault

Depth: **1879.3'**

Fault Dip = 20°
Rake = 0°

This thrust is in a shale bed immediately above a thin coal seam. Petals in the coal indicate that the direction of sHmax is normal to fault movement. This is a small-scale compressional feature.

In all of the coal beds that possess petal fractures, the strike of the coal cleating is parallel or nearly parallel to the strike of the petal fractures.

Petal Fractures

Parallel Shears

Depth: **1886' – 1888'** Host Rock: shale

Fracture dips: 50° - 55°

Some of the fractures from this interval have parallel dips and parallel rakes. Other fractures have a strike intersection of 30°. However the rakes of the discordant fractures are perpendicular to one another.

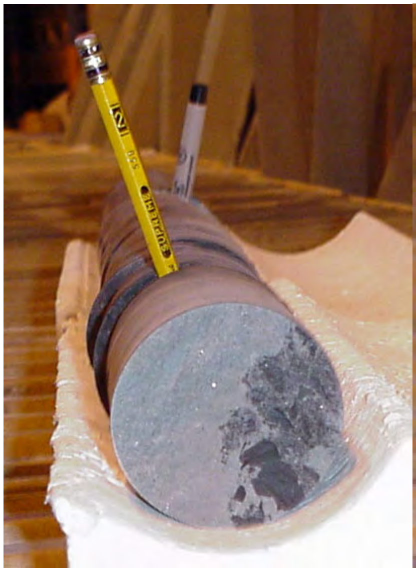

a.) Fracture Dip Directions of two fractures with a strike intersection of 30° are shown with a pen and pencil.

b.) The strike-orientation of Slickenlines on the same shears shown in a.) are now indicated with a pencil and pen. The fractures intersect at a 30° angle, The rakes of the fractures are normal to one another.

Petal Fracture

Depth: **1942'**
Host Rock: siltstone

The pencil on this petal fracture is normal to the petal strike and shows an orientation direction normal to sHmax. The pencil is parallel to a plume propagation direction on the fracture surface. The plume indicates that the fracture (which represents the Smax in the local stress region imposed on the formation by the weight of the bit) opened from right to left.

Shear Fracture with Respect to sHmax

Depth: 1942-1945

Fracture Characteristics:

Host Rock: Siltstone
Fracture Dip: 55°
Fracture Rake: 30°

The pencil shows the direction perpendicular to sHmax defined by the petal shown above. The Pen shows the strike direction of the shear. The strike of the shear is normal to sHmax.

Sear with possible reverse oblique slip

Depth: 1944.6

Photo of fracture surface shown in previous photo.

Host rock: Siltstone
Fracture Dip: 55°
Rake: 30°
Relative strike: Normal to sHmax

Irregular pattern on surface striations imply possible reverse oblique shear movement.

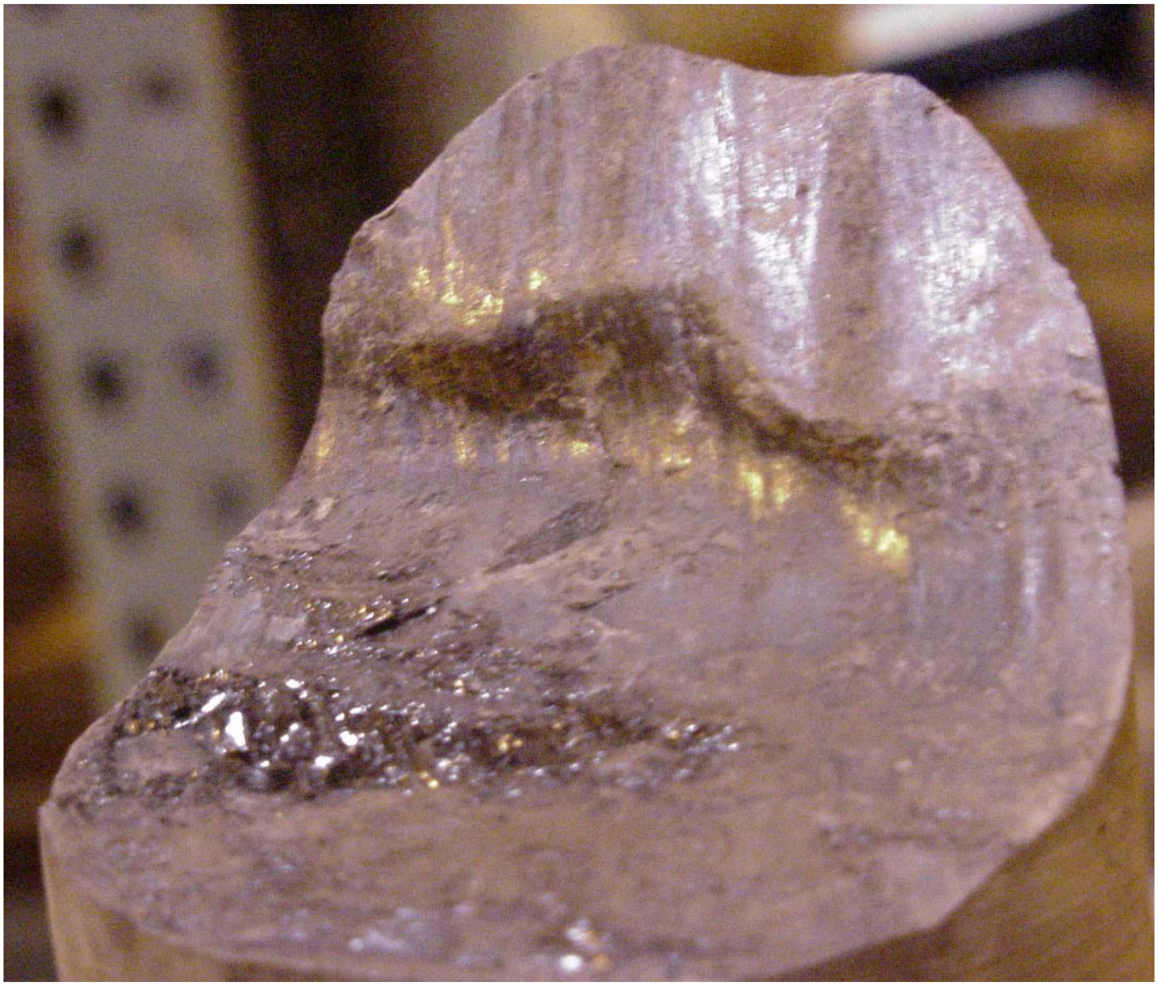

323

Sear with possible normal dip slip

Examples of Extension Fracture Characteristics and Fracture Relationships

This information is provided to document extension fracture characteristics and orientation information. Information is organized according to depth.

Extension Fracture

Depth: **1901.4'**

Fracture dip = 80°

Host Rock: Siltstone

This hairline fracture is associated with a plume (not well reveled in this photo) and patchy mineralization. When estimating the degree of fracture mineral filling, it is important to consider both sides of the core. Patches of "missing" mineral fracture filling on one side of the core are often found on the opposite side of the core.

Extension Fractures with a 90° intersection

Depth: **1949.7'**

Fracture dip = 80°
Fracture spacing = 0.7 ft.

Host Rock: Siltstone

Surface View of one Extension Fracture seen in previous photo

Depth: **1949.7'**

Fracture dip = 80°
Fracture spacing = 0.7 ft.
Lower fracture termination: subtle bed boundrary

Host Rock: Siltstone

Plume structure that propagated from bottom to top is apparent.

Intersecting Extension Fractures

Depth: 1957.6

Host Rock: Siltstone
Dip angles: 90° & 70°
Fracture terminations: in lithology

Dip strikes are parallel, but fractures dip in opposite directions with an intersection angle of

Surface View of one Extension Fracture seen in previous photo

Depth: **1957.6'**

Fracture dip = 70°

Host Rock: Siltstone

A plume structure that propagated horizontally is apparent. This surface shows patchy calcite fracture filling. Also the surface has an uneven oil stain that exhibits no to dull fluorescence.

Relationship of Extensional Fractures to Thrust Shears

Depth: 1987.1'

The upper blue pen shows the strike to two parallel hairline extension fractures:
Host rock: Sandstone
Fracture dip angles: 85°

The middle stick shows the strike of a small thrust that separates the sandstone bed from an underlying shale bed.
Dip Angle = 25°
Rake = 0°
The strike intersection of the extension fractures and this thrust is 30°.

The lower pencil shows the strike of a lower small thrust in a shale bed.
Dip Angle = 30°
Rake = 5°
The strike of the extension fractures is parallel to the strike of this thrust.

The relative strike between the two thrusts is 30°. See note at the bottom of page 4.

Relationship of Extensional Fractures to Bedding-Plane Slip Lineations

APPENDIX F

Core Log Reports: Ronald E. Graichen

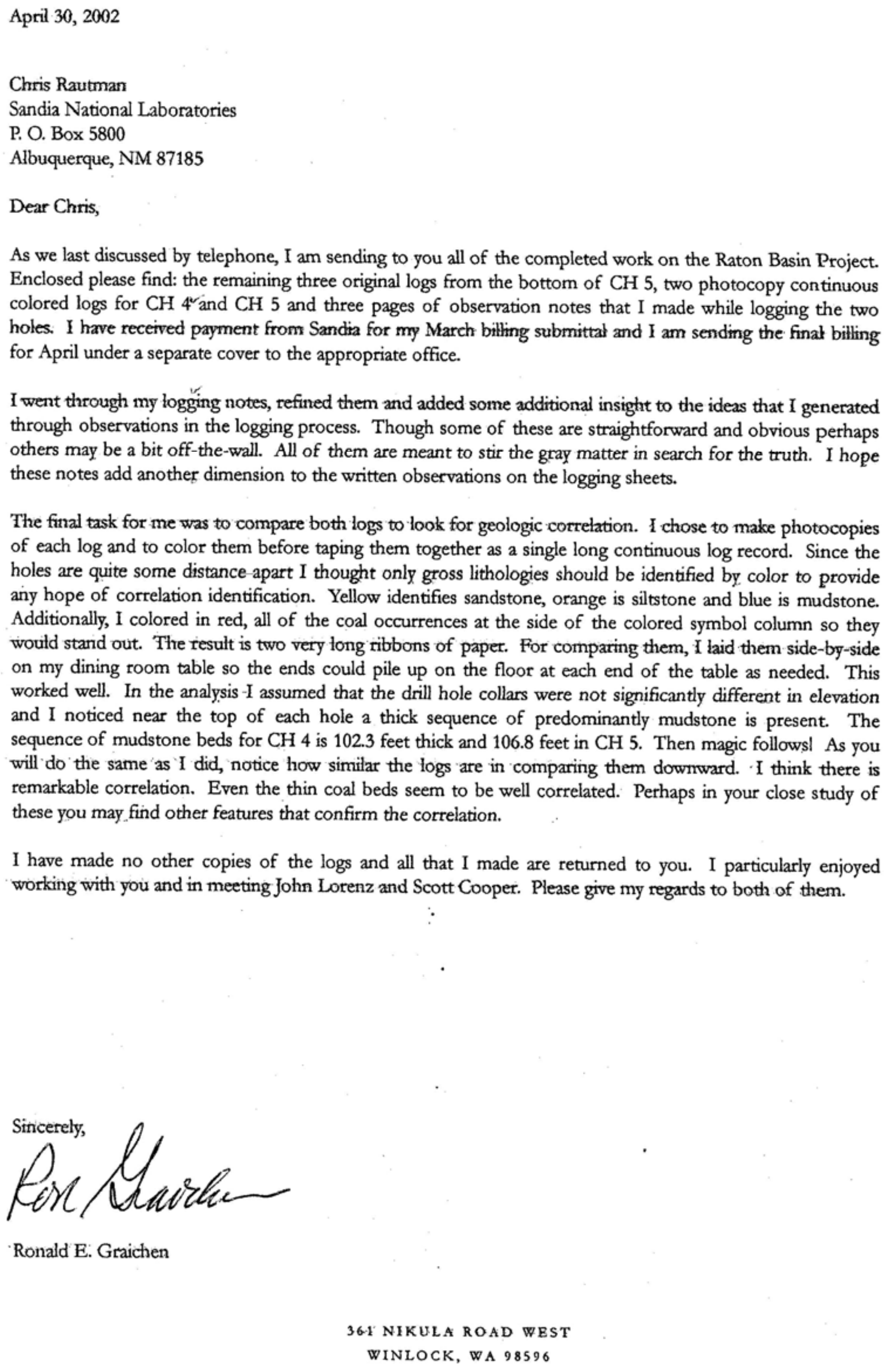

April 30, 2002

Chris Rautman
Sandia National Laboratories
P. O. Box 5800
Albuquerque, NM 87185

Dear Chris,

As we last discussed by telephone, I am sending to you all of the completed work on the Raton Basin Project. Enclosed please find: the remaining three original logs from the bottom of CH 5, two photocopy continuous colored logs for CH 4 and CH 5 and three pages of observation notes that I made while logging the two holes. I have received payment from Sandia for my March billing submittal and I am sending the final billing for April under a separate cover to the appropriate office.

I went through my logging notes, refined them and added some additional insight to the ideas that I generated through observations in the logging process. Though some of these are straightforward and obvious perhaps others may be a bit off-the-wall. All of them are meant to stir the gray matter in search for the truth. I hope these notes add another dimension to the written observations on the logging sheets.

The final task for me was to compare both logs to look for geologic correlation. I chose to make photocopies of each log and to color them before taping them together as a single long continuous log record. Since the holes are quite some distance apart I thought only gross lithologies should be identified by color to provide any hope of correlation identification. Yellow identifies sandstone, orange is siltstone and blue is mudstone. Additionally, I colored in red, all of the coal occurrences at the side of the colored symbol column so they would stand out. The result is two very long ribbons of paper. For comparing them, I laid them side-by-side on my dining room table so the ends could pile up on the floor at each end of the table as needed. This worked well. In the analysis I assumed that the drill hole collars were not significantly different in elevation and I noticed near the top of each hole a thick sequence of predominantly mudstone is present. The sequence of mudstone beds for CH 4 is 102.3 feet thick and 106.8 feet in CH 5. Then magic follows! As you will do the same as I did, notice how similar the logs are in comparing them downward. I think there is remarkable correlation. Even the thin coal beds seem to be well correlated. Perhaps in your close study of these you may find other features that confirm the correlation.

I have made no other copies of the logs and all that I made are returned to you. I particularly enjoyed working with you and in meeting John Lorenz and Scott Cooper. Please give my regards to both of them.

Sincerely,

Ron Graichen

Ronald E. Graichen

361 NIKULA ROAD WEST
WINLOCK, WA 98596

Notes: Core Hole 4

Sheet 1 Mudstone often has a breccia texture and it is easily broken during coring. The texture contains multiple orientation slickensides, interpreted to be caused by loading. Some siltstones display worm tracks or bioturbidite features.

Sheet 2 Carbonate in fractures in mudstone beds is discontinuous and patchy but much of this flakes off into the bottom of the core box. What amount of this coating is lost during drilling activity? A coal-like seam in medium to fine sandstone with 55 dip shows strike-slip slickensides indicating local horizontal stress.

Sheet 3 An 82-degree dip, planar slickensided surface shows up-dip drag indicating local reverse faulting.

Sheet 4 Sandstone beds are not fractured. Slickensides in mudstone are not logged unless there is a coating of carbonate on them; it infers a permeable fracture that permitted calcite deposition in a permeable structure. Many clayey slickensides show nearly dip slip movement (0 to 15 degrees). Coal seams are very thin to several millimeters and are common in the thicker mudstone units. Discordant dark "veins" are coal-like and may be stylolite type structures. Some of these do show, under a hand lens, dimple patterns on a broken surface.

Sheet 5 A vertical fracture in mudstone with minor calcite terminates at its top and bottom into mudstones with random orientation slickensides.

Sheet 6 Curved surface clay slickensides contained within compacted mudstone and not showing obvious open permeability do occur with occasional thin coal seams or "veinlets". Their discordant occurrence suggests migration of carbon (coal), and presumably water, during the compaction process. These also occur in coarse sandstone units. How did it get there without this process? This thesis accounts for non-conformable coal occurrences.

General observations not identified to individual log sheets though listed in sequence as observed in core hole 4 follow. Some features seen are repeated deeper in the hole and some are identified as also occurring in core hole 5.

Conjugate shears in mudstone with attendant tension fractures, in classic orientation, are found. The shears are fluted slickensides, usually 15 to 20 degrees rake from paralleling the dip orientation. Shear movement is assumed to be normal, the clay usually doesn't preserve directional evidence, though post mineral filling can show drag direction. A individual shear higher in this hole it did show evidence of this.

The thicker coals, greater than 0.2 feet thick, show orthogonal vertical fracturing (cleats?) with thin coatings of calcite. This is a common feature in core holes 4 and 5.

Vertical long fractures are seen in both core holes 4 and 5. Usually they are best formed in thick, coarse sandstone beds. These represent a vertical mobility opportunity for gas and fluid movement. Certainly the coarse sandstone itself is highly permeable. The high angle fractures are more predominant in mudstones but they are much shorter and are often inclined 5 to 20 degrees to the core axis.

Most measured structures terminate beyond the core boundary. Of the steep angled ones that do not, in sandstone vertical fractures often terminate as wispy fractures that end in the sandstone for no obvious reason, as might be expected of a tension gash created by regional stress. In mudstones, planar fractures are very thin (0.1 mm) and often terminate in organic trash bedding or into shear surfaces.

Mudstones containing coals (that have been sampled) tend to be more shale-like presumably because of increased organic carbon trash in the bedding. These units suffer more "disking" or close-spaced bedding separation caused from drilling activity.

Shearing in mudstones is generally curved in strike and dip. Less than 10 percent are planar.

Carbonate coating is most often as scaly patches, loosened from highly polished slickensides in mudstone. Drilling activity must remove some of this. The coatings usually adhere to fracture surfaces in coarser grained rock types.

Concretion nodules occur in both core holes 4 and 5. One in core hole 4 may be barite, but most appear to be ironstone. Several have star-like core openings later filled with calcite and some contain pyrite and calcite. They are reddish brown and are finely crystalline. In some they are bedding replacements without concretion form.

At 1000 feet in core hole 4 there is a consistent occurrence of vertical fractures in the sandstone beds. Even a 0.6 foot thick sandy bed contained by mudstone beds is fractured while the mudstone is not. This suggests that the plastic mudstone units transmit stress to fracture the more brittle sandstone beds.

The first sill is at 1146 feet in core hole 4. It is less than three feet thick and appears to be mildly chloritic altered (by organic acids?). Not one millimeter of bleaching occurs in black organic mudstone at the knife-edge contact. The sill contains calcite and reacts to HCl acid. The calcite was perhaps created by organic acid waters altering plagioclase to chlorite and calcite or it was deposited from migrating formational waters or both. Sill rocks do not appear to be good candidates for KAr age dating because of the alteration.

At 1600 feet in core hole 4, near vertical fracturing is en echelon. Individual fractures tend to split into two parallel fractures about one centimeter apart for part of the whole fracture length. On the larger scale, the fractures are en echelon, one will enter the core, pass through and exit with another coming in on the opposite side of the core, parallel to the first and repeating down hole. Some of the near vertical fracturing fades into siltstones and the latter may display a crude fabric paralleling the fracture.

Typically shear striations are fluted to wave-like, occurring at rake angles of 15 to 20 degrees to the dip angle. About 20 percent of slickensides are parallel or near parallel to the dip angle. Steeper angled shears at 45 to 90 degrees to the core axis may have strike oriented striations but these represent less than 3 percent of all.

At 1800 feet in core hole 4 the mudstones and siltstones are thick-bedded and they do not contain many slickensides. Drilling has caused breakage in these very brittle beds with the breaks occurring along pieces of carbon trash which generally lie perpendicular to the core axis. Drilling bit pressure has also created "petal" fractures or curving fractures that form sickle-shaped shards where these intersect bedding plane partings.

Vertical fractures tend to split into two fractures, a long planar one and an auxiliary one paralleling the parent but usually about a quarter of its length. The fracture separation is usually one half to one centimeter. Long fractures are often curved at their beginnings with a high angle to the core axis entering the core, curving into a vertical or near vertical fracture. I suspect this is a feature created by drilling. The vertical linear part of the fracture exists from regional tectonics and normally the terminations fade within the sandstone host as expected with a normal tension fracture. However, during the drilling process, as the drill bit pressure approaches the top of the tension fracture, a "petal effect" occurs to break the curved portion. Evidence for this is the edge of the vertical tension fracture is quite grainy, as would be expected in a "pull-apart" tension fracture. However, the edge of the curved is knife sharp indicative of shear stress.

The long vertical and near vertical fractures cannot be assumed to be oriented to perfect vertical drill core. Hardly any HQ or NQ core hole is vertical. And the greater the depth means the greater can be the orientation from vertical. Typically vertical core holes are not set perfectly vertical at the collar. The drilled hole orientation usually shows the effects within a few hundred feet of the collar of a right hand corkscrew because of rod rotation. Therefore, vertically appearing fractures, seen in a core box, especially from core at 1800 feet depth, are probably slightly inclined.

The following notes are made from logging of core hole 5.

Chris Rautman said he thought these core holes we logged were drilled with air rather than drilling fluids because of the presence of swelling clays. In starting to log core hole 5, I washed and scrubbed it to remove concealing muddy coatings and I was rewarded with a quickly developed fuzziness on the surface. I presume this is due to the presence of montmorillinite clay in the mudstone. The first six boxes (to 188.5 feet) contains very friable core and I question if this is a result of near surface weathering and related to clay swelling. Below 188.5 feet the core appears more competent, however wetting it produces the same swelling clay fuzziness. Swelling clays occur throughout the entire core length.

This core contains unbroken intervals with multiple internal slickensides. This is probably indicative of compaction and dewatering of the original sediment. The open fractures and slickensides mostly have calcite coatings and unlike core hole 4, these in core hole 5 are stained with iron oxide. Bedding partings in shale-like mudstone have the orange coatings even though the core is not naturally broken along bedding planes (in this shallow part of the hole bedding is near 90 degrees to the core axis). These microfractures are not readily observable in the unbroken core but show a permeability factor that is probably greater than within the lithologies in which they are contained. This is commonly displayed at 350 feet. At 370 feet there appears to be a diminishing of orange carbonate coatings; fractures in sandstones have none. In dark organic mudstones and siltstones the orange carbonate coatings are still present but much diminished to thin films of a few microns thickness. At 500 feet are seen hairline fractures 0.3 to 0.4 feet in length and 15 degrees to the core axis with iron oxide staining but little calcite.

Slickensides surfaces typically contain striations at 15 to 20 degrees to dip angle. About 10 percent have striations parallel or near parallel to the dip angle. Higher angle shear surfaces of 45 to 90 degrees to the core axis tend to have 45 degree rake striations and perhaps less than 3 percent of these have strike shears.

At 1,500 feet are seen long fractures paralleling the core axis for one page of core logging, followed by another page showing none then the next again with the parallel fractures. This suggests a set of close-spaced fractures separated laterally by a zone of none or few and farther removed by another close-spaced set of fractures. The vertical or near vertical fractures seen here and in core hole 4 also indicate a regional array of high angle fractures or fracture sets.

Well VPR CH-4

Raton Basin Project
Hole No: CH-4
Scale: 1" = 10' (1:120)
Sheet 1 of 34

Sandia National Laboratories
Logged by: Ron Graichen
Log Version:
Log Date: Mar. 5, 2002

Collar Elevation:
Bearing:
Inclination:
Total Depth:

Drill Site:
N:
E:
Started: 8-18-99
Completed 8-21-99

COMMENTS: all angles are measured to the 0° core axis.
Core Diam. 2.0"

Avg. Core Recovery/ Hole

Drilling Interval
% Core Recovered
Core Size
RQD
Sample Interval

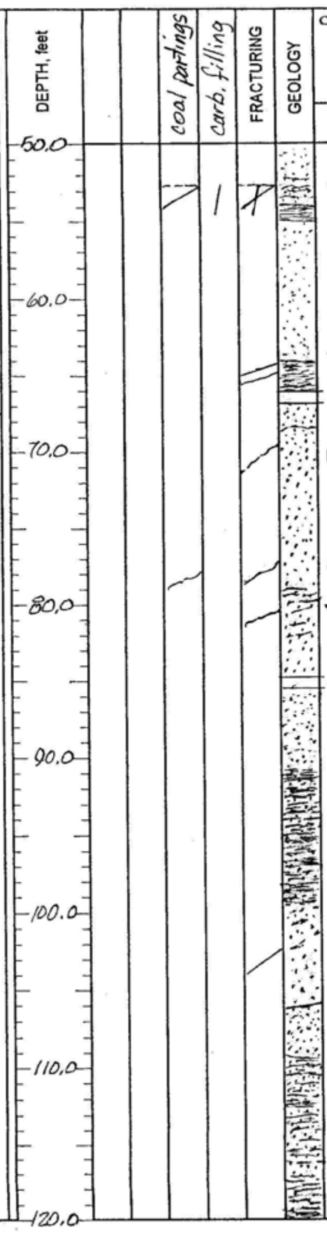

Descriptive Geology

Coring begins @ 50.0'

90° drill parting on thin black laminae, irregular grainey surface
62° wavey slicksides on hairline coal offset by carbonate healed
11° fracture 11°CA

clayey MED. SANDSTONE med. to dark gray, thick bedded

72° v. irregular, rubbly surfaces on two parallel fracts.
clayey zone 64' to the core loss, fragmented texture
66.2
66.8 lost core
wavey contact

10° irregular wavey surface in thick bed ss.

COARSE SANDSTONE lt. gray to tan, thick bedded
some shaley fragments 79-82'

66° v. wavey surf with slickensides along strike (90°) on thin coal seam

74° irregular surface - parting along bedding trend of fine sed. chips in ss. host.

84.8
85.6 core loss

MED TO SILTY SANDSTONE med. to dark gray, thick bedded.

gradational contact

56 planar but rough surface along local bedding - no filling

COARSE SANDSTONE tan to lt. gray, thick bedded

85' sharp contact, slightly wavey

45°-90° beds MED - SILTY SANDSTONE med to dk gray.
Some thin bedded silty zones disrupted w/ bioturbite structures ?

Sandia National Laboratories
Logged by: Ron Graichen
Log Version:
Log Date: Mar. 5, 2002

Raton Basin Project
Hole No: CH- 4
Scale: 1" = 10' (1:120)
Sheet 2 of 34

Drill Site:
N: E:
Started: 8-18-99
Completed 8-21-99

Collar Elevation:
Bearing:
Inclination:
Total Depth:

COMMENTS: all angles measured to the 0° core axis.

Avg. Core Recovery/ Hole

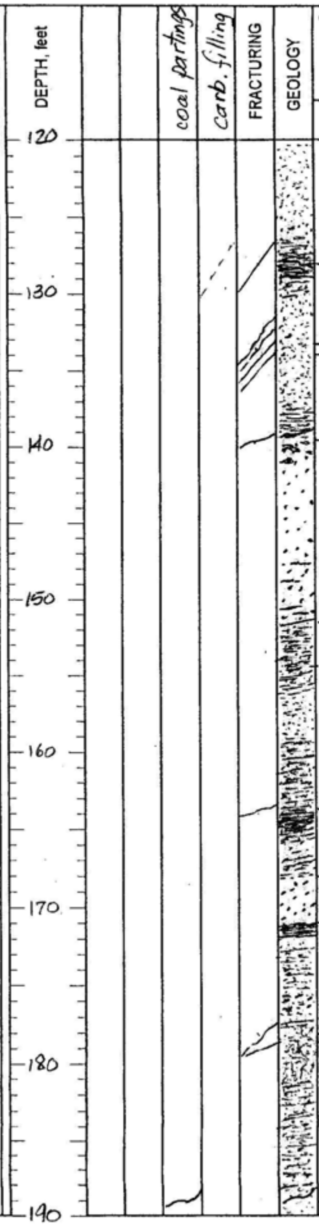

Descriptive Geology

Drilling Interval | % Core Recovered | Core Size | RQD | Sample Interval

MED TO SILTY SANDSTONE greenish gray to dark gray.
127.5'-129' is most clayey zone

128.1' 36° v. planar fract. Dissem patches of carbonate coating

133.3' 34° v. irregular surface fractures, drill induced along sed fabric.
134.0 42° & 45° dip slip & rake slip slickensides

139.8' _ 78° _ v. wavey surface _____ 139.7 gradational contact _____

COARSE SANDSTONE lt. gray, thick bedded
some v. coarse sand & pebbles

silty fragments @ 85°CA

151.7' _____ sharp contact 83° _____

MED TO SILTY SS dk gray green with 1-1½' beds of coarser sand & clayey silts & gradational med g. dk gray ss.

163.9' 70° irregular surface
← gradational into clayey siltstone w/ bioturbidite textures
← wavey darker silt thin beds & light colored coarser sands.

168.1 _____

COARSE SANDST. - bedding 60°CA

171.0 _____ sharp irregular contact _____
0.8' gray-black siltstone

MED TO FINE SS dk gray-green thick bedded, some jumbled texture - bioturbidites? appear to be worm trails

178.1' 36° irregular rough surface fracture
178.7' 69° irregular surface fracture
jumbled, fragmented texture

189.15' 55° on 1mm thick coal seam, Slickenside 75°CA, nearly strike slip

Raton Basin Project
Hole No: CH-4
Scale: 1" = 10' (1:120)
Sheet 3 of 34

Sandia National Laboratories
Logged by: Ron Graichen
Log Version:
Log Date: Mar. 5, 2002

Collar Elevation:
Bearing:
Inclination:
Total Depth:

Drill Site:
N: E:
Started: 8-18-99
Completed 8-21-99

COMMENTS: Very few fractures in this interval.

Avg. Core Recovery/ Hole

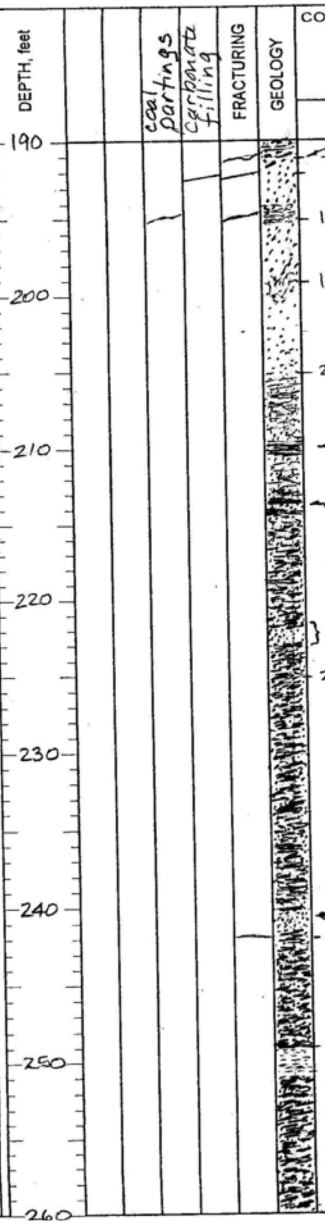

Descriptive Geology

191.25, 81° wavey surface fracture – no filling
192.1, 82° planar, slickensided carbonate coating, not parallel to
slicks upthrust in the dip direction.
195.0', 82° wavey surface, subtle slicks on 1/2 mm coal seam (?)
COARSE SANDSTONE lt to med. greenish gray
199.2'. 83° wavey parting surface
poor bedding parallels parting. Jumbled texture
possible bioturbidite.
small cut-fill channels & other irregular sediment structures.
205.3 gradual contact
black silty zone
4½" m.g. sandstone bed, thick bedded
MEDIUM TO SILTY SANDSTONE: dk greenish gray
Mostly thick bedded & jumbled texture.
coarse ss.
225.1', 86° possible natural parting
subtle 6" med-coarse ss. bed
242.0', 90° possible natural parting
249.0'
251.0' laminated bedding in f.g. sandstone & some small cut-fill structures.

Drilling Interval
% Core Recovered
Core Size
RQD
Sample Interval

Raton Basin Project
Hole No: CH - 4
Scale: 1" = 10' (1:120)
Sheet 4 of 34

Sandia National Laboratories
Logged by: Ron Graichen
Log Version:
Log Date: Mar. 5, 2002

Collar Elevation:
Bearing:
Inclination:
Total Depth:

Drill Site:
N: E:
Started: 8-18-99
Completed 8-21-99

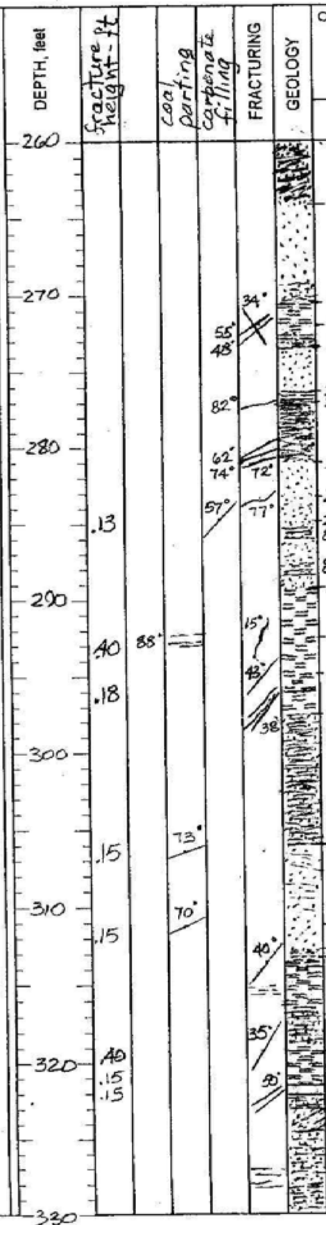

COMMENTS:

Avg. Core Recovery/ Hole

Descriptive Geology

264.0' — gradual contact

COARSE SANDSTONE: tan to lt. gray, thick bedded
thin dk gray laminations near bottom contact, wavey character

270.8' — gradual contact

272.3' MUDSTONE: dk brpwnish gray, minor ss. beds, brittle! irregular curved slicksurf fracts

273.8' — gradual contact

MED - COARSE SANDSTONE:

276.4' — sharp-healed contact

277.25 — mudstone - parting fracture

SILTSTONE: DK. brownish gray - easily broken by hand
abundant internal compression slickensides.

281.0' — gradual contact

FINE - MED. SANDSTONE med. to dk greenish gray localized thin bedding.

283.0' ← wavey surf. clayey fracture

284.4 ← .5 mm carbonate healed fract. 10% unfilled & open

84°
86° → thin bedding

289.3 — abrupt contact

MUDSTONE dk greenish gray

292.5'

295.0' wavey surface w/ dip direction slip striations

297.6 (3) parallel wavey surfaces - slicks — abrupt contact

FINE - SILTY SANDSTONE dk greenish gray
lacking bedding features
some thin beds w/ carbon trash as wavey patterns - not planar.

← 1mm coal seam - parting fracture

306' — gradual contact

MED. SANDSTONE tan to lt. gray

311.5' ← wavey surface coal parting fracture

312.6' slicks 40° fluted dip slip

313.3 — abrupt contact

← 315.4'-316 1 parting per 0.1 ft.

MUDSTONE & SILTY MUDS. dark gray, local
fissility due to thin coal seams 85-90° CA.

319.5' ← fluted slicks nearly dip slip

← parallel fluted slicksides nearly dip slip

← lost core 321.5 - 322.0'

323.0' —

324.2 — med. sandstone bed, irregular carbin laminations 70°CA.

327'-328' parting 90°CA each .15' aver.

← 329.0' 0.1' thick coal seam

Drilling Interval

% Core Recovered

Core Size

RQD

Sample Interval

Fracture photo record roll no.

photo 1 of 57° carb filled fract.

photo 2 of 15° slicks

photo 3 of 38° slicks pair

photo 4 of 35° slicks

Raton Basin Project
Hole No: CH-4
Scale: 1" = 10' (1:120)
Sheet 5 of 34

Sandia National Laboratories
Logged by: Ron Graichen
Log Version:
Log Date: Mar. 6. 2002

Collar Elevation:
Bearing:
Inclination:
Total Depth:

Drill Site:
N: E:
Started: 8-18-99
Completed 8-21-99

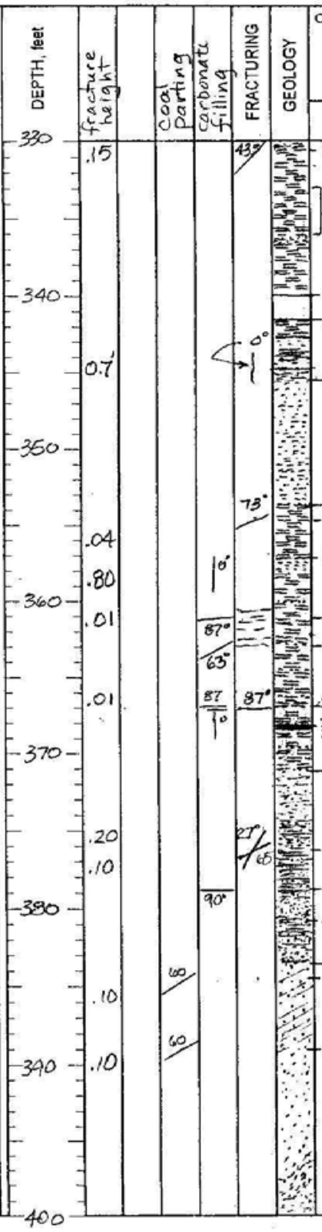

COMMENTS:
Mudstone slickenside with thin carbonate suggests open permeability on some structures. Fresh, bright slickensides are not considered as open fractures

Avg. Core Recovery/ Hole

Drilling Interval

% Core Recovered

Core Size

RQD

Sample Interval

Fracture Photo Record roll no.

Descriptive Geology

330.4' wavey slicks, mostly dip slip movement

MUDSTONE - SILTSTONE 328-336 is high carbon zone 90°CA with numerous 1-3mm coal seams.

333–336 ← bedding fracture separations each 0.1'-0.3'; each 0.1' @ 335'-336'

340.0 lost core

341.6

344.5'-345.2' vertical irregular surface fracture contained in mudstone bed & terminating against sandstone beds above & below. — Photo 7 & 8

345.5' ——— gradual contact ———

SANDSTONE fine-grained lt gray with dk gray silty laminations & v. thin beds. Bedding 90°CA. Bedding is wavey character. No natural fractures - only drilling induced parting along bedding

353.8' ——— sharp contact ———

354.7' ← wavey slicks w/ multiple striation strikes

MUDSTONE & SILTSTONE: dk gray - mostly mudstone

357.1 ← vertical, v. planar fracture 60% covered w/ brownish carbonate 0.1mm thick. Bottom .3' not broken - a hairline permeable fracture 0.1mm. Terminates top & bottom into irregular mudstone compaction slickensides. — photo 9, 10 0° fracture

361.2 ← v. thin carbonate coatings

362.9 ← slickenside dip slip

@ 360'-363' slickenside partings from drilling each 0.1-0.15 ft.

367.0' planar fracture w/ slickensides on coal/carbon also adjacent to 2mm thick carbonate seam.

368.1' 368.6' Two of these seams 1cm. apart, both solid calcite? — photo 11 of 87° fract. & CaCO3 Seams

coal seam removed for "desorp." 368.6-369.2 vertical fract. in coal planar, v. thin carb. coat. 50% filling

372.3' ——— gradational contact ———

FINE SANDSTONE some siltstone, lt gray - dk gray

376.5 cross cutting wavey slickensides

379.0 coal parting. An odd <1mm thick plane of coal striae (?)

381.0 strong slickensides on mudstone, slicks unidirectional 25° away from dip of fracture

383.6 ——— sharp contact ———

384.5 planar 1mm thick coal parting

SANDSTONE med. grained carbonate cement lt tan color, mostly thick bedded. Thin planar coal laminations throughout to 389 ft.

389.0 planar 1mm coal parting - drilling break

← wavey sed. bedding structures

← subtle bedding laminations of darker - organics ?, 80°CA.

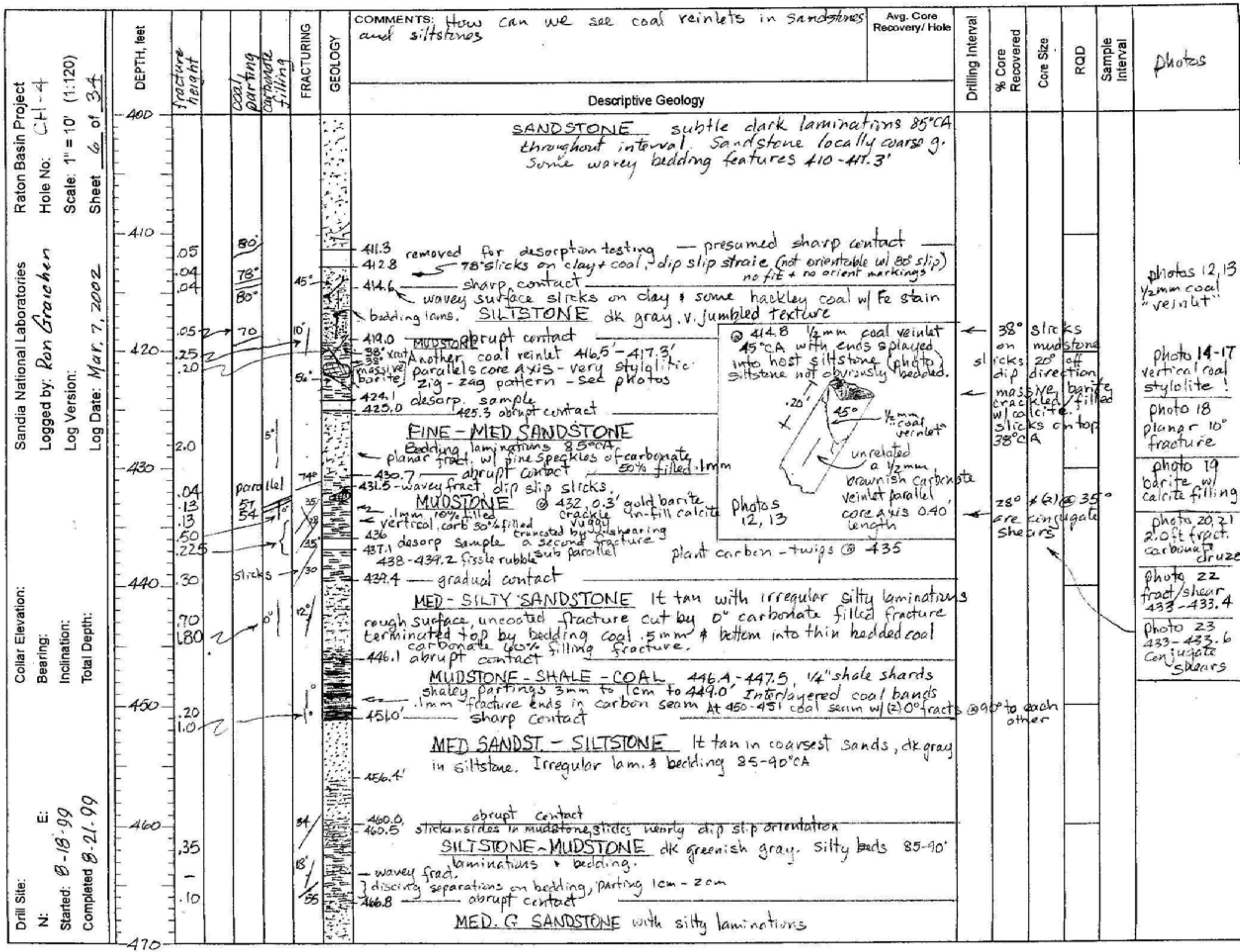

Raton Basin Project
Hole No: CH-4
Scale: 1" = 10' (1:120)
Sheet 6 of 34

Sandia National Laboratories
Logged by: Ron Graichen
Log Version:
Log Date: Mar. 7, 2002

Collar Elevation:
Bearing:
Inclination:
Total Depth:

Drill Site:
N: E:
Started: 8-18-99
Completed 8-21-99

COMMENTS: How can we see coal veinlets in sandstones and siltstones

Descriptive Geology

SANDSTONE subtle dark laminations 85°CA throughout interval. Sandstone locally coarse g. Some wavey bedding features 410-411.3'

411.3 removed for desorption testing — presumed sharp contact
412.8 78° slicks on clay + coal, dip slip straie (not orientable w/ 80° slip) no fit + no orient markings
414.6 sharp contact
wavey surface slicks on clay & some hackley coal w/ Fe stain
bedding lams. **SILTSTONE** dk gray. v. jumbled texture
419.0 MUDSTONE abrupt contact
38° xcut
38° Another coal veinlet 416.5'-417.3'
[massive barite] parallels core axis - very styloliltic zig-zag pattern - see photos
424.1 desorp. sample
425.0 425.3 abrupt contact

@ 414.8 ½mm coal veinlet 45°CA with ends splayed into host siltstone (photo) siltstone not obviously bedded.

a ½mm brownish carbonate veinlet parallel core axis 0.40' length

Photos 12, 13

FINE - MED SANDSTONE
Bedding laminations 85°CA
planar fract. w/ fine speckles of carbonate 50% filled .1mm
430.7 abrupt contact
431.5 - wavey fract dip slip slicks,
MUDSTONE @ 432, 0.3' gold barite crackle vuggy in-fill calcite
.1mm 10% filled
vertical, carb 30% filled truncated by shearing a second fracture sub parallel
436 desorp sample
437.1
438-439.2 fissle rubble
plant carbon - twigs @ 435
439.4 — gradual contact

MED - SILTY SANDSTONE It tan with irregular silty laminations
rough surface, uncoated fracture cut by 0° carbonate filled fracture terminated top by bedding coal .5mm & bottom into thin bedded coal carbonate 60% filling fracture.
446.1 abrupt contact

MUDSTONE - SHALE - COAL 446.4-447.5, ¼" shale shards
shaley partings 3mm to 1cm to 449.0' Interlayered coal bands
.1mm fracture ends in carbon seam At 450-451 coal seam w/ (2) 0° fracts @ 90° to each other
451.0' sharp contact

MED SANDST. - SILTSTONE It tan in coarsest sands, dk gray in siltstone. Irregular lam. & bedding 85-90°CA
456.4'
460.0 abrupt contact
460.5' slickensides in mudstone, slicks nearly dip slip orientation

SILTSTONE - MUDSTONE dk greenish gray. Silty beds 85-90° laminations & bedding.
— wavey fract.
} discing separations on bedding, parting 1cm - 2cm
466.8 abrupt contact

MED. G SANDSTONE with silty laminations

38° slicks on mudstone
slicks 20° off dip direction
massive barite crackled / filled w/ calcite. slicks on top 38°CA
28° & (2) @ 35° are conjugate shears

Photos

photos 12, 13 ½mm coal "veinlet"

photo 14-17 vertical coal stylolite !

photo 18 planar 10° fracture

photo 19 barite w/ calcite filling

photo 20, 21 2.0 ft fract. carbonate druze

photo 22 fract/shear 433-433.4

photo 23 433-433.6 Conjugate shears

Drill Site:
N:
E:
Started: 8-18-99
Completed 8-21-99

Collar Elevation:
Bearing:
Inclination:
Total Depth:

Sandia National Laboratories
Logged by: Ron Graichen
Log Version:
Log Date: Mar. 7, 2002

Raton Basin Project
Hole No: CH-4
Scale: 1" = 10' (1:120)
Sheet 7 of 34

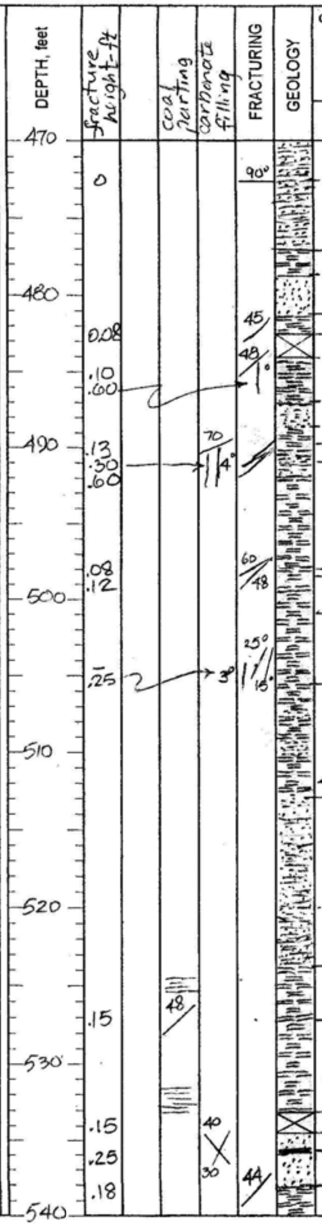

COMMENTS:

Avg. Core Recovery/ Hole

Descriptive Geology

472.6 maybe natural parting along bedding plane.

SILTSTONE light-dk gray bedding, wavey, irregular with some marine animal burrows?

477.2 — sharp contact

MUDSTONE

478.3 — sharp contact

MED G. SANDSTONE - w/ dark silty lams.

481.1 — sharp contact

mudstone 45° slicks, curving surface w/ slicks parallel to dip.

482.7 desorp. sample

484.0

485.8 - 486.4 vertical planar fracture - no coating, bounded by clayey laminations in bedding

487 — fine g. sandstone

488.6 —

489.2 curving slicks w/ 10% carb. filling. ← set of 3 subparallel slicks 45°CA on mudstone no filling

490.2 slicks; dip slip w/ 10% carbonate filling

SILTSTONES & MUDSTONES dk brownish gray

no natural fractures partings on bedding ea. 5-10cm. drill induced

498 498.2 slicks on claystone at rake to strike-dip.

501

rubblized - bad drilling; abundant discing possible shearing - clay slicks; 15° is near dip angle

← vertical planar fracture

505.6

512.7 is .15' coal seam w/ vertical fracts @ right ∠'s to each other.

512.9 — abrupt contact

MED - FINE G. SANDSTONE lt. gray with wavey laminations of dk gray silts. little drill breakage.

524 — gradational contact

← drilling caused partings on thin coal seams 4/.35'

527.6 slicks on 1mm coal seam "vein"

MUDSTONE - SILTSTONE dk gray moderate drill caused bedding parting 2-4/ft.

1-2mm coal bedding - drill discing 1/cm.

533.2 desorp sample

534.4 sharp contact

535.6 - 536 mudstone MED. G. SANDSTONE med. gray

fluted slicks - conjugate shears in mudstone

537.9 — abrupt contact

MUDSTONE

Drilling Interval

% Core Recovered

Core Size

RQD

Sample Interval

photos

Raton Basin Project
Hole No: CH-4
Scale: 1" = 10' (1:120)
Sheet 8 of 34

Sandia National Laboratories
Logged by: Ron Graichen
Log Version:
Log Date: Mar. 8, 2002

Collar Elevation:
Bearing:
Inclination:
Total Depth:

Drill Site:
N: E:
Started: 8-18-99
Completed 8-21-99

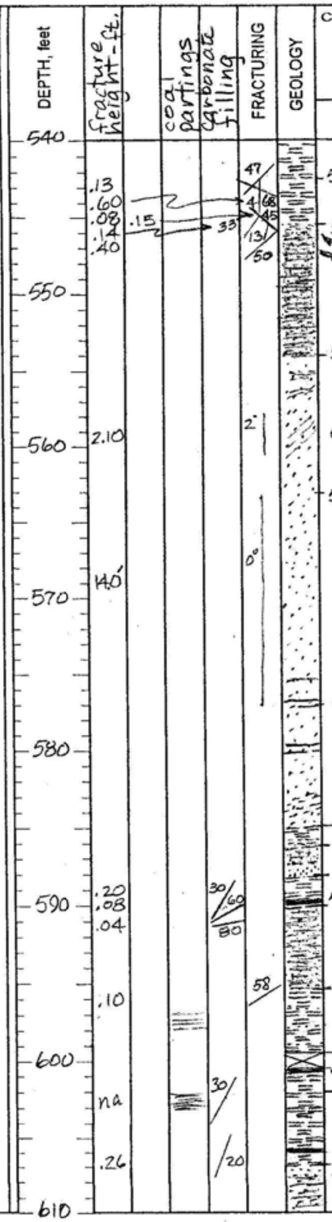

COMMENTS:

Descriptive Geology

Avg. Core Recovery/ Hole

MUDSTONE: @ 544.0, 0.25' barite, vuggy w/ pyrite

543.5 dip slip striations on mudstone, shear - conjugate shear to 68° with dip slip striae on non-carbonate mineral coating - down dip movement indicated. Vertical fract. open, .01mm as tension fract. ? tension fract. bounded by shears.

545.5' — gradational contact

← 45° clay slicks

← 50° planar fract in ss.

FINE SANDST + SILTST. well laminated bedding unfractured

554.1' — sharp contact

MED - COARSE SANDSTONE lt. gray thick bedded with localized intervals of darker finegrained thin beds + laminations

open rough surface fracture 558'-560'

563'

open rough surface fracture 14 feet long! unbounded, finally just wandered out of the core.

577' } 1mm - 3mm coal beds

585.0 — sharp contact
586.2 mudstone + siltstone

FINE SANDST - SILTSTONE irregular thin bedding + laminations

588.0 mudstone w/ 0.4' coal bed
coal
590.0

@ 590.4' thin fract. 50% carbonate filled
@ 590.0 same
@ 591.0 same
} v. planar

595.4 — abrupt contact
← wavey slicks near dip slip slicks
← S drilling induced discing on thin coal seams

MUDSTONE - SILTSTONE

599.7 desorp sample
600.7
coal
602.2 thin planar fract. 50% carbonate filled
← drilling discing on thin coal seams

← .3' coal seam w/ blocky vert. fracts @ 90°

607.1 — abrupt contact

← @ 605.0' planar unfilled fract. bounded by coal seams on upper term.

SILTSTONE as above

Drilling Interval

% Core Recovered

Core Size

RQD

Sample Interval

photos

photo 25
543.5
conjugate shears/tension fracture

Drill Site:
N: E:
Started: 8-18-99
Completed 8-21-99

Collar Elevation:
Bearing:
Inclination:
Total Depth:

Sandia National Laboratories
Logged by: Ron Graichen
Log Version:
Log Date: Mar. 8, 2002

Raton Basin Project
Hole No: CH-4
Scale: 1" = 10' (1:120)
Sheet 9 of 34

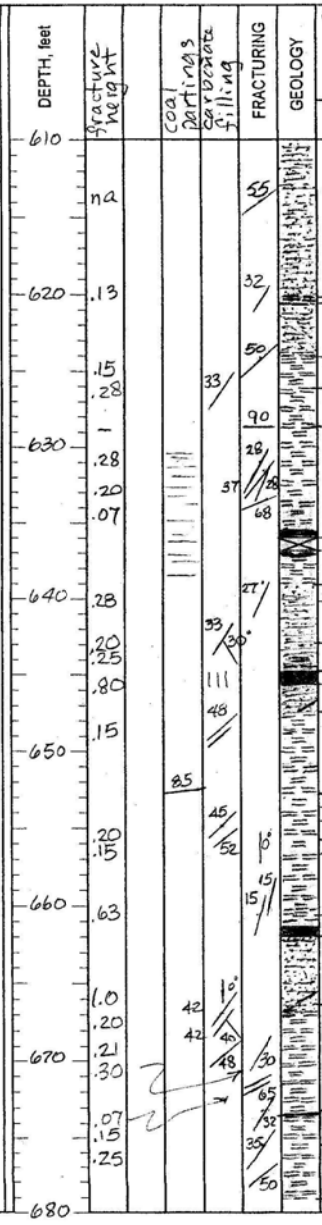

COMMENTS:

Avg. Core Recovery/ Hole

Descriptive Geology

← clay slicks

SILTSTONE med gray with darker fine beds & laminations of mudstone displaying wavey charactor.

620.1-620.6 mudstone bed containing planar fracture, uncoated terminated at 90° parting w/ plant organics.

624.0 — abrupt contact

← slicks 624.1', parallel dip, planar surface

626.2 thin V. planar fracture w/ 1-2% v.f.g carbonate

MUDSTONE dk browinsh gray

628.7 clay slicks

← 28° 37° slicks, V. nearly dip slip. All (3) generally parallel

drilling discing in shaley mudstone w/ coal seam partings 1cm-5cm.

slicks

635.9
636.9 desorp. sample, coal above & below w/ strong discing of core.

639'

640.1' clay slickensides, dip slip orientation

SILTSTONE med. to dk. gray

643' planar, dip slip slicks 40% thin carbonate filled

644.8'
645.6' coal bed, vertical fracts w/ carbonate coating

coal
647.5' — gradual contact

648.5' carbonate, 20% filling, planar slickensides – ~~nearly dip slip orient.~~ two parallel structures

MUDSTONE

653.0 slickensides on 1/2 mm coal seam

653.5 0.1' bedding replacement by barite (?)

654.4 — 25% carbonate filled slicks surf - slicks nearly @ dip direction.

656.0 – planar fract.

657.0 irregular 0.3 piece of f.g. barite (?)

planar fracture in

660.8 – 0.5' coal bed ← 0.2 bedding replace by barite (?)

662.1 — sharp contact

FINE-MED SANDSTONE with irregular thin beds & laminations of siltstone

← rough surface fract. 70% filled by carbonate – terminates in med. sandstone

– coal

667.4 — gradual contact

← pair slicks w/ carbonate 10% filling near dip slip striae

MUDSTONE dk brownish gray ← 40° fract. w/ druze carbonate 50% filled – v. planar & ⊥ slicks

669' planar fract

← pair, parallel planar fracts both 65°

672.5' slicks
coal

675 ← slicks parallel dip

679.5 – very gradational contact

SILTSTONE

Drilling Interval

% Core Recovered

Core Size

RQD

Sample Interval

photo record

photo 26
643'
carbonate slicks terminating fract.

photo 27
654.4'
carbonate on slicksides

Drill Site:
N: E:
Started: 8-19-99
Completed 8-21-99

Collar Elevation:
Bearing:
Inclination:
Total Depth:

Sandia National Laboratories
Logged by: Ron Graichen
Log Version:
Log Date: Mar. 8, 2002

Raton Basin Project
Hole No: CH-4
Scale: 1" = 10' (1:120)
Sheet 10 of 34

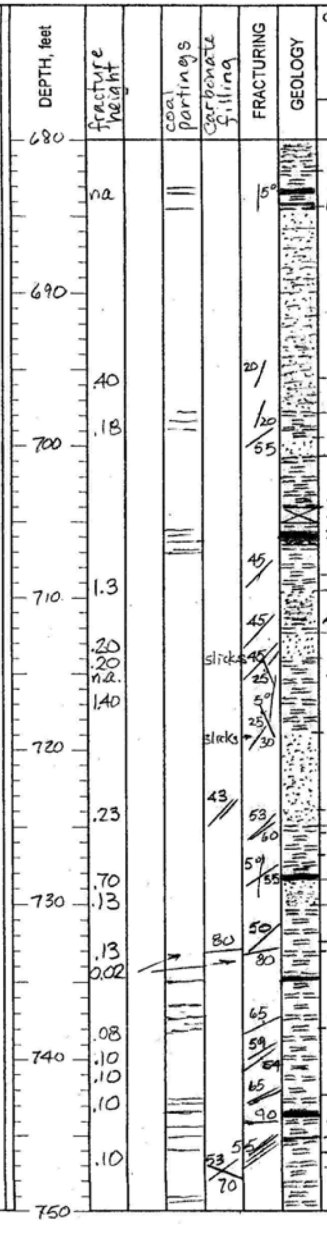

COMMENTS:
n.a. in fracture height means too hard to hold together to measure it.

Avg. Core Recovery/ Hole

Descriptive Geology

682 — abrupt contact SILTSTONE
— coal 0.4' 5° fracture, planar MUDSTONE
684.5 — abrupt contact

FINE SANDSTONE - SILTSTONE
lt. gray w/ darker finer-grained fine bedding & laminations, unbroken.

696.7 planar fracture w/ faint dusting of carbonate
698.0 —
699.4 — mudstone, minor coal beds 90°CA. slicks 55°CA, wavey surface - near parallel to dip
700.8 — abrupt contact

704.2
705.0 desorp sample
coal
706.2-706.5 desorp sample MUDSTONE dk brown gray
708.8' clayey slicks parallel dip
709.7 — gradual contact
← dip slip slicks along coal 'vein' SILTSTONE laminated & fine bedded
712.3 — gradual contact
FINE-MED SANDSTONE
714.0 — gradual contact
← planar 25° fract ⊥ to 45° slicks MUDSTONE
← 5° planar fract not bounded; 25° slicks parallel dip & @ 90° to strike of 5° fract wavey
719.1' — abrupt contact
SILTSTONE - FINE SS.

724.0 ← pair of parallel carb. coated slicks, fluted curvilinear near dip orient of slicks.
725.0 ← abrupt contact,
725.4 parallel slicks .4' apart MUDSTONE
727.0 planar fract. terminates in coal bed below, cross cut by 55° fract.
728.6 — 0.8' coal bed.
730.1 — fine SS.
732.6 ← smooth slicks, nearly planar. Two 80° slicks, one w/ carbonate 60% filling
733.2 ←
← 0.3' coal
738.0 ← near planar clay slicks, striae at rake angle to strike/dip
742.5 — pair of curviplanar slicks, 0.15' apart, parallel w/ rake slicks
← coal 0.4' thick. Blocky quadralateral vertical fracturing in coal seam.
← slicks
← coal
746.1' four clay slickenside slips, parallel & dip slip striae
747' carb. coated slicks as conjugate pair

Drilling Interval
% Core Recovered
Core Size
RQD
Sample Interval

photo record

photo 28
1.40', 5°
fracture

photo 29
pair of
shears 55°CA
@ 746.1 ft.

Drill Site:
N: E:
Started: 8-19-99
Completed 8-21-99

Collar Elevation:
Bearing:
Inclination:
Total Depth:

Sandia National Laboratories
Logged by: Ron Graichen
Log Version:
Log Date: Mar. 9, 2002

Raton Basin Project
Hole No: CH-4
Scale: 1" = 10' (1:120)
Sheet 11 of 34

DEPTH, feet | fracture height | coal partings | carbonate filling | FRACTURING | GEOLOGY | COMMENTS: | Avg. Core Recovery/ Hole | Drilling Interval | % Core Recovered | Core Size | RQD | Sample Interval | photos

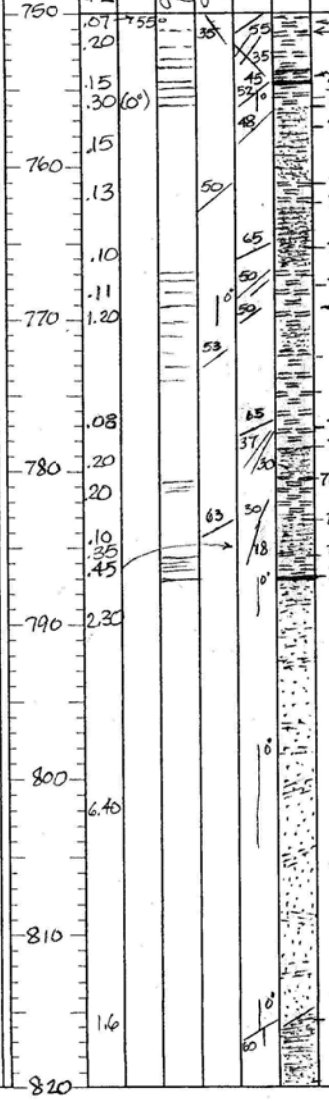

Descriptive Geology

←slicks on 55, 10% carb filling on 35° slicks
←751.0 pair of roughly slicksided shears 35°CA, parallel planar fract. 45° cont.

MUDSTONE dk gray with coal beds

←coal 0.1' & 0.6' 52° dip direct. slicks cut vertical planar fracture.

755.8
756.3 — abrupt contact

757.6 planar slicks

SILTS-FINE SS.

761.0
762.3 mudstone 762 smooth near planar slip w/ 10% carbonate filling

765.4 — abrupt contact @ contact 65° slicks.

768.0' (2) slicks 50° CA, parallel

SILTSTONES & MUDSTONES

←769-770.2 fract. w/ 10% carbonate, cross-cut shears no offset.

772.4 slicks near dip direction 25% carbonate filled.

777.4 mudstone ← near planar slicks
778.4 ← slicks in dip orientation fluted curvilinear surface
siltstone
780.5
mudstone
783.2 siltstone ← 30° slicksides near dip slip. 63° is 25% carb. filled.
785.5 ← 0.1' coal mudstone
18° fracture in sandstone core not broken
786.9 — ~~sharp~~ sharp contact

← rough surface fracture not coated

MED. G. - COARSE SANDSTONE

lt. tan with thin beds & laminations of silts @ variable 80-85° CA.

← same rough surface fracture

← vertical fracture cuts across contact, slightly offset by 65°CA slip

815.7 — sharp contact 60°CA

SILTSTONE med gray mostly unbroken & unfractured.

photos: photo 30 753' coal beds + core partings

Raton Basin Project
Hole No: CH-4
Scale: 1" = 10' (1:120)
Sheet 12 of 34

Sandia National Laboratories
Logged by: Ron Graichen
Log Version:
Log Date: Mar. 9, 2002

Collar Elevation:
Bearing:
Inclination:
Total Depth:

Drill Site:
N: E:
Started: 8-19-99
Completed 8-21-99

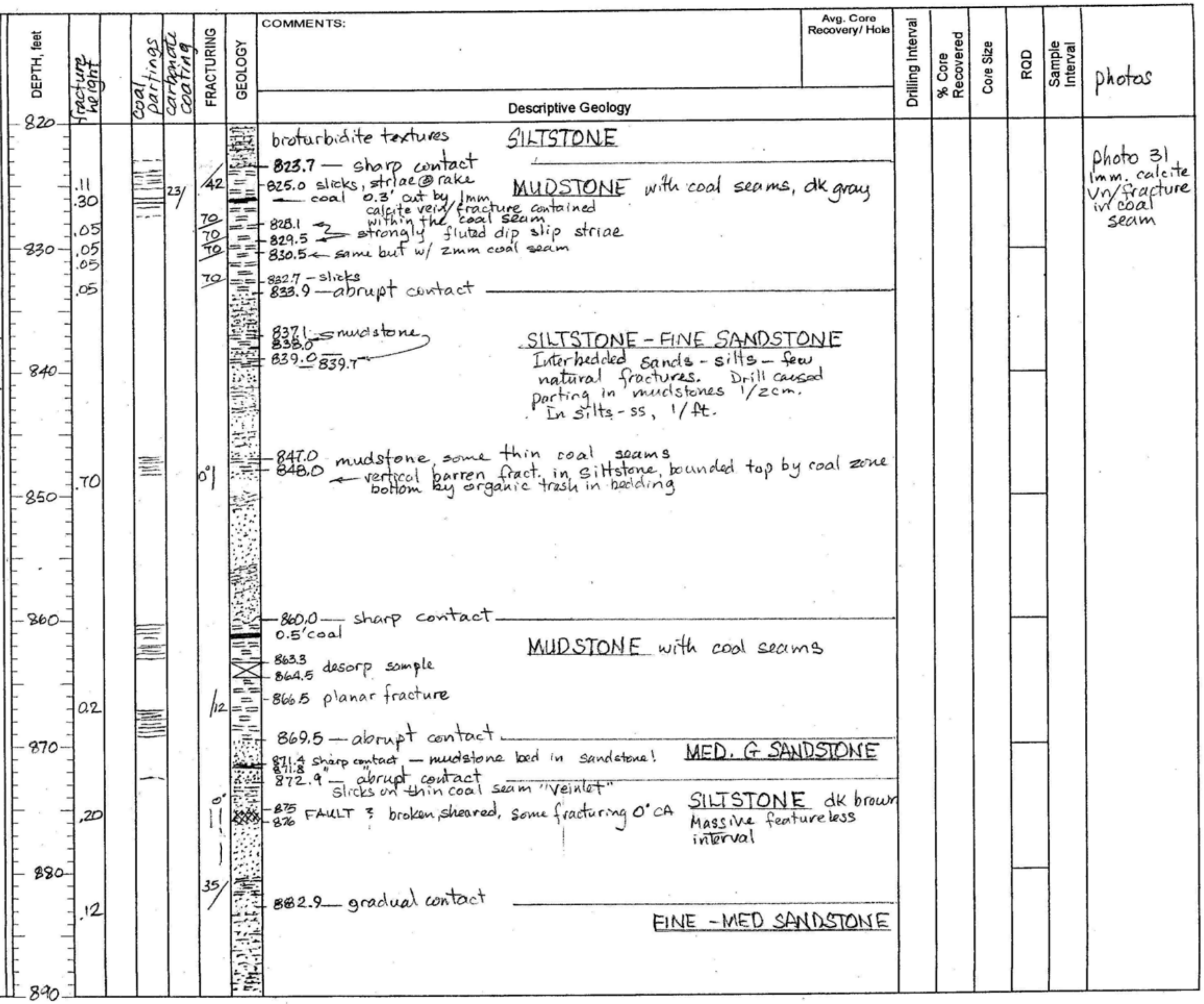

Descriptive Geology

broturbidite textures

SILTSTONE

823.7 — sharp contact

825.0 slicks, striae @ rake

← coal 0.3' cut by 1mm calcite vein/fracture contained within the coal seam

MUDSTONE with coal seams, dk gray

828.1, 829.5 — strongly fluted dip slip striae

830.5 ← same but w/ 2mm coal seam

832.7 – slicks

833.9 — abrupt contact

837.1, 838.0 — mudstone, 839.0 — 839.7

SILTSTONE - FINE SANDSTONE

Interbedded sands - silts - few natural fractures. Drill caused parting in mudstones 1/2cm. In silts - ss, 1/ft.

847.0 mudstone, some thin coal seams

848.0 ← vertical barren fract. in siltstone, bounded top by coal zone bottom by organic trash in bedding

860.0 — sharp contact

0.5' coal

MUDSTONE with coal seams

863.3, 864.5 desorp sample

866.5 planar fracture

869.5 — abrupt contact

871.4, 871.8 sharp contact — mudstone bed in sandstone!

MED. G SANDSTONE

872.9 — "abrupt contact" slicks on thin coal seam "veinlet"

875, 876 FAULT ? broken, sheared, some fracturing 0° CA

SILTSTONE dk brown

Massive featureless interval

882.9 — gradual contact

FINE - MED SANDSTONE

photo 31

1mm. calcite Vn/fracture in coal seam

Raton Basin Project
Hole No: CH-4
Scale: 1" = 10' (1:120)
Sheet 13 of 34

Sandia National Laboratories
Logged by: Ron Graichen
Log Version:
Log Date: Mar. 9, 2002

Collar Elevation:
Bearing:
Inclination:
Total Depth:

Drill Site:
N:
E:
Started: 8-18-99
Completed 8-21-99

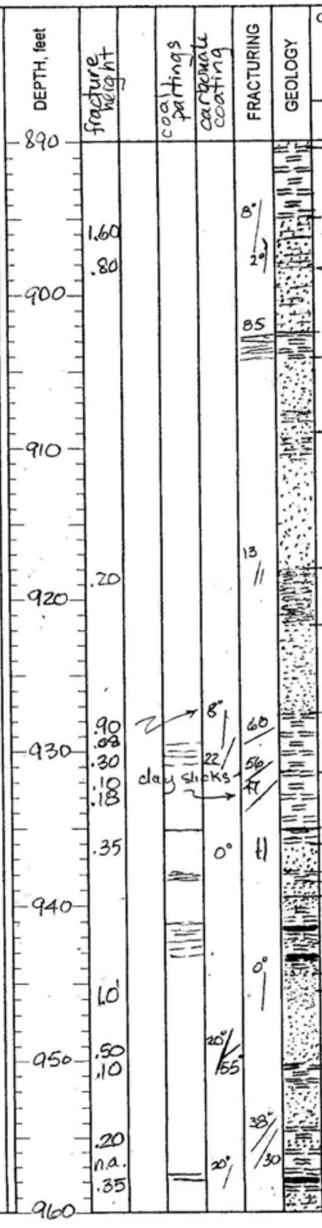

COMMENTS:

Avg. Core Recovery/ Hole

Descriptive Geology

890.4 — grad contact

MUDSTONE

895.1 — sharp contact
8° rough surface fracture
← rough surf fract. top curves out of core

FINE-MED G. SANDSTONE

902.4 slicks on contact
mudstone-siltstone, slicks surfaces every 1-2cm @ high angle CA
904.3

SILTSTONE dk gray
No natural fractures

909.0 — gradual contact

FINE SANDSTONE
Irregular bedding structures generally 90° CA.
No natural fractures.

918.1 — sharp wavey contact
v. thin fracts, end in SS.

SILTS.-Some SS.

← several <1mm coal veinlets as irregular wisps in whole core.

921.8 — gradual contact

FINE-MED.G. SS.
no natural structure

927.5 — gradual contact
← planar fracture, 10% carbonate filled, 60° slicks on mudstone, 931.8' string curving this cut by 22° fract w/ 10% carb. druze coating.
- shaley
← coal 0.1'

MUDSTONE

@936', two curving fracts nearly vertical; each 90° to the other, in sandstone.

936.0 — abrupt contact
med. sandstone
937.9 — sharp contact
938.4 — abrupt ← mudstone
939.5 ← sandstone

MED. G. SANDSTONE with mudstone beds.

0.4' coal, broken
943.5-944.0 coal - crumbled
944.6 — abrupt contact

SILTS.-MUDSTONE with coal

945.6 1ft long fract. in SS. no mineral

FINE SANDSTONE

← wavey surface slicks, paralled dip w/70% carbonate fill; 55° splays from the 20° slick
950.4 — gradual contact

SILTSTONE-MUDSTONE

← clay slicks, v. curving
← coal about 0.5'; 20° carbonate coated fracture 20% filled
contact

Drilling Interval	% Core Recovered	Core Size	RQD	Sample Interval	photos
					photo 32 897' SS. fracture deflected on siltstone bed photo 33-35 coal veinlet 907' photo 36 carbonate coated slicks 950'

Drill Site:
N:
E:
Started: 8-18-99
Completed 8-21-99

Collar Elevation:
Bearing:
Inclination:
Total Depth:

Sandia National Laboratories
Logged by: Ron Graichen
Log Version:
Log Date: Mar 11, 2002

Raton Basin Project
Hole No: CH-4
Scale: 1" = 10' (1:120)
Sheet 14 of 34

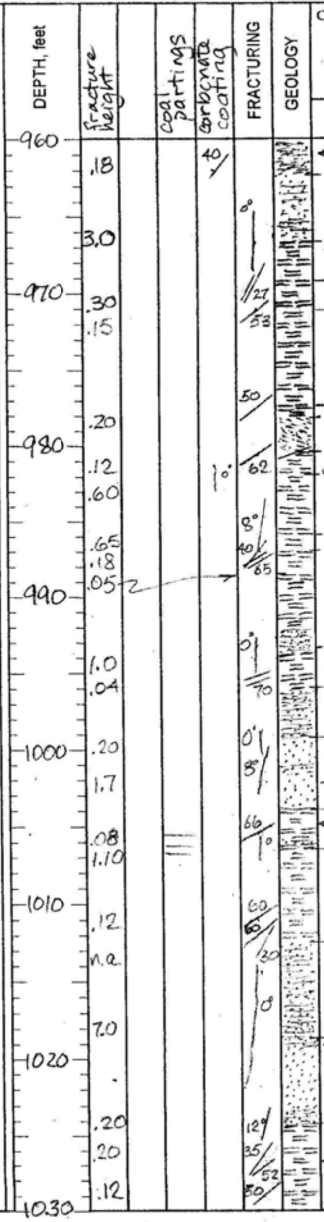

COMMENTS:

Avg. Core Recovery/ Hole

Descriptive Geology

←thin curving–Trace carb. coat fract. siltstone
-962.6' —— gradational contact
FINE –MED. SS.
S rough surface fracture no filling; continues into mudstone–both ends leave core
-966.9' ←— abrupt contact
} strong discing
368.9 } twin clay slicks, .1' apart, parallel, slicks near dip orient.
MUDSTONE brownish gray local shaley bedding & core fracturing along it due to drilling to 974'
-971.1' – clay slicks parallel dip.
-977.4' clay slicks near dip orient.
-978.2' — v. gradual contact
interbedded fine Sandstone & siltstone
-980.3' – sharp contact 65°CA
-982.0' slicks on contact
— v. irregular, fluted slicks, 30° carb. filled, striae 30° to vertical
MUDSTONE med gray – some silty beds within
-986'
-987' ← S 3 sets of slicks 40° & 65°CA. All have parallel slickensides at 45° rake, wavey fluted slicks, no filling
-993.3' ← S rough surface vertical fracture in sandy bed extending into mudstones, terminating on organic bed parting trace coal on fracture
← @ 995 pair of wavey clay slicks, rake striae
-996.1' ← abrupt contact
SILTSTONE with interbedded fine Sandstone beds, irregular wavey bedding common
-999.3' — sharp contact
← slightly curving fract on side of core
← rough fract 1001'-1002.6' MED. SANDSTONE
-1004.4' — v. sharp contact
← dip slip slicks
} high organic, some coal
-1006.7'
— 1005.6 vert. fract in sandy bed extends into mudstone below
MUDSTONE 1004.4 – 1006.7 high organic black w/ Tr. coal occurrences.
} shaley — S clay slicks near dip slip, parallel pair
-1012.7' —— abrupt contact
1014.5 – 1021.5 fracts parallel core. top of fract. filled w/ coal, dies out in ss.
SILTSTONE interbedded w/ f. ss toward contact
Some worm holes (3) filled w/ calcite & tr. pyrite
-1018.8' — gradual contact
SANDSTONE f. to med. g.
← S long fract. leaves core
-1024.6' — gradual contact
← fracture, no filling 1025.2' MUDSTONE shaley 1026'-1027'
-1027
← 2 slicks, near dip slip.

Drilling Interval	% Core Recovered	Core Size	RQD	Sample Interval	photos
					photo 1 981.6 carbonate filling clay slicks
					photo 2 vertical fracts. (2) 1 cm. apart

Drill Site:
N: E:
Started:
Completed

Collar Elevation:
Bearing:
Inclination:
Total Depth:

Sandia National Laboratories
Logged by: Ron Grainken
Log Version:
Log Date: Mar 11, 2002

Raton Basin Project
Hole No: CH-4
Scale: 1" = 10' (1:120)
Sheet 15 of 34

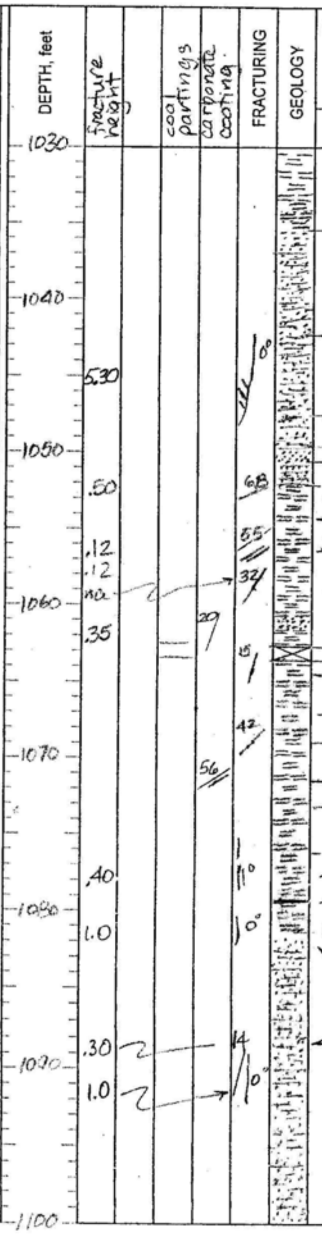

COMMENTS:

Avg. Core Recovery/ Hole

Descriptive Geology

MUDSTONE

1035.8' — gradational cont

FINE SANDSTONE - SILTSTONE

med. gray, w/ irregular bedding features, little natural fracturing

1042.3' — open vertical fracture, narrow half of core shows numerous petal fractures - caused by drilling; they only show on the narrow half

1047.6'

1049.6' fine sandstone
1050.8

1052.0 — gradual contact

v. wavey slides

MUDSTONE - some siltstones.

shaley

← pair of barren clay slicks, parallel

← clay slickensides.

← 20% filled fract. carbonate

1062.5' desorp. sample
1063.4'

1064.7 ← clay slickensides, v. irregular surface, slicks parallel dip.

shaley

1069' - fracture, uncoated, planar.

1071.3 50% carbonate filled slides — nearly planar. parallel pair

1073
shaley
1076

← 2 vertical fracts 1 cm. apart - no mineral coating. in black mudst.

← coal in high organic mudstone - black.

1081.4 — abrupt contact

← 1ft rough surface fract on edge of core, no filling.

SILTSTONE - FINE SANDSTONE

Drill induced parting in more shaley units 1 per .10 or .20 ft.

some irregular coal "veins"

← 14° dip slip slickenside at nearly right ∠ to fracture

Drilling Interval	% Core Recovered	Core Size	RQD	Sample Interval	photos
					photo 7,8 1046' petal fractures

Raton Basin Project
Hole No: CH-4
Scale: 1" = 10' (1:120)
Sheet 16 of 34

Sandia National Laboratories
Logged by:
Log Version:
Log Date: Mar 11, 2002

Collar Elevation:
Bearing:
Inclination:
Total Depth:

Drill Site:
N: E:
Started:
Completed

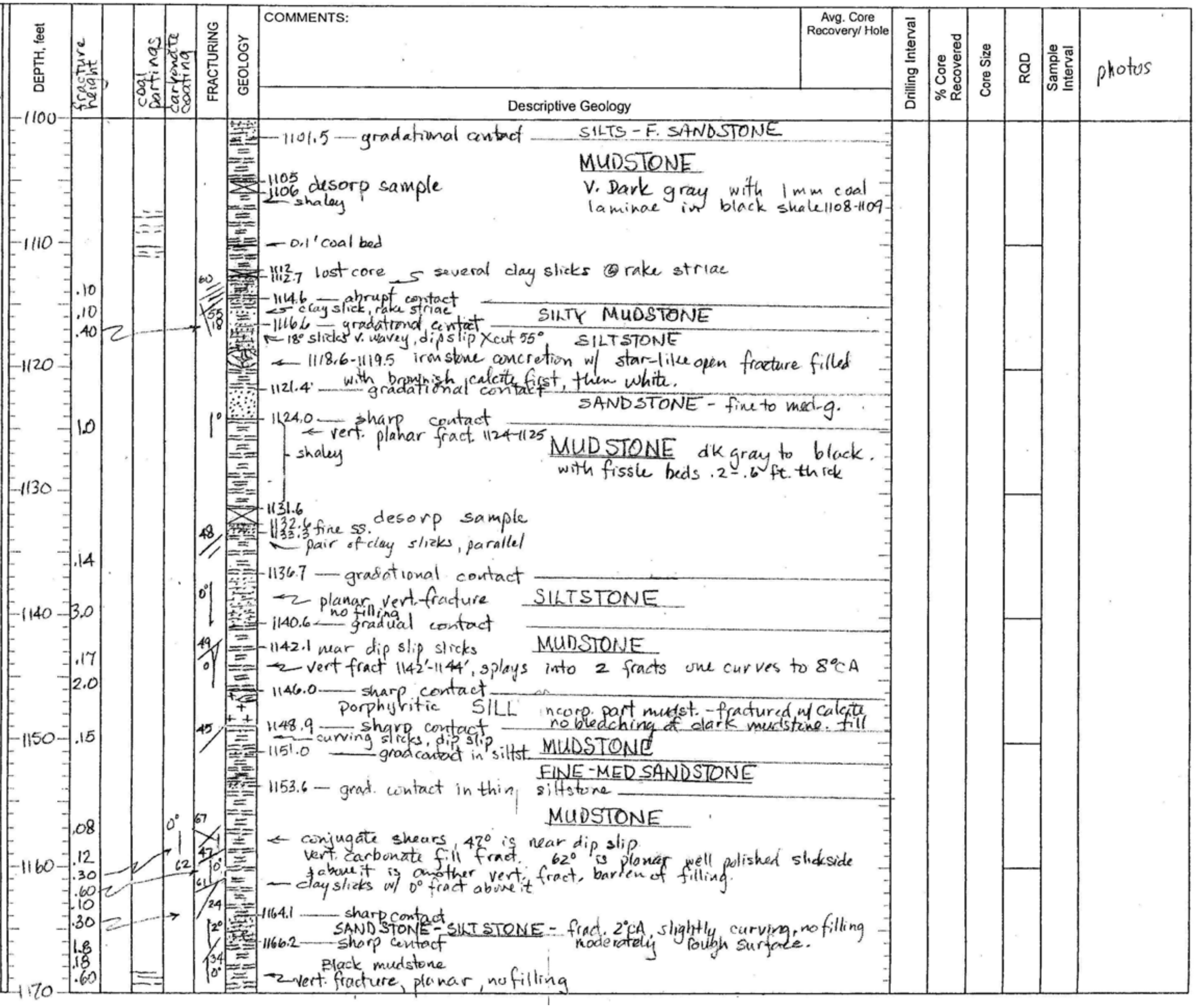

1101.5 — gradational contact — SILTS - F. SANDSTONE

MUDSTONE

1105
1106 desorp sample
← shaley

V. Dark gray with 1mm coal laminae in black shale 1108-1109

← 0.1' coal bed

1112
1112.7 lost core ← several clay slicks @ rake striae

1114.6 — abrupt contact
← clay slick, rake striae

SILTY MUDSTONE

1116.6 — gradational contact
← 18° slicks v. wavey, dip slip X cut 55°

SILTSTONE

← 1118.6-1119.5 ironstone concretion w/ star-like open fracture filled with brownish calcite first, then white.

1121.4' — gradational contact

SANDSTONE - fine to med-g.

1124.0 — sharp contact
← vert. planar fract. 1124-1125
shaley

MUDSTONE dk gray to black. with fissle beds .2-.6 ft. thick

1131.6
1132.6 fine ss. desorp sample
1133.3
← pair of clay slicks, parallel

1136.7 — gradational contact
← planar vert-fracture no filling

SILTSTONE

1140.6 — gradual contact

MUDSTONE

1142.1 near dip slip slicks
← vert fract 1142'-1144', splays into 2 fracts one curves to 8°CA

1146.0 — sharp contact

Porphyritic SILL ncorp. part mudst. - fractured w/ calcite fill no bleaching of dark mudstone.

1148.9 — sharp contact
← curving slicks, dip slip

MUDSTONE

1151.0 — grad contact in siltst

FINE-MED SANDSTONE

1153.6 — grad. contact in thin siltstone

MUDSTONE

← conjugate shears, 47° is near dip slip vert. carbonate fill fract. 62° is planar well polished slickside
& above it is another vert. fract, barren of filling.
← clay slicks w/ 0° fract above it

1164.1 — sharp contact

SANDSTONE - SILTSTONE - fract. 2°CA, slightly curving, no filling moderately rough surface.

1166.2 — sharp contact

Black mudstone
← vert. fracture, planar, no filling

Raton Basin Project
Hole No: CH-4
Scale: 1" = 10' (1:120)
Sheet 17 of 34

Sandia National Laboratories
Logged by: Ron Groichen
Log Version:
Log Date: Mar. 12, 2002

Collar Elevation: .
Bearing:
Inclination:
Total Depth:

Drill Site:
N:
E:
Started:
Completed

COMMENTS:
Better locate shale character with a column designation as such & column cartooning of it.
2.0' dia. core

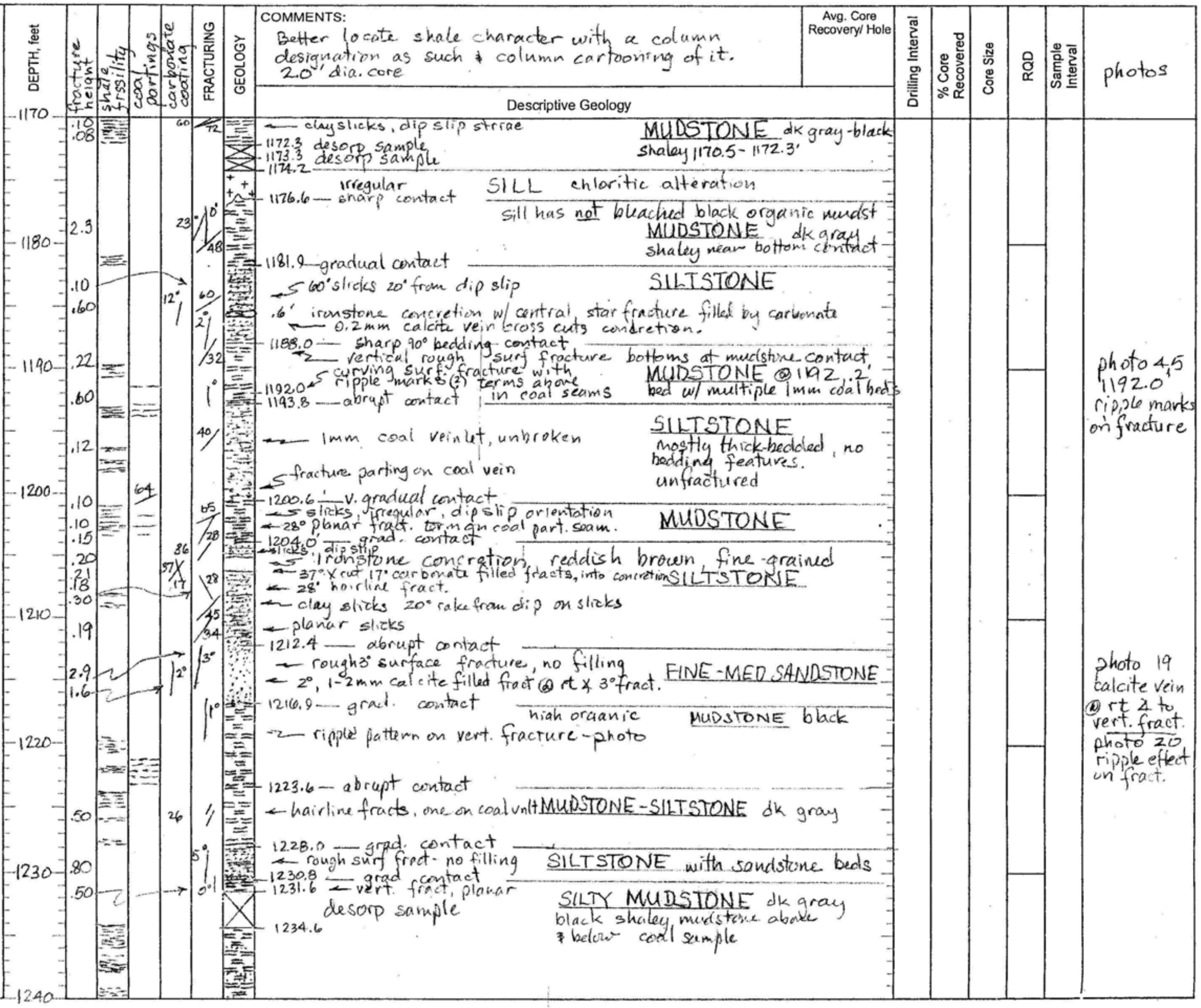

← clayslicks, dip slip strrae
1172.3 desorp sample
1173.3 desorp sample
1174.2
irregular
1176.6 — sharp contact
1181.9 — gradual contact
← 60° slicks 20° from dip slip
.6' ironstone concretion w/ central star fracture filled by carbonate
← 0.2mm calcite vein cross cuts concretion.
1188.0 — sharp 90° bedding contact
← vertical rough surf fracture bottoms at mudstone contact,
← curving surf. fracture with ripple marks(?) terms above in coal seams
1192.0
1193.8 — abrupt contact
← 1mm coal veinlet, unbroken
← fracture parting on coal vein
1200.6' — v. gradual contact
← slicks, irregular, dip slip orientation
← 28° planar fract. term on coal part. seam.
1204.0' — grad. contact
← slicks, dip slip
← Ironstone concretion, reddish brown, fine-grained
← 37° X cut 17° carbonate filled fracts, into concretion
← 28° hairline fract.
← clay slicks 20° rake from dip on slicks
← planar slicks
1212.4 — abrupt contact
← rough 3° surface fracture, no filling
← 2°, 1-2mm calcite filled fract @ rt ∡ 3° fract.
1216.9 — grad. contact
← ripple pattern on vert. fracture - photo
1223.6 — abrupt contact
← hairline fracts, one on coal vnlt
1228.0 — grad. contact
← rough surf fract - no filling
1230.8 — grad contact
1231.6 ← vert. fract, planar
desorp sample
1234.6

MUDSTONE dk gray-black
shaley 1170.5 - 1172.3'

SILL chloritic alteration

sill has not bleached black organic mudst
MUDSTONE dk gray
shaley near bottom contact

SILTSTONE

MUDSTONE @ 1192.2'
bed w/ multiple 1mm coal beds

SILTSTONE
mostly thick-bedded, no bedding features.
unfractured

MUDSTONE

fine-grained SILTSTONE

FINE-MED SANDSTONE

high organic MUDSTONE black

MUDSTONE-SILTSTONE dk gray

SILTSTONE with sandstone beds

SILTY MUDSTONE dk gray
black shaley mudstone above & below coal sample

photo 4,5
1192.0'
ripple marks on fracture

photo 19
calcite vein @ rt ∡ to vert. fract.
photo 20
ripple effect on fract.

Raton Basin Project
Hole No: CH-4
Scale: 1" = 10' (1:120)
Sheet 18 of 34

Sandia National Laboratories
Logged by: Ron Graichen
Log Version:
Log Date: Mar. 12, 2002

Collar Elevation:-
Bearing:
Inclination:
Total Depth:

Drill Site:
N: E:
Started:
Completed

COMMENTS: core dia. 2.0'

Avg. Core Recovery/ Hole

Drilling Interval | % Core Recovered | Core Size | RQD | Sample Interval | Photos

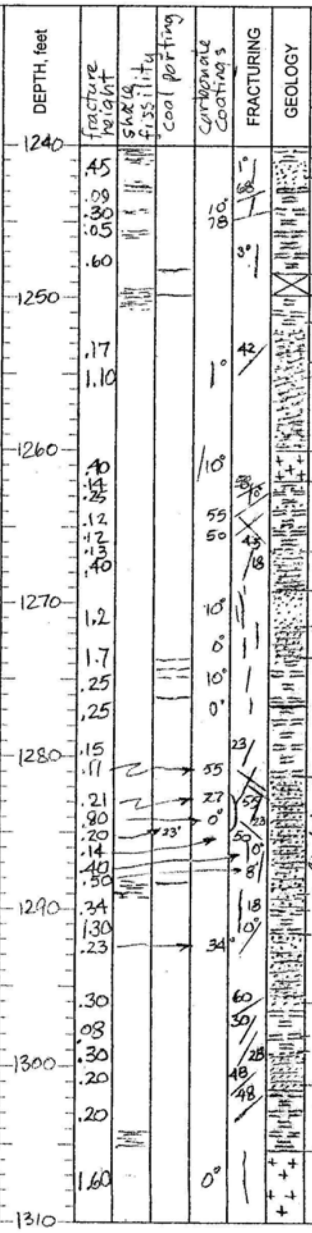

Descriptive Geology

1240.9 abrupt contact — mudstone

1242 sandstone bed, vert. fract. no filling

SILTSTONE - MUDSTONE dk gray to black

1248.3

1249.9 desorp sample

1251.4 — grad. contact

← planar slicks, striae 20° rake from dip

SILTSTONE - some fine sandst little fracturing

1254.2

← 0.2mm calcite vnlt cutting a poorly developed ironstone concretion

no bleaching of black siltstones on contact.

1260.0 — sharp contact

1mm calcite vn

SILL altered to chlorite, sill rock effervesces in HCl

1262.0 — sharp contact

← set of slicks

50°-45° conjugate shears

SILTY MUDSTONE

1266.7 — grad. contact

← planar fract.

SILTSTONE

1269.2 — abrupt contact

several close spaced 10° fracts, rough surface, no filling.

FINE — MED SANDSTONE

1271.5 — grad. contact

1271-1272' two parallel fracts 1cm. apart

SILTSTONE

1273.6 — grad. contact

MUDSTONE dk gray - black

← .2' coal seam

← planar fract.

1281.3 — gradual contact

← conjugate shears glassy slicks 27° is dip slip other's rake slip

SILTSTONE dk - med. gray

← 1283. arcuate fracture 0° to 30° and 0.80' long

← @ 1284 planar fract. 50° CA

← 1286.5 vert fract in SS w/ 15X30mm patch pyrite

← 1287, planar fract 8° CA

1289.0'

← planar fract. 18°

1290.0 mudstone

1291.7

1290-1291 vert fract, planar, no filling

1295.9 — gradual contact

1298' fluted polished slicks, dip slip

MUDSTONE black

1299' — abrupt contact

SILTSTONE

1301.6 — v. gradual contact

← planar slicks

MUDSTONE - black

1306.4 — sharp contact

← gently arcuate fracture in sill rock

SILL

photo 29 conjugate shears

photo 31 planar slickside shear

photo 33 arcuate fracture in sill

Drill Site:
N: E:
Started:
Completed

Collar Elevation:
Bearing:
Inclination:
Total Depth:

Sandia National Laboratories
Logged by: Ron Graichen
Log Version:
Log Date: Mar. 12, 2002

Raton Basin Project
Hole No: CH-4
Scale: 1" = 10' (1:120)
Sheet 19 of 34

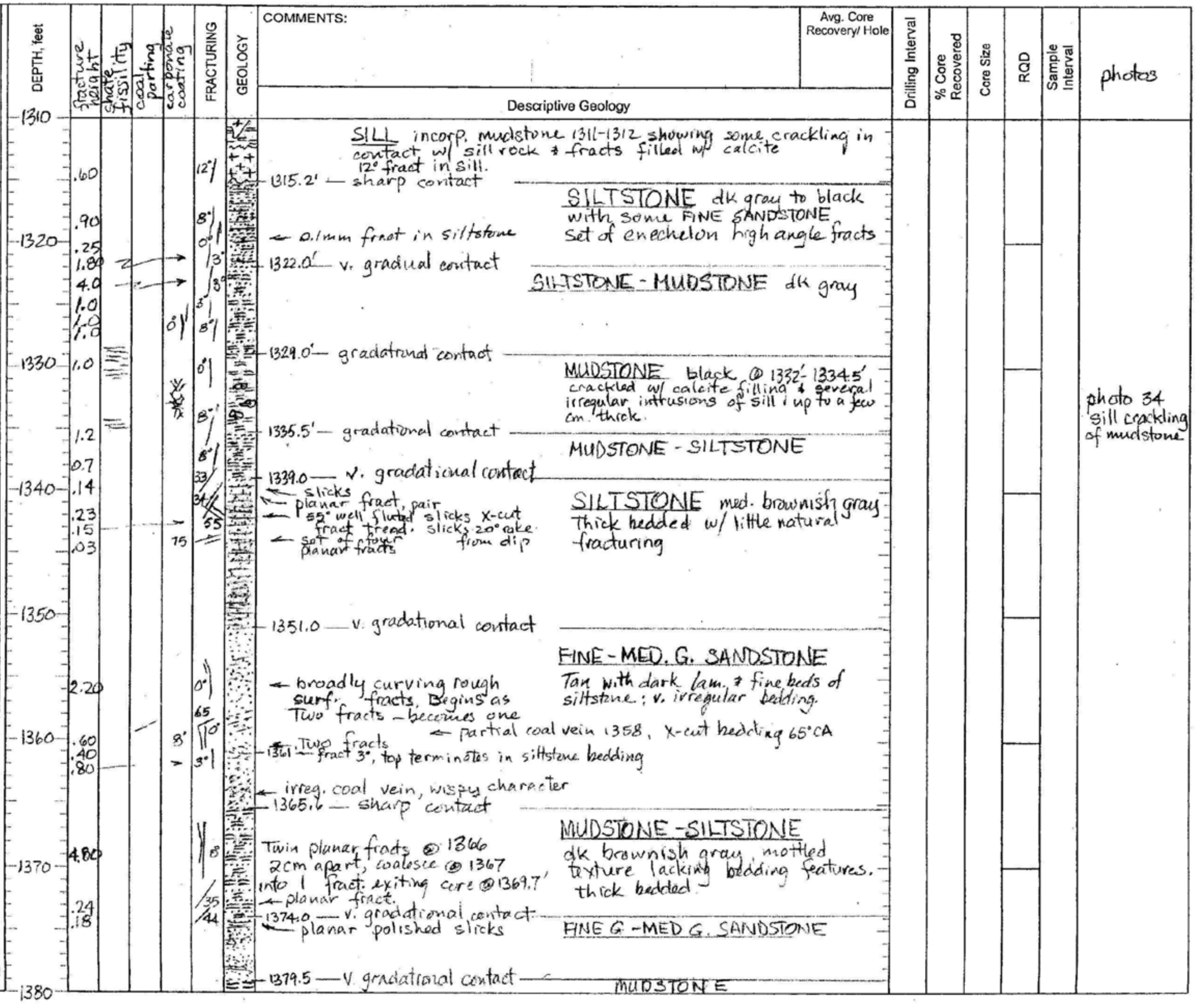

SILL incorp. mudstone 1311-1312 showing some crackling in contact w/ sill rock & fracts filled w/ calcite

12° fract in sill.

1315.2' — sharp contact

SILTSTONE dk gray to black with some FINE SANDSTONE Set of enechelon high angle fracts

← 0.1mm fract in siltstone

1322.0' — v. gradual contact

SILTSTONE - MUDSTONE dk gray

1329.0' — gradational contact

MUDSTONE black @ 1332'-1334.5' crackled w/ calcite filling & several irregular intrusions of sill i up to a few cm. thick.

1335.5' — gradational contact

MUDSTONE - SILTSTONE

1339.0 — v. gradational contact

← slicks

← planar fract, pair

← 55° well fluted slicks x-cut fract trend. slicks 20° rake from dip

← set of four planar fracts

SILTSTONE med. brownish gray Thick bedded w/ little natural fracturing

1351.0 — v. gradational contact

FINE - MED. G. SANDSTONE

Tan with dark lam. & fine beds of siltstone; v. irregular bedding.

← broadly curving rough surf. fracts. Begins as Two fracts — becomes one

← partial coal vein 1358, x-cut bedding 65°CA

1361 ← Two fracts
fract 3°, top terminates in siltstone bedding

← irreg. coal vein, wispy character

1365.6 — sharp contact

MUDSTONE - SILTSTONE

dk brownish gray mottled texture lacking bedding features. thick bedded

Twin planar fracts @ 1366 2cm apart, coalesce @ 1367 into 1 fract. exiting core @ 1369.7'

← planar fract.

1374.0 — v. gradational contact

← planar polished slicks

FINE G - MED G. SANDSTONE

1379.5 — V. gradational contact

MUDSTONE

photo 34
sill crackling
of mudstone

Sandia National Laboratories
Logged by: Ron Graichen
Log Version:
Log Date: Mar. 13, 2002

Raton Basin Project
Hole No: CH-4
Scale: 1" = 10' (1:120)
Sheet 20 of 34

Collar Elevation:
Bearing:
Inclination:
Total Depth:

Drill Site:
N: E:
Started:
Completed

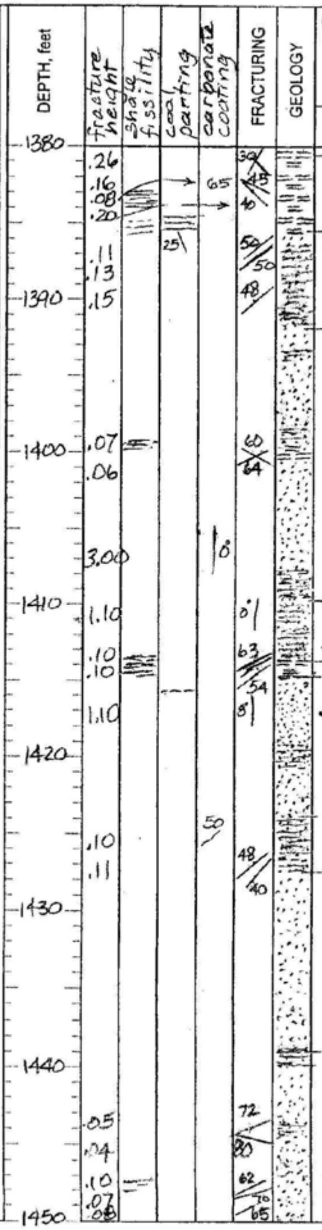

COMMENTS:

Avg. Core Recovery/ Hole

Descriptive Geology

1380.7 curving, wavey slicks near dip slip movement

45° planar fract, 65° slicks

@ 1382, planar fract.

MUDSTONE dkgray – black

@ 1384-1385 fract. ~~set~~ petal fracts (1) per 0.1ft, curvilinear 70°CA

1385.8 — abrupt contact

coal" vein" 25°CA ; 50° planar fract.

SILTSTONE med. gray poorly developed wispy bedding

planar rough surf fract.

1392.0 — sharp contact

MED. G. SANDSTONE

lt. gray color, not fractured wispy med. gray bedding

← 0.4' black shaley bed, cross-cutting slicks, rake angle slicks

broad curving fract. w/ 10% carb. filling one end, comes into core on top, curving to center & back out at bottom, Rough surf. patchy pyrite filling 1X3cm.

silty 1408-1409.8

1409.8 — abrupt contact

planar broad curving fract.

slicks 63°CA dip slip, pair .10' apart

SILTSTONE med. gray

1413.9 — abrupt contact

1415.9 — abrupt contact

MUDSTONE black

45°CA petal fracts in mudstone at right ∡s to slickensides 54°CA

petal fracts 1 to 2 cm apart

2 planar fract. rough surface.

FINE G. – MED G. SANDSTONE

some near 90°CA bedding with bioturbidite features. not fractured.

1423.8 — grad. contact

← wispy coal vein parting

slicks, wavey dip slip

1427.7 —

SILTSTONE

SANDSTONE med. gray

med. grained & fine grained

absolutely no natural fracturing!

1439.0' — sharp
1440.0 — sharp contacts - SILTSTONE

planar fracts in thin siltstone bed.

← slicks 62°, planar fract. 70°CA

planar fract. 65°CA

Drilling Interval

% Core Recovered

Core Size

RQD

Sample Interval

photos

Raton Basin Project
Hole No: CH-4
Scale: 1" = 10' (1:120)
Sheet 21 of 34

Sandia National Laboratories
Logged by: Ron Graichen
Log Version:
Log Date: Mar 13, 2002

Collar Elevation:
Bearing:
Inclination:
Total Depth:

Drill Site:
N: E:
Started:
Completed

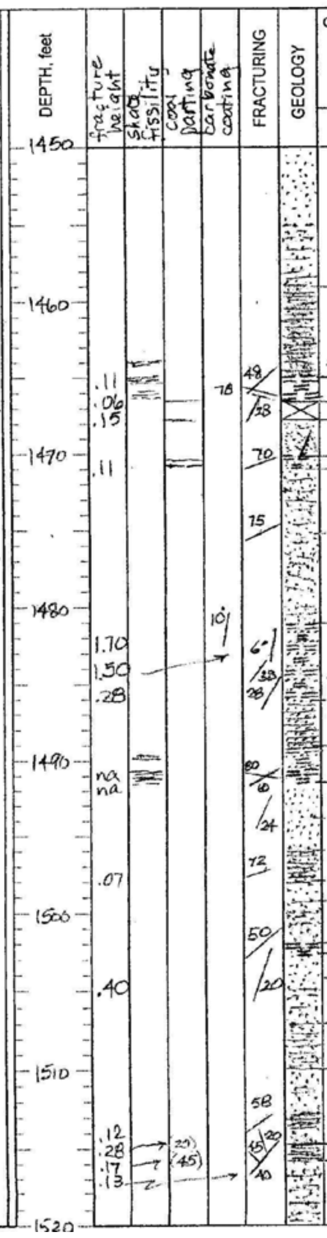

COMMENTS:

Avg. Core Recovery/ Hole

Descriptive Geology

cont. **SANDSTONE** lt. gray ss with darker, finer grained beds & laminations generally ⊥ CA. No natural fracturing

1459.0' — grad. contact

SILTSTONE

1465.1 v. wavey polished slicks, dip slip cut by pair of 78° slicks

1465.0 — sharp contact

MUDSTONE

1466.8
1467.8 desorp sample

sharp contact

1-2mm coal vn 25°CA

SANDSTONE fine to med. grain med. gray

1470.1
1471.0 black silty mudstone bed, sharp contacts
70° slicks, curved polished slicks

1475.4 planar fracture

1.7' rough surface fracture w/ heavy druze of calcite xtals — open 50% ?

1481.2 — gradational contact

SILTY MUDSTONE dk gray

1481.5 - 1483.0 planar fract. en echelon to 10° fract. above

clay slicks 38, 28 dip slip planar

1486.0 — grad. contact

SILTSTONE dk brown thick bedded mottled texture

1489.0 — abrupt contact

SILTY MUDSTONE dk brownish gray

conjugate shears in mudstone, interval rubblized

1491.5 — abrupt contact

SANDSTONE fine to med grained. Dull greenish gray localized subtle thin bedding

1493.8 planar fract. 30% pyrite filled

1496
1498 siltstone 72° slicks, curved dip slip

60° slicks, curved near dip slip

1502
1502.8 silty mudstone

1504.1 slicks 10° from dip slip, planar

1507 — grad. contact

no fracturing

SILTSTONE thick bedded dk gray mottled texture

1510 — grad. contact

SANDSTONE fine-med. grained

dip slip slicks, mildly fluted dip slip.

1514.5
1515.7 silty mudstone bed

40° v. irreg slicks offsetting 45° planar fracture

Drilling Interval
% Core Recovered
Core Size
RQD
Sample Interval
photos

photo 35
1504'
slickensides in thick-bed sandstone

Raton Basin Project
Hole No: CH4
Scale: 1" = 10' (1:120)
Sheet 22 of 34

Sandia National Laboratories
Logged by: Ron Graichen
Log Version:
Log Date: Mar 13, 2002

Collar Elevation:
Bearing:
Inclination:
Total Depth:

Drill Site:
N: E:
Started:
Completed

DEPTH, feet | fracture height | shale fissility | coal parting | carbonate coating | FRACTURING | GEOLOGY | COMMENTS: | Avg. Core Recovery/ Hole | Drilling Interval | % Core Recovered | Core Size | RQD | Sample Interval | photos

COMMENTS: core dia. 2.00 inches

Descriptive Geology

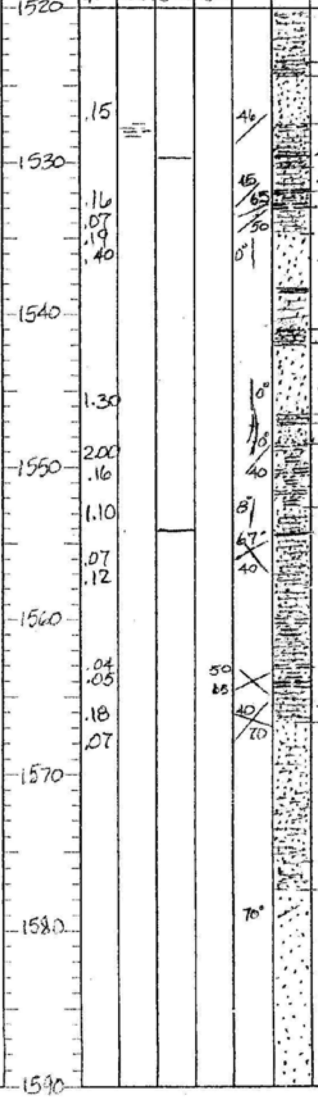

1523.7 – 1524.6 – siltstone, grad. contacts
slicks
1527.6 — grad. contact
thin coal 1529.5
rough slicks
1532 – 1533 silty mudstone ← 65° deeply fluted slicks ← 50° deeply fluted, dip slip slicks.
1534.9 — abrupt contact
← .1mm fract in SS. both top/bottom feather out in SS.
.2' mudstone bed
1541.0 – 1542.0 siltstone sharp contacts
Tr. pyrite in 1.3' fracture
1546.5 — abrupt contact
1547.2 siltstone
1548.6 fine SS.
← 40° planar fract
← 8° fract. rough surface
1552.8 — grad. contact fine sandstone
1554.3 — 0.1' coal bed
← cross cutting dip slip slicks
no fractures
cross-cutting dip slip slickensides
wavey. curving slicks 20° rake from dip
1566.8 — gradational contact
← 70° v. rough slickensides
no natural fractures
1577.6 — sharp contact
← wispy coal vein, not broken

cont. SANDSTONE

SILTSTONE brown thick bedded & mottled texture to 1532

dip slip, set of 3 parallel slip surfaces

SANDSTONE med. grained
lt. gray. Mostly wispy irregular bedding features. Little fracturing. Some worm burrow textures.
No fracturing.
Some wispy hairline carbon (coal) veinlets

SILTY MUDSTONE

SILTSTONE brown mottled texture thick bedded

SANDSTONE fine grained, some med. grained, interbedded with dk gray silty laminations, common. Some worm tracks

SANDSTONE coarse-grained lt. tan thick bedded lacking bedding features.
Weakly reactive carbonate cement

Raton Basin Project
Hole No: CH-4
Scale: 1" = 10' (1:120)
Sheet 23 of 34

Sandia National Laboratories
Logged by: Ron Graichen
Log Version:
Log Date: Mar. 14, 2002

Collar Elevation:
Bearing:
Inclination:
Total Depth:

Drill Site:
N:
E:
Started:
Completed

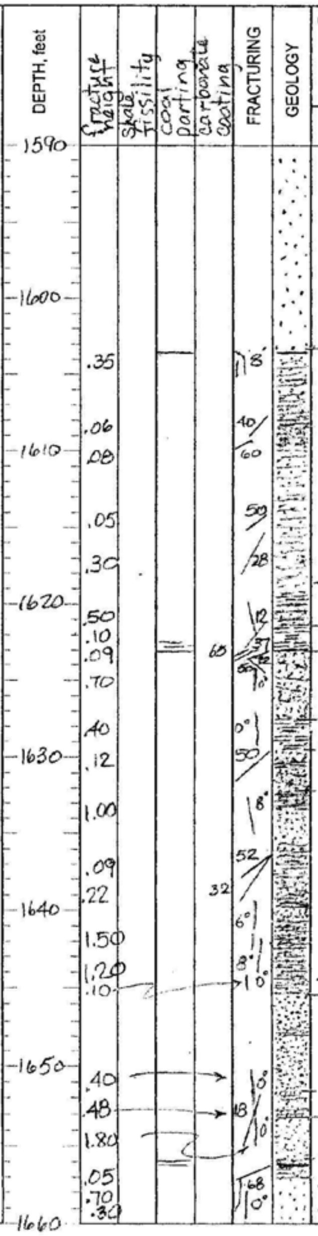

COMMENTS:

Avg. Core Recovery/ Hole

Descriptive Geology

cont. SANDSTONE coarse grained thick bedded

1603.6 —— sharp contact
SILTSTONE brownish gray thick bedded, w/ wispy faint carbon streaks – mostly high angle.
← 0.4' black mudstone w/ 1cm. coal seam
← pair of curving fracts - suspect drilling related.
← partially broken slickensides
Little-fracturing

poorly developed, curving slicks terminating against a coal vein
planar slicks, dip slip
← 0.1' ironstone concretionary band, rust red.
← long curving 12° fract, rough surf offset by 37° clayey slickensides
1621.7 —— sharp contact
MUDSTONE dk brown – black
1623.2 —— grad. contact
← 1cm. coal bed 65° pair of slicks .2' apart
← cross cutting slicks 72° & 60° in mudstone @ 1622.7; 0° vert. fract in coal zone extends into sandstone below
1627.4 silty mudstone
SANDSTONE med to c.g. with silty mudstone interbeds.
1629.5 ← curving slicks surface
one vert. fract. ends terminate in ss.
1632.2 —— gradual contact
gently curving rough surface fracture. Top fades into sandstone, bottom leaves core.
FINE SANDSTONE - SILTSTONE
Dip slip slicks
curving slicks 15° rake from dip
← long planar fracture, en echelon character - fracture parallels, faint carbon veinlets above it, photo
← a second enechelon fracture, on a larger scale than above.
← fracture in 0.1' ss bed, terminations deflected into silty laminae. photo
1645.4 —— grad. contact
SANDSTONE fine to med. grained.
← 0.4' rough surface fract. parallels wispy carbon trash occurrences above it.
1651.8 siltstone
1653.0 ←—— 18° dip slip slickensides dip slip; offsets 0° long fract.
fine sandstone
1655.9 siltstone ←—— 1-2mm coal seams in 0.3' black mudstone bed.
1657.0 —— sharp contact
← 68° slicks 10° from dip
← two 0° fracts rough surf., parallel
COARSE G. SANDSTONE

Drilling Interval
% Core Recovered
Core Size
RQD
Sample Interval
photos

photo 36
12° fracture terminated on slickside 1621 ft.

photo 1
enechelon fracture 1640'.
photo 2
1644.5'
fracture in SS. bed

Raton Basin Project
Hole No: CH-4
Scale: 1" = 10' (1:120)
Sheet 24 of 34

Sandia National Laboratories
Logged by: Ron Gratchen
Log Version:
Log Date: Mar 14, 2002

Collar Elevation:
Bearing:
Inclination:
Total Depth:

Drill Site:
N:
E:
Started:
Completed

DEPTH, feet	fracture height	shale fissility	coal parting	carbonate coating	FRACTURING	GEOLOGY	COMMENTS:	Descriptive Geology	Avg. Core Recovery/ Hole	Drilling Interval	% Core Recovered	Core Size	RQD	Sample Interval	photos
1660								cont. COARSE G. SANDSTONE tan thick bedded minor bedding features.							
	2.90				4°		long rough surface fract enters + leaves core.								
1670	4.00				0°		En echelon to one above	Only vertical fracturing							
							1675.6 — sharp contact 1677.0 silty mudstone								
1680							1680.0 planar slicks	F.G. SANDSTONE							
	.12				52 90°		1681.0 — abrupt contact								
			—				2cm. high carbon bed in silty mudstone bed.	SANDSTONE med. g.							
	.40				12°		single fract term. in SS.								
	1.50				0°		fract begins in silty bed, parallels core axis + exits core @ 18° angle long planar, rough surface								
							1687.5 — grad. contact								
1690	.16				48		planar slicks, some gouge	SILTSTONE - MUDSTONE							
	.23				38		wavey fluted slicks, dip slip 38°								
	1.70						1692.0 — V. grad contact second 38° slip curves into core axis and out of core - near dip slip slicks photo	MUDSTONE gray + brown gray							photo 3,4 curving slickensides
	.20				29										
	.15	≡			45										
					28		broken core 28° slicks, parallel pair 0.1' apart, slicks 20° from dip slip								
	.06			73			1699.0 — very grad contact								
1700	.04	≡			70		73° smooth planar rake slip								
	.03	≡		70				SILTSTONE							photo 5 wispy carbon trash in siltstone
	.10				35		multiple slicks orient. these most prominent - in mud stone bed 0.5' thick								
	.16			45	50		1706.0 — gradational contact								
	.12														
	.90			2°			rough surface fract gently curves out of core. Top fades into SS.	SANDSTONE fine-med grained lt. gray - not fractured							
1710															
							1712.0 1712.9 lost core drilling error								
1720															
	.11				60		1722.4 — sharp contact irregular rough slicks	SILTY MUDSTONE							
							1727.0 — V. grad. contact	F.G. SANDSTONE							
1730															

Raton Basin Project
Hole No: CH-4
Scale: 1" = 10' (1:120)
Sheet 25 of 34

Sandia National Laboratories
Logged by: Ron Graichen
Log Version:
Log Date: Mar. 14, 2002

Collar Elevation:
Bearing:
Inclination:
Total Depth:

Drill Site:
N:
E:
Started:
Completed

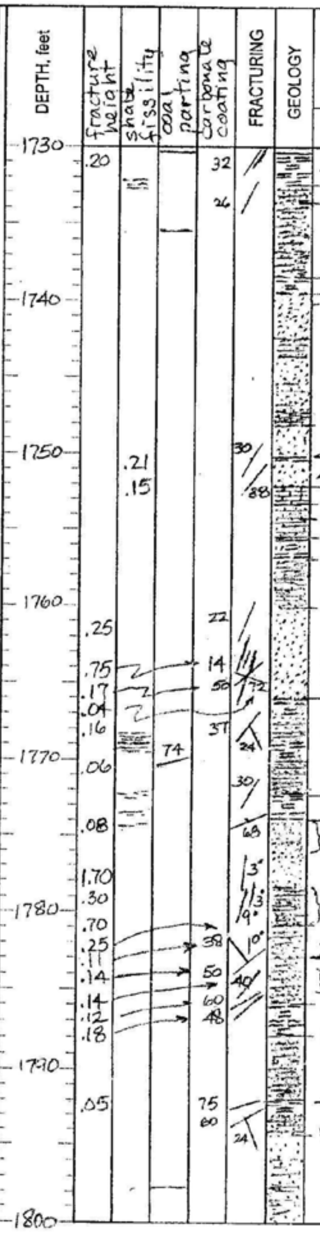

COMMENTS:
core condition poor 1730'–1732.5', drilling disturbed.

Avg. Core Recovery/ Hole

Descriptive Geology

← 1.5 mm coal seam ← sharp contact @ page break **MUDSTONE**
← pair of slicks, parallel 0.2 apart, slicks 20° dip
1732.4 — abrupt contact
1733.7 siltstone 26° planar fract. **FINE SANDSTONE**
worm bore pathways apparent - with carbon material outlining them.
1738.6 mudstone
1739.7 — abrupt contact
MED. G. SANDSTONE gray to dk gray where interbedded w/ fine sands
Little fracturing
1747.4
1748.1 siltstone
← rake slicks, wavey surface
1752.2 limestone concretion ?
1753.3
1754.5 — grad. contact
1755.5
1757.0 mudstone drill caused core parting one/3cm. aver.
SILTSTONE dk gray interbedded with f.g. sandstone, mostly thick bedded
no fracturing
1760.0 — sharp contact
fracture, may not be natural
set of 3 fracts' rough surface cross-cut by 2 slip surfaces 50° & 72°
FINE - MED G. SANDSTONE
1766.0 — sharp contact
1767.0 petal fracts in mudstone curving surfaces - 75° CA
SILTSTONE dk gray to dk brownish gray
← planar 37° slicks, 20° rake to dip
24° planar fracture ← 74° slicks along 3mm coal seam
1772.4 mudstone 1772-1773 multidirectional slickensides
1774.0 — abrupt contact
f.g. ← 68° clay slicks curving, dip slip
SANDSTONE fine to med. grained thick-bedded to 1778; interbedded with siltstones to 1781.
long rough surf fract. in/out core several parallel it.
interbedded silts/sands
1780.9 — gradational contact
← vert fract
← cross-cut slicks, both dip slip
MUDDY - SILTSTONE dk gray
clay slicks
1786.0 — abrupt contact
MUDSTONE rubblized by drilling
1788.0 — abrupt contact
SILTSTONE dk gray to mottled brownish gray
← multiple high angle slicks one/1-2cm; creating discing, ← clay slicks X-cutting 20° rake to dip.
1794.6 — grad contact
SANDSTONE fine to med. g. interbedded with med. gray silty beds - laminations ⊥ CA
parting ⊥ CA on organic laminae in 0.1' siltstone bed.

Drilling Interval
% Core Recovered
Core Size
RQD
Sample Interval

Photos

photo 6
@ 1736'
coal parting

photo 7
@ 1764
fracture set

photo 8
petal fracts
1766'

Sandia National Laboratories
Logged by: Ron Grigsby
Log Version:
Log Date: Mar 15, 2002

Raton Basin Project
Hole No: CH-4
Scale: 1" = 10' (1:120)
Sheet 26 of 34

Collar Elevation:
Bearing:
Inclination:
Total Depth:

Drill Site:
N: E:
Started:
Completed

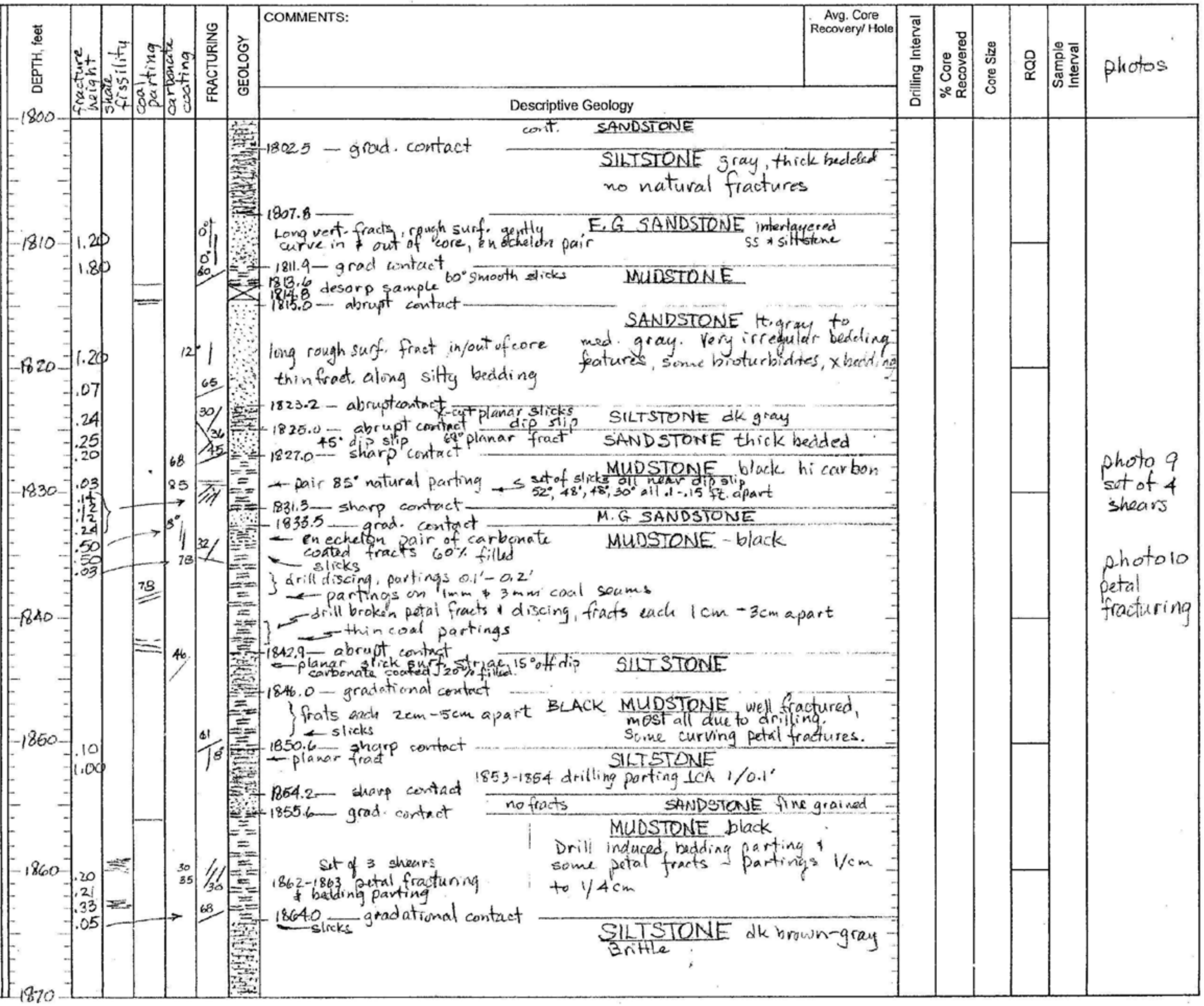

cont. SANDSTONE

1802.5 — grad. contact

SILTSTONE gray, thick bedded
no natural fractures

1807.8 —

Long vert. fracts, rough surf. gently curve in & out of core, en echelon pair

E.G SANDSTONE interlayered SS & siltstone

1811.9 — grad contact

60° smooth slicks

MUDSTONE

1813.6
1814.8 desorp sample

1815.0 — abrupt contact

SANDSTONE lt. gray to med. gray. Very irregular bedding features, some bioturbidites, x bedding

long rough surf. fract in/out of core

thin fract. along silty bedding

1823.2 — abrupt contact

X-cut planar slicks dip slip

SILTSTONE dk gray

1825.0 — abrupt contact

45° dip slip

68° planar fract

SANDSTONE thick bedded

1827.0 — sharp contact

MUDSTONE black hi carbon

← pair 85° natural parting

← set of slicks all near dip slip 52°, 48°, 48°, 30° all .1 - .15 ft. apart

1831.3 — sharp contact

M.G SANDSTONE

1833.5 — grad. contact

MUDSTONE - black

← en echelon pair of carbonate coated fracts 60% filled

← slicks

} drill discing, partings 0.1' - 0.2'

← partings on 1mm & 3mm coal seams

← drill broken petal fracts & discing, fracts each 1cm - 3cm apart

← thin coal partings

1842.9 — abrupt contact

← planar slick surf. striae 15° off dip carbonate coated 20% filled.

SILTSTONE

1846.0 — gradational contact

} frats each 2cm - 5cm apart

← slicks

BLACK MUDSTONE well fractured, most all due to drilling. Some curving petal fractures.

1850.6 — sharp contact

← planar fract

SILTSTONE

1853-1854 drilling parting ⊥CA 1/0.1'

1854.2 — sharp contact

no fracts

SANDSTONE fine grained

1855.6 — grad. contact

MUDSTONE black

Drill induced bedding parting & some petal fracts - partings 1/cm to 1/4cm

Set of 3 shears

1862-1863 petal fracturing & bedding parting

1864.0 — gradational contact

← slicks

SILTSTONE dk brown-gray Brittle

photo 9 set of 4 shears

photo 10 petal fracturing

Drill Site:
N:
E:
Started:
Completed

Collar Elevation:
Bearing:
Inclination:
Total Depth:

Sandia National Laboratories
Logged by: Ron Graichen
Log Version:
Log Date: Mar 15, 2002

Raton Basin Project
Hole No: CH-4
Scale: 1" = 10' (1:120)
Sheet 27 of 34

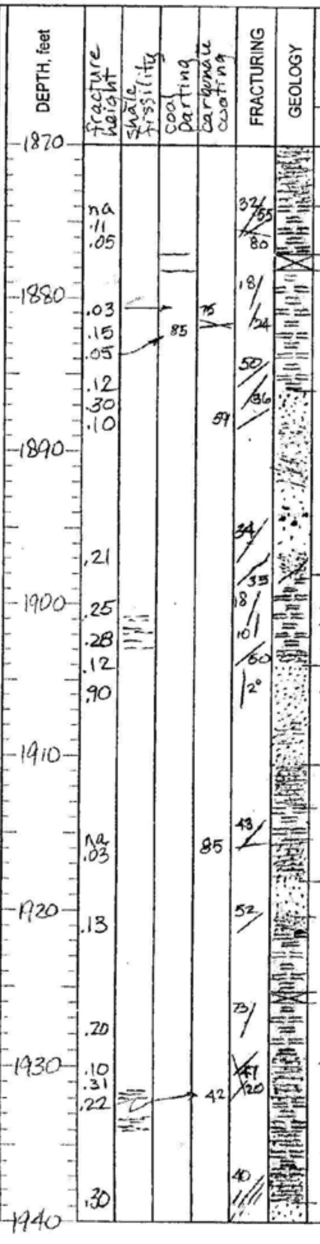

COMMENTS:

Avg. Core Recovery/ Hole

Descriptive Geology

cont. SILTSTONE dk gray mostly drill broken on bedding into 3cm - 5cm pieces

1874.0 — grad. contact
← natural planar fract.
← slicks x cutting

MUDSTONE black
some petal fracturing
abundant bedding parting due to drilling 2cm to 5cm.
carbon trash common

1877
1878 desorp sample
← slicks dip slip fluted
← planar fract
← x-cutting slicks carbonate filled
← slicks, striae 45° rake
1886.0 — v. grad. contact
← dip slip slicks
← planar slicks 20° rake from dip

some carbon trash in silty dk gray laminae

SANDSTONE dk silty & fine grained 1886 to 1891 becoming med. & coarse grained to 1895 & tan color.

pebble sized angular siltstone in c.g. ss.
← fract. planar along micaceous bedding plane
1898.0 sharp slickenside contact
v. wavey, polished slicks, general orientation

SILTSTONE - MUDSTONE
Black

← dip slip slicks
← 10° planar fract.
50° dip slip slicks
1904.0 — grad. contact
← long planar rough surf fract., fades into ss. above, leaves core below.

SANDSTONE tan with irregular gray silty bedding
Only 2° fracture present

1910.5 — abrupt contact
only drilling broken parting 0.1ft - 0.4ft SILTSTONE
1913.5 — abrupt contact
1915.4 — abrupt con multiple slicks Black MUDSTONE crumbly
← slicks
SILTSTONE
1918.0 — abrupt contact
no fractures SANDSTONE
1920.4 — sharp contact
← deeply fluted, dip slip slicks

MUDSTONE - SILTSTONE Black
1922 - 1924 drilling caused parting 0.1 ft to 0.2 ft spacing
also same 1926 - 1928, 1933 - 1934
1935 - 1936

1925.3
1925.9 desorp sample
← slicks, fluted dip slip
← very curvey slicks, dip slip 47°
← 20° cross-cuts 47, 42° slicks

← 40° shearing on contact mostly brittle rubble
1939.0 — abrupt contact SANDSTONE med. g.

Drilling Interval
% Core Recovered
Core Size
RQD
Sample Interval
photos

Raton Basin Project
Hole No: CH-4
Scale: 1" = 10' (1:120)
Sheet 28 of 34

Sandia National Laboratories
Logged by:
Log Version:
Log Date: Mar 16, 2002

Collar Elevation:
Bearing:
Inclination:
Total Depth:

Drill Site:
N:
E:
Started:
Completed

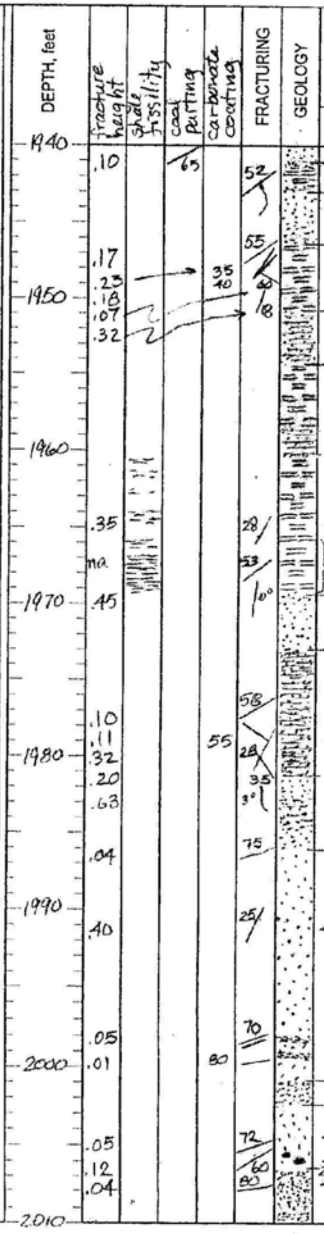

COMMENTS:

Avg. Core Recovery/ Hole

Descriptive Geology

1941.2 ← parting on coal seam 5mm
siltstone-mudstone 52° planar cont. fract.
1943.0 ← strongly curved slicks
no fractures

SANDSTONE med. grain lt. gray
several 1-3mm coal seams 60°CA

1946.5 — abrupt contact
← 55° slicks, planar @ 45° rake
← conjugate shears, slicks both dip slip

MUDSTONE dk gray
Broken

1950.9 — sharp contact
← slicks dip slip

SILTSTONE

1954.5 — abrupt contact
petal fracts. & core discing.
bedding partings 2-3cm apart in mudstone, wider in siltstone

MUDSTONE black

← shear slicks

← clay slicks, minor gouge
← core broken pieces

1969.5 — grad. contact
← vert. fract
no fractures

SANDSTONE med. g.

1973.0 — v. grad. contact

SILTSTONE

← dip slip. fluted slicks

← planar polished slicks
28° dip slip slicks
1981.5 — gradational contact
← 35°, 13, 90° strike change from 28
& v. wavey surface.
← planar, rough surface fracture; curves out of core

SANDSTONE fine to medium grained

1986.0 — v. grad contact
← fracture along f.g. carbon laminae - wavey surface.

SANDSTONE coarse to very coarse grained.
Tan color with bedding defined by finer grained seds. in thin beds and laminations.
Wavey, irregular bedding features common.

← v. rough fracture

sandstone not reactive to acid & impermeable

← wavey polished slicks on 2-4mm mudstone lamination, parallel pair 0.5' apart
← same

At 2006-2007.3', three beds 3mm to 5mm thick w/ pebble sized mudstone clasts

2001.0 — sharp contact
2002.7 — grad contact
fine-med. g. sandstone bed.

← fracture along v. thin carbon laminae
← slicks on 1mm coal seam
2007.5
← fract. on thin carbon laminae

sharp contact
SILTSTONE-FINE SANDSTONE

↙ bottom contact @ 2010-abrupt

Drilling Interval

% Core Recovered

Core Size

RQD

Sample Interval

photos

photo 11
1979.4 ft
slickensides
90° strike
difference

Sandia National Laboratories
Logged by: Ron Groichen
Log Version:
Log Date: Mar 10, 2002

Raton Basin Project
Hole No: CH4
Scale: 1" = 10' (1:120)
Sheet 29 of 34

Drill Site:
N: E:
Started:
Completed

Collar Elevation:
Bearing:
Inclination:
Total Depth:

COMMENTS: ,

Avg. Core Recovery/ Hole

Drilling Interval

% Core Recovered

Core Size

RQD

Sample Interval

DEPTH, feet	fracture height	shale fissility	coal parting	carbonate coating	FRACTURING	Descriptive Geology	photos
2010	—				90°	← hairline carbon trash parting SANDSTONE coarse to very coarse sandstone, thick bedded tan color	
	.04				76		
						arcuate rough surf. fract., terminates @ siltstone	
					18	2019.4 — sharp contact	
2020	.65					Siltstone + f.g. ss. dk brown SILTSTONE-FINE G. SANDSTONE	
					81	2022.0 — grad. contact	
	.20					← fract. in core, ends terminate in sandstone med to c.g. 2022-2024	
						2024.0	
	.04 .04			72 72		← cross-cutting 72° slicks	
						2027.4 — abrupt contact	
2030	.11					70, 90° coal partings on 3-4mm coal seams SANDSTONE tan, coarse to very coarse grained	
	.04		70	90	50	rough surface parting on carbon trash <1mm thick	
	.06		42		70	50° clay slicks parting on 2mm coal "vein"	
	.18				66	2035-2035.8 pebble size mudstone subangular clasts ← 66° planar slicks on 1mm mudstone laminae	
2040					75 63	fracture partings on carbon trash bedding laminae	
					8°	← coal patch = photo rough surface fracture	photo 12 coal patch
	.40						
	.08		65			← 65° parting on 3mm. coal seam	
2050					73	2049.7 — sharp contact 65° CA SILTSTONE dk gray	
	.05					2051.4 — sharp contact 85° CA	
	.06		72			← parting on wavy 1mm coal seam	
2060							
						2066.4 2067.4 siltstone	
2070	.90		70		5°	← linear, rough surface fract ; 70° coal parting on 2mm seam	
						2076.8 — desorp sample — sharp contact ?	
2080	.32			42		2078.2 ← slicks, 40° carbonate filled MUDSTONE Black	

Raton Basin Project
Hole No: CH-4
Scale: 1" = 10' (1:120)
Sheet 30 of 34

Sandia National Laboratories
Logged by: Ron Graichen
Log Version:
Log Date: Mar 16, 2002

Collar Elevation:
Bearing:
Inclination:
Total Depth:

Drill Site:
N:
E:
Started:
Completed

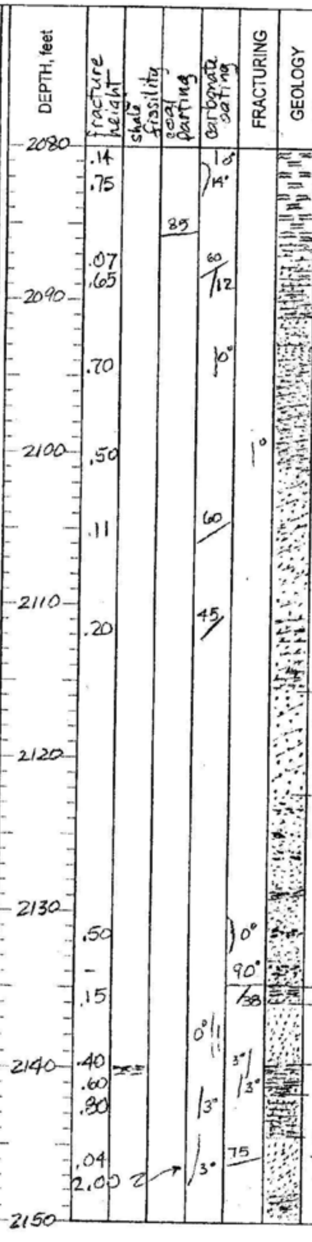

COMMENTS:

Avg. Core Recovery/ Hole

Descriptive Geology

← vert. fract 25% carb filled
← slicks curved as shown dip slip carbonate filled 25%
← 85° parting on 2mm coal seam

MUDSTONE black, brittle; bedding parting by drilling - 2cm-4cm apart are common, 83-85°CA

2086 — v. gradual contact

← 0.1mm calcite veinlet
60° dip slip slicks 25% carbonate filled

SILTSTONE black

2091.2 — gradual contact

← 0.1mm fract. 50% carb. filled not broken, slightly offset by 1mm-5mm coal bed.

FINE G. SANDSTONE lt gray interbedded with dk gray siltstone as bedding laminations and irregular wavey v. thin bedding. Not fractured, little parting.

← fract. in unbroken ss.

2101.0 — gradational contact

SANDSTONE med. grained lt. gray Bedding laminae typically 65 to 90°CA

← carbon/calcite parting 50% filled

No natural fracturing.

← planar fract. 25% carbonate filled in siltstone bed 0.2' thick

2115.8 — abrupt contact

70° bedding

SANDSTONE coarse grained thick bedded -

2122.3 — abrupt contact

SANDSTONE med. grained lt. gray with siltstone pebbles in bedding.
No natural fracturing

← rough surface fract in/out of core
slicks 90°CA @ contact; 38° planar fract.

2134.9
2135.9 muddy siltstone dk brown-gray

← 0.1mm en echelon calcite veinlets terminates fade out into bedding

2139.8 — abrupt contact
en echelon 0.1mm calcite vns

MUDSTONE dk gray to black

2141.9 — abrupt contact
← 1-2mm calcite veinlet

SILTSTONE to v.f. sandstone

2144.5 — grad. contact
← planar fract.
← 3° calcite vnlt 0.1mm

FINE SANDSTONE gray with some dk gray siltstone thin bedding.

Drilling Interval
% Core Recovered
Core Size
RQD
Sample Interval
photos

Drill Site: -
N: E:
Started:
Completed

Collar Elevation:
Bearing:
Inclination:
Total Depth:

Sandia National Laboratories
Logged by: Ron Graichen
Log Version:
Log Date: Mar 16, 2002

Raton Basin Project
Hole No: CH-4
Scale: 1" = 10' (1:120)
Sheet 31 of 34

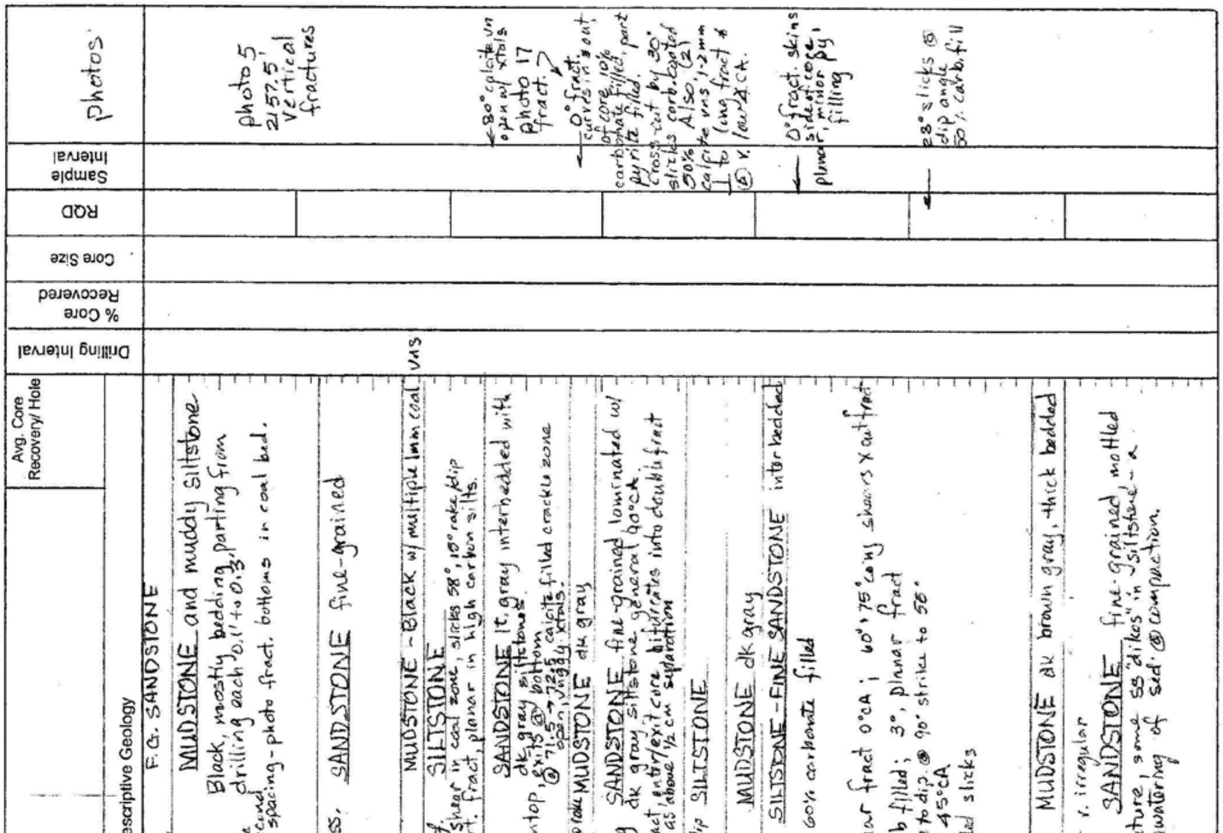

COMMENTS:

- 44° slicks, dip slip
- 2152.0 — sharp contact
- 50° slrcks 20° rake from dip planar
- 48° slicks, near dip slip, carbonate 30% filled.
- long planar fracture, local ripple mark texture & second parallel fract 3mm spacing - photo fract.
- soot black trace coal
- 2161.6 — grad. contact
- vert. fract. bottom facies into SS,
- 2167.0 — grad. contact
- 2168.4 — abrupt contact
- slicks 15° rake from dip, wavey surf. 30% carbonate filled
- 30° shear in coal zone, slicks 58°, 10° rake/dip vert. fract, planar in high carbon silts.
- 2172.5 — grad contact
- 1272.6 — 8° planar rough surf fract
- 1274.5 mudstone bed
- planar vert. fract. curves in cntop, exits @ bottom
- 80/60° conj shears, 120°is planar fract.
- 2178.0 — 53° carbonate 30% on slicks @ rake
- 2179.6 — abrupt contact
- rough surf. planar bifurcating fract. minor calcite @ bottom exit end.
- 4° long planar fract, entry/exit core, bifurcates into double fract
- 2185.4 — abrupt contact
- 50% carbonate filled slicks, dip slip
- 2188.5 — X-cut fract grad. cont
- 50° slick w/ 40% carb, rake and X cut fract
- 2190.8 — minor thin 1 mm coal
- 52° carbonate 50%
- twin 40° slicks, 20° rake/dip 60% carbonate filled
- 2197.0
- 2198.4 black mudstone, w/ few 1mm coals
- planar fract 0°cA; 60°, 75° conj shears X cut fract
- 55° slicks, 50% carb filled; 3°, planar fract
- 40° slicks 20° rake to dip. @ 90° strike to 56°
- (3) 0.1mm calcite vnlts 45°cA
- 35 + 10° carb. filled slicks
- 2208 — grad. contact
- 2210 — grad contact
- 35° 0.1mm calcite vnlt v. irregular
- 25°, 0.1mm calcite vnlt v. irregular
- long planar, rough surf fractures,

Descriptive Geology

F.G. SANDSTONE

MUDSTONE and muddy siltstone

Black, mostly bedding parting from drilling each 0.1' to 0.3', bottoms in coal bed.

SANDSTONE fine-grained

MUDSTONE - Black w/ multiple 1mm coal

SILTSTONE

SANDSTONE lt. gray interbedded with dk gray siltstones calcite filled crackle zone @ 71.5 → 72.5 open, vuggy xtals.

MUDSTONE dk gray

SANDSTONE fine-grained laminated w/ dk gray siltstone general 90°cA seal as above ½ cm separation

SILTSTONE

MUDSTONE dk gray

SILTSTONE - FINE SANDSTONE interbedded

MUDSTONE dk brown gray, thick bedded

SANDSTONE fine-grained mottled texture, some SS "dikes" in siltstone - a dewatering of sed @ compaction.

Photos

photo 5 2157.5' vertical fractures

80° calcite vn open w/ xtals photo 17 fract.

0° fract. curves in & out of core 10% carbonate filled, part pyrite filled. Cross cut by 30° slicks carb. coated 50% Also (2) calcite vns 1-2mm ⊥ to long fract & ⑤ v. low ∡ CA.

0° fract. skins side of core, planar, minor py filling

28° slicks ⑤ dip angle 50% carb. fill

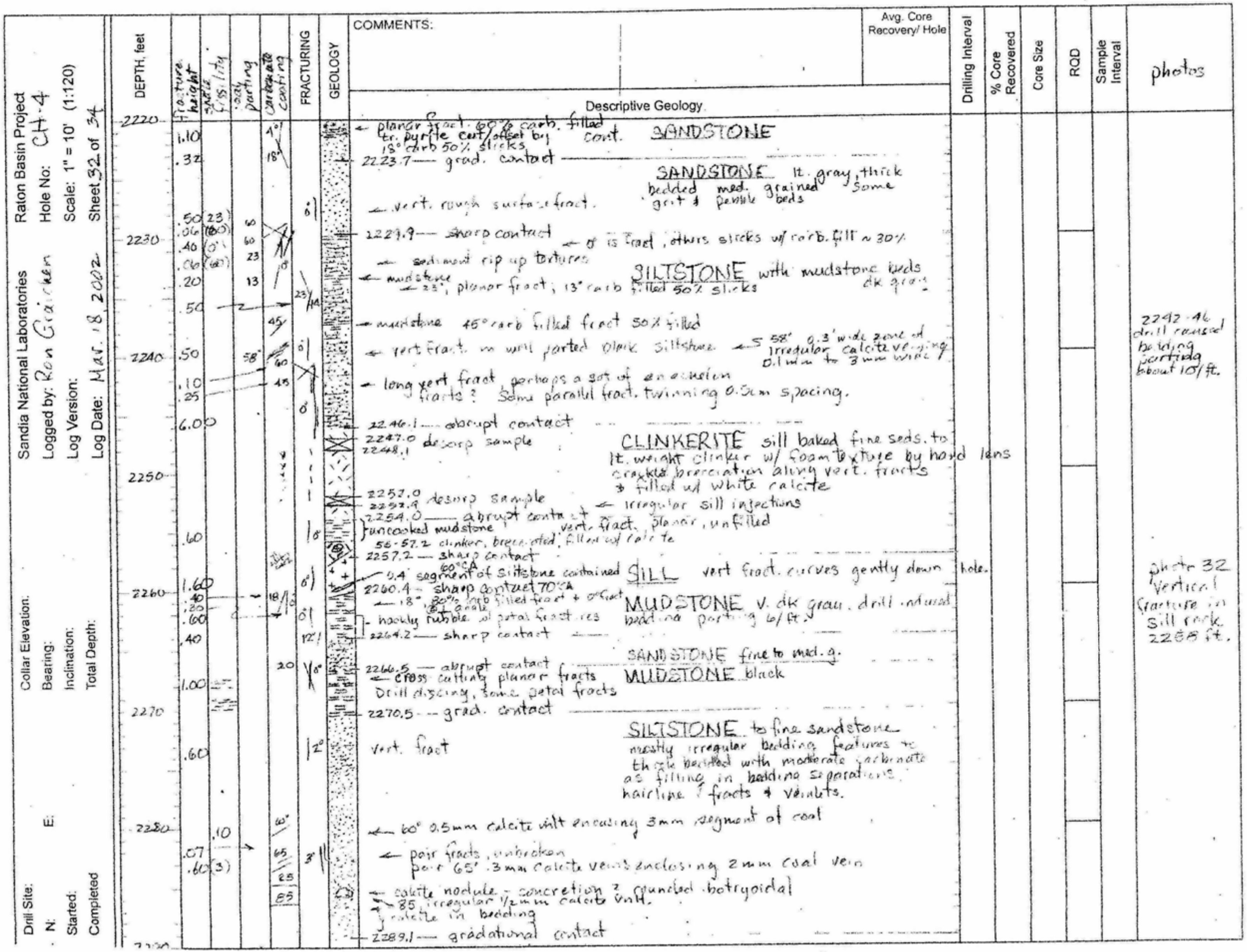

Drill Site:
N: E:
Started:
Completed

Collar Elevation:
Bearing:
Inclination:
Total Depth:

Sandia National Laboratories
Logged by: Ron Grigsby
Log Version:
Log Date: Mar. 18, 2002

Raton Basin Project
Hole No: CH-4
Scale: 1" = 10' (1:120)
Sheet 32 of 34

COMMENTS:

Avg. Core Recovery/ Hole

Drilling Interval | % Core Recovered | Core Size | RQD | Sample Interval | photos

Descriptive Geology

← planar fract. 60% carb. filled tr. pyrite cert/offset by 18° carb 50% slicks
cont. SANDSTONE
2223.7 — grad. contact

SANDSTONE lt. gray, thick bedded med. grained some grit & pebble beds

← vert. rough surface fract.

2229.9 — sharp contact
← 0° is fract, others slicks w/ carb. fill ~ 30%
← sediment rip up textures
← mudstone
← 23°, planar fract; 13° carb filled 50% slicks
SILTSTONE with mudstone beds dk gray

← mudstone 45° carb filled fract 50% filled
← vert fract. in well parted black siltstone
← 58° 0.3' wide zone of irregular calcite veining 0.1 mm to 3 mm wide

← long vert fract perhaps a set of en echelon fracts? Some parallel fract. twinning 0.5cm spacing.

2246.1 — abrupt contact
2247.0 – 2248.1 desorp sample

CLINKERITE sill baked fine seds. to lt. weight clinker w/ foam texture by hand lens crackle brecciation along vert. fracts & filled w/ white calcite

2252.0 – 2252.9 desorp sample
← irregular sill injections
2254.0 — abrupt contact
uncooked mudstone
vert. fract. planar, unfilled
56-57.2 clinker, brecciated, filled w/ calcite
2257.2 — sharp contact
0.4' segment of siltstone contained 60°CA
SILL vert fract. curves gently down hole.
2260.4 — sharp contact 70°CA
← 18°, 80% carb filled fract + 0° fract 60° angle
MUDSTONE v. dk gray. drill induced bedding parting 6/ft.
- hackly rubble w/ petal fractures
2264.2 — sharp contact

SANDSTONE fine to med. g.
2266.5 — abrupt contact
MUDSTONE black
← cross cutting planar fracts
Drill discing, some petal fracts
2270.5 — grad. contact

SILTSTONE to fine sandstone mostly irregular bedding features to thick bedded with moderate carbonate as filling in bedding separations, hairline fracts & veinlets.

vert. fract

← 60° 0.5mm calcite vnlt encasing 3mm segment of coal

← pair fracts, unbroken pair 65° .3mm calcite veins enclosing 2mm coal vein

← calcite nodule - concretion ? rounded botryoidal
← 85, irregular 1/2mm calcite vnlt.
calcite in bedding
2289.1 — gradational contact

2242-46 drill caused bedding parting about 10/ft.

photo 32 vertical fracture in sill rock 2258 ft.

Raton Basin Project
Hole No: CH4
Scale: 1" = 10' (1:120)
Sheet 33 of 34

Sandia National Laboratories
Logged by: Ron Graichen
Log Version:
Log Date: Mar 18, 2002

Collar Elevation:
Bearing:
Inclination:
Total Depth:

Drill Site:
N: E:
Started:
Completed

DEPTH, feet	fracture height	shale fissility	coal parting	carbonate coating	FRACTURING
2290					
	.20 .25 .30			60 10°	32
2300					
	.23			40	
2310				90° 30°	
2320					
	.10 .10			55	
2330					
	.03			70	
2340				85	
				85	
2350					
2360					

GEOLOGY

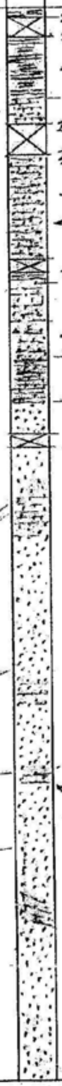

COMMENTS:

Avg. Core Recovery/ Hole

Descriptive Geology

2290.4 desorp sample
2292.0 irregular verning 1-3mm calcite

MUDSTONE black

← 1mm coal beds. ← 50° 0.5mm calcite veinlet & multiple horsetail vnlts splay from it.

2296.0 — grad. cont

← 32° planar slicks, 10°/dip

SILTSTONE dk gray-black

2197.7 desorp sample ← 0° calcitevein, gash fract. both ends fade in ss.
2194.8

calcite in bedding features, mottled & irregular

← slicks 90% coated w/ carbonate

2306.4 desorp sample
2307.5
2308.0 — abrupt contact

← two calcite veins in bedding
← broturbidite textures

SANDSTONE lt. gray with darker silty laminations & v. fine bedding.

dk brown thick bedded siltstone
— coal beds 1-2mm

2318.2 desorp sample
2319.2 — sharp contact ?

SANDSTONE formational contact ?
lt. brownish gray med. g. sandstone of uniform character w/ local "bug" remnants. Very little natural fracturing, no vertical fractures present

pair planar fracts

planar fract

parting on silty lamination

← fossil remnants, 1-2cm ovoids to bottom of hole.

Drilling Interval

% Core Recovered

Core Size

RQD

Sample Interval

photos

Drill Site:
N: E:
Started:
Completed

Collar Elevation:
Bearing:
Inclination:
Total Depth:

Sandia National Laboratories
Logged by: Ron Graichen
Log Version:
Log Date: Mar18, 2002

Raton Basin Project
Hole No: CH-4
Scale: 1" = 10' (1:120)
Sheet 34 of 34

DEPTH, feet
2360
2370

fracture height
shale fissility
coal parting
carbonate coating
FRACTURING
GEOLOGY
COMMENTS:
Avg. Core Recovery/ Hole
Descriptive Geology

cont! SANDSTONE, med. grained lt. brownish gray, uniform grain size. Thick bedded showing a few bioturbidite features & perhaps bug remnants.

No natural fracturing

2372.1 Bottom of Hole

Drilling Interval
% Core Recovered
Core Size
RQD
Sample Interval
photos

Well VPR CH-5

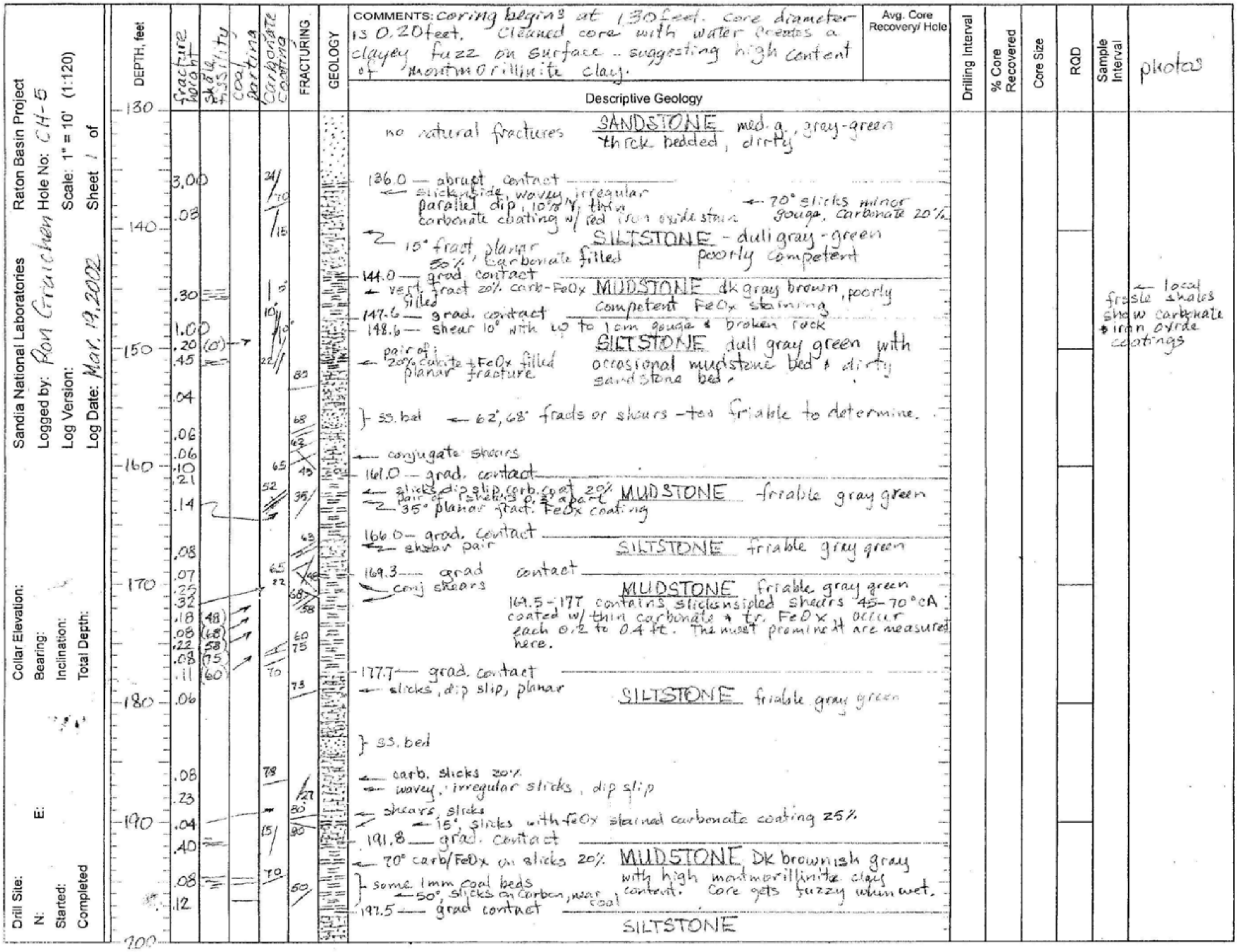

Sandia National Laboratories Raton Basin Project
Logged by: Ron Graichen Hole No: CH-5
Log Version: Scale: 1" = 10' (1:120)
Log Date: Mar. 19, 2002 Sheet 1 of

Drill Site: Collar Elevation:
N: E: Bearing:
Started: Inclination:
Completed Total Depth:

COMMENTS: coring begins at 130 feet. Core diameter is 0.20 feet. Cleaned core with water creates a clayey fuzz on surface - suggesting high content of montmorillinite clay.

Avg. Core Recovery/ Hole

Descriptive Geology

no natural fractures SANDSTONE med. g., gray-green thick bedded, dirty

136.0 — abrupt contact
← slickenside, wavey, irregular parallel dip, 10%, thin carbonate coating w/ red iron oxide stain
← 70° slicks minor gouge, carbonate 20%
⇄ 15° fract, planar 50% carbonate filled
SILTSTONE - dull gray-green poorly competent

144.0 — grad. contact
← vert. fract 20% carb-FeOx filled
MUDSTONE dk gray brown, poorly competent FeOx staining

147.6 — grad. contact
148.6 — shear 10° with up to 1 cm gouge & broken rock
SILTSTONE dull gray green with occasional mudstone bed & dirty sandstone bed.
← pair of: 20% calcite + FeOx filled planar fracture

} ss. bed ← 62°, 68° fracts or shears - too friable to determine.

← conjugate shears

161.0 — grad. contact
← slicks, dip slip, carb. coat 20% pair of shears 0.3' apart
⇄ 35° planar fract. FeOx coating
MUDSTONE friable gray green

166.0 — grad. contact
⇄ shear pair
SILTSTONE friable gray green

169.3 — grad contact
⇄ conj shears
MUDSTONE friable gray green
169.5 - 177 contains slickensided shears 45-70° CA coated w/ thin carbonate & tr. FeOx, occur each 0.2 to 0.4 ft. The most prominent are measured here.

177.7 — grad. contact
← slicks, dip slip, planar
SILTSTONE friable gray green

} ss. bed

← carb. slicks 20%
← wavey, irregular slicks, dip slip
⇄ shears, slicks
← 15°, slicks with FeOx stained carbonate coating 25%

191.8 — grad. contact
← 70° carb/FeOx on slicks 20%
MUDSTONE DK brownish gray with high montmorillinite clays content. Core gets fuzzy when wet.
} some 1mm coal beds
← 50°, slicks on carbon, near coal

197.5 — grad contact
SILTSTONE

← local friable shales show carbonate & iron oxide coatings

Drill Site:
N: E:
Started:
Completed

Collar Elevation:
Bearing:
Inclination:
Total Depth:

Sandia National Laboratories
Logged by: Ron Graichen
Log Version:
Log Date: Mar. 19, 2002

Raton Basin Project
Hole No: CH-5
Scale: 1" = 10' (1:120)
Sheet 2 of

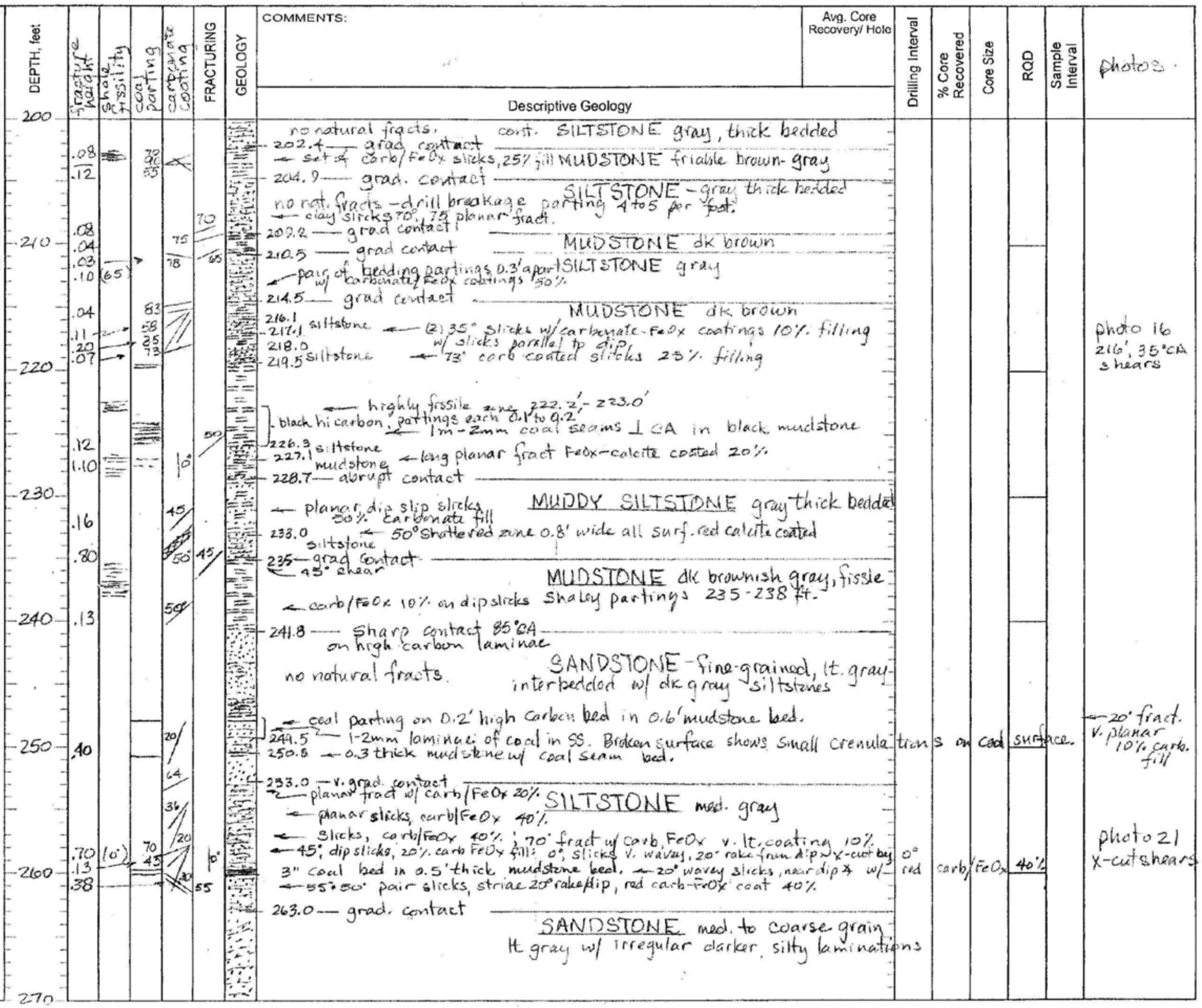

no natural fracts. cont. SILTSTONE gray, thick bedded
202.4 — grad contact
← set of carb/FeOx slicks, 25% fill MUDSTONE friable brown-gray
204.9 — grad. contact
SILTSTONE – gray thick bedded
no nat. fracts – drill breakage parting 4 to 5 per foot.
← clay slicks 70°, 75 planar fract.
209.2 — grad contact
MUDSTONE dk brown
210.5 — grad contact
SILTSTONE gray
← pair of bedding partings 0.3' apart w/ carbonate/FeOx coatings 50%
214.5 — grad contact
MUDSTONE dk brown
216.1
217.1 siltstone ← (2) 35° slicks w/ carbonate-FeOx coatings 10% filling w/ slicks parallel to dip
218.0
219.5 siltstone ← 73° carb coated slicks 25% filling

← highly fissile zone 222.2' – 223.0'
black hi carbon, partings each 0.1 to 0.2'
← 1m-2mm coal seams ⊥ CA in black mudstone
226.3 siltstone
227.1 mudstone ← long planar fract FeOx-calcite coated 20%
228.7 — abrupt contact
MUDDY SILTSTONE gray thick bedded
← planar, dip slip slicks 50% carbonate fill
233.0 ← 50° shattered zone 0.8' wide all surf. red calcite coated
siltstone
235 — grad contact
← 45° shear
MUDSTONE dk brownish gray, fissle
← carb/FeOx 10% on dip slicks Shaley partings 235-238 ft.
241.8 — sharp contact 85° CA on high carbon laminae
SANDSTONE – fine-grained, lt. gray interbedded w/ dk gray siltstones
no natural fracts.
← coal parting on 0.2' high carbon bed in 0.6' mudstone bed.
249.5 ← 1-2mm laminae of coal in SS. Broken surface shows small crenulations on coal surface.
250.8 ← 0.3 thick mudstone w/ coal seam bed.
253.0 — v. grad. contact
← planar fract w/ carb/FeOx 20% SILTSTONE med. gray
← planar slicks, carb/FeOx 40%.
← slicks, carb/FeOx 40%; 70° fract w/ carb, FeOx v. lt. coating 10%
← 45°, dip slicks, 20% carb FeOx fill; 0°, slicks v. wavy, 20° rake from dip ~ x-cut by 0° red carb/FeOx 40%
3" coal bed in 0.5' thick mudstone bed. ← 20° wavey slicks, near dip ∡ w/
← 55°, 50° pair slicks, striae 20° rake/dip, red carb-FeOx coat 40%
263.0 — grad. contact
SANDSTONE med. to coarse grain lt gray w/ irregular darker, silty laminations

photo 16
216', 35° CA shears

← 20° fract. v. planar 10% carb. fill

photo 21
X-cut shears

Raton Basin Project
Hole No: CH-5
Scale: 1" = 10' (1:120)
Sheet 3 of

Sandia National Laboratories
Logged by: Ron Graichen
Log Version:
Log Date: Mar. 20, 2002

Collar Elevation:
Bearing:
Inclination:
Total Depth:

Drill Site:
N: E:
Started:
Completed

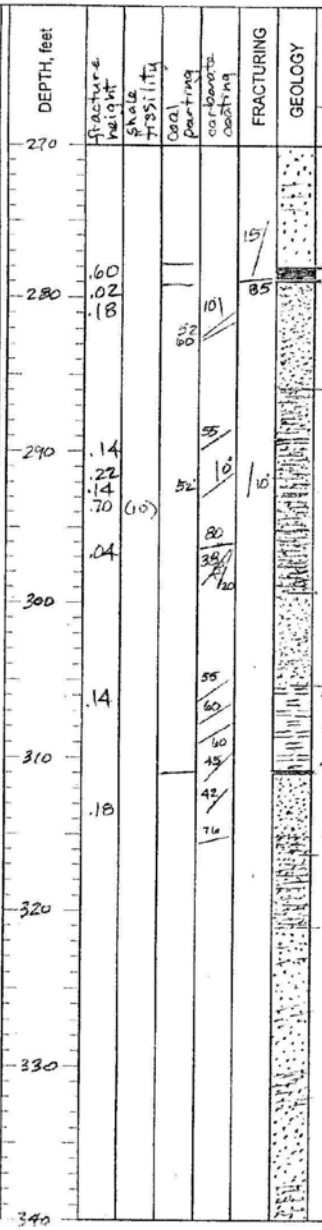

COMMENTS:

Avg. Core Recovery/ Hole

Descriptive Geology

cont. SANDSTONE

rough surf fracture

278.1 coal — sharp contact
279.0

10°, planar fract w/ red coating carb/FeOx 20%.
52, 60° red coat 20%, slicks.

SANDSTONE fine-grained, lt. gray grades into med. gray siltstone below

286.0 — v. grad. contact

slicks 20° rake/dip, red carb FeOx coating 20%.
vert fract red coat 20%
52° slicks, 15-20° to dip, red coated carb. FeOx 40%.
10° planar fract

SILTSTONE med. gray, generally not fractured

slicks w/ curb FeOx coat 30%.
88°, 20° rake/dip, carb FeOx coat 10%, 20°, 20° rake/dip, 20% coat, shattered. rock between shears.

299.5 — v. grad. contact

not fractured

SANDSTONE Some siltstone bed. fine grained, @ 301-305 laminations of siltstone 85°CA.

306.4 — abrupt contact
slicks v. irregular, near dip slip carb/FeOx 20% fill
60° slicks-gouge, striae 20° rake from dip 20% fill
0.4' coal
45°, v. irregular shear w/ carbonate FeOx 20%

MUDSTONE dk gray w/ coal beds

311.0 — sharp contact
fract, stepped, v. lt. coating carb FeOx = 10%
slicks, carb FeOx 10%.

SANDSTONE fine-grained lt. gray

316.4 — grad contact

no fractures

SILTSTONE gray - some broturbidite textures.

321.1 — grad. contact

SANDSTONE fine-grained, some broturbidite textures, irregular silty laminae. Unfractured.

Drilling Interval | % Core Recovered | Core Size | RQD | Sample Interval

photo 26
292'
carbonate FeOx coated slicks 15-20° rake to dip ∡.
photo 27
293' natural fract. & drill induced break.

Drill Site:
N: E:
Started:
Completed

Collar Elevation:
Bearing:
Inclination:
Total Depth:

Sandia National Laboratories
Logged by: Ron Graichen
Log Version:
Log Date: Mar. 20, 2002

Raton Basin Project
Hole No: CH-5
Scale: 1" = 10' (1:120)
Sheet 4 of

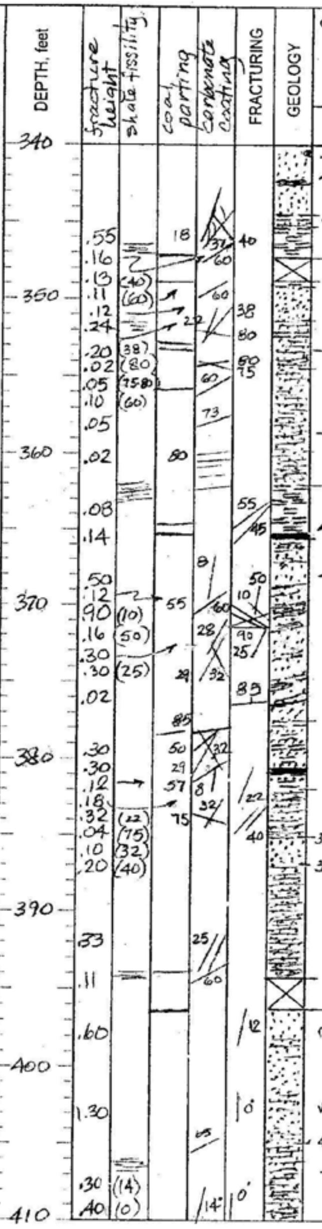

COMMENTS:

Avg. Core Recovery/ Hole

Descriptive Geology

Drilling Interval | % Core Recovered | Core Size | RQD | Sample Interval | photo

← carbonate-ironstone bedding replacement

cont. SANDSTONE

344.6 —— grad. contact

← multiple shear-fracture zone with carb/FeOx coatings ~40% fill

MUDSTONE @344.6 to coal is very well broken w/ every fract. & parting mineral coated

347.5 desorb sample

348.8

349.2 —— grad contact

f.g. sandstone ← 60° polished slicks, dip slip w/ 25% carb/FeOx

SILTSTONE and muddy siltstone

351.5

← Set of planar fracts 22°, 38°, 80° mineral coated 25-40%.

mineral coated fracts. 25-40% filled carbonate-FeOx

← 80° bedding partings, orange carb/FeOx coatings 10-20% all caused by drilling.

362.2 —— gradual contact

MUDSTONE with coal seams 363-364 brown-black, v. shaley

← 0.6' coal, 2cm bed partings above coal

365.7 —— abrupt contact

SANDSTONE with interbeds + laminations of dk gray siltstone

← 3mm wide fract 1mm open & calcite xtal druze — on both ribs

— rough surface fract 10°, cross cut by 50° fract. no mineral coating on either

28° calcite 80% filled fract

25° rough surf. fract.

Fract series: 60, 62, 72, 90 are all planar, non mineral

← @375, 0.3' carbonate-ironstone concretion - in bedding

85°; parting on sharp contact 2cm mudstone bed in med.g. tan sandstone

377.5 —— sharp contact

85° coal parting, 3mm coal bed.

50° slicks dip slip

0.5' coal seam 29°, 30° fracts, planar

MUDDY SILTSTONE - dk gray-black. Well fractured/sheared, all w/ v. thin orange coat carb-FeOx mineral filling (?) 20%.

382.0 —— grad contact

← 8° planar fract below coal, thin orange coat.

22° planar fract; 32°, 72° fracts w/ v. light carb-FeOx coatings - 20%

40° rough surf. fract.

385

m.g. sandstone

387

SILTSTONE laminated & thin beddes dk gray silts & lt gray v.f. sands Little natural fracturing.

25°, pair hairline fracts not broken, w/carb-FeOx fill

60°, planar fract carb FeOx coat 40%

394.3 desorb sample

396.3 —— sharp contact

rough surface fract.

SANDSTONE fine - med grained interbedded with darker silty beds & laminae Irregular bedding.

v. irregular, rough surface fract

65°, planar fract. thin carb FeOx coat 20%

405.0 —— abrupt contact

SILTSTONE gray

← minor shaley bedding parting w/ minor carb. FeOx coatins

← vert. fract skins side of core 14°,

photo 34 345' multiple fracts-shears

photo 35 brittle muddy siltstone fracts/shears w/ thin carbonate - iron oxide coatings

Raton Basin Project
Hole No: CH-5
Scale: 1" = 10' (1:120)
Sheet 5 of

Sandia National Laboratories
Logged by: Ron Graichen
Log Version:
Log Date: Mar. 21, 2002

Collar Elevation:
Bearing:
Inclination:
Total Depth:

Drill Site:
N:
E:
Started:
Completed

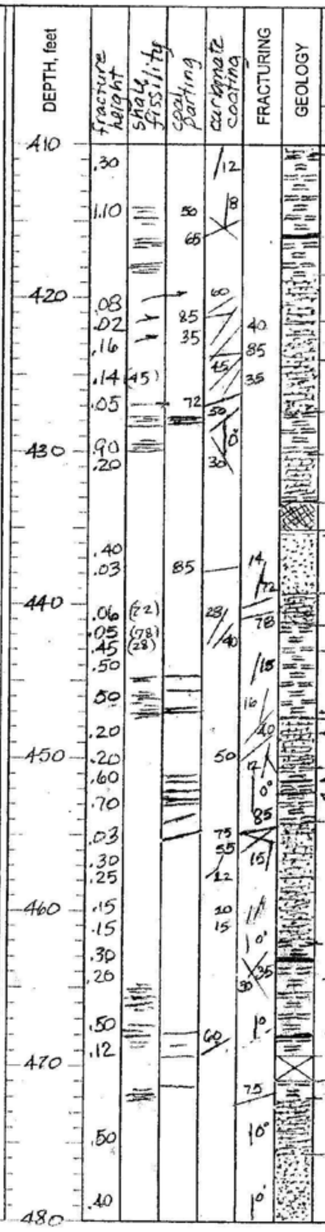

COMMENTS:

Descriptive Geology

410.5 contact gradational
← planar fract coated calcite FeOx bottom term. in bedding. 50%
← 60, 50 conj set shears 40% fill
0.2' coal bed

MUDSTONE dk gray to black. local strong bedding parting, 1/cm. parting surfaces are coated with orange, calcite-FeOx. Mostly parting from 411 - 419' is each 0.1' to 0.2'

418.5 — grad. contact

SILTSTONE

35° slicks, very curving surface, orange mineral coating 35% fill
← 40, 85 slicks 30% min.
← well broken - photo
@ 421.5' - 424.0' core is well fractured w/ 40% orange coating of carbonate - FeOx
72° slicks, 35% carb. fill

427.6 — grad contact
50° slicks 30° rake from dip 30% fill
0° fract. 30° fract 30% min. fill

MUDSTONE dk gray

430.2 — grad contact
not fractured

SILTSTONE - fine sandstone

433.3 — 433.0
ground up core & drill mud

Mudstone, most of interval destroyed but chips of mudstone & coal define unit

424.9 435.3
← 14 v. irregular fracture
85° planar fract 20% fill

SANDSTONE vfg to f.g sandstone

439.3 — grad contact
← slicks

SILTSTONE dk gray. To 440.8 formational breccia

441.4 — grad contact
← 28° slicks 20° off dip 30% carb fill

MUDSTONE Black. Abundant bedding parting
Wetted core swells - montmorillenite content!
Thin (2mm - 1cm) coal beds

bed parts - fracts abund - photo
← 16, planar fract. 40° curved fract.

447.4 — grad contact
← 40, 50 fracts

SILTSTONE

450.7 — grad contact
← coal 0.15'

MUDSTONE black, abund. bed parting & several en echelon fracts near parallel CA. some coal partings

454.0 — grad. contact
85° coal parting; 55, 75' are fracture sets
15° slicks, 20° off dip
22° curved slicks carb FeOx 30%.

SILTSTONE well fractured through 456 ft.

15°, 20°; irregular fracts FeOx but no carbonate

462.0 — v. grad. contact
0.3' coal bed
← conjugate shear set

MUDSTONE dk gray. locally fissle
Most fractures have FeOx only

← coal 2cm 60° slickensides dip slip coated carb. FeOx 25%.
469.6 desorb sample
471.1 75° - fract. FeOx coating tr. carb.

472.0 — v. grad. contact
0° planar fract fe coat.

SILTSTONE dk gray

475.7 — grad contact

SANDSTONE f.g & v.f.g. interbedded

vert fract

Avg. Core Recovery/ Hole
Drilling Interval
% Core Recovered
Core Size
RQD
Sample Interval
photo

photo 36
416 - 419
fracturing & bedding parting

photo 1
421.5 - 424'
well broken core

photo 2.
443 - 447
well broken core

photo 3
468'
fissle mudstone coal & vertical fracture

Raton Basin Project
Hole No: CH 5
Scale: 1" = 10' (1:120)
Sheet 6 of

Sandia National Laboratories
Logged by: Ron Grauchen
Log Version:
Log Date: MAR. 21, 2002

Collar Elevation:
Bearing:
Inclination:
Total Depth:

Drill Site:
N:
E:
Started:
Completed

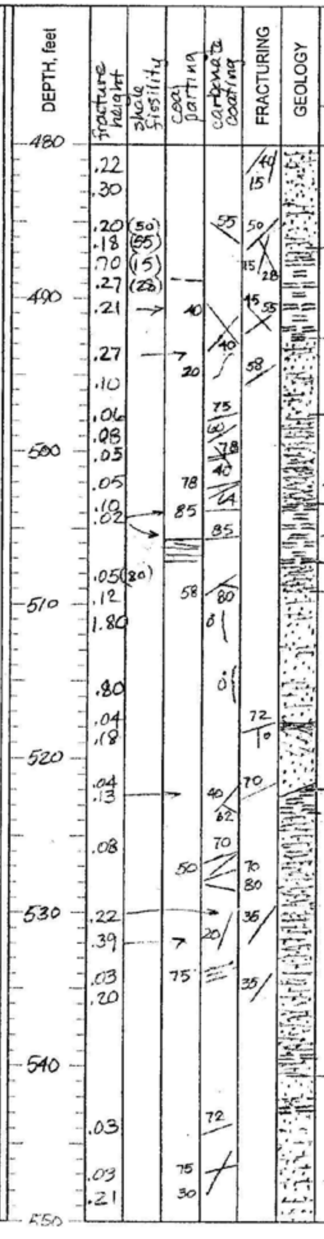

COMMENTS:

Avg. Core Recovery/ Hole

Descriptive Geology

← rough surf fract

SANDSTONE fine-grained lt. gray with irregular laminations of darker siltstone

no natural fractures

← fracts 70° disposed, one barren, one w/calcite 30%.

486.7 — v. gradational contact

MUDSTONE dk brownish gray

← 2cm coal seam

Well broken & sheared

← shear w/ carbonate 40°CA; conjugate pair Also, non carb coated pair 45/55° slicks 30° rake to dip

492.6 — grad. contact

← v. wavey 20° red stain carb. fracture; v. rough surface

SANDSTONE fine-grained

58, planar fract.

497.5 — grad. contact

SILTSTONE well fractured, some slickensides but not well developed, dull orange-carbonate-FeOx coating on all 30-40% (?)

← 64 curved slicks

503.3 — sharp contact

MUDSTONE dk brownish gray

85 minor shear surface

black carbonaceous zone w/ coals 1-2mm to 1cm. bed parting are 1-2cm.

507.0 — abrupt contact

58° shear offsets 80° fract

SILTSTONE

509.2 — abrupt contact

SANDSTONE lt. gray med. grained with laminations of siltstone to define bedding.

calcite filled rough fracture, top terminates in silt bed bottom exits core

← same, slices side of core, 1-2mm wide

← 0.6' mudstone bed 72° polished slick & vert. fract.

522.0 — abrupt contact 70°CA slickensides, rake movement

523.6 62°,40° polished slicks - rake movement. Bedding parting each 2-3cm.

70° fract.; 50° slicks dip slip.

SILTSTONE black high carbon w/coal mudstone to 523.6. Gray thick bedded moderately broken. Carbonate coatings are orange color & are generally 30-40% filling

80 polish slicks

35° polish slicks, rake striae

20° fracture, gently curved

75° set of fracts, carbonate fill 20%.

35° planar fract.

0.3' mudstone bed

540.9 — sharp contact

SANDSTONE lt gray med. grained

0.3 mudstone bed

72° slicks 20% carb. fill

Drilling Interval
% Core Recovered
Core Size
RQD
Sample Interval

photos

photo 4
487.5
fractures 90° disposed
15° ↑ 28°

photo 3
493.5
rough fracture

Drill Site:
N: E:
Started:
Completed

Collar Elevation:
Bearing:
Inclination:
Total Depth:

Sandia National Laboratories
Logged by: Ron Graichen
Log Version:
Log Date: Mar. 22, 2002

Raton Basin Project
Hole No: CH-5
Scale: 1" = 10' (1:120)
Sheet 7 of

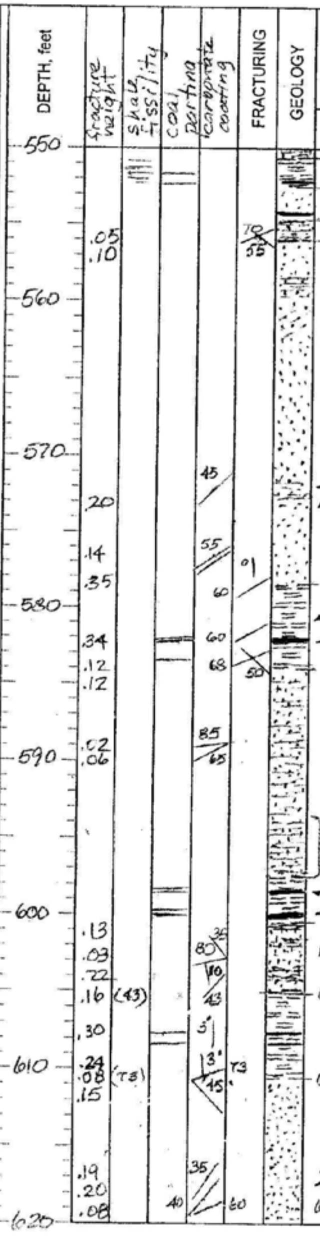

COMMENTS:

Avg. Core Recovery/ Hole

Descriptive Geology

550.7 — sharp contact
← 0.2' coal seam
552.6 — sharp contact
← 25 mm coal bed
654.7 siltstone
556.0
55°+70', polished slicks & rake 20° from dip

MUDSTONE w/ coal

SANDSTONE lt. tan, med. grained
dark silty laminae as irregular bedding,
Mostly thick bedded
+ unfractured.

no natural fractures

planar fract minor calcite coating 10%

vertical fract bounded by 55° fract above, fades into SS. below
578.4 — sharp contact 60°CA
60° slicks @ rake ∡
0.3' coal bed
← conjugate shear set
584.1 — abrupt contact

MUDSTONE dk gray to black
bedding parting common each 3cm-4cm.

SANDSTONE

calcite coated fracts 30%

silty
597.5 — abrupt contact
0.6' coal bed
600.5 — abrupt contact
10,35,80 are fractures w/v. light weak carbonate coating - 10% fill.
43° slicks
605.2 — sharp contact
0.2' coal
0.1' coal
45,73 planar fracts, light carb coat 20%.
610.5 — grad. contact

MUDSTONE black, mostly broken core
Bedding parting each 1cm-2cm

SILTSTONE-SANDSTONE interbedded

MUDSTONE dk gray to black
moderately fractured each 1cm - 2cm

SANDSTONE f. grained to v. f. grained
med. gray, thickbedded.
Unbroken.

carbonate coated fracts

60 slicks, gouge

Drilling Interval	% Core Recovered	Core Size	RQD	Sample Interval	photos
Pyrite	on	coal	fractures		
					photo 25 conjugate shears

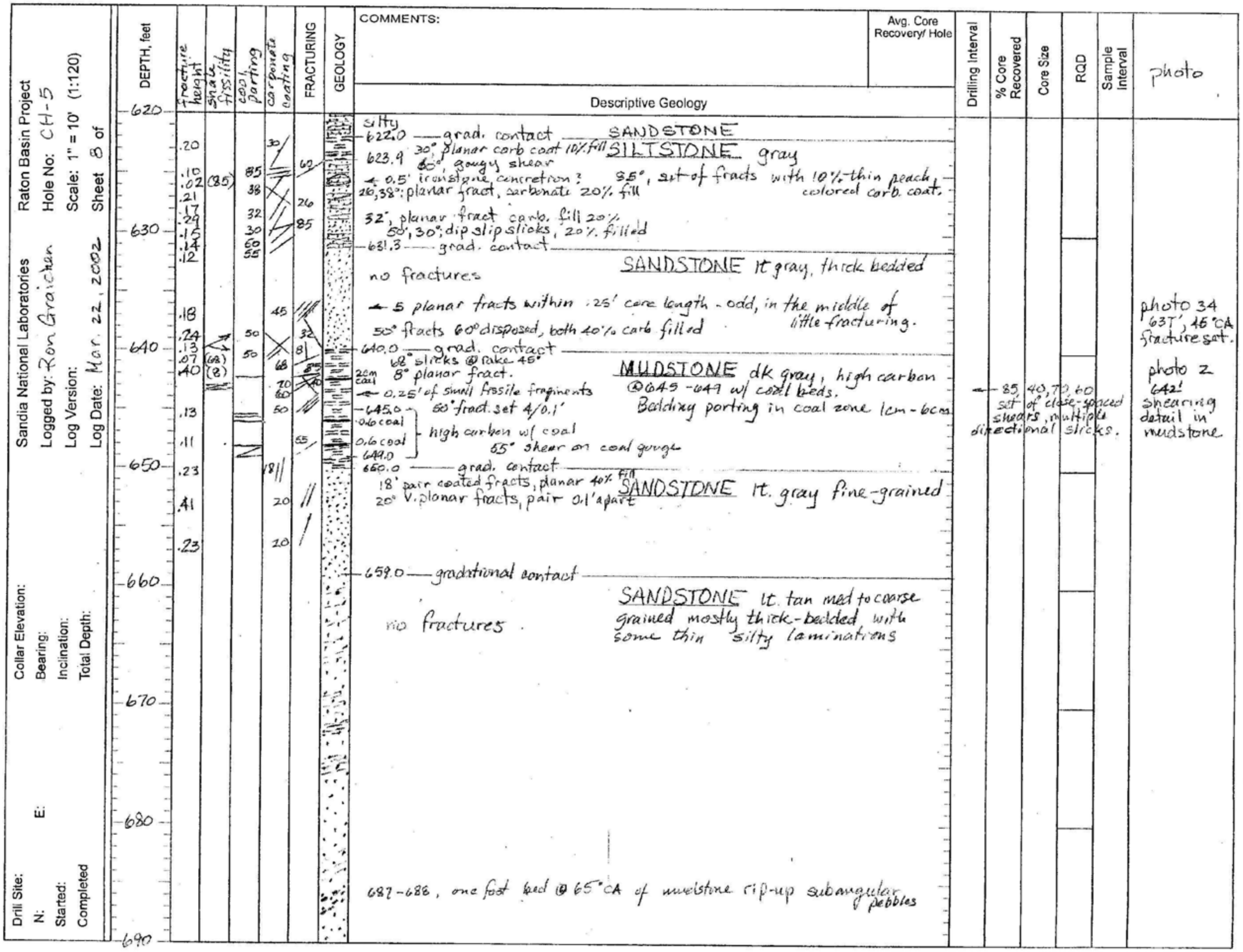

Sandia National Laboratories
Raton Basin Project
Logged by: Ron Graichen
Hole No: CH-5
Log Version:
Scale: 1" = 10' (1:120)
Log Date: Mar. 22, 2002
Sheet 8 of

Collar Elevation:
Bearing:
Inclination:
Total Depth:

Drill Site:
N:
E:
Started:
Completed

DEPTH, feet	fracture height	shale fissility	coal parting	carbonate coating	FRACTURING
620					
	.20			30	
	.10 .02	(85)	85		60
	.21		38		26
	.17 .29		32		85
630	.15 .14 .12		30 60 55		
	.18			45	
	.24 .13		50		32
640	.07 .40	(68) (8)	50	68	8 85 40
				70 60	
	.13			50	
	.11				55
650	.23			18	
	.41			20	
	.23			10	
660					
670					
680					
690					

COMMENTS:

Avg. Core Recovery/ Hole

Descriptive Geology

silty
622.0 —— grad. contact —— SANDSTONE
623.9 30° planar carb coat 10% fill SILTSTONE gray
60°, gougy shear
← 0.5' ironstone concretion? 35°, set of fracts with 10% thin peach colored carb. coat.
26,38°: planar fract, carbonate 20% fill
32°, planar fract carb. fill 20%
50°, 30°; dip slip slicks, 20% filled
631.3 —— grad. contact

SANDSTONE lt gray, thick bedded
no fractures
← 5 planar fracts within .25' core length - odd, in the middle of little fracturing.
50° fracts 60° disposed, both 40% carb filled

640.0 —— grad. contact
68° slicks @ rake 45°
2cm coal 8° planar fract.
MUDSTONE dk gray, high carbon @645 -649 w/ coal beds.
← 0.25' of small fissile fragments
Bedding parting in coal zone 1cm - 6cm
645.0 50° fract. set 4/0.1'
0.6 coal
0.6 coal
649.0 } high carbon w/ coal
55° shear on coal gouge
650.0 —— grad. contact
18° pair coated fracts, planar 40% fill
20° V. planar fracts, pair 0.1' apart
SANDSTONE lt. gray fine-grained

659.0 —— gradational contact
SANDSTONE lt. tan med to coarse grained mostly thick-bedded with some thin silty laminations
no fractures

687-688, one foot bed @ 65°CA of mudstone rip-up subangular pebbles

Drilling Interval	% Core Recovered	Core Size	RQD	Sample Interval	photo
←	85	40, 70, 60 set of close-spaced shears, multiple directional slicks.			photo 34 637', 45°CA fracture set. photo 2 642' shearing detail in mudstone

Drill Site:
N: E:
Started:
Completed

Collar Elevation:
Bearing:
Inclination:
Total Depth:

Sandia National Laboratories
Logged by: Ron Graichen
Log Version:
Log Date: Mar. 23, 2002

Raton Basin Project
Hole No: CH-5
Scale: 1" = 10' (1:120)
Sheet 9 of

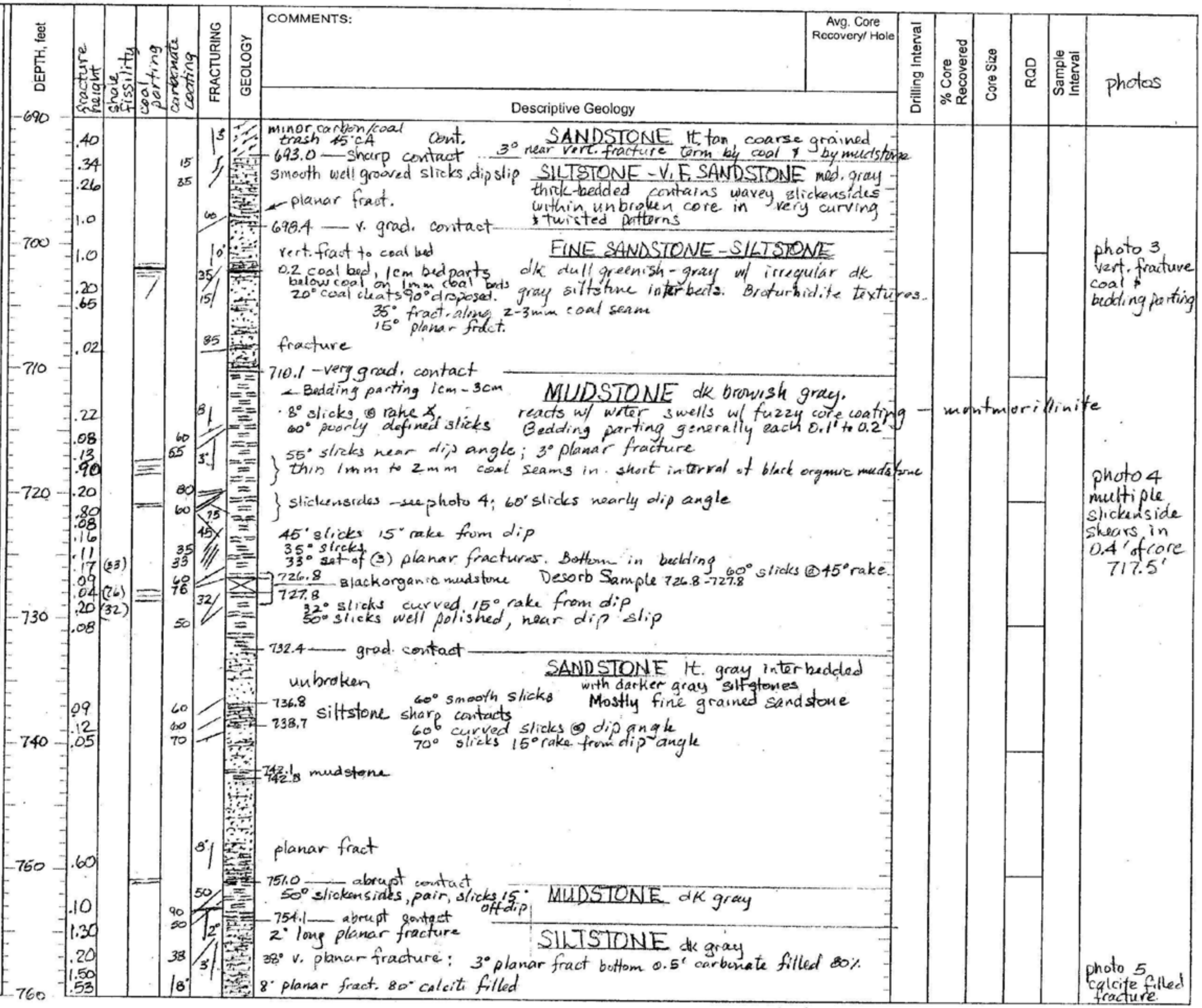

minor carbon/coal trash 45°CA
Cont.
693.0 — sharp contact
3° near vert. fracture term by coal & by mudstone

SANDSTONE lt. tan coarse grained

smooth well grooved slicks, dip slip

SILTSTONE - V. F. SANDSTONE med. gray thick-bedded contains wavey slickensides within unbroken core in very curving & twisted patterns

planar fract.

698.4 — v. grad. contact

vert. fract to coal bed
0.2 coal bed, 1cm bed parts below coal on 1mm coal beds
20° coal cleats 90° disposed.
35° fract. along 2-3mm coal seam
15° planar fract.

FINE SANDSTONE - SILTSTONE dk dull greenish-gray w/ irregular dk gray siltstone interbeds. Bioturbidite textures.

fracture

710.1 — very grad. contact

Bedding parting 1cm - 3cm
8° slicks @ rake ∡
60° poorly defined slicks
55° slicks near dip angle; 3° planar fracture
thin 1mm to 2mm coal seams in short interval of black organic mudstone
slickensides — see photo 4; 60° slicks nearly dip angle
45° slicks 15° rake from dip
35° slicks
33° set of (3) planar fractures. Bottom in bedding
60° slicks @ 45° rake.
726.8 Black organic mudstone Desorb Sample 726.8-727.8
727.8
32° slicks curved 15° rake from dip
50° slicks well polished, near dip slip

MUDSTONE dk browish gray. reacts w/ water swells w/ fuzzy core coating — montmorillinite
Bedding parting generally each 0.1' to 0.2'

732.4 — grad. contact

unbroken
736.8 siltstone sharp contacts
738.7
60° smooth slicks
60° curved slicks @ dip angle
70° slicks 15° rake from dip angle
742.1
742.8 mudstone
planar fract

SANDSTONE lt. gray interbedded with darker gray siltstones
Mostly fine grained sandstone

751.0 — abrupt contact
50° slickensides, pair, slicks 15° off dip

MUDSTONE dk gray

754.1 — abrupt contact
2° long planar fracture
38° v. planar fracture; 3° planar fract bottom 0.5' carbonate filled 80%
8° planar fract. 80° calcite filled

SILTSTONE dk gray

photo 3
vert. fracture
coal & bedding parting

photo 4
multiple slickenside shears in 0.4' of core
717.5'

photo 5
calcite filled fracture

Drill Site:
N: E:
Started:
Completed

Collar Elevation:
Bearing:
Inclination:
Total Depth:

Sandia National Laboratories
Logged by: Ron Graichen
Log Version:
Log Date: Mar 23, 2002

Raton Basin Project
Hole No: CH-5
Scale: 1" = 10' (1:120)
Sheet 10 of

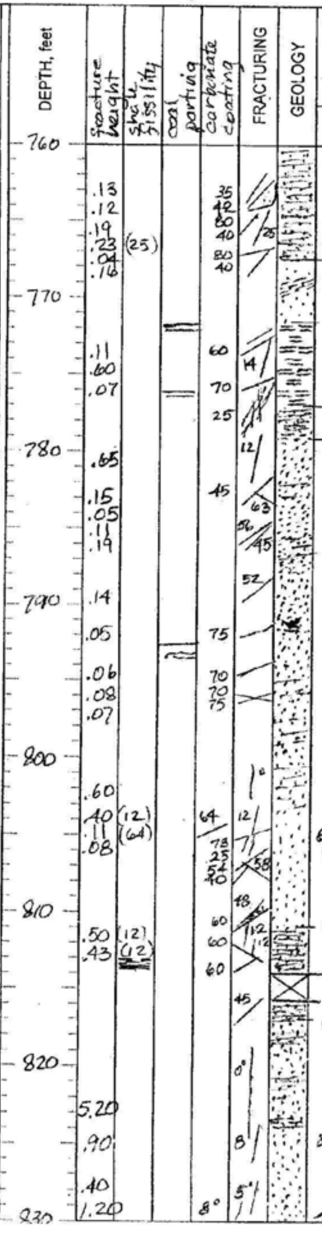

COMMENTS:

Avg. Core Recovery/ Hole

Descriptive Geology

cont. SILTSTONE thick bedded medium gray
35° smooth slicks 15° rake from dip.
42° slicks dip slip: 80° slicks convex dip angle 55°→80° dip slip slicks.
40°, 25° planar fractures, 25 has v. light carbonate coating
← fracture
767.5 — abrupt contact
40 slicks 15° rake from dip ∡
SANDSTONE med. grained, lt. tan thick bedded
771.4 — sharp contact
60° planar fract. pair
MUDSTONE dk gray to black
14° planar fract.
70° slicks, striae 10° from dip
777.0 — very grad. contact
← shear zone perhaps 0.2' true thickness - multiple shear orientations
779.0
SANDSTONE fine-grained, med. gray
long fluted slick shear
slicks 30° rake from dip
Siltstone 777 – 779 ft. Thick bedded
← 45° rake slicks; 63° fracture
56 planar fract; 45 gentle arcuate (across strike) fracture
planar fract
clot of coal with calcite filling cleats
← parting on 3mm coal seam; several other partings on irregular clots of coal.
planar fracture
← slickensides on 0.2' mudstone bed
vert fracture along side of core
64 fracture — parting along 2mm thick white calcite vein
73° planar slickensides, 12° planar fracture
25°, pair of parallel very rough irregular shears 20° rake from dip.
40° planar fracture; 54, 58° slicks w/ striae disposed 90° Some gouge
811.0 FAULT @ 810' grad. contact 0.15' true thickness gouge between 48°-60° slicks, striae @ dip ∡
SILTSTONE: dk gray, thick bedded
12° planar fracture; 60° slicks bounding 12° fract.
814.0 @ coal contact 0.2' of fissle shale as pile of flakes.
desorb sample
815.8
817.0 — v. grad. contact 45° planar fracture
SANDSTONE: interbedded siltstone & med. grained Sandstone
vertical fracture, partially filled w/ white calcite locally splayed.
8°, 5°, rough surface fracture, top term. in siltstone bed, bottom out of core
829.9 sharp contact with coal bed. 8° fracture to top of coal

Drilling Interval
% Core Recovered
Core Size
RQD
Sample Interval
photos

photo 6
25° shear zone 777'

photo 7
782
High angle shears.

photo 8
curved slicks around coal mass
792'

photo 10
810' fault

photo 12
Vertical fracture
820'

Sandia National Laboratories
Logged by: Ron Graichen
Log Version:
Log Date: Mar 25, 2002

Raton Basin Project
Hole No: CH5
Scale: 1" = 10' (1:120)
Sheet 11 of

Collar Elevation:
Bearing:
Inclination:
Total Depth:

Drill Site:
N: E:
Started:
Completed

DEPTH, feet	fracture height	shale fissility	coal parting	carbonate coating
830				
	.08			50°
	.12			50°
				55°
	.15			54°
840	.11			65
	.10			50
	.40	(10)		
	.20		25	
	.90			12
				3°
	.07			60
850	.07			55
	.40	(20)		45
	.23			
	.11		0°	
860	1.00			
	.60			
	.80	(15)		
	.18	(35)		55
	.07	(55)		60
	.07	(60)		70
	.07	(70)		70
	.08	(70)		75
	.04			85
870	.25			
	.09			70
	.03			85
880	.09			60
	.04			70
	.04			80
	.05			70
	.20			
	.28			
	.24	(20)		
890	.70	(0°)		
	.14			60
	.20			30
900				

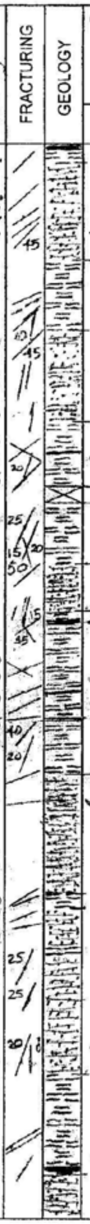

COMMENTS:

Avg. Core Recovery/ Hole

Descriptive Geology

← contact @ 0.4' coal-shale bed. Mudstone contact ~90°CA.
831.2 50° slicks, mudstone mod. broken w/ multiple slicks — **SILTSTONE**: dk gray, thick bedded
← 50° slicks dip slip & bumpy. Minor petal fracturing — Bedding parting from drilling each 0.1' - 0.2 ft.
← 54° rake slicks tightly curved; 45° dip slip slicks
837.7 —— gradational contact
← 1mm coal beds & 0.1'-0.2' partings — **MUDSTONE**: dk brownish gray-black
65° rough slicks, pair
10° planar fracture
842.0 —— grad-contact
45 slicks, planar-dip slip — **SANDSTONE**: fine grained, interbedded with siltstone
25 several parallel 0.1mm calcite mlts 90° disposed to 45° slicks & to long fractures.
12° fracts., rough surf. in SS. but planar in siltstone
3° fract. forks into two 1cm apart.
848.0 —— grad contact
← bed parts on 1mm coals. — **MUDSTONE**: dk gray-black
conjugate shear pair, both slicks dip slip, polished & warky. Strong bedding parting 853-855
← 1cm. coal, 20° fract. below it.
852.3 desorp. sample — 45° shear
853.4
26° fract. rusty coating
← cross-cutting planar fractures, rusty coatings 15°, 20°
857.7 —— grad. contact
50° slicks — 0° enechelon carbonate filled fractures in sandy zone.
15° set of close-spaced enechelon fracts — **SILTSTONE**
860.5 —— grad. contact
← 0.8' coal - sheared-broken — **MUDSTONE**: dk gray to black
55°, 35° shears in coal seam
60,70 conj shears, both dip slip
← 70° shear
0.4 coal - broken
← 75 slicks
867.5 0.25' thick coal ⊥n 85°CA bounded by ropy calcite veins, both contacts
40° slicks near dip slip.
20° fract. ← multiple coal seams 1mm - 2mm. - parting ea. 0.1 = 0.2 ft.
871.0 —— grad. contact
← 70° slicks, curved surface (photo) — **SILTSTONE**: dk gray
← minor slick
not fractured-sheared
879.0 mudstone bed 60°, 70° slickensides
880.0
60,70 both strongly curved along length of slicks, 25° dip change
mudstone
← planar fracture
← 2mm coal
planar fractures
890.5' —— grad contact
← several 1-2mm coals — **MUDSTONE**: dk gray - black. Bedding parting ea. cm in & coal seam zones, elsewhere ea. 0.1 to 0.2 ft.
pair 60° slicks
← 0.7' coal bed ← 30° shear | in coal seam
897.3' —— grad. contact
SILTSTONE gray interbedded with med. grained Sandstone & limey Sandstone

Drilling Interval	% Core Recovered	Core Size	RQD	Sample Interval	Photos
					photo 12 833.5 slickensided shears.
			reaction colored		string carbonate in light interbeds.
					photo 13 planar fracts 855.5 w/ rusty coatings
0.2	ft.				photo 14 868 coal seam w/ carbonate @ contacts.
					photo 15 871 slick surface

Drill Site:
N: E:
Started:
Completed

Collar Elevation:
Bearing:
Inclination:
Total Depth:

Sandia National Laboratories
Logged by: Ron Grauchen
Log Version:
Log Date: Mar. 25, 2002

Raton Basin Project
Hole No: CH-5
Scale: 1" = 10' (1:120)
Sheet 12 of

DEPTH, feet | fracture height | Shale fissility | coal parting | Carbonate coating | FRACTURING | GEOLOGY | COMMENTS: | Descriptive Geology | Avg. Core Recovery/ Hole | Drilling Interval | % Core Recovered | Core Size | RQD | Sample Interval | photos

DEPTH, feet: 900, 910, 920, 930, 940, 950, 960, 970

fracture height: .02, .28, .34, .10, .20, 1.80, 1.10, .26, .12, .09, .07, .70, .15, .18, .22, .09, .55, .04, .14, .23

Shale fissility: (.75), (.12)

Carbonate coating: 75, 55, 30°, 30, 60, 6°, 9°, 0, 58, 55, 65, 50, 35, 23, 75, 63, 55, 35

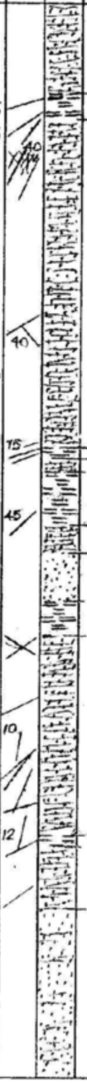

no fractures
75° slicks
906.0 —— grad. contact
907.7 —— grad. contact
55° slicks, 20° from dip ∡; 40° slicks v. wavey, 15° off dip ∡.
30° shear zone, slickenside rubble suggests FAULT ZONE 30°/CA.
no fractures
60°, slicks smooth dip slip, 40° is fracture
6° long planar fracture in & out of core over 1.80 ft.
thin white calcite coating perhaps 50% filled ?
9°, 0.1mm white calcite vein; 0° along side core, calcite vn 0.1mm
929.0 black mudstone w/ coal/near coal 0.3' thick cut by several 75° shear slicks.
929.8
930.8 —— grad contact
45° slicks, well curved 45° to 90°
934.2 — grad contact
siltstone
936.6
sandstone
939.1 —
mudstone
941.3 —
conjugate shears, slicks @ rake angle
65° slicks dip slip
} multiple shear surfaces
parting from drilling each 1cm – 3cm
10° planar fracture
← 949' fault 35°-50° shear pair & broken between them
23° slicks, 10° off dip
75° slicks planar, striae 40° rake from dip
954.3 — mudstone
955.0 —
12° planar fracture
55° smooth, slightly curved surface, dip slip
959.0 —— gradational contact
35° planar fract 25% calcite fill
no fractures

cont. <u>SILTSTONE</u>: interbedded silts and sands; some sands with strong carbonate acid reaction

<u>Mudstone-black nearly coal, shaley</u>

<u>SILTSTONE</u>: interbedded dk siltstone and lt gray sandstone & limey sandstone

<u>MUDSTONE</u>: black w/ multiple 1mm coal beds. local parting on coal

<u>SILTSTONE</u>: gray, thick bedded

<u>SANDSTONE</u>: Interbedded silts and sands, some sand with calcareous cement. Fine-grained-v.f. grained

Drill Site:
N:
E:
Started:
Completed

Collar Elevation:
Bearing:
Inclination:
Total Depth:

Sandia National Laboratories
Logged by: Ron Graichen
Log Version:
Log Date: Mar 26, 2002

Raton Basin Project
Hole No: CH-5
Scale: 1" = 10' (1:120)
Sheet 13 of

DEPTH, feet: 970, 980, 990, 1000, 1010, 1020, 1030, 1040

fracture height	shale fissility	coal parting	carbonate coating	FRACTURING
.21	(35)	35		45
.22	(6)	6	95	
.26				
.31	(30)		30	
.14	(45)		10	
1.25	(10)			
.15	→		33	
.60	(3)		0°	3° 12
.50	(0)		0°	
1.20	(0')			
.55	(14)		14	
.65	(4)		4	
			70	
			65	
.07	(65)	23 26		65
.11			14	45
1.20				0°
.02	(80)		55	80
.18	(55)		80	
.07			60	
.10			47	
.24			23	
.21			23	
				25
.41			35	
.20				
.30	(5)		60	
.26	(35)		5	35
.80	(0)			0

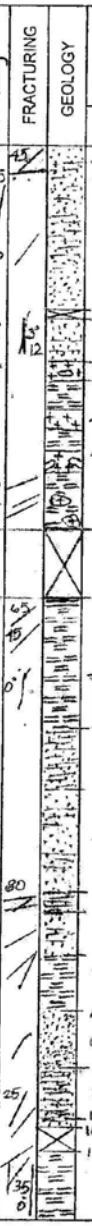

COMMENTS:

Avg. Core Recovery/ Hole

Descriptive Geology

35' planar fracture 25% carb. fill.
45' planar fracture; 85 planar slicks
6° planar fract. 50% fill; same 30°
10° calcite vein/fracture 100% fill bottoms in silty bedding

SANDSTONE: Cont. interbedded silts & calcareous sands. Poorly fractured - sheared.

33° stepped fracture

← 1mm. coal seam in sandstone

980.9 – 981.6 sample removed.
3° rough surf. fracture cross-cut by 12° parting on 2mm coal "vein" several parallel hairline calcite veinlets. & photos.

984.1
0°; hairline calcite vnlts 1.2 ft long. 0.60' long
sill
14' planar fract. 10% filled w/ calcite
4°, 0.1mm white calcite vn in dike rock
70° slicks @ rake & striae
65' slicks pair, rake & striae

MUDSTONE: Black carbonaceous with intrusive dikes - sills of dacite(?) No obvious cooking effects on black mudstone by sill. Sill must have been dry & the mudstone too. A chloritic green of sill rock suggests post implacement alteration - by organic acids ?

995.1
samples removed - desorbtion tests. ⓑ 994.0 is 0.12' coked coal bed ?

999.6 two coal beds, one remnant of removed sample; other 1cm thick.
← 1cm discing of core 1002-1003 on thin coals < 1mm. ← 65° planar slicks @ rake
23, 26' planar fracts w/ flakey carbonate coatings (which flakes off)
45° planar fract
← 14' carb. coated fract. 40% fill
dk gray ← 0° sinuous fracture; 0.1mm coal wisps in mudstone bedding plane.

1008.0 — grad contact

SILTSTONE: dk gray, thick bedded

no fractures - shears

1012.0 — grad contact

SANDSTONE: lt. gray with darker gray interbeds of siltstone: fine-grained Sands some carbonate cemented.

no fractures/shears

1018.8 – 1020.0 mudstone/siltstone/coal zone; 55° 80° slickensided shears & gouge
60° slicks, polished & planar

1023.0 — grad. contact

MUDSTONE: dk gray-brown somewhat friable

← planar fracture
23° slicks dip slip

1026.6 — grad. contact

FINE SANDSTONE: gray, thick-bedded

curving slick, striae curving too

1030.6 — grad. contact

SILTSTONE: gray, thick-bedded

25°, stepped fracture

1033.4 — grad. contact
1034.0 – 1035.9 desorb sample ← 35° slicks 20° off dip

MUDSTONE: dk gray-brown, friable

60° slicks, 20° off dip
5° slicks parallel core & curve into 35° slicks @ 45° rake
0° wavey, rough irregular slicks along side of core

Drilling Interval

% Core Recovered

Core Size

RQD

Sample Interval

photos

photo 16 982' coal vein parting.
photo 17. reverse side of 982' calcite vning
photo 18 984-993 sill intrusive
photo 19 slicks set 5°-35° 1036 ft.

Raton Basin Project
Hole No: CH-5
Scale: 1" = 10' (1:120)
Sheet 14 of

Sandia National Laboratories
Logged by: Ron Grauchen
Log Version:
Log Date: Mar. 26, 2002

Collar Elevation:
Bearing:
Inclination:
Total Depth:

Drill Site:
N: E:
Started:
Completed

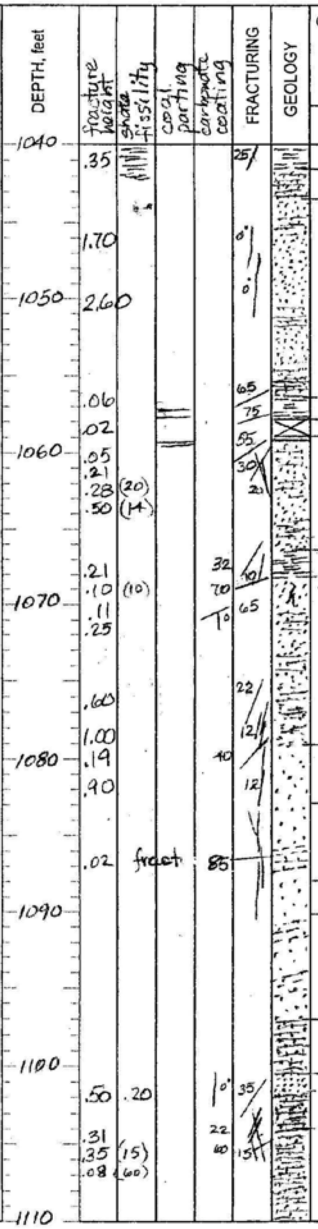

COMMENTS:

Avg. Core Recovery/ Hole

Descriptive Geology

1041.7 — grad. contact

Mudstone - cont. friable & highly broken-sheared siltstone gray, thick bedded, carbon trash random

1043.4 — grad. contact

long rough surface en echelon fractures

SANDSTONE: fine - med. grained some med. ss. highly calcareous Inter bedded w/ darker siltstones.

no fractures

← 65° polished slicks

1056.3' — abrupt contact

1057.9' 75° slicks Sample removed

1058.8' ——— 1058.9 sharp contact

MUDSTONE: black carbonaceous parting on 1cm. coal.

55° fracture.
30° planar fract.
20° fract 0.28 long, and 14° adjacent fract 0.50' long.

SILTSTONE: dk gray, thick-bedded

no fractures

1066.4 ← abrupt contact

Mudstone irreg. coal clot @ bottom contact.

1068.0 ← abrupt contact

← 32° polished dip slip slicks
10° planar fracture
0°; 65° planar fract. 50% filled

SANDSTONE: ← 70° slicks @ 40° rake
Irregular coal vein @ 1069'
Fine grained interbedded with dk gray siltstone

← rough surface fract

12° set of three long fractures

1079.0 — grad. contact

SANDSTONE: lt. tan med-coarse grained, generally thick bedded with occasional zones of fine grained dark sediment laminations.

1083
two long fractures parallel core & disposed nearly 90° to each other. Weaving auxillar(y) fractures create "spears" of rock
1088
single half (lengthwise) pc of core. photo
1090

no fractures

1097.1 — sharp contact

SILTSTONE: dk gray, thick bedded unfractured

1100.3
1100.7 sandstone; calcite vein - side of core 2mm.
← 22° dip slip slicks pair

← 35° curved surface slicks near dip slip.

15° pair fractures, planar ; 60° planar fracture

Drilling Interval

% Core Recovered

Core Size

RQD

Sample Interval

photo

photo 20
1069'
irregular
coal 'vein'

photo 21
1077' set
fractures.

photo 22
fracture
system
parallel cor
1080'-1089

photo 23
1088'-1090
long fractu

Raton Basin Project
Hole No: CH-5
Scale: 1" = 10' (1:120)
Sheet 15 of

Sandia National Laboratories
Logged by: Ron Graichen
Log Version:
Log Date: Mar 27, 2002

Collar Elevation:
Bearing:
Inclination:
Total Depth:

Drill Site:
N: E:
Started:
Completed

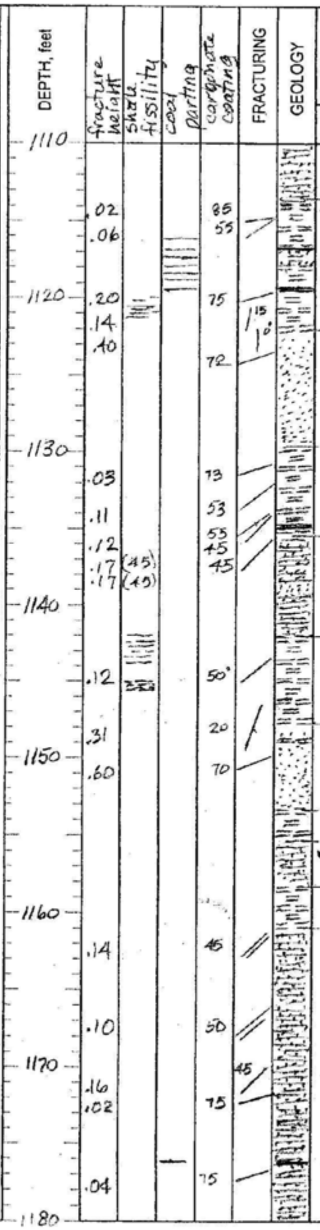

COMMENTS:

Avg. Core Recovery/ Hole

Descriptive Geology

55, 85 slicks — cont **SILTSTONE:** dk gray thick-bedded

1113.8 —— grad. contact

0.8' zone, badly broken sheared drilling rubble — **MUDSTONE:** black w/ coal, locally fissile, strong bedding parting 1cm to 0.1 ft. Numerous 1mm - 3mm coals

0.18' coal

0.5' coal, broken pcs.
75°, dip slip slicks

1122 0.4' of fissile shale

122.2 —— abrupt contact

planar fract. 0°, 15
72° slicks

SANDSTONE: interbedded fine sands and darker silts, irregular bedding textures.

1129.8 —— grad. contact

slicks, smooth dip slip striae — **MUDSTONE:** black, coal bearing

planar fract

coal broken — 1134.5 - 1135.5 mostly coal, too broken to determine thickness.

1135.6 —— grad contact

slicks on coal 55°, 45°
45° slicks, v. irregular, fluted — **SILTSTONE:** dk brown with bioturbidite features, thick-bedded, poorly fractured

1142.0 —— grad contact

slicks 20° rake from dip. — **MUDSTONE:** dk brown, shaley bedding parting common, each 1cm. - 0.1 ft.

1147.7 —— grad contact

20° fluted slickensides 10° off dip, along carbon remnant.
70°, planar slicks, dip slip — **SANDSTONE:** med. grained, interbedded w/ siltstone.

1153.6 —— grad contact — mudstone dk gray, some 0.1' bed parting

1155.3 —— grad contact

0.6' limey w/ cone in cone structure — **SILTSTONE:** gray thick bedded some bug tracks

1158.6 —— grad. contact — **MUDSTONE:** dk brown, 0.1 ft. bed parts.

1161.0 —— grad. contact

45° slicks dip slip, pair — **MUDDY SILTSTONE:** dk gray, thick bedded. almost a mudstone — ----- bedding parting is most common fracture @ 3-4/ft

pair of wavey slicks, dip slip + 15° rake ∡ from dip.

wavey slicks, 30° off dip
75° slicks, bumpy

1cm. coal
75° slicks, bumpy
contact @ 1180.0 ft

Drilling Interval	% Core Recovered	Core Size	RQD	Sample Interval	photos
					photo shear 1148'

Raton Basin Project
Hole No: CH 5
Scale: 1" = 10' (1:120)
Sheet 16 of ___

Sandia National Laboratories
Logged by: Ron Graichen
Log Version:
Log Date: Mar. 27, 2002

Collar Elevation:
Bearing:
Inclination:
Total Depth:

Drill Site:
N: E:
Started:
Completed

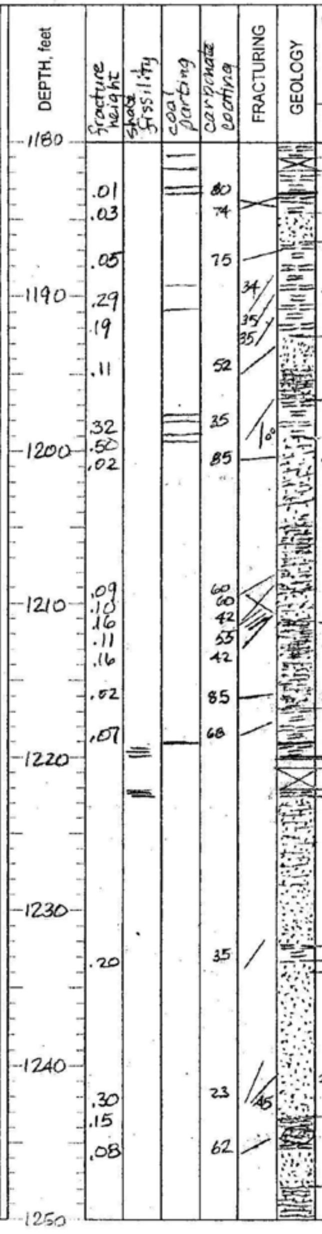

COMMENTS:

Avg. Core Recovery/ Hole

Descriptive Geology

1181.0 abrupt contact @ 1180.0 ft.
1181.9 → desorp sample
2cm coal

MUDSTONE: black
80, 74' slickensides, bumpy irregular patterns

1184.6 — grad. contact

SANDSTONE: med. grained, gray green

1186.5 — grad. contact
irregular slicks

MUDSTONE: dk gray to black
Two (2mm, 3mm) coals

← bumpy irregular slicks

1192.7 — grad contact
slicks 30° off dip ∠

FINE SANDSTONE - SILTSTONE: dk gray green

1196.8 ← grad contact
35° v. bumpy irregular slicks.

MUDSTONE: black carbonaceous
Several coal bed partings on bedding

1199.3 ← grad contact
← 0° planar fracture on side of core
← 85°, parting on 2mm coal

SANDSTONE: fine to med. grained
coarser sands lt. gray, inter bedded with
darker siltstones. Some thick-bedded
with bioturbidite features.

unfractured/sheared

slicks
conjugate shears, poor slick definition - at rake ∠s.

1211.3 — grad contact
55° set of (3) fractures - planar
42° planar fracture
85° part on carbon film in bedding

SILTSTONE: gray, thick bedded
locally sandstone

1216.8 — grad. contact
68° slicks 45° rake slicks.
← 1cm. coal

MUDSTONE: black w/ coal seams

1220.25 - 1220.55 removed
1220.8
1222.1 removed
1222.4 ← abrupt contact
shaley discing above & below coal

SANDSTONE: fine to med. grained,
interbedded w/ siltstones

not fractured

1232.3 mudstone
1233.3
1234.0 — abrupt contact
35° dip slip fluted slickensides

SANDSTONE: med. to coarse grained
lt. tan with minor f.g ss. & siltstone
laminations

23, irregular fracture on
silty-carbon layer v. rough surface: 45° parting on carbon layer

1243.1
← 0.5 ft. Ironstone concretionary deposit w/ central star fracturing
and calcite filling: 62° slicks @ 40° rake

1248.0 — grad. contact

SILTSTONE

Drilling Interval

% Core Recovered

Core Size

RQD

Sample Interval

photos

Drill Site:
N: E:
Started:
Completed

Collar Elevation:
Bearing:
Inclination:
Total Depth:

Sandia National Laboratories
Logged by: Ron Graichen
Log Version:
Log Date: Mar 27, 2002

Raton Basin Project
Hole No: CH-5
Scale: 1" = 10' (1:120)
Sheet 17 of

Drilling Interval	% Core Recovered	Core Size	RQD	Sample Interval	photos

COMMENTS: Avg. Core Recovery/ Hole

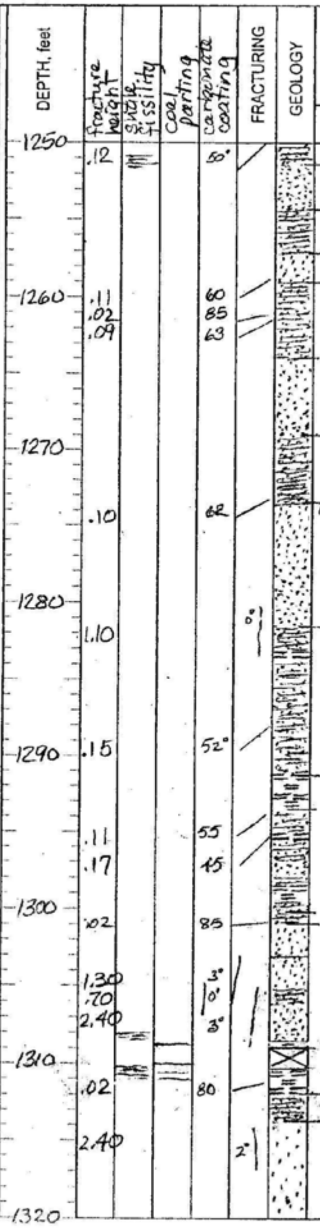

Descriptive Geology

1251.6 —— abrupt contact
SILTSTONE 50° mirror surface shear w/ gouge
thick-bedded
SANDSTONE: fine grained, gray brown

1254.2 —— grad. contact
SILTSTONE: dk gray, thick bedded

1257.1 —— grad. contact
SANDSTONE: fine-grained, gray

1259.0 —— grad contact
60° slicks @ dip ∡
SILTSTONE:
multiple orientation slicks. 85° wavey dip slip slicks.
Abundant carbon trash, random orientation

1264.0 —— grad contact
no fractures
SANDSTONE: med. gr. sandst is lt. gray interbedded with dk gray silts as laminations & thin beds disrupted by worm borings.

1269.0 —— grad. contact
no fractures
SILTSTONE: interbedded f.sands & silts becoming more Sandy toward 1273.5.

1273.5 —— grad contact
slicks on 1mm coal
SANDSTONE: fine-med. grained interbedded with dk gray siltstones.
no fractures

1281.7 —— abrupt contact
0° frat. skins side of core
SILTSTONE: dk gray, thick bedded bedding parting each 0.2'-0.4' average, caused by drilling. occasional petal fracture, drilling caused

slicks, wavey, dip slip

1291.4 —— grad contact
bedding parting each 1cm - 3 cm. 1191.8'- 1192.5'

1293.4 —— missing core
MUDSTONE - SILTSTONE: inter-bedded
wavey polished slicks
slicks 15° rake from dip, slick surfaces curves down dip 20° to 60°!

1301.4 ← siltstone
1302.0 —— grad. contact
85, slicks on bedding plane
SANDSTONE: med. g., lt. tan; enechelon fractures, 3° fractures are sub parallel, the 0° frac., 20% calcite filled. is at near right ∡ to 3° fracture strike.
siltstone 1306-1307

1308.6 —— abrupt contact
sample removed
1310.35 60° slicks on bedding
MUDSTONE: dk gray thin coals - 1mm
0.6' fissile shale below sample

1312.0 —— grad. contact
SILTSTONE: gray brown thick bedded random carbon trash.

1314.0 —— abrupt contact
SANDSTONE: coarse grained lt. tan, thick bedded
long rough surface fracture, to begins @ siltstone bed contact - bottom exits core

Drill Site:
N: E:
Started:
Completed

Collar Elevation:
Bearing:
Inclination:
Total Depth:

Sandia National Laboratories
Logged by: Ron Graichen
Log Version:
Log Date: Mar 28, 2002

Raton Basin Project
Hole No: CH-5
Scale: 1" = 10' (1:120)
Sheet 18 of

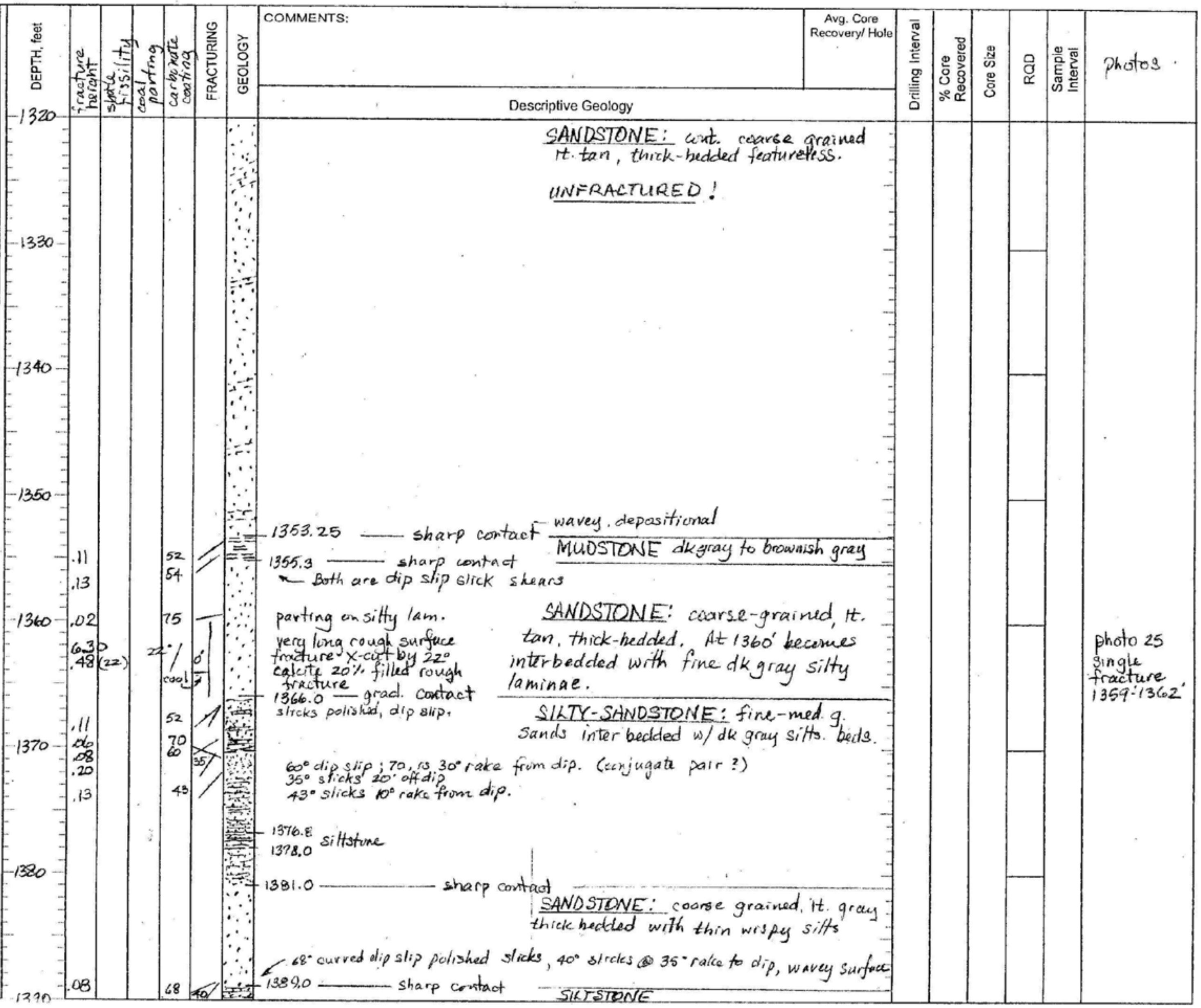

SANDSTONE: cont. coarse grained lt. tan, thick-bedded featureless.

UNFRACTURED!

1353.25 —— sharp contact wavey, depositional

MUDSTONE dk gray to brownish gray

1355.3 —— sharp contact
← Both are dip slip slick shears

SANDSTONE: coarse-grained, lt. tan, thick-bedded. At 1360' becomes interbedded with fine dk gray silty laminae.

parting on silty lam.
very long rough surface fracture X-cut by 22° calcite 20% filled rough fracture

photo 25 single fracture 1359-1362'

1366.0 — grad. contact
slicks polished, dip slip.

SILTY-SANDSTONE: fine-med. g. Sands interbedded w/ dk gray silts. beds.

60° dip slip; 70, 15 30° rake from dip. (conjugate pair ?)
35° slicks 20° off dip
43° slicks 10° rake from dip.

1376.8
1378.0 siltstone

1381.0 —— sharp contact

SANDSTONE: coarse grained, lt. gray thick bedded with thin wispy silts

68° curved dip slip polished slicks, 40° slicks @ 35° rake to dip, wavey surface

1389.0 —— sharp contact

SILTSTONE

Raton Basin Project
Hole No: CH-5
Scale: 1" = 10' (1:120)
Sheet 19 of

Sandia National Laboratories
Logged by: Ron Graichen
Log Version:
Log Date: Mar. 28, 2002

Collar Elevation:
Bearing:
Inclination:
Total Depth:

Drill Site:
N:
E:
Started:
Completed

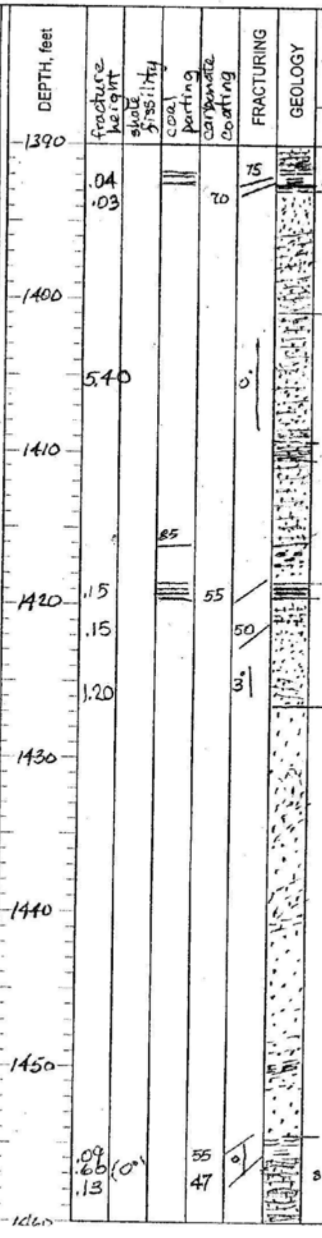

COMMENTS:

Avg. Core Recovery/ Hole

Descriptive Geology

several 1-2mm coals and **SILTSTONE-MUDSTONE:** dk gray to
0.15 coal at contact
1393 —— obrupt contact dk brownish gray + black
75° polished wavey, curving slick surface; 70° bumpy dipslip shear.
non-bedded, multiple random orientations of carbon trash in brownish gray f.g. Sandstone. **SANDSTONE:** fine-gr.

1401.0

long rough surface fracture, double split 1404-1405. 1cm apart and parallel
No other natural fracturing

1409.4 dk brown siltstone
1410.5

86° coal
Three 1cm. coals, one 0.25 ft broken coal.
55° slicks on coal: 1417-1418 subangular siltstone pebbles
1418.5
1419.4 coal beds
SANDSTONE: fine gr. to med. gr.
lt. gray interbedded w/ dk gray siltstone beds & laminations. Some bioturbidite textures.
rough surface, near dip slip striae.
planar fract, top begins in silty bed, bottom exits core.
1426.5 —— sharp contact ——

SANDSTONE: med. to coarse gr.
lt. gray thick bedded Sandstone
wispy silty bedding indicators show bedding folding – soft sediment deformation perhaps.

no fractures

1454.4 —— sharp contact ——
slicks 20° rake from dip
slicks 10° rake from dip
broad wavey
SILTSTONE: start of interval is 1½ ft of mudstone
Gray, thick-bedded: 0° planar fracture
Gradually becoming Sandstone @ 1460 ft

Drilling Interval
% Core Recovered
Core Size
RQD
Sample Interval
photos

Sandia National Laboratories
Logged by: Ron Graichen
Log Version:
Log Date: Mar 28, 2002

Raton Basin Project
Hole No: CH-5
Scale: 1" = 10' (1:120)
Sheet 2D of

Drill Site:
N:
E:
Started:
Completed
Collar Elevation:
Bearing:
Inclination:
Total Depth:

DEPTH, feet: 1460 – 1470 – 1480 – 1490 – 1500 – 1510 – 1520 – 1530

fracture height	shale fissility	coal parting	carbonate coating
.42 .40			12°
6.80			
.14			50°
.47			
.85 .63 .50			2° 8° 12°
.32 .45	(16) (8)		16° 8°
.11 .20 .10 .11			62 40 67 60
.12			50°
.12			50°
.15 .75 .16 .12			50 35 45

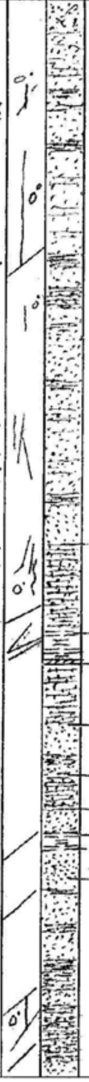

COMMENTS:

Avg. Core Recovery/ Hole

Descriptive Geology

contact
1459-1461, carbon trash @ random orientations.

SANDSTONE: fine to med. grained
Lt gray coarser sands interbedded with dk gray silts as fine beds & laminations
silty bedding generally 80-85°CA.

@ 466 two unbroken fractures, parallel CA 0.42' and 12°CA & 0.40'.

Long rough surface fracture, top begins as a "J" fracture @ 1476.4' and finally exits core in siltstone bed 1477.4'
Fracture length has a very gentle sinuous orientation

slicks. 10° rake from dip, planar surface

planar fracture in siltstone bed.

} minor random orientation carbon trash

Several fractures nearly parallel CA intersecting @ acute angles
2°, unbroken fracture top & bottom start & end in siltstone laminae
8°, V. rough surface, parallel strike to 2° structure
12°, planar, not rough & at about 10° strike variation from other fracts.

1495.4 —— abrupt contact
V. rough fracture 16°; 8° V. planar
← 0° very wavey, generally parallel core axis, 2-3mm wide, one side is homogeneous siltstone, the other is a jumbled, swirled & mixed texture siltstone
62°, slicks 20° from dip angle.

SILTSTONE: dk gray thick-bedded

1501.3 —— grad. contact

MUDSTONE: dk gray to black; 0.4' core missing as "N.Rec.", no recovery, coal 0.1' above, 0.2' below missing interval.

1503.4 —— grad. contact

set of slicks, all parallel 40°, 67°, 60° about 10°-15° rake from dip &

SILTSTONE: gray - thick bedded

1507.3 —— grad contact

SANDSTONE: silty to fine sandst.
random orientation carbon trash 1506-1509

1510.5 —— grad contact
4mm coal @ 1511'

SILTSTONE: gray, thick bedded, not fractured

1512.6 —— grad contact

SANDSTONE: med. gr.
50°, planar slicks 20° rake from dip

1514.3
1515.4 mudstone w/ 1-2mm coals
} irregular orientation carbon trash.

1517.2 —— sharp contact

wavy, bumpy slicks, dip slip

SANDSTONE - SILTSTONE: interbedded f.g. sandstone, lt. med. gray & darker siltst.

slicks 15° rake from dip; 0° planar fracture

35° dip slip hackly slicks
45° slicks 10° rake from dip.

Drilling Interval

% Core Recovered

Core Size

RQD

Sample Interval

photos

photo 26
unbroken fracture
photo 27
1489 ft
two fractures

photo 28
irregular coal "vein"
1496-1497.5'
photo 29
1502'
set of slicks

Drill Site:
N:
E:
Started:
Completed

Collar Elevation:
Bearing:
Inclination:
Total Depth:

Sandia National Laboratories
Logged by: Ron Graichen
Log Version:
Log Date: Apr. 2, 2002

Raton Basin Project
Hole No: CH-5
Scale: 1" = 10' (1:120)
Sheet 21 of

DEPTH, feet: 1530, 1540, 1550, 1560, 1570, 1580, 1590, 1600

fracture height	shale fissility	coal parting	carbonate coating	FRACTURING
.44			0°	
7.00			0°	
1.50(0°)				0°
2.20(3°)				3°
.90			0°	
1.20			0°	
2.00			0°	
1.60				2°
1.20			5°	3°
.42 (5°)				
.11				55
1.50				8°
.10			50	
.20			35	
.10			60	
.30			27	
.10			40 55	
.08			60	
.08			60	

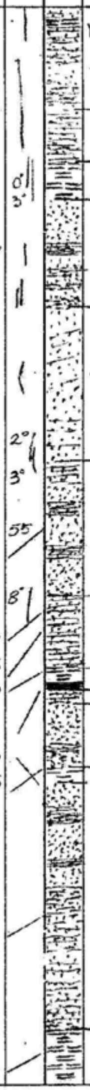

COMMENTS:

Avg. Core Recovery/ Hole

Descriptive Geology

planar vertical fracture. cont
← 0.4' mudstone, shaley parting

SANDSTONE- SILTSTONE interbedded.

← Long planar fract, locally double parallel fracts 0.5 cm apart. Top begins in siltstone bedding, bottom exits core.

1536.9 —— grad. contact

SILTSTONE: dk gray, thick-bedded

1540.0 —— abrupt contact

planar fracts. near parallel – 2 but diverging & exit core

MUDSTONE: dk gray-brown

1542.6 —— abrupt contact

SANDSTONE-SILTSTONE: interbedded

dk brown siltstone w/ several thin 1-2mm coals.

f.g. sands: ← 0° fract. begins & ends in silty bedding.

← 0° fract. doubles only in .35ft sandstone bed, 1cm. apart.

1549.4 —— abrupt contact

SANDSTONE: medium grained, lt. gray thick-bedded, calcareous cement

0°, aver. incl on sinuous fract. locally doubled. Fract. enters & leaves core domain

← Two enechelon & curving fractures similar to above, separated by ~ 2 cm. Minor pyrite on one

1559.6 —— abrupt contact

← 5°, 2mm white calcite vn.

SANDSTONE-SILTSTONE: interbedded Mostly fine grained sandstone

← planar slicks, dip slip, In siltstone bed.

1568.4 —— grad. contact

Planar fract enters core in SS, leaves in siltstone, siltstone w/ bedding parting due to drilling ea. 0.1ft only in length of fracture.

SILTSTONE: gray, thick bedded.

1573.0' ← mudstone

1574.1' 0.3ft thick coal bed

← 50° slicks, rough surface, striae @ dip 4.

35° slicks curved in strike, dipslip stride

1575.3 —— grad. contact

← 60° polished slicks, 15° rake from dip.

27° wavey surface, dip slip.

SANDSTONE: fine grained, gray, thick bedded

1579.5 —— gradational contact

1580.6 mudstone; 55° planar slicks 25° rake from dip

40° curving surface, slicks dip slip.

no fractures

SANDSTONE-SILTSTONE: interbedded f.g. sands and silts as fine bedding and laminations. Occasional v thin coal.

slicks near dip slip, gently curving surface!

1596.7 —— grad. contact

MUDSTONE: dk brownish gray Bedding parting common ea. 0.10ft ±

Drilling Interval

% Core Recovered

Core Size

RQD

Sample Interval

photos

photo 30 fracture doubles in sandstone bed, 1548-1549'

photo 31 1554 ft. sinuous fract. in SS.

Drill Site:
N: E:
Started:
Completed

Collar Elevation:
Bearing:
Inclination:
Total Depth:

Sandia National Laboratories
Logged by: Ron Graichen
Log Version:
Log Date: Apr. 2, 2002

Raton Basin Project
Hole No: CH-5
Scale: 1" = 10' (1:120)
Sheet 22 of

COMMENTS: Swelling clays common throughout hole length.
Core diameter 0.20 ft

Avg. Core Recovery/ Hole

DEPTH, feet | fracture height | shale fissility | coal parting | carbonate coating | FRACTURING | GEOLOGY

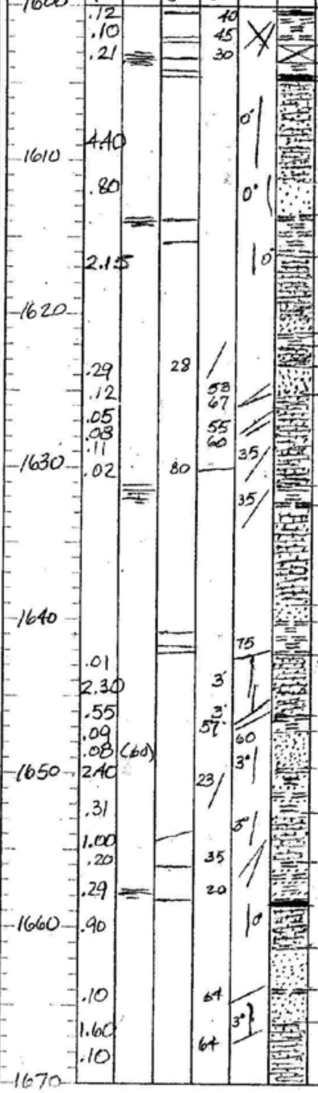

Descriptive Geology

← 0.3' coal
dip slip slicks, 40', 45' cont. **MUDSTONE:** black, coal bearing
1602.6 desorp sample
1603.3
1604.5 ← 0.35' coal
grad. contact

SILTSTONE - SANDSTONE: inter-bedded
Long planar, straight fracture. Top begins in siltstone bed, doubles for 0.7' & exits core @ bottom.
v. thin beds & laminations siltstone & v.f. sandstone

1611.3 abrupt contact
curved fracture in/out core domain
abrupt contact
SANDSTONE: med. grain, lt. gray
1613.4 1mm coal
← 4mm coal
MUDSTONE: dk gray; thick bedded.
1616.2 abrupt contact

SILTSTONE: dk gray, thick bedded

1621.3 mudstone - black - a few petal fractures. Drill discing ea 1 - 2cm.
1622.0 siltstone; 28° slicks 10° rake from dip; 30% calcite filling
1623.4 f.g. sandstone, thick bedded 58°, 67° slicks, both near dip slip
1625.0 56° curved slicks (in strike) striae @ dip ∡.; 60° slicks near dip slip

35° rough slicks; 80° is unbroken 2.5 mm wide calcite vn 100% fill.
1631.0 black mudstone
1632.5 35°, rough slicks

unbroken

1639.0 f.g. sandstone
1640.0 abrupt contact
bedding parting ea. 0.1 ft
1642.2 - abrupt
MUDSTONE: black, coal bearing ½-1mm
← 75° dip slip slickensides
SILTSTONE:

1646.0 abrupt contact
1647.2 mudstone 57°, curved (strike) slicks dip slip
SANDSTONE: f.g. interbedded w/ siltstone
60°, slicks @ 30° rake from dip
1649.6 abrupt

SILTY MUDSTONE some petal fracts.
3° long sinuous fract.; 23° slicks, 20% calcite filled. dip slip
1652.5 3° planar fract ends in coal parting
SILTSTONE: gray to dk. gray
thick-bedded
1655.8
SILTY MUDSTONE 1mm coal bed
35° & 20° slicks w/ striae 30° rake to dip.
1658.5 ← 0.4 ft coal - drill rubble
← 0° begins @ coal bed, planar fract.
1661.3 abrupt contact

SANDSTONE: fine-grained, thick bedded
1664.0 0.5' silty mudstone 64° planar dip slip slicks.
1666.0 grad. contact
64° planar dip slip, 3° fract terminates on slip.
SILTSTONE: 3° is a "J" fracture, coming into core on top - term on slick below.

Drilling Interval | % Core Recovered | Core Size | RQD | Sample Interval | Photos

photo 32
long fracture
1606-1609
shown in photo.

Sandia National Laboratories
Raton Basin Project
Logged by: Ron Graichen
Hole No: CH-5
Log Version:
Scale: 1" = 10' (1:120)
Log Date: April 3, 2002
Sheet 23 of

Drill Site:
Collar Elevation:
N:
E:
Bearing:
Started:
Inclination:
Completed
Total Depth:

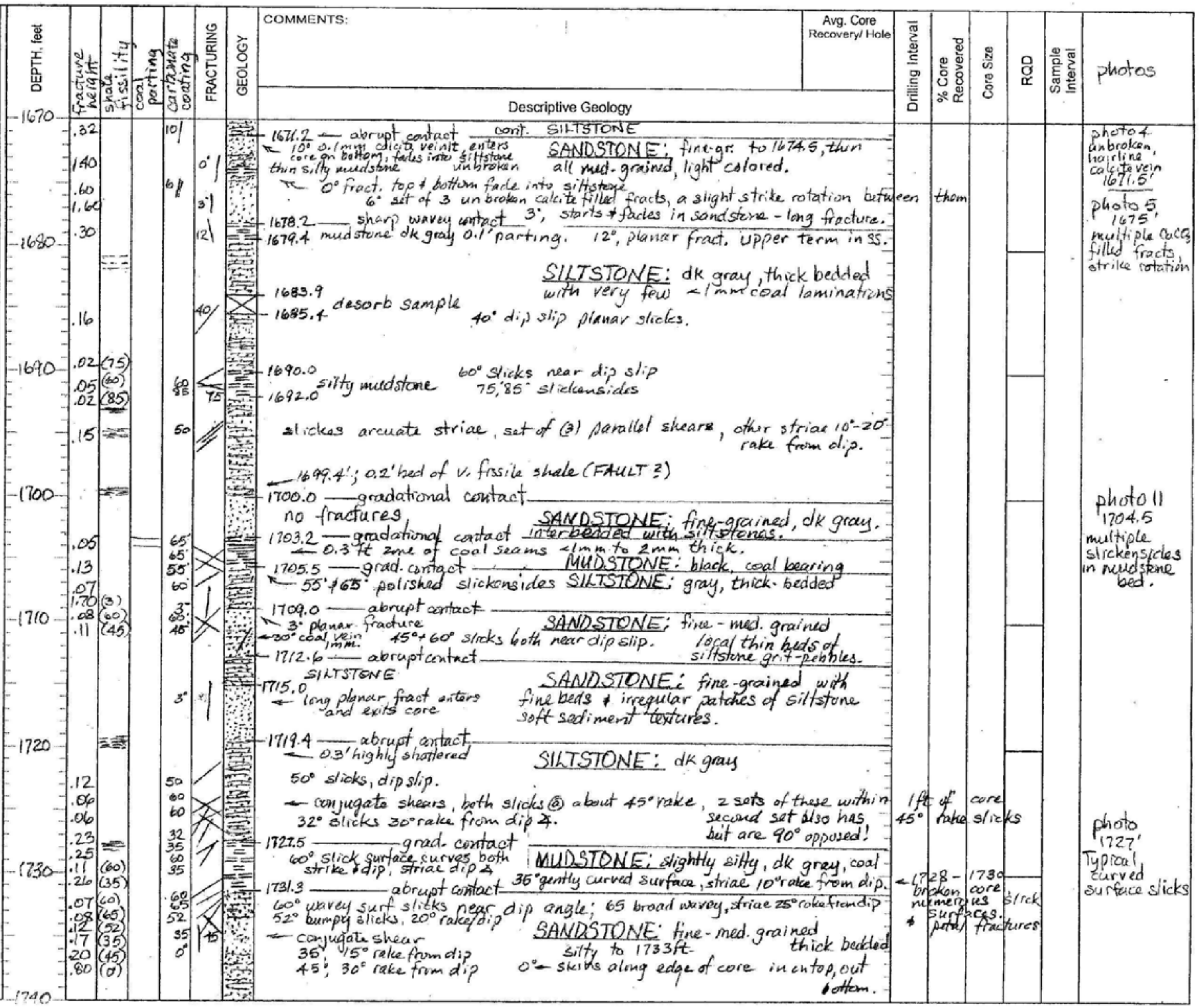

1671.2 — abrupt contact cont. SILTSTONE
← 10° 0.1mm calcite veinlt, enters core on bottom; fades into siltstone unbroken
thin silty mudstone
SANDSTONE: fine-gr. to 1674.5, then all med-grained, light colored.
← 0° fract. top & bottom fade into siltstone
6° set of 3 unbroken calcite filled fracts, a slight strike rotation between them
1678.2 — sharp wavey contact 3°, starts & fades in sandstone - long fracture.
1679.4 mudstone dk gray 0.1' parting. 12°, planar fract. upper term in SS.

SILTSTONE: dk gray, thick bedded with very few <1mm coal laminations
1683.9 desorb sample
1685.4
40° dip slip planar slicks.

1690.0 silty mudstone 60° slicks near dip slip
1692.0 75, 85° slickensides

slickes arcuate striae, set of (3) parallel shears, other striae 10°-20° rake from dip.

← 1699.4'; 0.2' bed of v. fissile shale (FAULT ?)
1700.0 — gradational contact
no fractures
SANDSTONE: fine-grained, dk gray. interbedded with siltstones.
1703.2 — gradational contact
← 0.3 ft zone of coal seams <1mm to 2mm thick.
1705.5 — grad. contact **MUDSTONE:** black, coal bearing
← 55° & 65° polished slickensides **SILTSTONE:** gray, thick-bedded
1709.0 — abrupt contact
← 3° planar fracture
← 30° coal vein 1mm.
45° + 60° slicks both near dip slip.
SANDSTONE: fine - med. grained local thin beds of siltstone grit-pebbles.
1712.6 — abrupt contact
SILTSTONE
1715.0
← long planar fract enters and exits core
SANDSTONE: fine-grained with fine beds & irregular patches of siltstone soft sediment textures.
1719.4 — abrupt contact
← 0.3' highly shattered
SILTSTONE: dk gray
50° slicks, dip slip.
← conjugate shears, both slicks @ about 45° rake, 2 sets of these within 1ft of core
32° slicks 30° rake from dip ∡. second set also has 45° rake slicks but are 90° opposed!
1727.5 — grad. contact
60° slick surface curves both strike & dip, striae dip ∡
MUDSTONE: slightly silty, dk grey, coal
35° gently curved surface, striae 10° rake from dip.
← 1728 - 1730 broken core numerous slick surfaces. & petal fractures
1731.3 — abrupt contact
60° wavey surf slicks near dip angle; 65 broad wavey, striae 25° rake from dip
52° bumpy slicks, 20° rake/dip
SANDSTONE: fine - med. grained thick bedded silty to 1733ft
← conjugate shear
35°, 15° rake from dip
45°, 30° rake from dip
0° ← skirts along edge of core in on top, out bottom.

photo 4 unbroken, hairline calcite vein 1671.5'

photo 5, 1675' multiple calcite filled fracts, strike rotation

photo 11 1704.5 multiple slickensides in mudstone bed.

photo 1727' Typical curved surface slicks

Raton Basin Project
Hole No: CH-5
Scale: 1" = 10' (1:120)
Sheet 24 of

Sandia National Laboratories
Logged by: Ron Graichen
Log Version:
Log Date: April 3, 2002

Collar Elevation:
Bearing:
Inclination:
Total Depth:

Drill Site:
N: E:
Started:
Completed

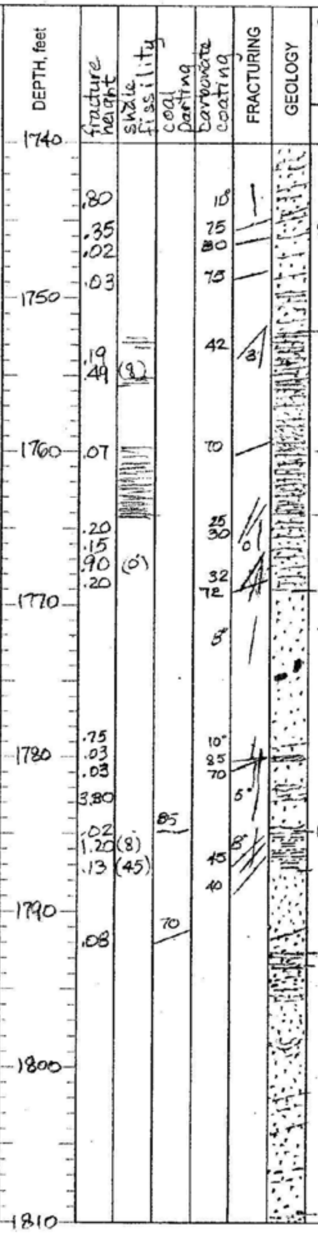

COMMENTS:

Avg. Core Recovery/ Hole

Descriptive Geology

cont. SANDSTONE: lt. tan med. grained becoming coarse grained 1746 – 1749.5'

rough surface fracture, top starts @ silty lamina, bottom exits core

80,75° parting on bumpy surface carbon trash laminae

← carbon parting

1752.0 —— sharp contact

slicks near dip slip bumpy surface.

SILTSTONE: gray, thick-bedded becomes very fine sandstone 1755 to 1760 ft, a brown-gray color

slightly wavey surface slicks, striae 20° rake from dip.

core appears to have been wetted during drilling – swelling clays have altered core to crumbly, friable pieces.

← slicks 25° are dip slip, 30° slicks variable.

← planar fract. top end rubble – so may be longer.

← curving surface (dip) near dip slip

← rubble, numerous but angle slick's, 10° to 20° CA

1769.1 —— abrupt contact 72° gently curved slicks

← rough surface fracture.

SANDSTONE: med. to coarse grained lt. tan, thick-bedded.

Two siltstone clasts; 0.14, 0.20 ft.

10° fracture, top begins on carbon trash bedding lamina & bottoms on siltstone bed or fragment.

← 3cm thick bed or fragment (?) siltstone w/ slicks at both top & bottom sharp contacts

5° fracture comes into core on top, through siltstone fragment & exits core on bottom. Fracture twinned parallel @ ½cm – 1cm apart for one foot below fragment/bed.

1784.8 —— sharp contact

← wavey surface 0.15 mm coal bed in SS. – parting

1787.2 —— abrupt contact

← 8° planar fract. enters core @ contact – exits below

45° slicks 20° rake from dip, cross-cut by fracture.

40° pair of parallel slicks, near dip slip.

1792.8 ← 70° parting on <1mm carbon trash bedding lamina.

1793.7 ← high carbon sandstone – black

SANDSTONE: med. to coarse grained Mostly lt. tan, thick-bedded with local wavey laminae of black carbon trash

no fractures

a few siltstone pebbles

1809.7 —— sharp contact —— FINE GRAINED SANDSTONE

Drilling Interval	% Core Recovered	Core Size	RQD	Sample Interval	photos
20°	rake/dip.				photo 19 siltstone clasts in sandstone
					photo 20 long fracture

Raton Basin Project
Hole No: CH - 5
Scale: 1" = 10' (1:120)
Sheet 25 of

Sandia National Laboratories
Logged by: Ron Grain
Log Version:
Log Date: April 4, 2002

Collar Elevation:
Bearing:
Inclination:
Total Depth:

Drill Site:
N: E:
Started:
Completed

DEPTH, feet	fracture height	shale fissility	coal parting	carbonate coating
1810				
	.90			0°
	3.30			13°
1820	.08			60°
	.20			40°
	.18			35°
	.28			12°
1830	.29			32°
	.20			8°
	.30			8°
1840				
			85	
	.02			
	.06			70
	.09			60
	1.00		10°	
1850	.07 (63)			10°
	.60 (10)			50
	.12 (60)			
1860				
1870	.09		55	
	.09		53	
	.08			
				57
			70	45
1880				

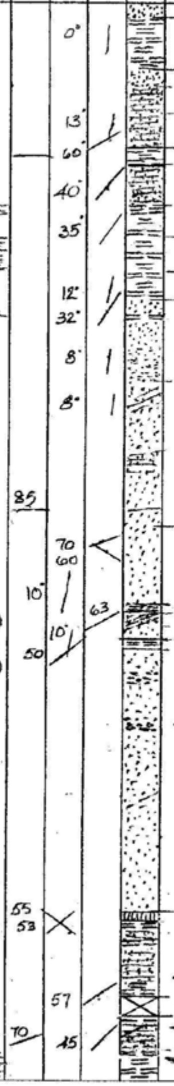

COMMENTS:

Avg. Core Recovery/ Hole

Descriptive Geology — f.g. SANDSTONE

1811.0 ——— abrupt contact
planar fract.

MUDSTONE: black, badly broken
driller pushed the bit too hard.

1814.4 ← sharp contact
1815.5 f. g. + med. g. sandstone

SILTSTONE: gray, thick bedded

broken 13°, slicks 15° rake/dip 60°, slicks 15° rake/dip
1819.5 black mudstone (2) 1/2 cm. coal seams at top of mudstone
1820.6

← planar slick surface striae dip slip.

1823.0 ——— grad. contact

35° slicks, dip slip

MUDSTONE: dk gray to black.
some petal fractures

swelling clays - drilling caused ?, Crumbly, drilling discing
12° planar fract.

1829.3 ——— sharp contact
32°, slicks, dip slip, planar surface

SANDSTONE: gray. Silty + fine grained to 1834.7; medium grained becoming coarser below.
Not fractured !

planar J fracture
1834.7
planar J fracture

← carbon trash bedding lamina - parting
1844 ← a few random 1cm rounded/subrounded siltstone pebbles in coarse-grained sandstone.
70° shear on siltstone bed.
60° parting on 3cm thick high carbon bed
10° rough surface fracture with 20% carbonate filling
1849.2 - 1849.7 silty bed.
1851.4 MUDSTNE 63°, polished planar slicks on carbon silty bed
1852.1 10° planar fracture in carbonaceous shale 10% carbonate filled
50° wavey surface. slicks, dip slip + bottom contact of mudstone bed.

mudstone pebble beds

0.85 ft nearly coal 55, 53° slicks 10° rake from dip, 100% coated w/ calcite
conjugate shear pair.

1868.9 ——— Sharp contact

SILTSTONE with mudstone beds, dk gray to black, mostly thick bedded.
petal fracts in mudstones.

57° planar slicks, 20° rake/dip

1874.7' desorp sample, a few inches of mudstone above + below sample.
1875.8 ← unbroken 6mm feathery calcite vein 65°CA
Hairline calcite in bedding partings.
1878.0 ——— grad contact
← coal lens up to 1cm.

MUDSTONE: dk gray

Drilling Interval | % Core Recovered | Core Size | RQD | Sample Interval | photos

photo 34, 1851.5'-1852' planar fracture in carbonaceous mudstone bed

Raton Basin Project
Hole No: CH-5
Scale: 1" = 10' (1:120)
Sheet 26 of

Sandia National Laboratories
Logged by: Ron Graichen
Log Version:
Log Date: April 4, 2002

Collar Elevation:
Bearing:
Inclination:
Total Depth:

Drill Site:
N:
E:
Started:
Completed

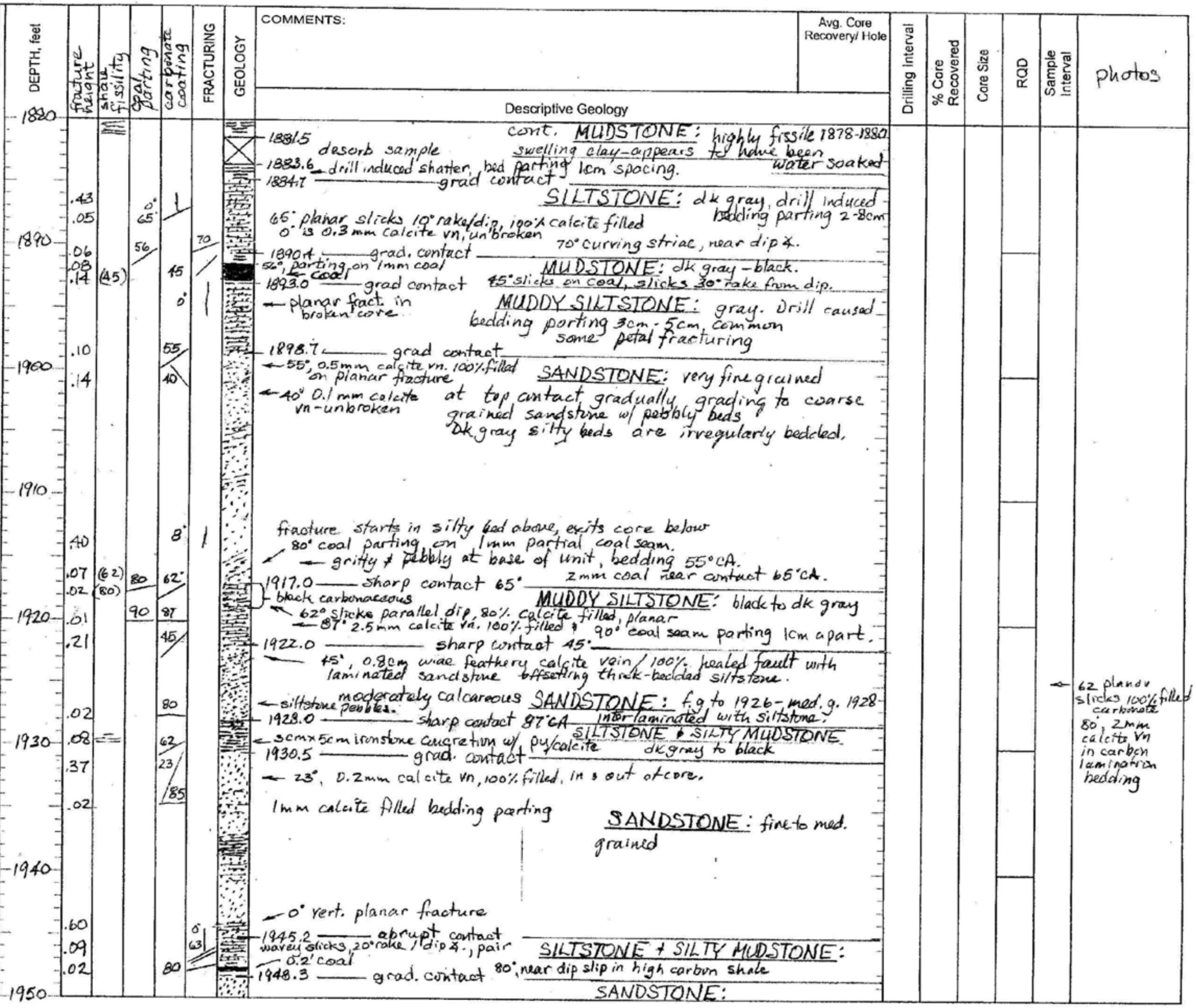

1881.5 desorb sample

1883.6 ← drill induced shatter, bed parting 1cm spacing.

1884.7 ——— grad contact

cont. MUDSTONE: highly fissile 1878-1880 swelling clay—appears to have been water soaked

SILTSTONE: dk gray, drill induced bedding parting 2-8cm

65° planar slicks 10° rake/dip, 100% calcite filled
0° is 0.3 mm calcite vn, unbroken
70° curving striae, near dip ∡.

1890.4 ——— grad. contact

56°, parting on 1mm coal
← coal

MUDSTONE: dk gray – black.
45° slicks on coal, slicks 30° rake from dip.

1893.0 ——— grad contact

← planar fract. in broken core

MUDDY SILTSTONE: gray. Drill caused bedding parting 3cm - 5cm, common some petal fracturing

1898.7 ——— grad contact

← 55°, 0.5mm calcite vn. 100% filled on planar fracture

SANDSTONE: very fine grained at top contact gradually grading to coarse grained sandstone w/ pebbly beds
Dk gray silty beds are irregularly bedded.

← 40° 0.1 mm calcite vn—unbroken

fracture starts in silty bed above, exits core below
↙ 80° coal parting on 1mm partial coal seam.
← gritty & pebbly at base of unit, bedding 55° CA.
2mm coal near contact 65° CA.

1917.0 ——— sharp contact 65°

black carbonaceous

MUDDY SILTSTONE: black to dk gray

← 62° slicks parallel dip, 80% calcite filled, planar
← 87° 2.5mm calcite vn. 100% filled & 90° coal seam parting 1cm apart.

1922.0 ——— sharp contact 45°

← 45°, 0.8cm wide feathery calcite vein / 100% healed fault with laminated sandstone offsetting thick-bedded siltstone.

← siltstone pebbles. moderately calcareous SANDSTONE: f.g to 1926 – med. g. 1928 interlaminated with siltstone.

1928.0 ——— sharp contact 87° CA

SILTSTONE & SILTY MUDSTONE dk gray to black

← 3cm x 5cm ironstone concretion w/ py/calcite

1930.5 ——— grad. contact

← 23°, 0.2mm calcite vn, 100% filled, in & out of core.

1mm calcite filled bedding parting

SANDSTONE: fine to med. grained

← 0° vert. planar fracture

1945.2 ——— abrupt contact

wavey slicks, 20° rake / dip ∡., pair

← 0.2' coal

SILTSTONE + SILTY MUDSTONE:
80°, near dip slip in high carbon shale

1948.3 ——— grad. contact

SANDSTONE:

← 62 planar slicks 100% filled carbonate
80°, 2mm calcite vn in carbon lamination bedding

Well VPR CH-7

Drill Site:
N: E:
Started:
Completed

Collar Elevation:
Bearing:
Inclination:
Total Depth:

Sandia National Laboratories
Logged by: CA Rautman
Log Version:
Log Date:

Raton Basin Project
Hole No: CH-7
Scale: 1" = 10' (1:120)
Sheet / of

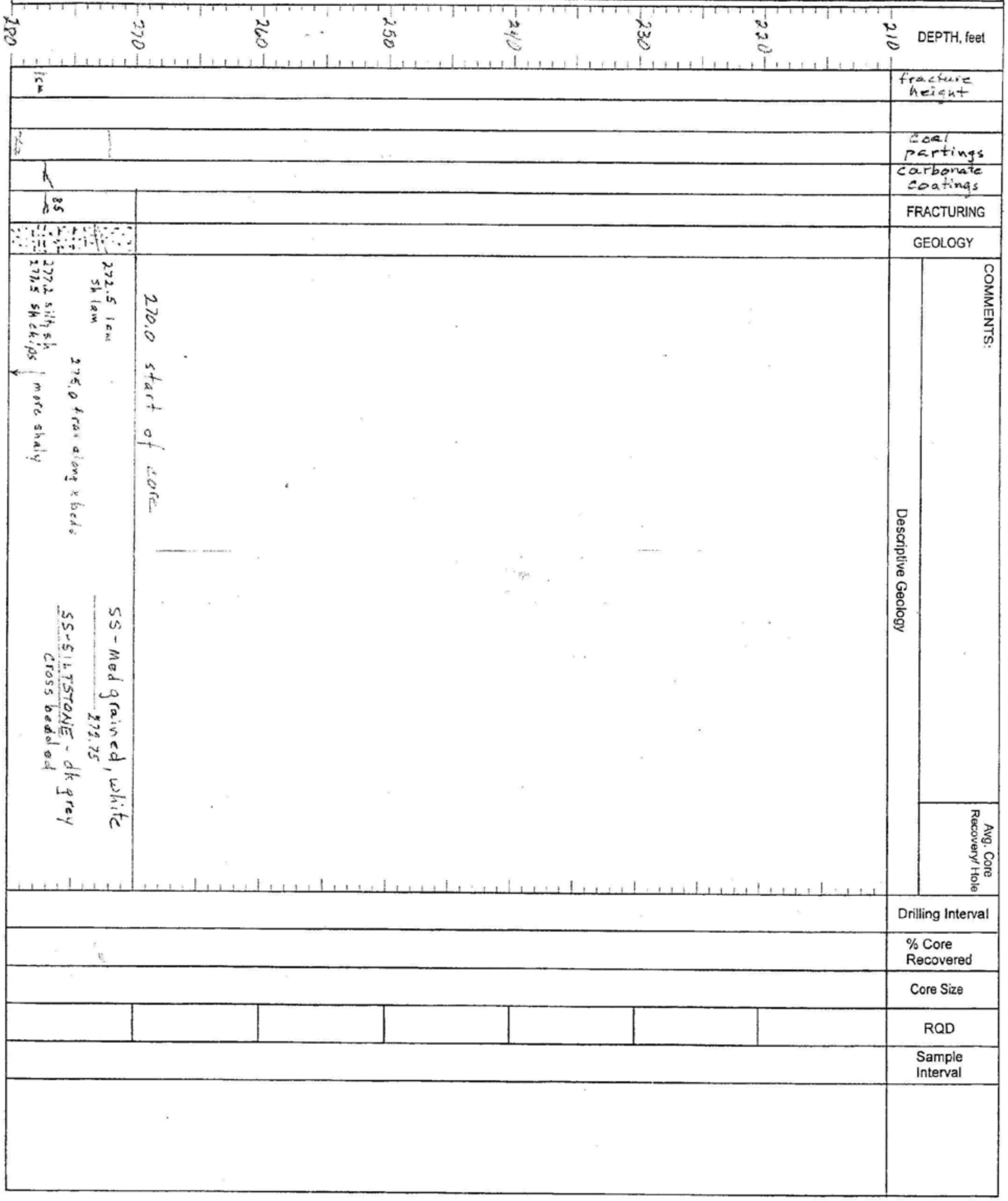

270.0 start of core

272.5 1cm sh lam

275.0 frax along x beds

277.2 silty sh

277.5 sh chips

more shaly

SS - Med grained, white

272.75

SS-SILTSTONE - dk grey cross bedded

Drill Site:
N: E:
Started:
Completed

Collar Elevation:
Bearing:
Inclination:
Total Depth:

Sandia National Laboratories
Logged by: C.A. Rautman
Log Version:
Log Date:

Raton Basin Project
Hole No: CH-7
Scale: 1" = 10' (1:120)
Sheet 2 of

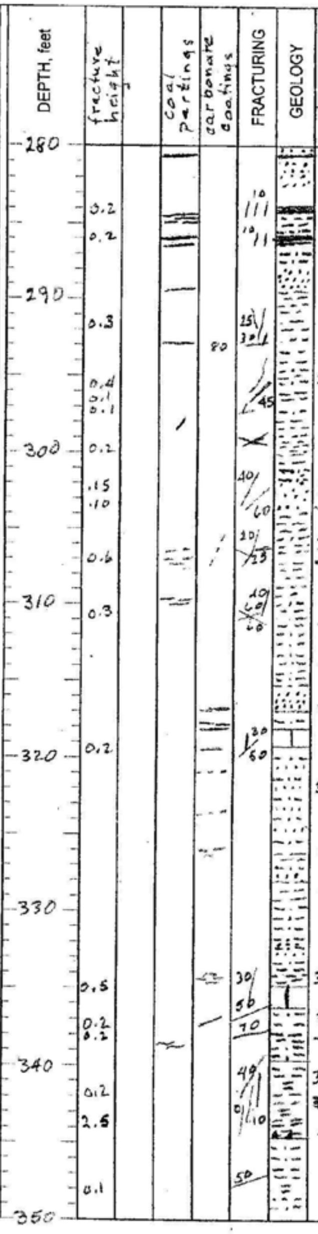

COMMENTS:

Descriptive Geology

coals exhibit orthogonal jtg; one dom.

283.6-284.0 coal, frax ~10° @ lam sp. incl frax incipient, stress relief?

disced along coaly ptgs 284.6 compact. slicks in sh.

xlam vfg ss

292 comp. slicks on high angle badly broken frax, multiple orient slicks ~ll dip; term against other frax

295 - post drilling curved frax 0-30° CA several similar frax

299.2 broken; conj sh, 60° weak compact slicks

302 ill defined, rough frax w/ suggestion of compact slicks ll dip

304.2 sharp contact ss/sltst

306 smooth slightly curved frac in silty mudstone; patchy CO3 discing term. against frax

306.5 conj compact slicks ~60

311 - conj slicks on comp frax

317.0 sharp base ss w/ coaly streaks

319.8-320.0 complex of ill-def compact slicks

322 - 0.3' burrowed vfg ss

326 - some discing

329.5 fluid escape strs

334.5 comp. slicks rake 30°

336.4 prom. long wavelength fluted slick 50° CA, flutes rake 30°

338 complex conj (?) comp slicks

340.4 - 40°

341.5-344 - intense comp. slicks grooves rake ~30° dip

344.0 shale bxa

SS - SLTST dk grey; local coarser white med ss layers 283.6

MUDSTONE w/ coal, siltst dk gr to black, carbonaceous,

288-289 fg ss xlam

292.9 end coaly intvl

MUDSTONE - SILTSTONE w/ local vfg ss more grn-grey, locally carbonaceous

mudstone - shaly intvls exhibit post-drilling dessication frax - incipient to well developed, mostly ~90 CA; ends may splay out into unfrax core

317.0

SILTSTONE - VFG SS mostly grey, carb. finely lam; locally burrowed

mostly brownish to blackis tones; some siltstones more green-grey

339.6

MUDSTONE

344.7

SILTSTONE + MUDSTONE

Avg. Core Recovery/ Hole

Drilling Interval

% Core Recovered

Core Size

RQD

Sample Interval

Roll 2

Photo 283.0 frax in coal

Photo 295.0 insip frax

Photo 305.5 w/co3 fill

318.2-319.2 No core C7-1

334.9-336.5 NO core C-7-2

Raton Basin Project
Hole No: CH-7
Scale: 1" = 10' (1:120)
Sheet 3 of

Sandia National Laboratories
Logged by: CHRautman
Log Version:
Log Date:

Collar Elevation:
Bearing:
Inclination:
Total Depth:

Drill Site:
N:
E:
Started:
Completed

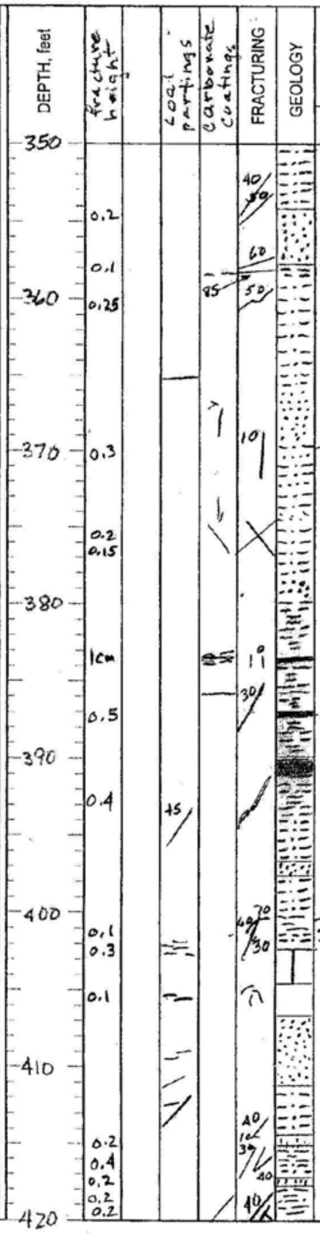

COMMENTS:

Avg. Core Recovery/ Hole

Drilling Interval

% Core Recovered

Core Size

RQD

Sample Interval

Descriptive Geology

354.7 indistinct rough comp frac

SILTSTONE

— indistinct

354.0 — SANDSTONE - white to ltgr med grained

— sharp base

357.9

360.2 irreg, stepped compac frac

SILTSTONE w/ lesser MUDSTONE, local vfg SS

locally finely lam

generally dkgrey

369.8 prom frac w/ comp slicks rake 20° + terminates at horiz break

375.4 conj comp frax w/slicks dips ~60° apart in plan CO_3 on one only 50-100% cov.

Photo 375.4'

379 - indistinct

some core loss 379-383 50-60%

MUDSTONE + COAL

386.6-387.5 poor coal + papery carb sh

390-391 poor coal + papery carb sh; disced

Photo 391' coal ptgs

393.0 v. irreg comp frac w/ poor slicks

393.6 indistinct

496.9-497.5 well lam vfg ss.

SILTSTONE w/ lesser sandstone + mudstone

mudstones are carb. + somewhat fissile

400.6 prom curved frac

papery sh.

401.3 incipient tight frac 30° CA - term at carb. ptg

402.4- 4038 "1.5' coal"

SS quite coarse locally (to med-crs sand)

404-406.5 complex intvl of compac frax w/slicks ~ll dip - many curved frax

406.9

indistinctly lam ss med grained fining upward 407-411 - redrilled

411.1

414.5-415.0 fg nonlam ss

← compac frax w/ slicks term at base ss

417.4-418.0 weakly lam fine ss

419 prom v. planar frac w/ <1mm CO_3 fill - 100% siltst

419.4 ratty comp frax w/ slicks ~40° slicks at

420'- papery silty sh

Photo 419.0'

Drill Site:
N: E:
Started:
Completed

Collar Elevation:
Bearing:
Inclination:
Total Depth:

Sandia-National Laboratories
Logged by: CARautman
Log Version:
Log Date:

Raton Basin Project
Hole No: CH-7
Scale: 1" = 10' (1:120)
Sheet 4 of

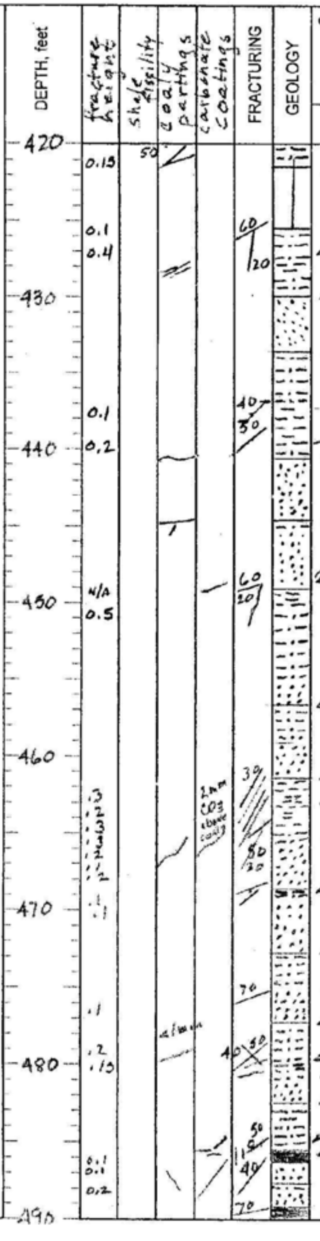

COMMENTS:

Avg. Core Recovery/ Hole

Descriptive Geology

421.6-425.6
No core
(ground)
426.2 - slick on comp. frac rake ~20°
426.9- irreg compfrax w/poor slicks

430.0 indistinct
vfg ss, betterlam at base, fining up
433.7 sharp contact

437.7 step frax 40°CA + term at horiz ptgs

439.7 prom planar frac w/comp slicks
440.8
SS, med-f. grained, fining upward
well lam white w/grey lam
444.7
SS, med-f. grained, fining up
4492 grn-grey to black at base
449.9 1mm CO3 veinlet in mudstone

456.8 sharp contact

461.5 sharp contact
← swarm of irreg comp frax in mudst

466.2 v. irreg coaly ptgs in ss
466.8 grooved slick? on frac in ss 30
468.3 sharp contact
468.7 - conj compact frax w/slicks ll dip
dips ~ 30° apart in plan
472.9 sharp contact

475.6 sh ptg

477.1 obscure contact

479.3 slicks ll dip - conj frax dips ~ 80 in plan
480.0 1-mm partially open frax 70 CA - comp. slicks
482.7 sharp contact 482 numerous post-drilling
incipient frax <1mm open
484.4
485.6-486.3 coal frax ll CA v. irreg fluted 50CA
487.6 frac w/CO3 ~ 75% slicks on comp. frac
in mudst abercoal
<1mm CO3 veinlets at
489.2-490 coaly mudst
[illegible]

440.8

SANDSTONES w/ SILTST
+ MUDST
grey + grn grey
series of pronounced
fining upward sequences
w/sharp± basal contacts
+ indistinct changes
to siltst + mudst upward
SS med-fine

several examples of
possible conj frac sets
w/ dips 40-50 w/ dip dir
at 50-80° to each other
in plan generally in
silty to muddy rx w/ comp
slicks near ll dip

482.7

SANDSTONE + COAL
med-fine ss
greyish coaly mudst
ss bioturb at base

Drilling Interval

% Core Recovered

Core Size

RQD

Sample Interval

Photo 437.7'
step frax

Photo 468.7'

Photo 484.4

Raton Basin Project
Hole No: VPR CH-7
Scale: 1" = 10' (1:120)
Sheet 5 of

Sandia National Laboratories
Logged by: HRautman
Log Version:
Log Date: 3-12-02

Collar Elevation:
Bearing:
Inclination:
Total Depth:

Drill Site:
N: E:
Started:
Completed

DEPTH, feet	fracture height	COMMENTS:	Photos
490	0.2	492.2 comp slicks pronounced bioturbation	
	0.1		
500	0.1 0.25	499.5 conj frax ~70 poorly dev 30% CO3 on one 500.7 slicks rake ~20° CO3 ~50%	
	.5 .2	505.8 - irreg curved comp frax w/ slicks 504.3-505 post drilling dessic breakage 506.4 slightly curved planar frac 100% CO3	Photo 504.7 Photo 506
510		SS 512.7 sharp contact 513-513.5 bioturb siltst 515.8 1cm CO3 stringer ⊥ CA; brecciated	
	0.2		
520	1.0	520-521 intense comp frax w/slicks 0-20°CA quite coaly mudst 526 - dessic breakage in mudst 526.6-528.6 broken intvl in coaly sh highly polished planes 30-70 CA	Photo 520
530		SS 533.6 sharp contact SS 539.1 sharp contact	Photo 528.5
540		med-fg v. muddy SS 545.8 indistinct contact	
550		vfg ss, silty 555.5 sharp contact 557.9 indistinct contact	
560			

Descriptive Geology

491.8

SILTSTONE
w/ fining upwards ss units + mudstone
thin carb shaly intvls
mostly dark gray
ss units white w/ shaly streaks + carb streaks

some mudstone intvls exhibit dessic-type breakage

carby sh intvls exhibit some weak fissility accentuated by coaly matl

Avg. Core Recovery/ Hole

Drilling Interval

% Core Recovered

Core Size

RQD

Sample Interval

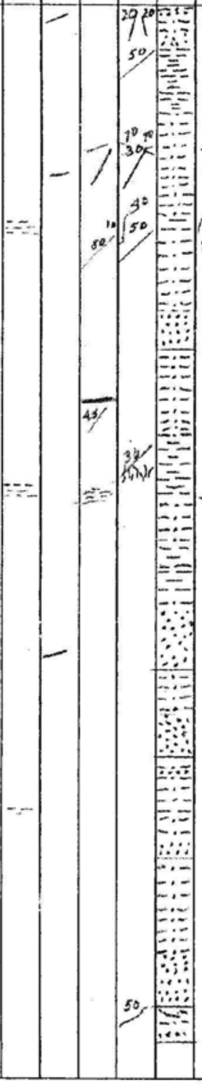

Drill Site:
N: E:
Started:
Completed

Collar Elevation:
Bearing:
Inclination:
Total Depth:

Sandia National Laboratories
Logged by: [illegible]
Log Version:
Log Date: 3-12-02

Raton Basin Project
Hole No: CH-7
Scale: 1" = 10' (1:120)
Sheet 6 of

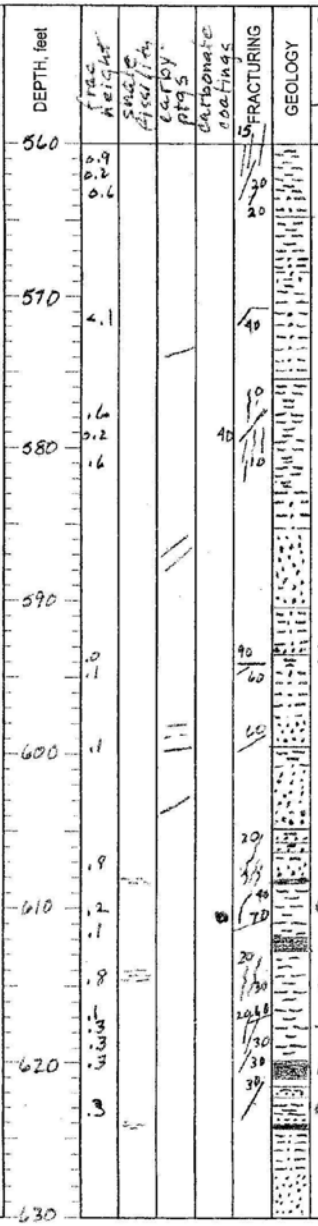

COMMENTS:

Avg. Core Recovery/ Hole

Descriptive Geology

560 – 561 15°CA frax ~ 1 cm apart
partial CO_3, quite irreg + feathered
slicks rake 20° 562.4 planar frac
564.8 indistinct

569 indistinct contact
570.5 slicked comp frac term
against horiz. break - drill induced

575.5 contact

580 - 582 broken - v. irreg compac frax
identifiable planes 0 - 30 CA
slicks II dip mudst exhibit bxa-like text
— 586.2 ss broken along coaly plant frag (post drill)
vfg silty dk gr ss mostly lam.

590.6 contact
— vfg lam ss
594.1 - slicks on frac 90 CA

— well lam fgss w/coaly stks
599.6 contact

604.9 contact
605.7 contact
607 - 607.5 - broken ~ 30° CA
607.5 - 607.8 coaly sh
610 curved frac along coaly frag, slicks
rake 90° to dip
611.9 - 612.8 v. shaly coal
614.5 slicks on frax 20-30°, conj 60° in plan
- 617.9 2 slicked frax ~ 60 apart in plan
slicks rake 30-40°
620.0 - 621.4 shaly coal; disced ~ 85 CA
622.9 slicks on comp frac
624.3 - 624.6 coaly shale

SILTSTONE w/ mudstone
+ local silty dk-gr vfg ss
fining upward sequences

606.3'
MUDSTONE +
Coaly Shale
abnt vitrinite
compaction slicks locally
throughout
numerous spun + ground intvls

624.6
SANDSTONE w/ mudst, sltst
fine - vfg lam, carb. stks

Drilling Interval

% Core Recovered

Core Size

RQD

Sample Interval

Photo 560.5

Photo 570.5

Photo 610.0

Photo 618±
and above

Sandia National Laboratories
Logged by: CARautman
Log Version:
Log Date: 3-12-02

Raton Basin Project
Hole No: CH-7
Scale: 1" = 10' (1:120)
Sheet 7 of

Drill Site:
N: E:
Started:
Completed

Collar Elevation:
Bearing:
Inclination:
Total Depth:

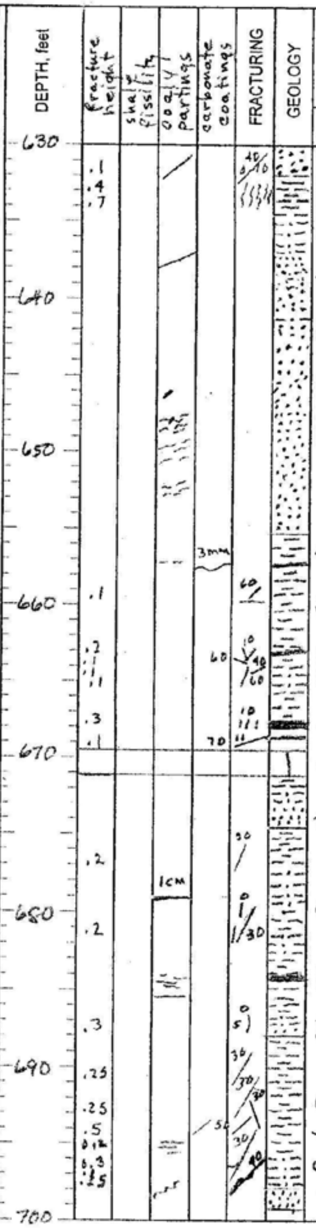

COMMENTS:

Avg. Core Recovery/ Hole

Descriptive Geology

SANDSTONE w/ much lesser siltstone + mudstone
mostly fine-vfg ss, lam w/shaly or coaly laminae
sparse coaly partings
much ss white - lt grey, siltstones more med grey
ss w/abnt coaly ptgs below 647.8

632-634 intensely broken slicks on frax planes ~ // dip

- 638.7 finely lam carby

652.8-655.7 darkgr coaly vfg ss - finely lam
656.5 - co3 veinlet incls sh frags
656.8 coaly

655.7 abrupt contact

MUDSTONE + SHALE
Black, org-rich + coaly mudstone + more fissile shale
some vfg ss + siltstone

(core loss) | disced || coaly streaks
659 weak slicks on 90° frax
662.8 coaly - intersecting frax w/ slicks
663.1-.3 coaly, comp frax - raking 10-30°
663.7 comp slicks 70° in plan

667.5-668.0 coal, cleats ~ .5-1 cm
668.8 comp slicks rake ~ 20-30°
668.2 coal w cleat 0 CA
coal removed

fluid escape shs at base
674.5

| disced

680, 682 compact slick, near 0 CA

| disced, coaly

686.8-687 slightly spiraling frac in silty vfg ss possibly drill?
688.0 contact

690.2, 690.5 conj frax w/ slicks raking 30 at ~ 80 in plan
~693.7 highly polished 80 frac w/CO3 coating
697.2 prom wavy frac w/ compac slicks ~ 40 CA raking 10-20°
white f-vfg ss, silty upward
699.3 sharp contact
696 frac ~ 70 CA prom concave w/ curve

Drilling Interval | % Core Recovered | Core Size | RQD | Sample Interval

Photo 631.3

Photo 662.9

669.4-671.1 coal removed

Raton Basin Project
Hole No: CH-7
Scale: 1" = 10' (1:120)
Sheet 8 of

Sandia National Laboratories
Logged by: JHRautman
Log Version:
Log Date: 3-18-02

Collar Elevation:
Bearing:
Inclination:
Total Depth:

Drill Site:
N: E:
Started:
Completed

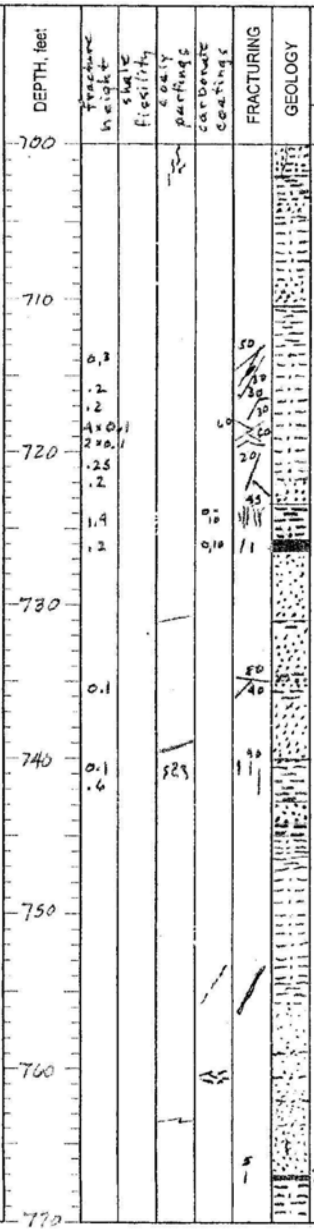

COMMENTS:

Avg. Core Recovery/ Hole

Drilling Interval
% Core Recovered
Core Size
RQD
Sample Interval

Descriptive Geology

699.8-701.9 - ? channel margin w/ ss/siltst on opp sides near vertical feature
701.9 contact
lam ↑ burrowed
703.9 contact

core loss

714 intersect frax ~20-30 in plan
weak comp slicks

716.2 30° frac term at bedding ptg 80 CA - strong slicks rake ‖ dip

717.7-718.2 broken zone 60CA at diff orient, multiple frax

721.3 comp slicks rake 20
721.7 45° Frac ~ 80 to frac at 721.3
723.5-725.7 shattered zone 0-10 CA <1cm apart
725.8-726.4 coal, cleat ~20CA sits on ss

726.4

SANDSTONE
dom. intvl.

SS, f-vfg, well lam at base, massive upward becoming v. coaly - shaly + bioturbated
731.1 sharp contact above ~728.2'

733.7 contact
734.9 contact
734.9 poor slicks rake 80-90°
735.4 ? petal frac in silty mudst
chip w/ prom curved lip at edge of core

~740.0

SILTSTONE + MUDSTONE
w/ v.fg ss
local more muddy org-rich intvls

740 contact
740.3 v. irreg near vert carb ptgs in mudst,
741.9 contact
742 multiple near vert frak in mudst term against ss bed below - v. irreg w/ coal matl
744.3 contact
745.0 contact

754.2 irreg frac 30° w/ 70° CO₃ cover

754.6
VFG SILTST + SS INTVL

760.5 CO₃-filled bx ‖ bedding ~2cm total thickness; CO₃ turns 90CA and feathers out
761.5-765.5 vfg ss gen. well lam, trace burrowing

767.0-767.3 COAL

767.1
COAL + MUDSTONE

Photo 701.5
(no frax) Photo 702-711
Photo 721.3
Photo 724.0
Photo 725.5
Photo 735.4
760.5 Photo
762.3 Photo

Drill Site:
N: E:
Started:
Completed

Collar Elevation:
Bearing:
Inclination:
Total Depth:

Sandia National Laboratories
Logged by: HA Routman
Log Version:
Log Date: 3-18-02

Raton Basin Project
Hole No: CH-7
Scale: 1" = 10' (1:120)
Sheet 9 of

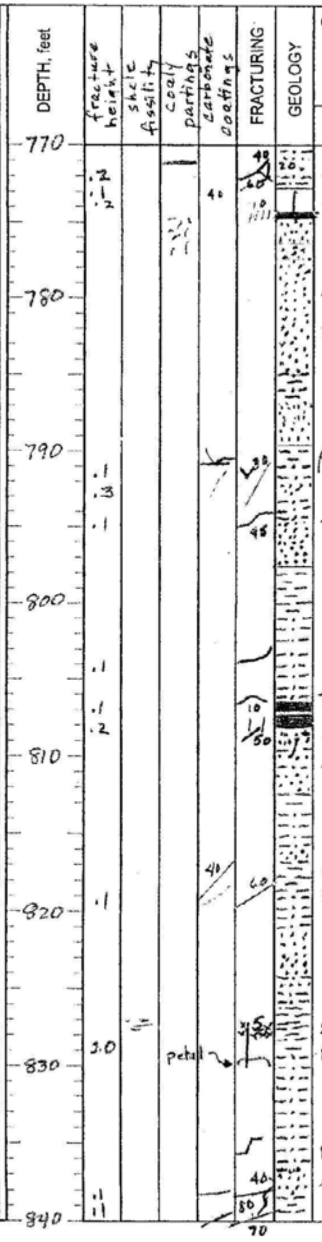

COMMENTS:

Avg. Core Recovery/ Hole

Descriptive Geology

770.5 shaly lam vfg ss/siltst.
— complex of small + incip frax in mudst
7729-774.3 No Core ill defined cleating 10°
v. coaly fg ss
776.5 indistinct (grad) contact
777.3 lam vfg ss w/ minimal carby matl below
778.8 abrupt change from lam ss → massive vfg ss w/prom irreg on frax // bedding
783 xlam
785 ill defined contact
791.7 intersect frax ~ 45 CA, oneplanar, other irreg
790.8 1-3 mm anast CO_3 veinlets // bedding
792.6 curved or folded frac 30°CA weak slicks rake ~ 20; fold axis or intersect line ~ // rake; 50-60% CO_3
794.2 compfrac w/ slicks trunc at internal bedding slicks rake 80
797.6 sharp contact
8033 petal frac 1-2 cm at lip
805.8 - quasi conical frac w/ slicks → 80 CA cuts bedding / plant frag
806.8-807.1 coal + carb mudst
807.4 - 808.0 coal
808.8 carby vfg ss/siltst
808.5 v. irreg frac w/ comp slicks in carby mudst - siltst.
811 petal-like frax broken to fit core into box ~ 1 cm ht.
810.6 scolithus-type burrow
818.0 1-2 mm tight CO_3 veinlet - white
818.9 highly polished frac, weak slicks rake ~ 10 30% CO_3?
med gr white ss ↑ fine vf
827.2-828.3 shattered zone fracs ~ // CA - bagged rubble w/ abnt slicks - soft mudst w/ dessic cracks └ post drilling
828.3-829.3 slightly twisted frac 5 CA term below at internal bedding in mudst plumose str on frac plane
828.6 distinct small ht petal frax forms lip - 2-3 mm at edge of core
distinct green cast below → 827.5
835 comp slicks
40° frac w/ comp slicks
838.0 839.9 80% + CO_3

COAL + MUDSTONE.

774.9

SANDSTONE - dom intvl

ss mostly f-vfg
greenish-grey
well lam, slightly silty
siltst also lam, grad to black mudst w/o fissility

Some ss assoc w/ coals quite carb, prob burrowed

797.6

SILTSTONE - dom intvl

w/ lesser vfg ss
mostly grn grey - black grey
contacts somewhat indistinct

possibly bentonitic?

Drilling Interval

% Core Recovered

Core Size

RQD

Sample Interval

772.9-774.3
spl C75

Photo 778.8

Photo 792.6

Photo 803.3
Photo 805.8

Photo 810.6'

Photo 828.6
Photo 829.3

Photo 835.1
837-840 core out of sequence

Drill Site:
N: E:
Started:
Completed

Collar Elevation:
Bearing:
Inclination:
Total Depth:

Sandia National Laboratories
Logged by:
Log Version:
Log Date:

Raton Basin Project
Hole No: CH-7
Scale: 1" = 10' (1:120)
Sheet 10 of

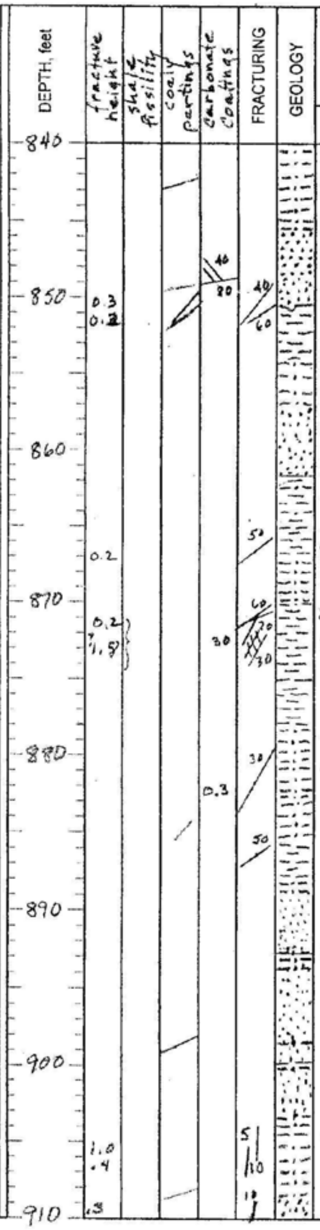

COMMENTS:
quite a few core segmts have slight petal-like frax char along post-drilling breaks - also where broken to fit box max ht ~ 2-3 mm

Avg. Core Recovery/ Hole

Descriptive Geology

845.0 weak flutes (scours) in mudst

248.8-849.1 3-2 mm CO_3 vainlets (tight)

850.3 + 851.2 v. coaly ptgs → frax

SILTSTONE - dom intvl
w/ lessar vfg ss
+ mudstone
mostly grn-grey

861.4 mod dist. break (contact)

866.5 comp slicks poorly dev.

871.0 poor comp slicks on intersect frax

871.4-974.0 many comp slicks at diverse orientations - mostly shattered

shaly bx?

881.3 2cm high petal frac at box break
881.8 v. long smooth frac

many drilling related curved frax petal-like

886.3 slicks rake 10-20

~888.3

bleached white ss to med grained

SANDSTONE - dom intvl

892.8 sharp contact

grey white ss

904 bagged rubble, mudst, dessic cracking
9047-905.2 long rough frac on side of core
906.6 1 cm petal frax on edge of core
907.4 crude breakouts (drilling) ~0-20 CA

Drilling Interval

% Core Recovered

Core Size

RQD

Sample Interval

Photo 850.4

Photo 881.3

Drill Site:
N: E:
Started:
Completed

Collar Elevation:
Bearing:
Inclination:
Total Depth:

Sandia National Laboratories
Logged by: Rautman
Log Version:
Log Date: 3-18-02

Raton Basin Project
Hole No: CH-7
Scale: 1" = 10' (1:120)
Sheet 11 of

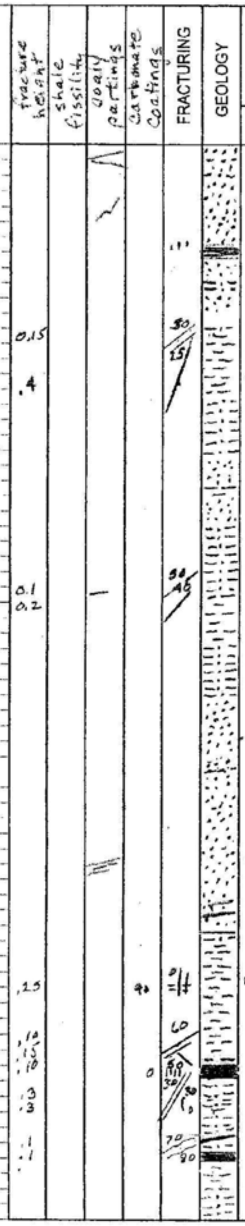

DEPTH, feet	COMMENTS: Descriptive Geology	Avg. Core Recovery/ Hole	Drilling Interval	% Core Recovered	Core Size	RQD	Sample Interval	
910	vfg silty SS, lam to massive carb streaks some quite carby							
	916.8-917.4 coal + carb mudst, poor cleats	916.8 SILTSTONE + SILTY MUDSTONE						
920	923 //frac planes ~1 cm apart							
	925.3 long rough frac							Photo 925.3
930								
940	939.1 polished frac w/ slicks rake 20 940.25 grooved frac w/ slicks amp grooves ~1-2cm							
	↑fine	945.5 SANDSTONE mostly white - lt gray massive, locally lam + silty fg - med gr. No Frax						
950	950.8-951.2 siltst intvl							
	955.6 carby ptgs 957-958 quite coarse - med SS 960.1 sh ptg 3mm							Photo 950.5-960.0
960		961.9 prom grad change MUDSTONE - black carb, silty						
	964-964.5 broken, faint slicks							
	smooth polished frax slicks rake ~20							Photo 969.2
970	269.4-270.9 ~0.5ft coal enclosed in carb mudstone - cleats OCA 0.5cm spacing 971.7 + 972.1 //frax at 30 CA 974.6 0.5 cm coal seam 80°CA 975.7-976.1 coal + carb mudst cleats ~OCA 975.0 - possible 2cm petal frac 975.1, 975.4 comp frax in mudst - highly polished surf w/ sed fluting + slicks	976.2 MUDSTONE/SILTST green-grey						Photo 970.5 Photo 972.0
980								

Raton Basin Project
Hole No: CH-7
Scale: 1" = 10' (1:120)
Sheet/2 of

Sandia National Laboratories
Logged by: CARautman
Log Version:
Log Date: 3-19-02

Collar Elevation:
Bearing:
Inclination:
Total Depth:

Drill Site:
N: E:
Started:
Completed

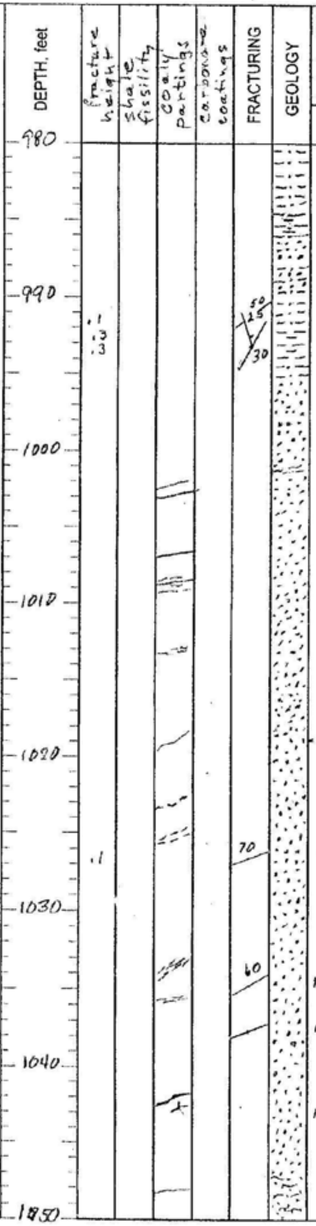

COMMENTS: Note: H_2O destroys highly polished surfaces in mudst

Avg. Core Recovery/ Hole

Descriptive Geology

MUDSTONE + SILTSTONE

grn-grey, also vfg silty ss

vfg sandy intvl, lam

~ 990.0 core out of place - conj 45° frax w/highly polished slick surfaces

992.7 + 992.9 conj frax irreg w/poor comp slicks

994.5 indistinct, grad. contact

vfg ss

SANDSTONE

locally silty + w/carb ptgs

1000.5-1001.0 silty, lam

some lam, mainly massive
coarse mica flakes on some ptgs

Frax only along coaly-micaceous ptgs - drill induced pref. planes ~ 80-85 CA = bedding

more massive intvls are bleached white

V. irreg break 60CA @ 1017

to med. grained, fining upward ill defined

fairly coarse - med grained ss

appears to be kaolin (clay) rich

local carby stringers + wisps up to 60° CA
core breaks pref along these ptgs + direction even in massive ss

1026.6 Nat frac, v. planar 70 CA
abnt amber grains - rutile?

No evidence of CO_3 coatings

fractures to fit core in box are closer to ⊥ CA but some breaks are ~70°

1034.7 Coring quite rough induced frac @ 60CA (typ)

1037.3 planar frac, natural 70 CA

1043.3 irreg clot of coaly matl.

1047.5-1051.3 - much more lam. w/ shaly-coaly wisps ~ 80-90 CA

Drilling Interval

% Core Recovered

Core Size

RQD

Sample Interval

988-990 core out of sequence - jumbled

995-997, core loss/ out of sequence

Photo 1017.0

Photo 1026.6

Photo 1027-4-1037.2

Photo 1041.9

Raton Basin Project
Hole No: CH-7
Scale: 1" = 10' (1:120)
Sheet 13 of

Sandia National Laboratories
Logged by:
Log Version:
Log Date:

Collar Elevation:
Bearing:
Inclination:
Total Depth:

Drill Site:
N: E:
Started:
Completed

COMMENTS: Note: compaction slicks appear to predate drilling induced breakage. - see 1090.4

Avg. Core Recovery/ Hole

Drilling Interval | % Core Recovered | Core Size | RQD | Sample Interval

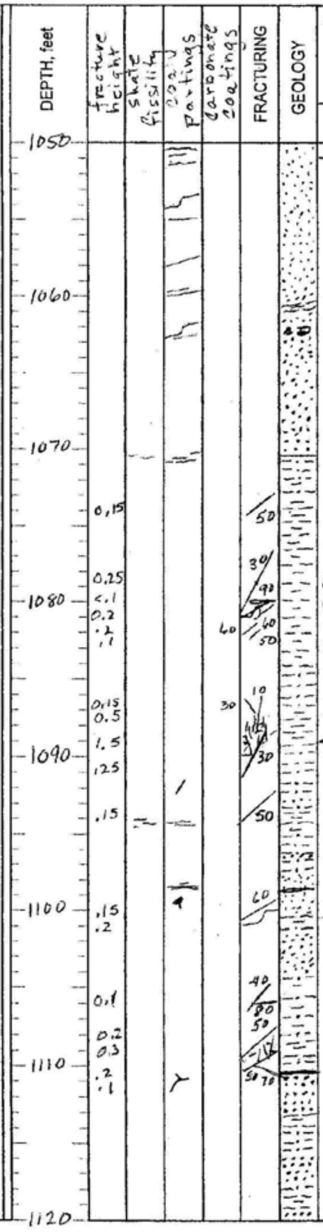

Descriptive Geology

↑ quite shaly + lam

SANDSTONE

1060.2 - 2-3 cm lam silty mudst.
1062.3-1062.8 shale/carb wisps and elongate sh chips to 0.25 x 2.0 cm

1070.4-1070.6 coaly mudst w/comp. slicks 60° CA

1070.4 - major lithologic change

MUDSTONE w/ lesser siltstone + silty vfg ss
v. dark grey - grn blk
coaly in part
abnt comp slicks

1078.5 v. planar frac, no discernible slicks
1079 highly polished frac 90 CA w/ comp slicks
1080.1 v. irreg core-induced frax w/ comp slicks
1082.7-1083.0 v. irreg core-induced fracs w/ slicks

1087.0 - intersecting frax, v. irreg comp slicks ~ 0° to dip
1087.6-1089.3 broken, v. irreg frax w/ slicks low angles to CA

1090.4 post drilling frac - curved ~ 60-20 CA, feathers out in center of core seg } has comp slicks raking 0°

1093.3 slicks rake ~ 0-5°

— 1096.5 lam vfg ss/sltst, disrupted lam

1098.2 ~ 3 cm coaly sh
Carby SS - choc brown
1100.5 sharp contact
1100.6 planar frac
1100.8 curved frac w/comp slicks stops at internal bedding

1109.0 smooth planar frac 50 CA; v. broken below to 1109.5, curving compac frax w/ slicks at diverse orientations generally ∥ dip
1110.4 2-3 cm muddy coal
v. carby vfg ss

1110.4

SILTSTONE w/ silty sandstone + minor mudstone
grey to grn-grey
less coaly below ~1113

↑ fining
well lam

mudstones not fract this intvl - except ⊥ CA drilling induced

Photo 1078.9
Photo 1087.0
Photo 1090.4
Photo 1100.8
Photo 1109.3 x 2

Drill Site:
N: E:
Started:
Completed

Collar Elevation:
Bearing:
Inclination:
Total Depth:

Sandia National Laboratories
Logged by:
Log Version:
Log Date:

Raton Basin Project
Hole No: CH-7
Scale: 1" = 10' (1:120)
Sheet 14 of

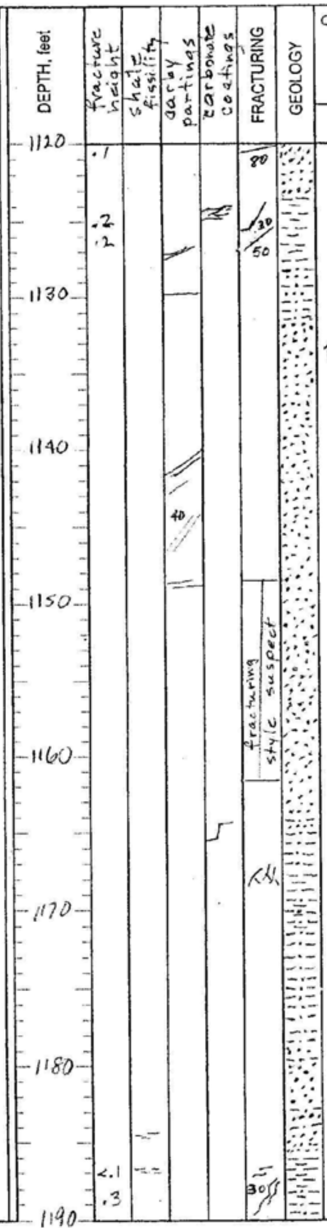

COMMENTS:

Avg. Core Recovery/ Hole

Drilling Interval

% Core Recovered

Core Size

RQD

Sample Interval

Descriptive Geology

fining — 1120.75 possible nat frac in SS ~ 80 CA, quite rough

1124.4-1124.5 - anast 2-3mm CO3 veinlets ~⊥ CA - tight

1125.2 - curved w/ damp slicks rake ~ 10-20

1126.2 highly polished, slicks ‖ dip

1127.3-.8 shale bxa ? text.

fining — much finer

1132-1133 partly distupted lam silty vfg ss

much lighter color

1mm micaceous, coaly ptgs 50-60°CA.

faint coaly ptgs ~ 40 CA

1132 grad contact

SANDSTONE

white to lt grey fine to med grained massive to weakly lam SS

~1148.5 at ~ this depth, sandstone becomes coarser (to med ss, ? crs) v. clayey and is broken up by swelling / hydration. Core in box breaks w/ spiral fracturing + as if case hardened, outer 3-5 mm all apparently assoc w/ core run 72 stops abruptly at run 73 - 1162.0'

?

Cleaned rock is well cemented med SS

1164.5-1165.0 pron. trans contact

1165.1 step frac w/slicks term int bedding

1167.0-1168.0 broken - abnt damp slicks on small frags 30-50 CA slicks ~‖ dip

1168-71 weak shale bxa texture in mudst

SILTSTONE w/ vfg ss + minor mudstone

v. dark grey-grn, locally carbonaceous, coaly plant frags

generally unfractured

slicks on small plane w/in core term on internal obscure bedding in app. massive sltst. mudst

vfg silty SS lam w/shaly streaks

1185.4-.8 clean vfg ss - lam

1185.9 fairly sharp contact slicks on internal planes

1188.8 irreg frac ~30 CA slicks ~‖ dip

Photo 1148.5-1157.2

Photo 1157.2-1166.3
Photo 1161.8

Drill Site:
N: E:
Started:
Completed

Collar Elevation:
Bearing:
Inclination:
Total Depth:

Sandia National Laboratories
Logged by: SAKautman
Log Version:
Log Date:

Raton Basin Project
Hole No: CH-7
Scale: 1" = 10' (1:120)
Sheet 15 of

DEPTH, feet | fracture height | Shale fissility | coaly partings | Carbonate coatings | FRACTURING | GEOLOGY | COMMENTS: | Avg. Core Recovery/ Hole | Descriptive Geology | Drilling Interval | % Core Recovered | Core Size | RQD | Sample Interval

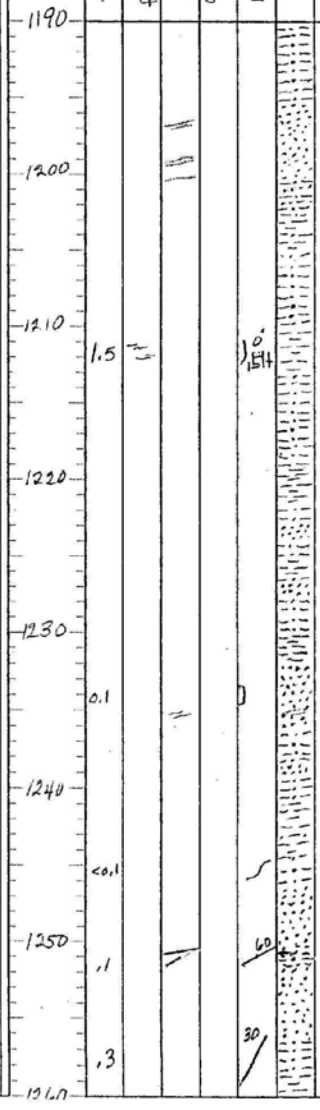

COMMENTS:

vfg silty ss quite lam w/ mud wisps, weak coaly ptgs

vfg siltyss + shaly siltst interlam on mm-cm scale

1212.0-1212.8 badly broken - mudst many comp. slicks, typ on frax ~ ll CA slicks may rake 0-20°

quite massive muddy siltst, no frax

vfg sandy intvl

1233.6 3 cm spall off side of core at OCA

vfg ss

1245.0 - partially penetrating comp slicks ~ ll dip

1251 weak comp slicks in silty intvl rate 0°

1251.3 - 1256.3 - much cleaner fg ss, white - v. lt grey

1257.2 somewhat irreg planar frac weak grooving ll dip

Descriptive Geology

SILTSTONE

Quite muddy locally grad into mudstone

Some vfg silty sandstone

all dark grey to grey grn

weak carb ptgs + plant frags

mudstones this intvl are probably silty and while darker grey than siltstones, do not fracture like less silty mudstones above

siltst + vfg silty ss interlam.

entire intvl quite massive and unfractured

~ 1246

SANDSTONE - dom intvl

vfg - fg ss, most silty + grn-grey, locally clean + whiter more typicall silty + inter lam w/ silty + muddy matl.

silty mudstones massive, not frac

Photo 1257.2

Photo 1259.0

Drill Site:
N: E:
Started:
Completed

Collar Elevation:
Bearing:
Inclination:
Total Depth:

Sandia National Laboratories
Logged by: CARautman
Log Version:
Log Date: 3-21-02

Raton Basin Project
Hole No: CH-7
Scale: 1" = 10' (1:120)
Sheet 16 of

DEPTH, feet	fracture height	shale fissility	coaly partings	carbonate coatings	FRACTURING	GEOLOGY	COMMENTS: Descriptive Geology	Avg. Core Recovery/ Hole	Drilling Interval	% Core Recovered	Core Size	RQD	Sample Interval	

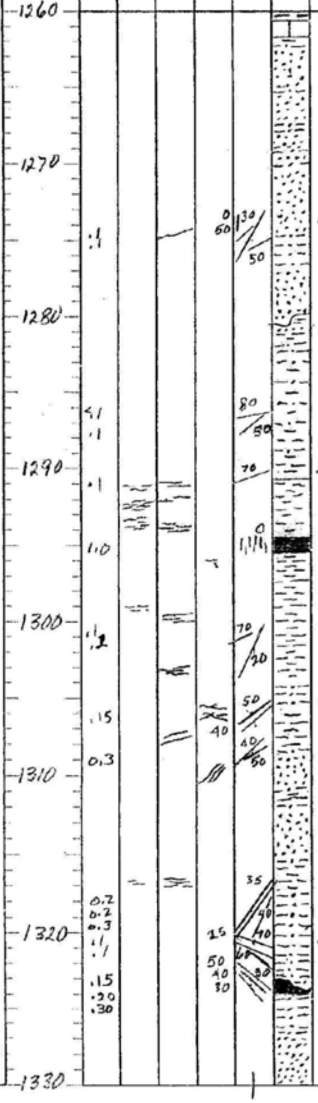

← dk grey carb mudst w/ polished fracks ~ 85CA missing intvl = coal?

↕ v.carb, vfg ss

vfg silty ss and muddy siltst interlam - wispy

1274.3-1274.5 drilling enhanced frac 0CA, silty interlayer

1275.1 - grooved comp slicks rake 0°
silty mudst.

1279.5-.7 sharp
scoured contact

1286.8, 1287.1 comp-type slicks
rake ~0° to dip

SILTSTONE + SILTY MUDSTONE

dk grey siltst + silty mudstone, becoming carb toward coaly intvl.

1290.5 comp slicks ll dip; just below 2 cm vfg ss layer, frac term at base of SS
1290.7, start of v.carby intvl

1294.4-1295.3 coal
cleats @ 0 CA <1cm apart
1297.0 v.carby mudst loses carb content

mudst, v.dk grey, probably silty
mostly unfrax except drilling ⊥ CA
1300.8 polished surface, no slicks
1301.6 irreg comp frax + slicks
1305.8-1306.3 zone of anast CO₃ veinlets .1-3mm
1305.3 comp clicks rake ~0°
1306.75 v. planar frac
1308.6 slightly irreg frac weak slicks ll dip
vfg ss, silty, dk gry

~1368.7

vfg ss, white

← bioturbated

1318.55, .85, 1319.8, 1320.8, 1321.3, 1321.7
v. planar frax w/ slicks 5-10 to dip
← conj sense of slip; slicks rake 20-30 re conj set
strike almost, but not parallel; 20°? rotation?

1322.8-1323.6 coal — v. steep contact ~20-30 CA
just above coal 1322.25, .35, .50
smooth planar frax, prog steeper dips
slicks rake ~80 to dip

1329.5 vert frax 0°CA see next page

1260.7-1261.8
C-7-6

Photo 1274.3

Photo 1290.5
mislabeled
1294.5

Photo 1295.0

Photo
1318.1-1321.7
Photo 1318.8',
1321.3'

Drill Site:
N: E:
Started:
Completed

Collar Elevation:
Bearing:
Inclination:
Total Depth:

Sandia National Laboratories
Logged by: CARautman
Log Version:
Log Date: 3-22-02

Raton Basin Project
Hole No: CH-7
Scale: 1" = 10' (1:120)
Sheet 17 of

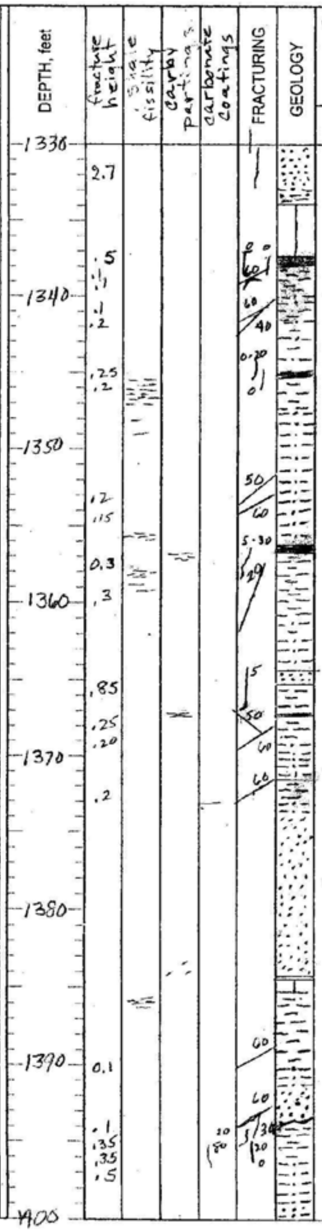

COMMENTS:

Avg. Core Recovery/ Hole

Drilling Interval | % Core Recovered | Core Size | RQD | Sample Interval

Descriptive Geology

~ 1329.5 - 1332.5 enechelon near-vert 0-10CA frax in SS, some open aperture to 1mm some CO3 fill - featherout above + below
numerous 2-3mm steps on plane

trans contact

SANDSTONE

~ 1333.6

— missing core presumed coal

no slicks
1337.6 - 38.1 2 ll frax on opp side of core, v. planar stepped, term at internal bedding

1341.6, .9 - quite smooth, planar frax

—40° frac term at int. bedding

MUDSTONE + SILTSTONE

v. carb, dk grew w/ poor coal & coaly mudstone

1345.5 - 1346 ext. carb mudst

1352.4, polished, planar slicks rake 30

1356.2 - .7 poor coal/carb sh.
1357.2 - irreg frac in coal - carby mudst - 5-30CA
1359.7 v. polished slightly fluted frac slicks rake 0

1363.6 grad contact ~0.1 to silty mudst
1364.2 knife-edge contact SS/mudst
1365.0 - 1365.8 v. planar, stepped frac; no slicks
1366.8 ext. carby mudst / coal ±
1368.8 conj frax w/ comp slicks rake 0
— strong lam siltst
1371.6 sharp contact
1372.6 comp slicks on planar frac

grad contact

SS, vfg, grey, silty more lam

SANDSTONE

↑ rapid decr in grain size

SS - med - crs grained, quite white
massive

1384.2 sharp contact
— sample presumed coal

1384.2

SILTSTONE, locally muddy

some quite carb + coaly, local vfg SS

all dk grey

— 1392.8 quite coarse
1393.3 sharp contact

fining up

1393.4 - 1395 intvl of complex comp-type frax - some planes v. planar some v. irreg.; w/slicks; one 20% CO3

fining up

Photo 1331
" 1332

1334.0 - 1337.3
sampls = coal

Photo 1337.7
Photo 1338.5

Photo 1365.5

1384.6 1385.4
spl C-7-9

Photo 1494.6
Photo 1495.0

Raton Basin Project
Hole No: CH-7
Scale: 1" = 10' (1:120)
Sheet 18 of

Sandia National Laboratories
Logged by: CARautman
Log Version:
Log Date: 3-22-02

Collar Elevation:
Bearing:
Inclination:
Total Depth:

Drill Site:
N: E:
Started:
Completed

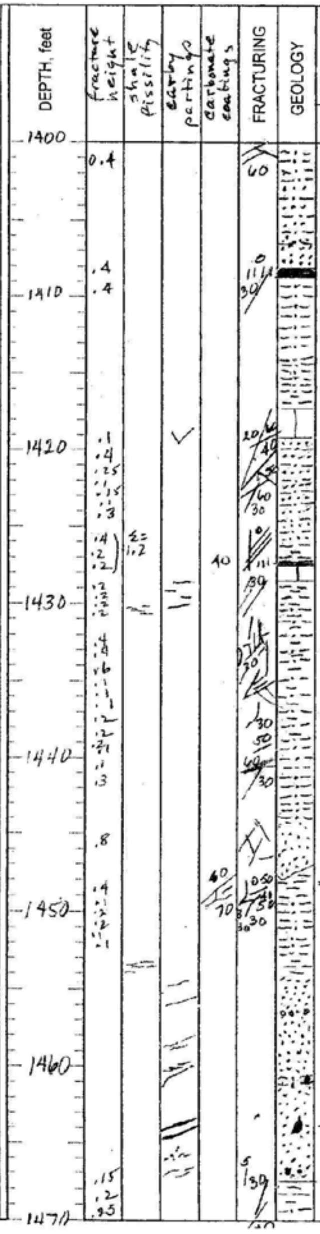

COMMENTS:

Avg. Core Recovery/ Hole

Descriptive Geology

1401.7 set of 3 conj frax - w/ comp slicks

1407.5-1408.3 quite coarse ~ med ss

fining up

sharpcontact

1408.3-.7 coal, 1cm cleats 0CA

1410.8 30 CA curved frac slicks rate 40-60dip rel to carb mat'l

SILTSTONE, muddy + muddy siltstone generally dk grey & carbonaceous

v. carb mudst

presumed coal

1420.2 20°CA, slicksrake 30°

1420.2-1422.1 atleast 6 frax vfg silty ss, dk grey w/ slicks 20-30° to dip quite planar, some conj.

presumed coal 1cm cleating 0-5 CA muddy coal above spl

v. carb mudst

intvl quite broken overall many frax ~ll, some ident conj rel. almost all frax w/ comp-type slicks irreg surfs, some stop at int. bedding

slicks rake 30

vfg-silty ss

fining up

fg ss w/ granules

1447.6-.8 1-3mm white CO3 veinlets

1456.4-.6 fine cangl w/ clasts to 3mm incl mudst & lags

fg ss w/ shaly laminae, wisps

4160.4-460.- v. carb + silty, w/ mudst clasts to 1-2cm

mudst clast 2cm

granules ~ carb streaks

1468.5 slicles rake 10°

1467.5 incipient open cracks just below ss siltst contact = stress relief

SANDSTONE - white - lt grey generally med - crs grained interbeds of more lam dk-grey silty - vfg ss some interbeds ~ muddy siltst.

SILTSTONE w/ ss

Drilling Interval

% Core Recovered

Core Size

RQD

Sample Interval

Photo 1401.7

Photo 1410.2

1417.4-1419.3 C-7-11

Photo 1419.8-1423.6

1427.7-1428.7 C-7-10

Raton Basin Project
Hole No: CH-7
Scale: 1" = 10' (1:120)
Sheet 19 of

Sandia National Laboratories
Logged by: CARautman
Log Version:
Log Date: 3-22-02

Collar Elevation:
Bearing:
Inclination:
Total Depth:

Drill Site:
N: E:
Started:
Completed

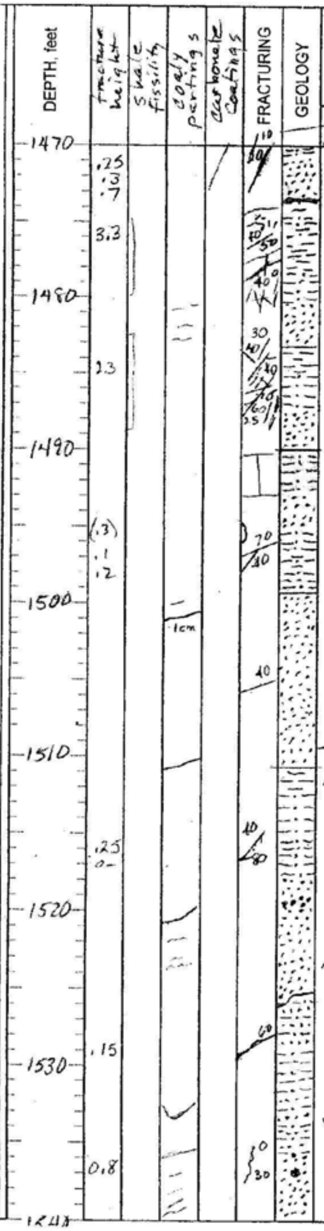

COMMENTS:

Avg. Core Recovery/ Hole

Drilling Interval

% Core Recovered

Core Size

RQD

Sample Interval

open
healed

Descriptive Geology

1471.35-1472.0 2-3mm partially open frac mostly healed by CO_3 - several mm openings

— fluid escape strs

1473.9 slicks on horiz curved frac

1476.8-1477 - broken zone

1477.3 v. irreg frax w/comp slicks

1475-76.3 odd bxe-like text in v. muddy siltst

SILTSTONE w/ SS

1477.3-1480.0 - v. broken zone intersect frax 0-30 CA, most w/ slicks ~0-10 CA where ID

1483.3 sharp contact

1484.8 horiz break - highly polished

1487.0 fluted frac ~40 CA sliks rake 30°

fining up

1490.0 Sharp contact

1490.0-1493 rubble -2.6' silty + muddy - dissintegrated to chips < 5mm

1495.2 v. irreg handling induced frac w/slick

1497.1, .3 slicks || dip

1499.4 sharp contact

SS, quite coarse

SANDSTONE

alt layers of white - lt grey coarse SS and dk-grey v. muddy or silty vfg SS

fining upward seqs w/ sharp bases

some granule zones

dk grey silty SS may exhibit dispersed white granules to 2mm - debris-flow deposits

1505.35 v. micaceous ptg 50CA

1505.7 - v. planar break 90CA = natural?

1506.1 - fluted break 50CA

Photo 1505.4
Photo 1505.7
Photo 1506.7

- 1509 coarse ss above, fine below

1510.7 sharp contact

fining up

slicks rake 0

← siltst quite muddy

1518.5-1519.3 granule zone

1526.6 sharp contact, crs SS over finer silty fgss

1528.6 - irreg frac, curved slicks rake 40-60'

silty SS, vfg v. carb, dk grey

← silty, lam vfg SS

1536.-1536.8 irreg rough frac at 1536.0 ends at coaly / sh ptg

Photo 1536.0

- 1cm mudst clast

white, lt grey crs SS

Drill Site:
N: E:
Started:
Completed

Collar Elevation:
Bearing:
Inclination:
Total Depth:

Sandia National Laboratories
Logged by: AHLautman
Log Version:
Log Date: 3-22-02

Raton Basin Project
Hole No: CH-7
Scale: 1" = 10' (1:120)
Sheet 20 of

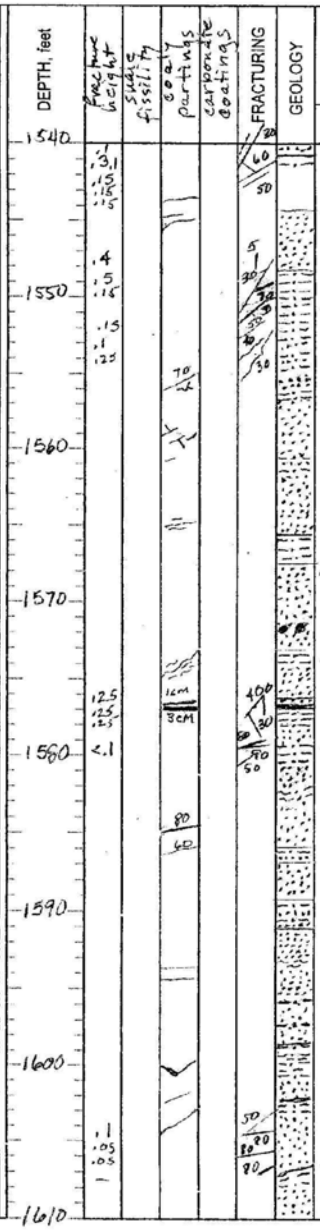

COMMENTS:

Avg. Core Recovery/ Hole

Drilling Interval | % Core Recovered | Core Size | RQD | Sample Interval

1541.8 slicks rake 0
incipient closed frac 1cm whole

Descriptive Geology

- small granules
- slicks rake 10°

1549.5 conj frax ~60° apart in plan

1447.7-1448.1: near vert frac
ends at contact w/ granule ss
slicks m 70° frac ~ 11 dip
1552.2 slicks rake 10
1553.7 slicks m 50° frac rake 40°

- 0.5 crs ss
- lam vfgss

med-crs ss

silty zone

crs white ss w/ sparse mud chips

1565.8 sharp contact
black carb siltst
1567.6 sharp contact

1571.6-72.4 intvl of mudst chips to 2cm
sharp contact 1573.1 +granules (feldspar?)

1577.1-.6 dk gr vfg ss
1577.5 intersect frax, slick on
40° frac rake to
79.5 horiz slicks rake ~ 20° in plan

1586-87 dkgr muddy siltst to crs ss ↑ fining

1589.2 sharp contact ? dk grey muddy siltst
1591.0 sharp contact vfg ss w/ granules

1592.8-93.1 wispy shaly/coaly lam

1695-97 lam; some disruption

1698.3 sharp contact

fining up

quite coarse ss
1602.5 sharp contact

v. carb ss/siltst.

1604.9, 1605.8 - v. planar frax w/
weak slicks - striations raking 50-60°
1606.8 partial comp slicks in mudst rake 10°
1606.8 sharp contact

fining up

quite coarse ss

- lam

1541
SANDSTONE
SILTSTONE, muddy
1543.7
SANDSTONE
1547.7
SILTSTONE
muddy dk grey
w/ granules
1565.1
SANDSTONE
1565.8
SILTSTONE, Carb
1567.6
SANDSTONE
white - lt grey, med-crs
alt w/ dk grey muddy -
siltstone - vfg ss w/
dispersed granules

Photo 1471.0

Photo 1548.8

Photo 1549.5

Photo 1548.4-1567.1

Sandia National Laboratories
Logged by: CAKRautman
Log Version:
Log Date: 4-3-0[illegible]

Raton Basin Project
Hole No: CH-7
Scale: 1" = 10' (1:120)
Sheet 21 of

Collar Elevation:
Bearing:
Inclination:
Total Depth:

Drill Site:
N: E:
Started:
Completed

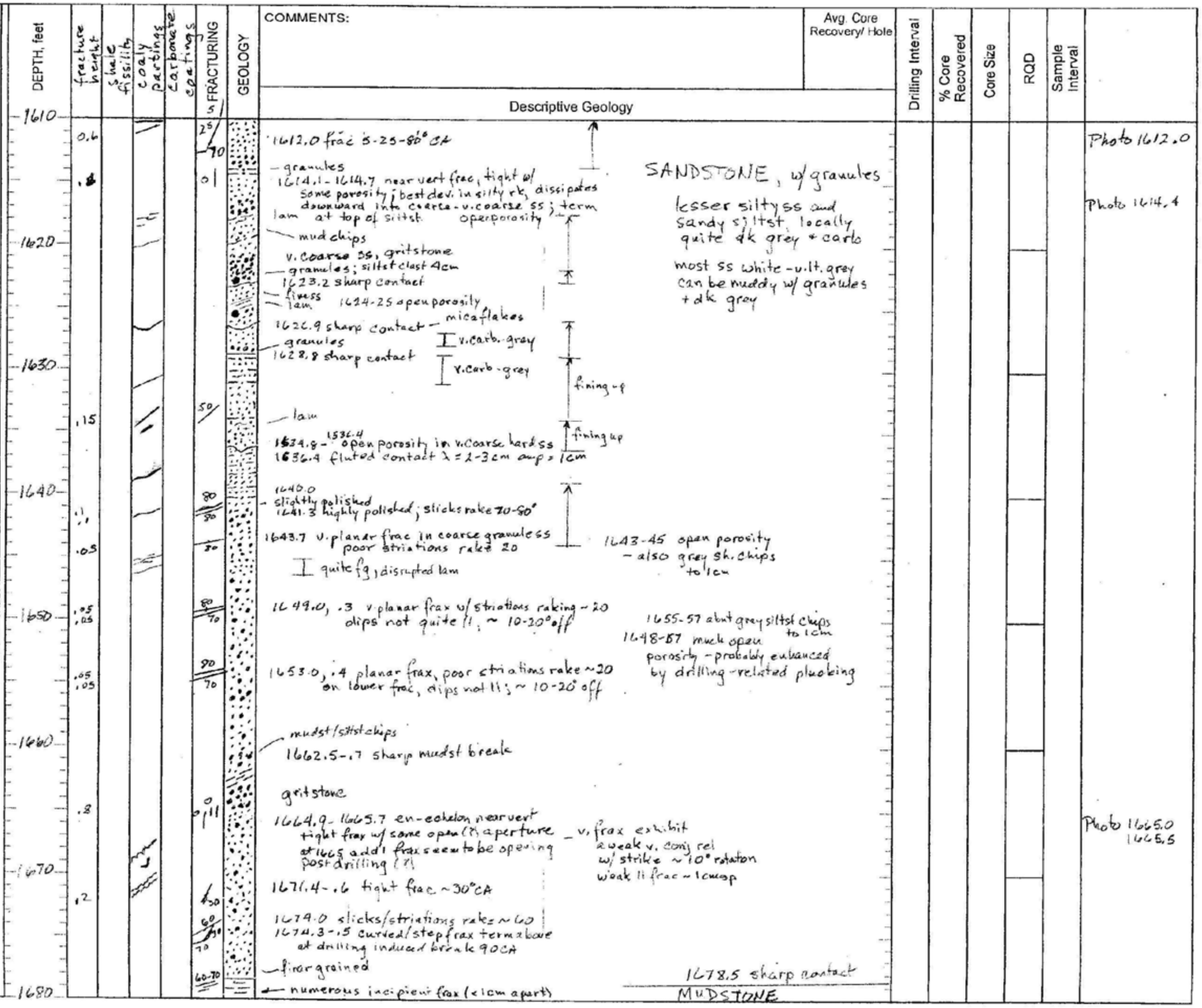

1612.0 frac 5-25-80° CA

- granules
1614.1-1614.7 near vert frac, tight w/ some porosity; best dev. in silty rk, dissipates downward into coarse-v.coarse ss; term at top of siltst. open porosity
- lam
- mud chips
v. coarse ss, gritstone
- granules; siltst clast 4cm
1623.2 sharp contact
- finess
- lam
1624-25 open porosity
1626.9 sharp contact - mica flakes
- granules
1628.8 sharp contact
v. carb. gray
v. carb - grey
- lam
1634.8 - 1536.4 open porosity in v. coarse hard ss
1636.4 fluted contact λ = 2-3cm amp = 1cm
1640.0 slightly polished
- 1641.3 highly polished; sticks rake 70-80°
1643.7 v. planar frac in coarse granuless poor striations rake 20
quite fg, disrupted lam
1649.0, .3 v. planar frax w/ striations raking ~20 dips not quite ‖; ~ 10-20° off
1653.0, .4 planar frax, poor striations rake ~20 on lower frac, dips not ‖; ~ 10-20° off
- mudst/siltst chips
1662.5-.7 sharp mudst break
gritstone
1664.9-1665.7 en-echelon near vert tight frax w/ some open (?) aperture at 1665 add'l frax seem to be opening post drilling (?)
1671.4-.6 tight frac ~30° CA
1674.0 slicks/striations rake ~60
1674.3-.5 curved/step frax term above at drilling induced break 90CA
- finer grained
← numerous incipient frax (< 1cm apart)

SANDSTONE, w/ granules

lesser silty ss and sandy siltst, locally quite dk grey + carb

most ss white-v.lt. grey can be muddy w/ granules + dk grey

1643-45 open porosity - also grey sh. chips to 1cm

1655-57 abnt grey siltst chips to 1cm
1648-57 much open porosity - probably enhanced by drilling-related plucking

- v. frax exhibit a weak v. conj rel w/ strike ~10° rotation
weak ‖ frac ~ 1cm sep

1678.5 sharp contact

MUDSTONE

Photo 1612.0

Photo 1614.4

Photo 1665.0
1665.5

Drill Site:
N: E:
Started:
Completed

Collar Elevation:
Bearing:
Inclination:
Total Depth:

Sandia National Laboratories
Logged by: CARautman
Log Version:
Log Date: 4-3-02

Raton Basin Project
Hole No: CH-7
Scale: 1" = 10' (1:120)
Sheet 22 of

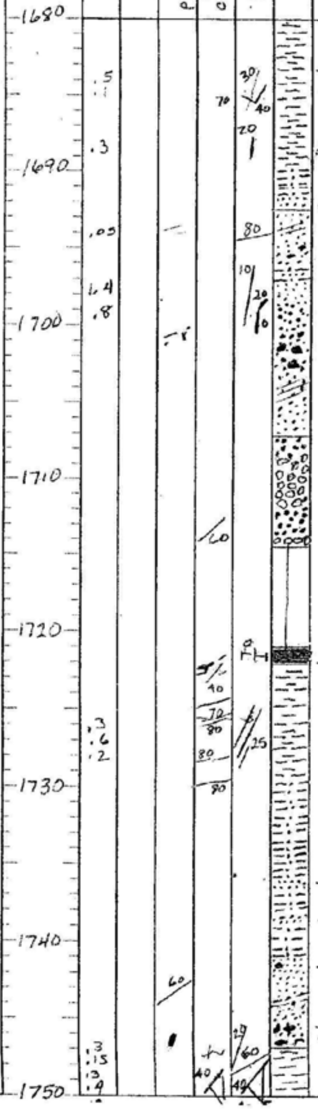

COMMENTS:

Avg. Core Recovery/ Hole

Drilling Interval

% Core Recovered

Core Size

RQD

Sample Interval

Descriptive Geology

broken/rubble

V. broken

only major frax inferred - rubble

quite massive

– colorchange

– lam

– siltst chips

1696.8-1698.2 slightly irreg, quite planar long frac; no coatings

1698.6-99.3 curved frac, CO_3 tight w/ some poros

1701 siltst-chip congl

1703 strongly lam

1707.3 abrupt change in grain size

1714.4(L)-1721.1 presumed coal

arg coal? - vert cleats

-1722.2 Coreloss

1722.3-.7 intvl of mm CO_3 veining

fining up cont?

rubble < 5cm

fining up

– well lam vfg ss w/softsed defm

– well lam vfg ss

– Some mud chips

1742.9-43.2 lam siltst, carb. 60 CA

mudst chips

1746.8 sharp contact, mudst chips

1747.0 comp slicks rake 5°

1748.0 good slicks rake 10°

crude fining up

multiple strikes w/ CO_3

1749.6 40° frac term 5° frac

weak CO_3

CO_3 ~1mm or less on 40° fracs ~ 80-100% coverage

MUDSTONE, silty at base to vfg carb. ss, black

Rubblized intvl exhibits breaks ⊥ and ∥ CA + at all angles; strong though frag comp slicks at all angles

1692.3 - fairly sharp contact

SANDSTONE - generally quite coarse to granules/grit stone white - lt grey, locally lam. some dr siltst chips

some open(?) porosity enhanced by plucking

CONGLOMERATE

COAL (?)

MUDSTONE + SILTSTONE

numerous 1-2mm CO_3 veinlets ~ ∥ bedding @ ~80 CA - seems to be reddish w/ FeOx

SANDSTONE

MUDSTONE

Coal Samples removed

Photo 1726.0
Photo 1727.0
Photo 1728.9

Drill Site:
N: E:
Started:
Completed

Collar Elevation:
Bearing:
Inclination:
Total Depth:

Sandia National Laboratories
Logged by: Rautman
Log Version:
Log Date: 4-3-02

Raton Basin Project
Hole No: CH-7
Scale: 1" = 10' (1:120)
Sheet 23 of

COMMENTS: long frac in ss exhibits poor match across frac plane - missing slivers ≈ // frax ?

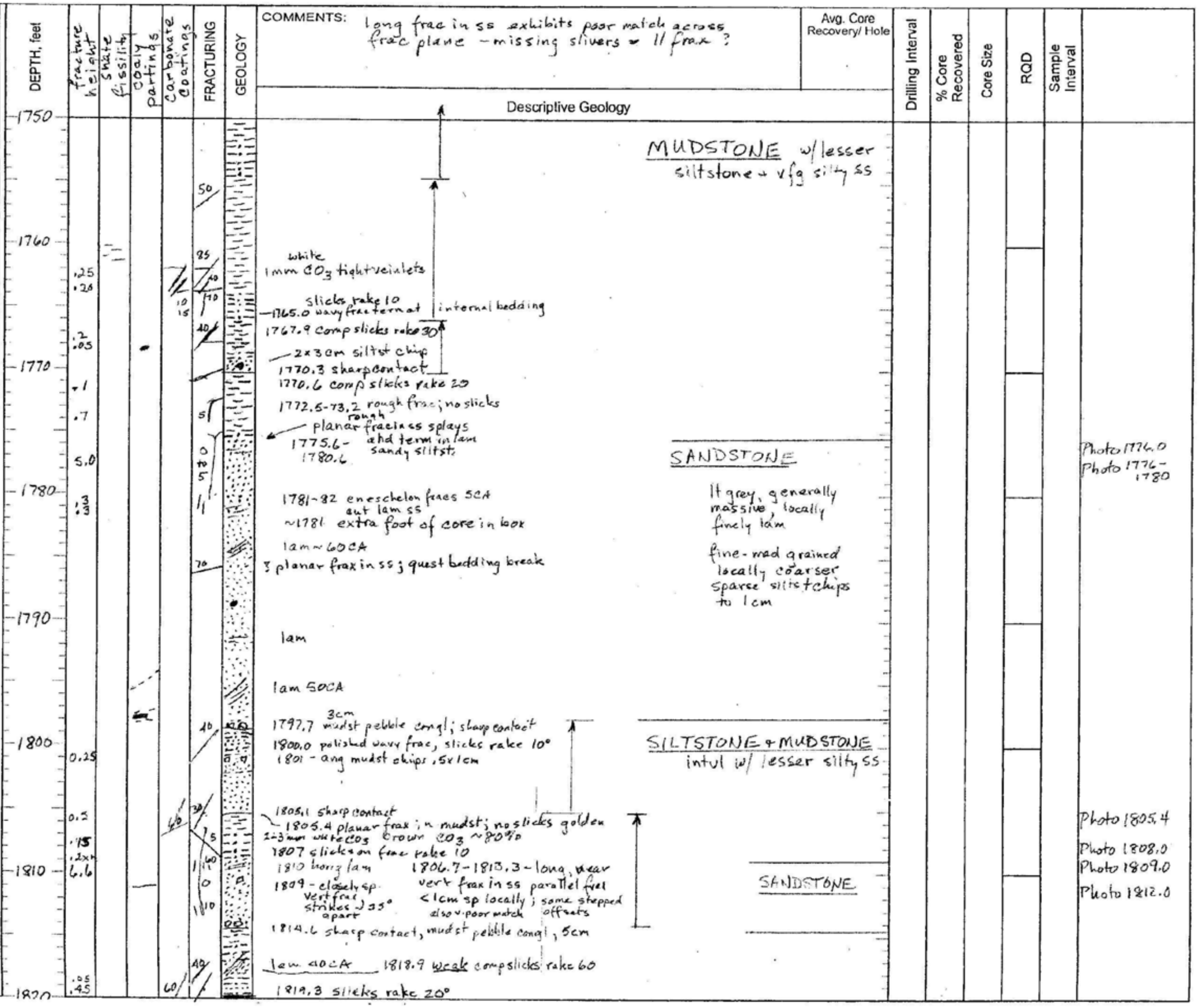

white 1mm CO3 tight veinlets

slicks rake 10

1765.0 wavy frac term at | internal bedding

1767.9 comp slicks rake 30

2x3cm siltst chip

1770.3 sharp contact

1770.6 comp slicks rake 20

1772.5-73.2 rough frac; no slicks

1775.6-1780.6 rough planar fracless splays and term in lam sandy siltst

1781-82 en eschelon fracs 5CA cut lam ss

~1781 extra foot of core in box

lam ~ 60CA

3 planar frax in ss; quest bedding break

lam

lam 50CA

1797.7 3cm mudst pebble congl; sharp contact

1800.0 polished wavy frac, slicks rake 10°

1801 - ang mudst chips .5x1cm

1805.1 sharp contact

1805.4 planar frax in mudst; no slicks golden brown CO3 ~80%

1-3mm white CO3

1807 slicks on frac rake 10

1810 horiz lam

1806.7-1813.3 - long, near vert frax in ss parallel frac <1cm sp locally; some stepped offsets also v. poor match

1809 - closely sp. vert frac, strikes ~35° apart

1814.6 sharp contact, mudst pebble congl, 5cm

lam 40CA

1818.9 weak comp slicks rake 60

1819.3 slicks rake 20°

MUDSTONE w/ lesser siltstone + vfg silty ss

SANDSTONE

lt grey, generally massive, locally finely lam

fine-med grained locally coarser sparse siltst chips to 1cm

SILTSTONE + MUDSTONE intvl w/ lesser silty ss

SANDSTONE

Photo 1776.0
Photo 1776-1780

Photo 1805.4
Photo 1808.0
Photo 1809.0
Photo 1812.0

Sandia National Laboratories

Raton Basin Project

Logged by: CARautman

Hole No: CH-7

Log Version:

Scale: 1" = 10' (1:120)

Log Date: 2-4-02

Sheet 24 of

Drill Site:

Collar Elevation:

N:

E:

Bearing:

Started:

Inclination:

Completed

Total Depth:

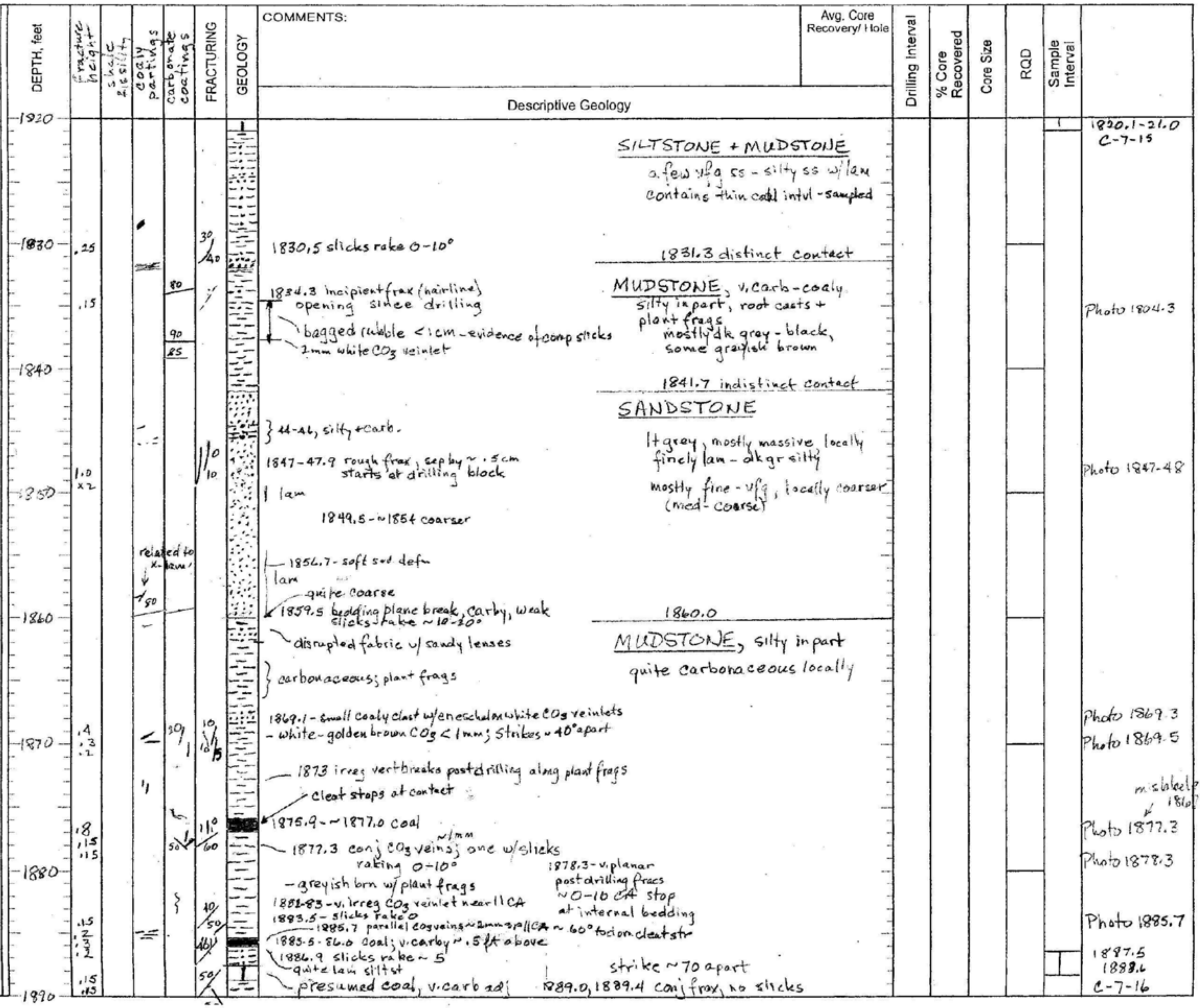

SILTSTONE + MUDSTONE

a few vfg ss - silty ss w/ lam

contains thin coal intvl - sampled

1830.5 slicks rake 0-10°

1831.3 distinct contact

MUDSTONE, v. carb - coaly

silty in part, root casts + plant frags

mostly dk grey - black, some grayish brown

1834.3 incipient frax (hairline) opening since drilling

bagged rubble < 1cm - evidence of comp slicks

1mm white CO_3 veinlet

1841.7 indistinct contact

SANDSTONE

lt grey, mostly massive locally finely lam - dk gr silty

mostly fine - vfg, locally coarser (med - coarse)

44-46, silty + carb.

1847-47.9 rough frax, sep by ~ .5 cm starts at drilling block

lam

1849.5 - ~1854 coarser

1856.7 - soft sed def

lam

quite coarse

1859.5 bedding plane break, carby, weak slicks - rake ~10-20°

1860.0

MUDSTONE, silty in part

quite carbonaceous locally

disrupted fabric w/ sandy lenses

carbonaceous; plant frags

1869.1 - small coaly clast w/ en eschelon white CO_3 veinlets

- white - golden brown CO_3 < 1mm; strikes ~ 40° apart

1873 irreg vert breaks post drilling along plant frags

cleat stops at contact

1875.9 - ~1877.0 coal

1877.3 conj CO_3 veins ~/mm; one w/ slicks raking 0-10°

1878.3 - v. planar post drilling fracs ~0-10 CA stop at internal bedding

- greyish brn w/ plant frags

1881-83 - v. irreg CO_3 veinlet near ll CA

1883.5 - slicks rake 0

1885.7 parallel CO_3 veins ~2mm sp ll CA ~ 60° to cleat str

1885.5 - 86.0 coal; v. carby ~ .5 ft above

1886.9 slicks rake ~ 5

quite lam siltst

presumed coal, v. carb adj

strike ~ 70 apart

1889.0, 1889.4 conj frax, no slicks

1820.1 - 21.0
C-7-15

Photo 1804.3

Photo 1847-48

Photo 1869.3

Photo 1869.5

mislabeled 1867.3

Photo 1877.3

Photo 1878.3

Photo 1885.7

1887.5
1888.6
C-7-16

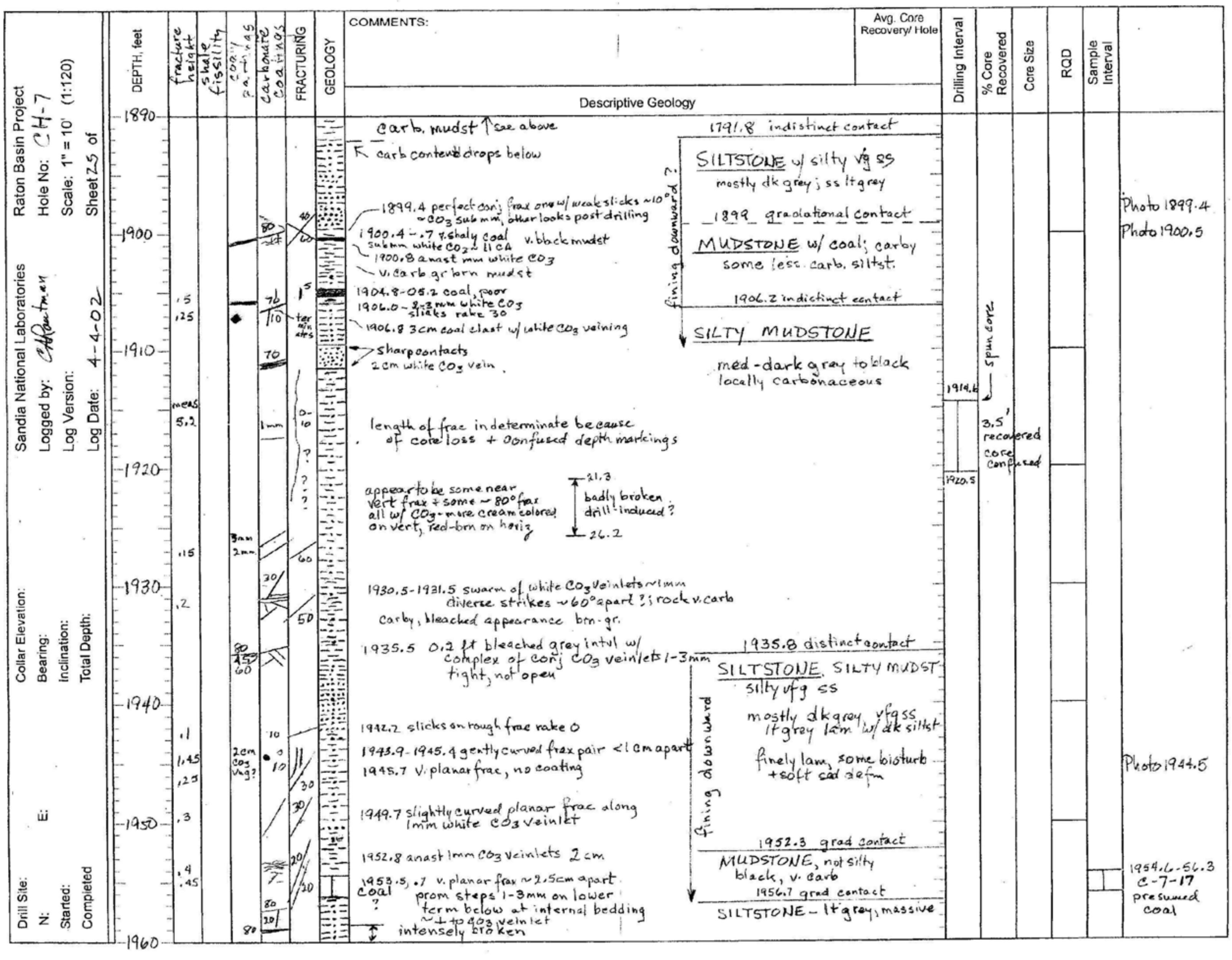

Raton Basin Project
Hole No: CH-7
Scale: 1" = 10' (1:120)
Sheet 25 of

Sandia National Laboratories
Logged by: CHBoutman
Log Version:
Log Date: 4-4-02

Collar Elevation:
Bearing:
Inclination:
Total Depth:

Drill Site:
N:
E:
Started:
Completed

COMMENTS:

carb. mudst ↑ see above

carb content drops below

1899.4 perfect conj frac one w/ weak slicks ~10° ~CO3 sub mm, other looks post drilling

1900.4 - .7 v. shaly coal v. black mudst
sub mm white CO2 ~ ⊥ CA

1900.8 anast mm white CO3

v. carb gr brn mudst

1904.8-05.2 coal, poor

1906.0 - 2-3 mm white CO3 slicks rake 30

1906.8 3cm coal clast w/ white CO3 veining

sharp contacts
2cm white CO3 vein

length of frac indeterminate because of core loss + confused depth markings

appear to be some near vert frax + some ~80° frax all w/ CO3 - more cream colored on vert, red-brn on horiz

21.3
badly broken drill-induced ?
26.2

1930.5-1931.5 swarm of white CO3 veinlets ~1mm diverse strikes ~60° apart ?; rock v. carb

carby, bleached appearance brn-gr.

1935.5 0.2 ft bleached grey intvl w/ complex of conj CO3 veinlets 1-3mm tight, not open

1942.2 slicks on rough frac rake 0

1943.9-1945.4 gently curved frax pair <1 cm apart

1945.7 v. planar frac, no coating

1949.7 slightly curved planar frac along 1mm white CO3 veinlet

1952.8 anast 1mm CO3 veinlets 2 cm

1953.5, .7 v. planar frax ~2.5cm apart
prom steps 1-3mm on lower
term below at internal bedding
~⊥ to CO3 veinlet

coal ?

intensely broken

Avg. Core Recovery/ Hole

Descriptive Geology

1791.8 indistinct contact

SILTSTONE w/ silty vfg ss
mostly dk grey; ss lt grey

1899 gradational contact

MUDSTONE w/ coal; carby
some less carb. siltst.

1906.2 indistinct contact

fining downward ?

SILTY MUDSTONE
med-dark gray to black
locally carbonaceous

1935.8 distinct contact

SILTSTONE, SILTY MUDST
silty vfg ss
mostly dk grey vfg ss
lt grey lam w/ dk siltst
finely lam, some bioturb
+ soft sed defm

fining downward

1952.3 grad contact

MUDSTONE, not silty
black, v. carb

1956.7 grad contact

SILTSTONE - lt grey, massive

spun core

3.5' recovered core confused

Photo 1899.4
Photo 1900.5
Photo 1944.5

1954.6-56.3
C-7-17
presumed coal

Drill Site:
N: E:
Started:
Completed

Collar Elevation:
Bearing:
Inclination:
Total Depth:

Sandia National Laboratories
Logged by: CARautman
Log Version:
Log Date: 4-4-02

Raton Basin Project
Hole No: CH-7
Scale: 1" = 10' (1:120)
Sheet 26 of 27

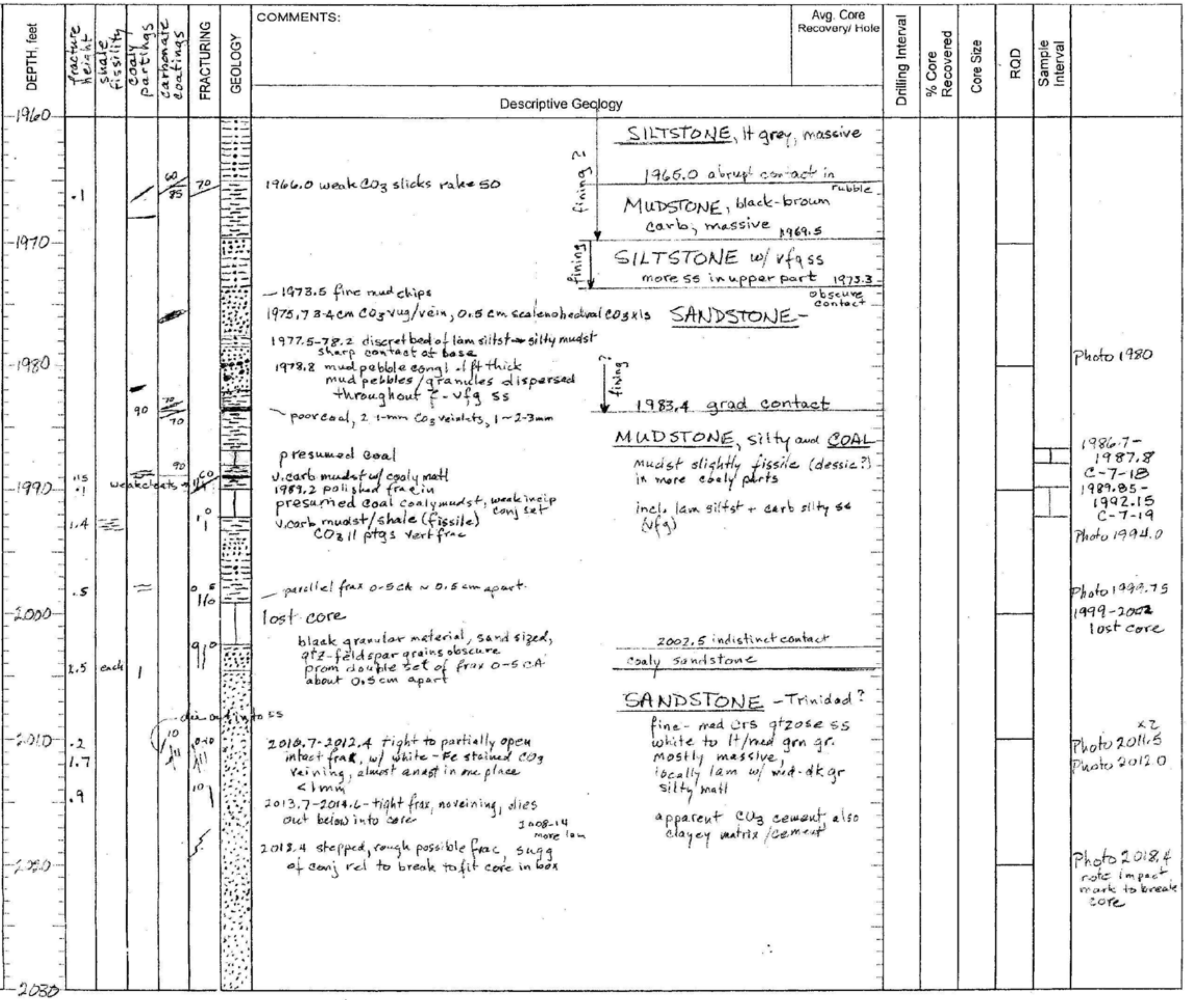

1966.0 weak CO3 slicks rake 50

— 1973.5 fine mud chips

1975.7 3-4 cm CO3 vug/vein, 0.5 cm scalenohedral CO3 xls

1977.5-78.2 discret bed of lam siltst → silty mudst
sharp contact at base

1978.8 mud pebble congl .1 ft thick
mud pebbles/granules dispersed
throughout f - vfg ss

~ poor coal, 2 1-mm CO3 veinlets, 1~2-3mm

presumed coal

v.carb mudst w/ coaly matl
1989.2 polished frac in
presumed coal coalymudst, weak incip conj set
v.carb mudst/shale (fissile)
CO3 // ptgs vert frac

— parallel frax 0-5 CA ~ 0.5 cm apart.

lost core

black granular material, sand sized,
qtz-feldspar grains obscure
prom double set of frax 0-5 CA
about 0.5 cm apart

2010.7-2012.4 tight to partially open
intact frac, w/ white - Fe stained CO3
veining, almost anast in one place
< 1 mm

2013.7-2014.6 - tight frax, no veining, dies
out below into core

2008-14
more lam

2018.4 stepped, rough possible frac, sugg
of conj rel to break to fit core in box

SILTSTONE, lt grey, massive

1966.0 abrupt contact in rubble

MUDSTONE, black-brown
carb, massive 1969.5

SILTSTONE w/ vfg ss
more ss in upper part 1973.3

obscure contact

SANDSTONE -

1983.4 grad contact

MUDSTONE, silty and COAL

mudst slightly fissile (dessic?)
in more coaly parts

incl. lam siltst + carb silty ss
(vfg)

2002.5 indistinct contact

coaly sandstone

SANDSTONE - Trinidad?

fine - med crs qtzose ss
white to lt/med grn gr.
mostly massive,
locally lam w/ med-dk gr
silty matl

apparent CO3 cement also
clayey matrix/cement

Photo 1980

1986.7 -
1987.8
C-7-18
1989.85 -
1992.15
C-7-19
Photo 1994.0

Photo 1999.75
1999-2002
lost core

x2
Photo 2011.5
Photo 2012.0

Photo 2018.4
note impact
mark to break
core

Drill Site:
N: E:
Started:
Completed

Collar Elevation:
Bearing:
Inclination:
Total Depth:

Sandia National Laboratories
Logged by: CAR Rautman
Log Version:
Log Date: 4-9-02

Raton Basin Project
Hole No: CH-7
Scale: 1" = 10' (1:120)
Sheet 27 of 27

DEPTH, feet: 2030, 2040, 2050, 2060, 2070, 2080, 2090, 2100

fracture height: 0.4

shale fissility

coaly partings

carbonate coatings

FRACTURING: 10

GEOLOGY

COMMENTS:

Descriptive Geology

SANDSTONE
quite massive grn-white
med ss, locally lam.

2037.5-2039 weak lam 70-90 CA, // handling-induced breaks-v. planar

2039.6-2040 partially open frac w/ en eschelon st; may have been initiated by breaking core to fit box

2043.2' E.O.H.

Avg. Core Recovery/ Hole

Drilling Interval

% Core Recovered

Core Size: 2.3+"

RQD

Sample Interval

Photo 2039.8

APPENDIX G

This appendix contains field data collected from 94 sites in the Raton Mesa area. Each entry consists of

- location ID
- latitude and longitude of the site
- an index map showing the location of the site in relation to Raton Mesa
- a rose diagram showing the distribution of fracture orientations at that location
- raw fracture data, including any notes concerning lithology, cross-cutting relationships, fracture fill minerals, etc.

Additional notes and photographs may be included for certain sites.

Fracture dips follow the right hand rule; that is, dip is in the direction 90 degrees clockwise from fracture azimuth.

Abbreviations used in this appendix:

VPA = Vermejo Park Anticline
ss = sandstone
frac = fracture

Location ID: 6/17/2003/1
Latitude: N 36.8883667
Longitude: W 104.9753333

Cliff exposure of Trinidad sandstone north of Vermejo Park Ranch office.

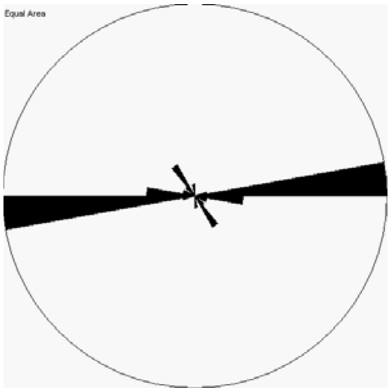

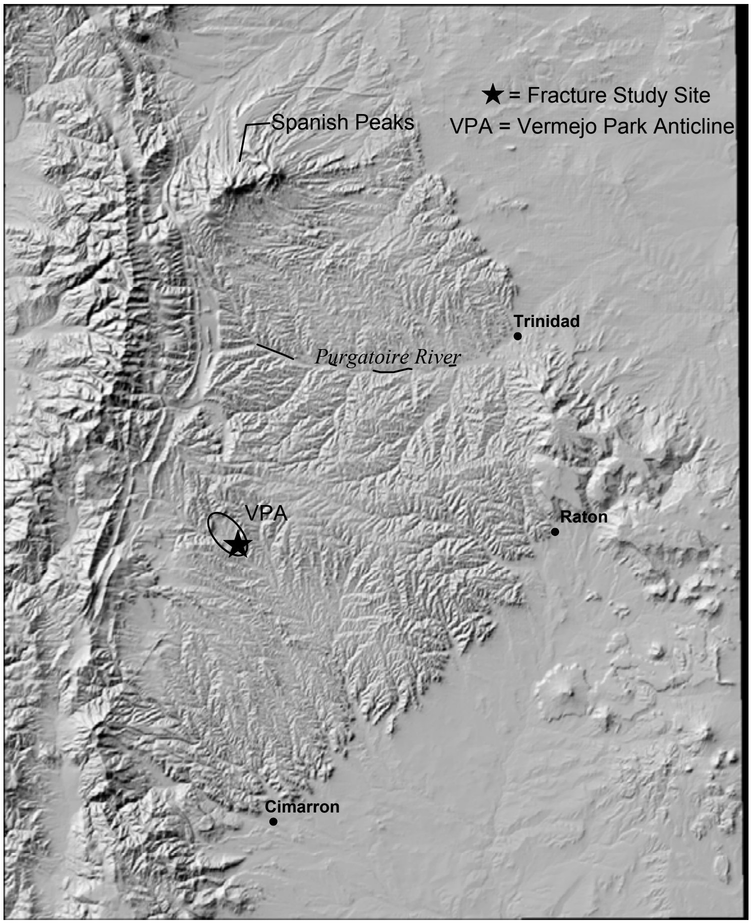

Notes:

Cliff exposure ~50 meters, bed thickness ~6 meters

E-W fracture set cuts ~15 meters of cliff

Fracture Data:

ID	Strike	Dip	Formation	Comment 1	Comment 2
6/17/2003/1	81	80	Trinidad		
6/17/2003/1	83	90	Trinidad		
6/17/2003/1	85	90	Trinidad		
6/17/2003/1	140	80	Trinidad		
6/17/2003/1	310	90	Trinidad		
6/17/2003/1	275	72	Trinidad		
6/17/2003/1	350	88	Trinidad		
6/17/2003/1	84	90	Trinidad		
6/17/2003/1	80	90	Trinidad		
6/17/2003/1	91	90	Trinidad		
6/17/2003/1	329	90	Trinidad		
6/17/2003/1	79	90	Trinidad		

6/17/2003/1	85	88	Trinidad	
6/17/2003/1	84	90	Trinidad	
6/17/2003/1	85	84	Trinidad	
6/17/2003/1	83	80	Trinidad	
6/17/2003/1	104	90	Trinidad	irregular, short
6/17/2003/1	87	90	Trinidad	
6/17/2003/1	118	90	Trinidad	irregular, short
6/17/2003/1	273	70	Trinidad	
6/17/2003/1	262	85	Trinidad	
6/17/2003/1	85	90	Trinidad	
6/17/2003/1	269	87	Trinidad	
6/17/2003/1	269	85	Trinidad	
6/17/2003/1	93	55	Trinidad	
6/17/2003/1	87	90	Trinidad	
6/17/2003/1	85	90	Trinidad	
6/17/2003/1	141	90	Trinidad	plume

Location ID: 6/17/2003/2
Latitude: N 36.92451667
Longitude: W 105.0168833

Spring Canyon

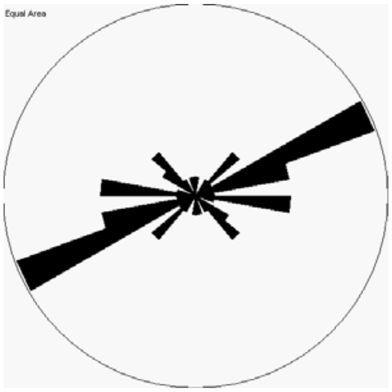

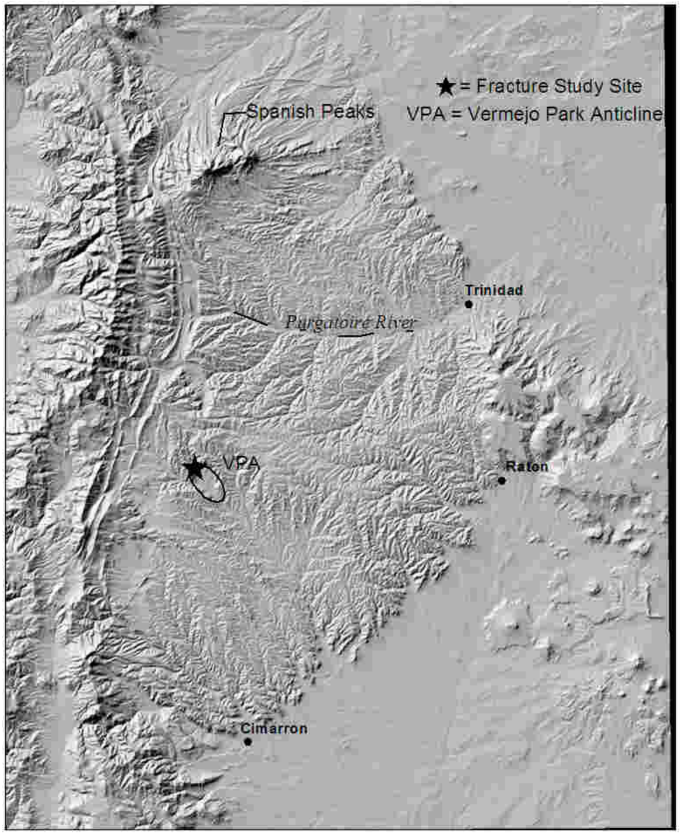

Notes:

Fracture Data:

ID	Strike	Dip	Formation	Comment 1	Comment 2
6/17/2003/2	66	64	Trinidad		
6/17/2003/2	66	64	Trinidad		
6/17/2003/2	73	61	Trinidad		
6/17/2003/2	59	90	Trinidad		
6/17/2003/2	45	76	Trinidad		
6/17/2003/2	41	78	Trinidad		
6/17/2003/2	31	78	Trinidad		
6/17/2003/2	48	60	Trinidad		
6/17/2003/2	62	74	Trinidad		
6/17/2003/2	64	62	Trinidad		
6/17/2003/2	68	64	Trinidad		
6/17/2003/2	70	65	Trinidad		
6/17/2003/2	68	63	Trinidad		
6/17/2003/2	67	90	Trinidad		
6/17/2003/2	72	78	Trinidad		
6/17/2003/2	89	64	Trinidad		

6/17/2003/2	94	70	Trinidad
6/17/2003/2	90	70	Trinidad
6/17/2003/2	70	70	Trinidad
6/17/2003/2	90	70	Trinidad
6/17/2003/2	70	70	Trinidad
6/17/2003/2	62	75	Trinidad
6/17/2003/2	62	75	Trinidad
6/17/2003/2	63	76	Trinidad
6/17/2003/2	306	66	Trinidad
6/17/2003/2	313	57	Trinidad
6/17/2003/2	6	90	Trinidad
6/17/2003/2	314	76	Trinidad
6/17/2003/2	305	70	Trinidad
6/17/2003/2	314	60	Trinidad
6/17/2003/2	322	75	Trinidad
6/17/2003/2	350	84	Trinidad
6/17/2003/2	280	55	Trinidad
6/17/2003/2	349	90	Trinidad
6/17/2003/2	278	90	Trinidad
6/17/2003/2	95	75	Trinidad

Location ID: 6/17/2003/3
Latitude: N 36.89933333
Longitude: W 105.0294333

Trinidad roadcut at west gate, thrust fault

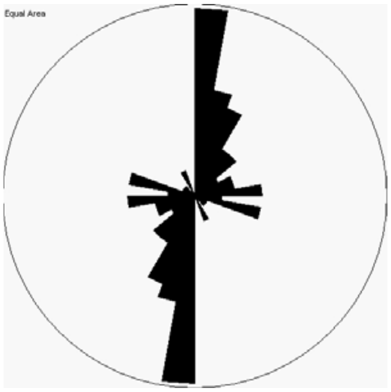

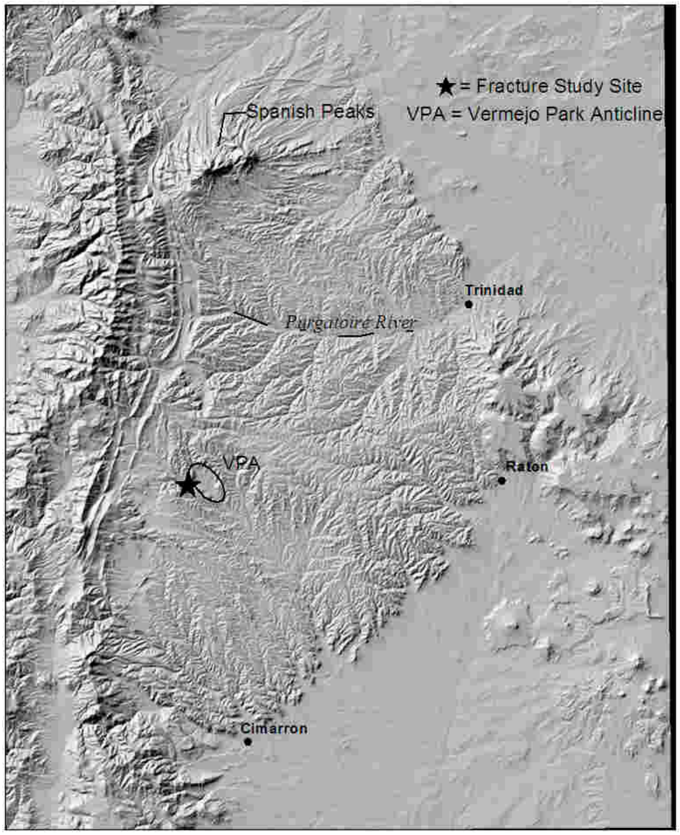

Notes:

Fracture Data:

ID	Strike	Dip	Formation	Comment 1	Comment 2
6/17/2003/3	82	90	Trinidad	plume	footwall of thrust
6/17/2003/3	200	82	Trinidad		footwall of thrust
6/17/2003/3	83	90	Trinidad	plume	footwall of thrust
6/17/2003/3	184	85	Trinidad		footwall of thrust
6/17/2003/3	282	60	Trinidad		footwall of thrust
6/17/2003/3	192	78	Trinidad		footwall of thrust
6/17/2003/3	93	90	Trinidad	plume	footwall of thrust
6/17/2003/3	90	90	Trinidad		footwall of thrust
6/17/2003/3	185	70	Trinidad	plume	footwall of thrust
6/17/2003/3	84	90	Trinidad	plume	footwall of thrust
6/17/2003/3	84	90	Trinidad		footwall of thrust
6/17/2003/3	200	60	Trinidad		footwall of thrust
6/17/2003/3	64	80	Trinidad	plume	footwall of thrust
6/17/2003/3	75	90	Trinidad		footwall of thrust
6/17/2003/3	202	64	Trinidad		footwall of thrust
6/17/2003/3	73	65	Trinidad		footwall of thrust
6/17/2003/3	216	68	Trinidad		footwall of thrust

6/17/2003/3	54	85	Trinidad		footwall of thrust
6/17/2003/3	212	64	Trinidad		footwall of thrust
6/17/2003/3	198	65	Trinidad		footwall of thrust
6/17/2003/3	7	76	Trinidad		hanging wall of thrust
6/17/2003/3	314	88	Trinidad		hanging wall of thrust
6/17/2003/3	334	90	Trinidad		hanging wall of thrust
6/17/2003/3	2	87	Trinidad		hanging wall of thrust
6/17/2003/3	9	90	Trinidad		hanging wall of thrust
6/17/2003/3	22	65	Trinidad		hanging wall of thrust
6/17/2003/3	5	58	Trinidad		hanging wall of thrust
6/17/2003/3	15	82	Trinidad		hanging wall of thrust
6/17/2003/3	82	88	Trinidad		hanging wall of thrust
6/17/2003/3	107	85	Trinidad		hanging wall of thrust
6/17/2003/3	6	88	Trinidad		hanging wall of thrust
6/17/2003/3	5	84	Trinidad		hanging wall of thrust
6/17/2003/3	4	88	Trinidad		hanging wall of thrust
6/17/2003/3	9	80	Trinidad		hanging wall of thrust
6/17/2003/3	8	86	Trinidad		hanging wall of thrust
6/17/2003/3	10	74	Trinidad		hanging wall of thrust
6/17/2003/3	10	88	Trinidad		hanging wall of thrust
6/17/2003/3	159	89	Trinidad		hanging wall of thrust
6/17/2003/3	109	80	Trinidad		hanging wall of thrust
6/17/2003/3	7	86	Trinidad		hanging wall of thrust
6/17/2003/3	70	90	Trinidad		hanging wall of thrust
6/17/2003/3	65	85	Trinidad		hanging wall of thrust
6/17/2003/3	13	86	Trinidad		hanging wall of thrust
6/17/2003/3	15	86	Trinidad		hanging wall of thrust
6/17/2003/3	6	89	Trinidad		hanging wall of thrust
6/17/2003/3	5	87	Trinidad		hanging wall of thrust
6/17/2003/3	57	80	Trinidad		hanging wall of thrust
6/17/2003/3	60	79	Trinidad		hanging wall of thrust
6/17/2003/3	20	72	Trinidad		hanging wall of thrust
6/17/2003/3	216	75	Trinidad		hanging wall of thrust
6/17/2003/3	100	85	Trinidad		associated with thrust
6/17/2003/3	103	85	Trinidad		associated with thrust
6/17/2003/3	34	60	Trinidad		associated with thrust
6/17/2003/3	113	90	Trinidad		associated with thrust
6/17/2003/3	44	70	Trinidad		associated with thrust
6/17/2003/3	48	70	Trinidad		associated with thrust
6/17/2003/3	127	90	Trinidad		associated with thrust
6/17/2003/3	24	50	Trinidad	slicked plane	
6/17/2003/3	44	60	Trinidad	plume	
6/17/2003/3	28	15	Trinidad	shear plane	
6/17/2003/3	44	20	Trinidad	shear plane	
6/17/2003/3	14	48	Trinidad	shear plane	

Location ID: 6/18/2003/1
Latitude: N 36.92393333
Longitude: W 105.0183667

Spring Canyon, west side

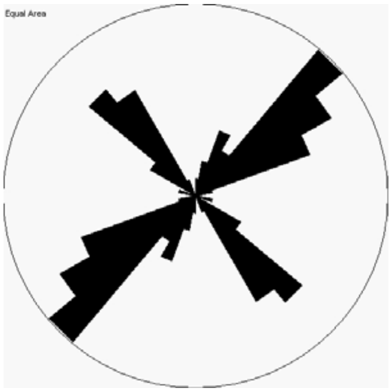

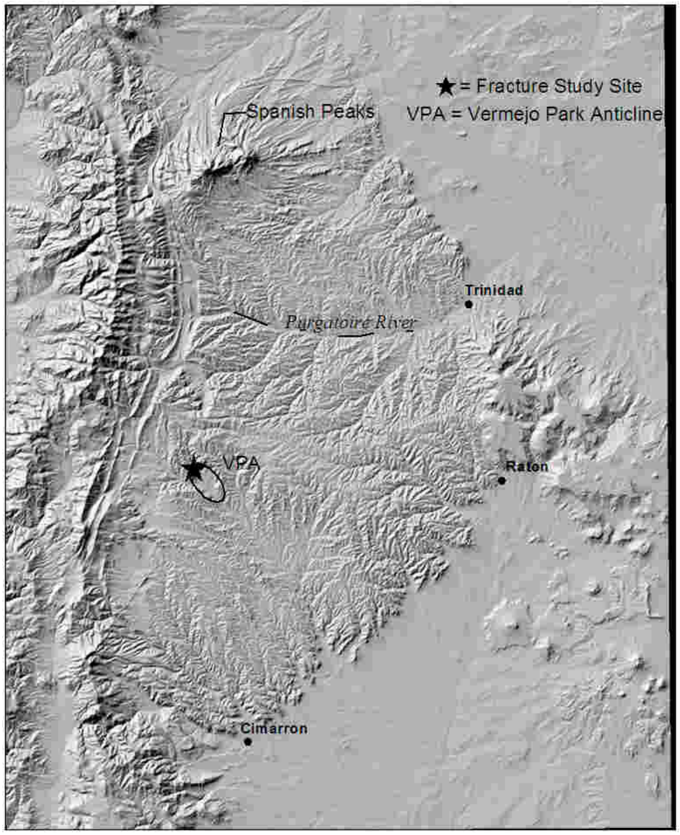

Notes:

Fracture Data:

ID	Strike	Dip	Formation	Comment 1
6/18/2003/1	47	52	Trinidad	
6/18/2003/1	145	87	Trinidad	plume
6/18/2003/1	38	48	Trinidad	
6/18/2003/1	45	60	Trinidad	
6/18/2003/1	47	65	Trinidad	
6/18/2003/1	60	68	Trinidad	
6/18/2003/1	64	50	Trinidad	
6/18/2003/1	48	64	Trinidad	
6/18/2003/1	63	62	Trinidad	
6/18/2003/1	59	64	Trinidad	
6/18/2003/1	49	68	Trinidad	
6/18/2003/1	56	62	Trinidad	
6/18/2003/1	48	58	Trinidad	
6/18/2003/1	140	90	Trinidad	
6/18/2003/1	45	78	Trinidad	
6/18/2003/1	44	66	Trinidad	
6/18/2003/1	53	68	Trinidad	

6/18/2003/1	42	58	Trinidad	
6/18/2003/1	55	67	Trinidad	
6/18/2003/1	56	71	Trinidad	
6/18/2003/1	332	78	Trinidad	
6/18/2003/1	57	67	Trinidad	
6/18/2003/1	55	65	Trinidad	
6/18/2003/1	50	67	Trinidad	
6/18/2003/1	38	42	Trinidad	
6/18/2003/1	60	61	Trinidad	shear zone
6/18/2003/1	48	40	Trinidad	shear zone
6/18/2003/1	39	80	Trinidad	fault
6/18/2003/1	316	90	Trinidad	pavement
6/18/2003/1	307	90	Trinidad	pavement
6/18/2003/1	310	90	Trinidad	pavement
6/18/2003/1	322	90	Trinidad	pavement
6/18/2003/1	318	90	Trinidad	pavement
6/18/2003/1	310	90	Trinidad	pavement
6/18/2003/1	326	90	Trinidad	pavement
6/18/2003/1	307	90	Trinidad	pavement
6/18/2003/1	323	90	Trinidad	pavement
6/18/2003/1	318	90	Trinidad	pavement
6/18/2003/1	319	90	Trinidad	pavement
6/18/2003/1	317	90	Trinidad	pavement
6/18/2003/1	329	90	Trinidad	pavement
6/18/2003/1	306	90	Trinidad	pavement
6/18/2003/1	318	90	Trinidad	pavement
6/18/2003/1	321	90	Trinidad	pavement
6/18/2003/1	18	90	Trinidad	pavement
6/18/2003/1	20	90	Trinidad	pavement
6/18/2003/1	25	90	Trinidad	pavement
6/18/2003/1	19	90	Trinidad	pavement
6/18/2003/1	21	90	Trinidad	pavement
6/18/2003/1	25	90	Trinidad	pavement
6/18/2003/1	8	90	Trinidad	pavement
6/18/2003/1	75	90	Trinidad	pavement
6/18/2003/1	64	90	Trinidad	pavement
6/18/2003/1	65	90	Trinidad	pavement
6/18/2003/1	67	90	Trinidad	pavement
6/18/2003/1	40	90	Trinidad	pavement
6/18/2003/1	286	90	Trinidad	pavement
6/18/2003/1	51	90	Trinidad	pavement

Location ID: 6/18/2003/2
Latitude: N 36.92228333
Longitude: W 105.0184833

Deep canyon south of Bartlett mine and 0.5 miles east of Spring Canyon

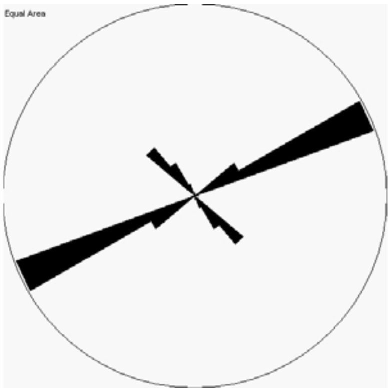

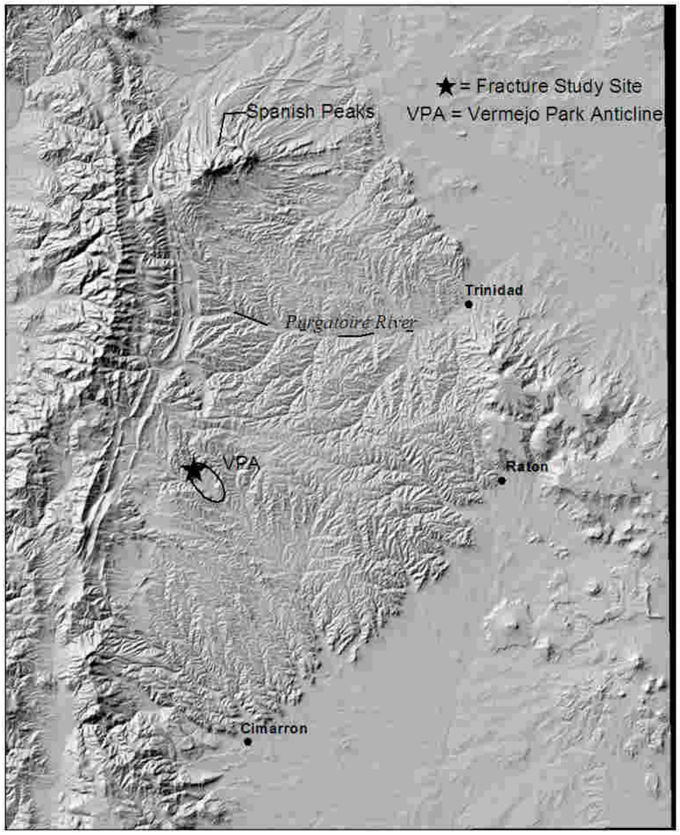

Notes:

Fracture Data:

ID	Strike	Dip	Formation	Comment 1
6/18/2003/2	62	65	Trinidad	
6/18/2003/2	65	76	Trinidad	
6/18/2003/2	62	66	Trinidad	
6/18/2003/2	66	70	Trinidad	
6/18/2003/2	60	68	Trinidad	plume
6/18/2003/2	60	73	Trinidad	
6/18/2003/2	61	66	Trinidad	
6/18/2003/2	58	70	Trinidad	
6/18/2003/2	61	72	Trinidad	
6/18/2003/2	61	72	Trinidad	
6/18/2003/2	62	68	Trinidad	
6/18/2003/2	62	73	Trinidad	
6/18/2003/2	61	69	Trinidad	
6/18/2003/2	60	69	Trinidad	
6/18/2003/2	58	70	Trinidad	
6/18/2003/2	60	73	Trinidad	
6/18/2003/2	330	90	Trinidad	

6/18/2003/2	311	90	Trinidad	
6/18/2003/2	320	90	Trinidad	
6/18/2003/2	321	90	Trinidad	plume
6/18/2003/2	318	90	Trinidad	IN THINNER BEDDED UNIT BELOW
6/18/2003/2	319	90	Trinidad	IN THINNER BEDDED UNIT BELOW
6/18/2003/2	319	90	Trinidad	IN THINNER BEDDED UNIT BELOW
6/18/2003/2	320	90	Trinidad	IN THINNER BEDDED UNIT BELOW
6/18/2003/2	318	90	Trinidad	IN THINNER BEDDED UNIT BELOW
6/18/2003/2	238	40	Trinidad	low angle planes
6/18/2003/2	57	25	Trinidad	low angle planes
6/18/2003/2	65	8	Trinidad	low angle planes

Location ID: 6/18/2003/3
Latitude: N 36.87598333
Longitude: W 105.1018667

Castle Rock

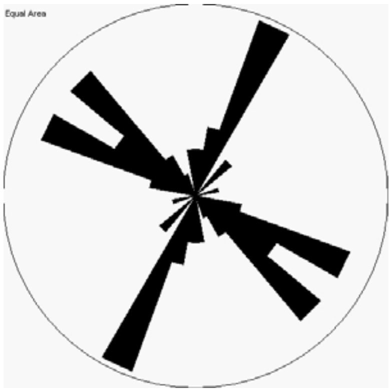

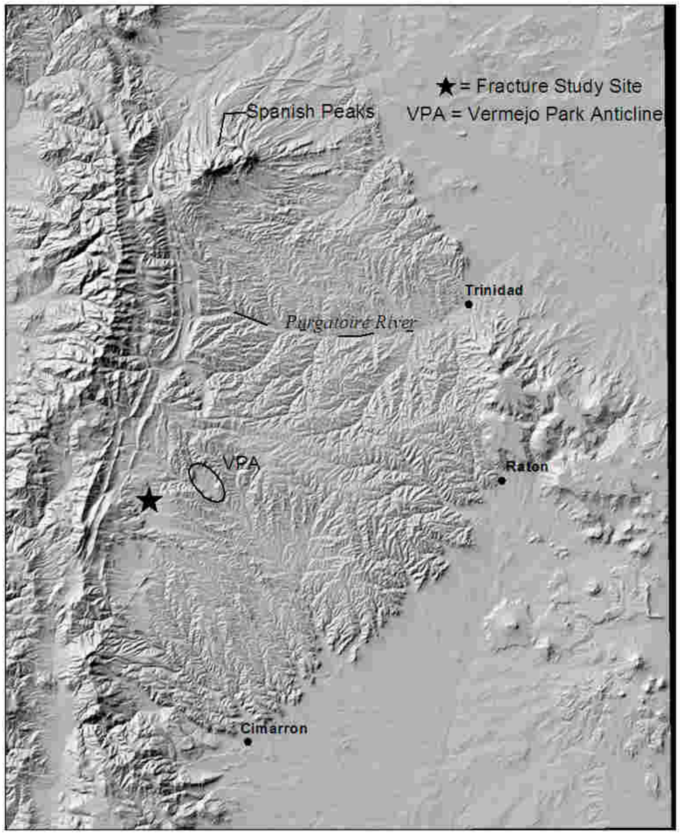

Notes:

Fracture Data:

ID	Strike	Dip	Formation	Comment 1
6/18/2003/3	305	90	Poison Canyon	SS
6/18/2003/3	292	90	Poison Canyon	SS
6/18/2003/3	108	90	Poison Canyon	SS
6/18/2003/3	291	90	Poison Canyon	SS
6/18/2003/3	286	90	Poison Canyon	SS
6/18/2003/3	124	90	Poison Canyon	SS
6/18/2003/3	6	90	Poison Canyon	SS
6/18/2003/3	158	90	Poison Canyon	SS
6/18/2003/3	293	90	Poison Canyon	SS
6/18/2003/3	306	90	Poison Canyon	SS
6/18/2003/3	202	90	Poison Canyon	SS
6/18/2003/3	258	90	Poison Canyon	SS
6/18/2003/3	297	90	Poison Canyon	SS
6/18/2003/3	353	90	Poison Canyon	SS
6/18/2003/3	118	90	Poison Canyon	6 cm carb shale layer
6/18/2003/3	131	90	Poison Canyon	6 cm carb shale layer

6/18/2003/3	130	90	Poison Canyon	6 cm carb shale layer
6/18/2003/3	134	90	Poison Canyon	6 cm carb shale layer
6/18/2003/3	136	90	Poison Canyon	6 cm carb shale layer
6/18/2003/3	118	90	Poison Canyon	6 cm carb shale layer
6/18/2003/3	132	90	Poison Canyon	6 cm carb shale layer
6/18/2003/3	130	90	Poison Canyon	6 cm carb shale layer
6/18/2003/3	112	90	Poison Canyon	6 cm carb shale layer
6/18/2003/3	134	90	Poison Canyon	6 cm carb shale layer
6/18/2003/3	141	90	Poison Canyon	6 cm carb shale layer
6/18/2003/3	149	90	Poison Canyon	6 cm carb shale layer
6/18/2003/3	18	90	Poison Canyon	SS pavement
6/18/2003/3	8	90	Poison Canyon	SS pavement
6/18/2003/3	23	90	Poison Canyon	SS pavement
6/18/2003/3	20	90	Poison Canyon	SS pavement
6/18/2003/3	41	90	Poison Canyon	SS pavement
6/18/2003/3	11	90	Poison Canyon	SS pavement
6/18/2003/3	29	90	Poison Canyon	SS pavement
6/18/2003/3	19	90	Poison Canyon	SS pavement
6/18/2003/3	40	90	Poison Canyon	SS pavement
6/18/2003/3	357	90	Poison Canyon	SS pavement
6/18/2003/3	22	90	Poison Canyon	SS pavement
6/18/2003/3	23	90	Poison Canyon	SS pavement
6/18/2003/3	120	90	Poison Canyon	SS pavement
6/18/2003/3	28	90	Poison Canyon	SS pavement
6/18/2003/3	21	90	Poison Canyon	SS pavement

Location ID: 6/19/2003/1
Latitude: N 36.87393333
Longitude: W 104.972

"The Steamboat"

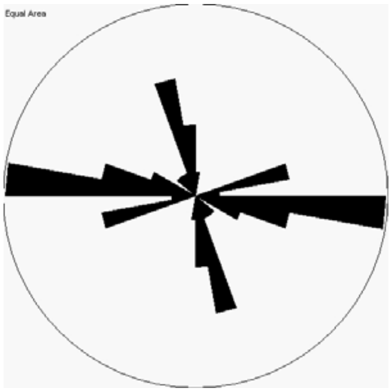

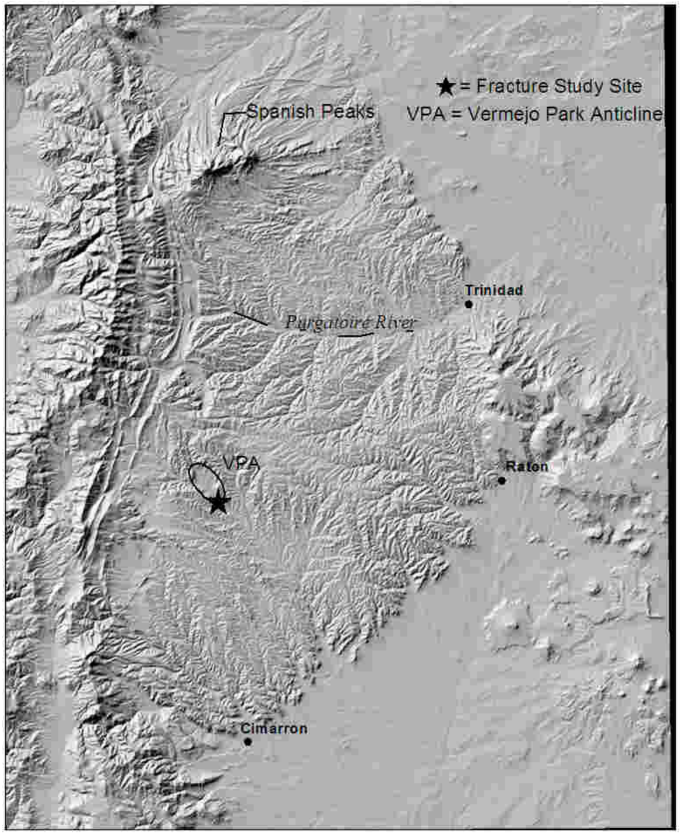

Notes:

Fracture Data:

ID	Strike	Dip	Formation
6/19/2003/1	110	90	Trinidad
6/19/2003/1	149	85	Trinidad
6/19/2003/1	319	90	Trinidad
6/19/2003/1	107	90	Trinidad
6/19/2003/1	92	90	Trinidad
6/19/2003/1	108	90	Trinidad
6/19/2003/1	158	90	Trinidad
6/19/2003/1	165	90	Trinidad
6/19/2003/1	108	90	Trinidad
6/19/2003/1	88	90	Trinidad
6/19/2003/1	110	90	Trinidad
6/19/2003/1	175	90	Trinidad
6/19/2003/1	5	90	Trinidad
6/19/2003/1	98	90	Trinidad
6/19/2003/1	172	90	Trinidad
6/19/2003/1	279	70	Trinidad

6/19/2003/1	90	90	Trinidad
6/19/2003/1	92	90	Trinidad
6/19/2003/1	168	85	Trinidad
6/19/2003/1	92	80	Trinidad
6/19/2003/1	94	80	Trinidad
6/19/2003/1	91	85	Trinidad
6/19/2003/1	171	90	Trinidad
6/19/2003/1	162	90	Trinidad
6/19/2003/1	100	90	Trinidad
6/19/2003/1	70	90	Trinidad
6/19/2003/1	165	90	Trinidad
6/19/2003/1	257	80	Trinidad
6/19/2003/1	347	90	Trinidad
6/19/2003/1	72	85	Trinidad
6/19/2003/1	73	80	Trinidad

Location ID: 6/19/2003/2
Latitude: N 36.87585
Longitude: W 104.9715333

North of Steamboat, north side of Vermejo River

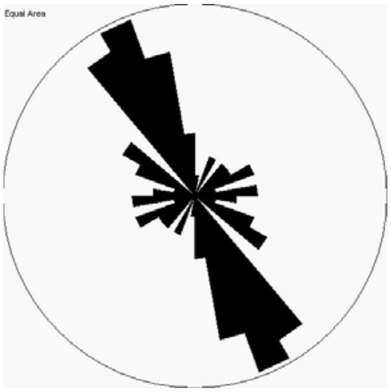

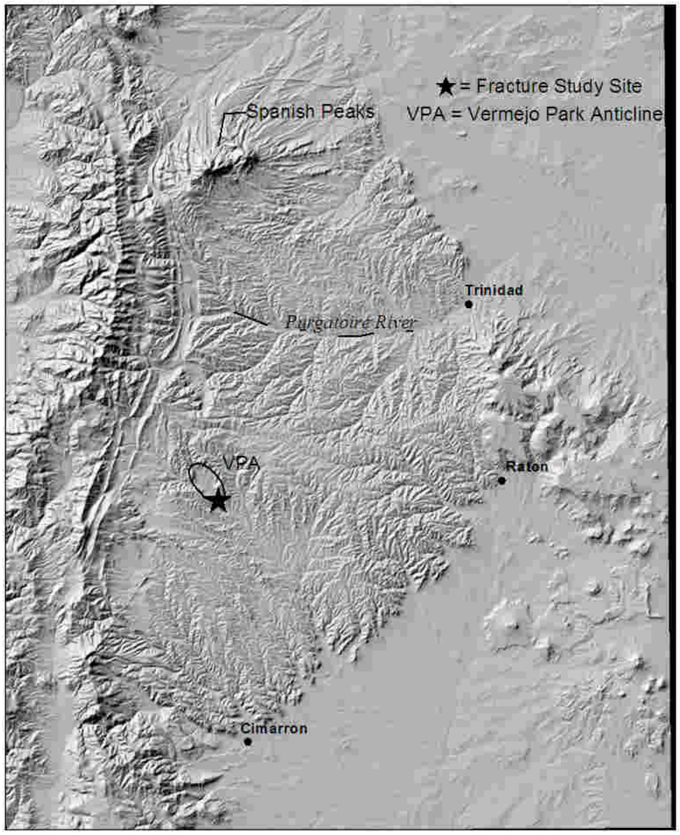

Notes:

Fracture Data:

ID	Strike	Dip	Formation	Comment 1	Comment 2
6/19/2003/2	98	85	Trinidad		
6/19/2003/2	350	80	Trinidad		
6/19/2003/2	69	90	Trinidad		
6/19/2003/2	9	90	Trinidad		
6/19/2003/2	83	85	Trinidad		
6/19/2003/2	342	85	Trinidad	plume	
6/19/2003/2	298	75	Trinidad		
6/19/2003/2	160	90	Trinidad	plume	
6/19/2003/2	82	80	Trinidad		
6/19/2003/2	327	70	Trinidad		
6/19/2003/2	53	90	Trinidad		
6/19/2003/2	142	90	Trinidad		
6/19/2003/2	158	90	Pierre		in thin bedded Pierre
6/19/2003/2	81	90	Pierre		in thin bedded Pierre
6/19/2003/2	163	90	Pierre		in thin bedded Pierre
6/19/2003/2	164	90	Pierre		in thin bedded Pierre
6/19/2003/2	167	90	Pierre		in thin bedded Pierre
6/19/2003/2	125	90	Pierre		in thin bedded Pierre

6/19/2003/2	27	90	Pierre		in thin bedded Pierre
6/19/2003/2	72	90	Pierre		in thin bedded Pierre
6/19/2003/2	158	90	Pierre		in thin bedded Pierre
6/19/2003/2	115	90	Pierre		in thin bedded Pierre
6/19/2003/2	120	90	Pierre		in thin bedded Pierre
6/19/2003/2	69	90	Pierre		in thin bedded Pierre
6/19/2003/2	141	90	Pierre		in thin bedded Pierre
6/19/2003/2	170	90	Pierre		in thin bedded Pierre
6/19/2003/2	167	90	Trinidad		in higher Trinidad unit, thin bedded, Oph.
6/19/2003/2	170	90	Trinidad		in higher Trinidad unit, thin bedded, Oph.
6/19/2003/2	41	90	Trinidad	irreg	in higher Trinidad unit, thin bedded, Oph.
6/19/2003/2	146	90	Trinidad		in higher Trinidad unit, thin bedded, Oph.
6/19/2003/2	123	90	Trinidad		in higher Trinidad unit, thin bedded, Oph.
6/19/2003/2	141	90	Trinidad		in higher Trinidad unit, thin bedded, Oph.
6/19/2003/2	150	90	Trinidad		in higher Trinidad unit, thin bedded, Oph.
6/19/2003/2	149	90	Trinidad		in higher Trinidad unit, thin bedded, Oph.
6/19/2003/2	150	90	Trinidad		in higher Trinidad unit, thin bedded, Oph.
6/19/2003/2	152	90	Trinidad		in higher Trinidad unit, thin bedded, Oph.
6/19/2003/2	122	90	Trinidad		in higher Trinidad unit, thin bedded, Oph.
6/19/2003/2	151	90	Trinidad		in higher Trinidad unit, thin bedded, Oph.
6/19/2003/2	25	90	Trinidad		in higher Trinidad unit, thin bedded, Oph.
6/19/2003/2	153	90	Trinidad		in higher Trinidad unit, thin bedded, Oph.
6/19/2003/2	157	90	Trinidad		in higher Trinidad unit, thin bedded, Oph.
6/19/2003/2	160	90	Trinidad		in higher Trinidad unit, thin bedded, Oph.
6/19/2003/2	141	90	Trinidad		in higher Trinidad unit, thin bedded, Oph.
6/19/2003/2	43	90	Trinidad		in higher Trinidad unit, thin bedded, Oph.
6/19/2003/2	149	90	Trinidad		in higher Trinidad unit, thin bedded, Oph.
6/19/2003/2	51	90	Trinidad		in higher Trinidad unit, thin bedded, Oph.
6/19/2003/2	106	90	Trinidad	w/calcite	in higher Trinidad unit, thin bedded, Oph.
6/19/2003/2	98	90	Trinidad	w/calcite	in higher Trinidad unit, thin bedded, Oph.
6/19/2003/2	64	90	Trinidad	w/calcite	in higher Trinidad unit, thin bedded, Oph.
6/19/2003/2	110	90	Trinidad	w/calcite	in higher Trinidad unit, thin bedded, Oph.
6/19/2003/2	150	90	Trinidad		in higher Trinidad unit, thin bedded, Oph.

Location ID: 6/19/2003/3
Latitude: N 36.87988333
Longitude: W 104.9697833

North of Steamboat, near top
of ridge, upper Vermejo/Raton

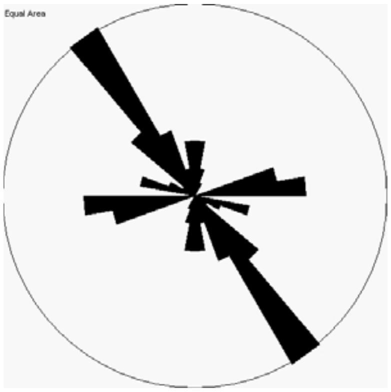

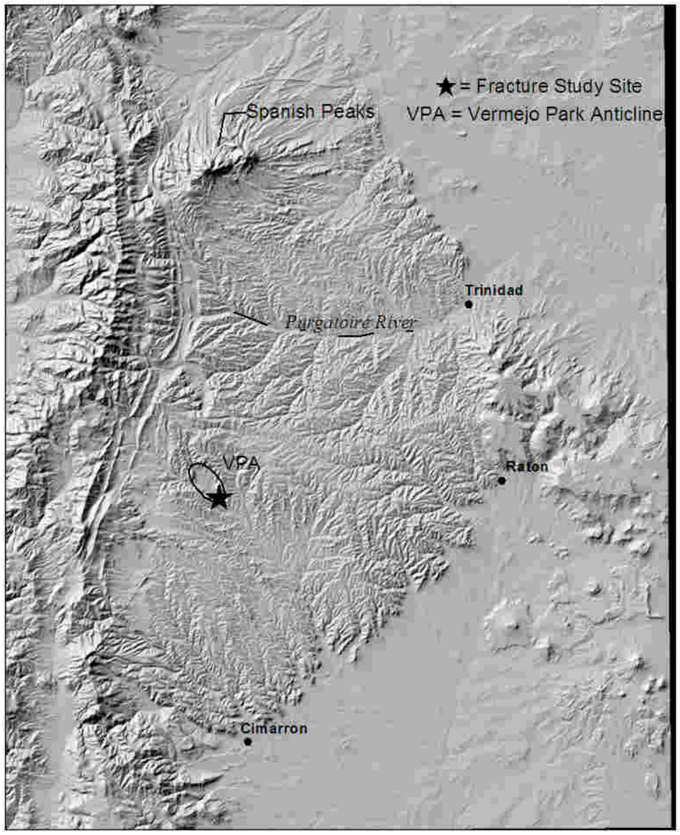

Notes:

Fracture Data:

ID	Strike	Dip	Formation	Comment 1	Comment 2	Comment 3
6/19/2003/3	102	90	Vermejo		coal cleats	
6/19/2003/3	118	90	Vermejo		coal cleats	
6/19/2003/3	17	90	Vermejo		coal cleats	
6/19/2003/3	28	90	Vermejo		coal cleats	
6/19/2003/3	107	90	Vermejo	face cleat	coal cleats	
6/19/2003/3	106	90	Vermejo		coal cleats	
6/19/2003/3	1	90	Vermejo		coal cleats	
6/19/2003/3	10	90	Vermejo		coal cleats	
6/19/2003/3	111	90	Vermejo		coal cleats	
6/19/2003/3	88	90	Vermejo		higher unit, shear	left lateral
6/19/2003/3	140	90	Vermejo		higher unit, shear	left lateral
6/19/2003/3	130	90	Vermejo		higher unit, shear	left lateral
6/19/2003/3	138	90	Vermejo		higher unit, shear	left lateral
6/19/2003/3	140	90	Vermejo		higher unit, shear	left lateral
6/19/2003/3	138	90	Vermejo		higher unit, shear	left lateral
6/19/2003/3	130	90	Vermejo		higher unit, shear	left lateral
6/19/2003/3	132	90	Vermejo		higher unit, shear	left lateral
6/19/2003/3	142	90	Vermejo		higher unit, shear	left lateral

6/19/2003/3	122	90	Vermejo	curves to 141 with no shear	higher unit, shear	right lateral
6/19/2003/3	140	90	Vermejo		higher unit, shear	right lateral
6/19/2003/3	80	90	Vermejo		higher unit, shear	right lateral
6/19/2003/3	133	90	Vermejo		higher unit, shear	right lateral
6/19/2003/3	162	90	Vermejo		higher unit, shear	unknown shear
6/19/2003/3	72	90	Vermejo		higher unit, shear	unknown shear
6/19/2003/3	176	90	Vermejo		higher unit, shear	unknown shear
6/19/2003/3	152	90	Vermejo		higher unit, shear	unknown shear
6/19/2003/3	155	90	Vermejo		higher unit, shear	unknown shear
6/19/2003/3	150	90	Vermejo		higher unit, shear	unknown shear
6/19/2003/3	158	90	Vermejo		higher unit, shear	unknown shear
6/19/2003/3	140	90	Vermejo		higher unit, shear	unknown shear
6/19/2003/3	142	90	Vermejo		higher unit, shear	unknown shear
6/19/2003/3	142	90	Vermejo		higher unit, shear	unknown shear
6/19/2003/3	142	90	Vermejo		higher unit, shear	unknown shear
6/19/2003/3	72	90	Vermejo			
6/19/2003/3	84	90	Vermejo			
6/19/2003/3	158	90	Vermejo			
6/19/2003/3	178	90	Vermejo			
6/19/2003/3	180	90	Vermejo			
6/19/2003/3	75	90	Vermejo			
6/19/2003/3	84	90	Vermejo			
6/19/2003/3	360	90	Vermejo			
6/19/2003/3	102	90	Vermejo			
6/19/2003/3	149	90	Vermejo			
6/19/2003/3	8	90	Vermejo			
6/19/2003/3	170	90	Vermejo			
6/19/2003/3	83	90	Vermejo			
6/19/2003/3	84	90	Vermejo			
6/19/2003/3	143	90	Vermejo			
6/19/2003/3	86	90	Vermejo			
6/19/2003/3	81	90	Vermejo			
6/19/2003/3	2	90	Vermejo			
6/19/2003/3	160	90	Vermejo			
6/19/2003/3	145	90	Vermejo			
6/19/2003/3	147	90	Vermejo			
6/19/2003/3	148	90	Vermejo			
6/19/2003/3	73	90	Vermejo			
6/19/2003/3	79	90	Vermejo			
6/19/2003/3	78	90	Vermejo	plume		
6/19/2003/3	170	90	Vermejo			
6/19/2003/3	145	90	Vermejo			

Location ID: 6/19/2003/4
Latitude: N 36.89371667
Longitude: W 104.9772333

Gazebo and trail to gazebo

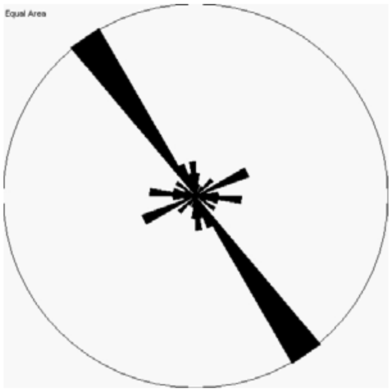

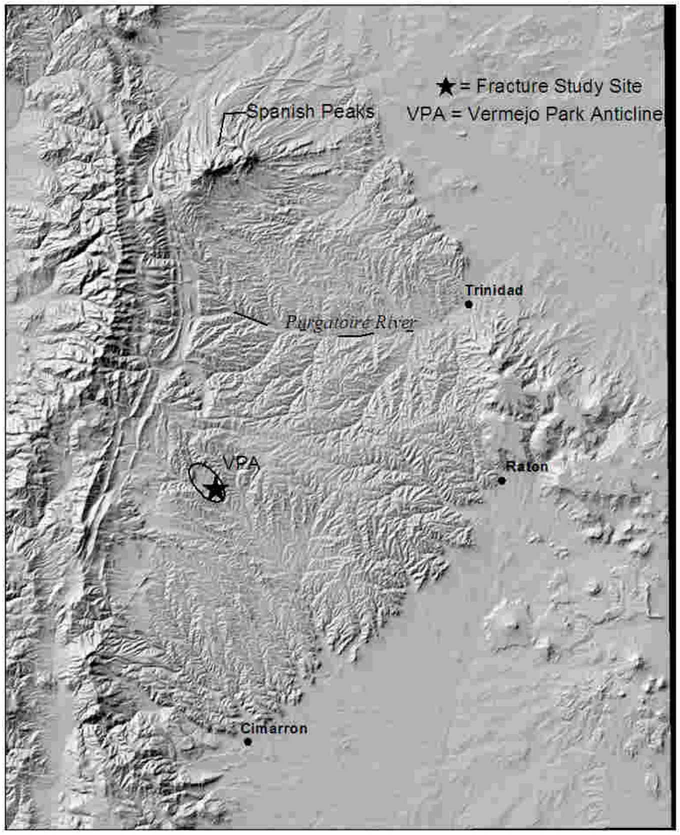

Notes:

Fracture Data:

ID	Strike	Dip	Formation	Comment 1	Comment 2
6/19/2003/4	5	90	Pierre	sill	
6/19/2003/4	142	90	Pierre	sill	
6/19/2003/4	48	90	Pierre	sill	
6/19/2003/4	128	90	Pierre	sill	
6/19/2003/4	127	90	Pierre	sill	
6/19/2003/4	143	90	Pierre	sill	
6/19/2003/4	144	90	Pierre	sill	
6/19/2003/4	141	90	Pierre	sill	
6/19/2003/4	143	90	Pierre	sill	
6/19/2003/4	68	90	Pierre	sill	
6/19/2003/4	67	90	Pierre	sill	
6/19/2003/4	149	90	Pierre	sill	
6/19/2003/4	112	90	Pierre	sill	
6/19/2003/4	62	90	Pierre	sill	
6/19/2003/4	103	90	Trinidad	in overlying Trinidad	plume
6/19/2003/4	69	90	Trinidad	in overlying Trinidad	plume
6/19/2003/4	81	90	Trinidad	in overlying Trinidad	plume
6/19/2003/4	3	90	Trinidad	in overlying Trinidad	plume

6/19/2003/4	178	90	Trinidad	in overlying Trinidad	plume
6/19/2003/4	173	90	Trinidad	in overlying Trinidad	plume
6/19/2003/4	81	90	Trinidad	in overlying Trinidad	plume
6/19/2003/4	163	90	Trinidad	in overlying Trinidad	plume
6/19/2003/4	171	90	Trinidad	in overlying Trinidad	plume
6/19/2003/4	159	90	Trinidad	in overlying Trinidad	plume
6/19/2003/4	72	90	Trinidad	in overlying Trinidad	plume
6/19/2003/4	103	90	Trinidad	in overlying Trinidad	left lateral shear
6/19/2003/4	67	90	Trinidad	in overlying Trinidad	plume
6/19/2003/4	142	90	Trinidad	pavement at Gazebo	plume
6/19/2003/4	143	90	Trinidad	pavement at Gazebo	plume
6/19/2003/4	144	90	Trinidad	pavement at Gazebo	plume
6/19/2003/4	141	90	Trinidad	pavement at Gazebo	plume
6/19/2003/4	143	90	Trinidad	pavement at Gazebo	plume
6/19/2003/4	141	90	Trinidad	pavement at Gazebo	plume
6/19/2003/4	143	90	Trinidad	pavement at Gazebo	plume
6/19/2003/4	43	90	Trinidad	pavement at Gazebo	
6/19/2003/4	140	90	Trinidad	pavement at Gazebo	plume
6/19/2003/4	38	90	Trinidad	pavement at Gazebo	irreg
6/19/2003/4	143	90	Trinidad	pavement at Gazebo	plume
6/19/2003/4	147	90	Trinidad	pavement at Gazebo	plume
6/19/2003/4	167	90	Trinidad	pavement at Gazebo	
6/19/2003/4	92	90	Trinidad	pavement at Gazebo	
6/19/2003/4	96	90	Trinidad	pavement at Gazebo	
6/19/2003/4	153	90	Trinidad	pavement at Gazebo	
6/19/2003/4	98	90	Trinidad	pavement at Gazebo	
6/19/2003/4	148	90	Trinidad	pavement at Gazebo	plume
6/19/2003/4	150	90	Trinidad	pavement at Gazebo	
6/19/2003/4	14	90	Trinidad	pavement at Gazebo	
6/19/2003/4	92	90	Trinidad	pavement at Gazebo	

Location ID: 6/19/2003/5
Latitude: N 36.8902
Longitude: W 104.6377667

"The Whale"

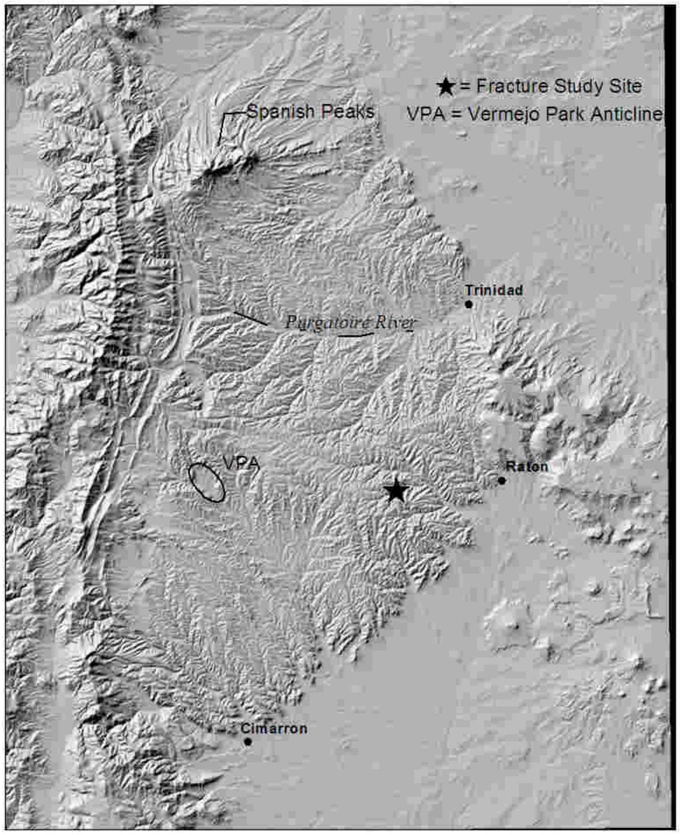

Notes:

Location ID: 6/20/2003/1
Latitude: N 36.88728333
Longitude: W 104.5661333

Hwy 555 east of whale, road cut (both sides) with coal

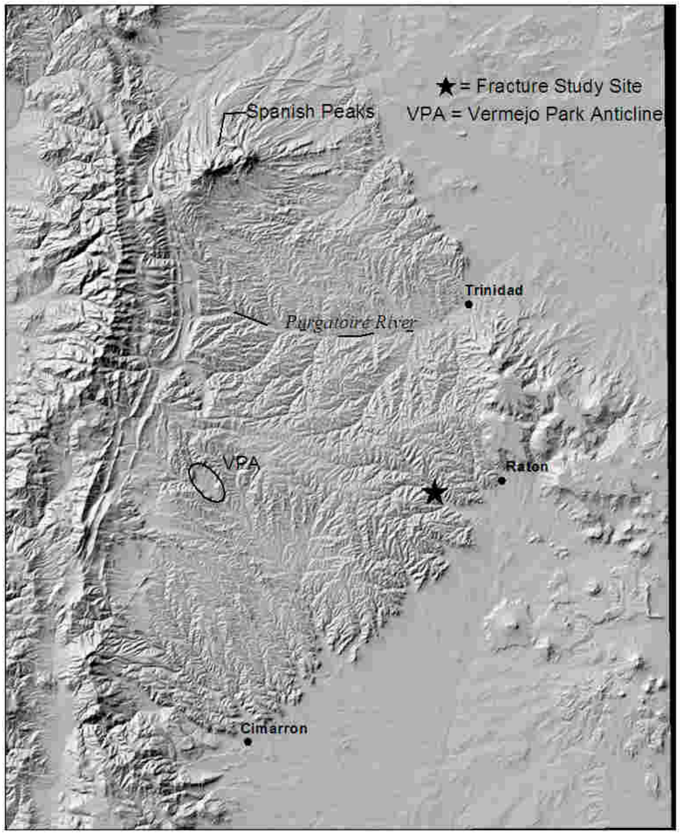

Notes:

Fracture Data:

ID	Strike	Dip	Formation	Comment 1	Comment 2
6/20/2003/1	100	90	Vermejo	face cleat	coal
6/20/2003/1	172	90	Vermejo		coal
6/20/2003/1	96	90	Vermejo		coal
6/20/2003/1	104	90	Vermejo		coal
6/20/2003/1	106	90	Vermejo		coal
6/20/2003/1	105	90	Vermejo		coal
6/20/2003/1	110	90	Vermejo		coal
6/20/2003/1	101	90	Vermejo		coal
6/20/2003/1	12	90	Vermejo		coal
6/20/2003/1	104	90	Vermejo		coal
6/20/2003/1	100	90	Vermejo		coal
6/20/2003/1	178	90	Vermejo		coal
6/20/2003/1	83	90	Vermejo		coal
6/20/2003/1	106	90	Vermejo		coal
6/20/2003/1	111	90	Vermejo		coal
6/20/2003/1	171	90	Vermejo		coal
6/20/2003/1	101	90	Vermejo		coal

6/20/2003/1	110	90	Vermejo		coal
6/20/2003/1	99	90	Vermejo		coal
6/20/2003/1	360	90	Vermejo		coal
6/20/2003/1	8	90	Vermejo		coal
6/20/2003/1	101	90	Vermejo	dominant	sand
6/20/2003/1	103	90	Vermejo		sand
6/20/2003/1	93	75	Vermejo		sand
6/20/2003/1	8	90	Vermejo	abuts 100 set	sand
6/20/2003/1	96	90	Vermejo		sand
6/20/2003/1	93	90	Vermejo	plume	sand
6/20/2003/1	94	90	Vermejo	plume	sand
6/20/2003/1	178	90	Vermejo		sand
6/20/2003/1	102	90	Vermejo		sand
6/20/2003/1	98	90	Vermejo		sand
6/20/2003/1	98	90	Vermejo		sand
6/20/2003/1	97	90	Vermejo		sand
6/20/2003/1	92	90	Vermejo		sand
6/20/2003/1	93	90	Vermejo		sand
6/20/2003/1	94	90	Vermejo		sand
6/20/2003/1	94	90	Vermejo	plume	sand
6/20/2003/1	175	90	Vermejo		sand
6/20/2003/1	98	90	Vermejo		sand
6/20/2003/1	98	90	Vermejo		sand
6/20/2003/1	179	90	Vermejo		sand
6/20/2003/1	96	90	Vermejo		sand
6/20/2003/1	90	90	Vermejo	plume and calcite mineralization in concretions	sand
6/20/2003/1	96	90	Vermejo		sand
6/20/2003/1	93	90	Vermejo		sand
6/20/2003/1	44	90	Vermejo		sand
6/20/2003/1	11	90	Vermejo		sand
6/20/2003/1	120	90	Vermejo		sand
6/20/2003/1	92	90	Vermejo		sand
6/20/2003/1	92	90	Vermejo		sand

Location ID: 6/20/2003/2
Latitude: N 36.89156667
Longitude: W 105.01145

Trinidad, south flank of VPA,
above water tank

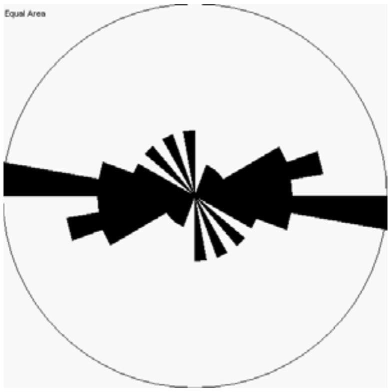

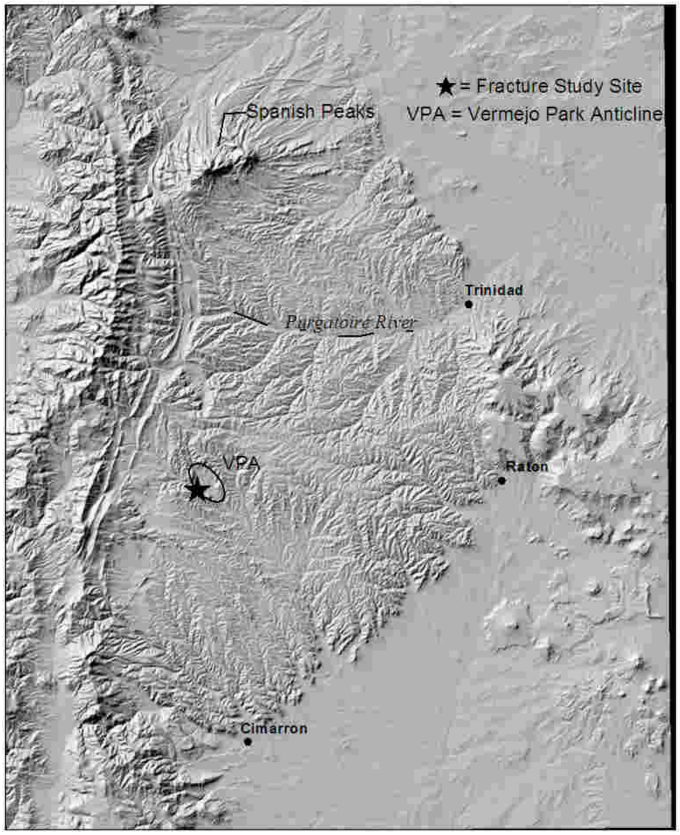

Notes:

Fracture Data:

ID	Strike	Dip	Formation	Comment 1
6/20/2003/2	40	90	Trinidad	
6/20/2003/2	97	90	Trinidad	
6/20/2003/2	99	90	Trinidad	
6/20/2003/2	91	90	Trinidad	
6/20/2003/2	93	90	Trinidad	
6/20/2003/2	103	90	Trinidad	
6/20/2003/2	20	90	Trinidad	
6/20/2003/2	58	90	Trinidad	
6/20/2003/2	114	90	Trinidad	
6/20/2003/2	97	90	Trinidad	
6/20/2003/2	107	90	Trinidad	
6/20/2003/2	79	90	Trinidad	
6/20/2003/2	79	90	Trinidad	
6/20/2003/2	69	90	Trinidad	w/3 generations of calcite, up to 1 cm thick
6/20/2003/2	61	90	Trinidad	w/calcite up to 5 cm, multiple generations
6/20/2003/2	60	90	Trinidad	
6/20/2003/2	158	90	Trinidad	

6/20/2003/2	107	90	Trinidad	
6/20/2003/2	138	90	Trinidad	
6/20/2003/2	37	90	Trinidad	
6/20/2003/2	113	90	Trinidad	
6/20/2003/2	152	90	Trinidad	
6/20/2003/2	95	90	Trinidad	
6/20/2003/2	80	90	Trinidad	
6/20/2003/2	85	90	Trinidad	
6/20/2003/2	79	90	Trinidad	
6/20/2003/2	85	90	Trinidad	
6/20/2003/2	318	80	Trinidad	
6/20/2003/2	79	90	Trinidad	
6/20/2003/2	179	90	Trinidad	plume
6/20/2003/2	179	90	Trinidad	plume

Location ID: 6/20/2003/3
Latitude: N 36.87141667
Longitude: W 104.9624

Reed Canyon

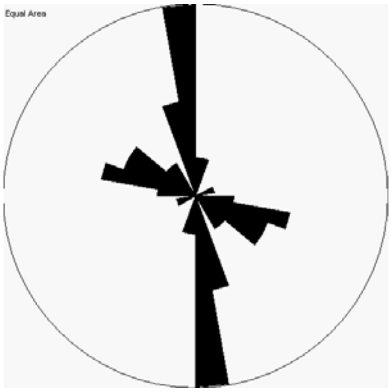

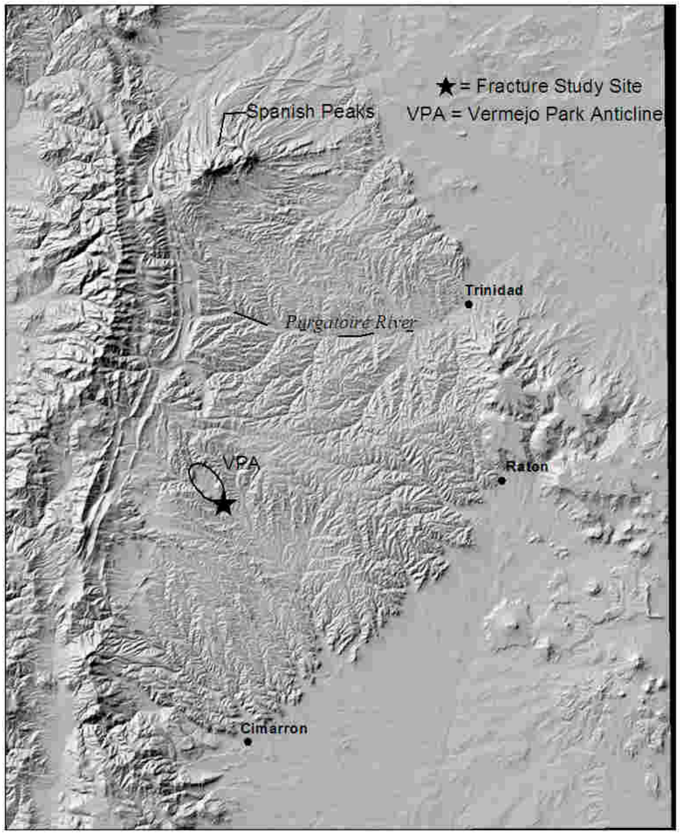

Notes:

Fracture Data:

ID	Strike	Dip	Formation	Comment 1	Comment 2	Comment 3
6/20/2003/3	109	90	Raton	horizontal shear		Raton Cong.
6/20/2003/3	125	90	Raton	left lateral shear	photo	Raton Cong.
6/20/2003/3	9	90	Raton	left lateral?		Raton Cong.
6/20/2003/3	108	90	Raton	right lateral shear		Raton Cong.
6/20/2003/3	102	90	Raton	right lateral shear		Raton Cong.
6/20/2003/3	93	90	Raton	right lateral shear		Raton Cong.
6/20/2003/3	114	90	Raton	right lateral shear		Raton Cong.
6/20/2003/3	116	90	Raton	right lateral shear		Raton Cong.
6/20/2003/3	74	90	Raton	right lateral?		Raton Cong.
6/20/2003/3	94	90	Raton	irreg		Raton Cong.
6/20/2003/3	115	90	Raton	near fault		Raton Cong.
6/20/2003/3	114	90	Raton	near fault		Raton Cong.
6/20/2003/3	60	90	Raton			Raton Cong.
6/20/2003/3	170	90	Raton			Raton Cong.
6/20/2003/3	169	90	Raton			Raton Cong.
6/20/2003/3	175	90	Raton			Raton Cong.
6/20/2003/3	177	90	Raton			Raton Cong.

6/20/2003/3	168	90	Raton		Raton Cong.
6/20/2003/3	172	90	Raton		Raton Cong.
6/20/2003/3	160	90	Raton		Raton Cong.
6/20/2003/3	176	90	Raton		Raton Cong.
6/20/2003/3	148	90	Raton		Raton Cong.
6/20/2003/3	106	90	Raton	east side of canyon	Raton Cong.
6/20/2003/3	173	90	Raton	east side of canyon	Raton Cong.
6/20/2003/3	125	90	Raton	east side of canyon	Raton Cong.
6/20/2003/3	178	90	Raton	east side of canyon	Raton Cong.
6/20/2003/3	147	90	Raton	east side of canyon	Raton Cong.
6/20/2003/3	176	90	Raton	east side of canyon	Raton Cong.
6/20/2003/3	120	90	Raton	east side of canyon	Raton Cong.
6/20/2003/3	10	90	Raton	east side of canyon	Raton Cong.
6/20/2003/3	168	90	Raton	east side of canyon	Raton Cong.
6/20/2003/3	103	90	Raton	east side of canyon	Raton Cong.
6/20/2003/3	134	90	Raton	east side of canyon	Raton Cong.
6/20/2003/3	124	90	Raton	east side of canyon	Raton Cong.
6/20/2003/3	160	90	Raton	east side of canyon	Raton Cong.
6/20/2003/3	171	90	Raton	east side of canyon	Raton Cong.
6/20/2003/3	136	90	Raton	east side of canyon	Raton Cong.
6/20/2003/3	179	90	Raton	east side of canyon	Raton Cong.
6/20/2003/3	5	90	Raton	east side of canyon	Raton Cong.
6/20/2003/3	16	90	Raton	east side of canyon	Raton Cong.

Location ID: 6/20/2003/4
Latitude: N 36.92183333
Longitude: W 104.8927833

Highway 555, Upper Raton?

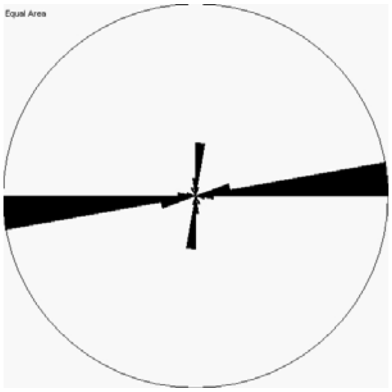

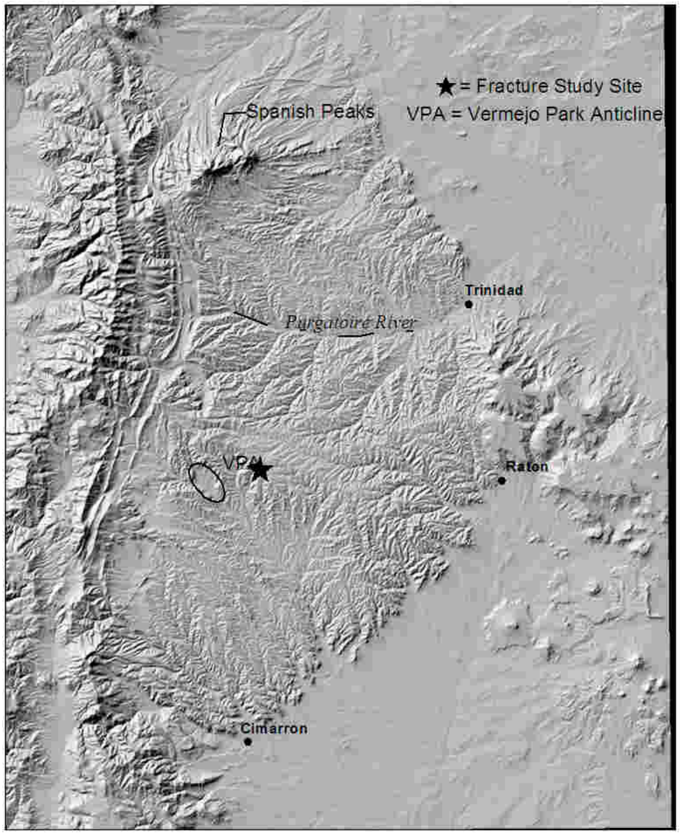

Notes:

Fracture Data:

ID	Strike	Dip	Formation	Comment 1	Comment 2
6/20/2003/4	2	90	Raton		ss
6/20/2003/4	88	90	Raton		ss
6/20/2003/4	82	90	Raton		ss
6/20/2003/4	171	90	Raton		ss
6/20/2003/4	180	90	Raton		ss
6/20/2003/4	89	90	Raton		ss
6/20/2003/4	81	90	Raton		ss
6/20/2003/4	90	90	Raton		ss
6/20/2003/4	3	90	Raton		ss
6/20/2003/4	94	90	Raton		ss
6/20/2003/4	1	90	Raton		ss
6/20/2003/4	83	90	Raton		ss
6/20/2003/4	175	90	Raton		ss
6/20/2003/4	88	90	Raton		ss
6/20/2003/4	82	90	Raton		ss
6/20/2003/4	5	90	Raton		ss
6/20/2003/4	80	90	Raton		ss

6/20/2003/4	80	90	Raton		ss
6/20/2003/4	88	90	Raton		ss
6/20/2003/4	9	90	Raton		ss
6/20/2003/4	89	90	Raton		ss
6/20/2003/4	10	90	Raton		ss
6/20/2003/4	108	90	Raton		ss
6/20/2003/4	76	90	Raton		ss
6/20/2003/4	80	90	Raton		ss
6/20/2003/4	78	90	Raton		ss
6/20/2003/4	150	90	Raton		ss
6/20/2003/4	79	90	Raton	face cleat (but cleat approx normal)	coal
6/20/2003/4	80	90	Raton		coal
6/20/2003/4	83	90	Raton		coal
6/20/2003/4	84	90	Raton		coal
6/20/2003/4	85	90	Raton		coal
6/20/2003/4	83	90	Raton		coal
6/20/2003/4	80	90	Raton		coal
6/20/2003/4	82	90	Raton		coal
6/20/2003/4	83	90	Raton		coal
6/20/2003/4	83	90	Raton		coal
6/20/2003/4	81	90	Raton		coal
6/20/2003/4	79	90	Raton		coal

Location ID: 6/25/2003/1
Latitude: N 36.92921667
Longitude: W 105.0213683

Spring Canyon, near Bartlett Mine

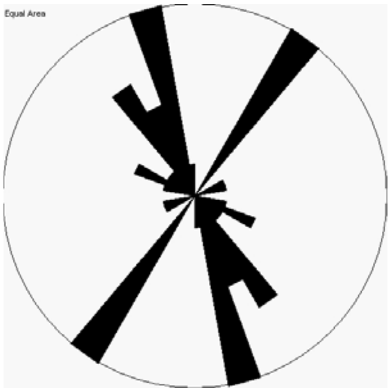

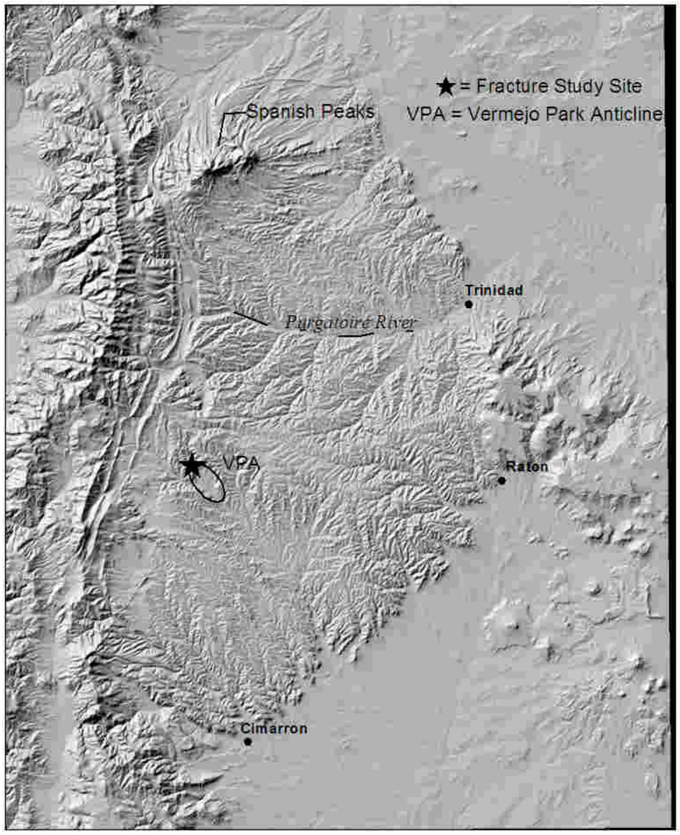

Notes:

Fracture Data:

ID	Strike	Dip	Formation	Comment 1	Comment 2
6/25/2003/1	348	70	Raton		Raton Conglomerate
6/25/2003/1	345	75	Raton		Raton Conglomerate
6/25/2003/1	341	70	Raton		Raton Conglomerate
6/25/2003/1	330	80	Raton		Raton Conglomerate
6/25/2003/1	359	85	Raton		Raton Conglomerate
6/25/2003/1	346	70	Raton		Raton Conglomerate
6/25/2003/1	340	70	Raton		Raton Conglomerate
6/25/2003/1	60	70	Raton	irregular	Raton Conglomerate
6/25/2003/1	38	65	Raton	irregular	Raton Conglomerate
6/25/2003/1	35	70	Raton	irregular	Raton Conglomerate
6/25/2003/1	336	80	Raton		Raton Conglomerate
6/25/2003/1	328	80	Raton		Raton Conglomerate
6/25/2003/1	332	80	Raton		Raton Conglomerate
6/25/2003/1	326	85	Raton		Raton Conglomerate
6/25/2003/1	340	80	Raton		Raton Conglomerate
6/25/2003/1	142	90	Raton		Raton Conglomerate
6/25/2003/1	131	75	Raton		Raton Conglomerate

6/25/2003/1	125	85	Raton		Raton Conglomerate
6/25/2003/1	148	90	Raton		Raton Conglomerate
6/25/2003/1	30	58	Raton		Raton Conglomerate
6/25/2003/1	115	78	Raton		Raton Conglomerate
6/25/2003/1	104	78	Raton		Raton Conglomerate
6/25/2003/1	114	78	Raton	possible LL shear	Raton Conglomerate
6/25/2003/1	70	55	Raton		Raton Conglomerate
6/25/2003/1	39	58	Raton		Raton Conglomerate
6/25/2003/1	30	70	Raton		Raton Conglomerate
6/25/2003/1	31	67	Raton		Raton Conglomerate

Location ID: 6/25/2003/2
Latitude: N 36.9106
Longitude: W 105.01655

West end of VP Anticline,
Trinidad

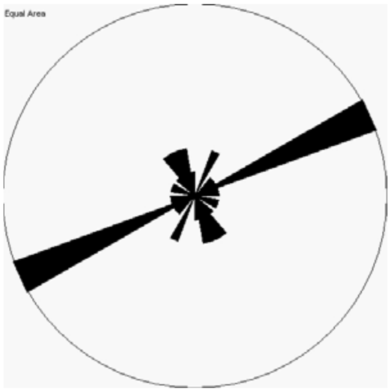

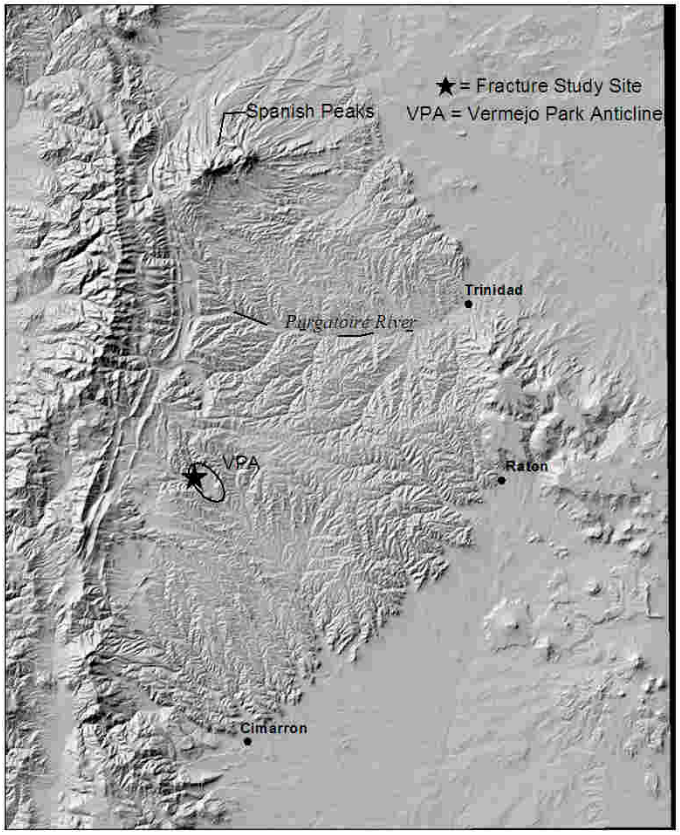

Notes:

Fracture Data:

ID	Strike	Dip	Formation	Comment 1
6/25/2003/2	250	85	Trinidad	
6/25/2003/2	20	70	Trinidad	
6/25/2003/2	150	85	Trinidad	
6/25/2003/2	115	90	Trinidad	
6/25/2003/2	62	88	Trinidad	
6/25/2003/2	28	63	Trinidad	
6/25/2003/2	345	85	Trinidad	
6/25/2003/2	132	74	Trinidad	
6/25/2003/2	62	80	Trinidad	
6/25/2003/2	165	88	Trinidad	
6/25/2003/2	62	83	Trinidad	
6/25/2003/2	58	80	Trinidad	
6/25/2003/2	108	90	Trinidad	
6/25/2003/2	140	90	Trinidad	
6/25/2003/2	60	74	Trinidad	
6/25/2003/2	352	85	Trinidad	irregular, curves to north
6/25/2003/2	48	68	Trinidad	plume

6/25/2003/2	338	80	Trinidad	
6/25/2003/2	82	76	Trinidad	
6/25/2003/2	328	85	Trinidad	narrow fracture cluster 15 cm wide containing > 10 fracs. Down to east displacement of 30 cm?
6/25/2003/2	64	85	Trinidad	down to south displacement of ~5 cm
6/25/2003/2	60	90	Trinidad	
6/25/2003/2	62	85	Trinidad	
6/25/2003/2	62	85	Trinidad	

Location ID: 6/25/2003/3
Latitude: N 36.91045
Longitude: W 105.0196333

West end of VPA, Raton Fm.

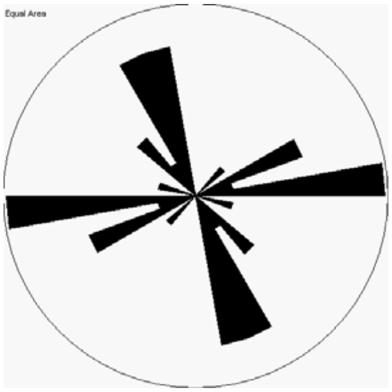

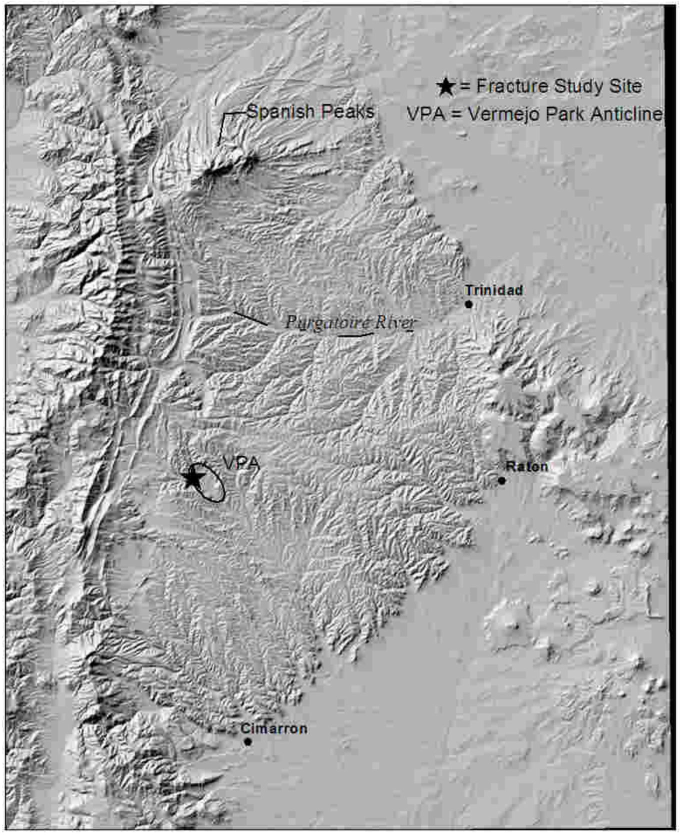

Notes:

Fracture Data:

ID	Strike	Dip (right hand rule)	Formation	Comment 1
6/25/2003/3	67	90	Raton	
6/25/2003/3	342	88	Raton	
6/25/2003/3	340	78	Raton	
6/25/2003/3	154	90	Raton	
6/25/2003/3	68	85	Raton	
6/25/2003/3	312	75	Raton	
6/25/2003/3	320	70	Raton	
6/25/2003/3	105	90	Raton	
6/25/2003/3	332	85	Raton	
6/25/2003/3	342	80	Raton	
6/25/2003/3	342	82	Raton	
6/25/2003/3	40	90	Raton	
6/25/2003/3	330	86	Raton	
6/25/2003/3	85	55	Raton	
6/25/2003/3	78	90	Raton	
6/25/2003/3	240	88	Raton	good horizontal shear lineations

6/25/2003/3	80	90	Raton
6/25/2003/3	80	90	Raton
6/25/2003/3	158	90	Raton
6/25/2003/3	85	90	Raton
6/25/2003/3	262	85	Raton
6/25/2003/3	136	90	Raton

Location ID: 6/26/2003/1
Latitude: N 36.90341667
Longitude: W 104.9783833

North side of VPA, west of gazebo, Trinidad and sill

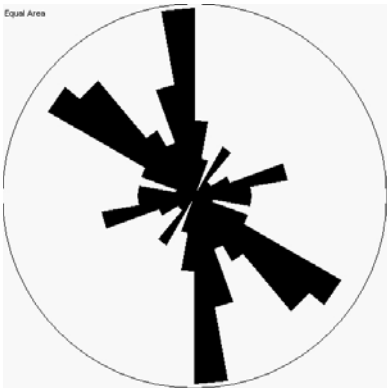

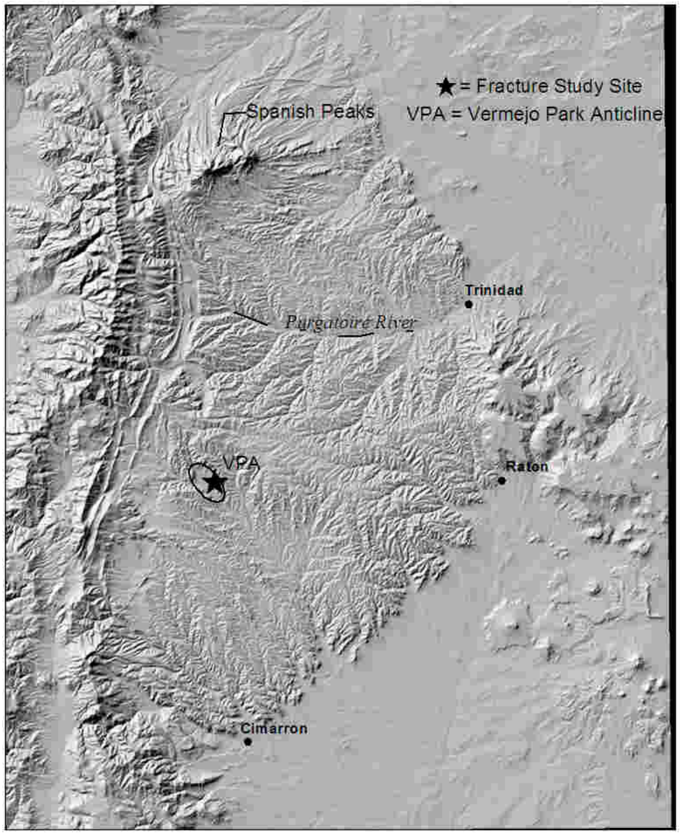

Notes:

Fracture Data:

ID	Strike	Dip	Formation	Comment 1	Comment 2
6/26/2003/1	158	90	Pierre	sill	w/calcite
6/26/2003/1	120	90	Pierre	sill	
6/26/2003/1	173	90	Pierre	sill	
6/26/2003/1	36	90	Pierre	sill	
6/26/2003/1	142	90	Pierre	sill	w/calcite
6/26/2003/1	121	90	Pierre	sill	
6/26/2003/1	169	90	Pierre	sill	plume
6/26/2003/1	120	90	Pierre	sill	
6/26/2003/1	152	42	Pierre	sill	
6/26/2003/1	120	90	Pierre	sill	
6/26/2003/1	71	90	Pierre	sill	w/calcite
6/26/2003/1	161	90	Pierre	sill	
6/26/2003/1	297	75	Pierre	sill	
6/26/2003/1	170	90	Pierre	sill	
6/26/2003/1	122	90	Pierre	sill	calcite vugs up to 3 cm across
6/26/2003/1	9	90	Pierre	sill	
6/26/2003/1	353	85	Pierre	sill	
6/26/2003/1	118	90	Pierre	sill	

6/26/2003/1	8	90	Pierre	sill	
6/26/2003/1	47	90	Pierre	sill	w/calcite
6/26/2003/1	310	70	Pierre	sill	w/calcite
6/26/2003/1	160	80	Trinidad	ss (thin bedded Trinidad)	
6/26/2003/1	92	90	Trinidad	ss (thin bedded Trinidad)	
6/26/2003/1	89	90	Trinidad	ss (thin bedded Trinidad)	
6/26/2003/1	71	90	Trinidad	ss (thin bedded Trinidad)	
6/26/2003/1	128	90	Trinidad	ss (thin bedded Trinidad)	
6/26/2003/1	63	90	Trinidad	ss (thin bedded Trinidad)	
6/26/2003/1	308	85	Trinidad	ss (thin bedded Trinidad)	
6/26/2003/1	79	90	Trinidad	ss (thin bedded Trinidad)	
6/26/2003/1	139	90	Trinidad	ss (thin bedded Trinidad)	
6/26/2003/1	32	90	Trinidad	ss (thin bedded Trinidad)	
6/26/2003/1	167	90	Trinidad	ss (thin bedded Trinidad)	
6/26/2003/1	310	80	Trinidad	ss (thin bedded Trinidad)	
6/26/2003/1	132	90	Trinidad	ss (thin bedded Trinidad)	
6/26/2003/1	57	90	Trinidad	ss (thin bedded Trinidad)	
6/26/2003/1	142	90	Trinidad	ss (thin bedded Trinidad)	
6/26/2003/1	252	80	Trinidad	ss (thin bedded Trinidad)	
6/26/2003/1	78	90	Trinidad	ss (thin bedded Trinidad)	
6/26/2003/1	292	85	Trinidad	ss (ophiomorph Trinidad)	
6/26/2003/1	60	20	Trinidad	ss (ophiomorph Trinidad)	
6/26/2003/1	358	88	Trinidad	ss (ophiomorph Trinidad)	
6/26/2003/1	100	90	Trinidad	ss (ophiomorph Trinidad)	
6/26/2003/1	270	8	Trinidad	ss (ophiomorph Trinidad)	
6/26/2003/1	175	80	Trinidad	ss (ophiomorph Trinidad)	
6/26/2003/1	160	90	Trinidad	ss (ophiomorph Trinidad)	
6/26/2003/1	175	90	Trinidad	ss (ophiomorph Trinidad)	
6/26/2003/1	175	90	Trinidad	ss (ophiomorph Trinidad)	
6/26/2003/1	170	90	Trinidad	ss (ophiomorph Trinidad)	
6/26/2003/1	88	90	Trinidad	ss (ophiomorph Trinidad)	
6/26/2003/1	177	90	Trinidad	ss (ophiomorph Trinidad)	
6/26/2003/1	92	90	Trinidad	ss (ophiomorph Trinidad)	
6/26/2003/1	37	20	Trinidad	ss (ophiomorph Trinidad)	
6/26/2003/1	300	62	Trinidad	ss (ophiomorph Trinidad)	
6/26/2003/1	315	80	Trinidad	ss (ophiomorph Trinidad)	
6/26/2003/1	315	85	Trinidad	ss (ophiomorph Trinidad)	
6/26/2003/1	318	85	Trinidad	ss (ophiomorph Trinidad)	
6/26/2003/1	162	90	Trinidad	ss (ophiomorph Trinidad)	
6/26/2003/1	84	90	Trinidad	ss (ophiomorph Trinidad)	
6/26/2003/1	332	85	Trinidad	ss (ophiomorph Trinidad)	
6/26/2003/1	136	90	Trinidad	ss (ophiomorph Trinidad)	
6/26/2003/1	2	90	Trinidad	ss (ophiomorph Trinidad)	
6/26/2003/1	10	90	Trinidad	ss (ophiomorph Trinidad)	
6/26/2003/1	175	90	Trinidad	ss (ophiomorph Trinidad)	
6/26/2003/1	142	90	Trinidad	ss (ophiomorph Trinidad)	
6/26/2003/1	120	90	Trinidad	ss (ophiomorph Trinidad)	
6/26/2003/1	322	80	Trinidad	ss (ophiomorph Trinidad)	
6/26/2003/1	10	90	Trinidad	ss (ophiomorph Trinidad)	
6/26/2003/1	180	90	Trinidad	ss (ophiomorph Trinidad)	

Location ID: 6/26/2003/2
Latitude: N 36.90678333
Longitude: W 104.9754667

North side of VPA, Vermejo and ? Raton

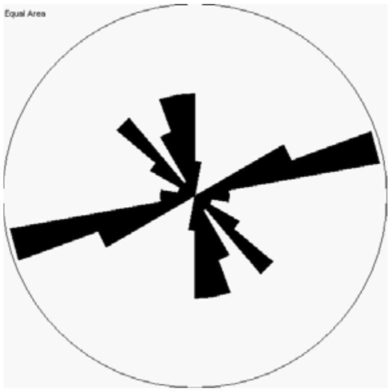

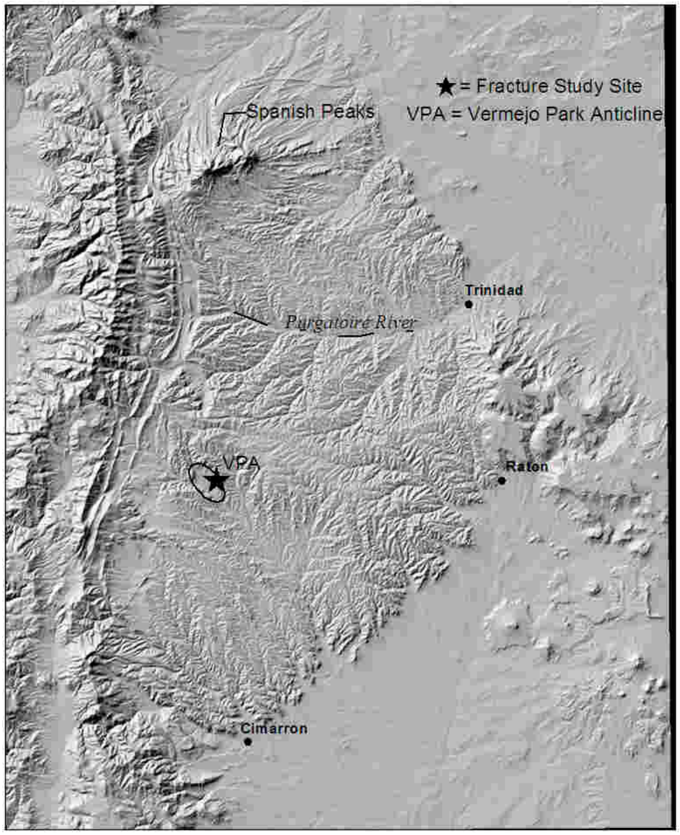

Notes:

Fracture Data:

ID	Strike	Dip	Formation	Comment 1	Comment 2
6/26/2003/2	72	85	Vermejo	ss (Vermejo)	w/calcite
6/26/2003/2	164	90	Vermejo	ss (Vermejo)	
6/26/2003/2	61	90	Vermejo	ss (Vermejo)	
6/26/2003/2	78	90	Vermejo	ss (Vermejo)	
6/26/2003/2	165	85	Vermejo	ss (Vermejo)	
6/26/2003/2	164	90	Vermejo	ss (Vermejo)	
6/26/2003/2	133	90	Vermejo	ss (Vermejo)	
6/26/2003/2	77	90	Vermejo	ss (Vermejo)	w/calcite
6/26/2003/2	129	85	Vermejo	ss (Vermejo)	
6/26/2003/2	263	85	Vermejo	ss (Vermejo)	
6/26/2003/2	163	90	Vermejo	ss (Vermejo)	
6/26/2003/2	162	85	Vermejo	ss (Vermejo)	
6/26/2003/2	259	85	Vermejo	ss (Vermejo)	
6/26/2003/2	163	90	Vermejo	ss (Vermejo)	w/calcite
6/26/2003/2	97	90	Vermejo	ss (Vermejo)	
6/26/2003/2	150	90	Vermejo	ss (Vermejo)	
6/26/2003/2	176	85	Vermejo	ss (Vermejo)	

6/26/2003/2	150	90	Vermejo	ss (Vermejo)	
6/26/2003/2	131	90	Vermejo	ss (Vermejo)	
6/26/2003/2	70	90	Vermejo	ss (Vermejo)	
6/26/2003/2	133	85	Vermejo	ss (Vermejo)	w/calcite
6/26/2003/2	79	90	Vermejo	ss (Vermejo)	
6/26/2003/2	133	85	Vermejo	ss (Vermejo)	
6/26/2003/2	79	90	Vermejo	ss (Vermejo)	
6/26/2003/2	130	85	Vermejo	ss (Vermejo)	
6/26/2003/2	80	90	Vermejo	ss (Vermejo)	w/calcite
6/26/2003/2	272	80	Raton	ss (basal Raton?)	
6/26/2003/2	8	90	Raton	ss (basal Raton?)	
6/26/2003/2	70	70	Raton	ss (basal Raton?)	
6/26/2003/2	173	90	Raton	ss (basal Raton?)	
6/26/2003/2	1	90	Raton	ss (basal Raton?)	
6/26/2003/2	65	90	Raton	ss (basal Raton?)	
6/26/2003/2	137	90	Raton	ss (basal Raton?)	
6/26/2003/2	79	90	Raton	ss (basal Raton?)	
6/26/2003/2	179	90	Raton	ss (basal Raton?)	
6/26/2003/2	140	90	Raton	ss (basal Raton?)	
6/26/2003/2	60	90	Raton	ss (basal Raton?)	
6/26/2003/2	174	90	Raton	ss (basal Raton?)	
6/26/2003/2	173	90	Raton	ss (basal Raton?)	
6/26/2003/2	65	90	Raton	ss (basal Raton?)	
6/26/2003/2	118	90	Raton	ss (basal Raton?)	
6/26/2003/2	109	90	Raton	ss (basal Raton?)	
6/26/2003/2	125	90	Raton	ss (basal Raton?)	
6/26/2003/2	70	90	Raton	ss (basal Raton?)	
6/26/2003/2	121	90	Raton	ss (basal Raton?)	
6/26/2003/2	69	90	Raton	ss (basal Raton?)	
6/26/2003/2	61	65	Raton	ss (basal Raton?)	
6/26/2003/2	158	90	Raton	ss (basal Raton?)	
6/26/2003/2	157	60	Raton	ss (basal Raton?)	
6/26/2003/2	355	75	Raton	ss (basal Raton?)	
6/26/2003/2	78	90	Raton	ss (basal Raton?)	

Location ID: 6/26/2003/4
Latitude: N 36.8659
Longitude: W 104.9966167

Juan Baca Canyon

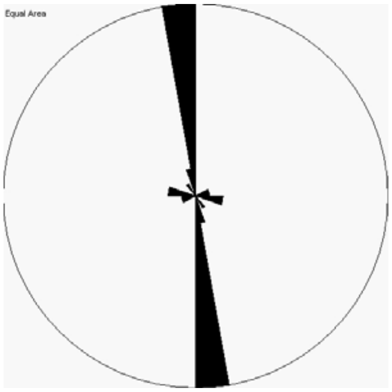

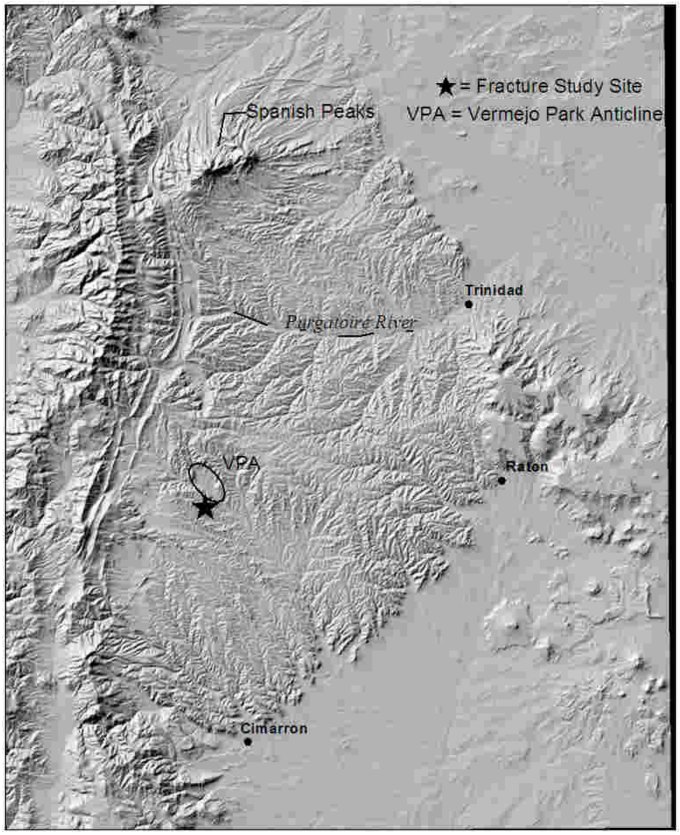

Notes:

Fracture Data:

ID	Strike	Dip	Formation	Comment 1
6/26/2003/4	176	80	unknown	ss (Raton? Vermejo?)
6/26/2003/4	173	90	unknown	ss (Raton? Vermejo?)
6/26/2003/4	350	85	unknown	ss (Raton? Vermejo?)
6/26/2003/4	172	90	unknown	ss (Raton? Vermejo?)
6/26/2003/4	283	80	unknown	ss (Raton? Vermejo?)
6/26/2003/4	172	90	unknown	ss (Raton? Vermejo?)
6/26/2003/4	75	90	unknown	ss (Raton? Vermejo?)
6/26/2003/4	173	90	unknown	ss (Raton? Vermejo?)
6/26/2003/4	168	90	unknown	ss (Raton? Vermejo?)
6/26/2003/4	179	90	unknown	ss (Raton? Vermejo?)
6/26/2003/4	67	90	unknown	ss (Raton? Vermejo?)
6/26/2003/4	170	85	unknown	ss (Raton? Vermejo?)
6/26/2003/4	96	90	unknown	ss (Raton? Vermejo?)
6/26/2003/4	173	90	unknown	ss (Raton? Vermejo?)
6/26/2003/4	171	90	unknown	ss (Raton? Vermejo?)
6/26/2003/4	170	80	unknown	ss (Raton? Vermejo?)
6/26/2003/4	88	90	unknown	ss (Raton? Vermejo?)

6/26/2003/4	178	90	unknown	ss (Raton? Vermejo?)
6/26/2003/4	172	90	unknown	ss (Raton? Vermejo?)
6/26/2003/4	173	90	unknown	ss (Raton? Vermejo?)
6/26/2003/4	288	80	unknown	ss (Raton? Vermejo?)
6/26/2003/4	146	90	unknown	ss (Raton? Vermejo?)
6/26/2003/4	97	90	unknown	ss (Raton? Vermejo?)
6/26/2003/4	168	90	unknown	ss (Raton? Vermejo?)

Location ID: 6/26/2003/5
Latitude: N 36.88328333
Longitude: W 105.10665

Castle Rock area, dike

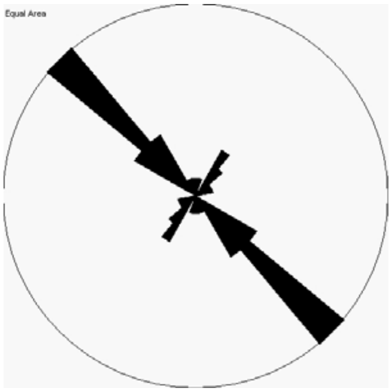

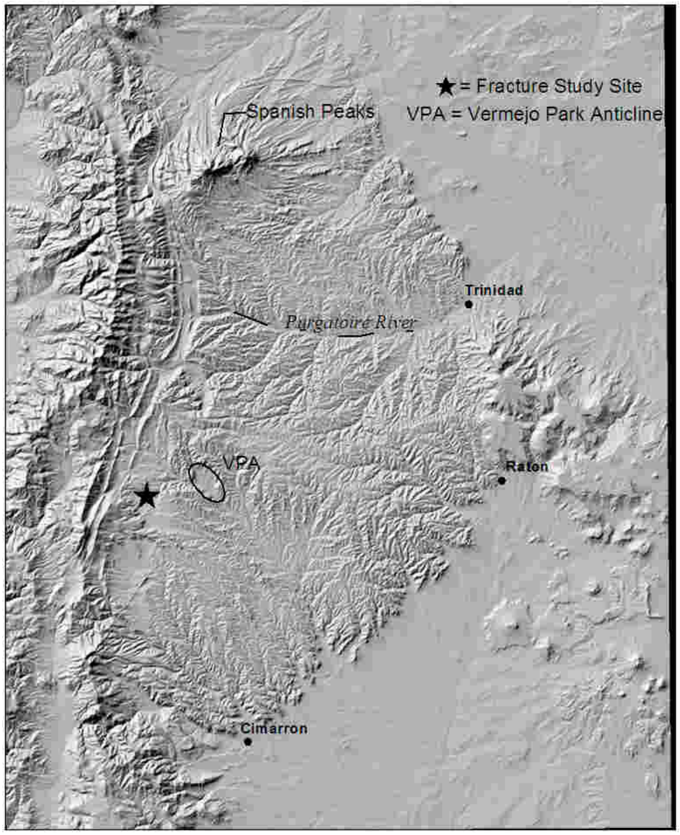

Notes:

Fracture Data:

ID	Strike	Dip	Formation	Comment 1	Comment 2
6/26/2003/5	132	90	Poison Canyon	ss (next to dike)	
6/26/2003/5	133	90	Poison Canyon	ss (next to dike)	
6/26/2003/5	135	90	Poison Canyon	ss (next to dike)	
6/26/2003/5	132	90	Poison Canyon	ss (next to dike)	
6/26/2003/5	37	90	Poison Canyon	ss (next to dike)	
6/26/2003/5	40	90	Poison Canyon	ss (next to dike)	
6/26/2003/5	41	90	Poison Canyon	ss (next to dike)	
6/26/2003/5	138	90	Poison Canyon	ss (poison canyon)	
6/26/2003/5	135	90	Poison Canyon	ss (poison canyon)	
6/26/2003/5	128	90	Poison Canyon	ss (poison canyon)	
6/26/2003/5	132	90	Poison Canyon	ss (poison canyon)	
6/26/2003/5	120	90	Poison Canyon	ss (poison canyon)	
6/26/2003/5	147	90	Poison Canyon	ss (poison canyon)	
6/26/2003/5	18	90	Poison Canyon	ss (poison canyon)	
6/26/2003/5	140	90	Poison Canyon	ss (poison canyon)	
6/26/2003/5	178	90	Poison Canyon	ss (poison canyon)	abuts 140

6/26/2003/5	150	90	Poison Canyon	ss (poison canyon)
6/26/2003/5	75	90	Poison Canyon	ss (poison canyon)
6/26/2003/5	128	90	Poison Canyon	ss (poison canyon)
6/26/2003/5	126	90	Poison Canyon	ss (poison canyon)
6/26/2003/5	164	90	Poison Canyon	ss (poison canyon)
6/26/2003/5	37	90	Poison Canyon	ss (poison canyon)
6/26/2003/5	7	90	Poison Canyon	ss (poison canyon)
6/26/2003/5	317	80	Poison Canyon	ss (poison canyon)
6/26/2003/5	35	90	Poison Canyon	ss (poison canyon)
6/26/2003/5	130	90	Poison Canyon	ss (poison canyon)
6/26/2003/5	132	90	Poison Canyon	ss (poison canyon)
6/26/2003/5	131	90	Poison Canyon	ss (poison canyon)
6/26/2003/5	148	90	Poison Canyon	ss (poison canyon)
6/26/2003/5	60	90	Poison Canyon	ss (poison canyon)
6/26/2003/5	58	90	Poison Canyon	ss (poison canyon)
6/26/2003/5	140	90	Poison Canyon	ss (poison canyon)

Location ID: 6/27/2003/1
Latitude: N 36.89768333
Longitude: W 104.583885

Highway 555, sills and coal dike

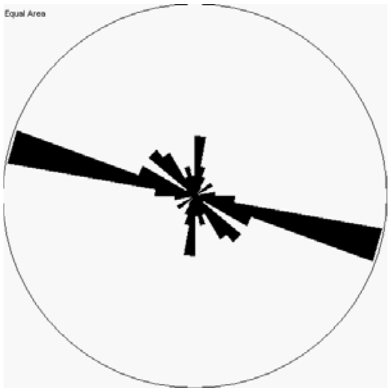

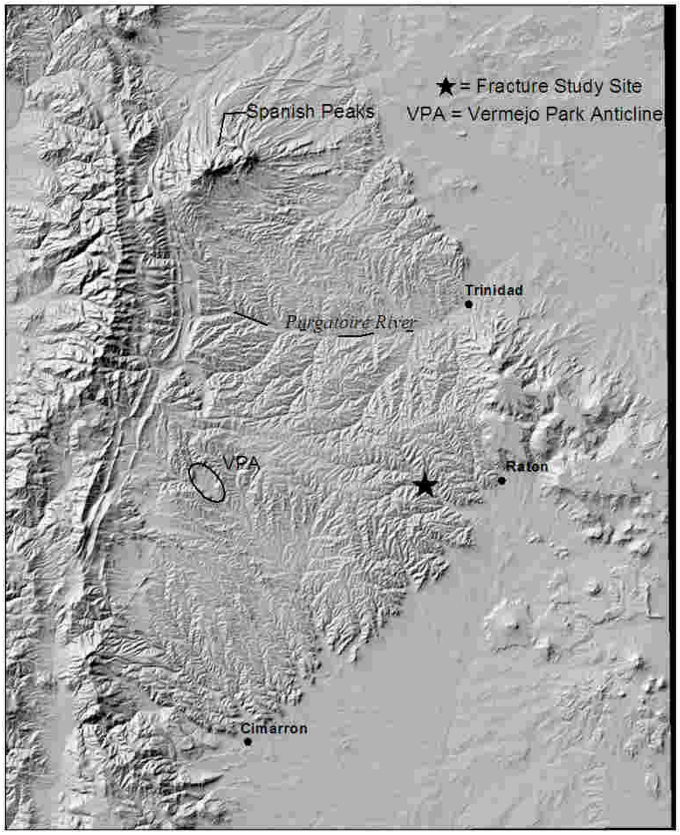

Notes:

Fracture Data:

ID	Strike	Dip	Formation	Comment 1	Comment 2
6/27/2003/1	108	90	unknown	sill	plume
6/27/2003/1	111	90	unknown	sill	plume
6/27/2003/1	38	90	unknown	sill	
6/27/2003/1	101	90	unknown	sill	
6/27/2003/1	163	90	unknown	sill	
6/27/2003/1	24	90	unknown	sill	
6/27/2003/1	172	90	unknown	sill	
6/27/2003/1	107	90	unknown	sill	
6/27/2003/1	102	90	unknown	sill	plume
6/27/2003/1	104	90	unknown	sill	
6/27/2003/1	107	90	unknown	sill	
6/27/2003/1	82	90	unknown	sill	
6/27/2003/1	89	90	unknown	sill	
6/27/2003/1	148	90	unknown	sill	
6/27/2003/1	10	90	unknown	sill	
6/27/2003/1	110	90	unknown	sill	
6/27/2003/1	318	78	unknown	sill	

6/27/2003/1	102	90	unknown	sill	plume
6/27/2003/1	91	90	unknown	sill	
6/27/2003/1	3	90	unknown	sill	
6/27/2003/1	94	90	unknown	sill	
6/27/2003/1	174	90	unknown	sill	
6/27/2003/1	102	90	unknown	sill	plume
6/27/2003/1	107	90	unknown	sill	plume
6/27/2003/1	8	90	unknown	sill	irregular
6/27/2003/1	110	90	unknown	sill	
6/27/2003/1	110	90	unknown	sill	
6/27/2003/1	109	90	unknown	sill	
6/27/2003/1	3	90	unknown	sill	
6/27/2003/1	2	90	unknown	sill	
6/27/2003/1	104	90	unknown	sill	
6/27/2003/1	24	90	unknown	sill	
6/27/2003/1	111	90	unknown	sill	plume
6/27/2003/1	109	90	unknown	sill	
6/27/2003/1	109	90	unknown	sill	
6/27/2003/1	1	80	unknown	sill	
6/27/2003/1	106	90	unknown	sill	
6/27/2003/1	5	90	unknown	sill	
6/27/2003/1	103	90	unknown	sill	
6/27/2003/1	277	68	unknown	siltstone	
6/27/2003/1	91	90	unknown	siltstone	
6/27/2003/1	152	90	unknown	siltstone	
6/27/2003/1	284	40	unknown	siltstone	
6/27/2003/1	194	90	unknown	siltstone	
6/27/2003/1	111	90	unknown	siltstone	
6/27/2003/1	136	90	unknown	siltstone	
6/27/2003/1	59	90	unknown	siltstone	
6/27/2003/1	13	90	unknown	siltstone	
6/27/2003/1	109	90	unknown	siltstone	
6/27/2003/1	142	90	unknown	siltstone	plume
6/27/2003/1	107	90	unknown	siltstone	
6/27/2003/1	142	90	unknown	siltstone	abuts 107
6/27/2003/1	155	90	unknown	siltstone	wrenched feature?
6/27/2003/1	168	90	unknown	siltstone	wrenched feature?
6/27/2003/1	148	90	unknown	siltstone	wrenched feature?
6/27/2003/1	143	90	unknown	siltstone	wrenched feature?
6/27/2003/1	160	90	unknown	siltstone	
6/27/2003/1	131	90	unknown	siltstone	
6/27/2003/1	109	90	unknown	siltstone	
6/27/2003/1	132	90	unknown	siltstone	
6/27/2003/1	58	65	unknown	siltstone	
6/27/2003/1	139	90	unknown	siltstone	
6/27/2003/1	136	90	unknown	siltstone	
6/27/2003/1	120	90	unknown	siltstone	

Location ID: 6/27/2003/2
Latitude: N 36.94733333
Longitude: W 104.81795

Canadian River valley, north side

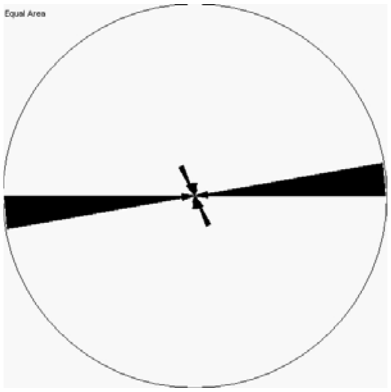

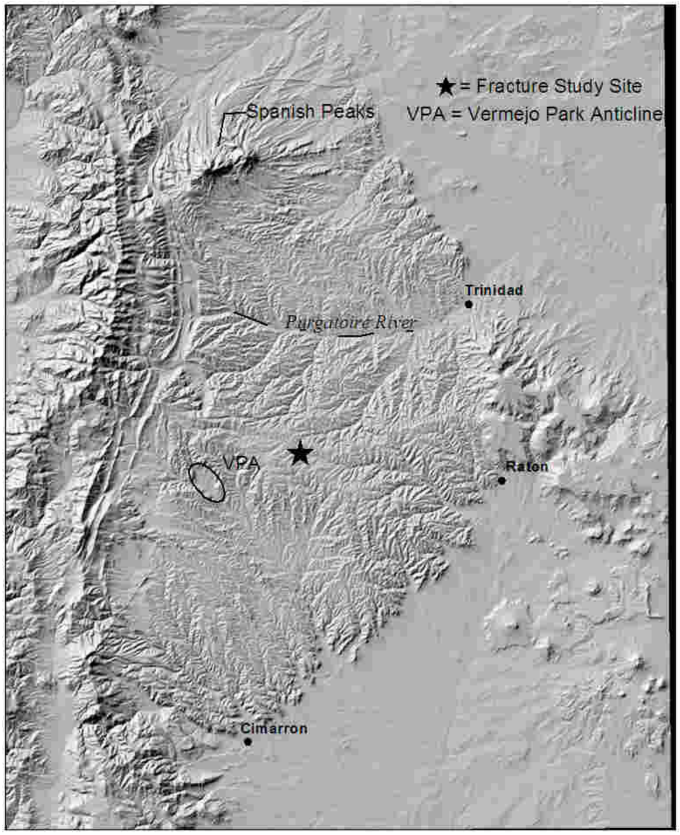

Notes:

Fracture Data:

ID	Strike	Dip	Formation	Comment 1
6/27/2003/2	269	85	Poison Canyon	siltstone
6/27/2003/2	147	90	Poison Canyon	siltstone
6/27/2003/2	263	80	Poison Canyon	siltstone
6/27/2003/2	84	90	Poison Canyon	siltstone
6/27/2003/2	89	90	Poison Canyon	siltstone
6/27/2003/2	18	90	Poison Canyon	siltstone
6/27/2003/2	265	80	Poison Canyon	siltstone
6/27/2003/2	86	90	Poison Canyon	siltstone
6/27/2003/2	265	75	Poison Canyon	siltstone
6/27/2003/2	266	85	Poison Canyon	siltstone
6/27/2003/2	89	90	Poison Canyon	siltstone
6/27/2003/2	1	90	Poison Canyon	siltstone
6/27/2003/2	81	90	Poison Canyon	siltstone
6/27/2003/2	83	85	Poison Canyon	siltstone
6/27/2003/2	83	90	Poison Canyon	siltstone
6/27/2003/2	79	85	Poison Canyon	ss
6/27/2003/2	172	90	Poison Canyon	ss

6/27/2003/2	261	88	Poison Canyon	ss
6/27/2003/2	88	90	Poison Canyon	ss
6/27/2003/2	89	90	Poison Canyon	ss
6/27/2003/2	2	90	Poison Canyon	ss
6/27/2003/2	83	90	Poison Canyon	ss
6/27/2003/2	79	90	Poison Canyon	ss
6/27/2003/2	163	90	Poison Canyon	ss
6/27/2003/2	261	80	Poison Canyon	ss
6/27/2003/2	269	75	Poison Canyon	ss
6/27/2003/2	171	90	Poison Canyon	ss
6/27/2003/2	85	90	Poison Canyon	ss
6/27/2003/2	82	75	Poison Canyon	ss
6/27/2003/2	85	55	Poison Canyon	ss
6/27/2003/2	84	90	Poison Canyon	ss
6/27/2003/2	156	90	Poison Canyon	ss
6/27/2003/2	82	75	Poison Canyon	ss
6/27/2003/2	150	90	Poison Canyon	ss
6/27/2003/2	158	90	Poison Canyon	ss
6/27/2003/2	273	85	Poison Canyon	ss
6/27/2003/2	80	90	Poison Canyon	ss
6/27/2003/2	90	90	Poison Canyon	ss
6/27/2003/2	160	80	Poison Canyon	ss
6/27/2003/2	82	90	Poison Canyon	ss
6/27/2003/2	145	90	Poison Canyon	ss
6/27/2003/2	84	90	Poison Canyon	ss
6/27/2003/2	83	90	Poison Canyon	ss
6/27/2003/2	83	90	Poison Canyon	ss
6/27/2003/2	156	85	Poison Canyon	ss
6/27/2003/2	85	90	Poison Canyon	ss
6/27/2003/2	151	80	Poison Canyon	ss

Location ID: 6/27/2003/3
Latitude: N 36.89768333
Longitude: W 104.9128833

Highway 555, coal

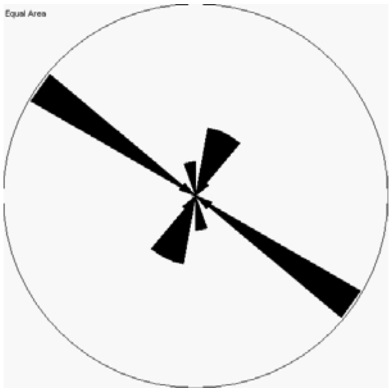

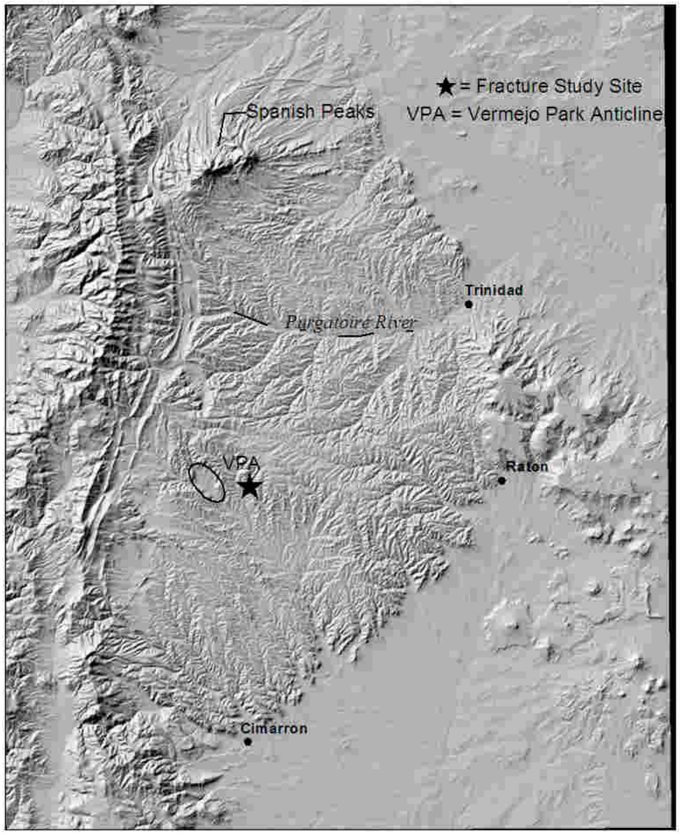

Notes:

Fracture Data:

ID	Strike	Dip	Formation	Comment 1
6/27/2003/3	34	90	unknown	coal
6/27/2003/3	35	90	unknown	coal
6/27/2003/3	120	90	unknown	coal
6/27/2003/3	136	90	unknown	coal
6/27/2003/3	118	90	unknown	coal
6/27/2003/3	122	90	unknown	coal
6/27/2003/3	123	90	unknown	coal
6/27/2003/3	125	90	unknown	coal
6/27/2003/3	122	90	unknown	coal
6/27/2003/3	123	90	unknown	coal
6/27/2003/3	121	90	unknown	coal
6/27/2003/3	19	90	unknown	coal
6/27/2003/3	21	90	unknown	coal
6/27/2003/3	15	90	unknown	coal
6/27/2003/3	20	90	unknown	coal
6/27/2003/3	43	90	unknown	coal
6/27/2003/3	38	90	unknown	coal

6/27/2003/3	35	90	unknown	coal
6/27/2003/3	175	90	unknown	coal
6/27/2003/3	170	90	unknown	coal
6/27/2003/3	161	90	unknown	coal
6/27/2003/3	28	90	unknown	coal
6/27/2003/3	25	90	unknown	coal
6/27/2003/3	126	90	unknown	coal
6/27/2003/3	126	90	unknown	coal
6/27/2003/3	166	90	unknown	coal
6/27/2003/3	129	90	unknown	coal
6/27/2003/3	14	90	unknown	coal
6/27/2003/3	127	90	unknown	coal
6/27/2003/3	10	90	unknown	coal

Location ID: 7/14/2003/1JL
Latitude: N 37.07161667
Longitude: W 103.9953167

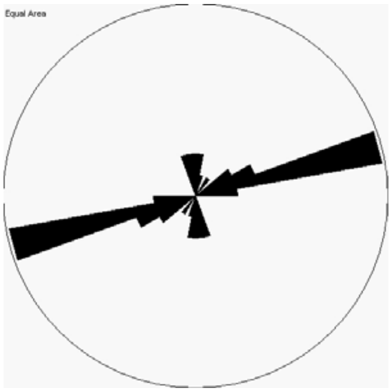

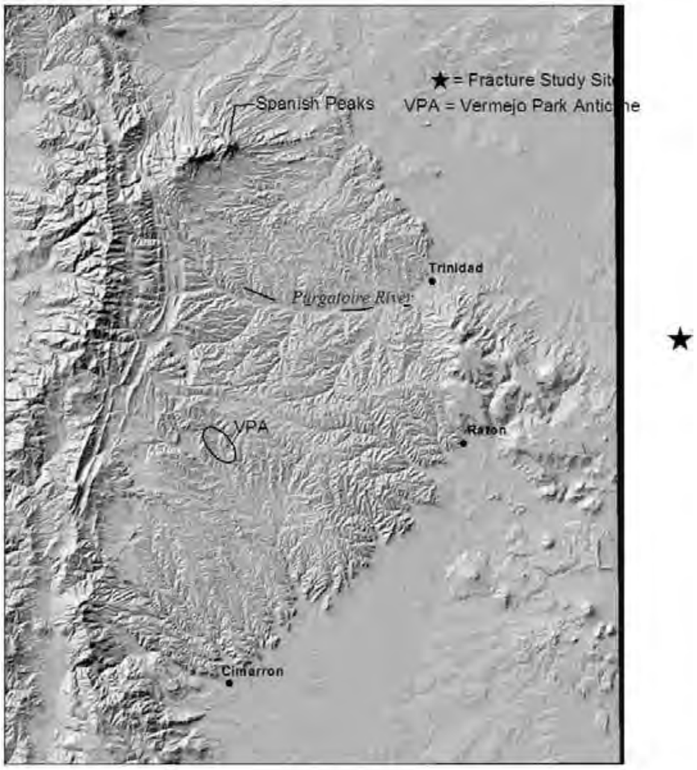

Notes:

Fracture Data:

ID	Strike	Dip	Formation	Comment 1
7/14/2003/1JL	72	90	Dakota	
7/14/2003/1JL	58	90	Dakota	
7/14/2003/1JL	60	90	Dakota	
7/14/2003/1JL	76	90	Dakota	
7/14/2003/1JL	71	90	Dakota	
7/14/2003/1JL	77	90	Dakota	
7/14/2003/1JL	79	90	Dakota	
7/14/2003/1JL	78	90	Dakota	
7/14/2003/1JL	80	90	Dakota	
7/14/2003/1JL	79	90	Dakota	
7/14/2003/1JL	70	90	Dakota	
7/14/2003/1JL	68	90	Dakota	
7/14/2003/1JL	57	90	Dakota	
7/14/2003/1JL	78	90	Dakota	
7/14/2003/1JL	80	90	Dakota	
7/14/2003/1JL	64	90	Dakota	RL
7/14/2003/1JL	168	90	Dakota	
7/14/2003/1JL	11	90	Dakota	
7/14/2003/1JL	1	90	Dakota	

7/14/2003/1JL	172	90	Dakota
7/14/2003/1JL	164	90	Dakota
7/14/2003/1JL	173	90	Dakota
7/14/2003/1JL	5	90	Dakota
7/14/2003/1JL	31	90	Dakota

Location ID: 7/14/2003/1MH
Latitude: N 36.85375
Longitude: W 105.1185833

West of Castle Rock park,
poison canyon

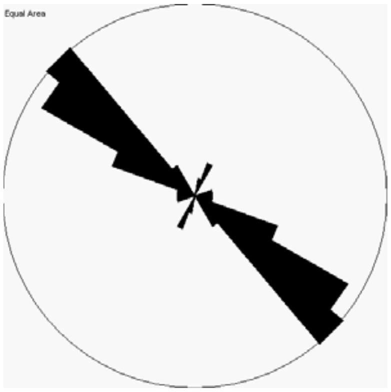

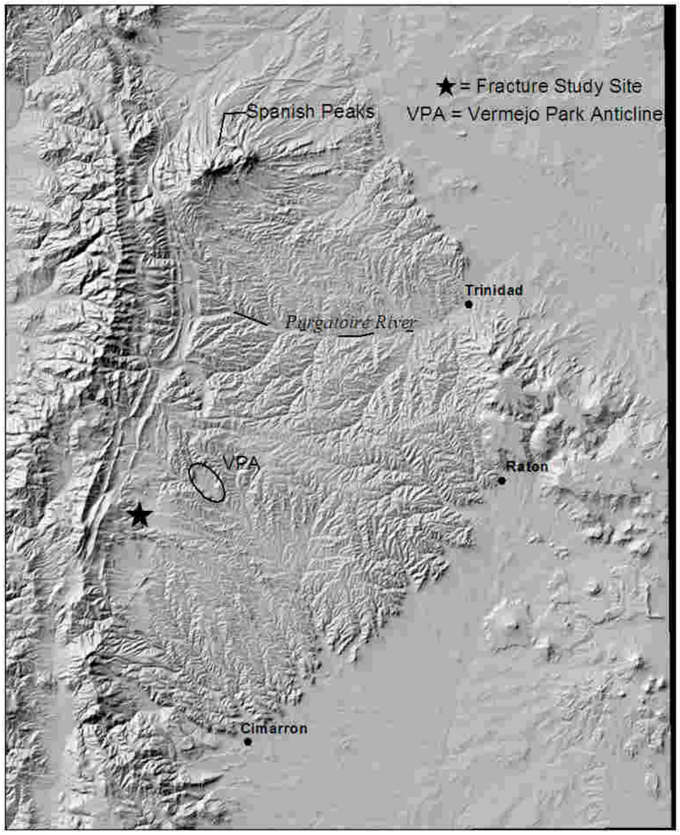

Notes:

Fracture Data:

ID	Strike	Dip	Formation	Comment 1
7/14/2003/1MH	312	82	Poison canyon	left lateral
7/14/2003/1MH	292	82	Poison canyon	
7/14/2003/1MH	313	80	Poison canyon	
7/14/2003/1MH	278	82	Poison canyon	
7/14/2003/1MH	307	90	Poison canyon	
7/14/2003/1MH	318	84	Poison canyon	
7/14/2003/1MH	70	54	Poison canyon	
7/14/2003/1MH	307	83	Poison canyon	
7/14/2003/1MH	300	84	Poison canyon	
7/14/2003/1MH	292	70	Poison canyon	
7/14/2003/1MH	13	85	Poison canyon	
7/14/2003/1MH	320	85	Poison canyon	
7/14/2003/1MH	304	90	Poison canyon	
7/14/2003/1MH	294	84	Poison canyon	
7/14/2003/1MH	310	90	Poison canyon	
7/14/2003/1MH	308	86	Poison canyon	
7/14/2003/1MH	310	90	Poison canyon	

7/14/2003/1MH	300	77	Poison canyon	
7/14/2003/1MH	313	88	Poison canyon	
7/14/2003/1MH	318	86	Poison canyon	
7/14/2003/1MH	308	85	Poison canyon	
7/14/2003/1MH	286	90	Poison canyon	
7/14/2003/1MH	305	82	Poison canyon	left lateral
7/14/2003/1MH	310	82	Poison canyon	
7/14/2003/1MH	310	78	Poison canyon	
7/14/2003/1MH	307	80	Poison canyon	
7/14/2003/1MH	314	80	Poison canyon	
7/14/2003/1MH	302	90	Poison canyon	
7/14/2003/1MH	320	90	Poison canyon	left lateral
7/14/2003/1MH	290	80	Poison canyon	right lateral
7/14/2003/1MH	295	90	Poison canyon	
7/14/2003/1MH	316	90	Poison canyon	
7/14/2003/1MH	267	90	Poison canyon	
7/14/2003/1MH	22	90	Poison canyon	
7/14/2003/1MH	28	90	Poison canyon	

Location ID: 7/14/2003/2JL
Latitude: N 36.8471
Longitude: W 103.9220167

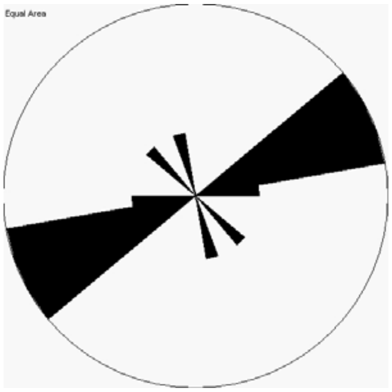

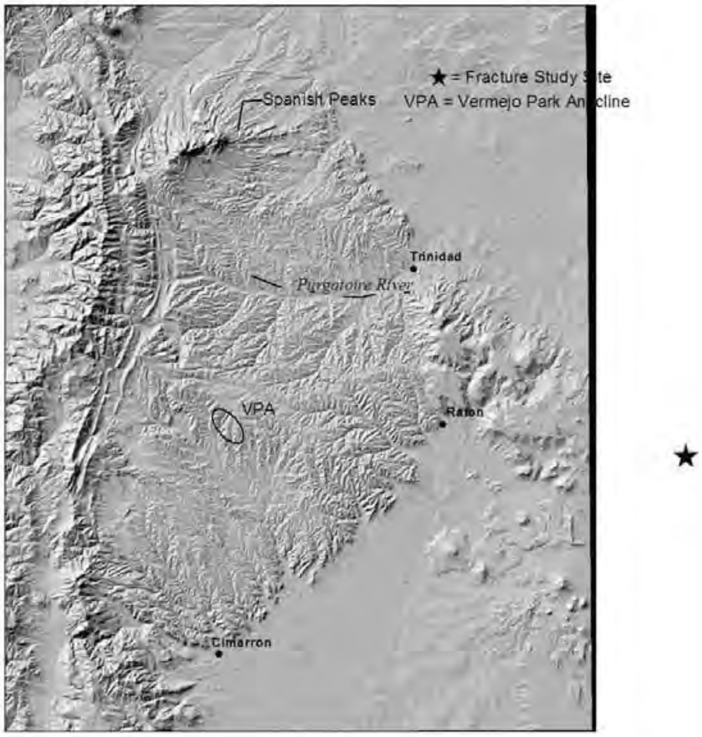

Notes:

Fracture Data:

ID	Strike	Dip	Formation	Comment 1
7/14/2003/2JL	70	90	Dakota	
7/14/2003/2JL	69	90	Dakota	
7/14/2003/2JL	130	90	Dakota	
7/14/2003/2JL	58	90	Dakota	
7/14/2003/2JL	57	90	Dakota	
7/14/2003/2JL	82	90	Dakota	
7/14/2003/2JL	160	90	Dakota	
7/14/2003/2JL	72	90	Dakota	
7/14/2003/2JL	64	90	Dakota	
7/14/2003/2JL	72	90	Dakota	LL
7/14/2003/2JL	50	90	Dakota	RL
7/14/2003/2JL	60	90	Dakota	

Location ID: 7/14/2003/3JL
Latitude: N 36.94171667
Longitude: W 104.28735

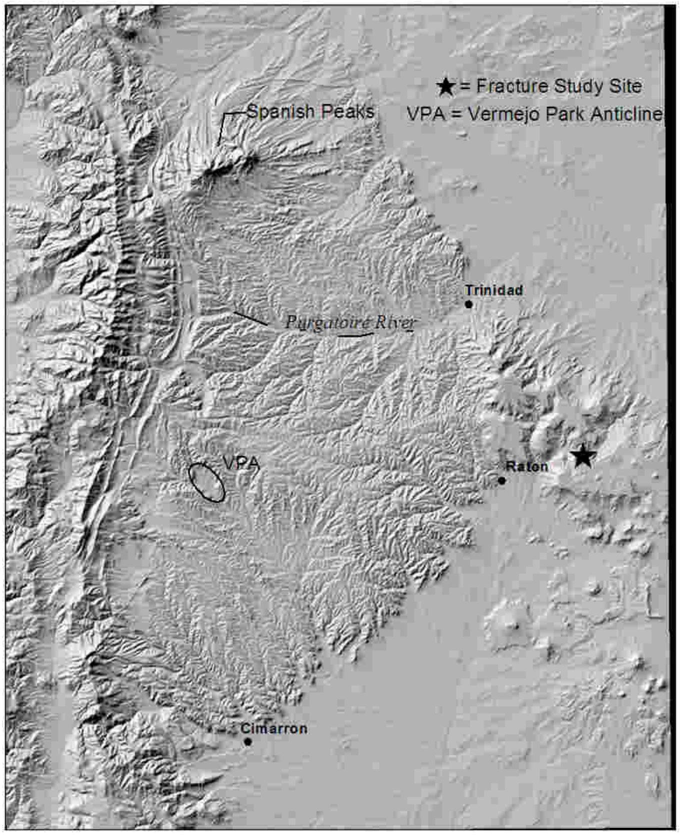

Notes:

Fracture Data:

ID	Strike	Dip	Formation
7/14/2003/3JL	160	90	Dakota
7/14/2003/3JL	30	90	Dakota
7/14/2003/3JL	115	90	Dakota
7/14/2003/3JL	12	90	Dakota
7/14/2003/3JL	120	90	Dakota
7/14/2003/3JL	91	90	Dakota
7/14/2003/3JL	23	90	Dakota
7/14/2003/3JL	109	90	Dakota
7/14/2003/3JL	106	90	Dakota
7/14/2003/3JL	107	90	Dakota
7/14/2003/3JL	103	90	Dakota
7/14/2003/3JL	138	90	Dakota
7/14/2003/3JL	143	90	Dakota
7/14/2003/3JL	129	90	Dakota
7/14/2003/3JL	154	90	Dakota
7/14/2003/3JL	108	90	Dakota
7/14/2003/3JL	110	90	Dakota

7/14/2003/3JL	100	90	Dakota
7/14/2003/3JL	28	90	Dakota
7/14/2003/3JL	129	90	Dakota
7/14/2003/3JL	103	90	Dakota
7/14/2003/3JL	110	90	Dakota

Location ID: 7/14/2003/4JL
Latitude: N 36.86993333
Longitude: W 104.0004167

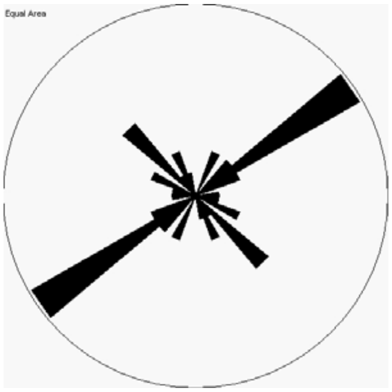

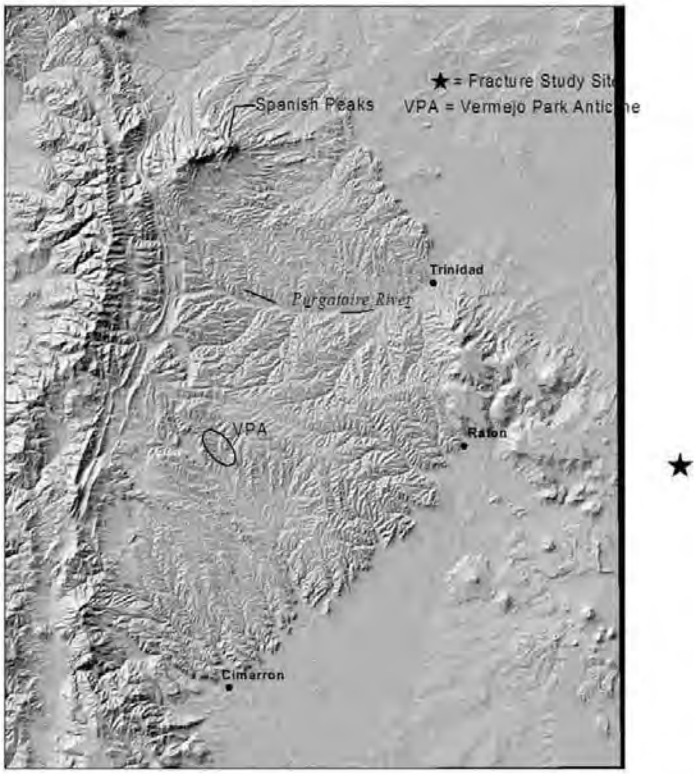

Notes:

Fracture Data:

ID	Strike	Dip	Formation
7/14/2003/4JL	93	90	Niobrara
7/14/2003/4JL	119	90	Niobrara
7/14/2003/4JL	119	90	Niobrara
7/14/2003/4JL	81	90	Niobrara
7/14/2003/4JL	102	90	Niobrara
7/14/2003/4JL	50	90	Niobrara
7/14/2003/4JL	51	90	Niobrara
7/14/2003/4JL	57	90	Niobrara
7/14/2003/4JL	51	90	Niobrara
7/14/2003/4JL	56	90	Niobrara
7/14/2003/4JL	66	90	Niobrara
7/14/2003/4JL	63	90	Niobrara
7/14/2003/4JL	57	90	Niobrara
7/14/2003/4JL	48	90	Niobrara
7/14/2003/4JL	51	90	Niobrara
7/14/2003/4JL	52	90	Niobrara
7/14/2003/4JL	49	90	Niobrara
7/14/2003/4JL	21	90	Niobrara
7/14/2003/4JL	24	90	Niobrara

7/14/2003/4JL	163	90	Niobrara
7/14/2003/4JL	153	90	Niobrara
7/14/2003/4JL	152	90	Niobrara
7/14/2003/4JL	143	90	Niobrara
7/14/2003/4JL	132	90	Niobrara
7/14/2003/4JL	130	90	Niobrara
7/14/2003/4JL	138	90	Niobrara
7/14/2003/4JL	130	90	Niobrara

Location ID: 7/16/2003/1JL
Latitude: N 37.33688333
Longitude: W 104.0709833

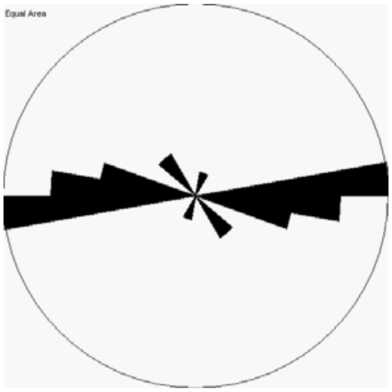

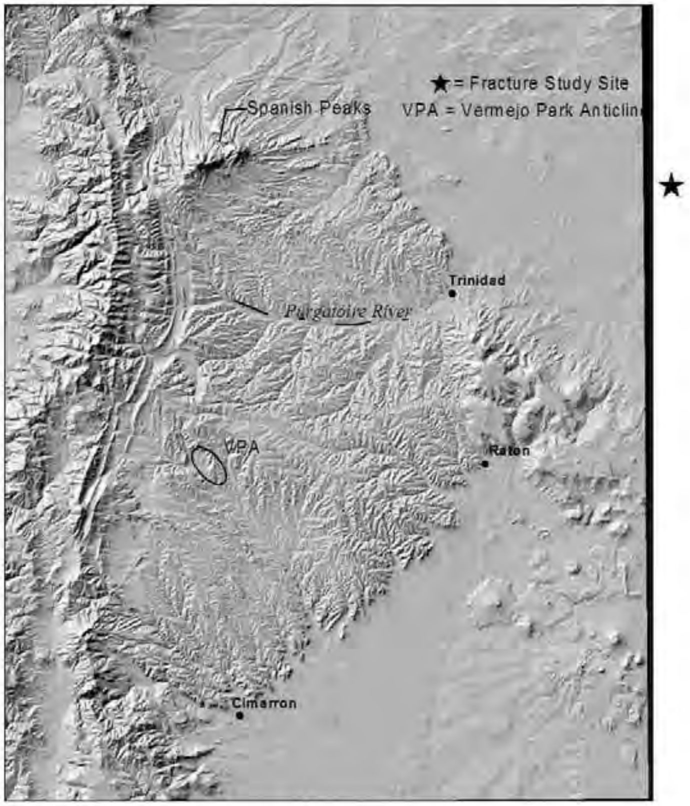

Notes:

Fracture Data:

ID	Strike	Dip	Formation
7/16/2003/1JL	87	90	Niobrara
7/16/2003/1JL	89	90	Niobrara
7/16/2003/1JL	88	90	Niobrara
7/16/2003/1JL	81	90	Niobrara
7/16/2003/1JL	81	90	Niobrara
7/16/2003/1JL	100	90	Niobrara
7/16/2003/1JL	132	90	Niobrara
7/16/2003/1JL	14	90	Niobrara
7/16/2003/1JL	142	90	Niobrara
7/16/2003/1JL	130	90	Niobrara
7/16/2003/1JL	101	90	Niobrara
7/16/2003/1JL	80	90	Niobrara
7/16/2003/1JL	109	90	Niobrara
7/16/2003/1JL	22	90	Niobrara
7/16/2003/1JL	96	90	Niobrara
7/16/2003/1JL	99	90	Niobrara
7/16/2003/1JL	93	90	Niobrara
7/16/2003/1JL	85	90	Niobrara

7/16/2003/1JL	92	90	Niobrara
7/16/2003/1JL	140	90	Niobrara
7/16/2003/1JL	105	90	Niobrara
7/16/2003/1JL	99	90	Niobrara
7/16/2003/1JL	94	90	Niobrara
7/16/2003/1JL	84	90	Niobrara

Location ID: 7/17/2003/1MH
Latitude: N 36.95443333
Longitude: W 105.1608267

“The Wall”, overturned Dakota Fm.

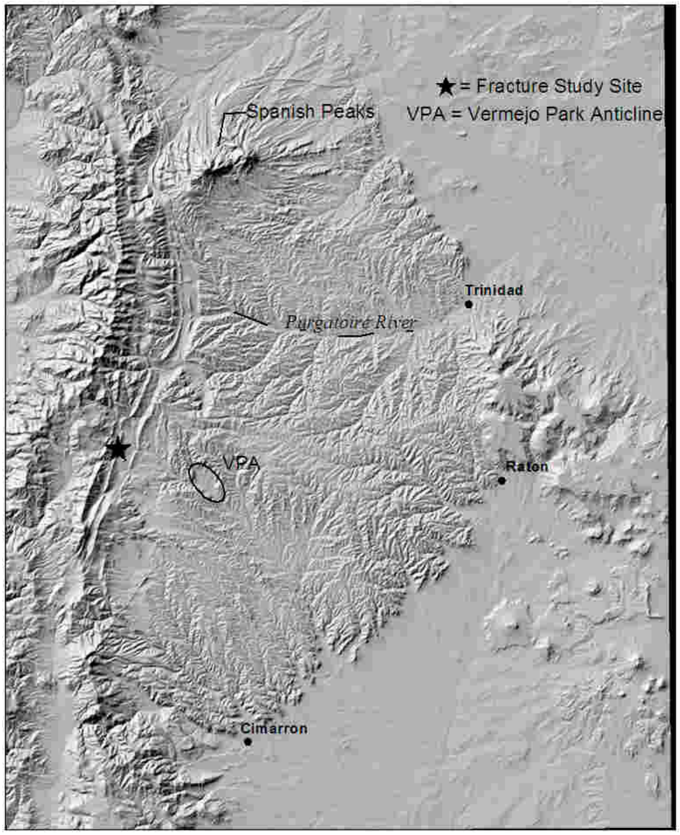

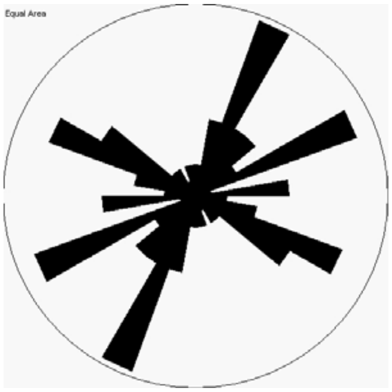

(data rotated to bed-horizontal)

Notes:

Fracture Data:

ID	Strike	Dip	Formation	Comment 1	Comment 2	Comment 3
7/17/2003/1MH	70	20	Dakota	Def. Band		
7/17/2003/1MH	168	72	Dakota	Def. Band		

7/17/2003/1MH	158	40	Dakota	Def. Band		
7/17/2003/1MH	296	10	Dakota	Def. Band		
7/17/2003/1MH	197	85	Dakota	Def. Band		
7/17/2003/1MH	183	40	Dakota	Def. Band		
7/17/2003/1MH	280	40	Dakota	Def. Band		
7/17/2003/1MH	312	68	Dakota	Def. Band		
7/17/2003/1MH	200	85	Dakota	Def. Band		
7/17/2003/1MH	29	90	Dakota	Def. Band		
7/17/2003/1MH	323	68	Dakota	Def. Band		
7/17/2003/1MH	337	55	Dakota	Def. Band		
7/17/2003/1MH	304	40	Dakota	Def. Band	chatter marks and dip slip lineations	
7/17/2003/1MH	297	38	Dakota	Def. Band		
7/17/2003/1MH	191	40	Dakota	Def. Band		
7/17/2003/1MH	332	48	Dakota	Def. Band		
7/17/2003/1MH	200	85	Dakota	Def. Band		
7/17/2003/1MH	358	64	Dakota	Def. Band		
7/17/2003/1MH	220	65	Dakota	Def. Band		
7/17/2003/1MH	188	50	Dakota	Def. Band		
7/17/2003/1MH	80	15	Dakota	Def. Band	fault	lineations strike 110
7/17/2003/1MH	325	75	Dakota	Def. Band		
7/17/2003/1MH	9	90	Dakota	Def. Band	vertical striations	
7/17/2003/1MH	339	78	Dakota	Def. Band		
7/17/2003/1MH	305	80	Dakota	Def. Band	10 parallel DB's parallel to bedding	
7/17/2003/1MH	215	30	Dakota	Def. Band		
7/17/2003/1MH	58	85	Dakota	Def. Band		
7/17/2003/1MH	328	5	Dakota	Def. Band		
7/17/2003/1MH	316	5	Dakota	Def. Band		
7/17/2003/1MH	344	30	Dakota	Def. Band		
7/17/2003/1MH	4	80	Dakota	Def. Band		
7/17/2003/1MH	80	90	Dakota	Def. Band		
7/17/2003/1MH	133	85	Dakota	Def. Band		
7/17/2003/1MH	178	90	Dakota	Def. Band		
7/17/2003/1MH	108	90	Dakota	Def. Band		
7/17/2003/1MH	358	78	Dakota	Def. Band		
7/17/2003/1MH	124	90	Dakota	Def. Band		
7/17/2003/1MH	117	90	Dakota	Def. Band		
7/17/2003/1MH	358	40	Dakota	Def. Band	lineations @ 90	
7/17/2003/1MH	331	50	Dakota	Def. Band		
7/17/2003/1MH	18	20	Dakota	Def. Band	lineations @ 115	
7/17/2003/1MH	130	80	Dakota	Def. Band		
7/17/2003/1MH	200	80	Dakota	Def. Band		
7/17/2003/1MH	330	30	Dakota	Def. Band	lineations @ 98	
7/17/2003/1MH	28	18	Dakota	Def. Band	lineations @100	
7/17/2003/1MH	143	62	Dakota	Fracture		
7/17/2003/1MH	80	90	Dakota	Fracture		
7/17/2003/1MH	153	62	Dakota	Fracture		

7/17/2003/1MH	359	8	Dakota	Fracture	
7/17/2003/1MH	171	70	Dakota	Fracture	
7/17/2003/1MH	82	60	Dakota	Fracture	
7/17/2003/1MH	29	38	Dakota	Fracture	
7/17/2003/1MH	107	90	Dakota	Fracture	
7/17/2003/1MH	41	30	Dakota	Fracture	w/shear; top block went SW
7/17/2003/1MH	92	72	Dakota	Fracture	
7/17/2003/1MH	38	15	Dakota	Fracture	
7/17/2003/1MH	108	90	Dakota	Fracture	
7/17/2003/1MH	11	20	Dakota	Fracture	
7/17/2003/1MH	99	90	Dakota	Fracture	
7/17/2003/1MH	286	85	Dakota	Fracture	
7/17/2003/1MH	22	25	Dakota	Fracture	
7/17/2003/1MH	290	73	Dakota	Fracture	
7/17/2003/1MH	72	50	Dakota	Fracture	
7/17/2003/1MH	103	90	Dakota	Fracture	
7/17/2003/1MH	99	90	Dakota	Fracture	
7/17/2003/1MH	30	10	Dakota	Fracture	
7/17/2003/1MH	300	72	Dakota	Fracture	
7/17/2003/1MH	302	85	Dakota	Fracture	
7/17/2003/1MH	30	70	Dakota	Fracture	
7/17/2003/1MH	28	32	Dakota	Fracture	
7/17/2003/1MH	138	90	Dakota	Fracture	
7/17/2003/1MH	6	40	Dakota	Fracture	
7/17/2003/1MH	119	90	Dakota	Fracture	
7/17/2003/1MH	290	85	Dakota	Fracture	
7/17/2003/1MH	311	38	Dakota	Fracture	
7/17/2003/1MH	305	40	Dakota	Fracture	
7/17/2003/1MH	17	70	Dakota	Fracture	fault w/gouge
7/17/2003/1MH	162	90	Dakota	Fracture	
7/17/2003/1MH	88	32	Dakota	Fracture	
7/17/2003/1MH	350	80	Dakota	Fracture	fault w/lineations trending 85
7/17/2003/1MH	5	25	Dakota	Fracture	
7/17/2003/1MH	32	10	Dakota	Fracture	lineations strike 108

Location ID: 7/17/2003/1RK
Latitude: N 36.96968333
Longitude: W 105.1221167

"Little Wall", basal Trinidad

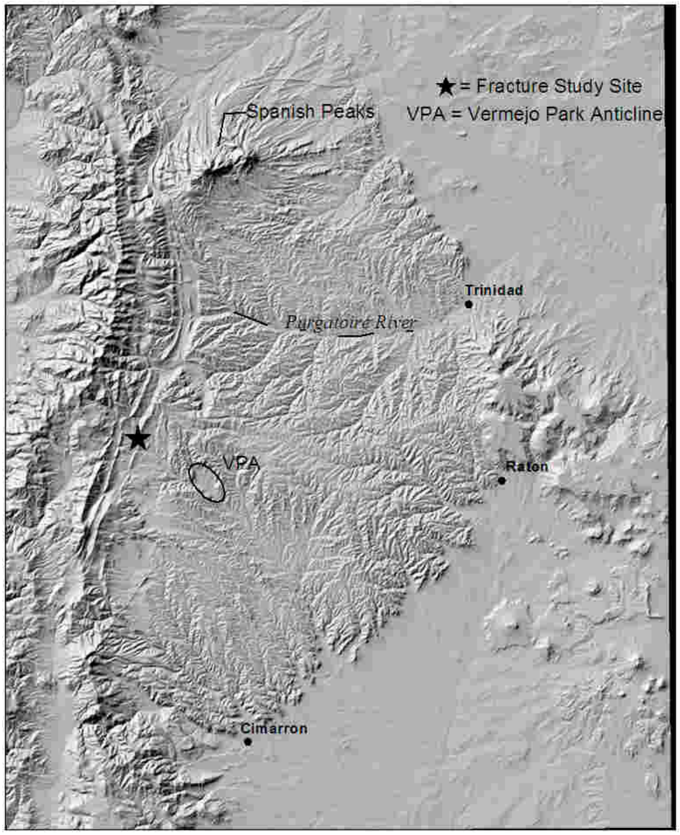

Notes:

Fracture Data:

ID	Strike	Dip	Formation	Comment 1	Comment 2
7/17/2003/RK	299	90	Trinidad	plume	terminates against 15/67NW
7/17/2003/RK	298	88	Trinidad		
7/17/2003/RK	297	81	Trinidad		
7/17/2003/RK	301	83	Trinidad		
7/17/2003/RK	294	80	Trinidad		
7/17/2003/RK	299	76	Trinidad	terminates against 11/52 NW	
7/17/2003/RK	112	86	Trinidad	swarm, 60 cm, 8 fracs	
7/17/2003/RK	116	84	Trinidad		
7/17/2003/RK	121	86	Trinidad		
7/17/2003/RK	119	83	Trinidad		
7/17/2003/RK	124	87	Trinidad		
7/17/2003/RK	124	83	Trinidad	plume	
7/17/2003/RK	201	59	Trinidad		
7/17/2003/RK	185	55	Trinidad	plume	
7/17/2003/RK	185	56	Trinidad	swarm, 60 cm, 8 fracs	
7/17/2003/RK	185	50	Trinidad		

7/17/2003/RK	179	62	Trinidad	
7/17/2003/RK	175	68	Trinidad	
7/17/2003/RK	186	64	Trinidad	
7/17/2003/RK	185	67	Trinidad	
7/17/2003/RK	183	65	Trinidad	
7/17/2003/RK	184	62	Trinidad	
7/17/2003/RK	191	59	Trinidad	terminates against 298/88
7/17/2003/RK	195	70	Trinidad	
7/17/2003/RK	189	70	Trinidad	
7/17/2003/RK	118	88	Trinidad	

Location ID: 7/17/2003/2MH
Latitude: N 36.95073333
Longitude: W 105.1356667

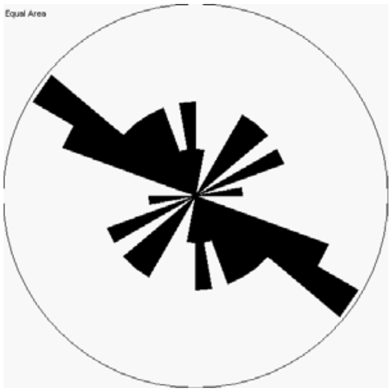

(data rotated to bed-horizontal)

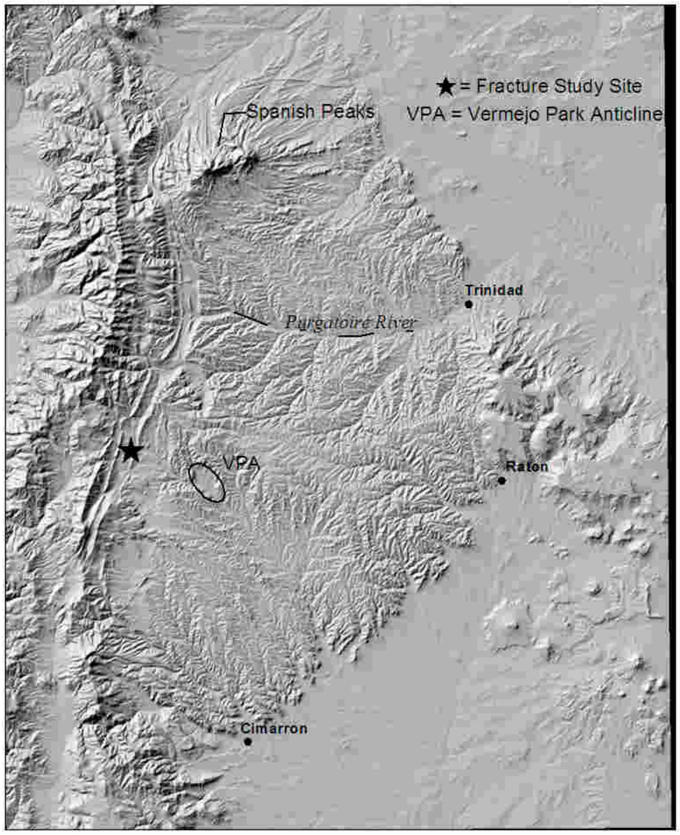

Notes:

Fracture Data:

ID	Strike	Dip	Formation	Comment 1	Comment 2
7/17/2003/2MH	140	90	Pierre		
7/17/2003/2MH	137	90	Pierre		
7/17/2003/2MH	132	90	Pierre		
7/17/2003/2MH	264	80	Pierre		
7/17/2003/2MH	228	60	Pierre		Basalt
7/17/2003/2MH	120	90	Pierre		Basalt
7/17/2003/2MH	228	68	Pierre		Basalt
7/17/2003/2MH	120	90	Pierre		Basalt
7/17/2003/2MH	115	90	Pierre		Basalt
7/17/2003/2MH	55	35	Pierre	plume (parallel to bedding)	Basalt
7/17/2003/2MH	162	65	Pierre	plume	Basalt
7/17/2003/2MH	210	58	Pierre		Basalt
7/17/2003/2MH	45	40	Pierre	w/frac fill	Basalt
7/17/2003/2MH	162	50	Pierre		Basalt
7/17/2003/2MH	130	75	Pierre	plume	Basalt
7/17/2003/2MH	164	75	Pierre		Basalt

7/17/2003/2MH	110	90	Pierre	Basalt
7/17/2003/2MH	302	85	Pierre	Basalt
7/17/2003/2MH	55	70	Pierre	Basalt
7/17/2003/2MH	152	80	Pierre	Basalt
7/17/2003/2MH	142	50	Pierre	Basalt
7/17/2003/2MH	288	80	Pierre	Basalt
7/17/2003/2MH	293	80	Pierre	Basalt
7/17/2003/2MH	146	70	Pierre	Basalt

Location ID: 7/17/2003/2RK
Latitude: N 36.95426667
Longitude: W 105.12385

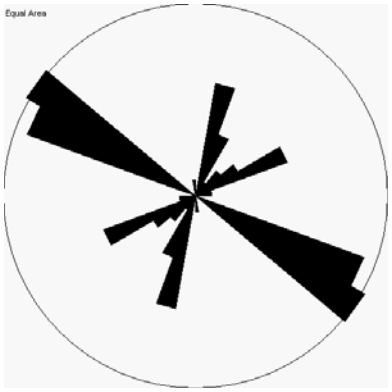

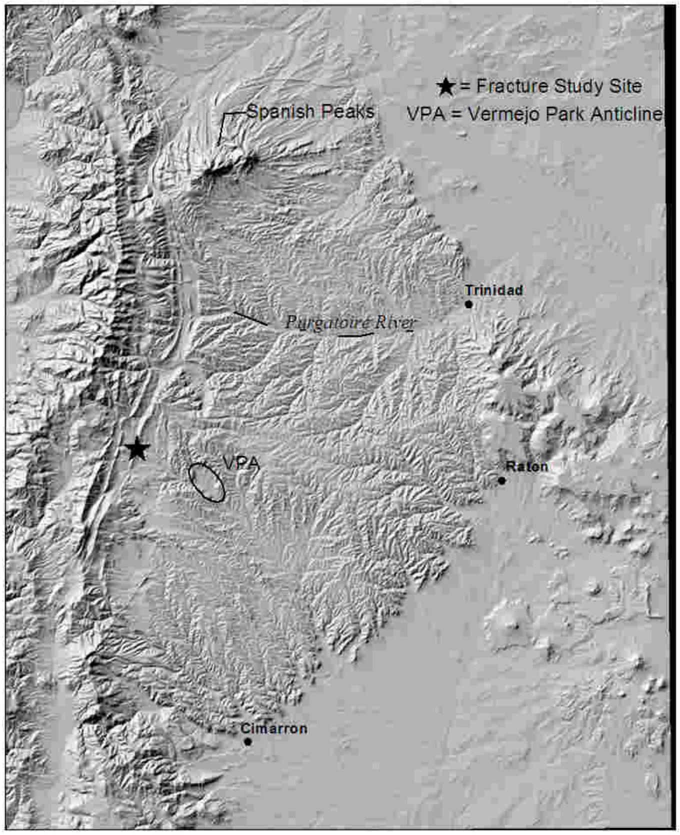

Notes:

Fracture Data:

ID	Strike	Dip	Formation	Comment 1
7/17/2003/2RK	196	61	Trinidad	
7/17/2003/2RK	208	65	Trinidad	
7/17/2003/2RK	196	68	Trinidad	
7/17/2003/2RK	194	68	Trinidad	
7/17/2003/2RK	193	69	Trinidad	
7/17/2003/2RK	223	72	Trinidad	
7/17/2003/2RK	14	74	Trinidad	
7/17/2003/2RK	201	74	Trinidad	
7/17/2003/2RK	205	74	Trinidad	
7/17/2003/2RK	243	76	Trinidad	
7/17/2003/2RK	246	76	Trinidad	
7/17/2003/2RK	224	77	Trinidad	
7/17/2003/2RK	245	78	Trinidad	
7/17/2003/2RK	237	78	Trinidad	
7/17/2003/2RK	249	78	Trinidad	terminates against 301
7/17/2003/2RK	205	80	Trinidad	
7/17/2003/2RK	238	80	Trinidad	

7/17/2003/2RK	243	82	Trinidad
7/17/2003/2RK	238	82	Trinidad
7/17/2003/2RK	197	82	Trinidad
7/17/2003/2RK	212	83	Trinidad
7/17/2003/2RK	119	83	Trinidad
7/17/2003/2RK	197	84	Trinidad
7/17/2003/2RK	118	85	Trinidad
7/17/2003/2RK	117	85	Trinidad
7/17/2003/2RK	117	85	Trinidad
7/17/2003/2RK	121	85	Trinidad
7/17/2003/2RK	121	85	Trinidad
7/17/2003/2RK	241	85	Trinidad
7/17/2003/2RK	124	85	Trinidad
7/17/2003/2RK	121	85	Trinidad
7/17/2003/2RK	255	86	Trinidad
7/17/2003/2RK	119	87	Trinidad
7/17/2003/2RK	129	87	Trinidad
7/17/2003/2RK	300	87	Trinidad
7/17/2003/2RK	115	88	Trinidad
7/17/2003/2RK	114	88	Trinidad
7/17/2003/2RK	118	88	Trinidad
7/17/2003/2RK	113	88	Trinidad
7/17/2003/2RK	121	88	Trinidad
7/17/2003/2RK	126	88	Trinidad
7/17/2003/2RK	125	88	Trinidad
7/17/2003/2RK	299	88	Trinidad
7/17/2003/2RK	300	90	Trinidad
7/17/2003/2RK	173	90	Trinidad
7/17/2003/2RK	302	90	Trinidad
7/17/2003/2RK	303	90	Trinidad
7/17/2003/2RK	89	90	Trinidad
7/17/2003/2RK	297	90	Trinidad

Location ID: 7/17/2003/3MH
Latitude: N 36.96061667
Longitude: W 105.1611167

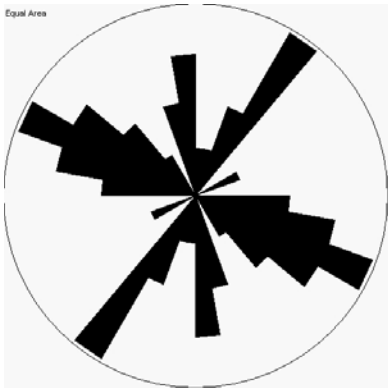

(data rotated to bed-horizontal)

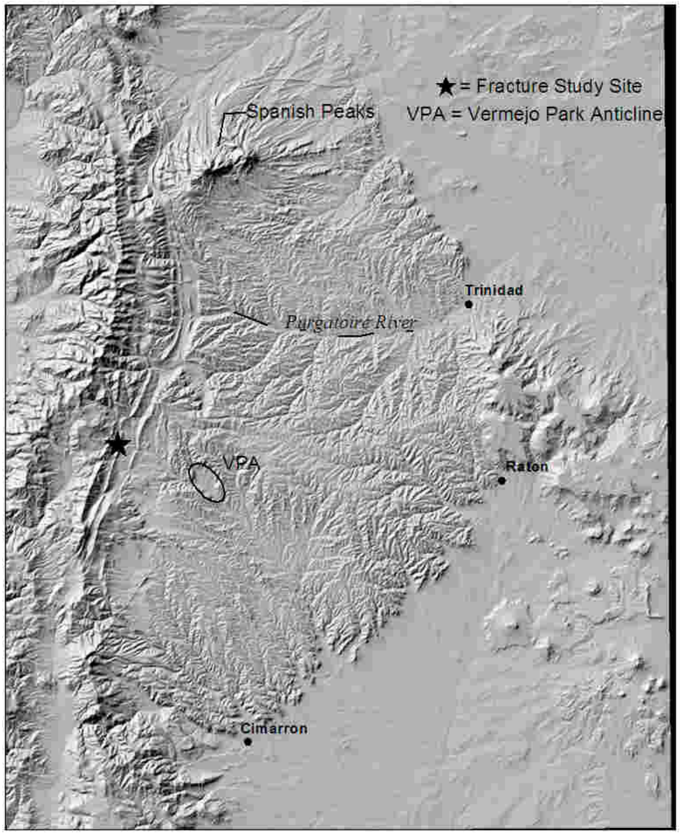

Notes:

Fracture Data:

ID	Strike	Dip	Formation	Comment 1	Comment 2
7/17/2003/3MH	306	85	Morrison		
7/17/2003/3MH	38	35	Morrison		
7/17/2003/3MH	61	45	Morrison		
7/17/2003/3MH	34	50	Morrison		
7/17/2003/3MH	42	60	Morrison		
7/17/2003/3MH	42	48	Morrison		
7/17/2003/3MH	123	80	Morrison	w/subvertical slickenlines, rake 66 NW, extensive	
7/17/2003/3MH	32	36	Morrison		
7/17/2003/3MH	118	90	Morrison	terminates against 25	
7/17/2003/3MH	310	65	Morrison	shear plane	puts rippled sand against conglomerate between two more competant beds
7/17/2003/3MH	80	70	Morrison		
7/17/2003/3MH	38	46	Morrison		
7/17/2003/3MH	104	75	Morrison	plume	
7/17/2003/3MH	313	85	Morrison		

7/17/2003/3MH	78	55	Morrison	
7/17/2003/3MH	118	82	Morrison	
7/17/2003/3MH	145	85	Morrison	
7/17/2003/3MH	94	58	Morrison	
7/17/2003/3MH	81	52	Morrison	
7/17/2003/3MH	88	56	Morrison	
7/17/2003/3MH	308	60	Morrison	terminates against 88
7/17/2003/3MH	130	90	Dakota	
7/17/2003/3MH	129	90	Dakota	
7/17/2003/3MH	128	25	Dakota	
7/17/2003/3MH	305	76	Dakota	
7/17/2003/3MH	315	55	Dakota	
7/17/2003/3MH	333	32	Dakota	
7/17/2003/3MH	159	88	Dakota	
7/17/2003/3MH	151	90	Dakota	
7/17/2003/3MH	298	60	Dakota	deformation band

Location ID: 7/17/2003/3RK
Latitude: N 36.77546667
Longitude: W 104.9213333

Van Bremmer Canyon

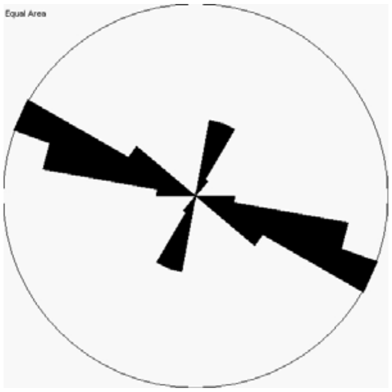

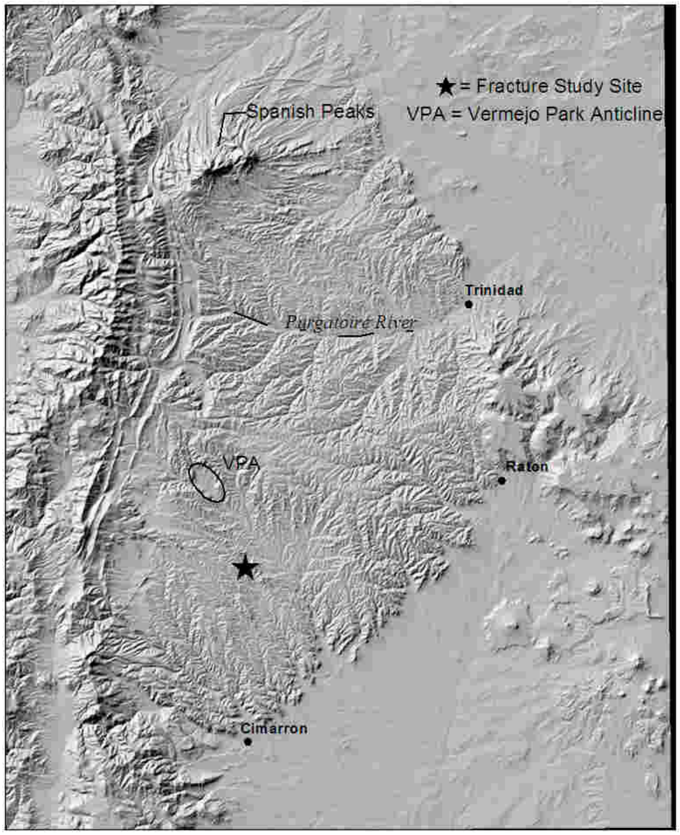

Notes:

Fracture Data:

ID	Strike	Dip	Formation	Comment 1
7/17/2003/3RK	19	90	Raton	terminates against 294
7/17/2003/3RK	294	82	Raton	
7/17/2003/3RK	215	84	Raton	plume
7/17/2003/3RK	108	85	Raton	
7/17/2003/3RK	17	88	Raton	terminates against 108
7/17/2003/3RK	291	85	Raton	plume
7/17/2003/3RK	298	83	Raton	plume
7/17/2003/3RK	207	80	Raton	terminates against 298
7/17/2003/3RK	115	86	Raton	
7/17/2003/3RK	308	90	Raton	
7/17/2003/3RK	277	78	Raton	
7/17/2003/3RK	27	90	Raton	
7/17/2003/3RK	289	90	Raton	
7/17/2003/3RK	204	80	Raton	
7/17/2003/3RK	288	81	Raton	
7/17/2003/3RK	294	85	Raton	
7/17/2003/3RK	285	82	Raton	

7/17/2003/3RK	208	85	Raton	
7/17/2003/3RK	287	90	Raton	
7/17/2003/3RK	199	86	Raton	terminates against 287
7/17/2003/3RK	282	90	Raton	
7/17/2003/3RK	196	88	Raton	
7/17/2003/3RK	104	87	Raton	
7/17/2003/3RK	109	89	Raton	
7/17/2003/3RK	293	86	Raton	
7/17/2003/3RK	117	78	Raton	
7/17/2003/3RK	303	90	Raton	
7/17/2003/3RK	300	90	Raton	
7/17/2003/3RK	127	85	Raton	
7/17/2003/3RK	294	90	Raton	
7/17/2003/3RK	116	88	Raton	
7/17/2003/3RK	278	84	Raton	
7/17/2003/3RK	293	85	Raton	

Location ID: 7/17/2003/4MH
Latitude: N 36.94815
Longitude: W 105.1182333

"Little Wall", Raton
Conglomerate

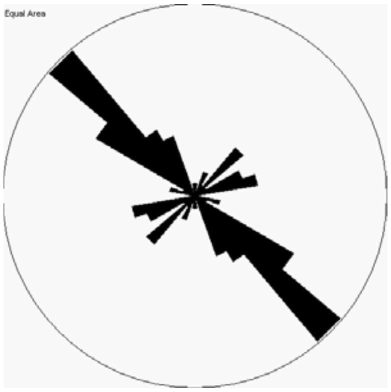

(data rotated to bed-horizontal)

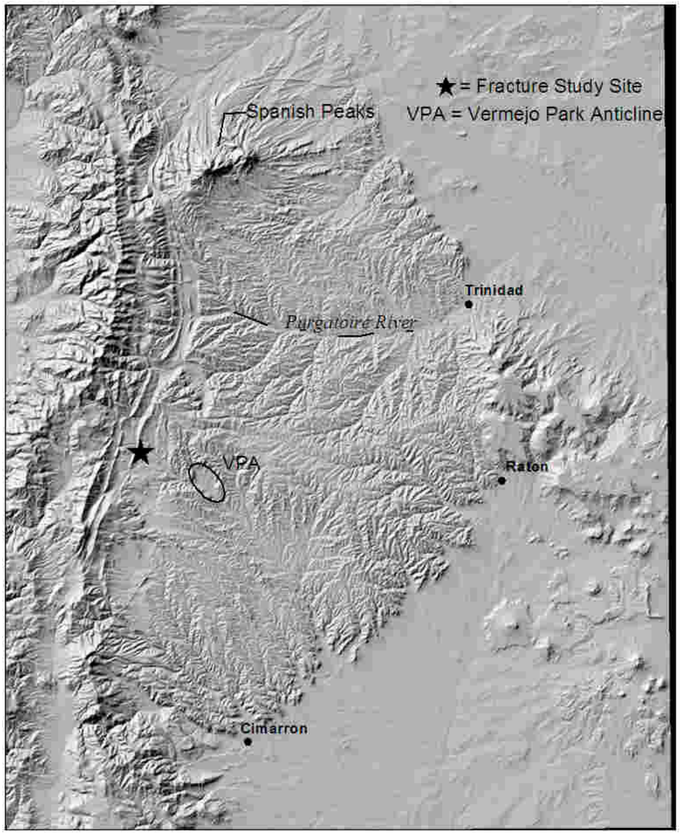

Notes:

Fracture Data:

ID	Strike	Dip	Formation	Comment 1	Comment 2
7/17/2003/4MH	128	60	Raton	Deformation band	Raton conglomerate
7/17/2003/4MH	270	45	Raton	Deformation band	Raton conglomerate
7/17/2003/4MH	58	90	Raton	Deformation band	Raton conglomerate
7/17/2003/4MH	262	75	Raton	Deformation band	Raton conglomerate
7/17/2003/4MH	262	75	Raton	Deformation band	Raton conglomerate
7/17/2003/4MH	263	60	Raton	Deformation band	Raton conglomerate
7/17/2003/4MH	70	90	Raton	Deformation band	Raton conglomerate
7/17/2003/4MH	58	70	Raton	Deformation band	Raton conglomerate
7/17/2003/4MH	60	20	Raton	Deformation band	Raton conglomerate
7/17/2003/4MH	45	90	Raton	Deformation band	Raton conglomerate
7/17/2003/4MH	125	90	Raton	Deformation band	Raton conglomerate
7/17/2003/4MH	45	90	Raton	Deformation band	Raton conglomerate
7/17/2003/4MH	62	90	Raton	Deformation band	Raton conglomerate
7/17/2003/4MH	60	90	Raton	Deformation band	Raton conglomerate
7/17/2003/4MH	148	90	Raton	left lateral	Raton conglomerate
7/17/2003/4MH	132	80	Raton	left lateral	Raton conglomerate
7/17/2003/4MH	140	90	Raton	left lateral	Raton conglomerate

7/17/2003/4MH	132	90	Raton	left lateral	Raton conglomerate
7/17/2003/4MH	134	90	Raton	left lateral	Raton conglomerate
7/17/2003/4MH	104	90	Raton	right lateral	Raton conglomerate
7/17/2003/4MH	152	90	Raton	right lateral	Raton conglomerate
7/17/2003/4MH	128	90	Raton	right lateral	Raton conglomerate
7/17/2003/4MH	140	90	Raton	right lateral	Raton conglomerate
7/17/2003/4MH	138	90	Raton	right lateral	Raton conglomerate
7/17/2003/4MH	138	90	Raton	right lateral	Raton conglomerate
7/17/2003/4MH	140	90	Raton		Raton conglomerate
7/17/2003/4MH	110	90	Raton		Raton conglomerate
7/17/2003/4MH	133	90	Raton		Raton conglomerate
7/17/2003/4MH	126	90	Raton		Raton conglomerate
7/17/2003/4MH	145	90	Raton		Raton conglomerate
7/17/2003/4MH	136	90	Raton		Raton conglomerate
7/17/2003/4MH	162	90	Raton		Raton conglomerate
7/17/2003/4MH	160	90	Raton		Raton conglomerate
7/17/2003/4MH	133	90	Raton		Raton conglomerate
7/17/2003/4MH	30	90	Raton		Raton conglomerate
7/17/2003/4MH	134	90	Raton		Raton conglomerate
7/17/2003/4MH	202	80	Raton		Raton conglomerate
7/17/2003/4MH	132	90	Raton		Raton conglomerate
7/17/2003/4MH	132	90	Raton		Raton conglomerate
7/17/2003/4MH	160	90	Raton		Raton conglomerate
7/17/2003/4MH	160	90	Raton		Raton conglomerate
7/17/2003/4MH	39	90	Raton		Raton conglomerate
7/17/2003/4MH	340	70	Raton		Raton conglomerate
7/17/2003/4MH	50	90	Raton		Raton conglomerate
7/17/2003/4MH	22	90	Raton		Raton conglomerate
7/17/2003/4MH	90	65	Raton		Raton conglomerate
7/17/2003/4MH	184	65	Raton		Raton conglomerate
7/17/2003/4MH	178	82	Raton		Raton conglomerate
7/17/2003/4MH	151	90	Raton		Raton conglomerate
7/17/2003/4MH	223	70	Raton		Raton conglomerate
7/17/2003/4MH	139	90	Raton		Raton conglomerate
7/17/2003/4MH	226	75	Raton		Raton conglomerate
7/17/2003/4MH	131	90	Raton		Raton conglomerate
7/17/2003/4MH	140	90	Raton		Raton conglomerate
7/17/2003/4MH	140	90	Raton		Raton conglomerate
7/17/2003/4MH	128	90	Raton		Raton conglomerate
7/17/2003/4MH	131	90	Raton		Raton conglomerate
7/17/2003/4MH	139	90	Raton		Raton conglomerate

Location ID: 7/17/2003/4RK
Latitude: N 36.60936667
Longitude: W 104.8205167

Van Bremmer Canyon

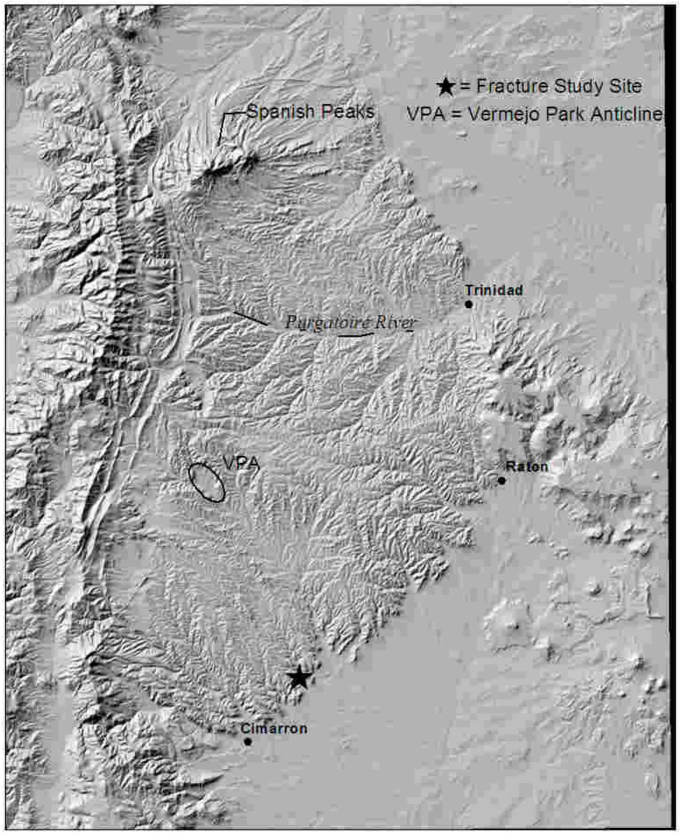

Notes:

Fracture Data:

ID	Strike	Dip	Formation	Comment 1	Comment 2	Comment 3
7/17/2003/4RK	354	76	Trinidad		1 m thick basal Trinidad	
7/17/2003/4RK	280	90	Trinidad		1 m thick basal Trinidad	
7/17/2003/4RK	285	85	Trinidad		1 m thick basal Trinidad	
7/17/2003/4RK	109	87	Trinidad		1 m thick basal Trinidad	
7/17/2003/4RK	110	85	Trinidad		1 m thick basal Trinidad	
7/17/2003/4RK	281	88	Trinidad		1 m thick basal Trinidad	
7/17/2003/4RK	286	90	Trinidad		1 m thick basal Trinidad	
7/17/2003/4RK	286	90	Trinidad		1 m thick basal Trinidad	
7/17/2003/4RK	285	88	Trinidad		1 m thick basal Trinidad	
7/17/2003/4RK	287	88	Trinidad		1 m thick basal Trinidad	
7/17/2003/4RK	357	88	Trinidad	terminates against 65	1 m thick basal Trinidad	
7/17/2003/4RK	109	88	Trinidad		1 m thick basal Trinidad	
7/17/2003/4RK	105	90	Trinidad		1 m thick basal Trinidad	
7/17/2003/4RK	285	90	Trinidad		1 m thick basal Trinidad	
7/17/2003/4RK	115	83	Trinidad	plume	1 m thick basal Trinidad	
7/17/2003/4RK	72	64	Trinidad		1 m thick basal Trinidad	

7/17/2003/4RK	280	90	Trinidad		1 m thick basal Trinidad	
7/17/2003/4RK	325	90	Trinidad		1 m thick basal Trinidad	
7/17/2003/4RK	41	81	Trinidad		1 m thick basal Trinidad	
7/17/2003/4RK	74	78	Trinidad		1 m thick basal Trinidad	
7/17/2003/4RK	285	90	Trinidad		1 m thick basal Trinidad	
7/17/2003/4RK	348	90	Trinidad		1 m thick basal Trinidad	
7/17/2003/4RK	294	85	Trinidad		8-9 m thick Trinidad	fractures do not cut through entire unit, several meter spacing
7/17/2003/4RK	360	85	Trinidad	terminates against 294	8-9 m thick Trinidad	
7/17/2003/4RK	298	86	Trinidad		8-9 m thick Trinidad	
7/17/2003/4RK	359	85	Trinidad		8-9 m thick Trinidad	
7/17/2003/4RK	275	90	Trinidad	plume	8-9 m thick Trinidad	
7/17/2003/4RK	273	90	Trinidad		8-9 m thick Trinidad	
7/17/2003/4RK	271	85	Trinidad		8-9 m thick Trinidad	
7/17/2003/4RK	289	86	Trinidad		8-9 m thick Trinidad	
7/17/2003/4RK	65	78	Trinidad		1 m thick basal Trinidad	
7/17/2003/4RK	281	85	concretion	plume		
7/17/2003/4RK	19	81	concretion	plume		
7/17/2003/4RK	297	88	concretion	plume		
7/17/2003/4RK	285	90	concretion	plume	calcite	
7/17/2003/4RK	285	88	concretion			
7/17/2003/4RK	280	90	concretion			
7/17/2003/4RK	317	90	concretion			
7/17/2003/4RK	299	87	concretion	plume		
7/17/2003/4RK	202	85	concretion			
7/17/2003/4RK	295	88	concretion	plume		

Location ID: 7/18/2003/1RK
Latitude: N 36.89425
Longitude: W 104.5738167

Vermejo Roadcut

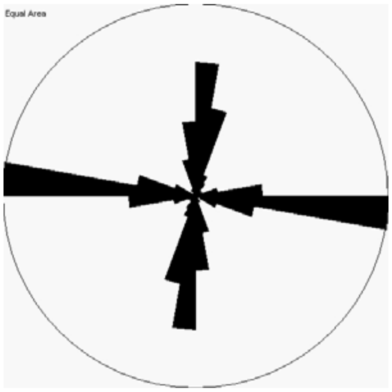

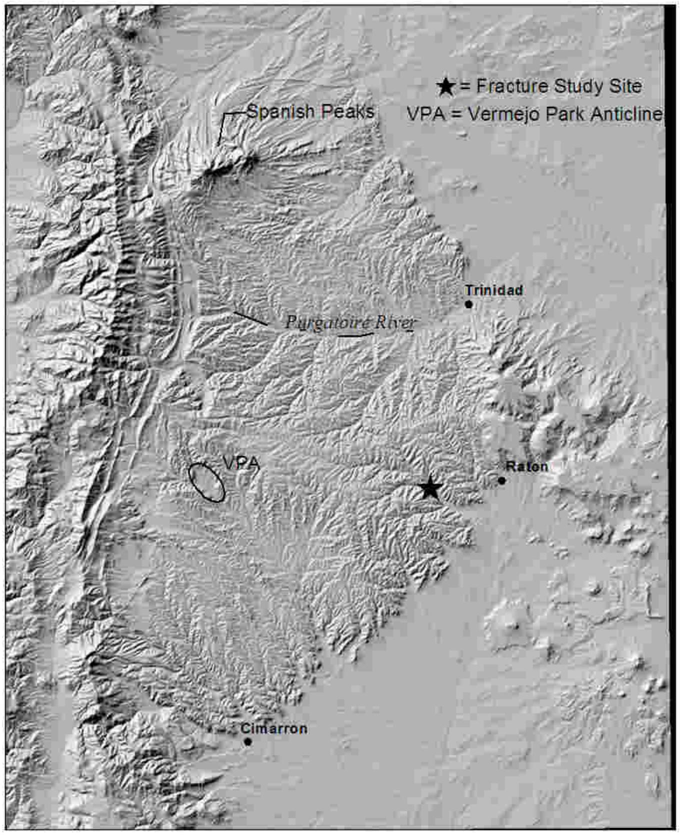

Notes:

Fracture Data:

ID	Strike	Dip	Formation
7/18/2003/1RK	180	60	Vermejo
7/18/2003/1RK	70	50	Vermejo
7/18/2003/1RK	348	50	Vermejo
7/18/2003/1RK	345	59	Vermejo
7/18/2003/1RK	90	30	Vermejo
7/18/2003/1RK	96	88	Vermejo
7/18/2003/1RK	84	90	Vermejo
7/18/2003/1RK	95	90	Vermejo
7/18/2003/1RK	296	82	Vermejo
7/18/2003/1RK	240	82	Vermejo
7/18/2003/1RK	97	88	Vermejo
7/18/2003/1RK	95	90	Vermejo
7/18/2003/1RK	99	90	Vermejo
7/18/2003/1RK	282	88	Vermejo
7/18/2003/1RK			Vermejo
7/18/2003/1RK	95	90	Vermejo
7/18/2003/1RK	96	89	Vermejo

7/18/2003/1RK	101	90	Vermejo
7/18/2003/1RK	100	88	Vermejo
7/18/2003/1RK	93	90	Vermejo
7/18/2003/1RK	104	90	Vermejo
7/18/2003/1RK	93	86	Vermejo
7/18/2003/1RK	94	90	Vermejo
7/18/2003/1RK	99	87	Vermejo
7/18/2003/1RK	277	87	Vermejo
7/18/2003/1RK	91	85	Vermejo
7/18/2003/1RK	99	90	Vermejo
7/18/2003/1RK	99	90	Vermejo
7/18/2003/1RK			Vermejo
7/18/2003/1RK	188	80	Vermejo
7/18/2003/1RK	1	79	Vermejo
7/18/2003/1RK	170	84	Vermejo
7/18/2003/1RK	210	83	Vermejo
7/18/2003/1RK	184	83	Vermejo
7/18/2003/1RK	42	68	Vermejo
7/18/2003/1RK	27	70	Vermejo
7/18/2003/1RK	13	90	Vermejo
7/18/2003/1RK	12	90	Vermejo
7/18/2003/1RK	10	90	Vermejo
7/18/2003/1RK	183	80	Vermejo
	180	90	Vermejo
7/18/2003/1RK	177	90	Vermejo
7/18/2003/1RK	11	90	Vermejo
7/18/2003/1RK	14	90	Vermejo
7/18/2003/1RK	10	85	Vermejo
7/18/2003/1RK	12	90	Vermejo
7/18/2003/1RK	3	85	Vermejo
7/18/2003/1RK	17	90	Vermejo
7/18/2003/1RK	19	68	Vermejo
7/18/2003/1RK	173	90	Vermejo
7/18/2003/1RK	2	90	Vermejo
7/18/2003/1RK	0	90	Vermejo
7/18/2003/1RK	95	90	Vermejo
7/18/2003/1RK	108	88	Vermejo
7/18/2003/1RK	96	90	Vermejo
7/18/2003/1RK	89	90	Vermejo
7/18/2003/1RK	290	83	Vermejo
7/18/2003/1RK	89	89	Vermejo
7/18/2003/1RK	90	90	Vermejo
7/18/2003/1RK	87	89	Vermejo
7/18/2003/1RK	93	89	Vermejo
7/18/2003/1RK	87	90	Vermejo
7/18/2003/1RK	90	89	Vermejo
7/18/2003/1RK	87	88	Vermejo
7/18/2003/1RK	83	90	Vermejo
7/18/2003/1RK	278	88	Vermejo
7/18/2003/1RK	92	87	Vermejo

7/18/2003/1RK	87	88	Vermejo
7/18/2003/1RK	90	88	Vermejo
7/18/2003/1RK	358	88	Vermejo
7/18/2003/1RK	11	84	Vermejo
7/18/2003/1RK	9	90	Vermejo
7/18/2003/1RK	2	90	Vermejo
7/18/2003/1RK	18	80	Vermejo
7/18/2003/1RK	185	85	Vermejo
7/18/2003/1RK	8	70	Vermejo
7/18/2003/1RK	4	83	Vermejo
7/18/2003/1RK	357	85	Vermejo
7/18/2003/1RK	356	80	Vermejo
7/18/2003/1RK	174	90	Vermejo
7/18/2003/1RK	4	81	Vermejo
7/18/2003/1RK	21	90	Vermejo
7/18/2003/1RK	355	86	Vermejo
7/18/2003/1RK	172	90	Vermejo
7/18/2003/1RK	335	90	Vermejo
7/18/2003/1RK	349	90	Vermejo
7/18/2003/1RK	92	40	Vermejo
7/18/2003/1RK	85	60	Vermejo
7/18/2003/1RK	78	45	Vermejo
7/18/2003/1RK	70	65	Vermejo
7/18/2003/1RK	344	90	Vermejo
7/18/2003/1RK	93	90	Vermejo
7/18/2003/1RK	12	90	Vermejo
7/18/2003/1RK	110	90	Vermejo
7/18/2003/1RK	106	90	Vermejo
7/18/2003/1RK	108	90	Vermejo
7/18/2003/1RK	3	90	Vermejo
7/18/2003/1RK	105	90	Vermejo
7/18/2003/1RK	1	30	Vermejo
7/18/2003/1RK	356	35	Vermejo
7/18/2003/1RK	5	34	Vermejo
7/18/2003/1RK	328	50	Vermejo
7/18/2003/1RK	7	30	Vermejo
7/18/2003/1RK	30	42	Vermejo
7/18/2003/1RK	25	40	Vermejo
7/18/2003/1RK	348	50	Vermejo

Location ID: 7/18/2003/2Rk
Latitude: N 36.66943333
Longitude: W 104.85115

Van Bremmer Canyon

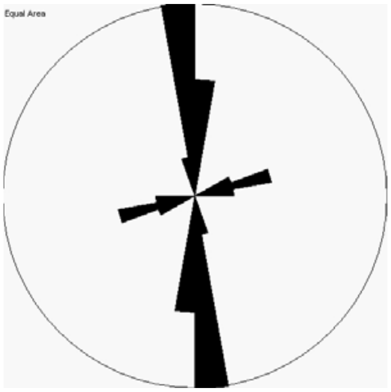

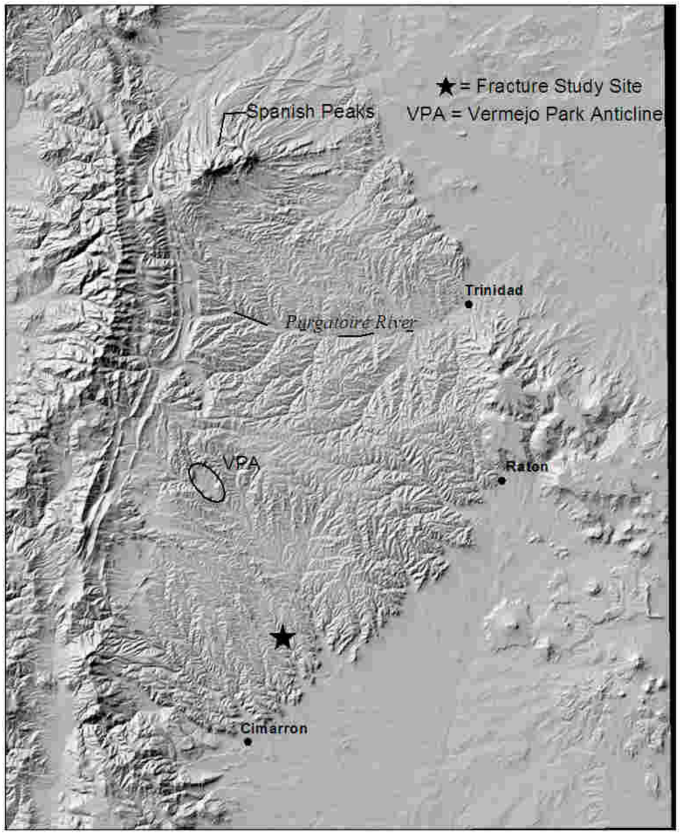

Notes:

Fracture Data:

ID	Strike	Dip	Formation	Comment 1
7/18/2003/2RK	170	29	Raton	
7/18/2003/2RK	1	50	Raton	
7/18/2003/2RK	180	28	Raton	
7/18/2003/2RK	345	50	Raton	
7/18/2003/2RK	1	44	Raton	
7/18/2003/2RK	354	25	Raton	flame structure
7/18/2003/2RK	350	29	Raton	
7/18/2003/2RK	350	44	Raton	
7/18/2003/2RK	265	25	Raton	
7/18/2003/2RK	355	55	Raton	
7/18/2003/2RK	242	75	Raton	
7/18/2003/2RK	256	75	Raton	
7/18/2003/2RK	256	65	Raton	

Location ID: 9/11/2002/2
Latitude: N 37.31316667
Longitude: W 104.6928333

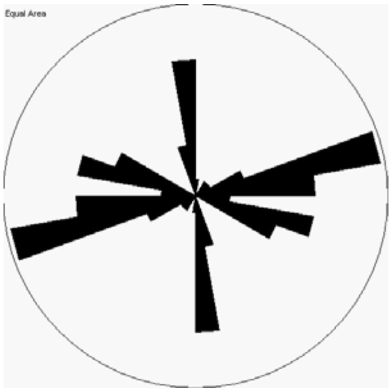

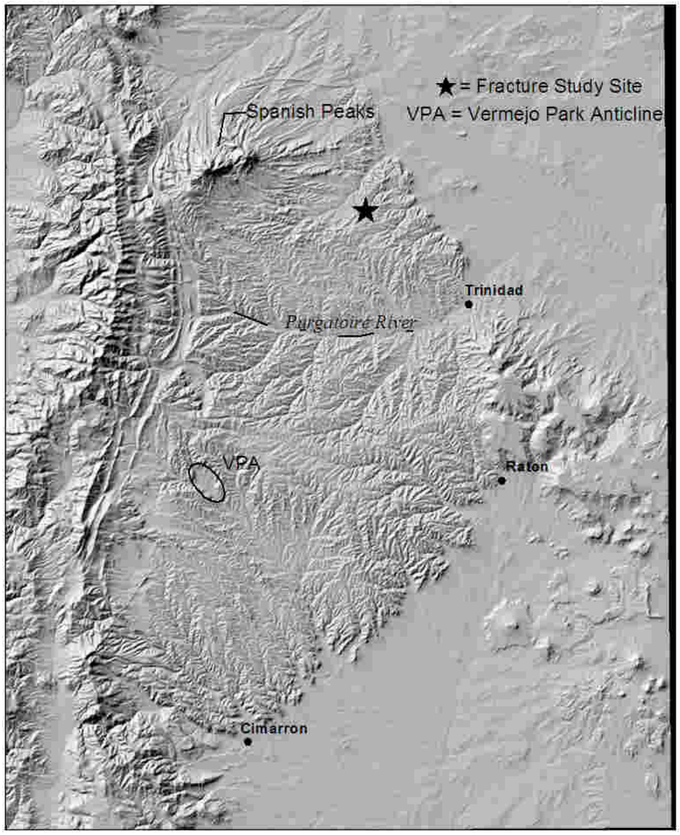

Notes:

Fracture Data:

ID	Strike	Dip	Formation
9/11/2002/2	252	90	Raton
9/11/2002/2	352	90	Raton
9/11/2002/2	350	90	Raton
9/11/2002/2	357	90	Raton
9/11/2002/2	48	90	Raton
9/11/2002/2	50	90	Raton
9/11/2002/2	76	90	Raton
9/11/2002/2	71	90	Raton
9/11/2002/2	101	90	Raton
9/11/2002/2	360	90	Raton
9/11/2002/2	87	90	Raton
9/11/2002/2	177	90	Raton
9/11/2002/2	107	90	Raton
9/11/2002/2	85	90	Raton
9/11/2002/2	109	90	Raton
9/11/2002/2	173	90	Raton
9/11/2002/2	90	90	Raton

9/11/2002/2	64	90	Raton
9/11/2002/2	111	90	Raton
9/11/2002/2	77	90	Raton
9/11/2002/2	113	90	Raton
9/11/2002/2	114	90	Raton
9/11/2002/2	79	90	Raton
9/11/2002/2	111	90	Raton
9/11/2002/2	81	90	Raton
9/11/2002/2	100	90	Raton
9/11/2002/2	348	90	Raton
9/11/2002/2	34	90	Raton
9/11/2002/2	350	90	Raton
9/11/2002/2	83	90	Raton
9/11/2002/2	108	90	Raton
9/11/2002/2	79	90	Raton
9/11/2002/2	69	90	Raton
9/11/2002/2	160	90	Raton
9/11/2002/2	83	90	Raton
9/11/2002/2	75	90	Raton
9/11/2002/2	73	90	Raton
9/11/2002/2	103	90	Raton
9/11/2002/2	187	90	Raton
9/11/2002/2	173	90	Raton
9/11/2002/2	70	90	Raton
9/11/2002/2	108	90	Raton
9/11/2002/2	77	90	Raton
9/11/2002/2	68	90	Raton
9/11/2002/2	81	90	Raton
9/11/2002/2	167	90	Raton
9/11/2002/2	97	90	Raton
9/11/2002/2	172	90	Raton
9/11/2002/2	83	90	Raton
9/11/2002/2	114	90	Raton
9/11/2002/2	71	90	Raton

Location ID: 9/11/2002/3
Latitude: N 37.31196667
Longitude: W 104.6947167

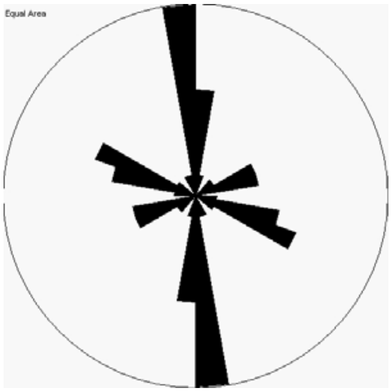

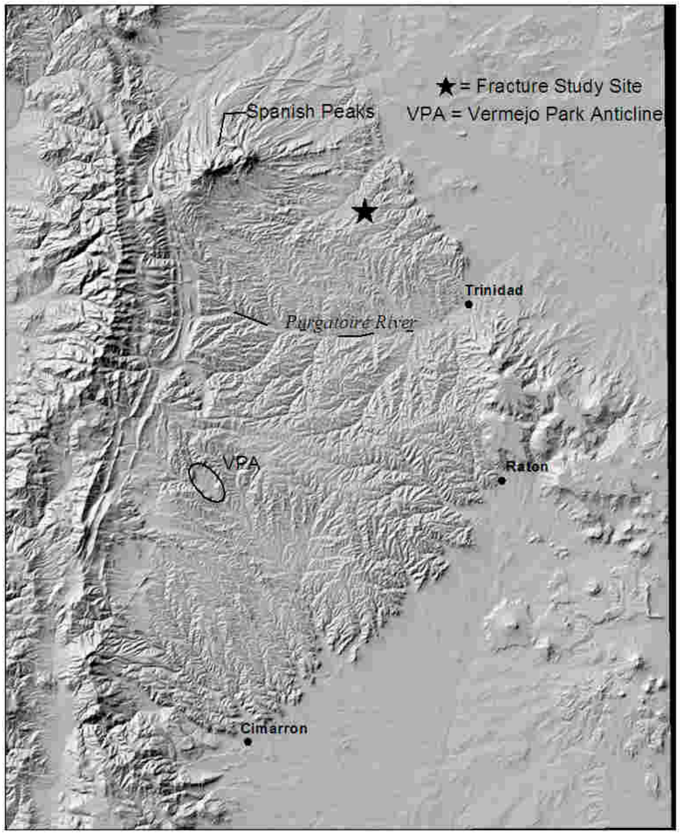

Notes:

Fracture Data:

ID	Strike	Dip	Formation	Comment 1
9/11/2002/3	357	90	unknown	
9/11/2002/3	1	90	unknown	
9/11/2002/3	334	90	unknown	
9/11/2002/3	59	90	unknown	
9/11/2002/3	68	90	unknown	
9/11/2002/3	46	90	unknown	
9/11/2002/3	358	90	unknown	
9/11/2002/3	62	90	unknown	
9/11/2002/3	350	90	unknown	
9/11/2002/3	70	90	unknown	
9/11/2002/3	98	90	unknown	
9/11/2002/3	357	90	unknown	
9/11/2002/3	102	90	unknown	
9/11/2002/3	107	90	unknown	
9/11/2002/3	292	90	unknown	
9/11/2002/3	356	90	unknown	
9/11/2002/3	309	90	unknown	

9/11/2002/3	293	90	unknown	
9/11/2002/3	5	90	unknown	
9/11/2002/3	113	90	unknown	
9/11/2002/3	351	90	unknown	across road in stream channel, thin bedded unit
9/11/2002/3	68	90	unknown	across road in stream channel, thin bedded unit
9/11/2002/3	359	90	unknown	across road in stream channel, thin bedded unit
9/11/2002/3	357	90	unknown	across road in stream channel, thin bedded unit
9/11/2002/3	2	90	unknown	across road in stream channel, thin bedded unit
9/11/2002/3	109	90	unknown	across road in stream channel, thin bedded unit
9/11/2002/3	112	90	unknown	across road in stream channel, thin bedded unit
9/11/2002/3	6	90	unknown	across road in stream channel, thin bedded unit
9/11/2002/3	2	90	unknown	across road in stream channel, thin bedded unit
9/11/2002/3	78	90	unknown	across road in stream channel, thin bedded unit
9/11/2002/3	113	90	unknown	across road in stream channel, thin bedded unit
9/11/2002/3	11	90	unknown	across road in stream channel, thin bedded unit
9/11/2002/3	77	90	unknown	across road in stream channel, thin bedded unit
9/11/2002/3	353	90	unknown	across road in stream channel, thin bedded unit
9/11/2002/3	349	90	unknown	across road in stream channel, thin bedded unit
9/11/2002/3	108	90	unknown	across road in stream channel, thin bedded unit

Location ID: 9/11/2002/5
Latitude: N 37.29438333
Longitude: W 104.8532333

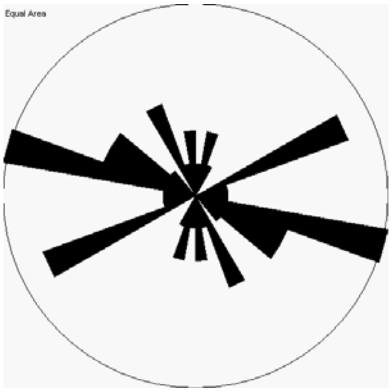

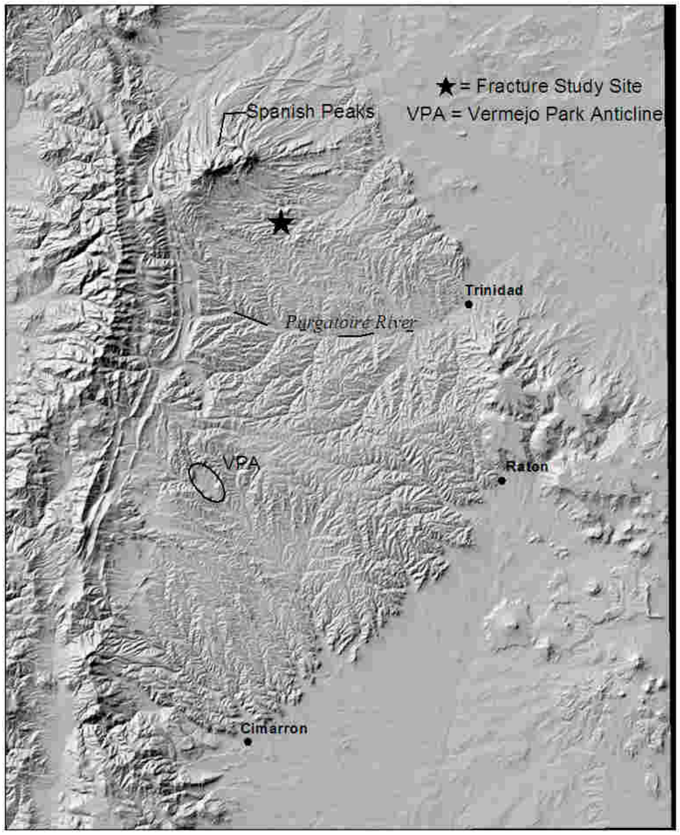

Notes:

Fracture Data:

ID	Strike	Dip	Formation
9/11/2002/5	103	90	Raton
9/11/2002/5	96	90	Raton
9/11/2002/5	122	90	Raton
9/11/2002/5	101	90	Raton
9/11/2002/5	82	90	Raton
9/11/2002/5	67	90	Raton
9/11/2002/5	352	90	Raton
9/11/2002/5	15	90	Raton
9/11/2002/5	62	90	Raton
9/11/2002/5	118	90	Raton
9/11/2002/5	125	90	Raton
9/11/2002/5	106	90	Raton
9/11/2002/5	157	90	Raton
9/11/2002/5	104	90	Raton
9/11/2002/5	70	90	Raton
9/11/2002/5	356	90	Raton
9/11/2002/5	67	90	Raton

9/11/2002/5	62	90	Raton
9/11/2002/5	342	90	Raton
9/11/2002/5	65	90	Raton
9/11/2002/5	334	90	Raton
9/11/2002/5	330	90	Raton
9/11/2002/5	17	90	Raton
9/11/2002/5	120	90	Raton
9/11/2002/5	104	90	Raton
9/11/2002/5	9	90	Raton
9/11/2002/5	113	90	Raton
9/11/2002/5	134	90	Raton
9/11/2002/5	115	90	Raton
9/11/2002/5	105	90	Raton
9/11/2002/5	22	90	Raton

Location ID: 9/12/2002/1
Latitude: N 36.5763
Longitude: W 104.9499167

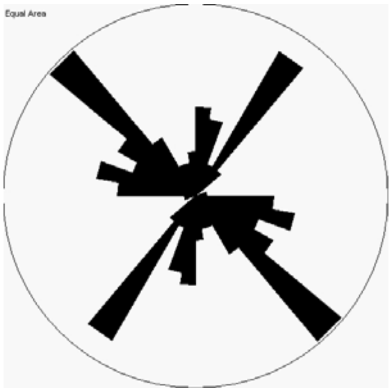

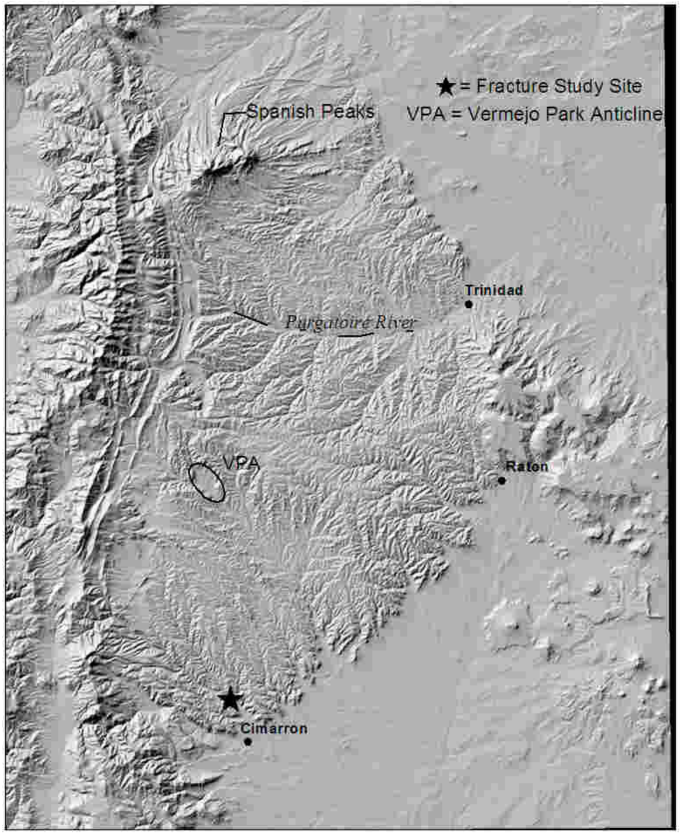

Notes:

Fracture Data:

ID	Strike	Dip	Formation	Comment 1	Comment 2
9/12/2002/1	216	15	Vermejo	Thrust	~5 m displacement
9/12/2002/1	122	90	Vermejo	away from thrust	Sandstone
9/12/2002/1	130	90	Vermejo	away from thrust	Sandstone
9/12/2002/1	31	90	Vermejo	away from thrust	Sandstone
9/12/2002/1	113	90	Vermejo	away from thrust	Sandstone
9/12/2002/1	47	90	Vermejo	away from thrust	Sandstone
9/12/2002/1	103	90	Vermejo	away from thrust	Sandstone
9/12/2002/1	30	90	Vermejo	away from thrust	Sandstone
9/12/2002/1	19	90	Vermejo	away from thrust	Sandstone
9/12/2002/1	22	90	Vermejo	away from thrust	Sandstone
9/12/2002/1	34	90	Vermejo	away from thrust	Sandstone
9/12/2002/1	110	90	Vermejo	away from thrust	Sandstone
9/12/2002/1	88	90	Vermejo	away from thrust	Sandstone
9/12/2002/1	99	90	Vermejo	away from thrust	Sandstone
9/12/2002/1	101	90	Vermejo	away from thrust	Sandstone
9/12/2002/1	114	90	Vermejo	away from thrust	Sandstone

9/12/2002/1	120	90	Vermejo	away from thrust	Sandstone
9/12/2002/1	105	90	Vermejo	away from thrust	Sandstone
9/12/2002/1	97	90	Vermejo	away from thrust	Sandstone
9/12/2002/1	100	90	Vermejo	away from thrust	Sandstone
9/12/2002/1	106	90	Vermejo	away from thrust	Sandstone
9/12/2002/1	142	90	Vermejo	away from thrust	Coal
9/12/2002/1	34	90	Vermejo	away from thrust	Coal
9/12/2002/1	39	90	Vermejo	away from thrust	Coal
9/12/2002/1	38	90	Vermejo	away from thrust	Coal
9/12/2002/1	42	90	Vermejo	away from thrust	Coal
9/12/2002/1	32	90	Vermejo	away from thrust	Coal
9/12/2002/1	30	90	Vermejo	away from thrust	Coal
9/12/2002/1	31	90	Vermejo	away from thrust	Coal
9/12/2002/1	28	90	Vermejo	away from thrust	Coal
9/12/2002/1	132	90	Vermejo	away from thrust	Coal
9/12/2002/1	130	90	Vermejo	away from thrust	Coal
9/12/2002/1	131	90	Vermejo	away from thrust	Coal
9/12/2002/1	132	90	Vermejo	away from thrust	Coal
9/12/2002/1	127	90	Vermejo	away from thrust	Coal
9/12/2002/1	173	90	Vermejo	away from thrust	Coal
9/12/2002/1	183	90	Vermejo	away from thrust	Coal
9/12/2002/1	184	90	Vermejo	away from thrust	Coal
9/12/2002/1	162	90	Vermejo	away from thrust	Coal
9/12/2002/1	176	90	Vermejo	away from thrust	Coal
9/12/2002/1	172	90	Vermejo	away from thrust	Coal
9/12/2002/1	179	90	Vermejo	away from thrust	Coal
9/12/2002/1	157	90	Vermejo	away from thrust	Coal
9/12/2002/1	156	90	Vermejo	away from thrust	Coal
9/12/2002/1	128	90	Vermejo	away from thrust	Coal
9/12/2002/1	137	90	Vermejo	away from thrust	Coal
9/12/2002/1	36	90	Vermejo	away from thrust	Coal
9/12/2002/1	33	90	Vermejo	away from thrust	Coal
9/12/2002/1	31	90	Vermejo	away from thrust	Coal
9/12/2002/1	33	90	Vermejo	away from thrust	Coal
9/12/2002/1	138	90	Vermejo	away from thrust	Coal
9/12/2002/1	140	90	Vermejo	away from thrust	Coal
9/12/2002/1	169	90	Vermejo	away from thrust	Coal
9/12/2002/1	182	90	Vermejo	away from thrust	Coal
9/12/2002/1	130	90	Vermejo	away from thrust	Coal
9/12/2002/1	133	90	Vermejo	away from thrust	Coal
9/12/2002/1	150	90	Vermejo	away from thrust	Coal
9/12/2002/1	40	90	Vermejo	away from thrust	Coal
9/12/2002/1	139	90	Vermejo	away from thrust	Coal
9/12/2002/1	188	90	Vermejo	away from thrust	Coal
9/12/2002/1	133	90	Vermejo	away from thrust	Coal
9/12/2002/1	18	90	Vermejo	away from thrust	Coal
9/12/2002/1	95	90	Vermejo	near fault, 5 m either side	Sandstone
9/12/2002/1	95	90	Vermejo	near fault, 5 m either side	Sandstone
9/12/2002/1	96	90	Vermejo	near fault, 5 m either side	Sandstone
9/12/2002/1	104	90	Vermejo	near fault, 5 m either side	Sandstone

9/12/2002/1	100	90	Vermejo	near fault, 5 m either side	Sandstone
9/12/2002/1	106	90	Vermejo	near fault, 5 m either side	Sandstone
9/12/2002/1	19	90	Vermejo	near fault, 5 m either side	Sandstone
9/12/2002/1	92	90	Vermejo	near fault, 5 m either side	Sandstone
9/12/2002/1	109	90	Vermejo	near fault, 5 m either side	Sandstone
9/12/2002/1	117	90	Vermejo	near fault, 5 m either side	Sandstone
9/12/2002/1	98	90	Vermejo	near fault, 5 m either side	Sandstone
9/12/2002/1	122	90	Vermejo	near fault, 5 m either side	Sandstone
9/12/2002/1	113	90	Vermejo	near fault, 5 m either side	Sandstone
9/12/2002/1	76	90	Vermejo	near fault, 5 m either side	Sandstone
9/12/2002/1	30	90	Vermejo	near fault, 5 m either side	Sandstone
9/12/2002/1	122	90	Vermejo	near fault, 5 m either side	Sandstone
9/12/2002/1	118	90	Vermejo	near fault, 5 m either side	Sandstone
9/12/2002/1	142	90	Vermejo	near fault, 5 m either side	Coal
9/12/2002/1	143	90	Vermejo	near fault, 5 m either side	Coal
9/12/2002/1	136	90	Vermejo	near fault, 5 m either side	Coal
9/12/2002/1	168	90	Vermejo	near fault, 5 m either side	Coal
9/12/2002/1	145	90	Vermejo	near fault, 5 m either side	Coal
9/12/2002/1	137	90	Vermejo	near fault, 5 m either side	Coal
9/12/2002/1	143	90	Vermejo	near fault, 5 m either side	Coal
9/12/2002/1	136	90	Vermejo	near fault, 5 m either side	Coal
9/12/2002/1	21	90	Vermejo	near fault, 5 m either side	Coal
9/12/2002/1	13	90	Vermejo	near fault, 5 m either side	Coal
9/12/2002/1	19	90	Vermejo	near fault, 5 m either side	Coal
9/12/2002/1	18	90	Vermejo	near fault, 5 m either side	Coal
9/12/2002/1	129	90	Vermejo	near fault, 5 m either side	Coal
9/12/2002/1	122	90	Vermejo	near fault, 5 m either side	Coal
9/12/2002/1	9	90	Vermejo	near fault, 5 m either side	Coal
9/12/2002/1	10	90	Vermejo	near fault, 5 m either side	Coal
9/12/2002/1	5	90	Vermejo	near fault, 5 m either side	Coal
9/12/2002/1	5	90	Vermejo	near fault, 5 m either side	Coal
9/12/2002/1	2	90	Vermejo	near fault, 5 m either side	Coal
9/12/2002/1	132	90	Vermejo	near fault, 5 m either side	Coal
9/12/2002/1	133	90	Vermejo	near fault, 5 m either side	Coal
9/12/2002/1	134	90	Vermejo	near fault, 5 m either side	Coal

Location ID: 9/12/2002/2
Latitude: N 36.58648333
Longitude: W 104.9785333

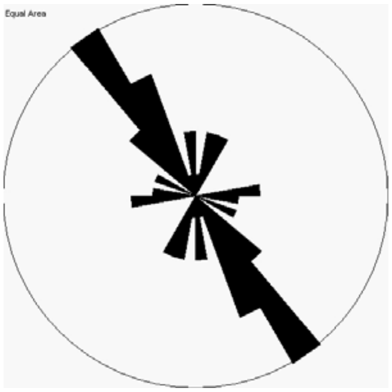

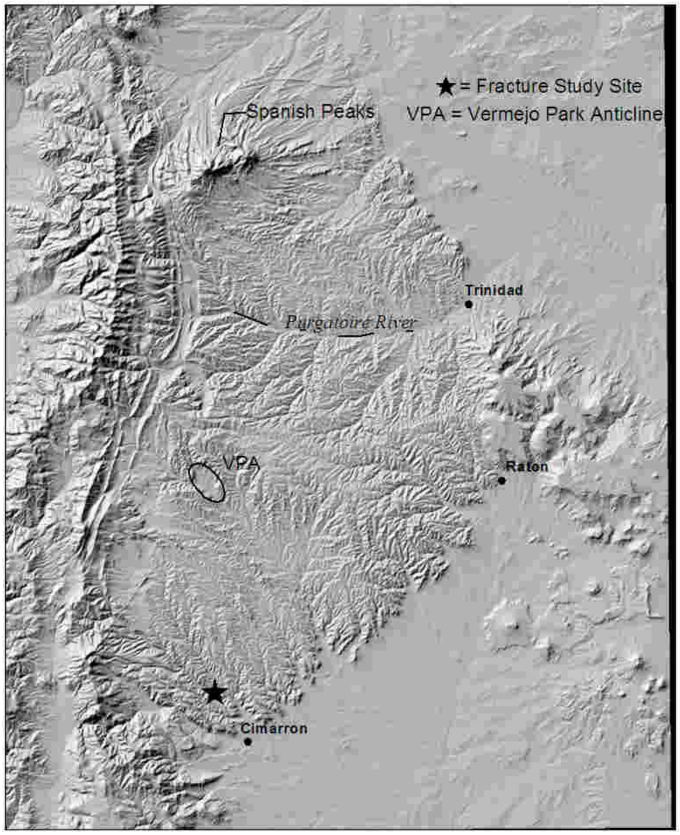

Notes:

Fracture Data:

ID	Strike	Dip	Formation	Comment 1
9/12/2002/2	134	90	Unknown	LL
9/12/2002/2	86	90	Unknown	
9/12/2002/2	22	90	Unknown	
9/12/2002/2	28	90	Unknown	RL
9/12/2002/2	10	90	Unknown	
9/12/2002/2	98	90	Unknown	RL
9/12/2002/2	138	90	Unknown	LL
9/12/2002/2	110	90	Unknown	RL
9/12/2002/2	87	90	Unknown	RL
9/12/2002/2	88	90	Unknown	RL
9/12/2002/2	147	90	Unknown	LL
9/12/2002/2	138	90	Unknown	LL
9/12/2002/2	138	90	Unknown	LL
9/12/2002/2	141	90	Unknown	LL
9/12/2002/2	160	90	Unknown	LL
9/12/2002/2	5	90	Unknown	

9/12/2002/2	153	90	Unknown	LL
9/12/2002/2	142	90	Unknown	LL
9/12/2002/2	149	90	Unknown	LL
9/12/2002/2	117	90	Unknown	RL
9/12/2002/2	145	90	Unknown	LL
9/12/2002/2	150	90	Unknown	
9/12/2002/2	142	90	Unknown	LL
9/12/2002/2	153	90	Unknown	
9/12/2002/2	150	90	Unknown	LL
9/12/2002/2	20	90	Unknown	
9/12/2002/2	143	90	Unknown	LL
9/12/2002/2	97	90	Unknown	RL
9/12/2002/2	156	90	Unknown	LL
9/12/2002/2	19	90	Unknown	
9/12/2002/2	148	90	Unknown	LL
9/12/2002/2	16	90	Unknown	
9/12/2002/2	352	90	Unknown	
9/12/2002/2	355	90	Unknown	
9/12/2002/2	150	90	Unknown	LL
9/12/2002/2	353	90	Unknown	
9/12/2002/2	143	90	Unknown	LL

Location ID: 9/12/2002/3
Latitude: N 36.78598333
Longitude: W 105.1858667

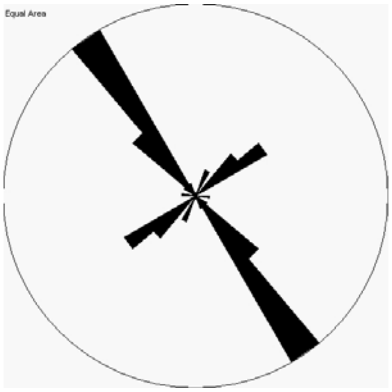

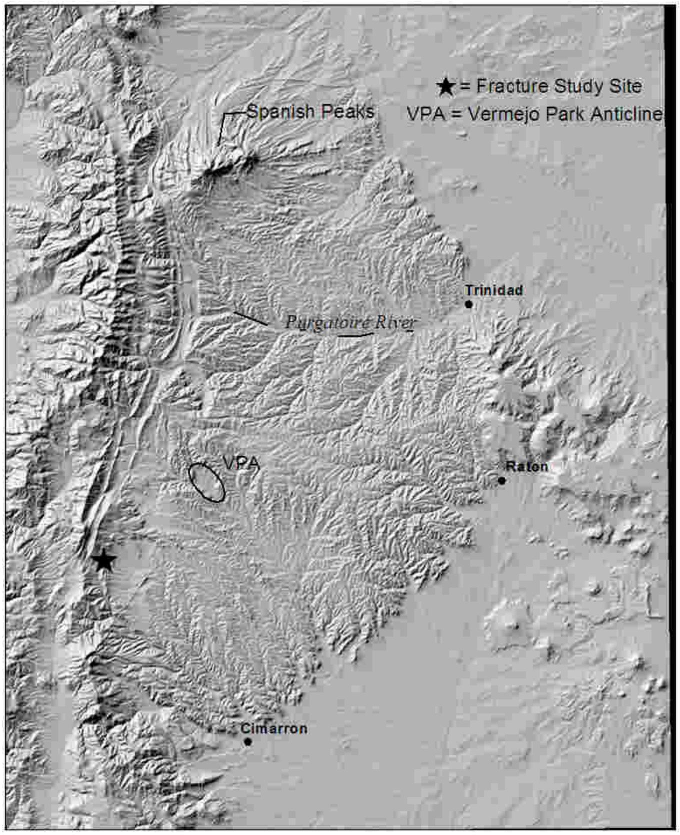

Notes:

Fracture Data:

ID	Strike	Dip	Formation
9/12/2002/3	145	90	Poison Canyon
9/12/2002/3	142	90	Poison Canyon
9/12/2002/3	147	90	Poison Canyon
9/12/2002/3	58	90	Poison Canyon
9/12/2002/3	147	90	Poison Canyon
9/12/2002/3	41	90	Poison Canyon
9/12/2002/3	97	90	Poison Canyon
9/12/2002/3	142	90	Poison Canyon
9/12/2002/3	137	90	Poison Canyon
9/12/2002/3	141	90	Poison Canyon
9/12/2002/3	145	90	Poison Canyon
9/12/2002/3	53	90	Poison Canyon
9/12/2002/3	147	90	Poison Canyon
9/12/2002/3	138	90	Poison Canyon
9/12/2002/3	146	90	Poison Canyon
9/12/2002/3	127	90	Poison Canyon
9/12/2002/3	25	90	Poison Canyon

9/12/2002/3	25	90	Poison Canyon
9/12/2002/3	139	90	Poison Canyon
9/12/2002/3	141	90	Poison Canyon
9/12/2002/3	143	90	Poison Canyon
9/12/2002/3	142	90	Poison Canyon
9/12/2002/3	141	90	Poison Canyon
9/12/2002/3	47	90	Poison Canyon
9/12/2002/3	145	90	Poison Canyon
9/12/2002/3	158	90	Poison Canyon
9/12/2002/3	47	90	Poison Canyon
9/12/2002/3	137	90	Poison Canyon
9/12/2002/3	136	90	Poison Canyon
9/12/2002/3	59	90	Poison Canyon
9/12/2002/3	57	90	Poison Canyon
9/12/2002/3	51	90	Poison Canyon
9/12/2002/3	53	90	Poison Canyon
9/12/2002/3	139	90	Poison Canyon
9/12/2002/3	48	90	Poison Canyon

Location ID: 9/12/2002/4
Latitude: N 36.77965
Longitude: W 105.1738333

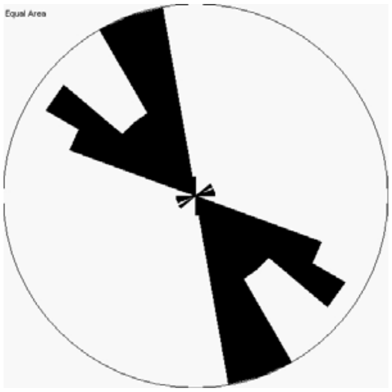

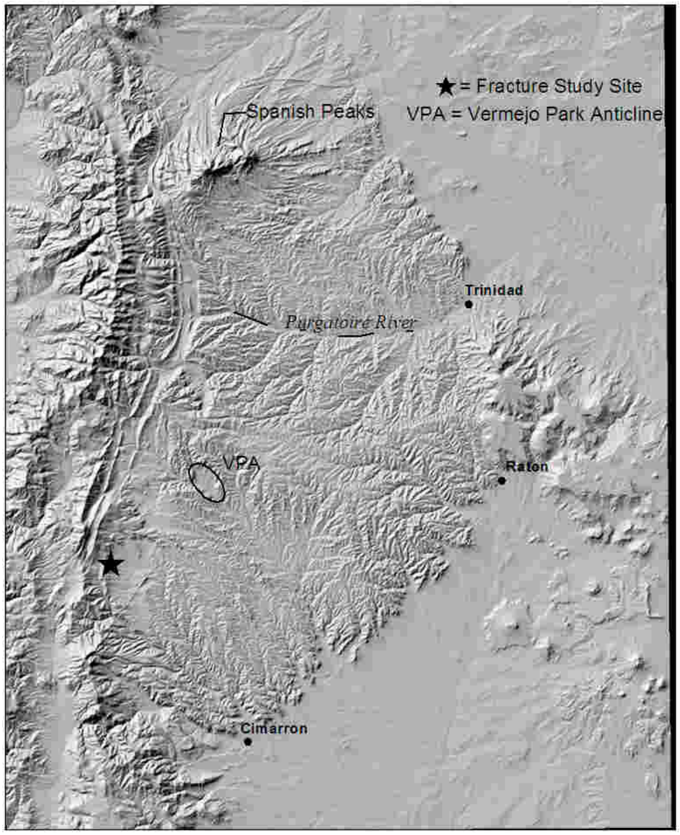

Notes:

Fracture Data:

ID	Strike	Dip	Formation	Comment 1
9/12/2002/4	152	90	Poison Canyon	LL
9/12/2002/4	128	90	Poison Canyon	RL
9/12/2002/4	114	90	Poison Canyon	
9/12/2002/4	164	90	Poison Canyon	
9/12/2002/4	168	90	Poison Canyon	
9/12/2002/4	148	90	Poison Canyon	
9/12/2002/4	122	90	Poison Canyon	
9/12/2002/4	58	90	Poison Canyon	
9/12/2002/4	130	90	Poison Canyon	
9/12/2002/4	152	90	Poison Canyon	
9/12/2002/4	131	90	Poison Canyon	
9/12/2002/4	144	90	Poison Canyon	
9/12/2002/4	153	90	Poison Canyon	
9/12/2002/4	132	90	Poison Canyon	
9/12/2002/4	152	90	Poison Canyon	
9/12/2002/4	153	90	Poison Canyon	

9/12/2002/4	78	90	Poison Canyon	
9/12/2002/4	160	90	Poison Canyon	
9/12/2002/4	154	90	Poison Canyon	
9/12/2002/4	162	90	Poison Canyon	
9/12/2002/4	85	90	Poison Canyon	
9/12/2002/4	167	90	Poison Canyon	
9/12/2002/4	120	90	Poison Canyon	
9/12/2002/4	161	90	Poison Canyon	
9/12/2002/4	115	90	Poison Canyon	LL
9/12/2002/4	161	90	Poison Canyon	
9/12/2002/4	161	90	Poison Canyon	LL
9/12/2002/4	116	90	Poison Canyon	LL
9/12/2002/4	116	90	Poison Canyon	LL
9/12/2002/4	126	90	Poison Canyon	
9/12/2002/4	160	90	Poison Canyon	
9/12/2002/4	149	90	Poison Canyon	LL
9/12/2002/4	121	90	Poison Canyon	
9/12/2002/4	120	90	Poison Canyon	
9/12/2002/4	145	90	Poison Canyon	
9/12/2002/4	118	90	Poison Canyon	
9/12/2002/4	174	90	Poison Canyon	
9/12/2002/4	153	90	Poison Canyon	LL
9/12/2002/4	151	90	Poison Canyon	LL
9/12/2002/4	122	90	Poison Canyon	
9/12/2002/4	121	90	Poison Canyon	LL
9/12/2002/4	111	90	Poison Canyon	LL
9/12/2002/4	145	90	Poison Canyon	LL
9/12/2002/4	114	90	Poison Canyon	LL
9/12/2002/4	138	90	Poison Canyon	LL
9/12/2002/4	158	90	Poison Canyon	LL
9/12/2002/4	128	90	Poison Canyon	LL
9/12/2002/4	162	90	Poison Canyon	LL
9/12/2002/4	132	90	Poison Canyon	LL
9/12/2002/4	150	90	Poison Canyon	LL

Location ID: 9/13/2002/1
Latitude: N 36.97386667
Longitude: W 104.3817

Sugarite

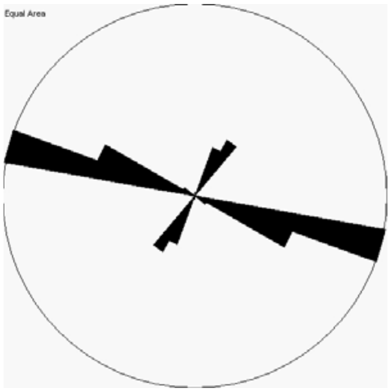

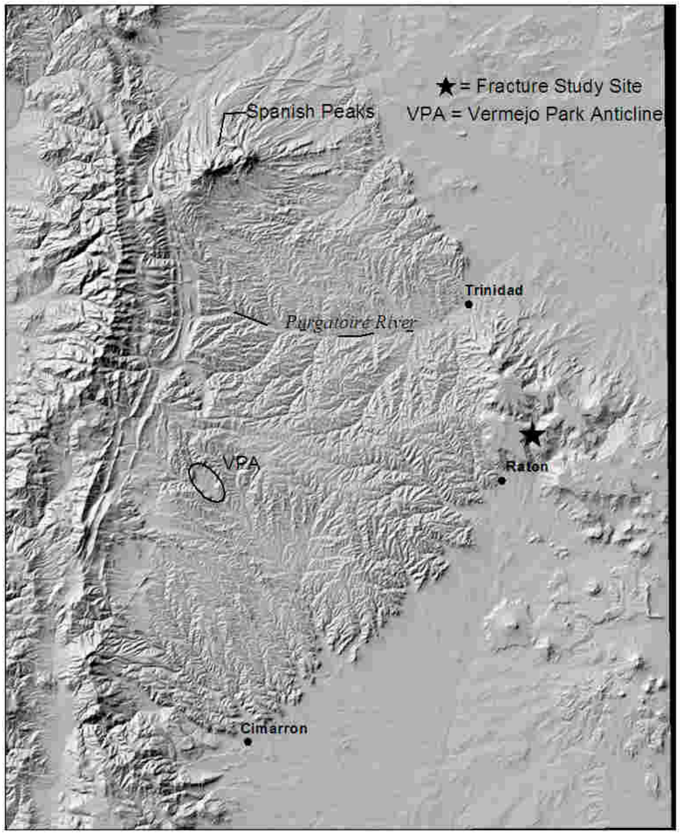

Notes:

Fracture Data:

ID	Strike	Dip	Formation	Comment 1
9/13/2003/1	108	90	Vermejo	
9/13/2003/1	107	90	Vermejo	
9/13/2003/1	28	90	Vermejo	RL
9/13/2003/1	115	90	Vermejo	
9/13/2003/1	30	90	Vermejo	
9/13/2003/1	32	90	Vermejo	
9/13/2003/1	120	90	Vermejo	
9/13/2003/1	27	90	Vermejo	
9/13/2003/1	103	90	Vermejo	
9/13/2003/1	106	90	Vermejo	
9/13/2003/1	108	90	Vermejo	
9/13/2003/1	34	90	Vermejo	
9/13/2003/1	103	90	Vermejo	
9/13/2003/1	105	90	Vermejo	
9/13/2003/1	111	90	Vermejo	
9/13/2003/1	31	90	Vermejo	
9/13/2003/1	106	90	Vermejo	

9/13/2003/1	25	90	Vermejo
9/13/2003/1	104	90	Vermejo
9/13/2003/1	119	90	Vermejo
9/13/2003/1	103	90	Vermejo
9/13/2003/1	110	90	Vermejo
9/13/2003/1	111	90	Vermejo
9/13/2003/1	104	90	Vermejo
9/13/2003/1	31	90	Vermejo
9/13/2003/1	106	90	Vermejo
9/13/2003/1	110	90	Vermejo
9/13/2003/1	108	90	Vermejo
9/13/2003/1	110	90	Vermejo
9/13/2003/1	29	90	Vermejo
9/13/2003/1	105	90	Vermejo
9/13/2003/1	110	90	Vermejo
9/13/2003/1	103	90	Vermejo

Location ID: 9/13/2002/2
Latitude: N 36.9835
Longitude: W 104.3720667

Lake Maloya spillway

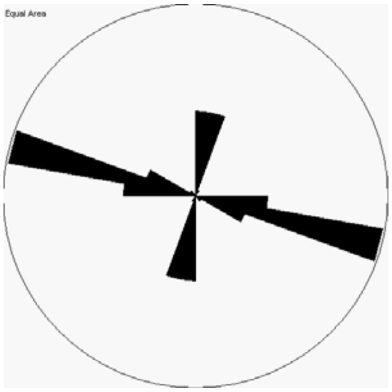

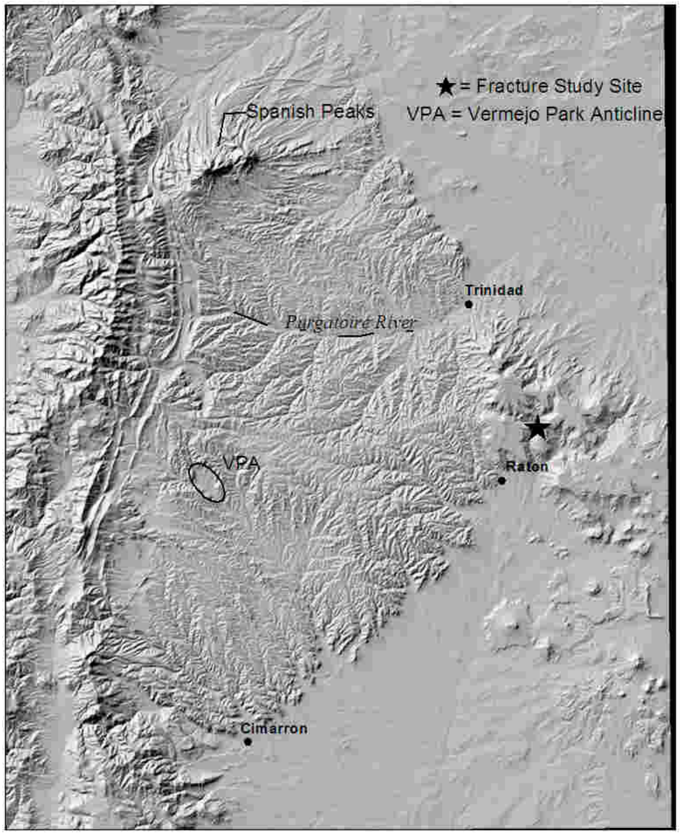

Notes:

Fracture Data:

ID	Strike	Dip	Formation	Comment 1
9/13/2002/2	110	90	Raton	Sandstone
9/13/2002/2	105	90	Raton	Sandstone
9/13/2002/2	109	90	Raton	Sandstone
9/13/2002/2	108	90	Raton	Sandstone
9/13/2002/2	108	90	Raton	Sandstone
9/13/2002/2	110	90	Raton	Sandstone
9/13/2002/2	114	90	Raton	Sandstone
9/13/2002/2	104	90	Raton	Sandstone
9/13/2002/2	104	90	Raton	Sandstone
9/13/2002/2	105	90	Raton	Sandstone
9/13/2002/2	111	90	Raton	Sandstone
9/13/2002/2	106	90	Raton	Sandstone
9/13/2002/2	109	90	Raton	Sandstone
9/13/2002/2	16	90	Raton	Sandstone
9/13/2002/2	97	90	Raton	Sandstone
9/13/2002/2	111	90	Raton	Sandstone

9/13/2002/2	100	90	Raton	Sandstone
9/13/2002/2	101	90	Raton	Sandstone
9/13/2002/2	104	90	Raton	Sandstone
9/13/2002/2	100	90	Raton	Sandstone
9/13/2002/2	110	90	Raton	Sandstone
9/13/2002/2	120	90	Raton	Sandstone
9/13/2002/2	111	90	Raton	Sandstone
9/13/2002/2	112	90	Raton	Sandstone
9/13/2002/2	100	90	Raton	Sandstone
9/13/2002/2	30	90	Raton	Sandstone
9/13/2002/2	97	90	Raton	Sandstone
9/13/2002/2	102	90	Raton	Coal
9/13/2002/2	109	90	Raton	Coal
9/13/2002/2	106	90	Raton	Coal
9/13/2002/2	107	90	Raton	Coal
9/13/2002/2	103	90	Raton	Coal
9/13/2002/2	103	90	Raton	Coal
9/13/2002/2	106	90	Raton	Coal
9/13/2002/2	105	90	Raton	Coal
9/13/2002/2	136	90	Raton	Coal
9/13/2002/2	100	90	Raton	Coal
9/13/2002/2	99	90	Raton	Coal
9/13/2002/2	98	90	Raton	Coal
9/13/2002/2	98	90	Raton	Coal
9/13/2002/2	99	90	Raton	Coal
9/13/2002/2	101	90	Raton	Coal
9/13/2002/2	102	90	Raton	Coal
9/13/2002/2	102	90	Raton	Coal
9/13/2002/2	101	90	Raton	Coal
9/13/2002/2	99	90	Raton	Coal
9/13/2002/2	99	90	Raton	Coal
9/13/2002/2	99	90	Raton	Coal
9/13/2002/2	97	90	Raton	Coal
9/13/2002/2	99	90	Raton	Coal
9/13/2002/2	102	90	Raton	Coal
9/13/2002/2	101	90	Raton	Coal
9/13/2002/2	8	90	Raton	Coal
9/13/2002/2	11	90	Raton	Coal
9/13/2002/2	10	90	Raton	Coal
9/13/2002/2	12	90	Raton	Coal
9/13/2002/2	7	90	Raton	Coal
9/13/2002/2	14	90	Raton	Coal
9/13/2002/2	9	90	Raton	Coal
9/13/2002/2	10	90	Raton	Coal
9/13/2002/2	9	90	Raton	Coal
9/13/2002/2	7	90	Raton	Coal
9/13/2002/2	4	90	Raton	Coal
9/13/2002/2	6	90	Raton	Coal
9/13/2002/2	5	90	Raton	Coal
9/13/2002/2	13	90	Raton	Coal

9/13/2002/2	7	90	Raton	Coal
9/13/2002/2	10	90	Raton	Coal
9/13/2002/2	8	90	Raton	Coal
9/13/2002/2	11	90	Raton	Coal
9/13/2002/2	10	90	Raton	Coal
9/13/2002/2	11	90	Raton	Coal
9/13/2002/2	12	90	Raton	Coal
9/13/2002/2	4	90	Raton	Coal
9/13/2002/2	9	90	Raton	Coal
9/13/2002/2	9	90	Raton	Coal
9/13/2002/2	11	90	Raton	Coal

Location ID: Maxwell
Latitude: N 36.59137
Longitude: W 104.35306

Niobrara LS East of Maxwell, road pavement

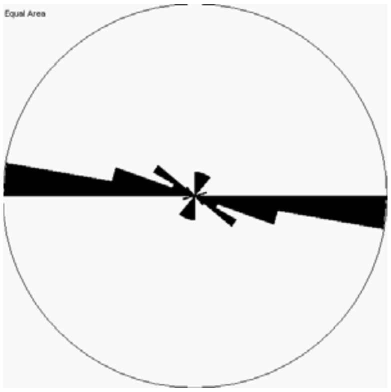

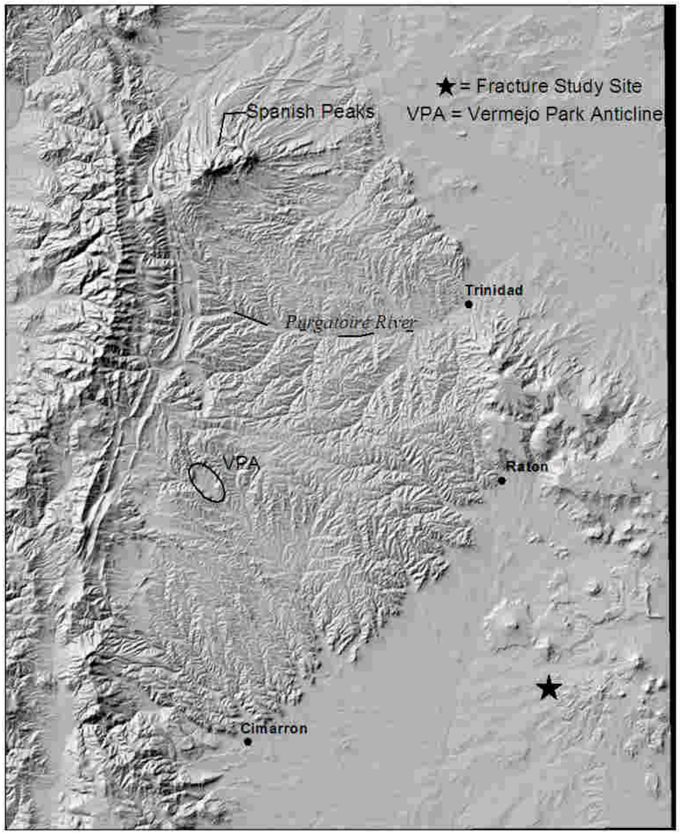

Notes:

Fracture Data:

ID	Strike	Dip	Formation	Comment 1
Maxwell	103	90	Niobrara	
Maxwell	92	90	Niobrara	
Maxwell	93	90	Niobrara	
Maxwell	119	90	Niobrara	
Maxwell	96	90	Niobrara	
Maxwell	96	90	Niobrara	
Maxwell	104	90	Niobrara	
Maxwell	127	90	Niobrara	
Maxwell	13	90	Niobrara	
Maxwell	21	90	Niobrara	
Maxwell	97	90	Niobrara	
Maxwell	104	90	Niobrara	
Maxwell	100	90	Niobrara	
Maxwell	99	90	Niobrara	
Maxwell	91	90	Niobrara	
Maxwell	90	90	Niobrara	

Maxwell	33	90	Niobrara	
Maxwell	130	90	Niobrara	
Maxwell	94	90	Niobrara	
Maxwell	95	90	Niobrara	
Maxwell	18	90	Niobrara	
Maxwell	96	90	Niobrara	
Maxwell	97	90	Niobrara	
Maxwell	93	90	Niobrara	
Maxwell	8	90	Niobrara	
Maxwell	105	90	Niobrara	
Maxwell	120	90	Niobrara	
Maxwell	74	90	Niobrara	
Maxwell	99	90	Niobrara	
Maxwell	100	90	Niobrara	
Maxwell	120	90	Niobrara	
Maxwell	126	90	Niobrara	
Maxwell	22	90	Niobrara	
Maxwell	93	90	Niobrara	
Maxwell	96	90	Niobrara	youngest
Maxwell	7	90	Niobrara	
Maxwell	30	90	Niobrara	
Maxwell	112	90	Niobrara	
Maxwell	102	90	Niobrara	

Location ID: RK1
Latitude: N 36.93011667
Longitude: W 105.0189833

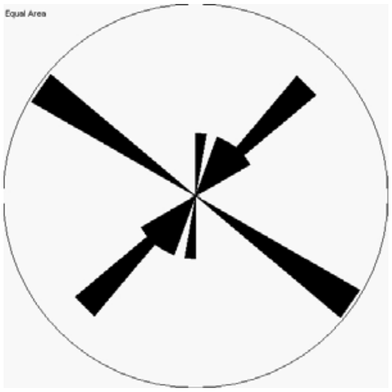

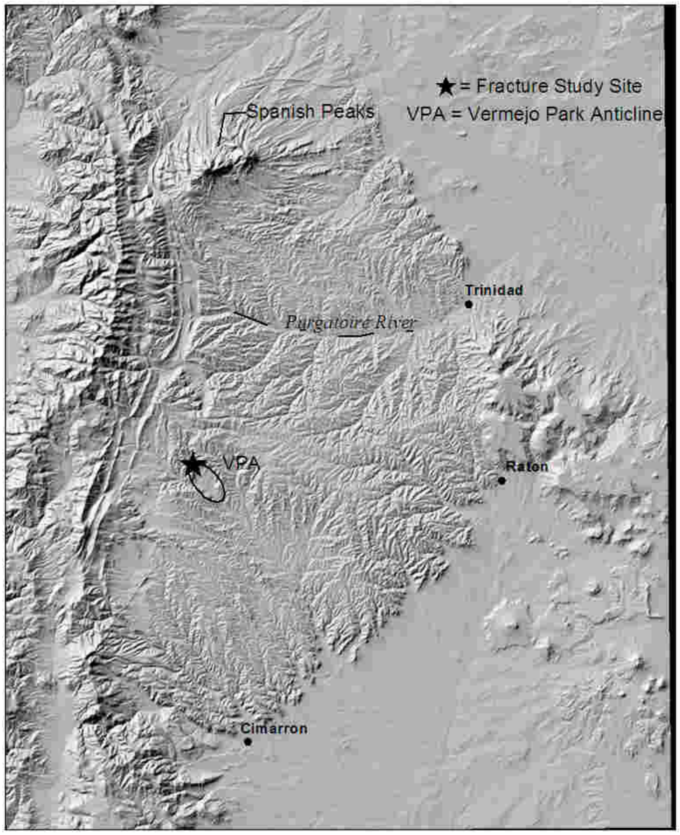

Notes:

Fracture Data:

ID	Strike	Dip	Formation
RK1	28	53	Raton
RK1	51	54	Raton
RK1	35	75	Raton
RK1	31	70	Raton
RK1	48	62	Raton
RK1	4	78	Raton
RK1	8	77	Raton
RK1	42	42	Raton
RK1	56	62	Raton
RK1	48	62	Raton
RK1	41	82	Raton
RK1	203	86	Raton
RK1	123	88	Raton
RK1	127	80	Raton
RK1	128	86	Raton
RK1	127	88	Raton
RK1	123	84	Raton

RK1	125	88	Raton
RK1	48	65	Raton

Location ID: RK2
Latitude: N 36.92536667
Longitude: W 104.9926333

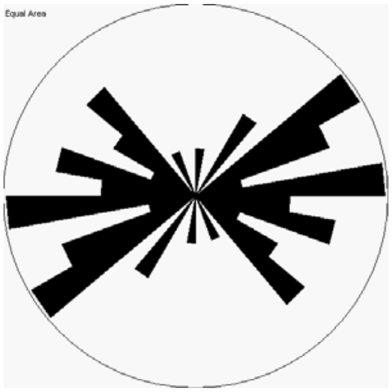

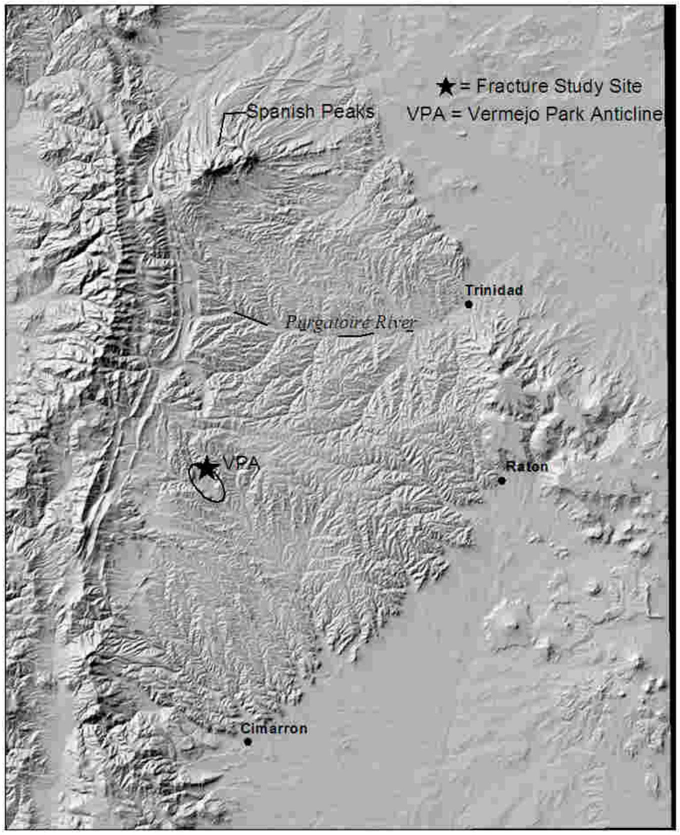

Notes:

Fracture Data:

ID	Strike	Dip	Formation
RK2	130	88	Trinidad
RK2	131	90	Trinidad
RK2	124	90	Trinidad
RK2	126	90	Trinidad
RK2	62	78	Trinidad
RK2	85	90	Trinidad
RK2	238	80	Trinidad
RK2	247	87	Trinidad
RK2	104	90	Trinidad
RK2	282	88	Trinidad
RK2	56	85	Trinidad
RK2	58	82	Trinidad
RK2	37	90	Trinidad
RK2	33	87	Trinidad
RK2	316	78	Trinidad
RK2	81	88	Trinidad
RK2	186	85	Trinidad

RK2	65	90	Trinidad
RK2	262	85	Trinidad
RK2	83	90	Trinidad
RK2	76	90	Trinidad
RK2	298	87	Trinidad
RK2	339	90	Trinidad
RK2	93	90	Trinidad
RK2	59	90	Trinidad
RK2	103	90	Trinidad
RK2	90	90	Trinidad

Location ID: RK3
Latitude: N 36.92548333
Longitude: W 104.99155

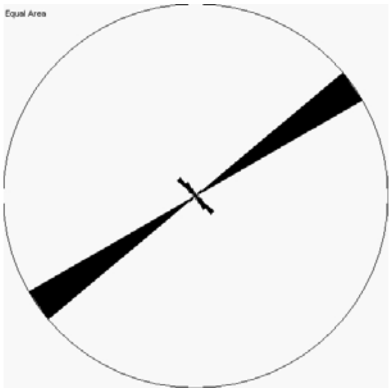

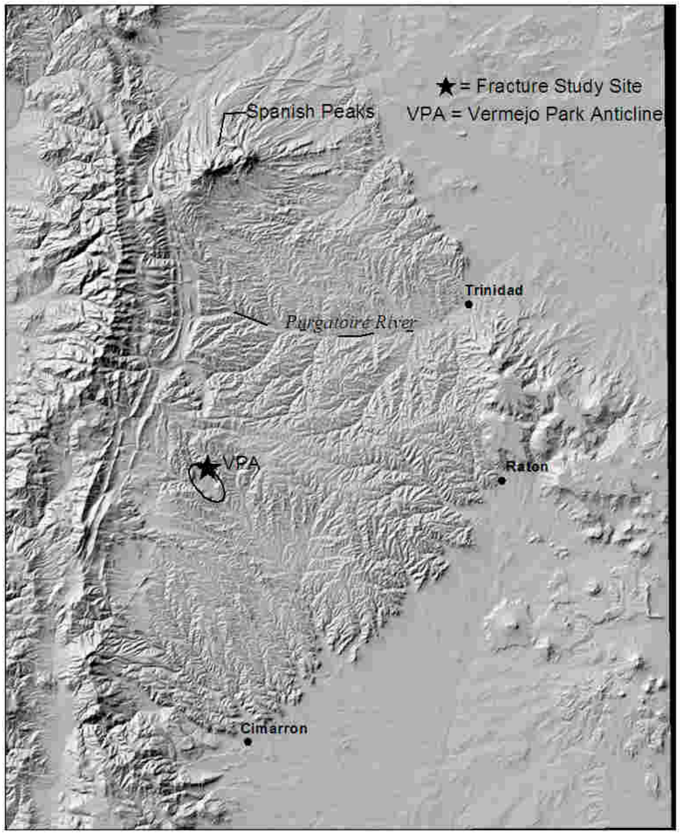

Notes:

Fracture Data:

ID	Strike	Dip	Formation	Comment 1
RK3	53	80	Trinidad	
RK3	54	80	Trinidad	
RK3	55	80	Trinidad	
RK3	54	80	Trinidad	
RK3	54	80	Trinidad	
RK3	52	80	Trinidad	
RK3	51	80	Trinidad	
RK3	53	80	Trinidad	
RK3	55	80	Trinidad	
RK3	56	80	Trinidad	
RK3	55	80	Trinidad	
RK3	55	80	Trinidad	
RK3	54	80	Trinidad	
RK3	53	80	Trinidad	
RK3	50	80	Trinidad	
RK3	58	80	Trinidad	
RK3	47	80	Trinidad	

RK3	50	80	Trinidad	
RK3	53	80	Trinidad	
RK3	52	80	Trinidad	
RK3	53	80	Trinidad	
RK3	54	80	Trinidad	
RK3	57	80	Trinidad	
RK3	56	80	Trinidad	
RK3	51	80	Trinidad	
RK3	148	88	Trinidad	
RK3	309	85	Trinidad	terminates against 58 degree set
RK3	138	86	Trinidad	terminates against 58 degree set
RK3	328	90	Trinidad	terminates against 58 degree set
RK3	312	90	Trinidad	terminates against 58 degree set
RK3	335	90	Trinidad	terminates against 58 degree set
RK3	135	85	Trinidad	terminates against 58 degree set

Location ID: RK4
Latitude: N 36.91711667
Longitude: W 104.9821

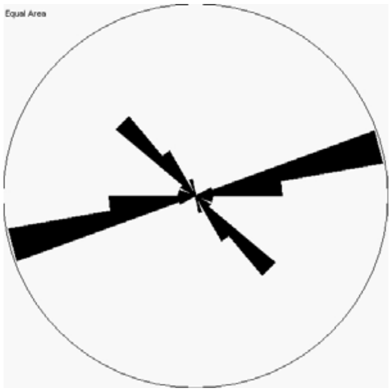

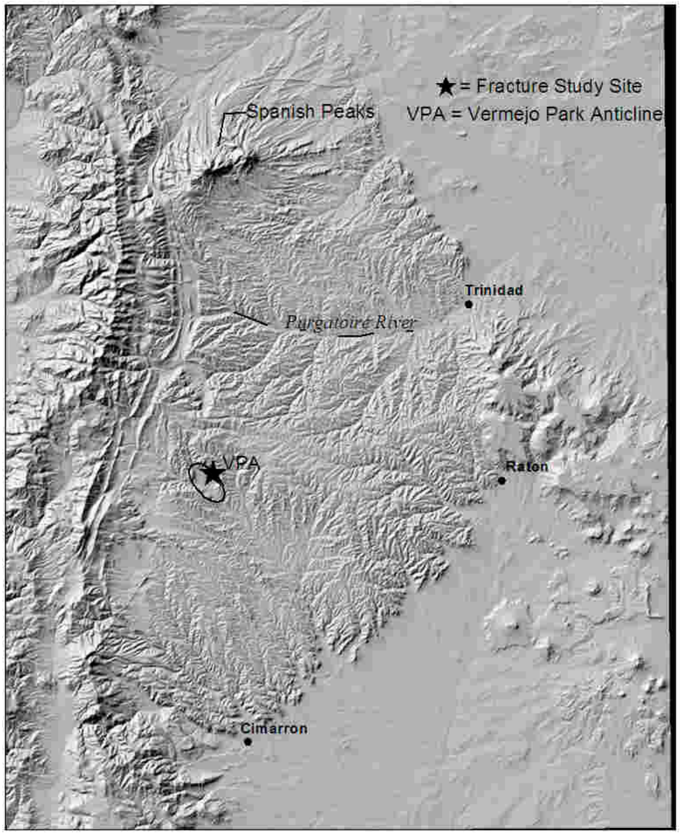

Notes:

Fracture Data:

ID	Strike	Dip	Formation
RK4	78	79	Trinidad
RK4	286	86	Trinidad
RK4	79	72	Trinidad
RK4	81	82	Trinidad
RK4	76	84	Trinidad
RK4	73	85	Trinidad
RK4	160	74	Trinidad
RK4	75	82	Trinidad
RK4	64	80	Trinidad
RK4	70	85	Trinidad
RK4	86	76	Trinidad
RK4	80	82	Trinidad
RK4	318	90	Trinidad
RK4	319	90	Trinidad
RK4	139	87	Trinidad
RK4	137	86	Trinidad
RK4	325	88	Trinidad

RK4	323	88	Trinidad
RK4	270	88	Trinidad
RK4	88	90	Trinidad
RK4	79	90	Trinidad
RK4	255	88	Trinidad
RK4	320	90	Trinidad
RK4	73	89	Trinidad
RK4	74	85	Trinidad
RK4	76	90	Trinidad
RK4	81	89	Trinidad
RK4	121	84	Trinidad
RK4	314	88	Trinidad
RK4	132	88	Trinidad

Location ID: RK5
Latitude: N 36.91441667
Longitude: W 104.9809

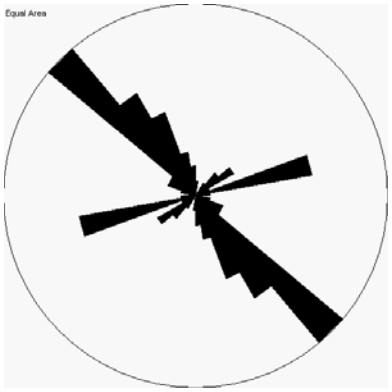

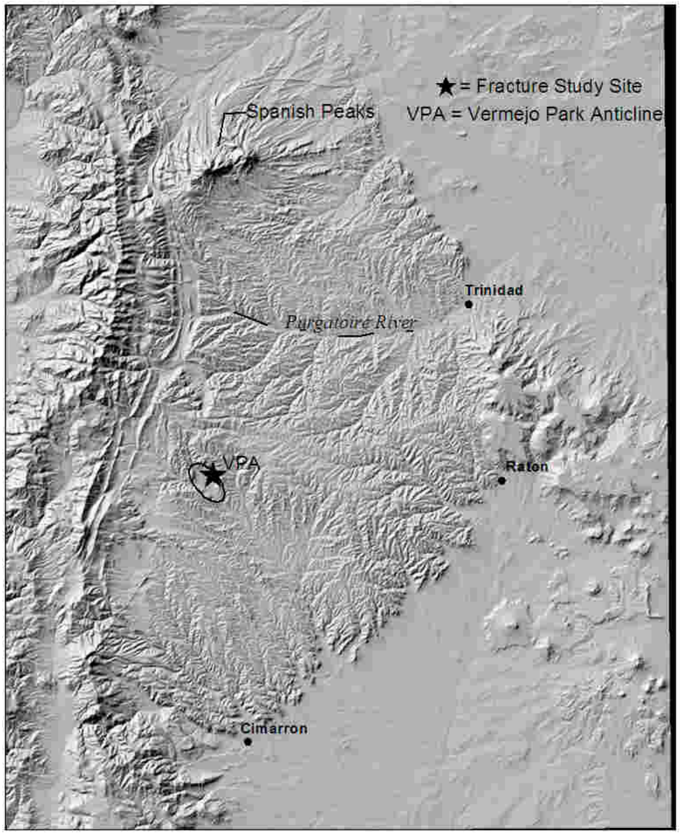

Notes:

Fracture Data:

ID	Strike	Dip	Formation	Comment 1	Comment 2
RK5	159	76	Trinidad		Trinidad
RK5	79	81	Trinidad		Trinidad
RK5	76	84	Trinidad		Trinidad
RK5	310	90	Trinidad		Trinidad
RK5	308	90	Trinidad		Trinidad
RK5	304	90	Trinidad		Trinidad
RK5	310	90	Trinidad		Trinidad
RK5	337	79	Trinidad		Trinidad
RK5	73	82	Trinidad		Trinidad
RK5	133	89	Trinidad		Trinidad
RK5	343	90	Trinidad		Trinidad
RK5	146	88	Trinidad		Trinidad
RK5	52	78	Trinidad		Trinidad
RK5	310	90	Trinidad		Trinidad
RK5	2	90	Trinidad		Trinidad
RK5	323	90	Trinidad		Trinidad
RK5	73	86	Trinidad		Trinidad

RK5	138	88	Trinidad		Trinidad
RK5	287	90	Trinidad		Trinidad
RK5	332	90	Trinidad		Trinidad
RK5	48	78	Trinidad		Trinidad
RK5	78	86	Trinidad		Trinidad
RK5	89	88	Trinidad		Trinidad
RK5	293	90	Trinidad		Trinidad
RK5	77	76	Trinidad		Trinidad
RK5	312	90	unknown	calcite	Sill
RK5	48	90	unknown	calcite	Sill
RK5	77	82	unknown	calcite	Sill
RK5	173	86	unknown	calcite	Sill
RK5	144	87	unknown		Sill
RK5	356	90	unknown		Sill
RK5	316	82	unknown		Sill
RK5	146	82	unknown		Sill
RK5	338	90	unknown		Sill
RK5	76	82	unknown		Sill
RK5	33	87	unknown	calcite	Sill
RK5	318	90	unknown		Sill
RK5	312	90	unknown		Sill
RK5	50	85	unknown		Sill
RK5	328	90	unknown		Sill
RK5	329	90	unknown		Sill
RK5	318	90	unknown		Sill
RK5	316	90	unknown		Sill
RK5	153	82	unknown		Sill
RK5	138	88	unknown		Sill
RK5	119	86	unknown	calcite	Sill
RK5	239	79	unknown		Sill
RK5	335	85	unknown		Sill
RK5	148	85	unknown		Sill
RK5	249	83	unknown		Sill
RK5	341	90	unknown		Sill
RK5	340	90	Trinidad		Trinidad
RK5	319	90	unknown		Sill
RK5	320	90	Trinidad		Trinidad

Location ID: RK6
Latitude: N 36.94926667
Longitude: W 105.1241

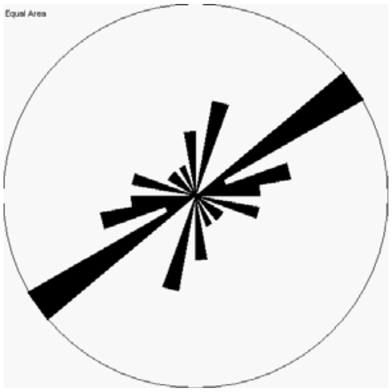

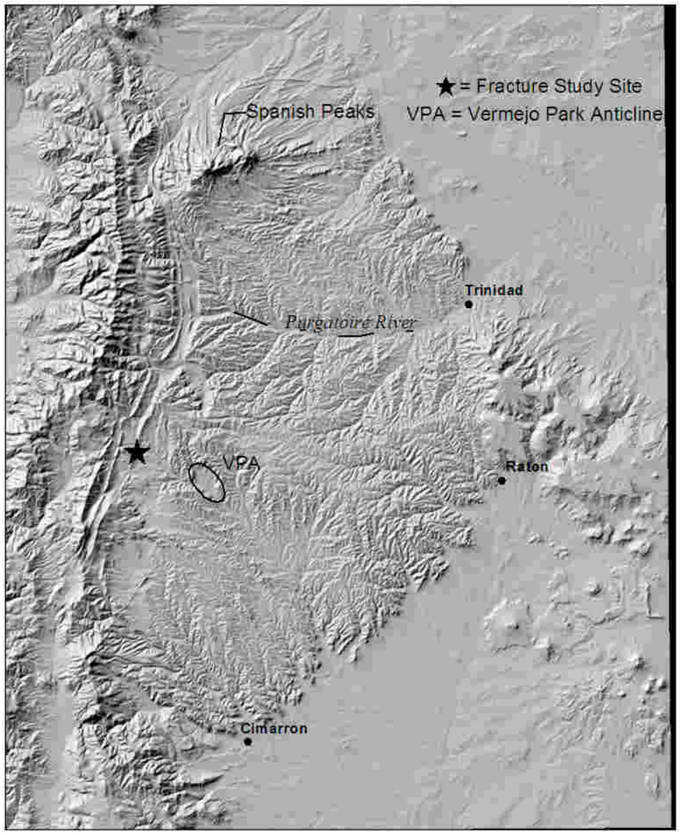

Notes:

Fracture Data:

ID	Strike	Dip	Formation	Comment 1
RK6	175	72	Trinidad	
RK6	12	16	Trinidad	Indications of shear, steps that suggest the overlying block moved up- westward perpendicular to steps, movement would be striking 282
RK6	12	14	Trinidad	Indications of shear, steps that suggest the overlying block moved up- westward perpendicular to steps, movement would be striking 283
RK6	10	16	Trinidad	Indications of shear, steps that suggest the overlying block moved up- westward perpendicular to steps, movement would be striking 284
RK6	287	65	Trinidad	Slightly arcuate, sheer steps suggest left lateral movement
RK6	261	88	Trinidad	Slightly arcuate, sheer steps suggest left lateral movement
RK6	74	86	Trinidad	
RK6	281	60	Trinidad	
RK6	75	88	Trinidad	
RK6	239	82	Trinidad	
RK6	269	85	Trinidad	
RK6	76	73	Trinidad	

RK6	150	82	Trinidad	
RK6	123	70	Trinidad	
RK6	232	64	Trinidad	
RK6	245	40	Trinidad	Reidel shear steps indicate upper block moving east, lineation perpendicular @ 332 deg
RK6	233	22	Trinidad	
RK6	56	73	Trinidad	
RK6	238	62	Trinidad	
RK6	237	14	Trinidad	
RK6	174	74	Trinidad	
RK6	314	90	Trinidad	

Location ID: RK7
Latitude: N 36.89911667
Longitude: W 104.5851167

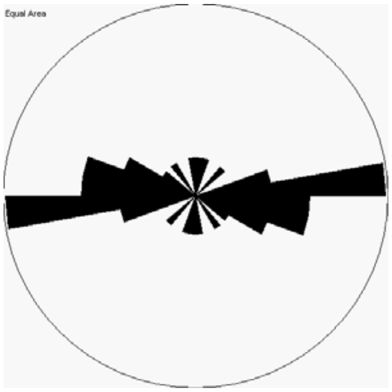

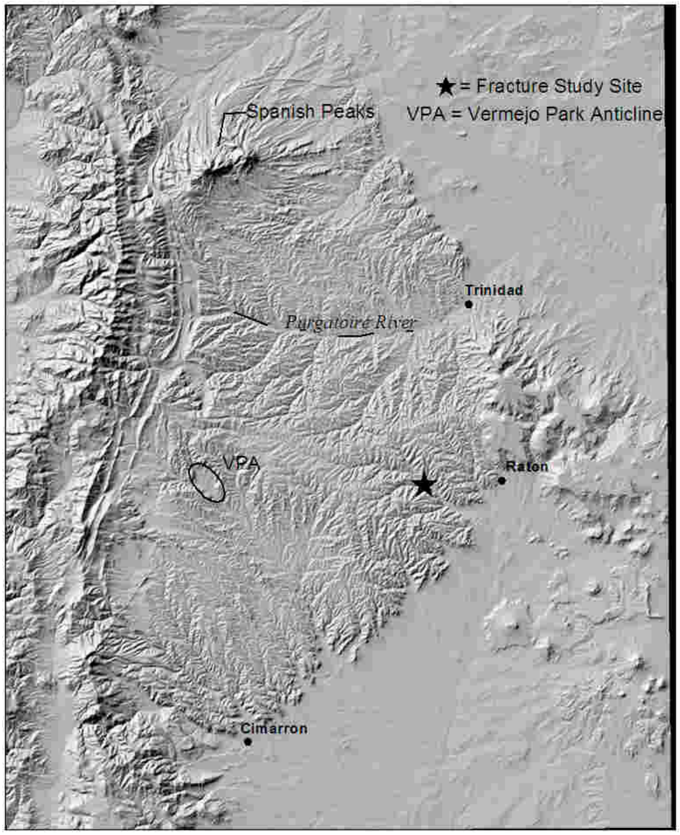

Notes:

Fracture Data:

ID	Strike	Dip	Formation	Comment 1
RK7	256	86	Vermejo	
RK7	269	82	Vermejo	
RK7	115	72	Vermejo	
RK7	293	84	Vermejo	
RK7	302	77	Vermejo	
RK7	262	76	Vermejo	
RK7	271	90	Vermejo	
RK7	42	90	Vermejo	terminates against EW set
RK7	277	86	Vermejo	
RK7	280	86	Vermejo	
RK7	283	88	Vermejo	
RK7	268	88	Vermejo	
RK7	267	88	Vermejo	
RK7	322	90	Vermejo	
RK7	12	90	Vermejo	terminates against EW set
RK7	76	87	Vermejo	
RK7	102	80	Vermejo	

RK7	93	72	Vermejo	
RK7	87	76	Vermejo	
RK7	4	88	Vermejo	
RK7	358	90	Vermejo	terminates against EW set

Location ID: RK8
Latitude: N 36.88196667
Longitude: W 104.55665

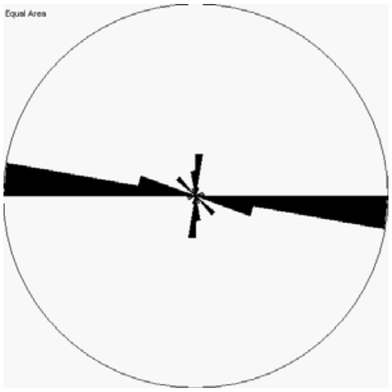

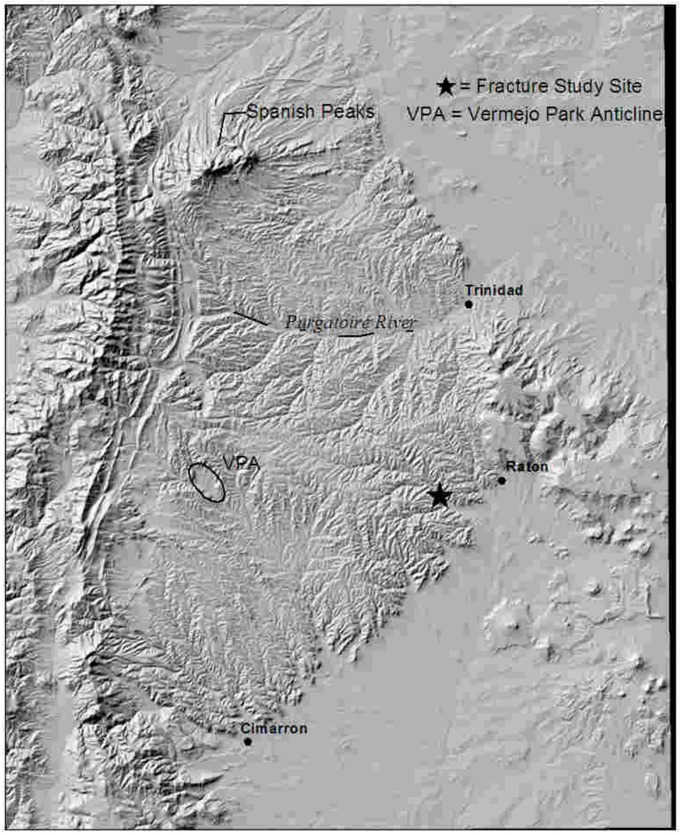

Notes:

Fracture Data:

ID	Strike	Dip	Formation	Comment 1
RK8	280	86	Trinidad	
RK8	91	86	Trinidad	
RK8	5	90	Trinidad	terminates against EW set
RK8	279	82	Trinidad	
RK8	285	90	Trinidad	
RK8	271	88	Trinidad	plume
RK8	101	86	Trinidad	
RK8	274	90	Trinidad	
RK8	184	82	Trinidad	
RK8	273	83	Trinidad	
RK8	278	90	Trinidad	
RK8	274	90	Trinidad	
RK8	184	82	Trinidad	
RK8	186	82	Trinidad	
RK8	373	83	Trinidad	
RK8	278	90	Trinidad	
RK8	274	90	Trinidad	

RK8	95	82	Trinidad	
RK8	271	86	Trinidad	
RK8	277	89	Trinidad	
RK8	179	88	Trinidad	
RK8	284	82	Trinidad	
RK8	286	89	Trinidad	
RK8	192	82	Trinidad	terminates against EW set
RK8	279	88	Trinidad	
RK8	99	88	Trinidad	
RK8	7	90	Trinidad	terminates against EW set
RK8	105	85	Trinidad	
RK8	283	88	Trinidad	
RK8	179	74	Trinidad	
RK8	277	90	Trinidad	
RK8	317	90	Trinidad	
RK8	317	90	Trinidad	
RK8	319	88	Trinidad	
RK8	330	90	Trinidad	
RK8	273	89	Trinidad	
RK8	273	90	Trinidad	
RK8	81	90	Trinidad	
RK8	96	86	Trinidad	
RK8	96	86	Trinidad	
RK8	98	88	Trinidad	
RK8	273	90	Trinidad	
RK8	68	90	Trinidad	
RK8	172	80	Trinidad	
RK8	278	88	Trinidad	
RK8	97	88	Trinidad	

Location ID: RK9
Latitude: N 36.89311667
Longitude: W 104.7512167

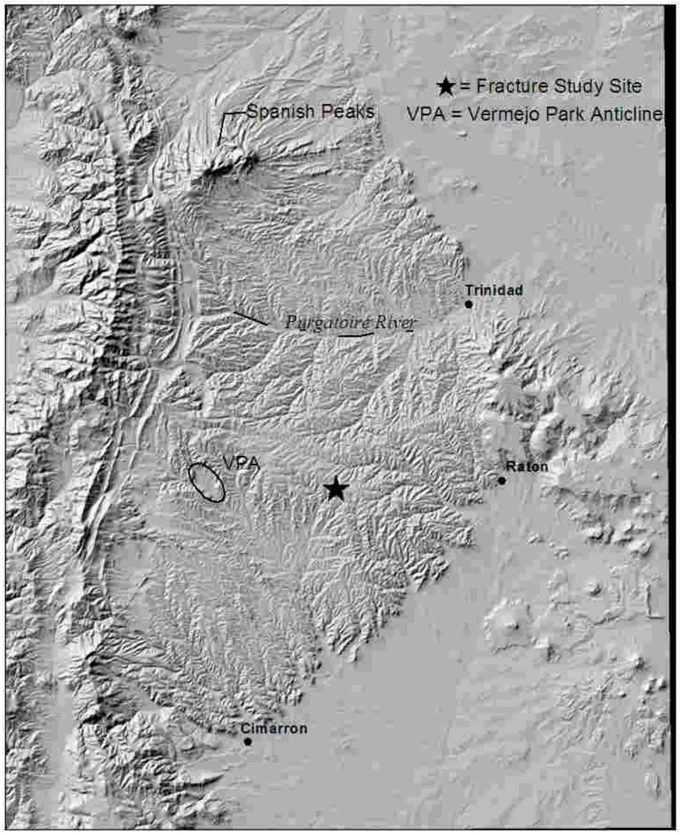

Notes:

Fracture Data:

Location ID: RK10
Latitude: N 36.88915
Longitude: W 104.7383833

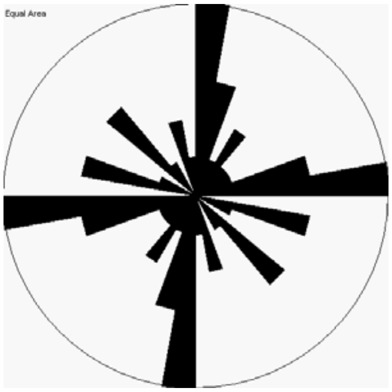

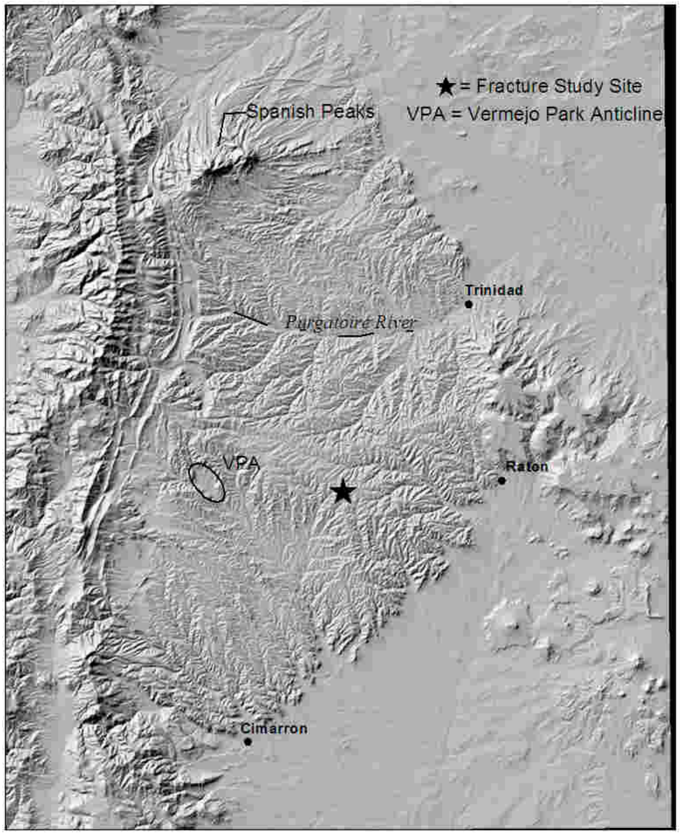

Notes:

Fracture Data:

ID	Strike	Dip	Formation	Comment 1
RK10	186	90	Poison Canyon	
RK10	35	90	Poison Canyon	
RK10	67	90	Poison Canyon	
RK10	14	90	Poison Canyon	
RK10	4	90	Poison Canyon	
RK10	78	90	Poison Canyon	
RK10	282	90	Poison Canyon	
RK10	1	90	Poison Canyon	
RK10	85	90	Poison Canyon	
RK10	81	90	Poison Canyon	
RK10	83	90	Poison Canyon	
RK10	25	90	Poison Canyon	
RK10	30	90	Poison Canyon	
RK10	310	90	Poison Canyon	
RK10	41	90	Poison Canyon	
RK10	19	90	Poison Canyon	
RK10	130	72	Poison Canyon	

RK10	132	70	Poison Canyon	
RK10	84	90	Poison Canyon	
RK10	86	90	Poison Canyon	
RK10	177	72	Poison Canyon	
RK10	239	75	Poison Canyon	
RK10	119	90	Poison Canyon	
RK10	325	90	Poison Canyon	
RK10	11	90	Poison Canyon	
RK10	8	90	Poison Canyon	
RK10	8	90	Poison Canyon	
RK10	106	88	Poison Canyon	
RK10	74	90	Poison Canyon	
RK10	344	90	Poison Canyon	terminates against 74
RK10	77	90	Poison Canyon	
RK10	342	90	Poison Canyon	terminates against 77
RK10	103	68	Poison Canyon	

Location ID: RK11
Latitude: N 36.89788333
Longitude: W 104.91455

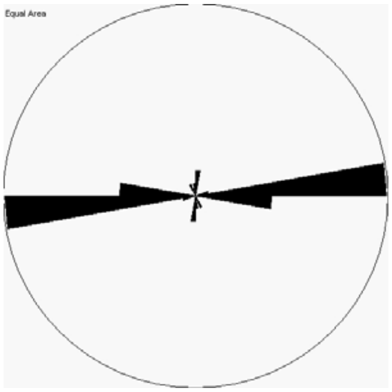

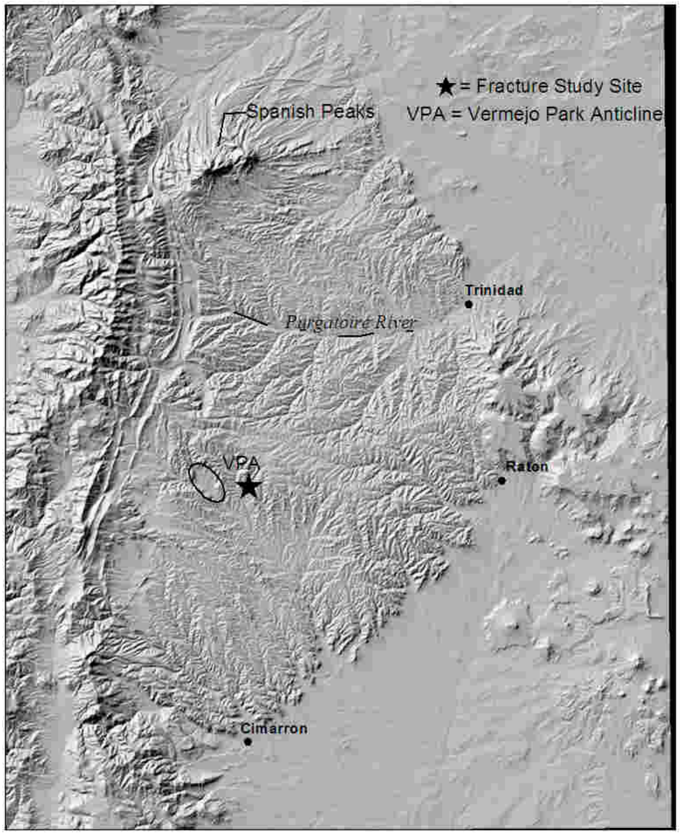

Notes:

Fracture Data:

ID	Strike	Dip	Formation	Comment 1
RK11	89	82	Vermejo	plume
RK11	82	80	Vermejo	plume
RK11	84	82	Vermejo	
RK11	84	75	Vermejo	4 cm normal displacement
RK11	87	82	Vermejo	
RK11	87	80	Vermejo	
RK11	268	85	Vermejo	38 cm normal displacement
RK11	275	88	Vermejo	
RK11	272	88	Vermejo	
RK11	80	82	Vermejo	
RK11	271	88	Vermejo	
RK11	86	84	Vermejo	
RK11	270	88	Vermejo	
RK11	85	82	Vermejo	
RK11	268	87	Vermejo	
RK11	95	90	Vermejo	
RK11	181	72	Vermejo	

RK11	85	86	Vermejo
RK11	89	87	Vermejo
RK11	89	88	Vermejo
RK11	175	86	Vermejo
RK11	79	90	Vermejo
RK11	187	68	Vermejo
RK11	85	90	Vermejo
RK11	159	75	Vermejo
RK11	95	86	Vermejo

Location ID: RK13
Latitude: N 36.89208333
Longitude: W 104.9776

Below and east of Gazebo, Trinidad

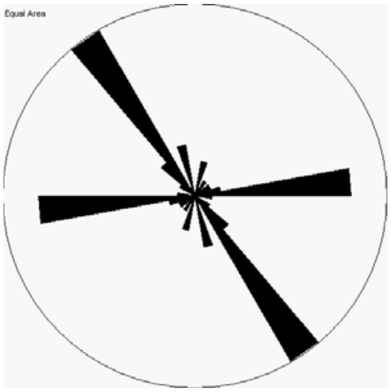

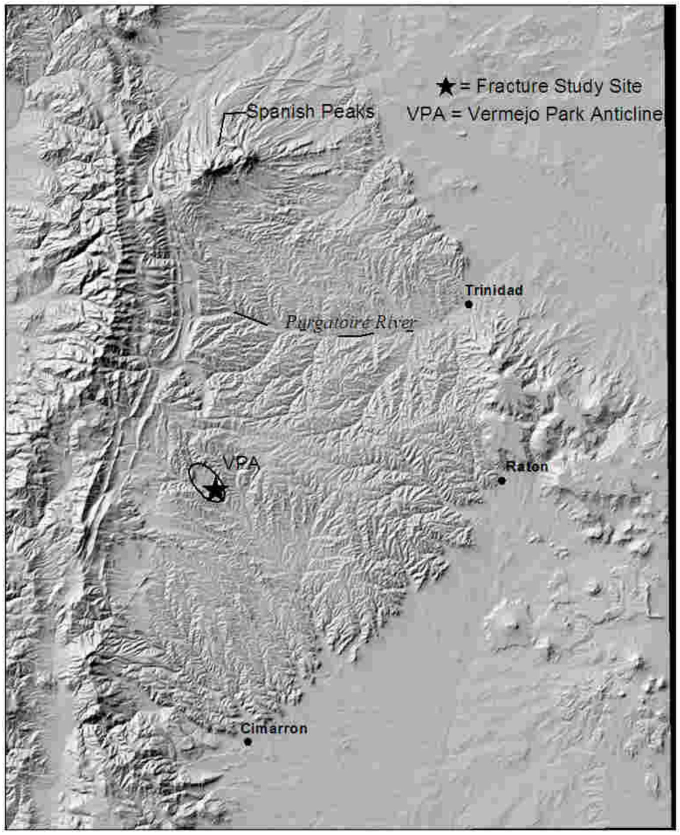

Notes:

Fracture Data:

ID	Strike	Dip	Formation	Comment 1	Comment 2	Comment 3
RK13	82	90	Trinidad			
RK13	22	90	Trinidad	terminates @ 82 degree fracture		
RK13	144	90	Trinidad			
RK13	82	88	Trinidad			
RK13	148	90	Trinidad			
RK13	56	86	Trinidad			
RK13	144	86	Trinidad			
RK13	134	90	Trinidad			
RK13	222	86	Trinidad			
RK13	265	82	Trinidad			
RK13	321	85	Trinidad			
RK13	141	90	Trinidad			
RK13	321	86	Trinidad			
RK13	83	54	Trinidad			
RK13	323	85	Trinidad			
RK13	10	90	Trinidad			

RK13	321	86	Trinidad	swarm of about 11 fractures, 18 cm wide, calcite		
RK13	314	63	Trinidad			
RK13	162	90	Trinidad			
RK13	150	74	Trinidad			
RK13	87	80	Trinidad			
RK13	137	90	Trinidad			
RK13	162	74	Trinidad			
RK13	322	80	Trinidad	swarm, over 18 cm wide, 9 fractures, cut through entire bed thickness ~15 m		
RK13	143	80	Trinidad			
RK13	38	35	Trinidad			
RK13	130	90	Trinidad			
RK13	84	90	Trinidad			
RK13	86	88	Trinidad			
RK13	164	74	Trinidad			
RK13	323	87	Trinidad			
RK13	65	83	Trinidad			
RK13	11	90	Trinidad			
RK13	323	88	Trinidad			
RK13	140	90	Trinidad			
RK13	88	65	Trinidad			
RK13	169	83	Trinidad			
RK13	88	76	Trinidad			
RK13	147	84	Trinidad			
RK13	321	90	Trinidad			
RK13	325	90	Trinidad			
RK13	321	90	Trinidad			
RK13	348	82	Trinidad			
RK13	169	60	Trinidad			
RK13	83	87	Trinidad			
RK13	125	90	Trinidad			
RK13	82	88	Trinidad			
RK13	39	90	Trinidad			
RK13	324	86	Trinidad	swarm, 33 cm, 8 fracs		
RK13	198	79	Trinidad			
RK13	92	73	Trinidad			
RK13	325	85	Trinidad	swarm, 13 cm, 6 fracs		
RK13	322	87	Trinidad	swarm, 15 cm, 5 fracs		
RK13	70	90	Trinidad	shear steps, right lateral	calcite up to 2 cm wide	large swarm zone 2 m wide
RK13	121	90	Trinidad	secondary fracture terminates against 70 degree	shear steps, left lateral	
RK13	83	53	Trinidad			
RK13	140	90	Trinidad			
RK13	86	60	Trinidad			
RK13	58	88	Trinidad			

RK13	242	72	Trinidad	
RK13	74	78	Trinidad	
RK13	76	85	Trinidad	plume
RK13	90	82	Trinidad	
RK13	83	83	Trinidad	
RK13	141	90	Trinidad	plume
RK13	269	82	Trinidad	
RK13	132	90	Trinidad	plume
RK13	145	85	Trinidad	
RK13	85	82	Trinidad	
RK13	85	79	Trinidad	
RK13	86	82	Trinidad	

Location ID: RK14
Latitude: N 36.82423333
Longitude: W 105.0835

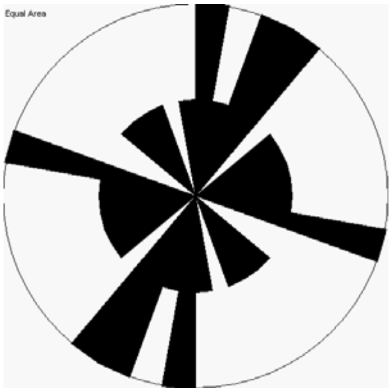

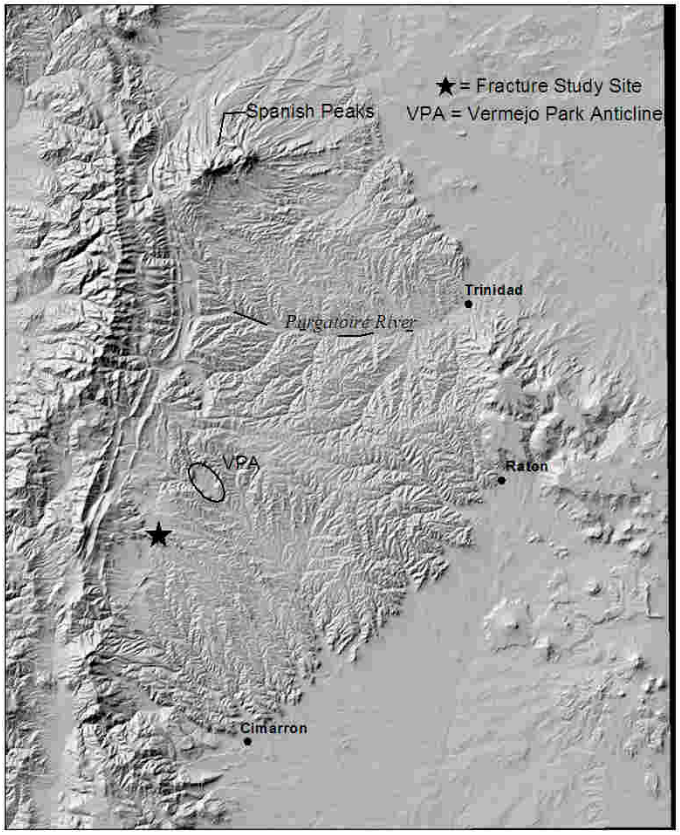

Notes:

Fracture Data:

ID	Strike	Dip	Formation
RK14	6	90	Poison Canyon
RK14	173	90	Poison Canyon
RK14	235	85	Poison Canyon
RK14	87	90	Poison Canyon
RK14	22	90	Poison Canyon
RK14	102	85	Poison Canyon
RK14	63	90	Poison Canyon
RK14	335	90	Poison Canyon
RK14	97	90	Poison Canyon
RK14	184	85	Poison Canyon
RK14	100	90	Poison Canyon
RK14	259	84	Poison Canyon
RK14	28	90	Poison Canyon
RK14	214	68	Poison Canyon
RK14	210	69	Poison Canyon
RK14	323	90	Poison Canyon
RK14	130	60	Poison Canyon
RK14	195	86	Poison Canyon

Location ID: RK15
Latitude: N 36.73605
Longitude: W 104.9645333

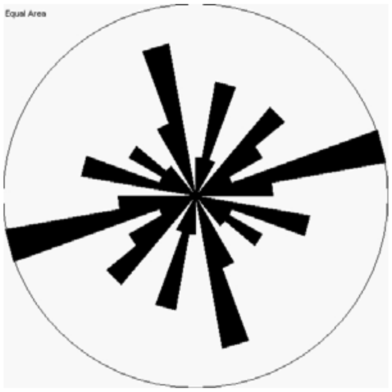

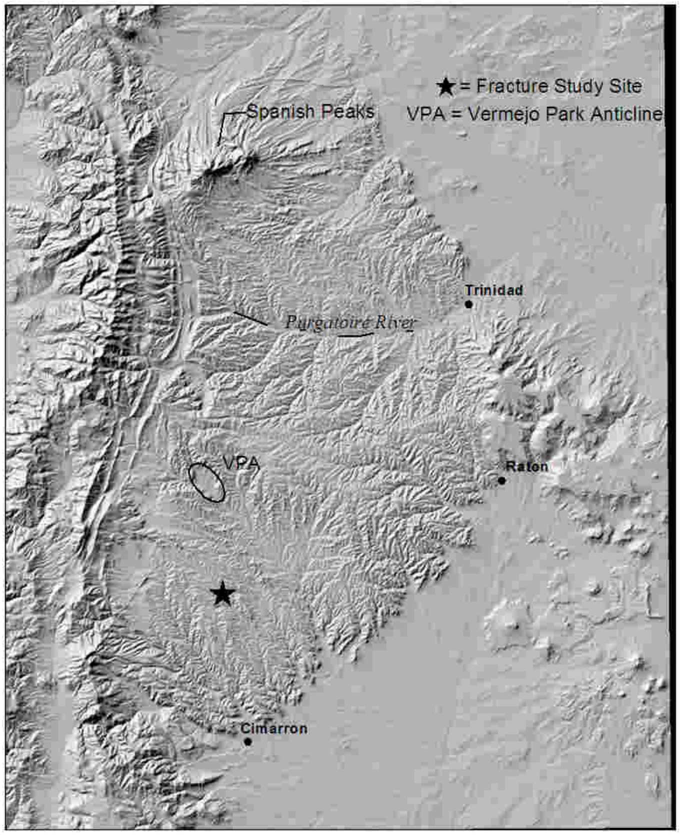

Notes:

Fracture Data:

ID	Strike	Dip	Formation
RK15	164	85	Raton
RK15	85	90	Raton
RK15	158	87	Raton
RK15	64	90	Raton
RK15	109	90	Raton
RK15	347	90	Raton
RK15	130	82	Raton
RK15	165	68	Raton
RK15	108	80	Raton
RK15	51	88	Raton
RK15	107	75	Raton
RK15	70	90	Raton
RK15	72	90	Raton
RK15	79	90	Raton
RK15	8	90	Raton
RK15	13	76	Raton
RK15	72	90	Raton

RK15	77	90	Raton
RK15	17	82	Raton
RK15	223	68	Raton
RK15	117	60	Raton
RK15	161	64	Raton
RK15	13	90	Raton
RK15	83	90	Raton
RK15	155	90	Raton
RK15	305	84	Raton
RK15	29	85	Raton
RK15	44	90	Raton
RK15	227	74	Raton
RK15	53	90	Raton
RK15	124	90	Raton

Location ID: RK16
Latitude: N 36.58628333
Longitude: W 104.8619167

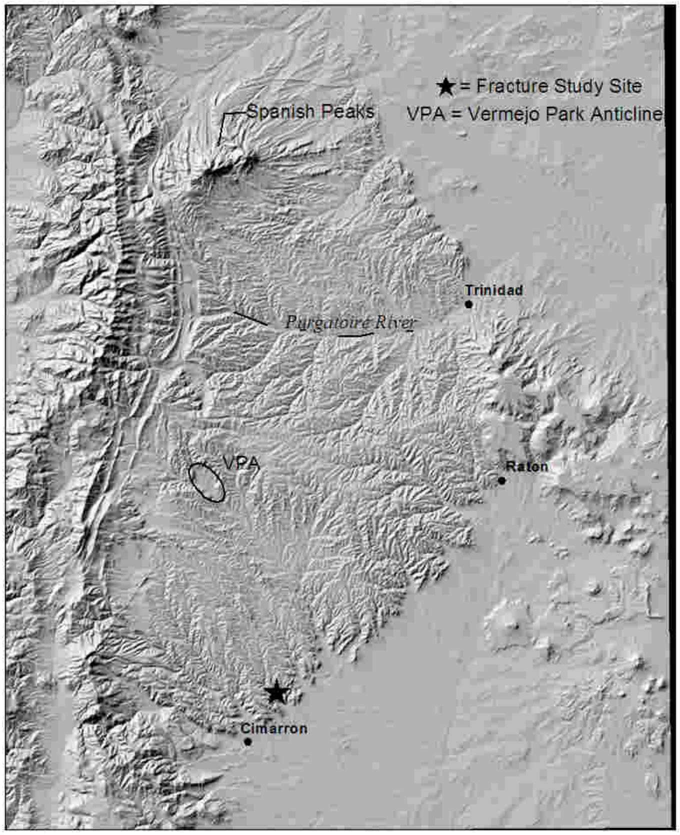

Notes:

Fracture Data:

ID	Strike	Dip	Formation	Comment 1
RK16	228	70	Trinidad	
RK16	92	90	Trinidad	
RK16	62	82	Trinidad	
RK16	198	48	Trinidad	
RK16	85	75	Trinidad	
RK16	191	79	Trinidad	
RK16	217	72	Trinidad	
RK16	51	90	Trinidad	
RK16	118	80	Trinidad	
RK16	118	85	Trinidad	
RK16	30	82	Trinidad	
RK16	122	90	Trinidad	
RK16	13	90	Trinidad	
RK16	18	90	Trinidad	
RK16	9	90	Trinidad	
RK16	18	90	Trinidad	
RK16	278	72	Trinidad	

RK16	280	80	Trinidad	plume
RK16	229	60	Trinidad	
RK16	198	83	Trinidad	
RK16	10	90	Trinidad	
RK16	13	90	Trinidad	
RK16	129	90	Trinidad	
RK16	115	90	Trinidad	
RK16	16	90	Trinidad	
RK16	295	90	Trinidad	plume
RK16	293	90	Trinidad	
RK16	115	88	Trinidad	
RK16	295	90	Trinidad	
RK16	299	90	Trinidad	
RK16	115	85	Trinidad	
RK16	152	90	Trinidad	
RK16	150	90	Trinidad	
RK16	115	90	Trinidad	
RK16	25	90	Trinidad	terminates against 115
RK16	121	90	Trinidad	
RK16	195	82	Trinidad	
RK16	118	75	Trinidad	
RK16	112	89	Trinidad	
RK16	116	82	Trinidad	
RK16	70	90	Trinidad	
RK16	122	72	Trinidad	plume
RK16	305	90	Trinidad	
RK16	115	88	Trinidad	
RK16	85	70	Trinidad	
RK16	71	70	Trinidad	

Location ID: RK17
Latitude: N 36.53773333
Longitude: W 104.88275

North of Highway 64, Trinidad
outcrop ~1 mile from road

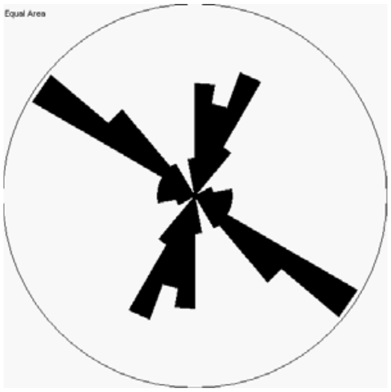

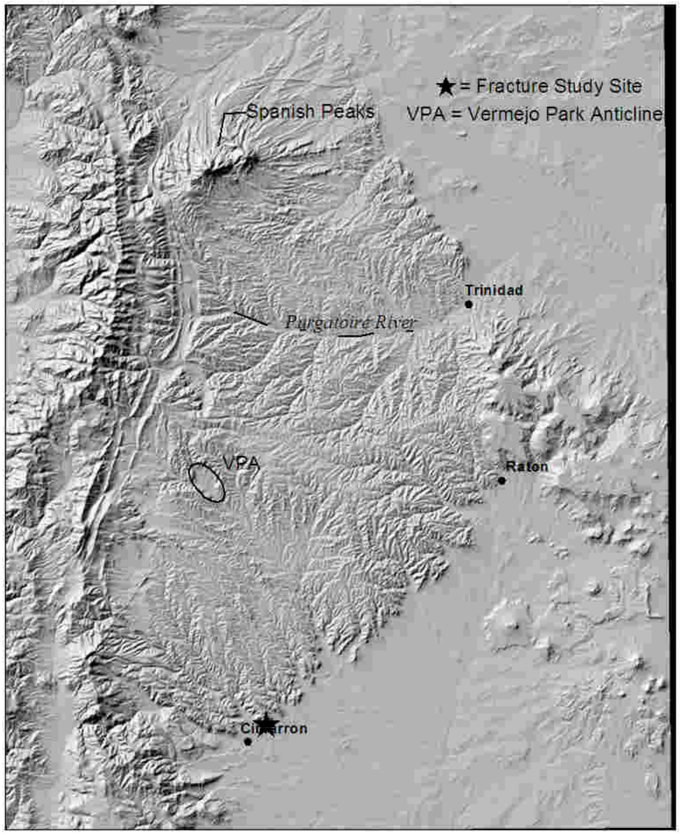

Notes:

Fracture Data:

ID	Strike	Dip	Formation	Comment 1
RK17	133	88	Trinidad	
RK17	63	78	Trinidad	
RK17	24	80	Trinidad	
RK17	28	79	Trinidad	
RK17	72	82	Trinidad	
RK17	93	67	Trinidad	
RK17	88	85	Trinidad	
RK17	31	90	Trinidad	
RK17	15	85	Trinidad	swarm, 11 cm, 6 fracs
RK17	24	84	Trinidad	swarm, 20 cm, 10 fracs
RK17	105	86	Trinidad	
RK17	1	90	Trinidad	
RK17	19	90	Trinidad	
RK17	278	90	Trinidad	
RK17	140	86	Trinidad	swarm, 1 m, 6 fracs
RK17	195	82	Trinidad	swarm, 15 cm, 7 fracs
RK17	24	72	Trinidad	swarm, 15 cm, 4 fracs

RK17	178	84	Trinidad	swarm, 15 cm, 5 fracs
RK17	6	90	Trinidad	
RK17	120	75	Trinidad	
RK17	12	90	Trinidad	
RK17	301	90	Trinidad	
RK17	127	86	Trinidad	
RK17	119	90	Trinidad	swarm, 1 m, >10 fracs
RK17	306	74	Trinidad	plume
RK17	130	88	Trinidad	
RK17	32	90	Trinidad	
RK17	20	84	Trinidad	
RK17	319	76	Trinidad	
RK17	145	75	Trinidad	
RK17	1	74	Trinidad	
RK17	318	85	Trinidad	
RK17	26	90	Trinidad	
RK17	133	84	Trinidad	
RK17	129	78	Trinidad	
RK17	109	90	Trinidad	
RK17	7	73	Trinidad	
RK17	136	85	Trinidad	
RK17	305	90	Trinidad	
RK17	9	85	Trinidad	terminates against 304/85 sw
RK17	10	80	Trinidad	terminates against 307/75 NE
RK17	0	82	Trinidad	
RK17	301	78	Trinidad	
RK17	89	90	Trinidad	
RK17	301	77	Trinidad	plume, calcite
RK17	35	80	Trinidad	terminates against 301
RK17	303	80	Trinidad	
RK17	350	82	Trinidad	
RK17	121	85	Trinidad	
RK17	20	79	Trinidad	terminates against 121
RK17	295	90	Trinidad	

Location ID: RK18
Latitude: N 36.86788333
Longitude: W 104.4991333

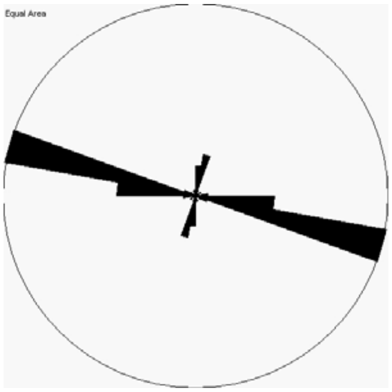

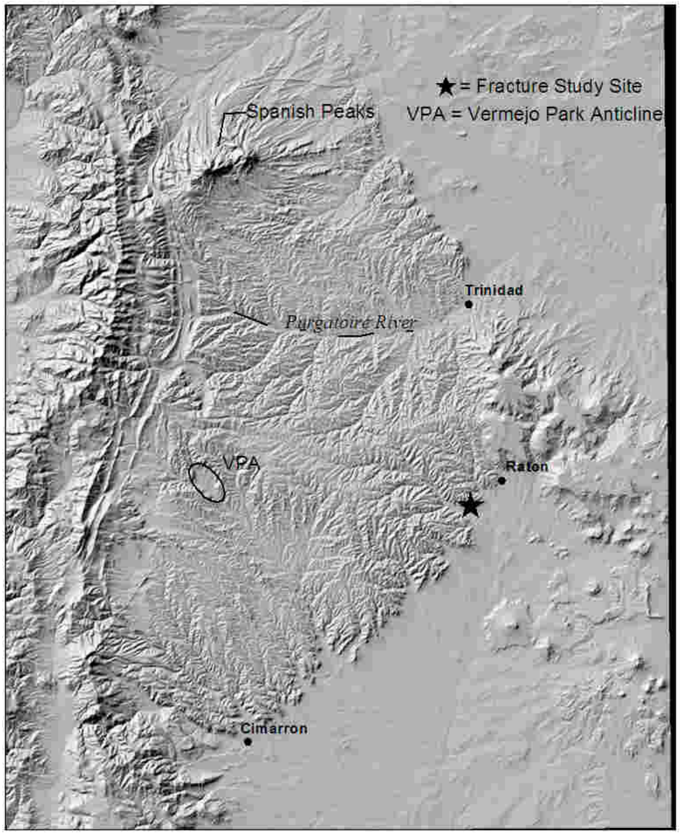

Notes:

Fracture Data:

ID	Strike	Dip	Formation	Comment 1	Comment 2
RK18	82	62	Trinidad		
RK18	93	90	Trinidad		
RK18	128	90	Trinidad		
RK18	107	88	Trinidad		
RK18	101	88	Trinidad		
RK18	115	90	Trinidad		
RK18	104	90	Trinidad		
RK18	107	90	Trinidad		
RK18	10	90	Trinidad	terminates against 104	
RK18	109	79	Trinidad		
RK18	106	90	Trinidad		
RK18	170	90	Trinidad		
RK18	93	90	Trinidad		
RK18	107	90	Trinidad		
RK18	93	90	Trinidad		
RK18	90	90	Trinidad		
RK18	101	90	Trinidad		

RK18	105	90	Trinidad		
RK18	109	90	Trinidad		
RK18	108	90	Trinidad		
RK18	108	90	Trinidad		
RK18	101	90	Trinidad		
RK18	109	88	Trinidad		
RK18	106	90	Trinidad		
RK18	115	90	Trinidad		
RK18	106	90	Trinidad		
RK18	23	90	Trinidad	terminate against EW set	
RK18	14	90	Trinidad	terminate against EW set	
RK18	15	90	Trinidad	terminate against EW set	
RK18	1	9	Trinidad	terminate against EW set	
RK18	4	88	Trinidad	terminate against EW set	
RK18	105	90	Trinidad		
RK18	109	90	Trinidad		
RK18	101	90	Trinidad		
RK18	103	90	Trinidad		
RK18	99	90	Trinidad		
RK18	10	90	Trinidad	terminates against 105	
RK18	14	80	Trinidad	terminates against 109	
RK18	9	90	Trinidad	terminates against 101	
RK18	14	86	Trinidad		
RK18	108	90	Trinidad		
RK18	92	90	Trinidad	swarm, 30 cm, 12 fracs	
RK18	93	90	Trinidad	w/ calcite	
RK18	91	85	Trinidad		
RK18	55	90	Trinidad		
RK18	165	90	Trinidad		
RK18	89	90	Trinidad		
RK18	97	87	Trinidad		thin unit below SS
RK18	16	88	Trinidad	terminates against 97	thin unit below SS
RK18	105	90	Trinidad		thin unit below SS
RK18	189	88	Trinidad	terminates against 105	thin unit below SS
RK18	102	90	Trinidad		thin unit below SS
RK18	7	90	Trinidad	terminates against 102	thin unit below SS
RK18	102	90	Trinidad		thin unit below SS
RK18	101	90	Trinidad		thin unit below SS
RK18	105	90	Trinidad		thin unit below SS
RK18	103	90	Trinidad		thin unit below SS
RK18	99	90	Trinidad		thin unit below SS
RK18	279	88	Trinidad		thin unit below SS
RK18	100	90	Trinidad		thin unit below SS
RK18	101	90	Trinidad		thin unit below SS
RK18	102	90	Trinidad		thin unit below SS
RK18	103	85	Trinidad	calcite	thin unit below SS
RK18	95	85	Trinidad	calcite	thin unit below SS
RK18	103	90	Trinidad		thin unit below SS
RK18	99	87	Trinidad		thin unit below SS

Location ID: RK19
Latitude: N 36.87838333
Longitude: W 104.9836667

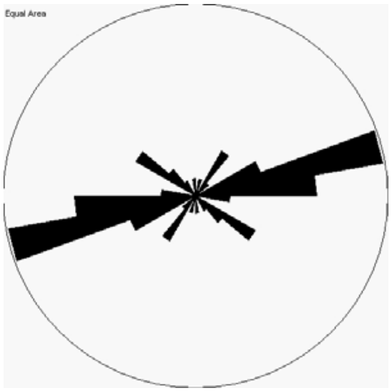

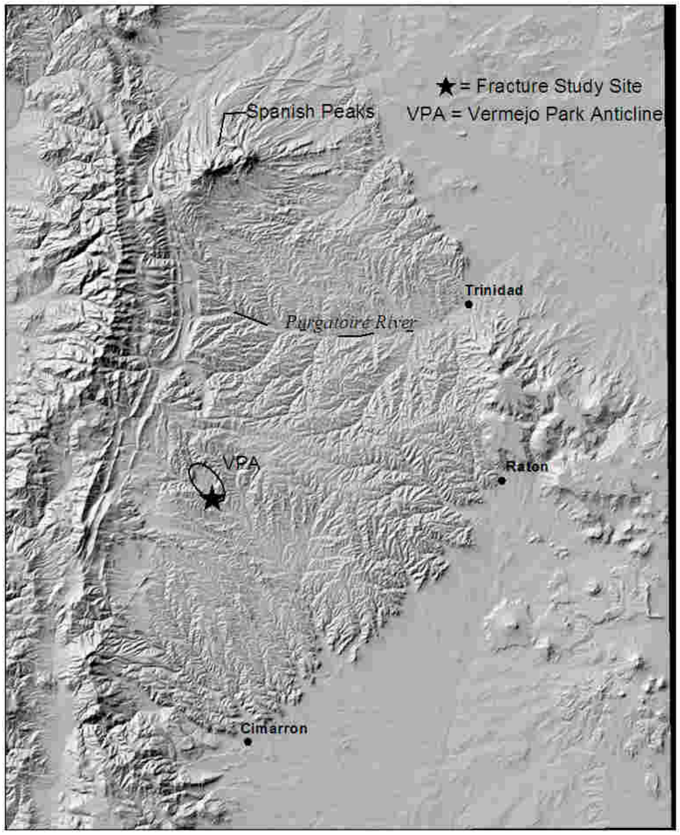

Notes:

Fracture Data:

ID	Strike	Dip	Formation	Comment 1
RK19	75	90	Trinidad	
RK19	78	90	Trinidad	
RK19	89	90	Trinidad	
RK19	92	90	Trinidad	plume
RK19	81	90	Trinidad	swarm, 15 cm, 3-4 fracs w/some calcite
RK19	266	88	Trinidad	
RK19	82	90	Trinidad	
RK19	77	90	Trinidad	
RK19	319	85	Trinidad	
RK19	83	90	Trinidad	swarm, 30 cm, 15 fracs
RK19	99	85	Trinidad	
RK19	85	88	Trinidad	
RK19	12	79	Trinidad	
RK19	357	83	Trinidad	
RK19	123	90	Trinidad	
RK19	252	75	Trinidad	
RK19	77	85	Trinidad	

RK19	124	90	Trinidad	
RK19	128	90	Trinidad	
RK19	212	88	Trinidad	
RK19	70	90	Trinidad	
RK19	75	80	Trinidad	
RK19	252	88	Trinidad	calcite
RK19	213	85	Trinidad	
RK19	63	84	Trinidad	
RK19	323	84	Trinidad	
RK19	68	76	Trinidad	plume
RK19	70	84	Trinidad	
RK19	77	76	Trinidad	
RK19	67	80	Trinidad	
RK19	80	76	Trinidad	
RK19	72	85	Trinidad	
RK19	220	83	Trinidad	
RK19	124	90	Trinidad	
RK19	218	86	Trinidad	
RK19	318	86	Trinidad	
RK19	63	90	Trinidad	

Location ID: RK20
Latitude: N 36.91148333
Longitude: W 105.08735

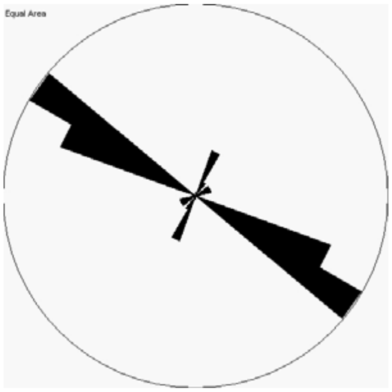

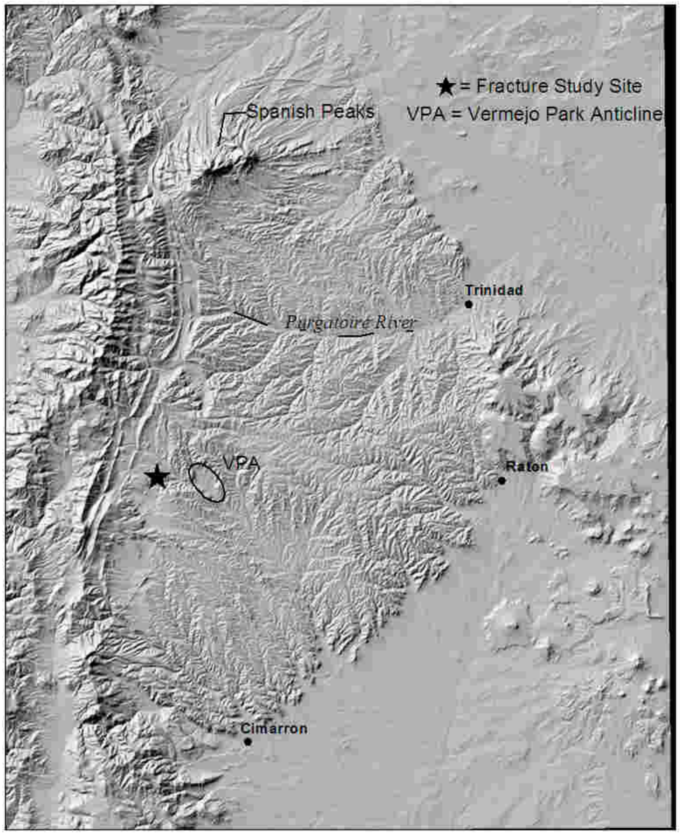

Notes:

Fracture Data:

ID	Strike	Dip	Formation	Comment 1	Comment 2
RK20	309	88	unknown		Raton? Vermejo?
RK20	306	85	unknown	plant trace fossil	Raton? Vermejo?
RK20	294	84	unknown		Raton? Vermejo?
RK20	302	84	unknown		Raton? Vermejo?
RK20	296	86	unknown		Raton? Vermejo?
RK20	301	85	unknown		Raton? Vermejo?
RK20	306	84	unknown	plume	Raton? Vermejo?
RK20	299	84	unknown		Raton? Vermejo?
RK20	23	80	unknown		Raton? Vermejo?
RK20	297	86	unknown	terminates against 35/86 SE	Raton? Vermejo?
RK20	301	88	unknown	plume	Raton? Vermejo?
RK20	306	86	unknown		Raton? Vermejo?
RK20	292	82	unknown		Raton? Vermejo?
RK20	290	88	unknown		Raton? Vermejo?
RK20	28	80	unknown		Raton? Vermejo?
RK20	216	75	unknown		Raton? Vermejo?
RK20	301	87	unknown		Raton? Vermejo?

RK20	113	90	unknown		Raton? Vermejo?
RK20	301	84	unknown	terminates against 27/89 NW	Raton? Vermejo?
RK20	119	90	unknown		Raton? Vermejo?
RK20	305	78	unknown		Raton? Vermejo?
RK20	61	90	unknown		Raton? Vermejo?
RK20	302	89	unknown		Raton? Vermejo?
RK20	75	90	unknown		Raton? Vermejo?
RK20	201	85	unknown		Raton? Vermejo?
RK20	301	90	unknown		Raton? Vermejo?
RK20	230	89	unknown		Raton? Vermejo?
RK20	115	87	unknown		Raton? Vermejo?

Location ID: RK21
Latitude: N 36.90858333
Longitude: W 105.0499667

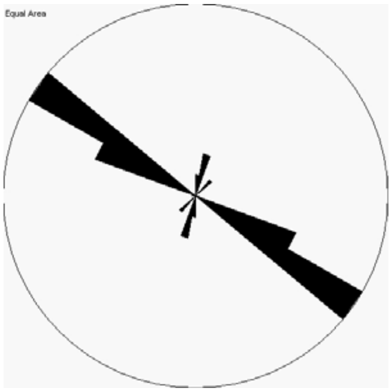

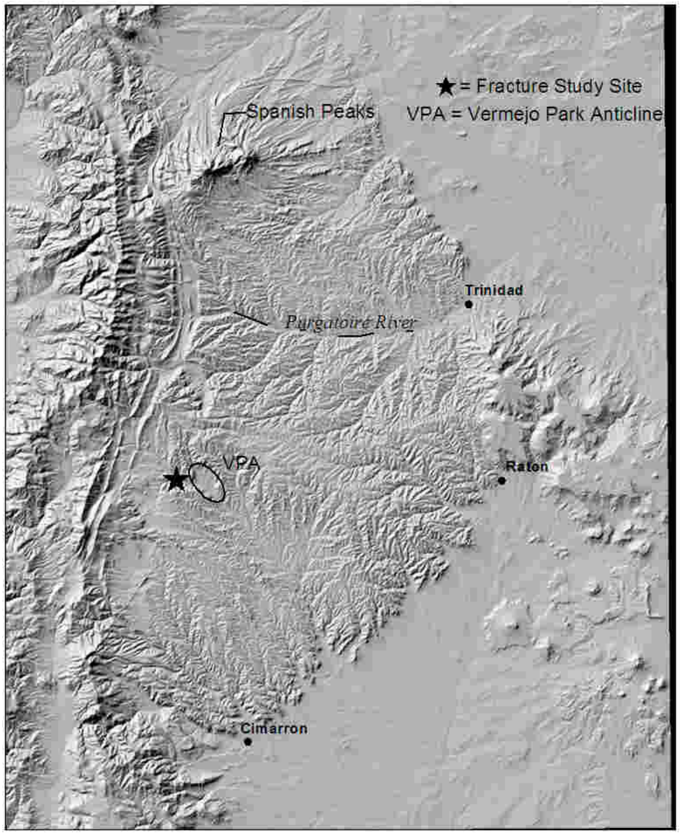

Notes:

Fracture Data:

ID	Strike	Dip	Formation	Comment 1	Comment 2
RK21	301	84	Raton		
RK21	118	90	Raton		
RK21	301	88	Raton	terminates against 25/80	
RK21	5	80	Raton		
RK21	13	80	Raton		
RK21	308	78	Raton	terminates against 34/85 SE	
RK21	119	90	Raton		
RK21	302	88	Raton	terminates against 19/85 NW	
RK21	118	86	Raton		
RK21	300	90	Raton	terminates against 40/80 SE	plume
RK21	119	90	Raton		
RK21	305	87	Raton		
RK21	303	86	Raton		
RK21	122	90	Raton		
RK21	43	90	Raton		
RK21	14	75	Raton		

RK21	296	86	Raton
RK21	301	87	Raton

Location ID: RK22
Latitude: N 36.84831667
Longitude: W 104.9277833

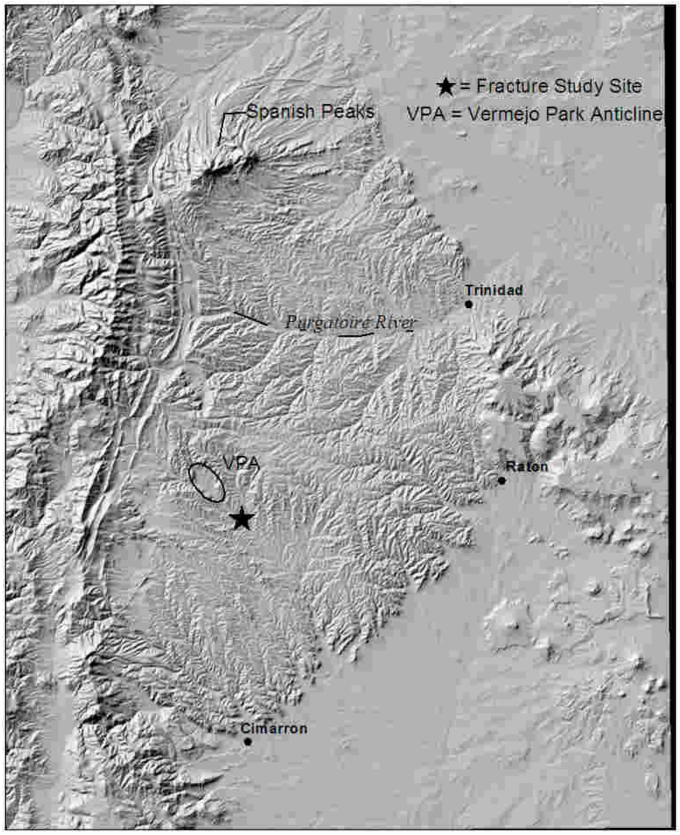

Notes:

Fracture Data:

ID	Strike	Dip	Formation	Comment 1	Comment 2
RK22	80	90	unknown		Vermejo?
RK22	81	90	unknown		Vermejo?
RK22	186	86	unknown		Vermejo?
RK22	160	90	unknown		Vermejo?
RK22	83	86	unknown		Vermejo?
RK22	84	81	unknown		Vermejo?
RK22	341	90	unknown	terminates against 271/90	Vermejo?
RK22	152	90	unknown		Vermejo?
RK22	180	87	unknown		Vermejo?
RK22	356	90	unknown		Vermejo?
RK22	82	90	unknown		Vermejo?
RK22	83	90	unknown		Vermejo?
RK22	175	89	unknown		Vermejo?
RK22	79	90	unknown		Vermejo?
RK22	325	90	unknown		Vermejo?
RK22	85	85	unknown		Vermejo?

RK22	320	88	unknown		Vermejo?
RK22	356	90	unknown		Vermejo?
RK22	313	88	unknown		Vermejo?
RK22	271	82	unknown		Vermejo?
RK22	165	80	unknown		Vermejo?
RK22	326	75	unknown		Vermejo?
RK22	174	83	unknown	terminates against 93/79	Vermejo?
RK22	273	79	unknown		Vermejo?

Location ID: SC1
Latitude: N 37.13128333
Longitude: W 104.00545

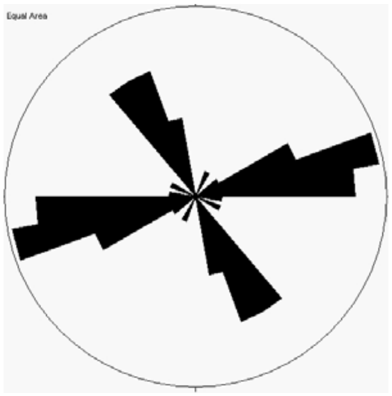

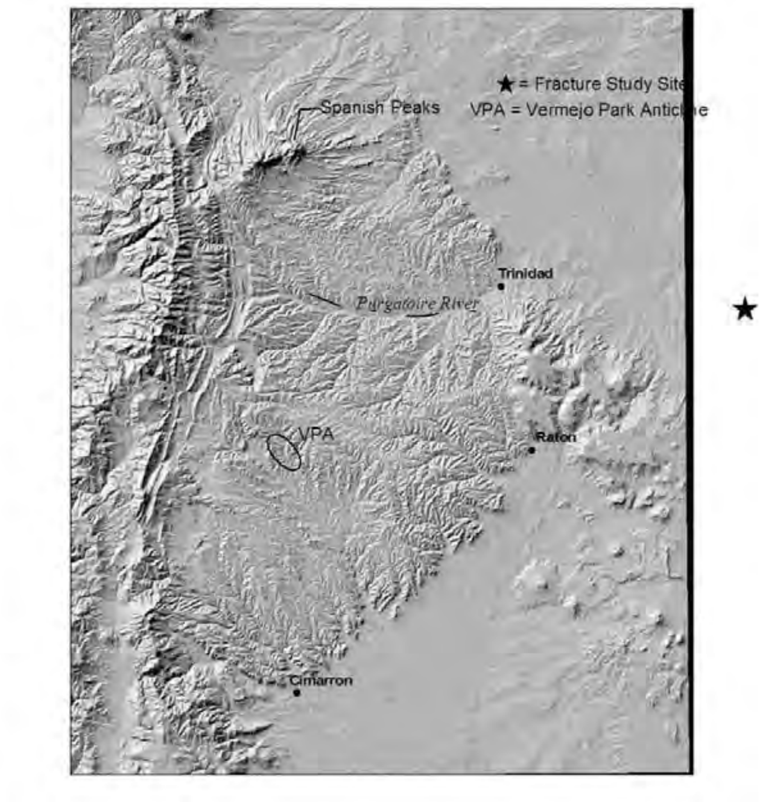

Notes:

Fracture Data:

ID	Strike	Dip	Formation
SC1	266	90	Dakota
SC1	260	90	Dakota
SC1	265	90	Dakota
SC1	264	90	Dakota
SC1	269	90	Dakota
SC1	338	80	Dakota
SC1	334	72	Dakota
SC1	339	76	Dakota
SC1	328	69	Dakota
SC1	339	75	Dakota
SC1	252	90	Dakota
SC1	24	90	Dakota
SC1	342	90	Dakota
SC1	63	90	Dakota
SC1	321	90	Dakota
SC1	58	90	Dakota
SC1	332	90	Dakota
SC1	251	90	Dakota
SC1	250	90	Dakota

SC1	323	90	Dakota
SC1	259	90	Dakota
SC1	254	90	Dakota
SC1	254	90	Dakota
SC1	349	90	Dakota
SC1	321	90	Dakota
SC1	67	90	Dakota
SC1	68	90	Dakota
SC1	321	90	Dakota
SC1	296	90	Dakota
SC1	67	90	Dakota
SC1	74	90	Dakota
SC1	271	90	Dakota
SC1	84	90	Dakota
SC1	345	90	Dakota

Location ID: SC2
Latitude: N 37.12718333
Longitude: W 104.0216333

Highway 160, east of Trinidad, CO
Dakota Fm.

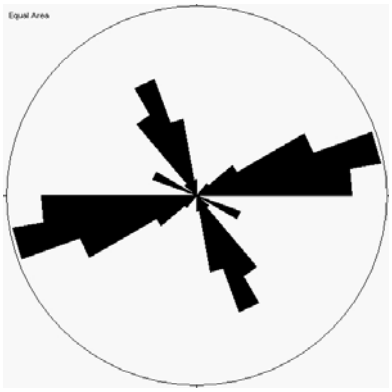

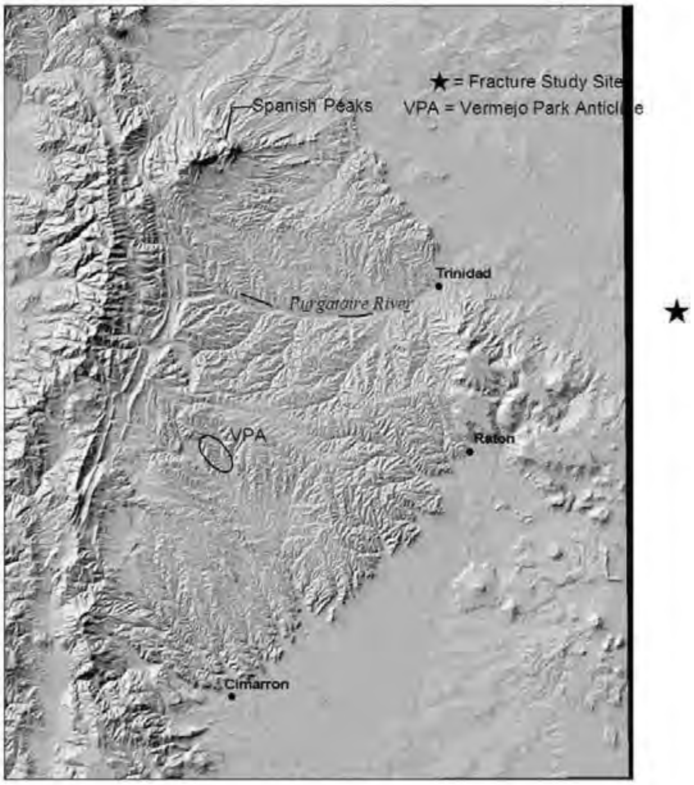

Notes:

Fracture Data:

ID	Strike	Dip	Formation	Comment 1	Comment 2
SC2	330	90	Dakota		
SC2	327	90	Dakota		
SC2	341	90	Dakota		
SC2	335	90	Dakota		
SC2	338	90	Dakota		
SC2	351	90	Dakota		
SC2	341	90	Dakota		
SC2	249	90	Dakota		
SC2	247	90	Dakota		
SC2	248	90	Dakota		
SC2	323	90	Dakota		
SC2	232	90	Dakota		
SC2	321	90	Dakota		
SC2	249	90	Dakota		
SC2	247	90	Dakota		
SC2	331	90	Dakota		
SC2	40	90	Dakota		
SC2	59	90	Dakota		
SC2	325	90	Dakota		

SC2	234	90	Dakota	
SC2	338	90	Dakota	
SC2	63	90	Dakota	
SC2	334	90	Dakota	
SC2	325	90	Dakota	
SC2	345	90	Dakota	
SC2	324	90	Dakota	
SC2	340	90	Dakota	
SC2	312	90	Dakota	
SC2	334	90	Dakota	
SC2	340	90	Dakota	
SC2	331	90	Dakota	
SC2	291	90	Dakota	
SC2	290	90	Dakota	
SC2	294	90	Dakota	
SC2	62	90	Dakota	
SC2	72	90	Dakota	
SC2	76	90	Dakota	
SC2	75	90	Dakota	
SC2	77	90	Dakota	
SC2	74	90	Dakota	
SC2	85	90	Dakota	
SC2	82	90	Dakota	
SC2	80	90	Dakota	
SC2	85	90	Dakota	
SC2	89	90	Dakota	
SC2	68	90	Dakota	
SC2	82	90	Dakota	
SC2	72	90	Dakota	
SC2	71	90	Dakota	
SC2	79	90	Dakota	
SC2	72	90	Dakota	
SC2	82	90	Dakota	
SC2	83	90	Dakota	
SC2	77	90	Dakota	
SC2	84	90	Dakota	
SC2	76	90	Dakota	
SC2	83	90	Dakota	
SC2	79	90	Dakota	
SC2	254	90	Dakota	coal cleat
SC2	342	90	Dakota	coal cleat
SC2	352	90	Dakota	coal cleat
SC2	18	90	Dakota	coal cleat
SC2	3	90	Dakota	coal cleat
SC2	355	90	Dakota	coal cleat
SC2	77	90	Dakota	coal cleat
SC2	354	90	Dakota	coal cleat
SC2	280	90	Dakota	coal cleat
SC2	342	90	Dakota	coal cleat
SC2	337	90	Dakota	coal cleat

SC2	245	90	Dakota	coal cleat	
SC2	38	90	Dakota	coal cleat	
SC2	310	90	Dakota	coal cleat	
SC2	26	90	Dakota	coal cleat	
SC2	28	90	Dakota	coal cleat	
SC2	68	90	Dakota	coal cleat	
SC2	73	90	Dakota	coal cleat	
SC2	65	90	Dakota	coal cleat	
SC2	61	90	Dakota	coal cleat	
SC2	266	90	Dakota		
SC2	260	90	Dakota		
SC2	265	90	Dakota		
SC2	264	90	Dakota		
SC2	269	90	Dakota		
SC2	338	80	Dakota		
SC2	334	72	Dakota		
SC2	339	76	Dakota		
SC2	328	69	Dakota		
SC2	339	75	Dakota		
SC2	252	90	Dakota		
SC2	24	90	Dakota		
SC2	342	90	Dakota		
SC2	63	90	Dakota		
SC2	321	90	Dakota		
SC2	58	90	Dakota		
SC2	332	90	Dakota		
SC2	251	90	Dakota		
SC2	250	90	Dakota		
SC2	323	90	Dakota		
SC2	259	90	Dakota		
SC2	254	90	Dakota		
SC2	254	90	Dakota		
SC2	349	90	Dakota		
SC2	321	90	Dakota		
SC2	67	90	Dakota		
SC2	68	90	Dakota		
SC2	321	90	Dakota		
SC2	296	90	Dakota		
SC2	67	90	Dakota		
SC2	74	90	Dakota		
SC2	271	90	Dakota		
SC2	84	90	Dakota		
SC2	345	90	Dakota		
SC2	68	90	Dakota		MM374
SC2	77	90	Dakota		MM374
SC2	65	90	Dakota		MM374
SC2	67	90	Dakota		MM374
SC2	69	90	Dakota		MM374
SC2	92	90	Dakota		MM374
SC2	65	90	Dakota		MM374

SC2	81	90	Dakota	MM374
SC2	68	90	Dakota	MM374
SC2	79	90	Dakota	MM374
SC2	79	90	Dakota	MM374
SC2	75	90	Dakota	MM374
SC2	88	90	Dakota	MM374
SC2	340	90	Dakota	MM374
SC2	282	90	Dakota	MM374
SC2	336	90	Dakota	MM374
SC2	68	90	Dakota	MM374
SC2	87	90	Dakota	MM374
SC2	86	90	Dakota	MM374
SC2	84	90	Dakota	MM374
SC2	78	90	Dakota	MM374
SC2	76	90	Dakota	MM374
SC2	286	90	Dakota	MM374
SC2	76	90	Dakota	MM374
SC2	88	90	Dakota	MM374
SC2	85	90	Dakota	MM374
SC2	61	90	Dakota	MM374
SC2	62	90	Dakota	MM374
SC2	67	90	Dakota	MM374
SC2	63	90	Dakota	MM374
SC2	340	90	Dakota	MM374
SC2	333	90	Dakota	MM374
SC2	76	90	Dakota	MM374
SC2	81	90	Dakota	MM374
SC2	327	90	Dakota	MM374
SC2	324	90	Dakota	MM374
SC2	335	90	Dakota	MM374
SC2	327	90	Dakota	MM374
SC2	337	90	Dakota	MM374
SC2	330	90	Dakota	MM374
SC2	328	90	Dakota	MM374
SC2	303	90	Dakota	MM374
SC2	315	90	Dakota	MM374
SC2	315	90	Dakota	MM374
SC2	315	90	Dakota	MM374
SC2	310	90	Dakota	MM374
SC2	340	90	Dakota	MM374
SC2	325	90	Dakota	MM374
SC2	316	90	Dakota	MM374
SC2	325	90	Dakota	MM374
SC2	329	90	Dakota	MM374
SC2	329	90	Dakota	MM374
SC2	317	90	Dakota	MM374
SC2	330	90	Dakota	MM374
SC2	333	90	Dakota	MM374
SC2	321	90	Dakota	MM374
SC2	62	90	Dakota	MM374

SC2	65	90	Dakota	MM374
SC2	332	90	Dakota	MM374
SC2	318	90	Dakota	MM374
SC2	325	90	Dakota	MM374
SC2	332	90	Dakota	MM374
SC2	326	90	Dakota	MM374
SC2	337	90	Dakota	MM374
SC2	324	90	Dakota	MM374
SC2	315	90	Dakota	MM374
SC2	42	90	Dakota	MM374
SC2	310	90	Dakota	MM374
SC2	326	90	Dakota	MM374
SC2	327	90	Dakota	MM374
SC2	320	90	Dakota	MM374
SC2	318	90	Dakota	MM374
SC2	327	90	Dakota	MM374
SC2	325	90	Dakota	MM374
SC2	323	90	Dakota	MM374
SC2	330	90	Dakota	MM374
SC2	68	90	Dakota	MM374
SC2	75	90	Dakota	MM374
SC2	350	90	Dakota	MM374
SC2	336	72	Dakota	mm375
SC2	155	74	Dakota	mm375
SC2	332	80	Dakota	mm375
SC2	78	90	Dakota	mm375
SC2	337	74	Dakota	mm375
SC2	79	90	Dakota	mm375
SC2	81	90	Dakota	mm375
SC2	262	87	Dakota	mm375
SC2	156	75	Dakota	mm375
SC2	335	78	Dakota	mm375
SC2	81	90	Dakota	mm375
SC2	335	90	Dakota	mm375
SC2	76	90	Dakota	mm375
SC2	314	90	Dakota	mm375
SC2	59	90	Dakota	mm375
SC2	70	90	Dakota	mm375
SC2	329	90	Dakota	mm375
SC2	73	90	Dakota	mm375
SC2	60	90	Dakota	mm375
SC2	338	90	Dakota	mm375
SC2	71	90	Dakota	mm375
SC2	15	90	Dakota	mm375
SC2	61	90	Dakota	mm375
SC2	63	90	Dakota	mm375
SC2	324	90	Dakota	mm375
SC2	81	90	Dakota	mm375
SC2	351	90	Dakota	mm375

Location ID: SC3
Latitude: N 37.18996667
Longitude: W 104.1549833

Highway 160, east of Trinidad, CO
Niobrara Fm.

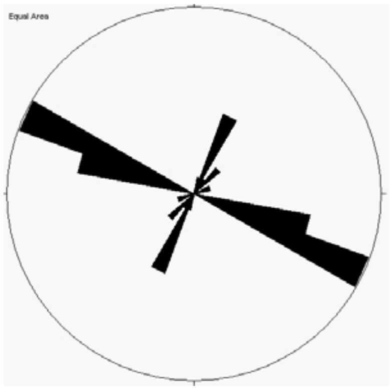

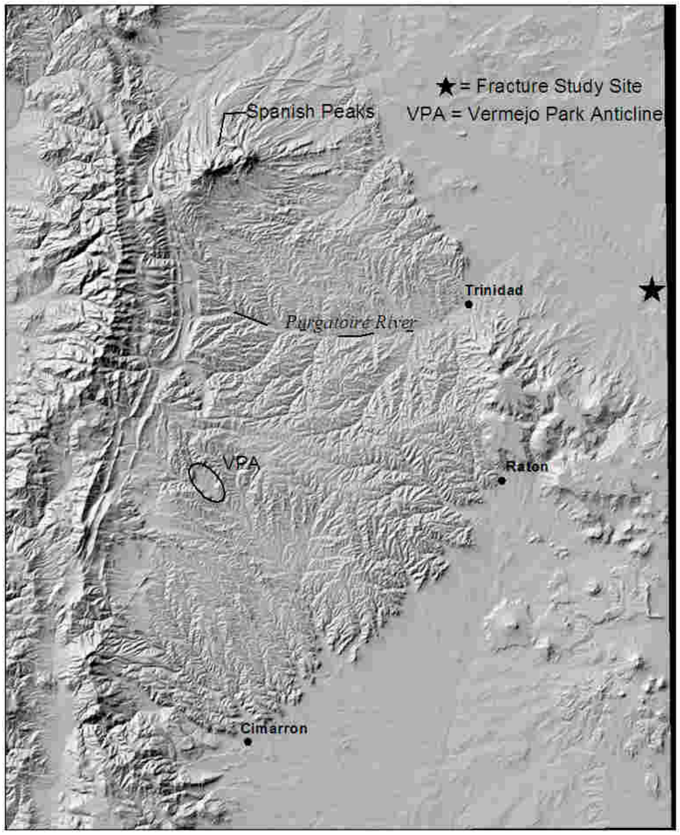

Notes:

Fracture Data:

ID	Strike	Dip	Formation
SC3	290	90	Niobrara
SC3	286	90	Niobrara
SC3	296	90	Niobrara
SC3	288	90	Niobrara
SC3	294	90	Niobrara
SC3	24	90	Niobrara
SC3	26	90	Niobrara
SC3	23	90	Niobrara
SC3	290	90	Niobrara
SC3	289	90	Niobrara
SC3	291	90	Niobrara
SC3	288	90	Niobrara
SC3	289	90	Niobrara
SC3	19	90	Niobrara
SC3	47	90	Niobrara
SC3	291	90	Niobrara
SC3	298	90	Niobrara

SC3	294	90	Niobrara
SC3	40	90	Niobrara
SC3	21	90	Niobrara
SC3	287	90	Niobrara
SC3	27	90	Niobrara
SC3	79	90	Niobrara
SC3	281	90	Niobrara
SC3	295	90	Niobrara
SC3	69	90	Niobrara
SC3	297	90	Niobrara
SC3	294	90	Niobrara
SC3	32	90	Niobrara
SC3	292	90	Niobrara
SC3	288	90	Niobrara
SC3	288	90	Niobrara
SC3	294	90	Niobrara
SC3	288	90	Niobrara
SC3	293	90	Niobrara
SC3	293	90	Niobrara
SC3	293	90	Niobrara
SC3	293	90	Niobrara
SC3	294	90	Niobrara
SC3	290	90	Niobrara
SC3	287	90	Niobrara
SC3	291	90	Niobrara
SC3	290	90	Niobrara
SC3	283	90	Niobrara
SC3	284	90	Niobrara
SC3	293	90	Niobrara
SC3	293	90	Niobrara
SC3	23	90	Niobrara
SC3	287	90	Niobrara
SC3	287	90	Niobrara
SC3	298	90	Niobrara
SC3	290	90	Niobrara
SC3	284	90	Niobrara
SC3	284	90	Niobrara
SC3	285	90	Niobrara
SC3	286	90	Niobrara
SC3	285	90	Niobrara
SC3	272	90	Niobrara
SC3	268	90	Niobrara
SC3	284	90	Niobrara
SC3	284	90	Niobrara
SC3	288	90	Niobrara
SC3	289	90	Niobrara
SC3	271	90	Niobrara
SC3	250	90	Niobrara
SC3	221	90	Niobrara
SC3	295	90	Niobrara

SC3	292	90	Niobrara
SC3	287	90	Niobrara
SC3	295	90	Niobrara
SC3	295	90	Niobrara
SC3	295	90	Niobrara
SC3	295	90	Niobrara
SC3	287	90	Niobrara
SC3	266	90	Niobrara
SC3	74	90	Niobrara
SC3	92	90	Niobrara
SC3	91	90	Niobrara
SC3	87	90	Niobrara
SC3	90	90	Niobrara
SC3	91	90	Niobrara
SC3	110	90	Niobrara
SC3	98	90	Niobrara
SC3	97	90	Niobrara
SC3	112	90	Niobrara
SC3	113	90	Niobrara
SC3	108	90	Niobrara
SC3	109	90	Niobrara
SC3	118	90	Niobrara
SC3	118	90	Niobrara
SC3	114	90	Niobrara
SC3	112	90	Niobrara
SC3	118	90	Niobrara
SC3	117	90	Niobrara
SC3	111	90	Niobrara
SC3	107	90	Niobrara
SC3	111	90	Niobrara
SC3	37	90	Niobrara
SC3	21	90	Niobrara
SC3	29	90	Niobrara
SC3	119	90	Niobrara
SC3	109	90	Niobrara
SC3	105	90	Niobrara
SC3	23	90	Niobrara
SC3	98	90	Niobrara
SC3	108	90	Niobrara
SC3	103	90	Niobrara
SC3	15	90	Niobrara
SC3	18	90	Niobrara
SC3	30	90	Niobrara
SC3	350	90	Niobrara
SC3	118	90	Niobrara
SC3	106	90	Niobrara
SC3	8	90	Niobrara
SC3	111	90	Niobrara
SC3	112	90	Niobrara
SC3	2	90	Niobrara

SC3	111	90	Niobrara
SC3	101	90	Niobrara
SC3	107	90	Niobrara
SC3	109	90	Niobrara
SC3	350	90	Niobrara
SC3	13	90	Niobrara
SC3	19	90	Niobrara
SC3	100	90	Niobrara
SC3	107	90	Niobrara
SC3	109	90	Niobrara
SC3	346	90	Niobrara
SC3	17	90	Niobrara
SC3	103	90	Niobrara
SC3	107	90	Niobrara
SC3	109	90	Niobrara
SC3	110	90	Niobrara
SC3	110	90	Niobrara
SC3	111	90	Niobrara
SC3	22	90	Niobrara
SC3	20	90	Niobrara
SC3	107	90	Niobrara
SC3	108	90	Niobrara
SC3	16	90	Niobrara
SC3	350	90	Niobrara
SC3	105	90	Niobrara
SC3	114	90	Niobrara
SC3	108	90	Niobrara
SC3	108	90	Niobrara
SC3	107	90	Niobrara
SC3	24	90	Niobrara
SC3	25	90	Niobrara
SC3	106	90	Niobrara
SC3	105	90	Niobrara
SC3	104	90	Niobrara
SC3	102	90	Niobrara
SC3	15	90	Niobrara
SC3	20	90	Niobrara
SC3	110	90	Niobrara
SC3	106	90	Niobrara
SC3	355	90	Niobrara
SC3	22	90	Niobrara
SC3	112	90	Niobrara
SC3	104	90	Niobrara
SC3	105	90	Niobrara
SC3	21	90	Niobrara
SC3	22	90	Niobrara
SC3	24	90	Niobrara
SC3	104	90	Niobrara
SC3	106	90	Niobrara
SC3	108	90	Niobrara

SC3	18	90	Niobrara
SC3	19	90	Niobrara

Location ID: SC4
Latitude: N 37.12551667
Longitude: W 104.7874833

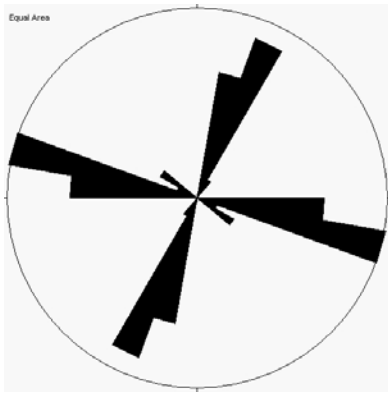

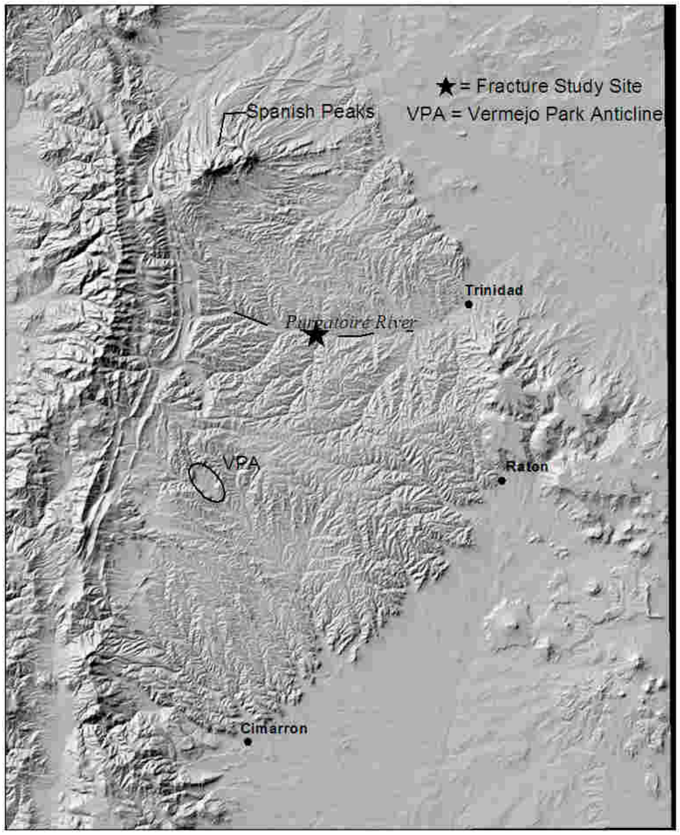

Notes:

Fracture Data:

ID	Strike	Dip	Formation	Comment 1
SC4	20	90	Raton	Sandstone
SC4	294	90	Raton	Sandstone
SC4	287	90	Raton	Sandstone
SC4	278	90	Raton	Sandstone
SC4	300	90	Raton	Sandstone
SC4	278	90	Raton	Sandstone
SC4	25	90	Raton	Sandstone
SC4	25	90	Raton	Sandstone
SC4	19	90	Raton	Sandstone
SC4	15	90	Raton	Sandstone
SC4	276	90	Raton	Sandstone
SC4	18	90	Raton	Sandstone
SC4	287	90	Raton	Sandstone
SC4	12	90	Raton	Sandstone
SC4	303	90	Raton	Sandstone
SC4	18	90	Raton	Sandstone
SC4	279	90	Raton	Sandstone

SC4	27	90	Raton	Sandstone
SC4	19	90	Raton	Sandstone
SC4	34	90	Raton	Sandstone
SC4	275	90	Raton	Sandstone
SC4	284	90	Raton	Sandstone
SC4	283	90	Raton	Sandstone
SC4	283	90	Raton	Sandstone
SC4	29	90	Raton	Sandstone
SC4	27	90	Raton	Sandstone
SC4	25	90	Raton	Sandstone
SC4	287	90	Raton	Sandstone
SC4	285	90	Raton	Sandstone
SC4	285	90	Raton	Sandstone
SC4	278	90	Raton	Sandstone
SC4	29	90	Raton	Sandstone
SC4	284	90	Raton	Sandstone
SC4	17	90	Raton	Sill
SC4	305	90	Raton	Sill
SC4	318	90	Raton	Sill
SC4	359	90	Raton	Sill
SC4	319	90	Raton	Sill
SC4	32	90	Raton	Sill
SC4	318	90	Raton	Sill
SC4	274	90	Raton	Sill
SC4	91	90	Raton	Sill
SC4	312	90	Raton	Sill
SC4	215	90	Raton	Sill
SC4	311	90	Raton	Sill
SC4	14	90	Raton	Sill
SC4	309	90	Raton	Sill
SC4	292	90	Raton	Sill
SC4	23	90	Raton	Sill
SC4	303	90	Raton	Sill
SC4	36	90	Raton	Sill
SC4	86	90	Raton	Sill
SC4	276	90	Raton	Sill
SC4	21	90	Raton	Sill
SC4	345	90	Raton	Sill
SC4	274	90	Raton	Sill
SC4	25	90	Raton	Sill
SC4	273	90	Raton	Sill
SC4	28	90	Raton	Sill
SC4	31	90	Raton	Sill
SC4	272	90	Raton	Sill
SC4	271	90	Raton	Sill
SC4	10	90	Raton	Sill
SC4	29	90	Raton	Sill
SC4	66	90	Raton	Sill
SC4	87	90	Raton	Sill
SC4	304	90	Raton	Sill

SC4	35	90	Raton	Sill
SC4	87	90	Raton	Sill
SC4	37	90	Raton	Sill
SC4	35	90	Raton	Sill
SC4	31	90	Raton	Sill
SC4	295	90	Raton	Sill
SC4	17	90	Raton	Sill
SC4	300	90	Raton	Sill
SC4	294	90	Raton	Sill
SC4	301	90	Raton	Sill
SC4	303	90	Raton	Sill
SC4	301	90	Raton	Sill
SC4	316	90	Raton	Sill
SC4	1	90	Raton	Sill
SC4	301	90	Raton	Sill
SC4	301	90	Raton	Coal cleats
SC4	45	90	Raton	Coal cleats
SC4	293	90	Raton	Coal cleats
SC4	301	90	Raton	Coal cleats
SC4	26	90	Raton	Coal cleats
SC4	77	90	Raton	Coal cleats
SC4	15	90	Raton	Coal cleats
SC4	31	90	Raton	Coal cleats
SC4	294	90	Raton	Coal cleats
SC4	303	90	Raton	Coal cleats
SC4	303	90	Raton	Coal cleats
SC4	16	90	Raton	Coal cleats
SC4	325	90	Raton	Coal cleats
SC4	72	90	Raton	Coal cleats
SC4	325	90	Raton	Coal cleats
SC4	24	90	Raton	Coal cleats
SC4	301	90	Raton	Coal cleats
SC4	19	90	Raton	Coal cleats
SC4	329	90	Raton	Coal cleats
SC4	298	90	Raton	Coal cleats
SC4	303	90	Raton	Coal cleats
SC4	78	90	Raton	Coal cleats
SC4	76	90	Raton	Coal cleats
SC4	296	90	Raton	Coal cleats
SC4	82	90	Raton	Coal cleats
SC4	82	90	Raton	Coal cleats
SC4	355	90	Raton	Coal cleats
SC4	325	90	Raton	Coal cleats
SC4	330	90	Raton	Coal cleats
SC4	84	90	Raton	Coal cleats
SC4	11	90	Raton	Coal cleats
SC4	33	90	Raton	Coal cleats

Location ID: SC5
Latitude: N 37.13101667
Longitude: W 104.53315

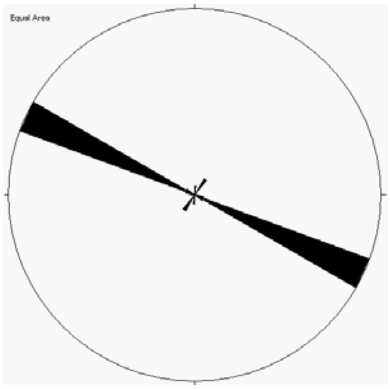

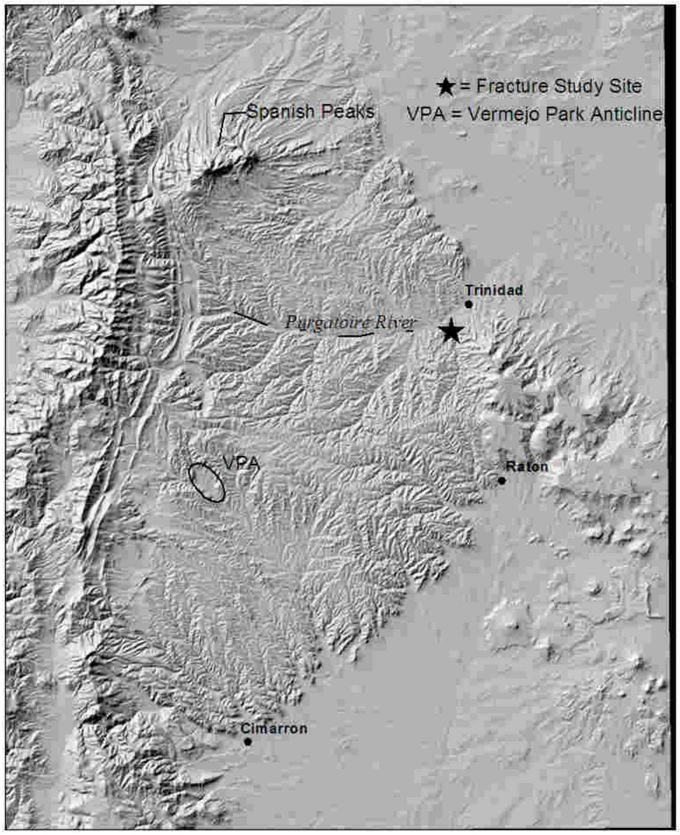

Notes:

Fracture Data:

ID	Strike	Dip	Formation	Comment 1
SC5	290	90	Vermejo	Sandstone
SC5	291	90	Vermejo	Sandstone
SC5	291	90	Vermejo	Sandstone
SC5	293	90	Vermejo	Sandstone
SC5	296	90	Vermejo	Sandstone
SC5	298	90	Vermejo	Sandstone
SC5	297	90	Vermejo	Sandstone
SC5	297	90	Vermejo	Sandstone
SC5	293	90	Vermejo	Sandstone
SC5	296	90	Vermejo	Sandstone
SC5	291	90	Vermejo	Sandstone
SC5	300	90	Vermejo	Sandstone
SC5	298	90	Vermejo	Sandstone
SC5	30	90	Vermejo	Sandstone
SC5	297	90	Vermejo	Sandstone
SC5	291	90	Vermejo	Sandstone
SC5	39	90	Vermejo	Sandstone

SC5	289	90	Vermejo	Sandstone
SC5	290	90	Vermejo	Sandstone
SC5	293	90	Vermejo	Sandstone
SC5	8	90	Vermejo	Sandstone
SC5	291	90	Vermejo	Sandstone
SC5	295	90	Vermejo	Sandstone
SC5	290	90	Vermejo	Sandstone
SC5	291	90	Vermejo	Sandstone

Location ID: SC6
Latitude: N 37.1580333
Longitude: W 104.5821667

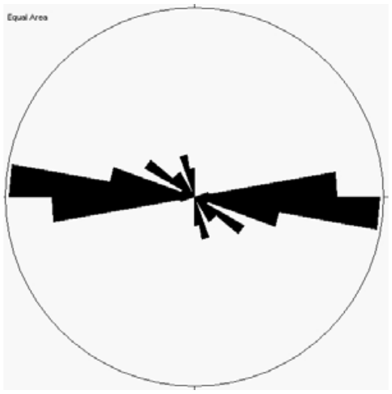

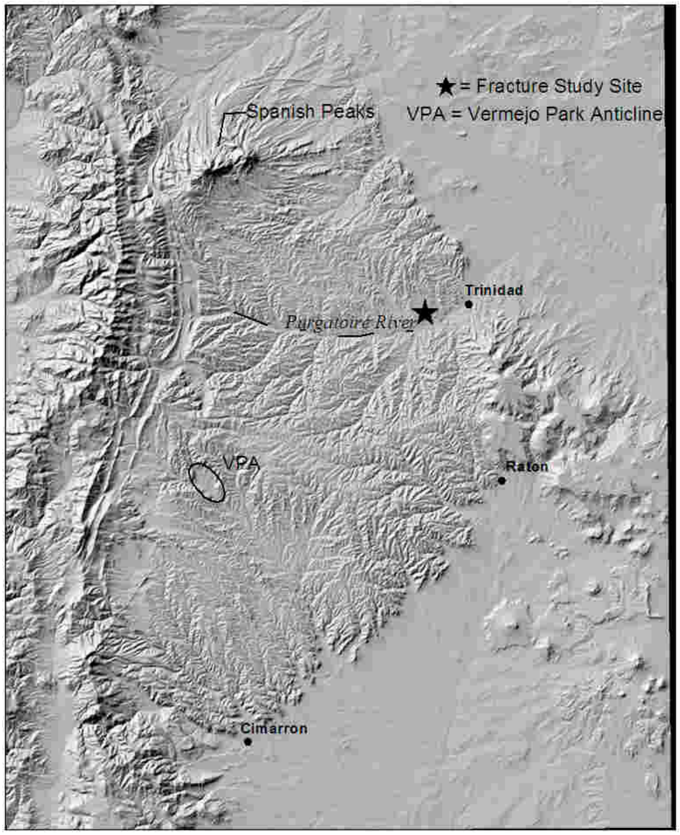

Notes:

Fracture Data:

ID	Strike	Dip	Formation	Comment 1
SC6	340	90	unknown	sandstone
SC6	82	90	unknown	sandstone
SC6	99	90	unknown	sandstone
SC6	84	90	unknown	sandstone
SC6	90	90	unknown	sandstone
SC6	355	90	unknown	sandstone
SC6	349	90	unknown	sandstone
SC6	88	90	unknown	sandstone
SC6	103	90	unknown	sandstone
SC6	79	90	unknown	sandstone
SC6	100	90	unknown	sandstone
SC6	109	90	unknown	sandstone
SC6	93	90	unknown	sandstone
SC6	90	90	unknown	sandstone
SC6	89	90	unknown	sandstone
SC6	92	90	unknown	sandstone
SC6	137	90	unknown	sandstone

SC6	120	90	unknown	sandstone
SC6	102	90	unknown	sandstone
SC6	91	90	unknown	sandstone
SC6	91	90	unknown	sandstone
SC6	128	90	unknown	sandstone
SC6	121	90	unknown	sandstone
SC6	93	90	unknown	sandstone
SC6	87	90	unknown	sandstone
SC6	88	90	unknown	sandstone
SC6	109	90	unknown	sandstone
SC6	108	90	unknown	sandstone
SC6	97	90	unknown	sandstone
SC6	92	90	unknown	sandstone
SC6	141	90	unknown	sandstone
SC6	88	90	unknown	sandstone
SC6	89	90	unknown	sandstone
SC6	97	90	unknown	sandstone
SC6	117	90	unknown	sandstone
SC6	84	90	unknown	sandstone
SC6	345	90	unknown	sandstone
SC6	329	90	unknown	sandstone
SC6	93	90	unknown	sandstone
SC6	138	90	unknown	sandstone
SC6	121	90	unknown	sandstone
SC6	91	90	unknown	sandstone
SC6	87	90	unknown	sandstone
SC6	351	90	unknown	sandstone

Location ID: SC7
Latitude: N 37.11378333
Longitude: W 104.5205167

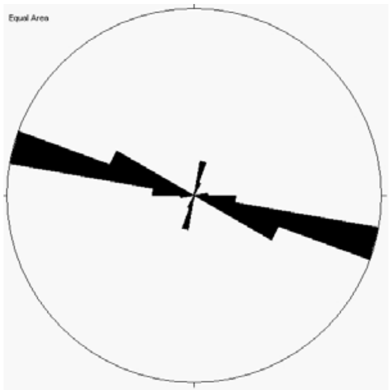

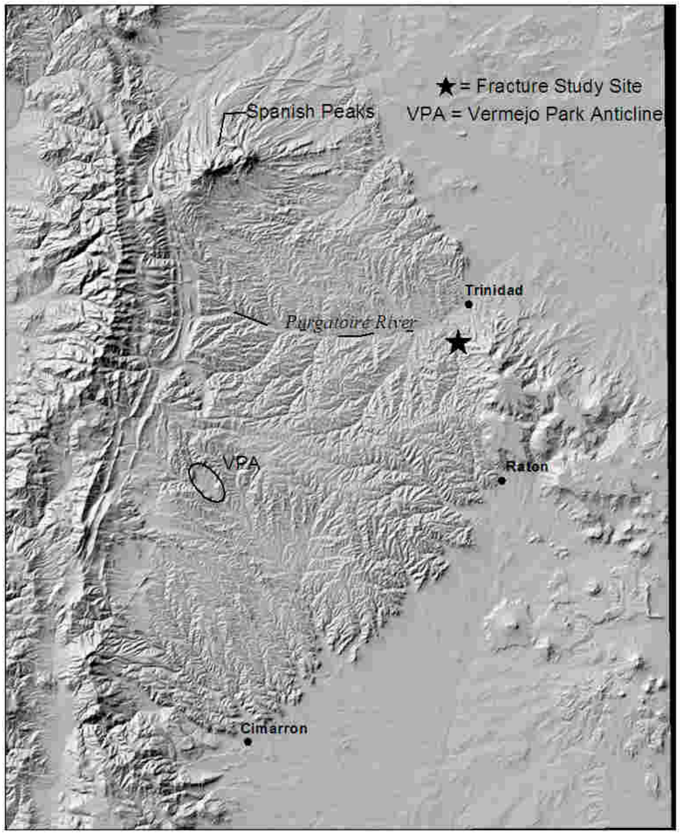

Notes:

Fracture Data:

ID	Strike	Dip	Formation	Comment 1
SC7	283	90	Vermejo	sandstone
SC7	287	90	Vermejo	sandstone
SC7	286	90	Vermejo	sandstone
SC7	286	90	Vermejo	sandstone
SC7	285	90	Vermejo	sandstone
SC7	289	90	Vermejo	sandstone
SC7	286	90	Vermejo	sandstone
SC7	285	90	Vermejo	sandstone
SC7	282	90	Vermejo	sandstone
SC7	285	90	Vermejo	sandstone
SC7	292	90	Vermejo	sandstone
SC7	290	90	Vermejo	sandstone
SC7	288	90	Vermejo	sandstone
SC7	297	90	Vermejo	sandstone
SC7	292	90	Vermejo	sandstone
SC7	281	90	Vermejo	sandstone
SC7	279	90	Vermejo	sandstone

SC7	291	90	Vermejo	sandstone
SC7	285	90	Vermejo	sandstone
SC7	290	90	Vermejo	sandstone
SC7	18	90	Vermejo	sandstone
SC7	295	90	Vermejo	sandstone
SC7	25	90	Vermejo	sandstone
SC7	288	90	Vermejo	sandstone
SC7	296	90	Vermejo	sandstone
SC7	16	90	Vermejo	sandstone
SC7	286	90	Vermejo	sandstone
SC7	285	90	Vermejo	sandstone
SC7	292	90	Vermejo	sandstone
SC7	286	90	Vermejo	sandstone
SC7	26	90	Vermejo	sandstone
SC7	288	90	Vermejo	sandstone
SC7	278	90	Vermejo	sandstone
SC7	285	90	Vermejo	sandstone
SC7	280	90	Vermejo	sandstone
SC7	281	90	Vermejo	sandstone
SC7	281	90	Vermejo	sandstone
SC7	293	90	Vermejo	sandstone
SC7	268	90	Vermejo	sandstone
SC7	268	90	Vermejo	sandstone
SC7	290	90	Vermejo	sandstone
SC7	289	90	Vermejo	sandstone
SC7	292	90	Vermejo	sandstone
SC7	291	90	Vermejo	sandstone
SC7	286	90	Vermejo	sandstone
SC7	15	90	Vermejo	sandstone
SC7	277	90	Vermejo	sandstone
SC7	11	90	Vermejo	sandstone
SC7	289	90	Vermejo	sandstone
SC7	11	90	Vermejo	sandstone
SC7	289	90	Vermejo	sandstone
SC7	286	90	Vermejo	sandstone
SC7	276	90	Vermejo	sandstone
SC7	279	90	Vermejo	sandstone
SC7	279	90	Vermejo	sandstone
SC7	279	90	Vermejo	coal cleats
SC7	283	90	Vermejo	coal cleats
SC7	283	90	Vermejo	coal cleats
SC7	283	90	Vermejo	coal cleats
SC7	284	90	Vermejo	coal cleats
SC7	281	90	Vermejo	coal cleats
SC7	282	90	Vermejo	coal cleats
SC7	283	90	Vermejo	coal cleats
SC7	285	90	Vermejo	coal cleats
SC7	283	90	Vermejo	coal cleats
SC7	286	90	Vermejo	coal cleats
SC7	287	90	Vermejo	coal cleats

SC7	287	90	Vermejo	coal cleats
SC7	288	90	Vermejo	coal cleats
SC7	286	90	Vermejo	coal cleats
SC7	285	90	Vermejo	coal cleats
SC7	286	90	Vermejo	coal cleats
SC7	290	90	Vermejo	coal cleats
SC7	281	90	Vermejo	coal cleats
SC7	284	90	Vermejo	coal cleats
SC7	288	90	Vermejo	coal cleats
SC7	287	90	Vermejo	coal cleats
SC7	285	90	Vermejo	coal cleats
SC7	287	90	Vermejo	coal cleats
SC7	282	90	Vermejo	coal cleats
SC7	283	90	Vermejo	coal cleats
SC7	8	90	Vermejo	coal cleats
SC7	13	90	Vermejo	coal cleats
SC7	13	90	Vermejo	coal cleats
SC7	13	90	Vermejo	coal cleats
SC7	10	90	Vermejo	coal cleats
SC7	17	90	Vermejo	coal cleats
SC7	9	90	Vermejo	coal cleats
SC7	13	90	Vermejo	coal cleats
SC7	10	90	Vermejo	coal cleats
SC7	10	90	Vermejo	coal cleats
SC7	12	90	Vermejo	coal cleats
SC7	12	90	Vermejo	coal cleats
SC7	14	90	Vermejo	coal cleats
SC7	9	90	Vermejo	coal cleats
SC7	14	90	Vermejo	coal cleats
SC7	6	90	Vermejo	coal cleats
SC7	8	90	Vermejo	coal cleats
SC7	16	90	Vermejo	coal cleats
SC7	11	90	Vermejo	coal cleats
SC7	15	90	Vermejo	coal cleats
SC7	13	90	Vermejo	coal cleats
SC7	11	90	Vermejo	coal cleats
SC7	6	90	Vermejo	coal cleats
SC7	268	54	Vermejo	faults in coal
SC7	343	48	Vermejo	faults in coal
SC7	284	40	Vermejo	faults in coal
SC7	57	50	Vermejo	faults in coal
SC7	42	45	Vermejo	faults in coal
SC7	259	45	Vermejo	faults in coal
SC7	18	50	Vermejo	faults in coal
SC7	109	55	Vermejo	faults in coal
SC7	283	40	Vermejo	faults in coal
SC7	328	50	Vermejo	faults in coal
SC7	84	88	unknown	dike

Location ID: SC8
Latitude: N 36.3526
Longitude: W 104.6014

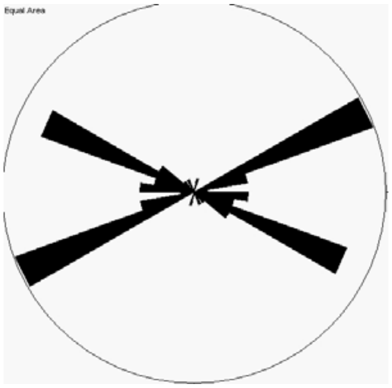

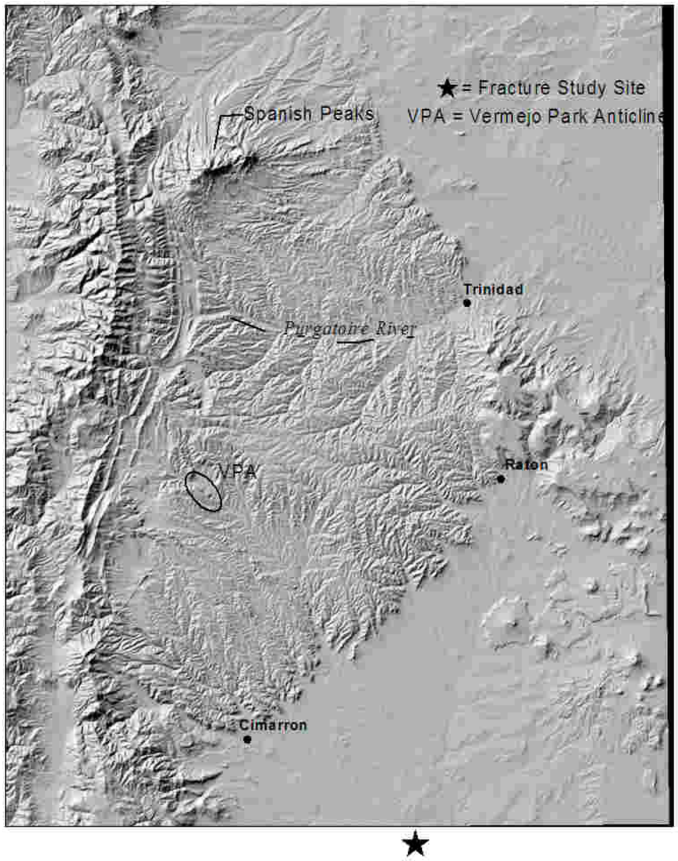

Notes:

Fracture Data:

ID	Strike	Dip	Formation	Comment 1
SC8	280	90	Niobrara	
SC8	289	90	Niobrara	
SC8	250	90	Niobrara	
SC8	10	90	Niobrara	
SC8	251	90	Niobrara	
SC8	278	90	Niobrara	
SC8	308	90	Niobrara	
SC8	258	90	Niobrara	
SC8	300	90	Niobrara	
SC8	309	90	Niobrara	
SC8	245	90	Niobrara	
SC8	299	90	Niobrara	
SC8	247	90	Niobrara	
SC8	248	90	Niobrara	
SC8	292	90	Niobrara	
SC8	248	90	Niobrara	
SC8	292	90	Niobrara	

SC8	290	90	Niobrara	
SC8	290	90	Niobrara	
SC8	330	90	Niobrara	
SC8	298	90	Niobrara	
SC8	243	90	Niobrara	
SC8	244	90	Niobrara	
SC8	248	90	Niobrara	
SC8	298	90	Niobrara	
SC8	299	90	Niobrara	
SC8	249	90	Niobrara	
SC8	297	90	Niobrara	
SC8	296	90	Niobrara	
SC8	245	90	Niobrara	
SC8	279	90	Niobrara	
SC8	294	90	Niobrara	
SC8	243	90	Niobrara	
SC8	242	90	Niobrara	
SC8	252	90	Niobrara	
SC8	278	90	Niobrara	
SC8	315	90	Niobrara	
SC8	241	90	Niobrara	
SC8	269	90	Niobrara	
SC8	242	90	Niobrara	
SC8	277	90	Niobrara	
SC8	245	90	Niobrara	
SC8	289	90	Niobrara	
SC8	292	90	Niobrara	
SC8	344	70	Niobrara	fault
SC8	327	50	Niobrara	fault
SC8	29	50	Niobrara	fault
SC8	210	48	Niobrara	fault
SC8	185	60	Niobrara	fault

Location ID: SC9a
Latitude: N 36.9043167
Longitude: W 104.4462833

Goat Hill overlook, Vermejo coal

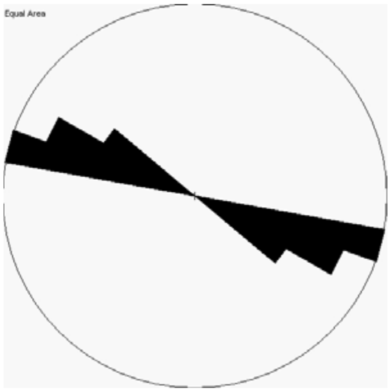

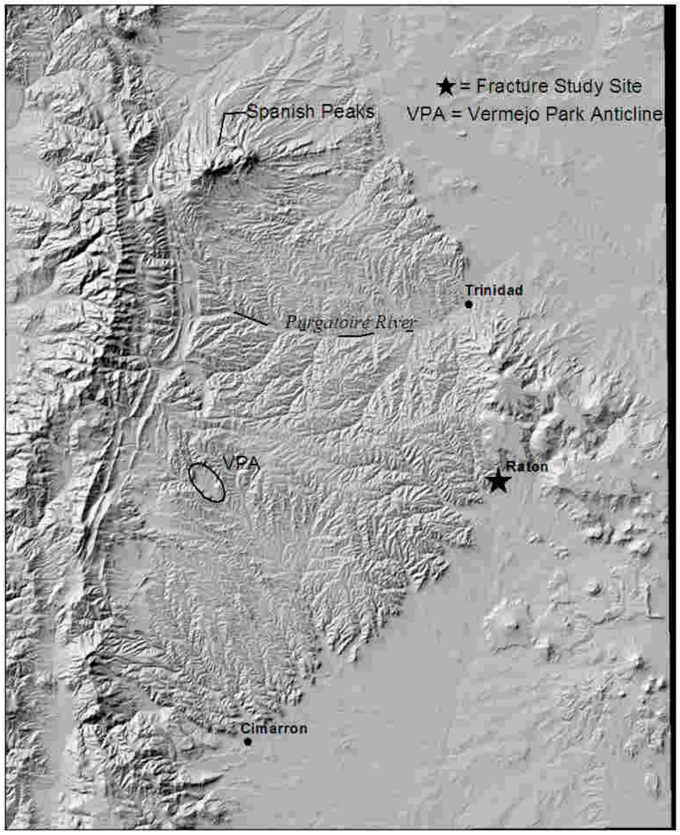

Notes:

Fracture Data:

ID	Strike	Dip	Formation
SC9a	283	82	Vermejo
SC9a	283	82	Vermejo
SC9a	282	84	Vermejo
SC9a	282	84	Vermejo
SC9a	283	82	Vermejo
SC9a	283	82	Vermejo
SC9a	284	82	Vermejo
SC9a	284	81	Vermejo
SC9a	284	80	Vermejo
SC9a	284	82	Vermejo
SC9a	302	79	Vermejo
SC9a	300	79	Vermejo
SC9a	302	76	Vermejo
SC9a	306	86	Vermejo
SC9a	299	84	Vermejo
SC9a	306	76	Vermejo
SC9a	300	72	Vermejo

SC9a	288	80	Vermejo
SC9a	296	79	Vermejo
SC9a	294	79	Vermejo
SC9a	296	85	Vermejo
SC9a	297	81	Vermejo
SC9a	297	85	Vermejo
SC9a	294	85	Vermejo
SC9a	295	82	Vermejo
SC9a	293	68	Vermejo

Location ID: SC9b
Latitude: N 36.9043167
Longitude: W 104.4462833

Goat Hill overlook, sandstone

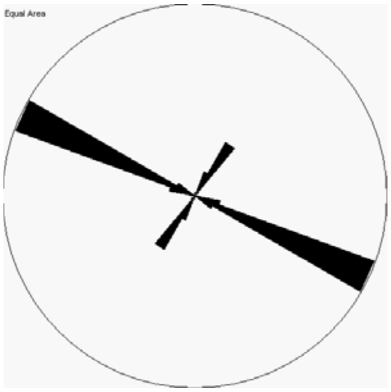

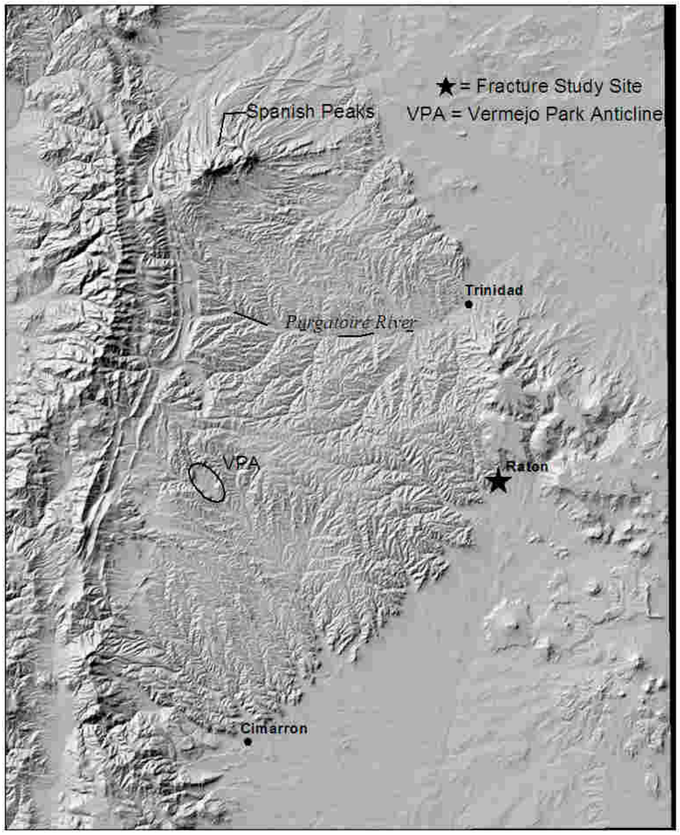

Notes:

Fracture Data:

ID	Strike	Dip	Formation	Comment 1
SC9b	289	90	Unknown	Vermejo or Trinidad
SC9b	287	90	Unknown	Vermejo or Trinidad
SC9b	292	90	Unknown	Vermejo or Trinidad
SC9b	295	90	Unknown	Vermejo or Trinidad
SC9b	296	90	Unknown	Vermejo or Trinidad
SC9b	299	90	Unknown	Vermejo or Trinidad
SC9b	299	90	Unknown	Vermejo or Trinidad
SC9b	298	90	Unknown	Vermejo or Trinidad
SC9b	298	90	Unknown	Vermejo or Trinidad
SC9b	299	90	Unknown	Vermejo or Trinidad
SC9b	302	90	Unknown	Vermejo or Trinidad
SC9b	287	90	Unknown	Vermejo or Trinidad
SC9b	298	90	Unknown	Vermejo or Trinidad
SC9b	300	90	Unknown	Vermejo or Trinidad
SC9b	299	90	Unknown	Vermejo or Trinidad
SC9b	298	90	Unknown	Vermejo or Trinidad
SC9b	297	90	Unknown	Vermejo or Trinidad

SC9b	296	90	Unknown	Vermejo or Trinidad
SC9b	293	90	Unknown	Vermejo or Trinidad
SC9b	295	90	Unknown	Vermejo or Trinidad
SC9b	299	90	Unknown	Vermejo or Trinidad
SC9b	296	90	Unknown	Vermejo or Trinidad
SC9b	296	90	Unknown	Vermejo or Trinidad
SC9b	300	90	Unknown	Vermejo or Trinidad
SC9b	296	90	Unknown	Vermejo or Trinidad
SC9b	290	90	Unknown	Vermejo or Trinidad
SC9b	300	90	Unknown	Vermejo or Trinidad
SC9b	296	90	Unknown	Vermejo or Trinidad
SC9b	297	90	Unknown	Vermejo or Trinidad
SC9b	294	90	Unknown	Vermejo or Trinidad
SC9b	295	90	Unknown	Vermejo or Trinidad
SC9b	299	90	Unknown	Vermejo or Trinidad
SC9b	289	90	Unknown	Vermejo or Trinidad
SC9b	299	90	Unknown	Vermejo or Trinidad
SC9b	299	90	Unknown	Vermejo or Trinidad
SC9b	299	90	Unknown	Vermejo or Trinidad
SC9b	299	90	Unknown	Vermejo or Trinidad
SC9b	293	90	Unknown	Vermejo or Trinidad
SC9b	295	90	Unknown	Vermejo or Trinidad
SC9b	295	90	Unknown	Vermejo or Trinidad
SC9b	290	90	Unknown	Vermejo or Trinidad
SC9b	293	90	Unknown	Vermejo or Trinidad
SC9b	293	90	Unknown	Vermejo or Trinidad
SC9b	289	90	Unknown	Vermejo or Trinidad
SC9b	293	90	Unknown	Vermejo or Trinidad
SC9b	299	90	Unknown	Vermejo or Trinidad
SC9b	26	90	Unknown	Vermejo or Trinidad
SC9b	27	90	Unknown	Vermejo or Trinidad
SC9b	27	90	Unknown	Vermejo or Trinidad
SC9b	31	90	Unknown	Vermejo or Trinidad
SC9b	30	90	Unknown	Vermejo or Trinidad
SC9b	34	90	Unknown	Vermejo or Trinidad
SC9b	36	90	Unknown	Vermejo or Trinidad
SC9b	35	90	Unknown	Vermejo or Trinidad
SC9b	30	90	Unknown	Vermejo or Trinidad
SC9b	28	90	Unknown	Vermejo or Trinidad
SC9b	31	90	Unknown	Vermejo or Trinidad
SC9b	36	90	Unknown	Vermejo or Trinidad
SC9b	25	90	Unknown	Vermejo or Trinidad
SC9b	30	90	Unknown	Vermejo or Trinidad
SC9b	30	90	Unknown	Vermejo or Trinidad
SC9b	33	90	Unknown	Vermejo or Trinidad
SC9b	32	90	Unknown	Vermejo or Trinidad
SC9b	44	90	Unknown	Vermejo or Trinidad

Location ID: SC10
Latitude: N 37.02858333
Longitude: W 103.9583167

Dakota pavement

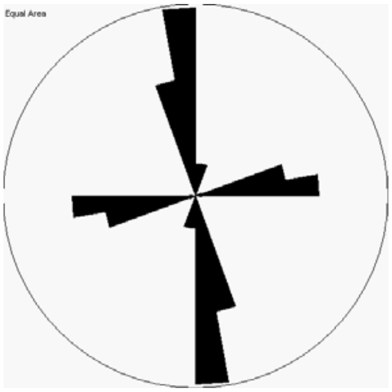

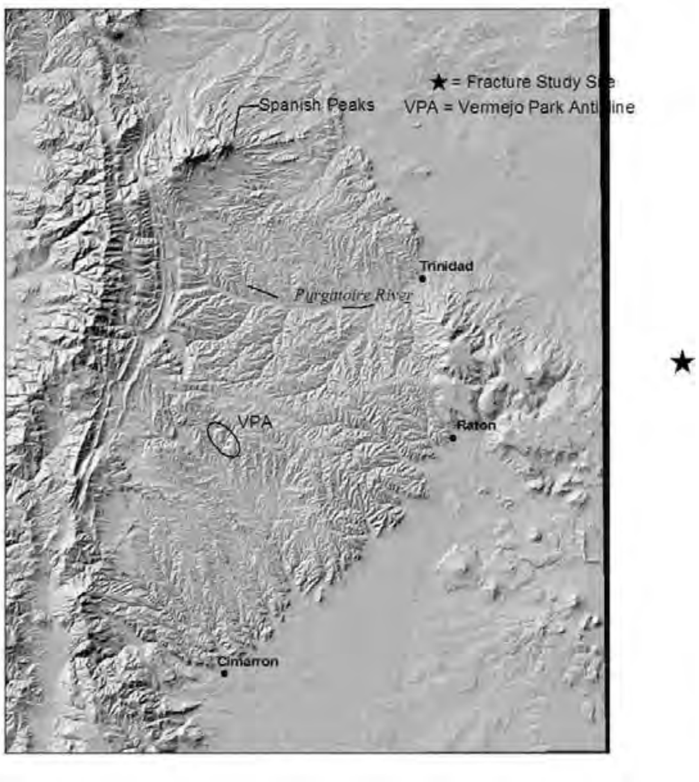

Notes:

Fracture Data:

ID	Strike	Dip	Formation
SC10	350	90	Dakota
SC10	348	90	Dakota
SC10	358	90	Dakota
SC10	358	90	Dakota
SC10	356	90	Dakota
SC10	357	90	Dakota
SC10	10	90	Dakota
SC10	355	90	Dakota
SC10	354	90	Dakota
SC10	358	90	Dakota
SC10	358	90	Dakota
SC10	10	90	Dakota
SC10	354	90	Dakota
SC10	2	90	Dakota
SC10	357	90	Dakota
SC10	2	90	Dakota
SC10	348	90	Dakota
SC10	357	90	Dakota
SC10	352	90	Dakota
SC10	346	90	Dakota

SC10	347	90	Dakota
SC10	347	90	Dakota
SC10	347	90	Dakota
SC10	349	90	Dakota
SC10	347	90	Dakota
SC10	345	90	Dakota
SC10	355	90	Dakota
SC10	347	90	Dakota
SC10	349	90	Dakota
SC10	345	90	Dakota
SC10	345	90	Dakota
SC10	357	90	Dakota
SC10	358	90	Dakota
SC10	357	90	Dakota
SC10	19	90	Dakota
SC10	355	90	Dakota
SC10	359	90	Dakota
SC10	2	90	Dakota
SC10	8	90	Dakota
SC10	6	90	Dakota
SC10	12	90	Dakota
SC10	10	90	Dakota
SC10	354	90	Dakota
SC10	355	90	Dakota
SC10	356	90	Dakota
SC10	356	90	Dakota
SC10	350	90	Dakota
SC10	349	90	Dakota
SC10	352	90	Dakota
SC10	354	90	Dakota
SC10	348	90	Dakota
SC10	344	90	Dakota
SC10	350	90	Dakota
SC10	352	90	Dakota
SC10	354	90	Dakota
SC10	345	90	Dakota
SC10	346	90	Dakota
SC10	84	90	Dakota
SC10	80	90	Dakota
SC10	76	90	Dakota
SC10	68	90	Dakota
SC10	76	90	Dakota
SC10	76	90	Dakota
SC10	75	90	Dakota
SC10	84	90	Dakota
SC10	82	90	Dakota
SC10	82	90	Dakota
SC10	83	90	Dakota
SC10	84	90	Dakota
SC10	86	90	Dakota

SC10	83	90	Dakota
SC10	79	90	Dakota
SC10	75	90	Dakota
SC10	80	90	Dakota
SC10	73	90	Dakota
SC10	72	90	Dakota
SC10	76	90	Dakota
SC10	70	90	Dakota
SC10	71	90	Dakota
SC10	71	90	Dakota
SC10	82	90	Dakota
SC10	81	90	Dakota
SC10	79	90	Dakota
SC10	75	90	Dakota
SC10	84	90	Dakota
SC10	84	90	Dakota
SC10	85	90	Dakota
SC10	86	90	Dakota
SC10	87	90	Dakota
SC10	82	90	Dakota
SC10	86	90	Dakota
SC10	90	90	Dakota

Location ID: SC11
Latitude: N 37.1601667
Longitude: W 104.9422

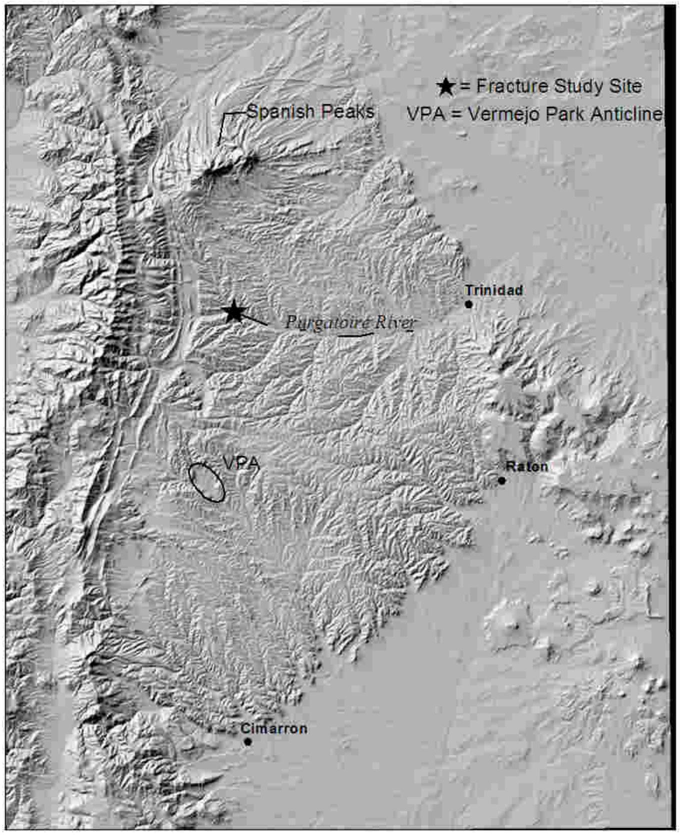

Notes:

Fracture Data:

ID	Strike	Dip	Formation
SC11	22	90	unknown
SC11	23	90	unknown
SC11	29	90	unknown
SC11	27	90	unknown
SC11	24	90	unknown
SC11	31	90	unknown
SC11	27	90	unknown
SC11	18	90	unknown
SC11	28	90	unknown
SC11	25	90	unknown
SC11	13	90	unknown
SC11	25	90	unknown
SC11	18	90	unknown
SC11	23	90	unknown
SC11	26	90	unknown
SC11	24	90	unknown
SC11	22	90	unknown

SC11	24	90	unknown
SC11	20	90	unknown
SC11	25	90	unknown
SC11	25	90	unknown
SC11	290	90	unknown
SC11	311	90	unknown
SC11	296	90	unknown
SC11	311	90	unknown
SC11	295	90	unknown
SC11	278	90	unknown
SC11	278	90	unknown
SC11	277	90	unknown
SC11	282	90	unknown
SC11	285	90	unknown
SC11	279	90	unknown
SC11	289	90	unknown
SC11	289	90	unknown
SC11	289	90	unknown
SC11	279	90	unknown
SC11	279	90	unknown
SC11	280	90	unknown
SC11	286	90	unknown
SC11	281	90	unknown

Location ID: SC12
Latitude: N 37.3586333
Longitude: W 104.7036167

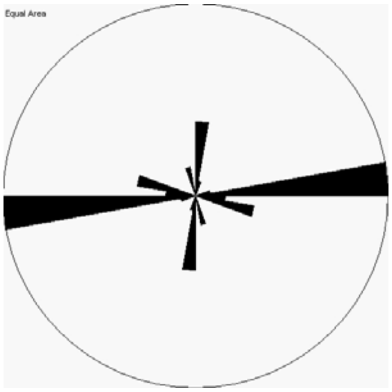

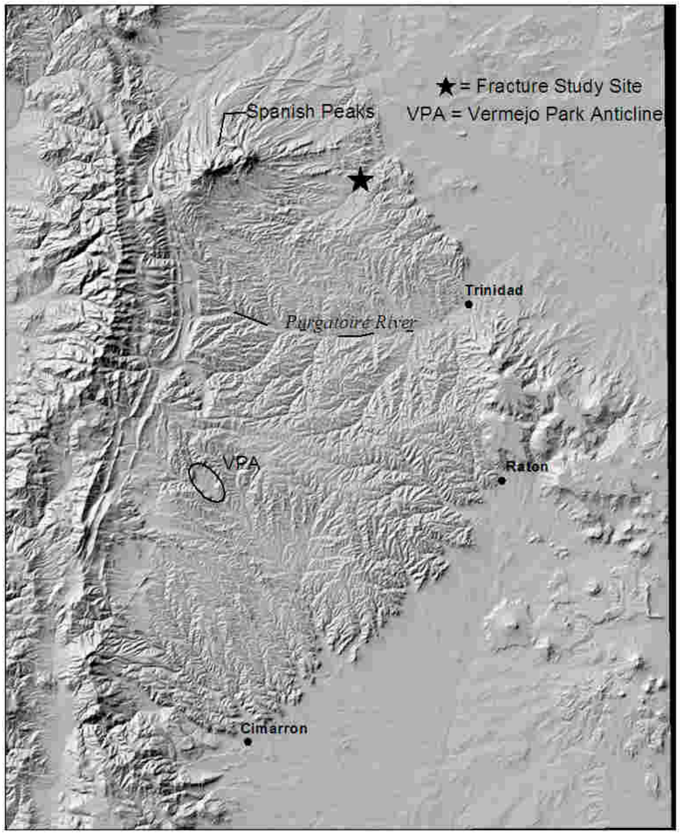

Notes:

Fracture Data:

ID	strike	dip	Formation	Comment 1	Comment 2
SC12	348	90	unknown	ss capped by quaternary alluvium	Raton Fm.?
SC12	8	90	unknown	ss capped by quaternary alluvium	Raton Fm.?
SC12	2	90	unknown	ss capped by quaternary alluvium	Raton Fm.?
SC12	346	90	unknown	ss capped by quaternary alluvium	Raton Fm.?
SC12	12	90	unknown	ss capped by quaternary alluvium	Raton Fm.?
SC12	4	90	unknown	ss capped by quaternary alluvium	Raton Fm.?
SC12	6	90	unknown	ss capped by quaternary alluvium	Raton Fm.?
SC12	2	90	unknown	ss capped by quaternary alluvium	Raton Fm.?
SC12	86	90	unknown	ss capped by quaternary alluvium	Raton Fm.?
SC12	89	90	unknown	ss capped by quaternary alluvium	Raton Fm.?
SC12	281	90	unknown	ss capped by quaternary alluvium	Raton Fm.?
SC12	87	90	unknown	ss capped by quaternary alluvium	Raton Fm.?
SC12	89	90	unknown	ss capped by quaternary alluvium	Raton Fm.?
SC12	90	90	unknown	ss capped by quaternary alluvium	Raton Fm.?
SC12	281	90	unknown	ss capped by quaternary alluvium	Raton Fm.?
SC12	281	90	unknown	ss capped by quaternary alluvium	Raton Fm.?
SC12	280	90	unknown	ss capped by quaternary alluvium	Raton Fm.?

SC12	84	90	unknown	ss capped by quaternary alluvium	Raton Fm.?
SC12	276	90	unknown	ss capped by quaternary alluvium	Raton Fm.?
SC12	84	90	unknown	ss capped by quaternary alluvium	Raton Fm.?
SC12	89	90	unknown	ss capped by quaternary alluvium	Raton Fm.?
SC12	88	90	unknown	ss capped by quaternary alluvium	Raton Fm.?
SC12	87	90	unknown	ss capped by quaternary alluvium	Raton Fm.?
SC12	88	90	unknown	ss capped by quaternary alluvium	Raton Fm.?
SC12	70	90	unknown	ss capped by quaternary alluvium	Raton Fm.?
SC12	89	90	unknown	ss capped by quaternary alluvium	Raton Fm.?
SC12	87	90	unknown	ss capped by quaternary alluvium	Raton Fm.?
SC12	84	90	unknown	ss capped by quaternary alluvium	Raton Fm.?

Location ID: SC13
Latitude: N 36.91998333
Longitude: W 104.4485833

Raton on-ramp to I-25

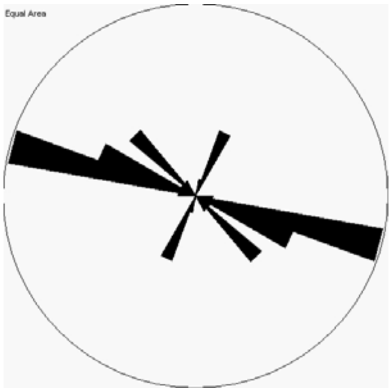

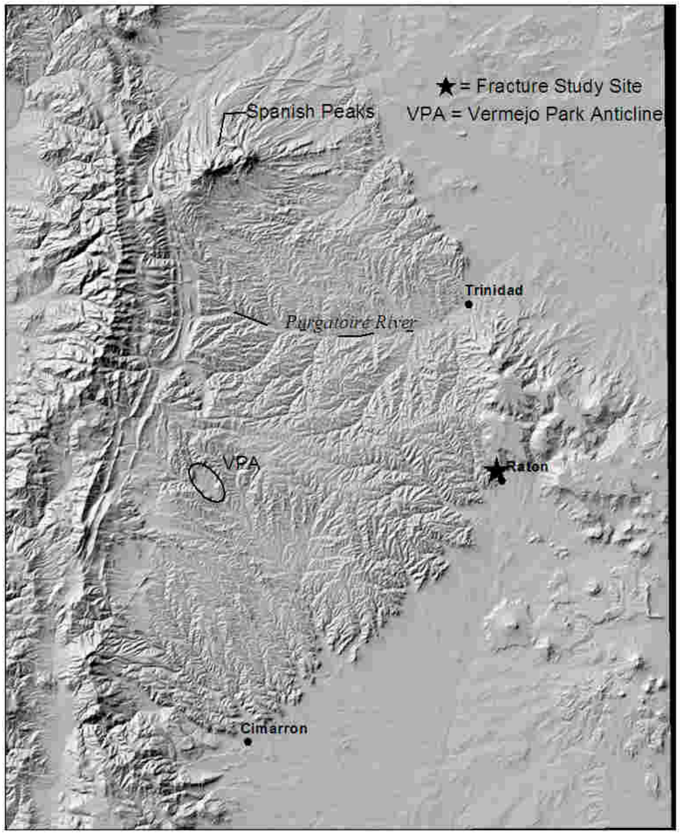

Notes:

Fracture Data:

ID	Strike	dip	Formation	Comment 1
SC13	290	90	Trinidad	
SC13	286	90	Trinidad	
SC13	292	90	Trinidad	
SC13	289	90	Trinidad	
SC13	292	90	Trinidad	
SC13	289	90	Trinidad	
SC13	284	90	Trinidad	
SC13	286	90	Trinidad	
SC13	297	90	Trinidad	
SC13	284	90	Trinidad	
SC13	27	90	Trinidad	
SC13	19	90	Trinidad	
SC13	20	90	Trinidad	
SC13	21	90	Trinidad	
SC13	314	90	Trinidad	
SC13	289	90	Trinidad	thick ss unit above
SC13	287	90	Trinidad	thick ss unit above

SC13	287	90	Trinidad	thick ss unit above
SC13	287	90	Trinidad	thick ss unit above
SC13	279	90	Trinidad	thick ss unit above
SC13	293	90	Trinidad	thick ss unit above
SC13	284	90	Trinidad	thick ss unit above
SC13	293	90	Trinidad	thick ss unit above
SC13	312	90	Trinidad	thick ss unit above
SC13	326	90	Trinidad	thick ss unit above
SC13	310	90	Trinidad	thick ss unit above
SC13	21	90	Trinidad	thick ss unit above
SC13	303	90	Trinidad	thick ss unit above
SC13	314	90	Trinidad	thick ss unit above
SC13	314	90	Trinidad	thick ss unit above

Location ID: SC14
Latitude: N 36.9316333
Longitude: W 104.4583167

I-25 roadcut, just before mp 456

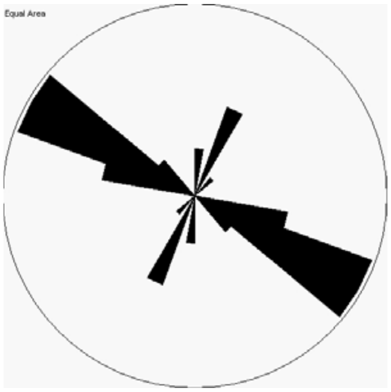

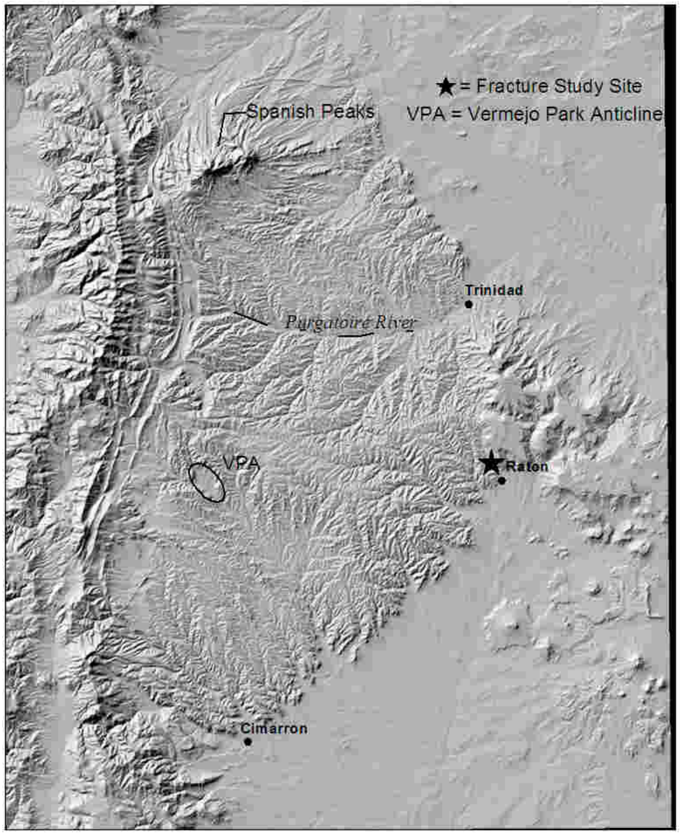

Notes:

Fracture Data:

ID	Strike	Dip	Formation	Comment 1
SC14	289	90	unknown	vermejo or raton?
SC14	290	90	unknown	vermejo or raton?
SC14	42	90	unknown	vermejo or raton?
SC14	288	90	unknown	vermejo or raton?
SC14	308	90	unknown	vermejo or raton?
SC14	285	90	unknown	vermejo or raton?
SC14	29	90	unknown	vermejo or raton?
SC14	302	90	unknown	vermejo or raton?
SC14	298	90	unknown	vermejo or raton?
SC14	294	90	unknown	vermejo or raton?
SC14	303	90	unknown	vermejo or raton?
SC14	1	90	unknown	vermejo or raton?
SC14	307	90	unknown	vermejo or raton?
SC14	295	90	unknown	vermejo or raton?
SC14	295	90	unknown	vermejo or raton?
SC14	314	90	unknown	vermejo or raton?
SC14	296	90	unknown	vermejo or raton?

SC14	291	90	unknown	vermejo or raton?
SC14	304	90	unknown	vermejo or raton?
SC14	310	90	unknown	vermejo or raton?
SC14	303	90	unknown	vermejo or raton?
SC14	22	90	unknown	vermejo or raton?
SC14	308	90	unknown	vermejo or raton?
SC14	1	90	unknown	vermejo or raton?
SC14	289	90	unknown	vermejo or raton?
SC14	22	90	unknown	vermejo or raton?
SC14	307	90	unknown	vermejo or raton?
SC14	24	90	unknown	vermejo or raton?
SC14	291	90	unknown	vermejo or raton?

Location ID: SC15
Latitude: N 36.6563
Longitude: W 104.76545

Dawson cemetery

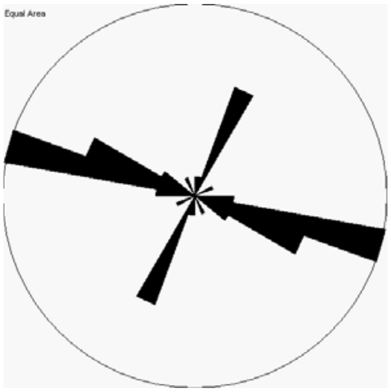

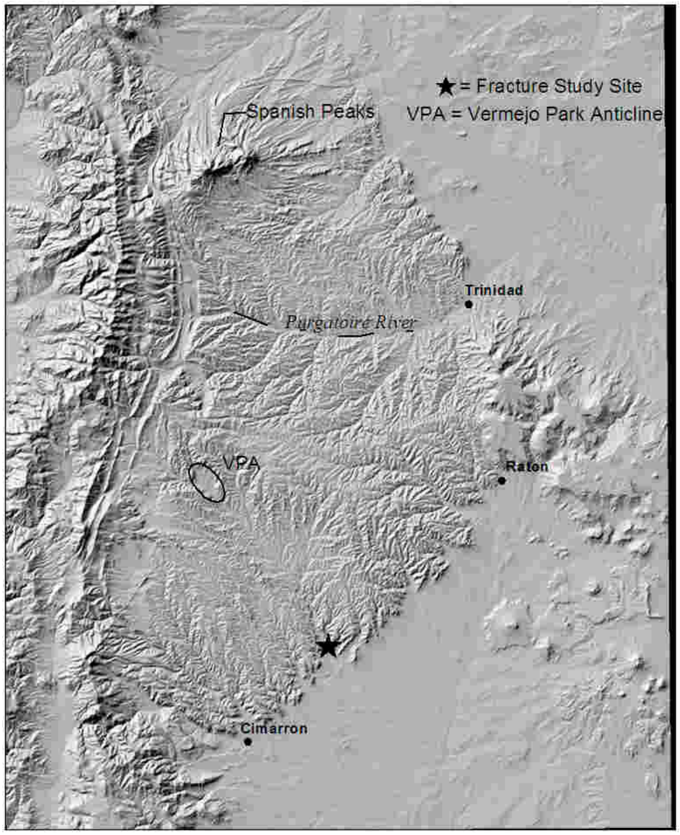

Notes:

Fracture Data:

ID	Strike	Dip	Formation
SC15	292	90	Trinidad
SC15	308	90	Trinidad
SC15	309	90	Trinidad
SC15	283	90	Trinidad
SC15	285	90	Trinidad
SC15	288	90	Trinidad
SC15	281	90	Trinidad
SC15	291	90	Trinidad
SC15	288	90	Trinidad
SC15	275	90	Trinidad
SC15	292	90	Trinidad
SC15	289	90	Trinidad
SC15	284	90	Trinidad
SC15	332	90	Trinidad
SC15	290	90	Trinidad
SC15	288	90	Trinidad
SC15	295	90	Trinidad

SC15	288	90	Trinidad
SC15	291	90	Trinidad
SC15	288	90	Trinidad
SC15	277	90	Trinidad
SC15	20	90	Trinidad
SC15	24	90	Trinidad
SC15	24	90	Trinidad
SC15	16	90	Trinidad
SC15	24	90	Trinidad
SC15	20	90	Trinidad
SC15	27	90	Trinidad
SC15	3	90	Trinidad
SC15	63	90	Trinidad

Location ID: SC16
Latitude: N 37.04026667
Longitude: W 104.5124667

I-25 S, 2 miles before exit 2

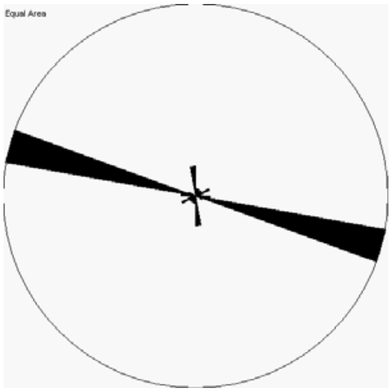

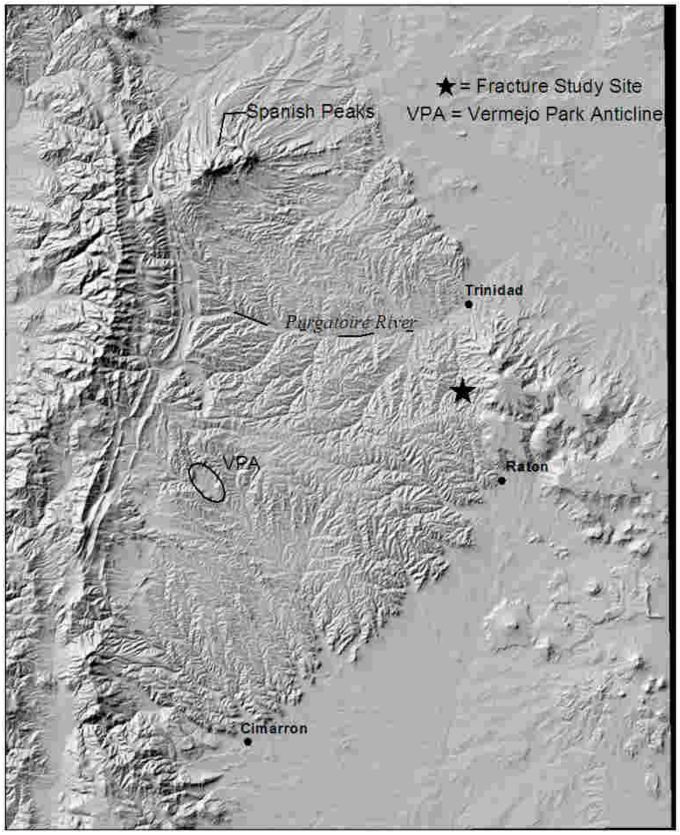

Notes:

- Lower Raton, interbedded ss and mudstone
- 40-50 meters of railroad cut
- fine grained, well cemented
- numerous plumes
- 280 fracture set oldest

Fracture Data:

ID	Strike	Dip	Formation
SC16	288	90	Raton
SC16	286	90	Raton
SC16	289	90	Raton
SC16	356	90	Raton
SC16	2	90	Raton
SC16	289	90	Raton
SC16	282	90	Raton
SC16	60	90	Raton
SC16	282	90	Raton
SC16	51	90	Raton
SC16	278	90	Raton
SC16	65	90	Raton
SC16	285	90	Raton

SC16	276	90	Raton
SC16	280	90	Raton
SC16	288	90	Raton
SC16	48	90	Raton
SC16	282	90	Raton
SC16	250	90	Raton
SC16	282	90	Raton
SC16	289	90	Raton
SC16	283	90	Raton
SC16	19	90	Raton
SC16	284	90	Raton
SC16	289	90	Raton
SC16	291	90	Raton
SC16	26	90	Raton
SC16	287	90	Raton
SC16	357	90	Raton
SC16	286	90	Raton
SC16	359	90	Raton
SC16	285	90	Raton
SC16	289	90	Raton
SC16	351	90	Raton
SC16	288	90	Raton
SC16	287	90	Raton
SC16	284	90	Raton
SC16	283	90	Raton
SC16	287	90	Raton
SC16	286	90	Raton
SC16	282	90	Raton

Location ID: SC17
Latitude: N 37.033033
Longitude: W 104.50445

RR Road, east of Morley ruins

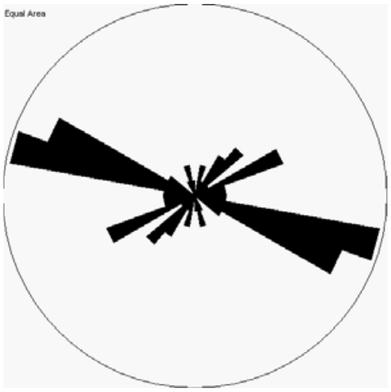

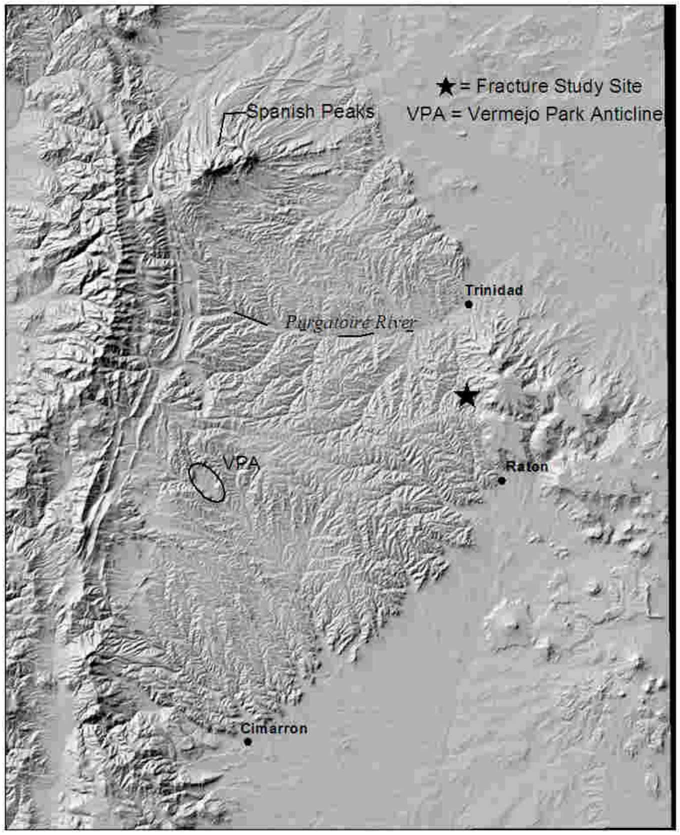

Notes:

- *Ophiomorpha* present, less numerous than Dawson
- Moderately well cemented

Fracture Data:

ID	Strike	Dip	Formation
SC17	35	90	Trinidad
SC17	71	90	Trinidad
SC17	285	90	Trinidad
SC17	34	90	Trinidad
SC17	36	90	Trinidad
SC17	292	90	Trinidad
SC17	62	90	Trinidad
SC17	41	90	Trinidad
SC17	295	90	Trinidad
SC17	288	90	Trinidad
SC17	58	90	Trinidad
SC17	288	90	Trinidad
SC17	15	90	Trinidad
SC17	75	90	Trinidad
SC17	296	90	Trinidad
SC17	294	90	Trinidad

SC17	288	90	Trinidad
SC17	29	90	Trinidad
SC17	292	90	Trinidad
SC17	342	90	Trinidad
SC17	284	90	Trinidad
SC17	303	90	Trinidad
SC17	290	90	Trinidad
SC17	276	90	Trinidad
SC17	292	90	Trinidad
SC17	288	90	Trinidad
SC17	263	90	Trinidad
SC17	297	90	Trinidad
SC17	44	90	Trinidad
SC17	284	90	Trinidad
SC17	287	90	Trinidad
SC17	165	90	Trinidad
SC17	282	90	Trinidad
SC17	224	90	Trinidad
SC17	287	90	Trinidad
SC17	11	90	Trinidad
SC17	249	90	Trinidad
SC17	335	90	Trinidad
SC17	299	90	Trinidad
SC17	269	90	Trinidad
SC17	305	90	Trinidad
SC17	243	90	Trinidad
SC17	282	90	Trinidad
SC17	249	90	Trinidad
SC17	240	90	Trinidad
SC17	350	90	Trinidad
SC17	40	90	Trinidad
SC17	292	90	Trinidad
SC17	285	90	Trinidad
SC17	278	90	Trinidad
SC17	243	90	Trinidad

Location ID: SC18
Latitude: N 37.0515
Longitude: W 104.5226167

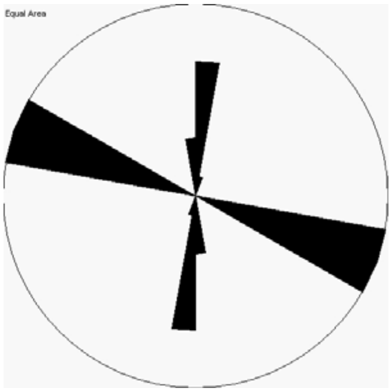

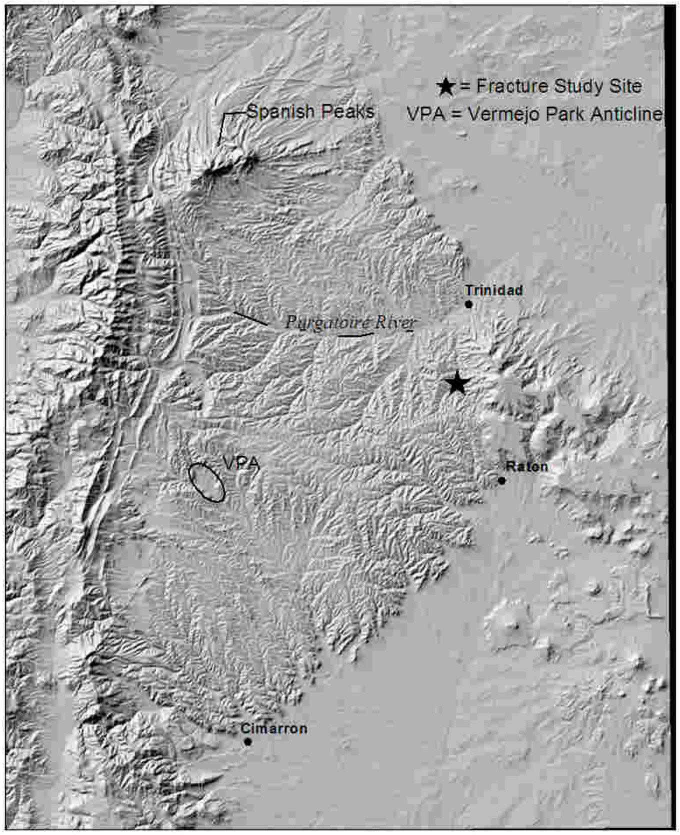

Notes:

- Syn-depositional thrust fault
- Basal Raton unit, some interbedding
- Carbonaceous shale under ss

Fracture Data:

ID	Strike	Dip	Formation
SC18	292	90	Raton
SC18	292	90	Raton
SC18	17	90	Raton
SC18	291	90	Raton
SC18	6	90	Raton
SC18	299	90	Raton
SC18	287	90	Raton
SC18	2	90	Raton
SC18	290	90	Raton
SC18	7	90	Raton
SC18	292	90	Raton
SC18	286	90	Raton
SC18	294	90	Raton
SC18	4	90	Raton
SC18	294	90	Raton

SC18	359	90	Raton
SC18	288	90	Raton
SC18	287	90	Raton
SC18	284	90	Raton
SC18	358	90	Raton
SC18	290	90	Raton
SC18	5	90	Raton
SC18	287	90	Raton
SC18	294	90	Raton
SC18	7	90	Raton
SC18	287	90	Raton
SC18	359	90	Raton
SC18	286	90	Raton
SC18	1	90	Raton
SC18	288	90	Raton
SC18	282	90	Raton

Location ID: SC19
Latitude: N 37.03231667
Longitude: W 104.5018833

I-25 N, south of chart 18, dike

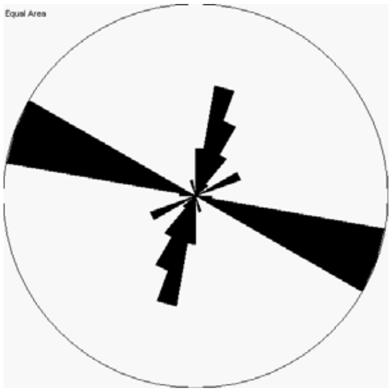

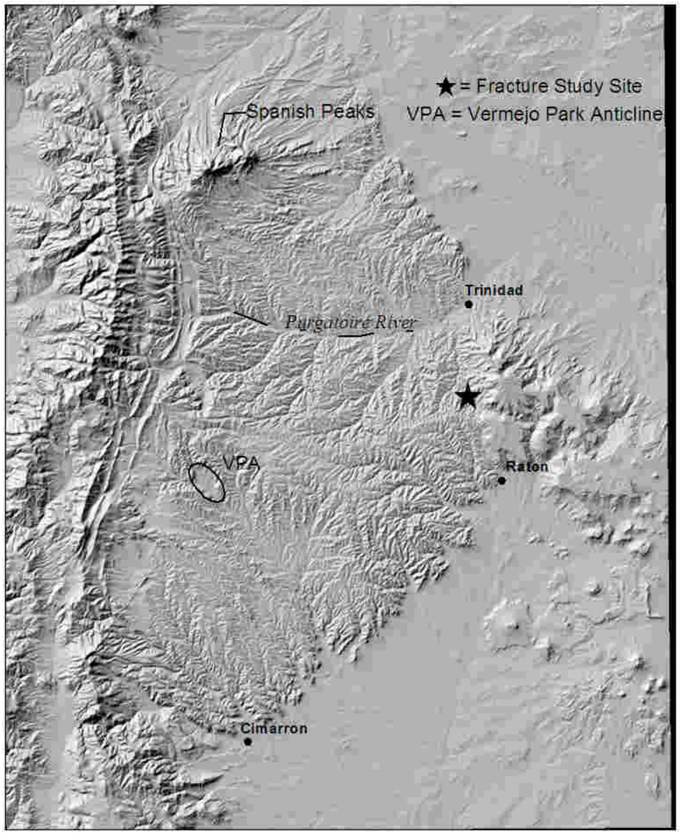

Notes:

- Vermejo ss, measured below 4-5 m coal bed
- Dike strikes 287; mm-scale crystals

Fracture Data:

ID	Strike	Dip	Formation	Comment 1
SC19	104	90	Vermejo	
SC19	185	90	Vermejo	
SC19	94	90	Vermejo	
SC19	4	90	Vermejo	
SC19	21	90	Vermejo	
SC19	280	90	Vermejo	
SC19	287	90	Vermejo	
SC19	40	90	Vermejo	
SC19	290	90	Vermejo	
SC19	287	90	Vermejo	
SC19	287	90	Vermejo	
SC19	218	90	Vermejo	
SC19	347	90	Vermejo	
SC19	10	90	Vermejo	
SC19	5	90	Vermejo	
SC19	287	90	Vermejo	

SC19	283	90	Vermejo	
SC19	287	90	Vermejo	
SC19	16	90	Vermejo	
SC19	292	90	Vermejo	
SC19	17	90	Vermejo	
SC19	290	90	Vermejo	
SC19	15	90	Vermejo	
SC19	290	90	Vermejo	
SC19	288	90	Vermejo	
SC19	20	90	Vermejo	
SC19	290	90	Vermejo	
SC19	12	90	Vermejo	
SC19	293	90	Vermejo	
SC19	296	90	Vermejo	
SC19	33	90	Vermejo	coal above ss
SC19	109	90	Vermejo	coal above ss
SC19	30	90	Vermejo	coal above ss
SC19	27	90	Vermejo	coal above ss
SC19	116	90	Vermejo	coal above ss
SC19	114	90	Vermejo	coal above ss
SC19	20	90	Vermejo	coal above ss
SC19	22	90	Vermejo	coal above ss
SC19	293	90	Vermejo	coal above ss
SC19	291	90	Vermejo	
SC19	15	90	Vermejo	
SC19	298	90	Vermejo	
SC19	62	90	Vermejo	lower ss unit
SC19	60	90	Vermejo	lower ss unit
SC19	11	90	Vermejo	lower ss unit
SC19	285	90	Vermejo	lower ss unit
SC19	60	90	Vermejo	lower ss unit
SC19	283	90	Vermejo	lower ss unit

Location ID: SC20
Latitude: N 37.02145
Longitude: W 104.49175

I-25 N exit 2

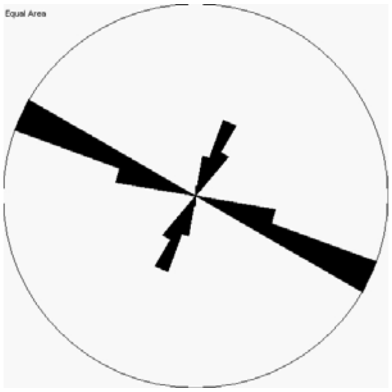

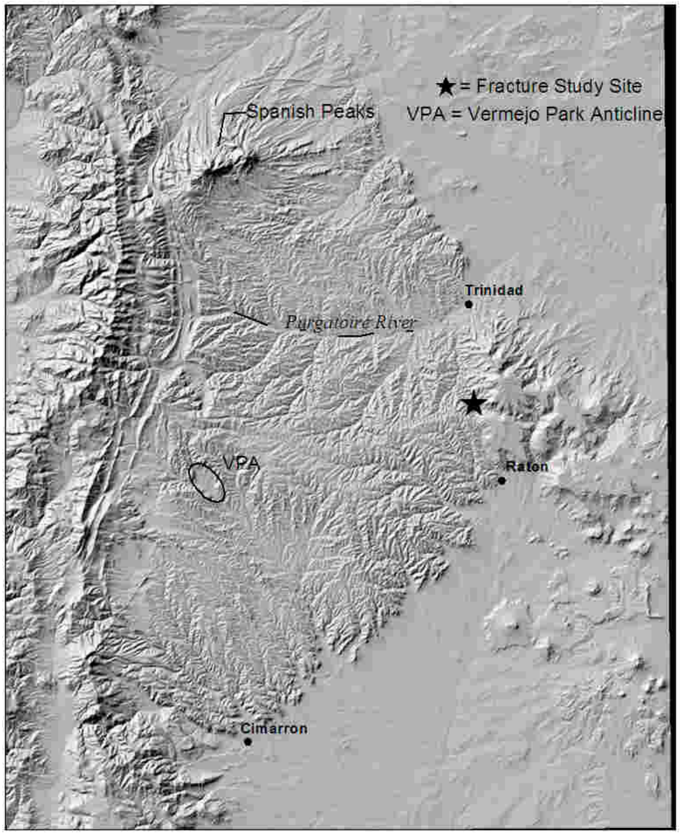

Notes:

- ~1 m thick bed of basal Raton
- well cemented
- iron oxide and calcite cement mineralization
- extension fractures, plumes
- 20 degree fracture set is younger than 290 set

Fracture Data:

ID	Strike	Dip	Formation	Comment 1
SC20	299	90	Raton	Basal raton sand?
SC20	293	90	Raton	Basal raton sand?
SC20	290	90	Raton	Basal raton sand?
SC20	31	90	Raton	Basal raton sand?
SC20	287	90	Raton	Basal raton sand?
SC20	18	90	Raton	Basal raton sand?
SC20	287	90	Raton	Basal raton sand?
SC20	21	90	Raton	Basal raton sand?
SC20	29	90	Raton	Basal raton sand?
SC20	293	90	Raton	Basal raton sand?
SC20	25	90	Raton	Basal raton sand?
SC20	20	90	Raton	Basal raton sand?

SC20	291	90	Raton	Basal raton sand?
SC20	293	90	Raton	Basal raton sand?
SC20	296	90	Raton	Basal raton sand?
SC20	31	90	Raton	Basal raton sand?
SC20	293	90	Raton	Basal raton sand?
SC20	290	90	Raton	Basal raton sand?
SC20	22	90	Raton	Basal raton sand?
SC20	298	90	Raton	Basal raton sand?
SC20	39	90	Raton	Basal raton sand?
SC20	28	90	Raton	Basal raton sand?
SC20	295	90	Raton	Basal raton sand?
SC20	37	90	Raton	Basal raton sand?
SC20	298	90	Raton	Basal raton sand?
SC20	13	90	Raton	Basal raton sand?
SC20	297	90	Raton	Basal raton sand?
SC20	288	90	Raton	coals above
SC20	289	90	Raton	coals above
SC20	287	90	Raton	coals above
SC20	289	90	Raton	coals above
SC20	292	90	Raton	coals above
SC20	290	90	Raton	coals above
SC20	296	90	Raton	coals above
SC20	290	90	Raton	coals above
SC20	292	90	Raton	coals above
SC20	289	90	Raton	coals above
SC20	288	90	Raton	coals above
SC20	290	90	Raton	coals above
SC20	17	90	Raton	coals above
SC20	32	90	Raton	coals above
SC20	9	90	Raton	coals above
SC20	13	90	Raton	coals above
SC20	21	90	Raton	coals above
SC20	23	90	Raton	coals above

DISTRIBUTION

61	Sandia National Labs	
	MS 0373	John Holland 09127 (2)
	0706	Chris Rautman 06113 (2)
	0750	Scott Cooper 06116 (20)
		John Lorenz (25)
		James Herrin (2)
		Greg Elbring (1)
	0751	Bill Olsson 06117 (2)
	0778	Bill Arnold 06851 (2)
	9018	Central Technical Files 8945-1 (3)
2	M3669	Los Alamos National Laboratory Attn: J.C. Stevenson, WDP-WD M. George, M4 P.O. Box 1663 Los Alamos, NM 87545
3	M0830	Lawrence Livermore National Laboratory Attn: R.F. Chatham, L125 (2) A.B. Palmen, L394 P.O. Box 808 Livermore, CA 94550
6	M0701	US Department of Energy Attn: Maj. Gen. W.W. Hoover Washington, DC 20545
1	M0800	J.S. Kendall, 8417
1	M0800	P.R. Walker, 8417
1	M0800	Central Technical Files, 8945-1
5	MS 0314	L.G. Grant, 9811
		0574 D.R. Jones, 5941
8	0827	J.R. Dallas, 1502 Attn: R. Collier
1	0832	A.T. Walker, 6503
1	0841	E.R. Farmer, 3340 Attn: D.G. Anderson, 3341
2	0899	Technical Library, 9616
1	0161	Patent and Licensing Office, 11500

4 Vermejo Park Ranch
Attn: Rich Larsen (2)
Gus Holm (2)
P.O. Drawer E
Raton, NM 87740

5 El Paso Production Company
Attn: Kenneth Whetstone
Nine Greenway Plaza
Houston, Tx 77046

2 New Mexico Bureau of Geology and Mineral Resources
Attn: Ron Broadhead
Tom Engler, Chair, Petroleum and Natural Gas Engineering Department
801 Leroy Place
Socorro, NM 87801

1 Devon Energy Corporation
Attn: Curt McKinney
20 North Broadway
Oklahoma City, OK 73102-8260

1 Connie Knight
1800 Washington Ave
Golden, CO 80401